THE JOURNAL
OF
CHEMICAL PHYSICS

VOLUME 21, NUMBER 10 OCTOBER, 1953

# A Study of the Infrared Spectrum of the Amide Group*†

HARRY LETAW, JR.‡ AND ARMIN H. GROPP
*Department of Chemistry, University of Florida, Gainesville, Florida*
(Received April 2, 1953)

The very strong 1560-cm$^{-1}$ band of the N-substituted amide group has been assigned previously either to $\nu$(C−N) or to $\delta$(N−H). This investigation consisted of a study of the frequency shifts of this and other bands in the infrared spectra of several N-butyl- and N,N-dibutyl-ethanamides upon substitution of chlorine and fluorine in the 2 position. On the basis of these shifts and other properties of the band in question, observed in the spectra both of the pure compounds and of their $CCl_4$ solutions, it is concluded that the $\nu$(C−N) assignment is correct. The apparent absence of the corresponding band from the spectrum of the N,N-disubstituted amide group is explained by the accidental degeneracy of $\nu$(C=O) and $\nu$(C−N). Other bands were cataloged and assigned where possible.

## INTRODUCTION

THE problems of particular interest in the present research were the assignment of the very strong 1560-cm$^{-1}$ band which occurs in the spectra of the N-monosubstituted amides and the explanation of the absence of this band from the spectra of the N,N-disubstituted amides. Perhaps the most thorough interpretations are those of Richards and Thompson[1] and Lenormant.[2] The former have assigned the band in question to $\delta$(N−H), while the latter states that it is $\nu$(C−N). These opinions will be examined in detail in the light of the evidence brought out in the present investigation.

Previous investigations of this problem have usually centered about differences between the spectra of similar compounds with various groups substituted upon the amido-nitrogen. The present communication is a report of a study of the infrared spectra of several 2-halogeno-ethanamides, both N-butyl- and N,N-dibutyl-substituted. These series of compounds were selected because they made possible the observation of the effect of a gradual change in the electronegativity of a substituent in a previously neglected position on the molecule upon the characteristic infrared bands of the amide group.

## EXPERIMENTAL

The infrared spectrograms were obtained by use of Perkin-Elmer Model 21 and Model 12-C spectrometers. The latter instrument was made available to us by the Glidden Corporation's Naval Stores Research Laboratories in Jacksonville, Florida. Sodium chloride optics were used throughout this research.

TABLE I. $\nu$(N−H) of some N-butyl-ethanamides.

| Compound | Frequency (cm$^{-1}$) Pure | Dilute | Frequency increase (cm$^{-1}$) |
|---|---|---|---|
| N-butyl-ethanamide | 3279 (s) | 3436 (m) | 157 |
| | 3086 (m) | | 350 |
| N-butyl-2-chloro-ethanamide | 3257 (s) | 3413 (m) | 156 |
| | 3067 (m) | | 346 |
| N-butyl-2,2-dichloro-ethanamide | 3257 (s) | 3425 (m) | 168 |
| | 3067 (m) | | 358 |
| N-butyl-2-chloro-2-fluoro-ethanamide | 3268 (s) | 3425 (m) | 157 |
| | 3067 (m) | | 358 |
| N-butyl-2,2-difluoro-ethanamide | 3425 (m) | 3425 (m) | 0 |
| | 3268 (s) | | 157 |
| | 3086 (m) | | 339 |
| N-butyl-2,2,2-trifluoro-ethanamide | 3289 (s) | 3425 (m) | 136 |
| | 3086 (m) | | 339 |

* Presented in part at the 318th Meeting of the American Physical Society, Durham, North Carolina, March 26–28, 1953.
† Abstracted from a dissertation presented by H.L. in partial fulfilment of the requirements for the Ph.D. degree.
‡ U. S. Atomic Energy Commission Predoctoral Fellow, 1950–1952. Now at the University of Illinois, Urbana, Illinois.
[1] R. E. Richards and H. W. Thompson, J. Chem. Soc. (London) 1947, 1248.
[2] H. Lenormant, Ann. chim. 5, 459 (1950).

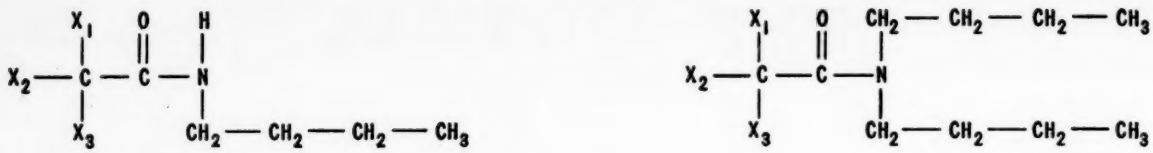


| $X_1$ | $X_2$ | $X_3$ |
|---|---|---|
| H | H | H |
| H | H | Cl |
| H | Cl | Cl |
| H | F | Cl |
| H | F | F |
| F | F | F |

FIG. 1. Schematic structural formulas of (a) the N-butyl-ethanamides and (b) the N,N-dibutyl-ethanamides.

The compounds studied, prepared by Dr. P. Tarrant and co-workers of this laboratory, were N-butyl-ethanamide, N-butyl-2-chloro-ethanamide, N-butyl-2,2-dichloro-ethanamide, N-butyl-2-chloro-2-fluoro-ethanamide, N-butyl-2,2-difluoro-ethanamide, N-butyl-2,2,2-trifluoro-ethanamide, and the corresponding N,N-dibutyl-ethanamides. The structural formulas of these compounds are illustrated in Fig. 1.

Each compound except N-butyl-2,2-dichloro-ethanamide was investigated in the pure liquid state at 25°C. The exceptional compound, being a solid at this temperature, was run as a highly concentrated mull in $CCl_4$. A demountable cell was used for this work. Several dilutions of each compound were prepared in $CCl_4$ and run with solvent compensation. The lowest concentration investigated, usually about 0.006$M$, was such that further shifts in dilution-sensitive band frequencies were not observed in more dilute samples.

Because of the nature of the problem, greatest emphasis was placed upon the bands occurring in the carbonyl region; however, other bands were studied also.

## RESULTS

The N-butyl series of compounds presented the characteristic $\nu$(N−H) in the region of 3200 $cm^{-1}$. The frequencies of the two bands typical of perturbation due to hydrogen bonding and the single band resulting from dissociation are given in Table I. The disappearance of the lower frequency bands upon dilution and the appearance of the unperturbed $\nu$(N−H) was quite gradual throughout. In general, the band of lower frequency tended to decrease in intensity at the more rapid rate.

A set of weak bands appeared in the spectra of the N,N-dibutyl-ethanamides near 3300–3500 $cm^{-1}$. Those of lower frequency increased virtually monotonically from 3257 to 3332 $cm^{-1}$. They are identified as harmonics of the band which progresses from 1647 to 1689 $cm^{-1}$. The higher frequency band occurs in the neighborhood of 3448 $cm^{-1}$. This is near the monomeric $\nu$(N−H) observed in the other series. In view of the fact that this absorption is quite weak and that other bands which might be attributed to the presence of the N-butyl ethanamides are absent, it is unlikely that these are due to such impurities. It is evident that small quantities of such materials would be virtually completely hydrogen bound. This indicates that the frequency cited is incorrect for $\nu$(N−H) under these conditions. Although these could be water bands, the frequency is somewhat higher in the case of the latter than that ob

TABLE II. Low-intensity, high-frequency bands of some N,N-dibutyl-ethanamides.

| Compound | Frequency ($cm^{-1}$) |
|---|---|
| N,N-dibutyl-ethanamide | 3436 (w)<br>3257 (vw<br>1727 (vw |
| N,N-dibutyl-2-chloro-ethanamide | 3448 (w)<br>3287 (w)<br>1733 (w) |
| N,N-dibutyl-2,2-dichloro-ethanamide | 3390 (vw<br>3289 (w)<br>1754 (w) |
| N,N-dibutyl-2-chloro-2-fluoro-ethanamide | 3413 (vw<br>3279 (w)<br>1770 (w) |
| N,N-dibutyl-2,2-difluoro-ethanamide | 3472 (vw<br>3300 (vw<br>1764 (w) |
| N,N-dibutyl-2,2,2-trifluoro-ethanamide | 3472 (vw<br>3322 (w)<br>1776 (vw |

served here. The variation in frequency from compound to compound is beyond the limits of probable error. It is possible that these bands are harmonics; however, we were unable to assign them. The frequency data on these two bands and a weak, unassigned band appearing in the neighborhood of 1750 $cm^{-1}$ are in Table II. The latter does not appear to be a fundamental although a harmonic at 3448 $cm^{-1}$ could imply that it is.

$\nu$(C—H) was assigned to three bands. A shoulder of medium intensity occurs at 2924 $cm^{-1}$, a strong band at 2915 $cm^{-1}$, and a band of medium intensity at 2849 $cm^{-1}$. These frequencies are invariant under dilution and are adhered to within narrow limits by all species of both series of compounds. There is no apparent difference in the bands of compounds into which halogen substituents have been introduced even though one would expect a highly activated 2 hydrogen to give rise to a shifted $\nu$(C—H). Such an observation would perhaps be impossible in view of the overwhelming intensities of like vibrations in the butyl groups.

TABLE III. $\nu$(C=O) of some N-butyl-ethanamides.

| Compound | Frequency ($cm^{-1}$) Pure | Dilute | Frequency increase ($cm^{-1}$) |
|---|---|---|---|
| N-butyl-ethanamide | 1658 (vs) | 1686 (vs) | 28 |
| | 1645 (vs) | | 41 |
| N-butyl-2-chloro-ethanamide | 1661 (vs) | 1686 (vs) | 25 |
| | 1653 (vs) | | 33 |
| N-butyl-2,2-dichloro-ethanamide | 1692 (vs) | 1706 (vs) | 14 |
| | 1675 (vs) | | 31 |
| N-butyl-2-chloro-2-fluoro-ethanamide | 1692 (vs) | 1712 (vs) | 20 |
| | 1678 (vs) | | 34 |
| N-butyl-2,2-difluoro-ethanamide | 1684 (vs) | 1718 (vs) | 34 |
| | 1675 (vs) | | 43 |
| N-butyl-2,2,2-trifluoro-ethanamide | 1718 (vs) | 1736 (vs) | 18 |
| | 1706 (vs) | | 30 |

Tables III and IV contain the frequency data for $\nu$(C=O) and the 1562 $cm^{-1}$ bands appearing in the spectra of the N-butyl-ethanamides. The shifts in frequency upon dilution are also indicated. It should be noted that a rather detailed study of the structure of these bands has been carried out.

A previously unreported phenomenon was observed in the spectra of N,N-dibutyl-2,2-dichloro-ethanamide, N,N-dibutyl-2-chloro-2-fluoro-ethanamide, and N,N-dibutyl-2,2-difluoro-ethanamide. Upon dilution, the band near 1670 $cm^{-1}$ is found to split. This split is roughly symmetrical about the frequency of the band observed in the spectrum of the pure material. The higher frequency portion is of lower intensity. The frequency data in this region for all of the N,N-dibutyl compounds are given in Table V. The other three members of the series did not show either a split or a significant shift of the frequency of this band upon dilution. Highest definition was found in the case of N,N-dibutyl-2,2-dichloro-ethanamide. Structure of the band for this compound is shown in Fig. 2.

TABLE IV. $\nu$(C—N) of some N-butyl-ethanamides.

| Compound | Frequency ($cm^{-1}$) Pure | Dilute | Frequency decrease ($cm^{-1}$) |
|---|---|---|---|
| N-butyl-ethanamide | 1565 (vs) | 1502 (s) | 63 |
| | 1555 (vs) | | 53 |
| | 1546 (s) | | 44 |
| N-butyl-2-chloro-ethanamide | 1563 (s) | 1515 (s) | 48 |
| | 1552 (vs) | | 37 |
| | 1546 (vs) | | 31 |
| N-butyl-2,2-dichloro-ethanamide | 1563 (vs) | 1513 (s) | 50 |
| | 1552 (s) | | 39 |
| | 1548 (s) | | 35 |
| | 1527 (s) | | 14 |
| N-butyl-2-chloro-2-fluoro-ethanamide | 1562 (vs) | 1515 (s) | 47 |
| | 1553 (s) | | 38 |
| | 1549 (s) | | 34 |
| N-butyl-2,2-difluoro-ethanamide | 1566 (vs) | 1524 (s) | 42 |
| | 1554 (vs) | | 30 |
| N-butyl-2,2,2-trifluoro-ethanamide | 1564 (vs) | 1524 (s) | 40 |
| | 1557 (vs) | | 33 |

Extremely intense bands occurred in the spectra of all of the compounds containing fluorine. The frequencies and relative intensities of these bands are tabulated in Table VI. As would be expected on the basis of data pertaining to simpler compounds containing fluorine,[3] the $\nu$(C—F) frequencies progressively increase with the substitution of additional fluorine. Fuson and coworkers[4] have recently stated that compounds containing a perfluoromethyl group bonded to a carbon atom will have two $\nu$(C—F) about 50 $cm^{-1}$ apart in the

TABLE V. $\nu$(C=O), $\nu$(C—N) of some N,N-dibutyl-ethanamides.

| Compound | Frequency ($cm^{-1}$) Pure | Dilute | Frequency shift ($cm^{-1}$) |
|---|---|---|---|
| N,N-dibutyl-ethanamide | 1647 (vs) | 1647 (vs) | 0 |
| N,N-dibutyl-2-chloro-ethanamide | 1658 (vs) | 1656 (vs) | −2 |
| N,N-dibutyl-2,2-dichloro-ethanamide | 1667 (vs) | 1684 (s) | +17 |
| | | 1658 (vs) | −9 |
| N,N-dibutyl-2-chloro-2-fluoro-ethanamide | 1675 (vs) | 1686 (s) | +11 |
| | | 1664 (vs) | −11 |
| N,N-dibutyl-2,2-difluoro-ethanamide | 1675 (vs) | 1686 (m) | +11 |
| | | 1667 (vs) | −8 |
| N,N-dibutyl-2,2,2-trifluoro-ethanamide | 1689 (vs) | 1692 (vs) | +3 |

[3] Smith, Brown, Nielsen, Smith, and Liang, J. Chem. Phys. **20**, 473 (1952); Smith, Saunders, Nielsen, and Ferguson, J. Chem. Phys. **20**, 847 (1952).

[4] Fuson, Josien, Jones, and Lawson, J. Chem. Phys. **20**, 1627 (1952).

1150–1300 $cm^{-1}$ range. This prediction is borne out by the data obtained in this investigation.

A strong absorption band found in the neighborhood of 1408–1460 $cm^{-1}$ in the spectra of all of the compounds studied is assumed to be due to $\delta(C-H)$. Assignment is made on the basis of the analysis of propane[5] in which methylene deformations and assymetric methyl deformations occur at 1465, 1468, and 1470 $cm^{-1}$. We have been unable to find any statement in the literature with respect to the assignment of $\delta(N-H)$ to this broad (on the order of 100 $cm^{-1}$ at half-height) band.

It was found that a band occurred at about 1380 $cm^{-1}$ in all cases. A similar band occurs in the spectrum of acetamide and has been assigned by Davies and Hallam[6] to $\nu(C-N)$. We found no change in the frequency of this band upon dilution. In subsidiary spectrograms, it was found that this band occurs nearly identically in form and in relative intensity in *n*-butanol and in the three *n*-butyl-, *n*-hexyl-, and *n*-octyl-amines. Bands at 1370 and 1375 $cm^{-1}$ in the propane spectrum are assigned to symmetrical deformations of the methyl groups.[5] This evidence has led us to assign this band to $\delta(C-H)$.

A band found in the 1300–1320 $cm^{-1}$ range in the spectra of all compounds studied is somewhat confusing. The analogous band of acetamide is assigned to the symmetrical $\delta(C-H)$.[6] We have found this band in the amines and in the alcohol mentioned above. It is more intense in the secondary amines than it is in the primary and even more so in the tertiary. Though this band has no obvious counterpart in the spectrum of propane, we are inclined to agree with the assignment of Davies and Hallam.[6]

A rather broad resolved pair of bands centering about 1250 $cm^{-1}$ is assigned to rocking or wagging methyl and methylene vibrations. The corresponding vibrations in propane[5] are displaced to lower frequencies by about 70

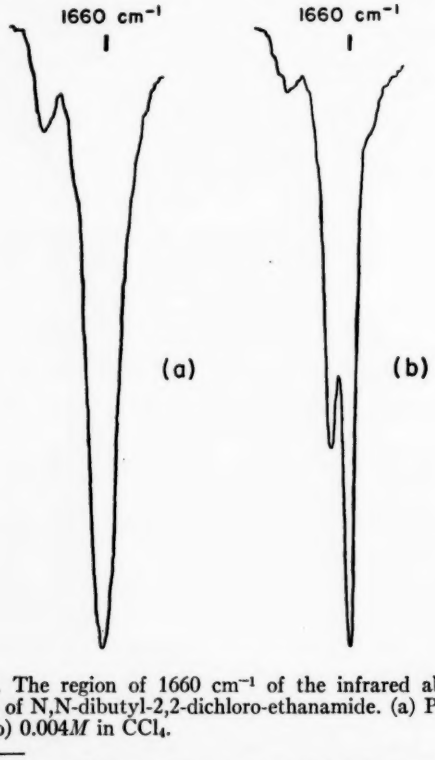


FIG. 2. The region of 1660 $cm^{-1}$ of the infrared absorption spectrum of N,N-dibutyl-2,2-dichloro-ethanamide. (a) Pure compound. (b) 0.004*M* in $CCl_4$.

TABLE VI. $\nu(C-F)$ of some 2-fluoro-ethanamides.

| Compound | Frequency ($cm^{-1}$) Pure | Dilute |
|---|---|---|
| N-butyl-2-chloro-2-fluoro-ethanamide | 1112 (m)<br>1087 (s)<br>1062 (vs)<br>1036 (m) | 1080 (w)<br>1052 (vs) |
| N,N-dibutyl-2-chloro-2-fluoro-ethanamide | 1112 (m)<br>1094 (vs)<br>1075 (s)<br>1056 (m)<br>1024 (w) | 1112 (w)<br>1096 (m)<br>1062 (vs)<br>1024 (w) |
| N-butyl-2,2-difluoro-ethanamide | 1136 (vs)<br>1107 (vs)<br>1088 (vs)<br>1065 (vs) | 1110 (vs)<br>1107 (vs)<br>1085 (vs)<br>1065 (vs) |
| N,N-dibutyl-2,2-difluoro-ethanamide | 1117 (vs)<br>1060 (vs) | 1106 (s)<br>1056 (vs) |
| N-butyl-2,2,2-trifluoro-ethanamide | 1208 (vs)<br>1182 (vs)<br>1163 (vs) | 1202 (s)<br>1163 (vs) |
| N,N-dibutyl-2,2,2-trifluoro-ethanamide | 1202 (vs)<br>1179 (vs)<br>1140 (vs)<br>1130 (vs) | 1205 (vs)<br>1179 (s)<br>1140 (vs)<br>1126 (s) |

TABLE VII. Average vibrational frequencies of the N-butyl-ethanamides.

| Frequency ($cm^{-1}$) | Relative intensity | Assignment |
|---|---|---|
| 3425 | (m) | $\nu(N-H)$ (monomer) |
| 3270 | (s) | $\nu(N-H)$ (linear dimer) |
| 3076 | (m) | $\nu(N-H)$ (cyclic dimer) |
| 2924 | (sh) | $\nu(C-H)$ |
| 2915 | (s) | $\nu(C-H)$ |
| 2849 | (m) | $\nu(C-H)$ |
| 1707 | (vs) | $\nu(C=O)$ (monomer) |
| 1684 | (vs) | $\nu(C=O)$ (cyclic dimer) |
| 1672 | (vs) | $\nu(C=O)$ (linear dimer) |
| 1564 | (vs) | $\nu(C-N)$ (cyclic dimer) |
| 1554 | (vs) | $\nu(C-N)$ (linear N—H—O) |
| 1547 | (s) | $\nu(C-N)$ (linear N—H—N) |
| 1516 | (s) | $\nu(C-N)$ (monomer) |
| 1408–1460 | (s) | $\delta(C-H)$, $\delta(N-H)$ |
| 1380 | (m) | $\delta(C-H)$ |
| 1300–1320 | (m) | $\delta(C-H)$ |
| 1250 | (m) | $w,r(C-H)$ |
| 1208–1163 | (vs) | $\nu(C-F)$ ($CF_3$) |
| 1136–1065 | (vs) | $\nu(C-F)$ ($CF_2$) |
| 1112–1036 | (vs) | $\nu(C-F)$ (CClF) |
| 1065–1095 | (m) | $\nu(C-N)$ (butyl-N) |

[5] G. Herzberg, *Molecular Spectra and Molecular Structure* (D. Van Nostrand Company, Inc., New York, 1945), Vol. II.

[6] M. Davies and H. E. Hallam, Trans. Faraday Soc. 47, 1170 (1951).

$cm^{-1}$. In some of the compounds, these bands are masked by $\nu$(C−F).

The N-butyl-ethanamides absorb in the 1065–1095 $cm^{-1}$ region while the analogous vibration occurs at 1098–1122 $cm^{-1}$ in the other series of compounds. We have assigned these bands to $\nu$(C−N) of the butyl-nitrogen bond although the frequency is somewhat higher than would be expected. These frequencies are quite near to those assigned to methyl and methylene rocking modes in other compounds and could possibly be so identified.

Several other bands were observed throughout the remainder of the sodium chloride region in all of the compounds studied. Insufficient data are at hand to permit the assignment of these vibrations.

## DISCUSSION

The easily identified $\nu$(N−H) frequencies have been recorded in Table I. There is no question as to the assignment of the band found at higher dilutions; however, evidence has been presented elsewhere[7] with respect to the nature of the bands found in the spectra of the pure substances and the configuration of the N-alkyl-amides which is at variance with previous conclusions. Mizushima *et al.*,[7] have postulated that the trans-form alone exists in N-methyl-ethanamide. As a result, they exclude the possibility of the formation of a cyclic dimer in concentrated solutions. They have identified both the 3086 and 3270 $cm^{-1}$ bands as $\nu$(N−H) of the associated molecules. Other investigators[2,8,9] have stated that the lower frequency band is due to cyclic dimers and the higher frequency to linear configurations. In the present research, it was noted that the lower frequency band was of lower relative intensity than was the higher and that, upon dilution, the former was the first to vanish. In the absence of a more suitable explanation of the origin of the 3086 $cm^{-1}$ band, we have chosen to identify it with $\nu$(N−H) perturbed through cyclic dimerization. A significant argument in favor of this interpretation is that the frequency shift of this band upon dilution is nearly double that of the higher frequency band. It has been shown that the absolute values of frequency shifts in infrared spectra have little obvious significance;[10] however, the relative frequency shifts are applicable to the calculation of energies.[11,12] One would expect the

TABLE VIII. Average vibrational frequencies of the N,N-dibutyl-ethanamides.

| Frequency ($cm^{-1}$) | Relative intensity | Assignment |
|---|---|---|
| 3438 | (vw) | 1754 $cm^{-1}$ harmonic (?) |
| 3289 | (w) | 1668 $cm^{-1}$ harmonic |
| 2924 | (sh) | $\nu$(C−H) |
| 2915 | (s) | $\nu$(C−H) |
| 2849 | (m) | $\nu$(C−H) |
| 1754 | (w) | (?) |
| 1668 | (vs) | $\nu$(C=O), $\nu$(C−N) |
| 1408–1460 | (s) | $\delta$(C−H) |
| 1380 | (m) | $\delta$(C−H) |
| 1300–1320 | (m) | $\delta$(C−H) |
| 1250 | (m) | $w,r$(C−H) |
| 1205–1126 | (vs) | $\nu$(C−F) ($CF_3$) |
| 1106–1056 | (vs) | $\nu$(C−F) ($CF_2$) |
| 1112–1024 | (vs) | $\nu$(C−F) (CClF) |
| 1098–1122 | (m) | $\nu$(C−N) (butyl-N) |

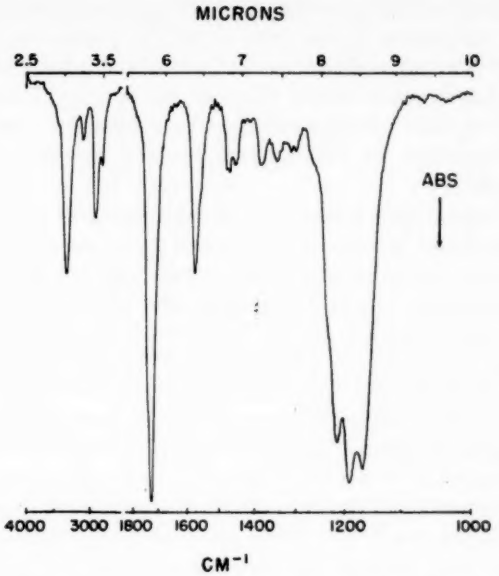


FIG. 3. Absorption spectrum of pure N-butyl-2,2,2-trifluoro-ethanamide.

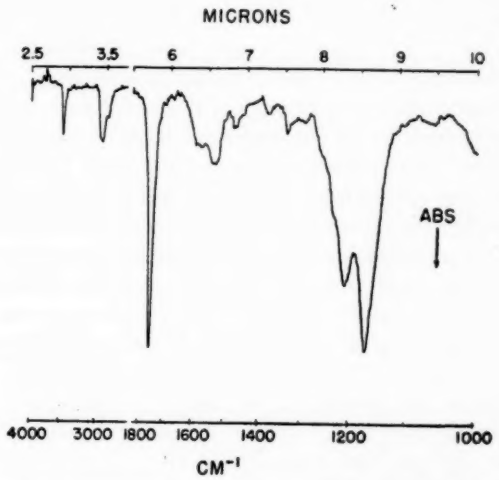


FIG. 4. Absorption spectrum of 0.004*M* N-butyl-2,2,2-trifluoro-ethanamide in $CCl_4$.

[7] Mizushima, Simanouti, Nagakura, Kurutani, Tsuboi, Baba, and Fujioka, J. Am. Chem. Soc. **72**, 3490 (1950); Mizushima, Shimanouchi, Tsuboi, Sugita, Kurosaki, Mataga, and Souda, J. Am. Chem. Soc. **74**, 4639 (1952).

[8] Buswell, Krebs, and Rodebush, J. Phys. Chem. **44**, 1126 (1940).

[9] S. E. Darmon and G. B. B. M. Sutherland, Nature **164**, 440 (1949).

[10] M. Davies, Ann. Repts. on Progr. Chem. (Chem. Soc. London) **43**, 5 (1946).

[11] R. M. Badger and S. H. Bauer, J. Chem. Phys. **5**, 839 (1937).

[12] R. M. Badger, J. Chem. Phys. **8**, 288 (1940).

additional stabilization of the hydrogen bond resulting from cyclization to contribute to the energy to this extent. Though a direct comparison of the intensities of these bands is not wholly justified, the entropy decrease resulting from cyclization might be expected to inhibit the formation of this species despite the favorable energetics.

In Table III it is seen that the frequency of $\nu$(C=O) of the dilute N-butyl-ethanamides increases to higher values as the electronegativities of the halogen substituents increase. The trifluoro derivative absorbs at 1736 $cm^{-1}$ upon dilution after a shift of 18–30 $cm^{-1}$. Upon dilution in $CCl_4$, $\nu$(C=O) of $CF_3COOH$ changed from 1785 to 1810 $cm^{-1}$, a comparable shift.[4] For the lower fatty acids in dilute dioxane solutions, Batuev[13] found the upper frequency limits of this band to be 1740 $cm^{-1}$ with shifts of 70–84 $cm^{-1}$ in going to the pure materials. This general pattern agrees with the data in Table III in that the frequency shifts upon dilution steadily decrease with increasing halogenation. The anomalous case, N-butyl-2,2-difluoro-ethanamide may be explained readily. Reference to Table I indicates the presence in the spectrum of a pure sample of this compound of unperturbed $\nu$(N−H). It is evident that the highly activated 2 hydrogen has displaced amido-hydrogen from bonding sites available to it in other compounds. This being the case, the hydrogen bond formed is of higher stability and the observed shift is greater than predicted. The presence of a considerable amount of bonded amido-hydrogen indicates that the conventional dimers are also present. A rather broad (for this band) shoulder centered at 1700 $cm^{-1}$ possibly accounts for the missing $\nu$(C=O) modes. Previous experiments[6] have shown that the amides are virtually completely associated in the pure state and in concentrated solutions in $CCl_4$. One would not expect the monomeric $\nu$(N−H) to indicate the presence of unassociated molecules.

This decrease in the shift in frequency upon dilution would indicate that a saturation effect is taking place; that is, that the hydrogen bond is less stable as a result of the competition for the electron cloud of oxygen. Simply on the basis of the relative magnitudes of the shifts observed, we have identified the associated $\nu$(C=O) which occurs at the higher frequency with the linear dimer and the other with the cyclic dimer.

In the introduction it was stated that the origin of the bands appearing near 1560 $cm^{-1}$ in the spectra of the N-butyl-ethanamides is quite controversial. Lenormant[2] and Randall *et al.*,[14] have argued that this band is probably characteristic of the amido $\nu$(C−N). Richards and Thompson[1] and others have assigned it to $\delta$(N−H). The latter argument seems to find its strength in the following reasoning. The primary amines absorb broadly in this neighborhood with the band being rather certainly due to this deformation. In acetamide,[6] the frequency and structure of the band are virtually unchanged with respect to the amines. In view of the absence of such a band from the spectra of N,N-disubstituted amides and since one would expect to find $\delta$(N−H) in this region of the spectra of the N-monosubstituted amides, the band is so assigned.

Evidence contrary to this assertion centers about deuterization experiments and the substitution of halogen atoms upon the nitrogen. Edsall and Scheinberg[15] studied the infrared spectra of $CH_3NH_2$ and $CH_3ND_2$. They found that the introduction of deuterium shifted $\delta$(N−H) to lower frequencies by a factor of 1.33–1.36 and shifted $\nu$(C−N) to lower frequencies by a factor of 1.05. Upon deuterization of N-monosubstituted amides, Lenormant[2] found the 1560 $cm^{-1}$ band to be shifted to lower frequencies by a factor of 1.05. Analogous conclusions have been reached by Fuson[4] in the cases of $CF_3COOH$ and $CF_3COOD$. Lenormant[2] observed the spectrum of N-bromo-ethanamide and found the 1560 $cm^{-1}$ band to be totally absent. Such a substituent would be expected to reduce the double-bond character of the carbon-nitrogen linkage and shift the characteristic absorption of that bond to much lower frequencies. A further objection[14] to the $\delta$(N−H) assignment lies in the absence of a band at 1560 $cm^{-1}$ from the spectra of lactams such as the cyclic monomer of 6-amino-hexanoic acid. Although this compound would be expected to possess $\delta$(N−H) in any event, one can readily see that the assumption of partial double-bond character by the amido-carbon-nitrogen bond could be forbidden structurally. Although Richards and Thompson[1] have observed that the substitution of electrophilic groups upon the amido-nitrogen sometimes decreases the frequency of this band, we feel that the evidence in the case of N-bromo-ethanamide is completely unambiguous.

Upon dilution, the frequency of this band is found to shift to lower values. The data recorded in Table IV clearly indicate the behavior of this band with the introduction of halogen into the methyl group. A detailed discussion of the somewhat discontinuous behavior of this band with increasing electronegativity of substituents requires further experimental data.

The structure of this band in the spectra of the pure compounds can be correlated with the dimers expected to be present. It is necessary to point out that the 1527-$cm^{-1}$ band of N-butyl-2,2-dichloro-ethanamide is not explained. This compound, being solid at 25°C was investigated in the form of a $CCl_4$ mull. We have tentatively considered this band to be characteristic of some vibration which appears only in the solid state.

We assign the 1564-, 1554-, and 1547-$cm^{-1}$ bands to $\nu$(C−N) in the dimers involving cyclic N−H—O, linear N−H—O and N−H—N hydrogen bonds, respectively. $\nu$(C−N) of the monomer reaches a maximum value after the fourth member of the series and

[13] M. I. Batuev, Compt. rend. acad. sci. U.R.S.S. **53**, 507 (1946).
[14] Randall, Fowler, Fuson, and Dangl, *Infrared Determination of Organic Structures* (D. Van Nostrand Company, Inc., New York, 1949).
[15] J. T. Edsall and H. Scheinberg, J. Chem. Phys. **8**, 520 (1940).

remains constant in frequency thereafter. This indicates the relative involvement of the lone pair of electrons of nitrogen in the bond. One would expect the nitrogen to lose the power to compete with oxygen in dimer formation. The frequencies of the monomeric $\nu(C=O)$ in Table III show that no saturation of the shift occurs. This is a reflection of the presence of a lone pair of electrons even when a pure double bond exists. Recognizing the probable occurrence of only two other important dimers in the series, we have arbitrarily chosen that band which is shifted to the greatest extent upon dilution as that of the cyclic dimer.

In view of the broadness and complexity of the band at 1408–1460 $cm^{-1}$, and because of the results of the deuterization experiments discussed above, we believe that the missing $\delta(N-H)$ is included here with $\delta(C-H)$.

When one has accepted as reasonably certain the assignment of the 1560-$cm^{-1}$ band to $\nu(C-N)$, it becomes necessary to explain the absence of this band from the spectra of the N,N-disubstituted amides. With the substitution of an alkyl group upon the nitrogen of acetamide, $\nu(C-N)$ shifts to frequencies which are higher by about 175 $cm^{-1}$. Substitution of still another alkyl group would be expected to shift this band to still higher frequencies. The only band of any consequence in this region is at about 1650 $cm^{-1}$ and is usually assigned to $\nu(C=O)$.[1,2] On the basis of plausibility, we believe that $\nu(C=O)$ and $(C-N)$ give rise to an accidentally degenerate band. Thus, the additional alkyl group has shifted $\nu(C-N)$ about 90 $cm^{-1}$ higher or half as much as the first alkyl group did. $\nu(C=O)$ was decreased about 14 $cm^{-1}$ in the first case and 40 $cm^{-1}$ in the second. Though the directions and magnitudes of these shifts are reasonable, it is not improbable that the resonance of these fundamentals to some extent forces the superposition of frequencies. It is possible that the two bands found in the neighborhood of 3400 $cm^{-1}$ are overtones of these vibrations.

In Table V and, for example, in Fig. 2, one sees that this band splits in the spectra of dilute solutions of three of the compounds. This split, being of the order of 20 $cm^{-1}$, is probably concealed by the structure of the band in the pure compounds. Each of the three compounds possesses an active hydrogen capable of participating in a hydrogen bond. Though this perturbation might be expected in some of the cases to be smaller than that resulting from amido-hydrogen interactions, it should be sufficient to mask the split.

The presence of this split leads one to suspect the existence of isomeric forms of these compounds. It is evident that the salient difference between the compounds exhibiting the split and those which do not is the presence in the former of active 2 hydrogens. The interaction between these atoms and the oxygen should result in the existence of rotational isomers. This coupled with the repulsion of the halogen and oxygen atoms should give rise to two potential wells of unequal depth rotated 180° apart. It is seen that the higher frequency band of the split pair remains virtually constant in frequency but decreases in intensity in going up the series. The lower frequency band behaves oppositely.[16]

The field interaction through the hydrogen bond and the induction of the halogens through the chain serve to balance one another in the *cis*-form. This explains the relatively constant frequency of the higher frequency band. In the *trans*-form, the interaction with the oxygen is actually only the absence of repulsion. As a result, the monotonic increases of both $\nu(C-N)$ and $\nu(C=O)$ remain matched. It is interesting to note that the frequency of the degenerate band, 1647 $cm^{-1}$, is quite close to a generally accepted value of 1650 $cm^{-1}$ for $\nu(C=N)$.[17]

Utilizing the techniques of Badger and Bauer,[11,12] one can estimate the strengths of the hydrogen bonds formed in the N-butyl series. The average shift found upon destruction of the cyclic dimer was of the order of 350 $cm^{-1}$, while that observed for acetamide[6] was about 260 $cm^{-1}$. Since it was found that the heat of formation of the hydrogen bond in the latter compound is about 1.1 kcal/bond-mole,[6] it is estimated that the value in the compounds investigated in this research is about 1.5 kcal/bond-mole.

The general chemical and physical behaviors of N-monosubstituted amides and N,N-disubstituted amides are clarified by the assignment of the 1560-$cm^{-1}$ band in the former to $\nu(C-N)$ and the postulate of the degeneracy of $\nu(C=O)$ and $\nu(C-N)$ in the latter. Previously anomalous spectra such as that of diketopiperazine[2] are readily understood in the light of these concepts.

## ACKNOWLEDGMENTS

We gratefully acknowledge the kindness of Professor H. S. Gutowsky of the University of Illinois in reading the manuscript and that of Professor G. B. B. M. Sutherland of the University of Michigan for a profitable discussion early in the research with one of us (H. L.). Dr. Paul Tarrant of this laboratory not only provided the compounds studied but also assisted us in many phases of this investigation. We wish to acknowledge the helpfulness of Dr. J. P. Bain in making available to us the single-beam instrument and facilities of the Naval Stores Laboratories of the Glidden Corporation. Mr. E. W. McKisson and Mr. R. S. Silas provided invaluable aid in the Infrared Laboratory of the University of Florida.

[16] A serious difficulty in this interpretation is the absence of a similar split in the spectra of the N-butyl series. Such a split could be masked by the natural band width if it were of slightly smaller magnitude due to the less negative character of the oxygen. An alternate explanation of the split is that it is a resolution of the accidental degeneracy. Though we have been unable to devise an entirely consistent model, it is seen that a perturbation of the existing resonance could account for such a resolution.

[17] R. C. Johnson, *An Introduction to Molecular Spectra* (Methuen, London, 1949).

# The Volume Exclusion Effect in Flexible Chains*

HUBERT M. JAMES
*Purdue University, W. Lafayette, Indiana*
(Received May 11, 1953)

The volume exclusion effect in a chain of small impenetrable spheres is treated by two methods—one based on derivation of a Fokker-Planck equation by consideration of the number of ways in which a chain can be extended by adding another sphere without violating the volume exclusion condition, and the other based on the calculation of the number of excluded configurations as a function of chain extension. Both approaches lead, in the first approximation, to the same simple analytic form for the distribution of chain extensions $r$, and to the prediction that $\langle r^2 \rangle$ will increase faster than the number of spheres in the chain. Volume exclusion does not merely change the distribution function by a scale factor, as is assumed in the theory of Flory; there is a relatively large decrease in the probability of small extensions. The present theory is compared in detail with that of Hermans, Klamkin, and Ullman, which is superficially similar in appearance, but fundamentally quite different in character and result.

## 1. INTRODUCTION

IT is well known that the distribution of extensions (end-to-end distances) of a polymer chain in solution will be affected by interactions between different portions of the chain, and, in particular, by the fact that two elements of the chain cannot occupy the same volume. Attempts to treat the volume exclusion effect theoretically have, however, led to a remarkable series of discordant results. Attempts to discuss the distribution of chain extensions $r$ by construction and solution of a Fokker-Planck equation have usually[1–3] led to the conclusion that $\langle r^2 \rangle$ increases proportionally to the number $N$ of essentially independent elements, or links, in the chain. Alternative methods, based on attempts to calculate the number of configurations excluded by the volume effect, as a function of the mean dimensions of the molecule, have usually[4–6] indicated that volume exclusion tends to make $\langle r^2 \rangle$ increase faster than $N$. Recently, Grimley[7] has used a Fokker-Planck equation to derive a value for $\langle r^2 \rangle$ that increases faster than $N$ and resembles rather closely a form found by Bueche, using the other approach.[8] However, both methods seem to be in need of clarification and extension.

This paper begins with a treatment of the distribution of chain extensions through derivation of a Fokker-Planck equation. This approach to the problem, based on consideration of the number of ways in which a chain can be extended by the addition of links without violating the volume exclusion conditions, simplifies the analysis and leads to a Fokker-Planck equation that differs in important respects from those previously considered. A simple analytic solution of this equation, valid in the first approximation, is found. An alternative treatment of the problem, based on calculation of the number of excluded configurations as a function of chain extension, is then carried through, and yields exactly the same form for the distribution function. The methods concur in predicting that $\langle r^2 \rangle$ will increase faster than $N$, and that volume exclusion produces an important change in the form of the distribution of extensions, rather than the mere change of scale assumed in the theory of Flory. The present theory is compared in detail with that of Hermans, Klamkin, and Ullman. It is shown that the basic assumptions of the two theories, despite a considerable formal similarity, are fundamentally different; it is for this reason that the volume exclusion effects predicted by the two theories are different in magnitude and character.

## 2. INTEGRAL FORMULATION OF THE THEORY

As a model of a free polymer molecule of $N$ links we shall take a string of $N+1$ small impenetrable spheres of diameter $A$. Instead of treating the distance between adjacent spheres in the chain as fixed (as Hermans, Klamkin, and Ullman do), we shall take the displacement $\mathbf{s}$ along each such link as variable, with the *a priori* probability density function for $\mathbf{s}$ given, in the absence of volume exclusion, by

$$g(\mathbf{s}) = \left(\frac{3}{2\pi}\right)^{\frac{3}{2}} \exp(-\tfrac{3}{2}s^2). \tag{1}$$

We thus take as our unit of length the rms distance between adjacent spheres in the chain, in the absence of volume exclusion. From Eq. (1) it follows that the relative number of configurations of the chain with displacement $\mathbf{r}$ between any pair of $t$th neighbors is given exactly, again in the absence of volume exclusion effects, by

$$f_0(t;\mathbf{r}) = \left(\frac{3}{2\pi t}\right)^{\frac{3}{2}} \exp\left(-\frac{3}{2}\frac{r^2}{t}\right), \tag{2}$$

even for small values of $t$.

* Work supported by U. S. Office of Naval Research.
[1] J. J. Hermans, Rec. trav. chim. **69**, 220 (1950).
[2] H. Hadwiger, Makromol. Chem. **5**, 148 (1951).
[3] Hermans, Klamkin, and Ullman, J. Chem. Phys. **20**, 1360 (1952).
[4] P. J. Flory, J. Chem. Phys. **17**, 303 (1949).
[5] P. J. Flory and T. G. Fox, Jr., J. Am. Chem. Soc. **73**, 1904 (1951).
[6] F. Bueche, J. Chem. Phys. **21**, 205 (1953).
[7] T. B. Grimley, J. Chem. Phys. **21**, 185 (1953).
[8] Compare Eq. (5) of reference 7, and the last equation of page 207 of reference 6. Grimley's $\beta_1$ is $-v$ in Bueche's notation.

Our problem is now to find the relative number of configurations of a chain of $N$ links, $N+1$ spheres, with displacement $\mathbf{r}$ between the end spheres, taking account of the effects of volume exclusion. We first consider a chain of $t$ links. Let one end sphere, the 0th, have its center fixed at the origin. Let

$$dC=f(t;\mathbf{r})d\mathbf{r} \tag{3}$$

be the relative number of configurations of the chain, computed with due regard for volume exclusion, such that the other end sphere, the $t$th sphere, has its center at point $\mathbf{r}$ to within $d\mathbf{r}$. Considering all these configurations, let $\psi(t;\mathbf{s},\mathbf{r})$ be the fraction of cases in which one can add to this chain another sphere, the $(t+1)$st, displaced from the $t$th sphere by an amount $\mathbf{s}$, without overlapping any other sphere in the chain. The relative number of configurations of the enlarged chain with the $t$th sphere at point $\mathbf{r}-\mathbf{s}$ within $d\mathbf{r}$, and the $(t+1)$st sphere displaced further by an amount $\mathbf{s}$ to within $d\mathbf{s}$, is then

$$f(t;\mathbf{r}-\mathbf{s})d\mathbf{r}\psi(t;\mathbf{s},\mathbf{r}-\mathbf{s})g(\mathbf{s})d\mathbf{s}.$$

The total relative number of configurations of the extended chain with the $(t+1)$st sphere at $\mathbf{r}$ to within $d\mathbf{r}$, which is $f(t+1;\mathbf{r})d\mathbf{r}$, is obtained on summing over all $d\mathbf{s}$. Thus one finds

$$f(t+1;\mathbf{r})=\int d\mathbf{s}f(t;\mathbf{r}-\mathbf{s})g(\mathbf{s})\psi(t;\mathbf{s},\mathbf{r}-\mathbf{s}). \tag{4}$$

We now consider the form of $\psi(t;\mathbf{s},\mathbf{r})$. First of all, $\psi$ will certainly vanish if $s<A$, since the presence of the $t$th sphere at $\mathbf{r}$ will then prevent the placing of the $(t+1)$st sphere at $\mathbf{r}+\mathbf{s}$. To take account of the volumes occupied by other spheres, we define a function $F$ such that

$$dP=F(t;\mathbf{r},\mathbf{r}+\mathbf{s})d\mathbf{s} \tag{5}$$

is the probability of finding any sphere except the $t$th in a chain of $t$ links with its center at $\mathbf{r}+\mathbf{s}$ to within $d\mathbf{s}$, when the $t$th sphere has its center fixed at $\mathbf{r}$. $F(t;\mathbf{r},\mathbf{r}+\mathbf{s})$ is to be computed taking account of all volume exclusion effects *except those due to the end spheres*, 0 *and* $t$. (For $s>A$, $F$ will be nearly equal to the corresponding density function $F'$ that also takes account of volume exclusion by the end spheres; it is, however, continuous and nearly constant through the small volume where $s<A$, whereas $F'$ would be discontinuous and identically zero in this volume.) Now the $(t+1)$st sphere can be placed at the point $\mathbf{r}+\mathbf{s}$ without overlapping any of these other spheres, provided no sphere has its center in a spherical volume

$$v=(4/3)\pi A^3, \tag{6}$$

eight times the volume of a single sphere, about the point in question. The fraction of cases in which this occurs is approximately

$$1-vF'(t;\mathbf{r},\mathbf{r}+\mathbf{s})\cong 1-vF(t;\mathbf{r},\mathbf{r}+\mathbf{s}),$$

if $v$ is small and $s>A$. As a basic assumption of the theory, we therefore take

$$\psi(t;\mathbf{s},\mathbf{r})=\begin{cases}1-vF(t;\mathbf{r},\mathbf{r}+\mathbf{s}), & (s>A),\\ 0, & (s<A).\end{cases} \tag{7}$$

Introduction of Eq. (7) into Eq. (4) yields

$$f(t+1;\mathbf{r})=\int d\mathbf{s}f(t;\mathbf{r}-\mathbf{s})g(\mathbf{s})[1-vF(t;\mathbf{r}-\mathbf{s},\mathbf{r})]$$
$$-vf(t;\mathbf{r})g(0)[1-vF(t;\mathbf{r},\mathbf{r})], \tag{8}$$

where the integral is over all $\mathbf{s}$, and the last term is the correction for the vanishing of $\psi$ in the little sphere $s<A$. Neglecting the term involving $v^2$, we obtain

$$f(t+1;\mathbf{r})=\int d\mathbf{s}f(t;\mathbf{r}-\mathbf{s})g(\mathbf{s})-vg(0)f(t;\mathbf{r})$$
$$-v\int d\mathbf{s}f(t;\mathbf{r}-\mathbf{s})g(\mathbf{s})F(t;\mathbf{r}-\mathbf{s},\mathbf{r}). \tag{9}$$

This is the basic integral formula of the present theory. The first term gives the relative number of ways of placing the $(t+1)$st sphere at $\mathbf{r}$, when volume exclusion is neglected; the second term corrects for volume exclusion by the $t$th sphere, and the last term corrects for the volume exclusion effect of the other spheres.

In the absence of volume exclusion, Eq. (9) becomes

$$f(t+1;\mathbf{r})=\int d\mathbf{s}f(t;\mathbf{r}-\mathbf{s})g(\mathbf{s}). \tag{10}$$

Construction of successive $f$'s by repeated use of this formula, starting with $f(1;\mathbf{s})=g(\mathbf{s})$, gives

$$f(t;\mathbf{r})=f_0(t;\mathbf{r}), \quad (v=0). \tag{11}$$

Our problem is to determine the effect of the correction terms involving $v$ in such an iterative calculation.

### 3. AVERAGE DENSITY OF OTHER SPHERES NEAR THE END SPHERE

The function $F(t;\mathbf{r}-\mathbf{s},\mathbf{r})$ plays a fundamental rôle in this theory, and an understanding of its qualitative characteristics is essential for what follows. Strictly, $F(t;\mathbf{r}-\mathbf{s},\mathbf{r})$ is the average density of spheres about the point $\mathbf{r}$, for a chain of spheres with ends fixed at 0 and $\mathbf{r}-\mathbf{s}$, when volume exclusion is taken into account for all but the fixed end spheres. Complete development of the theory would require relation of this quantity to the functions $f(p;\mathbf{r})$, or its calculation by other means. As a first approximation, however, it is natural to replace $F(t;\mathbf{r}-\mathbf{s},\mathbf{r})$ by the corresponding sphere density $F_0(t;\mathbf{r}-\mathbf{s},\mathbf{r})$ computed with neglect of volume exclusion. A study of $F_0$ also provides information required for deriving with appropriate accuracy the Fokker-Planck equation corresponding to Eq. (9). We therefore turn to a study of this function.

When volume exclusion is neglected, the probability density for finding the $j$th sphere at the point $\mathbf{r}$ is easily found as

$$h_j(t;\,\mathbf{r}-\mathbf{s},\,\mathbf{r})=\frac{f_0(j;\,\mathbf{r})f_0(t-j;\,\mathbf{s})}{\int d\mathbf{R}f_0(j;\,\mathbf{R})f_0(t-j;\,\mathbf{R}-\mathbf{r}+\mathbf{s})}. \quad (12)$$

One obtains

$$h_j(t;\,\mathbf{r}-\mathbf{s},\,\mathbf{r})=\left(\frac{3}{2\pi}\right)^{\frac{3}{2}}\left[\frac{t}{j(t-j)}\right]^{\frac{3}{2}}$$
$$\times\exp\left[\frac{3}{2t}|\mathbf{r}-\mathbf{s}|^2\right]\exp\left[-\frac{3}{2}\frac{r^2}{j}\right]\exp\left[-\frac{3}{2}\frac{s^2}{t-j}\right], \quad (13)$$

and can then compute

$$F_0(t;\,\mathbf{r}-\mathbf{s},\,\mathbf{r})=\sum_{j=1}^{t-1}h_j(t;\,\mathbf{r}-\mathbf{s},\,\mathbf{r}). \quad (14)$$

Hermans, Klamkin, and Ullman have replaced such a sum over $j$ by an integration from $j=0$ to $j=t$, and have evaluated the integral.[9] However, such an integral approximation to $F_0(t;\,\mathbf{r}-\mathbf{s},\,\mathbf{r})$ does not converge for $\mathbf{r}=0$ or $\mathbf{s}=0$, and is not adequate for our purposes. We must therefore reconsider the problem.

In the absence of volume exclusion, the distribution function $f_0(t;\,\mathbf{r})$ is of significant magnitude only for $r^2$ of the order of $t$ or less. Even in the presence of volume exclusion, one can expect to limit attention to values of $r$ of the order of $t^{\frac{1}{2}}$ or less. It will also be noted that in Eq. (9) only values of $s$ of the order of 1 play a significant role, since $g(\mathbf{s})$ becomes very small when $s$ is large. We therefore seek an approximation to $F_0$ valid for $r$ of the order of $t^{\frac{1}{2}}$ or less, and for $s$ of the order of 1.

Since $t$ will be large for almost all steps in the iterative calculation, we shall be content with an approximation to $F_0$ good to terms of the order of $t^{-\frac{1}{2}}$, or $r/t=(r^2/t)^{\frac{1}{2}}t^{-\frac{1}{2}}$ or $st^{-\frac{1}{2}}$.

We first define the function

$$\rho_0(r)=\left(\frac{3}{2\pi}\right)^{\frac{3}{2}}\sum_{j=1}^{\infty}\frac{1}{j^{\frac{3}{2}}}\exp\left[-\frac{3}{2}\frac{r^2}{j}\right]. \quad (15)$$

This is the average density of spheres, computed without volume exclusion, produced at point $\mathbf{r}$ by an infinite chain with one end fixed at the origin. We shall need only the following properties of $\rho_0(r)$:

$$\rho_0(0)=\left(\frac{3}{2\pi}\right)^{\frac{3}{2}}\zeta\left(\frac{3}{2}\right)=2.612\left(\frac{3}{2\pi}\right)^{\frac{3}{2}}; \quad (16)$$

$\zeta(\frac{3}{2})$ being the Riemann zeta function;

$$\int d\mathbf{r}g(\mathbf{r})\rho_0(r)=\left(\frac{3}{2\pi}\right)^{\frac{3}{2}}\sum_{j=1}^{\infty}\frac{1}{(j+1)^{\frac{3}{2}}}$$
$$=\left(\frac{3}{2\pi}\right)^{\frac{3}{2}}\left[\zeta\left(\frac{3}{2}\right)-1\right]; \quad (17)$$

$$\rho_0(r)\cong\left(\frac{3}{2\pi}\right)^{\frac{3}{2}}\int_0^{\infty}dj\frac{1}{j^{\frac{3}{2}}}\exp\left[-\frac{3}{2}\frac{r^2}{j}\right]=\frac{3}{2\pi}\frac{1}{r}, \quad (18)$$

if $r\ll 1$.

From Eqs. (13) and (14) it follows that

$$F_0(t;\,\mathbf{r}-\mathbf{s},\,\mathbf{r})=\exp\left\{-\frac{3}{t}(\mathbf{r}\cdot\mathbf{s})\right\}$$
$$\times\left(\frac{3}{2\pi}\right)^{\frac{3}{2}}\sum_{j=1}^{t-1}\left[\frac{t^{\frac{1}{2}}(t-j)}{j^{\frac{3}{2}}(t-j)^{\frac{3}{2}}}+\frac{t^{\frac{1}{2}}j}{j^{\frac{3}{2}}(t-j)^{\frac{3}{2}}}\right]$$
$$\times\exp\left\{-\frac{3r^2(t-j)}{2tj}\right\}\exp\left\{-\frac{3s^2j}{2t(t-j)}\right\}. \quad (19)$$

Defining

$$H(t;r,s)=\left(\frac{3}{2\pi}\right)^{\frac{3}{2}}\sum_{j=1}^{t-1}\frac{1}{j^{\frac{3}{2}}}\left[\frac{t}{t-j}\right]^{\frac{1}{2}}$$
$$\times\exp\left\{-\frac{3r^2(t-j)}{2tj}\right\}\exp\left\{-\frac{3s^2j}{2t(t-j)}\right\}, \quad (20)$$

we can write Eq. (19) as

$$F_0(t;\,\mathbf{r}-\mathbf{s},\,\mathbf{r})=\exp\left\{-\frac{3}{t}(\mathbf{r}\cdot\mathbf{s})\right\}$$
$$\times[H(t;r,s)+H(t;s,r)]. \quad (21)$$

The first term on the right comes from the first term in the square bracket of Eq. (19), and consists mainly of contributions to the sphere density by spheres with $j<t/2$; the second term arises from the second term in the square bracket of Eq. (19), on change of the variable of summation from $j$ to $t-j$, and consists primarily of contributions by spheres with $j>t/2$.

To evaluate $H(t;r,s)$, we divide it into three parts:

$$S_1(r)=\left(\frac{3}{2\pi}\right)^{\frac{3}{2}}\sum_{j=1}^{I}\frac{1}{j^{\frac{3}{2}}}\left[\frac{t}{t-j}\right]^{\frac{1}{2}}\exp\left\{-\frac{3r^2(t-j)}{2tj}\right\}, \quad (22)$$

where $I$ is the integer nearest $t^{\frac{1}{2}}$,

$$S_2(r)=\left(\frac{3}{2\pi}\right)^{\frac{3}{2}}\sum_{j=I+1}^{t-1}\frac{1}{j^{\frac{3}{2}}}\left[\frac{t}{t-j}\right]^{\frac{1}{2}}\exp\left\{-\frac{3r^2(t-j)}{2tj}\right\}, \quad (23)$$

$$S_3(r,s)=\left(\frac{3}{2\pi}\right)^{\frac{3}{2}}\sum_{j=1}^{t-1}\frac{1}{j^{\frac{3}{2}}}\left[\frac{t}{t-j}\right]^{\frac{1}{2}}\exp\left\{-\frac{3r^2(t-j)}{2tj}\right\}$$
$$\times\left[\exp\left\{-\frac{3s^2j}{2t(t-j)}\right\}-1\right]. \quad (24)$$

[9] See reference 3, Eqs. (35) and (35a), with $p=0$, for an evaluation of $F_0(t;\,\mathbf{r},\,\mathbf{r}+\mathbf{s})=F_0(t;\,\mathbf{r},\,\mathbf{R})$ by this method. In Eq. (35a), $\mathbf{R}+\mathbf{r}$ should be replaced by $\mathbf{R}-\mathbf{r}$.

One can easily show that

$$S_1(r)=\left(\frac{3}{2\pi}\right)^{\frac{3}{2}}\sum_{j=1}^{t}\frac{1}{j^{\frac{3}{2}}}\exp\left\{-\frac{3}{2}\frac{r^2}{j}\right\}+O(t^{-\frac{1}{2}}) \quad (25)$$

for all $r$.[10] $S_2(r)$ can be approximated by an integral over $j$, convergent for all $r$, with error of the same order of magnitude:

$$S_2(r)=\left(\frac{3}{2\pi}\right)^{\frac{3}{2}}\int_{t/(t^{\frac{1}{2}}+1)}^{t}dj\frac{1}{j^{\frac{3}{2}}}\left[\frac{t}{t-j}\right]^{\frac{1}{2}} \times\exp\left\{-\frac{3r^2(t-j)}{2tj}\right\}+O(t^{-\frac{1}{2}}). \quad (26)$$

On introduction of the variable of integration $z=tj/(t-j)$, this becomes

$$S_2(r)=\left(\frac{3}{2\pi}\right)^{\frac{3}{2}}\int_{t^{\frac{1}{2}}}^{\infty}dz\frac{1}{z^{\frac{3}{2}}}\exp\left\{-\frac{3}{2}\frac{r^2}{z}\right\}+O(t^{-\frac{1}{2}})$$

$$=\left(\frac{3}{2\pi}\right)^{\frac{3}{2}}\sum_{j=t+1}^{\infty}\frac{1}{j^{\frac{3}{2}}}\exp\left\{-\frac{3}{2}\frac{r^2}{j}\right\}+O'(t^{-\frac{1}{2}}). \quad (27)$$

We thus find

$$S_1(r)+S_2(r)=\rho_0(r)+O(t^{-\frac{1}{2}}). \quad (28)$$

To evaluate $S_3(r, s)$, one can approximate the sum in Eq. (24) by the integral from $j=1$ to $j=t$, convergent for all $r$ and $s$. Introduction of $z=tj/(t-j)$ as the variable of integration yields

$$S_3(r, s)\cong\left(\frac{3}{2\pi}\right)^{\frac{3}{2}}\int_{0}^{\infty}dz\frac{1}{z^{\frac{3}{2}}}\exp-\left\{\frac{3}{2}\frac{r^2}{z}\right\} \times\left[\exp\left\{-\frac{3}{2}\frac{s^2}{t^2}z\right\}-1\right], \quad (29)$$

with error of the order of $1/t$ or less so long as $r$ and $s$ are of the order of $t^{\frac{1}{2}}$ or less. The integration is elementary, and yields

$$S_3(r, s)=\frac{3}{2\pi}\frac{1}{r}[\exp\{-3rs/t\}-1]+O(t^{-1}). \quad (30)$$

For $r$ of the order of $t^{\frac{1}{2}}$, $s$ of the order of 1, we thus have

$$S_3(r, s)\cong-\frac{9}{2\pi}\frac{s}{t}+O(t^{-1}), \quad (31)$$

which is negligible for our purposes. On the other hand,

$$S_3(s, r)\cong-\frac{9}{2\pi}\frac{r}{t} \quad (31a)$$

is of the order of $t^{-\frac{1}{2}}$, and must be retained.

[10] An upper limit on the correction sum is conveniently obtained by replacing $r^2$ in each term of the sum by the value $2j/3$ that maximizes (very nearly) that particular term.

We have thus obtained

$$H(t; r, s)=\rho_0(r)+\frac{3}{2\pi}\frac{1}{r}[\exp\{-3rs/t\}-1]+O(t^{-\frac{1}{2}}). \quad (32)$$

On introducing this result into Eq. (21), and retaining appropriate terms in the expansion of the exponential, one finds, with the desired accuracy,

$$F_0(t; \mathbf{r}-\mathbf{s}, \mathbf{r})\cong\rho_0(r)+\rho_0(s)-\frac{3}{t}(\mathbf{r}\cdot\mathbf{s})\rho_0(s)-\frac{9}{2\pi}\frac{r}{t}, \quad (33)$$

for $s$ of the order of 1 and $r$ of the order of $t^{\frac{1}{2}}$ or less. Thus the average density of spheres at $\mathbf{r}$, a distance $r$ from one end of the long chain and $s$ from the other, is approximately equal to the average density, $\rho_0(r)+\rho_0(s)$, that would be produced there by an infinite chain with ends fixed at the origin and at $\mathbf{r}-\mathbf{s}$. The significant correction terms represent

(a) a distortion of the distribution of spheres near the end of the chain fixed at $\mathbf{r}-\mathbf{s}$, which changes sign when $\mathbf{s}$ is reversed, and

(b) a decrease in the sphere density that is essentially independent of $s$, but varies with $r$.

On use of Eq. (18), we obtain a result valid for large $r$:

$$F_0(t; \mathbf{r}-\mathbf{s}, \mathbf{r})\cong\rho_0(s)-\frac{3}{t}(\mathbf{r}\cdot\mathbf{s})\rho_0(s)+\frac{3}{2\pi}\frac{1}{r}-\frac{9}{2\pi}\frac{r}{t}. \quad (34)$$

Thus $F_0(t; \mathbf{r}-\mathbf{s}, \mathbf{r})$ can be expressed as the average sphere density produced at $\mathbf{r}$ by an infinite chain with one end free and the other end fixed at $\mathbf{r}-\mathbf{s}$, plus correction terms due to the fact that the chain is finite and has its other end fixed at the origin. The correction terms are all of the order of $t^{-\frac{1}{2}}$ when $r$ is of the order of $t^{\frac{1}{2}}$.

The above results, derived for $v=0$, suggest that in the presence of volume exclusion one can write, with corresponding accuracy,

$$F(t; \mathbf{r}-\mathbf{s}, \mathbf{r})\cong\rho(s)-\frac{1}{t}\alpha(v, r)(\mathbf{r}\cdot\mathbf{s})\rho(s)+G(t; r). \quad (35)$$

Here $\rho(s)$ is the density of spheres at $\mathbf{s}$ due to an infinite chain with one end fixed at the origin, when volume exclusion is taken into account, except for the end sphere; $\alpha(v, r)$ is an unknown function of its arguments, of the order of 1; and $G(t; r)$ is a correction term of the order of $t^{-\frac{1}{2}}$, varying slowly with $r$.

## 4. DERIVATION OF THE FOKKER-PLANCK EQUATION

We shall now derive the Fokker-Planck equation corresponding to the basic integral equation, Eq. (9), assuming that $F(t; \mathbf{r}-\mathbf{s}, \mathbf{r})$ has the form indicated in Eq. (35). As in Sec. 3, we shall desire an approximation accurate for $r$ of the order of $t^{\frac{1}{2}}$, and for $t$ large.

Let the components of $\mathbf{s}$ be $\xi_1$, $\xi_2$, $\xi_3$, and the compo-

nents of $\mathbf{r}$ be $x_1$, $x_2$, $x_3$. Then

$$f(t;\mathbf{r}-\mathbf{s})=f(t;\mathbf{r})-\sum_i \xi_i\frac{\partial f(t;\mathbf{r})}{\partial x_i}+\tfrac{1}{2}\sum_i\sum_j \xi_i\xi_j\frac{\partial^2 f(t;\mathbf{r})}{\partial x_i\partial x_j}+\cdots. \quad (36)$$

In the absence of volume exclusion, $f=f_0$, this is a rapidly convergent expansion when $\xi_i$ is of the order of 1 and $x_i$ is of the order of $t^{\frac{1}{2}}$, since $\partial f_0/\partial x_i$ is then of the order of $t^{-\frac{1}{2}}f_0$ and $\partial^2 f_0/\partial x_i\partial x_j$ is of the order of $t^{-1}f_0$. Even in the presence of volume exclusion, one can expect the terms to have the same relative magnitude. Introducing Eqs. (35) and (36) into Eq. (9), and remembering that $g(\mathbf{s})$ is spherically symmetric and that

$$\int d\mathbf{s}g(\mathbf{s})=\int d\mathbf{s}s^2g(\mathbf{s})=1, \quad (37)$$

we obtain

$$f(t+1;\mathbf{r})=f(t;\mathbf{r})+\tfrac{1}{6}\nabla^2 f(t;\mathbf{r})+O(t^{-2}f)-vg(0)f(t;\mathbf{r})-v\left\{\int d\mathbf{s}\rho(s)g(\mathbf{s})+G(t;r)\right\}f(t;\mathbf{r})+O(vt^{-1}f). \quad (38)$$

Since $\partial^2 f_0/\partial t^2$ is of the order of $t^{-2}f_0$, we can expect to replace $f(t+1;\mathbf{r})-f(t;\mathbf{r})$ by $\partial f/\partial t$ with error of the order of $t^{-2}f$. On neglecting terms of the order of $t^{-2}f$ and $vt^{-1}f$, we thus obtain the Fokker-Planck equation

$$\frac{\partial f}{\partial t}-\tfrac{1}{6}\nabla^2 f=-v\left[g(0)+\int d\mathbf{s}\rho(s)g(\mathbf{s})+G(t;r)\right]f(t;\mathbf{r}), \quad (39)$$

or, by Eq. (35),

$$\frac{\partial f}{\partial t}-\tfrac{1}{6}\nabla^2 f=-v\left[g(0)+\int d\mathbf{s}\rho(s)g(\mathbf{s})-\rho(0)+F(t;\mathbf{r},\mathbf{r})\right]f(t;\mathbf{r}). \quad (40)$$

The larger terms in Eq. (39), involving constant multipliers of $f(t;\mathbf{r})$, affect the magnitude of $f$ but not its form; thus they do not affect the calculation of $\langle r^n\rangle$. They can be eliminated from consideration by defining

$$\phi(t;\mathbf{r})=\exp\left\{vt\left[g(0)+\int d\mathbf{s}\rho(s)g(\mathbf{s})\right]\right\}f(t;\mathbf{r}). \quad (41)$$

Equation (39) then becomes simply

$$\frac{\partial\phi}{\partial t}-\tfrac{1}{6}\nabla^2\phi=-vG(t;r)\phi(t;\mathbf{r}), \quad (42)$$

with the term on the right of the order of $vt^{-\frac{1}{2}}\phi$ for $r$ of the order of $t^{\frac{1}{2}}$.

## 5. APPROXIMATE TREATMENT OF THE VOLUME EXCLUSION EFFECT

To obtain a treatment of the volume exclusion effect in the first approximation, we replace the quantities $F(t;\mathbf{r}-\mathbf{s},\mathbf{r})$, or $\rho(s)$ and $G(t;r)$, in the correction term of the Fokker-Planck equation by the corresponding quantities $F_0$, $\rho_0$, $G_0$ computed without taking account of volume exclusion. Introduction of Eq. (34) into Eq. (40), and use of Eqs. (1), (16), and (17) yields

$$\frac{\partial f}{\partial t}-\tfrac{1}{6}\nabla^2 f=-vF_0(t;\mathbf{r},\mathbf{r})f(t;\mathbf{r}), \quad (43)$$

or

$$\frac{\partial f}{\partial t}-\tfrac{1}{6}\nabla^2 f=-v\left[\rho_0(0)+\frac{3}{2\pi}\frac{1}{r}-\frac{9}{2\pi}\frac{r}{t}\right]f(t;\mathbf{r}). \quad (44)$$

When $v=0$ the appropriate solution of this equation is $f(t;\mathbf{r})=f_0(t;\mathbf{r})$ [Eq. (2)]. For $v>0$ the corresponding exact solution has the form $f=f_0(t;\mathbf{r})T(t)R(r)$:

$$f(t;\mathbf{r})=\left[\frac{3}{2\pi t}\right]^{\frac{3}{2}}\exp\left[-\frac{3}{2}\frac{r^2}{t}\right]\times\exp\left[-\left\{v\rho_0(0)-\frac{27}{8\pi^2}v^2\right\}t\right]\exp\left[\frac{9}{2\pi}vr\right]. \quad (45)$$

In order to concentrate attention on the form of this distribution, we express the spatial dependence in units appropriate to each value of $t$. Let

$$\xi=\left[\frac{3}{2t}\right]^{\frac{1}{2}}\mathbf{r}. \quad (46)$$

In the absence of volume exclusion, the relative number of chain configurations with given $\xi$ to within $d\xi$ is $D_0(\xi)d\xi$, where the density function in $\xi$ space is

$$D_0(\xi)=\pi^{-\frac{3}{2}}\exp[-\xi^2] \quad (47)$$

for all $t$. In the presence of volume exclusion the corresponding density function, as given by Eq. (45), is

$$D(t;\xi)=\pi^{-\frac{3}{2}}\exp[-v\rho_0(0)t]\exp[-(\xi-\lambda)^2], \quad (48)$$

where

$$\lambda=\left(\frac{27}{8\pi^2}\right)^{\frac{1}{2}}vt^{\frac{1}{2}}. \quad (49)$$

If one assumes that there are $W$ ways of placing the $(t+1)$st sphere with respect to the $t$th sphere, in the absence of volume exclusion, and that $g(\mathbf{s})$ gives the relative density of these positions, one can take as the absolute number of chain configurations with $\xi$ to within $d\xi$

$$dC=W^tD(t;\xi)d\xi; \quad (50)$$

the total number of configurations for the chain then becomes

$$C=W^t \exp[-v\rho_0(0)t]4\pi^{-\frac{1}{2}} \times\int_0^\infty d\xi\xi^2 \exp[-(\xi-\lambda)^2]. \quad (51)$$

In Eq. (51), the dependence of the integral on $v$ and $t$ is relatively unimportant, compared to that of the first exponential. Thus the first exponential in Eq. (51) or Eq. (48) represents the well-known fact that volume exclusion reduces the total number of configurations possible for a chain of $t$ unit by approximately a factor of the form $x^t$. That such a factor will appear in the present theory is clear when one remembers that the average density of other spheres around the end sphere, $F(t;\mathbf{r}-\mathbf{s},\mathbf{r})\cong\rho(s)$, is nearly independent of $\mathbf{r}$ and $t$ in the important ranges of these variables. The presence of the other spheres reduces the number of ways in which each additional sphere can be added to the chain by a factor that is nearly independent of $r$ and $t$, and is approximated by the constant $x$. Here we have found

$$x=\exp[-v\rho_0(0)]. \quad (52)$$

This form of this result should not lead one to the conclusion that the reduction factor is determined entirely by the sphere density at $s=0$; physically, it is obvious that the factor will depend on the whole density distribution for $s$ of the order of 1. A more general form for the reduction factor appears in Eq. (41):

$$x=\exp\left[-v\left\{g(0)+\int d\mathbf{s}\rho(s)g(\mathbf{s})\right\}\right]. \quad (53)$$

Equations (52) and (53) happen to give the same result for the special density function $\rho_0(s)$.

In addition to reducing the total number of chain configurations, volume exclusion changes the form of the distribution function for chain extensions. This change, expressed in the last factor of Eq. (45), and in the replacement of $\xi$ by $\xi-\lambda$ in passing from Eq. (47) to Eq. (48), consists in an increase of the relative weight of chain configurations with large $r$ or $\xi$. The general character of this change is, of course, to be expected, since the configurations with small $r$ are on the average more compact, more closely coiled, than the configurations with large $r$, and a larger fraction of them will be eliminated by the volume exclusion effect. In the present theory, this change in the distribution arises from the term $G(t;r)$ in the sphere density, which contributes the last two terms to Eq. (44). The function $G(t;r)$ expresses the increase in the average density of spheres around the end sphere as $r$ decreases. Because of this larger sphere density, the number of ways of passing from a configuration of a chain of $p$ spheres to a configuration of a chain of $(p+1)$ spheres is smaller when $r$ is small than it is when $r$ is large. The total change in $f(t;\mathbf{r})$ due to volume exclusion then appears as the cumulative effect of this factor, as the chain is built up sphere by sphere, in favoring configurations with large $r$.

Equations (48) and (49) indicate that the form of the distribution function is determined by the value of $\lambda$, or of $vt^{\frac{1}{2}}$. It will be noted that the change in this distribution due to volume exclusion is not approximated by a change of scale, as is assumed by Flory.[4] Instead, the maximum density in $\xi$-space shifts to larger values of $\xi$ as $vt^{\frac{1}{2}}$ increases, and the distribution assumes a quite different character from the usual Gaussian function when $vt^{\frac{1}{2}}$ is of the order of 1.

For comparison with experiment, the most interesting quantity derived from the theory is [see Eq. (48)]

$$\langle r^2\rangle_t=\frac{3t}{2}\langle\xi^2\rangle_t=\frac{2t}{3}\frac{\int_0^\infty d\xi\xi^4\exp[-(\xi-\lambda)^2]}{\int_0^\infty d\xi\xi^2\exp[-(\xi-\lambda)^2]}. \quad (54)$$

A straightforward calculation yields

$$\langle r^2\rangle_t=t\cdot\frac{[1+4\lambda^2+(4/3)\lambda^4](\pi^{\frac{1}{2}}/2)\{1+I(\lambda)\}+[(5/3)\lambda+\frac{2}{3}\lambda^3]\exp(-\lambda^2)}{(1+2\lambda^2)(\pi^{\frac{1}{2}}/2)\{1+I(\lambda)\}+\lambda\exp(-\lambda^2)}, \quad (55)$$

where $I(\lambda)$ is the probability integral,

$$I(\lambda)=\frac{2}{\pi^{\frac{1}{2}}}\int_0^\lambda \exp(-x^2)dx. \quad (56)$$

In the present units, $\langle r^2\rangle=t$ when $v=0$; the second factor on the right of Eq. (55) then gives the correction for volume exclusion. For small $\lambda$, one finds

$$\langle r^2\rangle_t=t\left\{1+\frac{4}{3\pi^{\frac{1}{2}}}\lambda+\left(2-\frac{16}{3\pi}\right)\lambda^2+\cdots\right\} =t+\frac{4}{3}\left(\frac{3}{2\pi}\right)^{\frac{1}{2}}vt^{\frac{1}{2}}+\cdots. \quad (57)$$

To the approximation on the second line, this agrees with the result of Grimley.[7] For larger $\lambda$, the exponential terms in both numerator and denominator of Eq. (55) rapidly become negligible, and one finds, with an error of less than 1 percent for $\lambda\geq 1$,

$$\langle r^2\rangle_t=t(1+4\lambda^2+(4/3)\lambda^4)/(1+2\lambda^2). \quad (58)$$

For $\lambda\ll 1$, this yields

$$\langle r^2\rangle\cong\tfrac{2}{3}\lambda^2t=\frac{9}{4\pi^2}v^2t^2. \quad (59)$$

The range of applicability of Eq. (59) will be discussed in Sec. 7.

Increase of $\langle r^2 \rangle$ faster than $t$ means that one cannot describe volume exclusion effects adequately in terms of an increase in the effective link length of the chain, or in terms of interactions of each link with a fixed number, however large, of its neighbor links. In other words, it is an essential feature of volume exclusion that it is an interaction of every portion of the chain with every other. In terms of the present theory, this appears in the fact that the function $G_0(t;r)$, which determines the volume exclusion effect on the form of the distribution, is a sum of contributions from all parts of the chain; indeed, the term $-9r/2\pi t$ comes mainly from the half of the chain nearer the $t$th link, while the term $\frac{3}{2}\pi r$ comes mainly from the other half.

## 6. AN ALTERNATIVE TREATMENT OF THE VOLUME EXCLUSION EFFECT

The theory of the volume exclusion effect will now be worked out from a quite different point of view,[11] which, however, leads to exactly the same distribution of extensions.

The relative number of configurations for a chain of $t$ links with extension $\mathbf{r}$, computed without volume exclusion, is given by $f_0(t;\mathbf{r})$. Let $p(t;r)$ be the fraction of these configurations in which the volume exclusion condition is not violated for any pair of spheres. Then

$$f(t;\mathbf{r}) = f_0(t;\mathbf{r})p(t;r). \tag{60}$$

We now make the following approximations in calculating $p(t;r)$.

(a) Let $P_{mn}(t;r)$ be the very small probability, proportional to $v$, that a configuration of a chain of $t$ links with extension $r$ will be eliminated from consideration by overlap of the $m$th and $n$th spheres. The probability that it will not be thus eliminated can then be written with good accuracy as

$$p_{mn} = \exp\{-P_{mn}(t;r)\}. \tag{61}$$

In computing the probability $p(t;r)$ that *no* volume exclusion condition is violated, we treat the probabilities $p_{mn}$ as independent, to obtain

$$p(t;r) = \exp\{-\sum_{m=1}^{t}\sum_{n=0}^{m-1} P_{mn}(t;r)\}. \tag{62}$$

The exponent in this equation is proportional to $v$; a more accurate calculation would change it only by terms involving higher powers of $v$.

(b) We compute the probability $P_{mn}$ for overlapping of the $m$th and $n$th spheres, $(m>n)$, neglecting the volume exclusion effect so far as all other spheres are concerned. (This corresponds to the approximation of replacing $F$ by $F_0$ in Sec. 5.) Since $P_{mn}$ is the fraction of the configurations in which the center of the $n$th sphere lies within a small volume $v$ about the center of the $m$th sphere, we have

$$P_{mn}(t;r) = v\frac{\int d\mathbf{r}_m f_0(n;\mathbf{r}_m) f_0(m-n;0) f_0(t-m;\mathbf{r}-\mathbf{r}_m)}{\int d\mathbf{r}_m \int d\mathbf{r}_n f_0(n;\mathbf{r}_n) f_0(m-n;\mathbf{r}_m-\mathbf{r}_n) f_0(t-m;\mathbf{r}-\mathbf{r}_m)}, \tag{63}$$

or after a little calculation,

$$P_{mn}(t;r) = v\left(\frac{3}{2\pi}\right)^{\frac{3}{2}}\left[\frac{1}{(m-n)(t-m+n)}\right]^{\frac{3}{2}} \times \exp\left\{-\frac{3(m-n)}{2t(t-m+n)}r^2\right\}. \tag{64}$$

To this approximation, $P_{mn}$ thus depends only on $|m-n|$, and not on $m$ and $n$ separately.

By Eq. (64), the double sum in Eq. (62) contains $t+1-(m-n)$ equal terms corresponding to interactions between $(m-n)$th neighbors. The double sum can then be reduced to a single sum over values of $m-n=j$. Writing for the number of $j$th neighbors $t-j$, rather than the exact $t+1-j$, we obtain

$$p(t;r) = \exp\left\langle -vt\sum_{j=1}^{t-1}\left(\frac{3}{2\pi}\right)^{\frac{3}{2}}\frac{1}{j^{\frac{3}{2}}}\left[\frac{t}{t-j}\right]^{\frac{3}{2}} \times \exp\left\{-\frac{3jr^2}{2t(t-j)}\right\}\right\rangle. \tag{65}$$

[11] This approach has been indicated, but not developed, by Bueche in reference 6.

The sum contains no term with $j=t$, since $P_{t,0}$ is not given by Eq. (64), but vanishes for $r>A$. By Eqs. (20) and (32) we have then

$$\left.\begin{aligned} p(t;r) &= \exp[-vtH(t;0,r)] \\ &= \exp\left[-v\rho_0(0)t + \frac{9}{2\pi}vr\right], \end{aligned}\right\} \tag{66}$$

with neglect of terms of the order of $vt^{\frac{1}{2}}$. Equation (60) becomes, on use of Eqs. (2) and (66),

$$f(t;\mathbf{r}) = \left(\frac{3}{2\pi t}\right)^{\frac{3}{2}} \exp[-v\rho_0(0)t] \exp\left[-\frac{3}{2}\frac{r^2}{t} + \frac{9}{2\pi}vr\right]. \tag{67}$$

This is identical with the solution [Eq. (45)] of the Fokker-Planck equation, except for the multiplier $\exp[27v^2t/8\pi^2]$, which is a term of a sort that is not given reliably by either theory, and does not affect the calculation of $\langle r^n \rangle$.

## 7. RANGE OF APPLICABILITY OF THE THEORY

The theory here presented has been designed to be valid primarily for $r$ of the order of $t^{\frac{1}{2}}$ or less. Terms in

the equations of Secs. 3 and 4 have been classified, and have been neglected or retained, according to their orders of magnitude in this range, for small $v$ and large $t$. Both the general theory of Sec. 4 and the approximate distribution function derived in Secs. 5 and 6 thus cease to be valid when $r$ greatly exceeds $t^{\frac{1}{2}}$; in other words, one can expect these theories to be satisfactory only when the probabilities for chain extensions much greater than $t^{\frac{1}{2}}$ are so small that they need not be calculated accurately.

The approximate theory of Sec. 5 gives an indication, probably quite accurate, as to the significance of this limitation. The distribution function of Eq. (48) has its maximum for $\xi=\lambda$, and is small outside the range of validity of the theory ($\xi$ of the order of 1) only if $\lambda$ is of the order of 1 or less. Thus the present theory is valid only for $vt^{\frac{1}{2}}$ of the order of 1 or less; it is valid in the limit of small $v$, for fixed $t$, but not in the limit of large $t$ for fixed small $v$.

From this it follows that Eq. (59) cannot be regarded as a limiting form for $\langle r^2\rangle$ as $t$ increases. Granted the approximations made in Secs. 5 and 6, the validity of Eq. (59) follows for fixed values of $\lambda$ greater than 1 by enough to make Eq. (59) a good approximation, but not for values of $\lambda$ increasing faster than some quite small power of $t$. Thus Eq. (59) may be a good approximation in a limited range of $\lambda$ and $t$ without, however, contradicting the conclusion of Rubin, that in three-dimensional problems $\langle r^2\rangle$ can increase no faster than $t^{\frac{1}{2}}$ in the limit of large $t$.[12]

In the theory developed in Sec. 4, the assumption concerning $\psi(t;\mathbf{s},\mathbf{r})$ in Eq. (7) neglects terms of the order of $v^2$, which would appear in a more careful treatment of the probability of finding the volume $v$ unoccupied by other spheres; terms of the same order are neglected in passing from Eq. (8) to Eq. (9). To include these terms in the calculation would introduce, on the right of Eq. (38), terms in which $f$ is multiplied by constants of the order of $v^2$, and terms in which the variable multiplier is of the order of $v^2t^{-\frac{1}{2}}$. In deriving Eq. (39) we have thus neglected terms on the right with constant multipliers of the order of $v^2$, while retaining the dominant constant multiplier of the order of $v$; we have also neglected variable multipliers of the order of $t^{-2}$, $v^2t^{-\frac{1}{2}}$, and $vt^{-1}$, while retaining the dominant variable multiplier, $G(t;r)$, of the order of $vt^{-\frac{1}{2}}$. The terms with variable multipliers are the ones that determine the form of the distribution, which should thus be determined with good accuracy, in the range under consideration, so long as both $v$ and $t^{-\frac{1}{2}}$ are small. The neglected term with constant multiplier $Cv^2$ would change the magnitude of $f$ by a factor $\exp[Cv^2t]$ which is not necessarily close to 1; however, such a factor is still of entirely secondary importance in determining the magnitude of $f$, so long as $v$ is small.

It is not immediately clear what further limitations there may be on the accuracy of the approximate theories of Secs. 5 and 6. In both cases, the effect of volume exclusion for each pair of spheres is estimated by neglecting the volume exclusion effect for all other pairs. In consequence, these theories probably overestimate the effect of volume exclusion. In Sec. 5, in replacing the exact function $F(t;\mathbf{r}-\mathbf{s},\mathbf{r})$ by the approximate $F_0(t;\mathbf{r}-\mathbf{s},\mathbf{r})$, we replace $\rho(s)$ by the obviously more compact distribution $\rho_0(s)$ computed without volume exclusion, and $G(t;r)$ by $G_0(t;r)$. Replacement of $\rho(s)$ by $\rho_0(s)$ will lead to an overestimate of the rate at which the number of configurations is reduced by volume exclusion, but one that does not appear to be important.[13] The nature of the difference between $G(t;r)$ and $G_0(t;r)$ is less obvious. The difference will vanish in the limit of small $v$ for fixed large $t$; thus our results should be valid for small $vt^{\frac{1}{2}}$. An estimate of the accuracy of this theory (and that of Sec. 6) for $vt^{\frac{1}{2}}$ of the order of 1 must await development of these theories in a higher approximation.

A discussion of the relation of this theory to experiment will not be undertaken here. Comments and references to the experimental results are to be found in the paper of Hermans, Klamkin, and Ullman.[3]

## 8. COMPARISON OF THE PRESENT THEORY WITH THAT OF HERMANS, KLAMKIN, AND ULLMAN

The formal basis of the present theory resembles that of Hermans, Klamkin, and Ullman, but the results are entirely different. It therefore seems desirable to discuss in detail the quite fundamental differences in the two theories.

The difference in the chain model is minor, and appears to be of no significance: the present theory deals with links of variable length with *a priori* weights described by $g(\mathbf{s})$, whereas the theory of HKU treats the links as having constant length.

The present theory determines the distribution of distances between the end spheres of a chain by con-

[12] R. J. Rubin, J. Chem. Phys. **20**, 1940 (1952). It should be noted, however, that Rubin's upper limit on $\langle r^2\rangle$ is based on an assumption that is not mathematically rigorous. Rubin assumes that the introduction of volume exclusion between the $m$th and $n$th spheres will produce the greatest increment in $\langle r^2\rangle$ if this particular interaction is the first to be introduced. In Sec. 6 we have dealt, not merely with the value of $\langle r^2\rangle$, but with the whole distribution of extensions for a chain of $t$ links. The interaction of the $m$th and $n$th spheres introduced into this distribution a factor $\exp\{-P_{mn}(t;r)\}$, which increases monotonely from a value a little less than 1 toward the limit 1, as $r\to\infty$. Rubin's assumption is, essentially, that introduction of such a factor into the distribution will increase $\langle r^2\rangle$ by a greater amount if the distribution is originally of the form $f_0(t;\mathbf{r})$ than it will if the distribution is initially of the form $f_0(t;\mathbf{r})\varphi(r)$, where $\varphi(r)$ is a function that, like a product of factors $\exp\{-P_{ij}(t;r)\}$, increases monotonely toward the value 1 as $r\to\infty$. That this is not a mathematically rigorous assumption is easily shown by a counter-example, in which one replaces both $\exp\{-P_{mn}(t;r)\}$ and $\varphi(r)$ by $1-\beta\exp(-\alpha r^2)$, with $\alpha$ and $\beta$ both small.

[13] The value of $x$ [Eq. (53)] is determined by the value of $\rho(s)$ for $s$ of the order of 1. In this range, $\rho(s)$ is primarily a sum of contributions from spheres near the end sphere. These contributions will be modified by volume exclusion in much the same way as $f(t;\mathbf{r})$ for small $t$ [see Eq. (45)]. It therefore appears that, in the important range of $s$, $\rho(s)\cong\rho_0(s)$, so long as $v$ is small.

sidering the relative number of ways, $f(t;\mathbf{r})$, in which one can build up a chain of $t$ links with extension $\mathbf{r}$ by adding spheres one at a time. At each step, one takes account of the volume exclusion interaction between the newly added sphere and all spheres previously added to the chain; in the end one has thus taken account of the interactions between every pair of spheres. The function $f(t;\mathbf{r})$ is subject to no normalization condition, and $\int d\mathbf{r} f(t;\mathbf{r})$ decreases nearly exponentially with increasing $t$.

In the theory of HKU, attention is fixed on a complete chain of $N+1$ spheres. The distribution of distances $\mathbf{r}$ between the $(t+1)$st and $p$th spheres within the chain is then computed from the distribution of distances between the $t$th and $p$th spheres by an integral formula resembling Eq. (4) of the present paper. Since the function $f(\mathbf{r}, t-p)$ defined by HKU is a probability density function, it is subject to the normalization condition $\int d\mathbf{r} f(\mathbf{r}, t-p)=1$ for all $t-p$.

The difference in normalization of the functions $f$ in the two theories follows from the different assumptions made concerning the function $\psi$.

In the present theory, $\psi(t;\mathbf{s},\mathbf{r})$ is the fraction of cases in which one can add the $(t+1)$st sphere at point $\mathbf{r}+\mathbf{s}$, when the $t$th sphere is at point $\mathbf{r}$. Thus $\psi$ is always less than 1; neither $\psi$ nor $\psi(t;\mathbf{s},\mathbf{r})g(\mathbf{s})$ satisfies any normalization condition. The form of $\psi$ assumed in Eq. (7) is not a mere ansatz, but follows from consideration of the volume exclusion conditions that may prevent the placing of the $(t+1)$st sphere at $\mathbf{r}+\mathbf{s}$.

In the theory of HKU the function $\psi(\mathbf{s},\mathbf{r})d\mathbf{s}$ (with an unexpressed dependence on $p$, $t$, $N$) gives the probability that the $(t+1)$st sphere will be found at $\mathbf{r}+\mathbf{s}$ to within $d\mathbf{s}$ when the $t$th sphere is found at $\mathbf{r}$. It is subject to the normalization condition $\int d\mathbf{s}\psi(\mathbf{s},\mathbf{r})\equiv 1$, which assures the normalization of the successive $f$'s determined by the integral formula. Concerning their $\psi$, HKU make the following assumption:

$$\psi(\mathbf{s},\mathbf{r})=\beta[1-vF(\mathbf{r}+\mathbf{s})], \tag{68}$$

where $F(\mathbf{r}+\mathbf{s})$ is the sphere density at $\mathbf{r}+\mathbf{s}$ when the $t$th sphere is at $\mathbf{r}$. This is of essentially the same form as Eq. (7) of the present paper, except for the presence of the normalization factor $\beta$, which depends (tacitly) on $p$, $t$, $N$, and $\mathbf{r}$. In physical significance, however, this assumption is by no means equivalent to Eq. (7), and the fundamental difference in the theories enters at this point.

To make this clear, we may consider the probability distribution $\psi$ of HKU from another point of view. Let the $p$th sphere of the chain be fixed at the origin, and the $t$th sphere be fixed at $\mathbf{r}$; then $\psi(\mathbf{s},\mathbf{r})d\mathbf{s}$ is the fraction of the configurations of the chain with the $(t+1)$st sphere at $\mathbf{r}+\mathbf{s}$ to within $d\mathbf{s}$, when *all* volume exclusion interactions in the chain are taken into account. In the absence of volume exclusion, the number of such configurations will be the same for all directions of $\mathbf{s}$, and $\psi$ becomes constant. In the presence of volume exclusion, then, $\psi$ must be proportional to the fraction of these chain configurations that are not eliminated by any volume exclusion condition. The variation of $\psi$ with $\mathbf{s}$ should thus represent the change with $\mathbf{s}$ of the fraction of configurations eliminated by all volume exclusion interactions, involving the "tail" of $p$ spheres with the $p$th sphere fixed at the origin, the chain of $t-p$ spheres stretching from the origin to the point $\mathbf{r}$, and the "tail" of $N-t$ spheres with one end fixed at $\mathbf{r}+\mathbf{s}$. It is clear that *this number will vary primarily because a change in* $\mathbf{s}$ *changes the probability of volume exclusion interaction between the chain stretching from the origin to* $\mathbf{r}$ *and the "tail" stretching out from the point* $\mathbf{r}+\mathbf{s}$. In general, both of these chain sections will include a great many spheres distributed through a relatively large volume.[14] In assuming that their $\psi$ has the form given in Eq. (68) [an ansatz which they do not discuss in detail], HKU in effect take the probability of volume exclusion interaction between large and extended distributions of spheres to be just $v$ times the sphere density at $\mathbf{r}+\mathbf{s}$. This assumption seems difficult to justify; certainly it follows less clearly from the model than does the basic assumption of the present paper, that the probability of interference with the placing of a single sphere at $\mathbf{r}+\mathbf{s}$ is proportional to the sphere density at that point.

Although the basic formulas of HKU differ from those of the present paper only in an apparently trivial normalization factor in $\psi$, the effect of this factor on the results is enormous, and by no means limited to the normalization of the distribution function. The variable normalization factor eliminates from the Fokker-Planck equation of HKU what would otherwise be the dominant term—the term that is the basis of the present theory—and they predict a volume exclusion effect that is of a smaller order of magnitude, and of different character.

Finally, it may be emphasized that the advantage of the point of view employed in this paper is that it permits consideration of volume exclusion interactions for one sphere at a time, whereas the approach of HKU logically involves one in consideration of the interactions between all spheres at the same time.

[14] In using the method of HKU one can choose $p=0$, to eliminate one tail, and can let $t\to N+1$ to obtain a result comparable to that of the present paper. However, in most of the intermediate steps of their calculation the tail beyond the $t$th sphere must contain a considerable fraction of the total chain.

# Rate of Association of Methyl Radicals

G. B. KISTIAKOWSKY AND E. KIRK ROBERTS*
*Gibbs Memorial Laboratory, Harvard University, Cambridge, Massachusetts*
(Received July 10, 1953)

The recombination rate constant of methyl radicals has been redetermined by the intermittent illumination method as $3.7\times10^{13}$ cc/mole sec at 165°, after a correction for the concurrent formation of methane. The recombination rate constant of deuterated methyl radicals has been found to have a substantially identical value. The dependence of these second-order rate constants on total pressure was studied over the range of 1- to 10-mm acetone pressure. Both rate constants were found to decrease identically with pressure. The form of their pressure dependence agrees with deductions from the "third-body" stabilization theory. It is shown that the absolute magnitude of the recombination rate constants, their near-identity and their identical decrease with pressure are all consistent with theoretical predictions, provided the methyl radicals form a loosely bound critical complex, in which they carry out essentially unhindered rotations. Recent literature data on the recombination of methyl radicals are reviewed, and it is shown that they are not in serious disagreement with the present measurements.

SEVERAL seemingly conflicting measurements have been reported in the recent literature on the rate of formation of ethane by the recombination of methyl radicals. Using the photochemical rotating sector technique with acetone and dimethyl mercury vapors at pressures of 10 to 50 mm and at 125 to 220°C, Gomer[1] obtained $4.5\times10^{13}$ cc/mole sec for the recombination rate constant. Miller and Steacie[2] measured the ratio of the rate constants of the methyl radical recombination and their reaction with nitric oxide at a pressure of 4.5 mm of mercury dimethyl at room temperature; this result was used by Durham and Steacie[3] to calculate the rate constant of the recombination reaction as $1.1\times10^{12}$ cc/mole sec by combining it with their measurements of the rate of the reaction of methyl radicals with nitric oxide (0.2 mm of dibutyl peroxide being the source of radicals). Lossing, Ingold, and Tickner[4,5] determined the recombination rate constant as $5.1\times10^{12}$ cc/mole sec, by a mass spectrometric technique in the presence of 15 mm of helium and only a few microns pressure of organic vapors. The radicals were generated by thermal decomposition at 850–975°C. Ingold and Lossing,[6] refining this technique, reported that upon reducing the temperature to 160°, the recombination rate constant rose to about $1.3\times10^{13}$ cc/mole sec. These values of the rate constant correspond to collision yields of 0.01 to 0.36 for an assumed cross section of 3.5A, but may be mutually consistent if the association rate constant is pressure and temperature dependent. A pressure dependence above *ca* 20 mm of acetone or dimethyl mercury is definitely ruled out by careful measurements of the ratio of the recombination and hydrogen abstraction reactions of methyl radicals carried out in the Noyes[7] and the Steacie[8] laboratories. Such dependence, however, may become significant at still lower pressures, and so account for the different collision yields mentioned above.

To shed further light on the mechanism of this reaction, the recombination rate of methyl radicals was compared in the present experiments to that of deuterated methyls. Furthermore, the pressure dependence of the recombination reactions was explored down to 1-mm total pressure.

The theory of the rotating sector as applied to the photolysis of acetone has been summarized elsewhere.[1] In brief, there are three important reactions involving methyl radicals in the photolysis of acetone,

$$(CH_3)_2CO+h\nu\rightarrow 2CH_3+CO, \quad (1)$$

$$2CH_3\rightarrow C_2H_6; \quad R(C_2H_6)=k_2[CH_3]^2, \quad (2)$$

$$CH_3+(CH_3)_2CO\rightarrow CH_4+CH_2COCH_3;$$
$$R(CH_4)=k_3[(CH_3)][(CH_3)_2CO]. \quad (3)$$

In the event that reaction (3) occurs to a much lesser extent than reaction (2), the recombination rate constant is given by

$$k_2=1/[4\tau^2R(C_2H_6)_s], \quad (4)$$

where $\tau$ is the mean life of the methyl free radicals, determined from the comparison of the rates of methane production under conditions of intermittent and steady illumination, while $R(C_2H_6)_s$ is the rate of ethane production with steady illumination. The theory, from which the equations relating the methane production to the radical lifetime and the duration of illumination are derived, has been worked out by Dickinson.[9]

* Present address: Chemistry Department, Middlebury College, Middlebury, Vermont.

[1] R. Gomer and G. B. Kistiakowsky, J. Chem. Phys. **19**, 85 (1951).
[2] D. M. Miller and E. W. R. Steacie, J. Chem. Phys. 7**319**, (1951).
[3] R. W. Durham and E. W. R. Steacie, J. Chem. Phys. **20**, 582 (1952).
[4] F. P. Lossing and A. W. Tickner, J. Chem. Phys. **20**, 907 (1952).
[5] Lossing, Ingold, and Tickner, Disc. Faraday Soc. **14**, 34 (1953).
[6] K. U. Ingold and F. P. Lossing, J. Chem. Phys. **21**, 308 (1953).
[7] W. A. Noyes and L. M. Dorfman, J. Chem. Phys. **16**, 788 (1948).
[8] A. F. Trotman-Dickenson and E. W. R. Steacie, J. Chem. Phys. **18**, 1097 (1950).
[9] W. A. Noyes and P. A. Leighton, *The Photochemistry of Gases* (Reinhold Publishing Corporation, New York, 1941), pp. 202–209.

TABLE I. Experiments with intermittent illumination of $(CH_3)_2CO$ at 30-mm pressure. Rates expressed as mole $cc^{-1}$ $sec^{-1}$.

| Run | Temp. °C | $R(C_2H_6)$ | $R(CH_4)$ | $R(CO)$ | $\frac{R(CH_4)_i}{R(CH_4)_s}$ | Sector speed (rpm) |
|---|---|---|---|---|---|---|
| 1 | 165 | $117.\times10^{-12}$ | $11.7\times10^{-12}$ | $133.\times10^{-12}$ | | |
| 2 | 165 | 30.2 | 4.05 | 34.5 | 0.344 | 218 |
| 3 | 165 | 25.6 | 4.34 | 30.1 | 0.381 | 218 |
| 4 | 165 | 109. | 11.6 | 123. | | |
| 5 | 165 | 27.5 | 3.36 | 32. | 0.286 | 55.6 |
| 6 | 165 | 28.3 | 3.58 | 31.8 | 0.303 | 89.6 |
| 7 | 165 | 113. | 11.6 | 129. | | |
| 8 | 165 | 27.2 | 4.26 | 32.1 | 0.361 | 301 |
| 9 | 165 | 27.4 | 3.10 | 31.7 | 0.276 | 48.0 |
| 10 | 165 | 113. | 11.4 | 129. | | |
| 11 | 165 | 26.4 | 4.70 | 32.4 | 0.419 | 582 |
| 12 | 165 | 30.6 | 4.31 | 36.0 | 0.359 | 287 |
| 13 | 165 | 128. | 12.1 | 144. | | |
| 14 | 165 | 31.5 | 3.60 | 36.0 | 0.299 | 89.8 |
| 15 | 135 | 28.6 | 1.97 | 30.8 | 0.337 | 89.8 |
| 16 | 135 | 114. | 5.89 | 122. | | |
| 17 | 135 | 29.0 | 2.22 | 31.4 | 0.372 | 287 |
| 18 | 135 | 28.6 | 2.80 | 31.8 | 0.469 | 940 |
| 19 | 135 | 113. | 5.86 | 121. | | |
| 20 | 135 | 28.4 | 1.78 | 30.4 | 0.303 | 55.5 |
| 21 | 135 | 27.8 | 2.42 | 31.0 | 0.403 | 581 |
| 22 | 135 | 112. | 5.91 | 121. | | |
| 23 | 135 | 28.2 | 2.84 | 31.6 | 0.476 | 581 |

In order to account for the pressure dependence of the recombination rate constant, a more detailed mechanism including deactivation by a third body is required,

$$2CH_3 \rightarrow C_2H_6^* \quad (k_a), \tag{5}$$

$$C_2H_6^* \rightarrow 2CH_3 \quad (k_b), \tag{6}$$

$$C_2H_6^* + M \rightarrow C_2H_6 + M \quad (k_c). \tag{7}$$

If we apply the steady-state assumption to the energy-rich ethane molecules $C_2H_6^*$,

$$R(C_2H_6) = k_2[CH_3]^2 = \frac{k_a[M]}{k_b/k_c + [M]}[CH_3]^2. \tag{8}$$

In the present low-pressure experiments, it has been possible to determine only the ratio $k_2/k_3^2$, so that when acetone is assumed to be the third body,

$$\frac{k_2}{k_3^2} = \frac{k_a/k_3^2[(CH_3)_2CO]}{k_b/k_c + [(CH_3)_2CO]} = \frac{R(C_2H_6)}{R(CH_4)^2}[(CH_3)_2CO]^2 \tag{9}$$

and

$$\frac{k_3^2}{k_2} = \frac{k_3^2}{k_a} + \frac{k_3^2 k_b}{k_a k_c}\frac{1}{[(CH_3)_2CO]}. \tag{10}$$

It is assumed that $k_3$ is pressure independent, since it is associated with a metathetical reaction.

## EXPERIMENTAL

The deuterated acetone was prepared by the method of Reitz;[10] 1.4 grams of Mallinckrodt analytical reagent acetone was refluxed with 2 grams of 99.8 percent $D_2O$ obtained from the Stuart Oxygen Company with a few drops of concentrated $H_2SO_4$ added. The mixture was then passed twice over fresh Drierite by distillation at reduced pressure, the acetone being received at $-195°$. The refluxing and distillation was repeated four times, using 2 grams of fresh $D_2O$ and a few drops of $H_2SO_4$ each time. According to the distribution ratio calculated by Reitz, $D/H$ in acetone: $D/H$ in water = 0.8, 95 percent of the hydrogen atoms of the original acetone should be replaced by deuterium. This means that 85 percent of the methyl radicals produced would be completely deuterated, and that practically all of the remainder would have only one normal hydrogen atom. The infrared spectrum of the deuterated acetone was compared with that of normal acetone, confirming the calculated extent of the deuteration reaction.

The deuterated acetone, as well as the normal acetone, were dried over Drierite and distilled once in vacuum at $-78°$ and then thoroughly outgassed at $-78°$ before each series of runs.

The $CO_2$ used as an inert gas in the low-pressure runs was obtained from the third quarter of a small piece of commercial dry ice which was allowed to evaporate in vacuum. The portion saved was distilled once at $-115°$ and was outgassed before each use at $-195°$.

TABLE II. Experiments with intermittent illumination of $(CD_3)_2CO$ at 30-mm pressure. Rates expressed as mole $cc^{-1}$ $sec.^{-1}$

| Run | Temp. °C | $R(C_2D_6)$ | $R(CD_4)$ | $R(CO)$ | $\frac{R(CD_4)_i}{R(CD_4)_s}$ | Sector speed (rpm) |
|---|---|---|---|---|---|---|
| 24 | 165 | $116.\times10^{-12}$ | $2.72\times10^{-12}$ | $119.\times10^{-12}$ | | |
| 25 | 165 | 28.1 | 1.13 | 30.1 | 0.414 | 377 |
| 26 | 165 | 28.5 | 1.00 | 30.1 | 0.370 | 249 |
| 27 | 165 | 114. | 2.71 | 118. | | |
| 28 | 165 | 28.7 | 0.834 | 30.1 | 0.309 | 89.6 |
| 29 | 165 | 28.7 | 1.24 | 30.8 | 0.461 | 961 |
| 30 | 165 | 115. | 2.67 | 119. | | |
| 31 | 165 | 28.8 | 0.777 | 30.0 | 0.292 | 48.0 |
| 32 | 165 | 28.6 | 1.16 | 30.6 | 0.442 | 582 |
| 33 | 165 | 117. | 2.64 | 122. | | |
| 34 | 165 | 28.9 | 0.900 | 30.7 | 0.341 | 154 |
| 35 | 165 | 29.6 | 0.825 | 31.1 | 0.313 | 89.8 |
| 36 | 165 | 115. | 2.60 | 121. | | |
| 37 | 165 | 30.2 | 1.02 | 32.0 | 0.383 | 287 |
| 38 | 195 | 28.5 | 2.48 | 32.2 | 0.432 | 581 |
| 39 | 195 | 117. | 5.77 | 126. | | |
| 40 | 195 | 25.8 | 1.79 | 28.4 | 0.329 | 89.8 |
| 41 | 195 | 28.1 | 2.64 | 32.1 | 0.479 | 940 |
| 42 | 195 | 118. | 5.50 | 127. | | |
| 43 | 195 | 28.3 | 2.07 | 31.4 | 0.380 | 250 |

[10] O. Reitz, Z. physik. Chem. **A179**, 119 (1937).

The experimental arrangement and methods used in the rotating sector experiments were the same as those developed by Gomer.[1] For the low-pressure runs, the cylindrical reaction flask was replaced by a spherical quartz flask, most of the experiments being made with one of 523 cc volume and a few with a 165-cc flask. These flasks were placed in a large furnace made from copper pipe and heated electrically through a Sola voltage regulator transformer. Several copper fins were placed in the open end of the furnace, between the flask and the mercury lamp, to reduce convection currents and improve temperature uniformity. Exploration with a thermocouple of the region of the furnace occupied by the flasks showed that the temperature was uniform to 0.5°.

The unfiltered output of a Cooper-Hewitt 110-volt dc mercury lamp was used as the light source. The lamp was stabilized by a large inductance, and its output was kept constant manually, using the photocell arrangement described by Gomer.[1] In two runs a Lectromesh screen interposed between the lamp and the reaction cell reduced the light intensity by a factor of nearly 10.

In the low-pressure runs with added $CO_2$, the acetone and $CO_2$ were measured separately, before being transferred to a mixing chamber incorporated in the vacuum system. After mixing, the gases were allowed to expand into the reaction cell. In the analysis of the reaction products it was necessary to eliminate some of the $CO_2$ carried over with the ethane. This was done by passing the mixture over KOH at −150°. A check on the accuracy of this separation was obtained by adding some $CO_2$ to the reaction mixture after the exposure of acetone alone; the error in the final result was less than 5 percent.

## RESULTS AND DISCUSSION

The runs with the rotating sector were performed in series of three, the second of which was with steady illumination and provided a value for methane production to be compared with those of the first and third runs using intermittent illumination. The sector was cut so that the ratio of the dark period to the light period was 3:1. The exposure time in each series was so regulated as to obtain nearly equal quantities of methane in the three runs. The results of the rotating sector experiments are shown in Tables I and II and in Figs. 1 and 2. In order to correct for any variation in light intensity between the runs with steady and with intermittent illumination, the ratio of the rates of methane production with intermittent and steady illumination, $R(CH_4)_i/R(CH_4)_s$, was multiplied by the factor $1/0.99$ $(R(CO)_s/4R(CO)_i)^{\frac{1}{2}}$, where 0.99 is the average value of $(R(CO)_s/4R(CO)_i)^{\frac{1}{2}}$ for all runs. This correction is applied because with steady illumination the rate of methane production is proportional to the square root of the absorbed light intensity, provided that the ratio of methane to ethane is small.

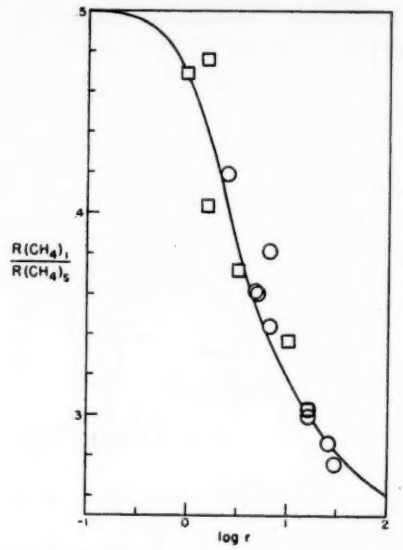


FIG. 1. The effect of flicker frequency upon the yield of methane from $CH_3$ radicals. ○ runs at 165° corresponding to $\tau=5.2$ msec. □ runs at 135° corresponding to $\tau=8.2$ msec. $\tau$=ratio of light period to the mean life $\tau$ of the radicals.

The lifetime of the methyl radicals was obtained from the best fit of the experimental data to the theoretical curve of Dickinson. The rate of ethane formation used in calculating the recombination rate constant is the average observed rate of formation with steady illumination.

A summary of the free radical lifetimes and recombination rate constants deduced from equations given above appears in Table III. The experimental error in the rate constants at 165° is about 15 percent, whereas at the other temperatures with fewer experimental points it is about 30 percent.

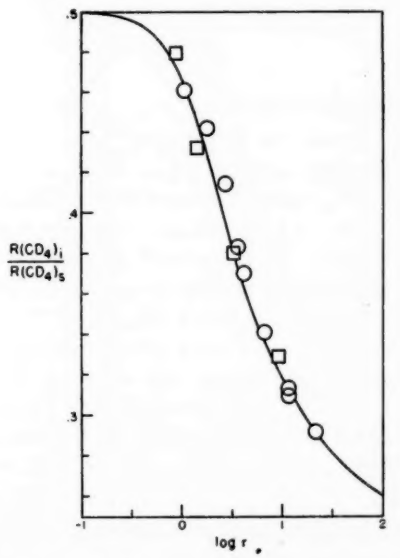


FIG. 2. The effect of flicker frequency upon the yield of methane from $CD_3$ radicals. ○ runs at 165° corresponding to $\tau=7.3$ msec. □ runs at 195° corresponding to $\tau=9.1$ msec.

Table III shows the rate constant for ordinary methyls at 165° to be much larger than the other values given. As shown by Table I this appears to be due to the breakdown of the assumptions made in deriving Dickinson's formula, namely, a negligible formation of methane. The effect of intermittent illumination has been worked out, therefore, for a kinetic mechanism more nearly representing the conditions encountered at 165°. Assuming that the only reactions involving methyl radicals are those given by Eqs. (1)–(3), it follows that during a light period:

$$\frac{d[CH_3]}{dt}=2R(CO)-2k_2[CH_3]^2-k_3[CH_3][(CH_3)_2CO] \quad (11)$$

and during a dark period:

$$-\frac{d[CH_3]}{dt}=2k_2[CH_3]^2+k_3[CH_3][(CH_3)_2CO]. \quad (12)$$

If we assume further that the acetone concentration remains constant, integrate these equations and solve them for the instantaneous methyl radical concentration, it is found that, during a light period,

$$[CH_3]_l=-\frac{b}{4k_2}-\frac{Q}{4k_2}\frac{1+Ye^{Qt}}{1-Ye^{Qt}}, \quad (13)$$

and during a dark period,

$$[CH_3]_d=\frac{b[CH_3]_0'}{(b+c[CH_3]_0')e^{bt}-c[CH_3]_0'}, \quad (14)$$

where

$$b=k_3[(CH_3)_2CO],$$

$$c=2k_2,$$

$$Q=[b^2+8cR(CO)]^{\frac{1}{2}},$$

$$Y=\frac{2c[CH_3]_0+b-Q}{2c[CH_3]_0+b+Q},$$

$[CH_3]_0$ = methyl radical concentration at the beginning of a light period, and

$[CH_3]_0'$ = methyl radical concentration at the beginning of a dark period.

TABLE III. Uncorrected association rate constants.

| Radical | Temp. | Lifetime (msec) | $k_2$ cc/mole, sec |
|---|---|---|---|
| $CH_3$ | 135 | 8.2 | $3.3\times10^{13}$ |
| $CH_3$ | 165 | 5.2 | $8.0\times10^{13}$ |
| $CD_3$ | 165 | 7.3 | $4.1\times10^{13}$ |
| $CD_3$ | 195 | 9.1 | $2.6\times10^{13}$ |

Equations (13) and (14) can be used to calculate the methyl radical concentration at the beginning of the light and dark periods by the method of successive approximations. At the sector speeds for which these calculations have been carried out, the methyl concentration at the end of a light period is the same as the methyl concentration with steady illumination within 1 percent. An integration of the expressions (13) and (14) for the instantaneous methyl radical concentration, over the light and the dark periods, respectively, gives the average methyl radical concentrations. During the light period,

$$\overline{[CH_3]_l}=-\frac{b}{2c}+\frac{1}{2ct}\ln\frac{(e^{Qt}-Y)(1-Ye^{-Qt})}{(1-Y)^2} \quad (15)$$

and during the dark period,

$$\overline{[CH_3]_d}=-\frac{b}{c}+\frac{1}{pct}\ln\frac{(b+c[CH_3]_0')e^{pbt}-c[CH_3]_0'}{b}, \quad (16)$$

where $p=3$ is the ratio of the length of the dark period to the length of the light period. The average methyl radical concentration with intermittent illumination is given by

$$[CH_3]_i=\frac{[CH_3]_l+p[CH_3]_d}{p+1}. \quad (17)$$

The average methyl radical concentration with steady illumination $[CH_3]_s$ can be obtained from Eq. (13) by setting $t=\infty$.

A trial value of $k_2$ is then chosen, and from this $k_3$ is calculated, since the ratio $k_3/k_2^{\frac{1}{2}}$ is known from the runs with steady illumination. Then Eqs. (13)–(17) are used to calculate the ratio $[CH_3]_i/[CH_3]_s$, which should equal the experimental ratio $R(CH_4)_i/R(CH_4)_s$, since the average rate of methane production is proportional to the average methyl radical concentration, with either steady or intermittent illumination. New trial values of $k_2$ are tested until a value is found such that

$$([CH_3]_i)/([CH_3]_s)=[R(CH_4)_i]/[R(CH_4)_s]. \quad (18)$$

These calculations have been carried out for runs 12 and 13 with normal methyl radicals, and for runs 26 and 27 with deuterated methyl radicals. These runs were chosen for three reasons: (1) they fit well on the curves, (2) they occur near the inflection point of the curves, where the magnitude of the recombination rate constant has the greatest effect on the average methyl radical concentration with intermittent illumination, and (3) the runs have comparable experimental methane ratios. It was found that the recombination rate constant of normal methyl radicals at 165° must be reduced to $4.2\times10^{13}$ cc/mole sec, corresponding to a mean lifetime of 6.7 msec, in order that Eq. (18) be satisfied. This is a reduction of 50 percent compared to the value obtained by using the formulas of Dickinson.

TABLE IV. The effect of total pressure on the recombination rate constant.

| Run | Pressure acetone $CO_2$ (mm) | Temp. °C | Exposure time (min) | $R(C_2H_6)$ | $R(CH_4)$ mole/cc sec | $R(CO)$ | $k_2/k_3^2$ |
|---|---|---|---|---|---|---|---|
| 44 | 10 | 215 | 8 | $17.4\times10^{-12}$ | $4.65\times10^{-12}$ | $22.1\times10^{-12}$ | 0.410 |
| 45 | 10 | 189 | 8 | 18.7 | 2.82 | 21.6 | 0.435 |
| 46 | 8 | 184 | 8 | 16.2 | 2.00 | 18.2 | 0.391 |
| 47 | 6 | 183 | 8 | 13.1 | 1.43 | 14.6 | 0.331 |
| 48 | 4 | 185 | 8 | 10.1 | 0.953 | 11.3 | 0.278 |
| 49 | 3 | 179 | 8 | 8.31 | 0.624 | 9.00 | 0.230 |
| 50 | 2 | 176 | 12 | 6.61 | 0.392 | 7.00 | 0.181 |
| 51 | 1 | 170 | 20 | 3.87 | 0.176 | 4.06 | 0.100 |
| 52 | 2 | 174 | 6 | 6.49 | 0.401 | 6.90 | 0.156 |
| 53 | 15 | 173 | 5 | 27.1 | 3.71 | 31.2 | 0.410 |
| 54 | 12 | 171 | 6 | 22.3 | 2.58 | 25.3 | 0.405 |
| 55 | 10 | 223 | 5 | 16.1 | 5.48 | 22.2 | 0.0292 |
| 56 | 8 | 232 | 6 | 13.2 | 4.81 | 18.3 | 0.0271 |
| 57 | 6 | 235 | 6 | 10.5 | 3.52 | 14.4 | 0.0253 |
| 58 | 4 | 237 | 6 | 8.06 | 2.27 | 10.5 | 0.0221 |
| 59 | 3 | 239 | 6 | 6.74 | 1.72 | 8.75 | 0.0193 |
| 60 | 2 | 238 | 8 | 5.46 | 1.18 | 6.67 | 0.0144 |
| 61 | 1 | 241 | 10 | 3.40 | 0.597 | 4.07 | 0.0096 |
| 62[a] | 8 | 241 | 20 | 0.658 | 1.27 | 1.67 | 0.0264 |
| 63[a] | 2 | 238 | 90 | 0.380 | 0.288 | 0.639 | 0.0168 |
| 64 | 1.5 | 239 | 8 | 4.37 | 0.837 | 5.26 | 0.0138 |
| 65 | 2 | 241 | 8 | 4.87 | 1.10 | 6.05 | 0.0162 |
| 66[b] | 4 | 241 | 12 | 10.3 | 2.98 | 13.4 | 0.0187 |
| 67[b] | 8 | 239 | 6 | 14.3 | 5.80 | 20.1 | 0.0256 |
| 68[b] | 2 | 239 | 20 | 6.59 | 1.22 | 7.96 | 0.0166 |
| 69[b] | 4 | 237 | 12 | 9.85 | 2.54 | 12.6 | 0.0216 |
| 70[b] | 2 | 237 | 20 | 6.67 | 1.24 | 7.96 | 0.0155 |
| 71 | 6 9.9 | 241 | 6 | 10.2 | 3.88 | 14.2 | 0.0245 |
| 72 | 1 8.6 | 242 | 10 | 3.26 | 0.490 | 3.80 | 0.0142 |
| 73 | 1 38. | 242 | 10 | 3.59 | 0.512 | 4.29 | 0.0143 |
| 74 | 1 37. | 242 | 10 | 3.44 | 0.476 | 4.05 | 0.0159 |
| 75[c] | 2 45. | 242 | 8 | 4.54 | 1.12 | 5.97 | 0.0152 |
| 76 | 1 39. | 244 | 10 | 3.27 | 0.478 | 4.02 | 0.0160 |
| 77 | 6 38. | 241 | 6 | 9.20 | 3.61 | 13.5 | 0.0257 |
| | | | | Deuteroacetone | | | |
| 78 | 6 | 237 | 10 | 12.5 | 1.23 | 13.6 | 0.260 |
| 79 | 2 | 237 | 15 | 5.89 | 0.351 | 6.25 | 0.168 |
| 80 | 10 | 237 | 6 | 17.3 | 2.18 | 19.6 | 0.321 |
| 81 | 1 | 238 | 20 | 3.88 | 0.193 | 4.09 | 0.095 |
| 82 | 4 | 238 | 10 | 9.41 | 0.731 | 10.2 | 0.257 |
| 83 | 1.5 | 239 | 18 | 4.99 | 0.260 | 5.32 | 0.156 |
| 84 | 1.1 | 240 | 20 | 4.15 | 0.210 | 4.40 | 0.113 |

[a] Light intensity reduced by Lectromesh screen.
[b] Reaction carried out in 165-cc cell.
[c] $CO_2$ added after exposure.

On the other hand, the rate constant for deuterated methyl radicals becomes $3.8\times10^{13}$ cc/mole sec, thus changing by less than the experimental error from the value obtained directly from the Dickinson formulas. This small change is the result of the comparatively insignificant yield of methane from deuterated methyls at 165°. Accordingly it may be safely assumed that the other values of Table III would not be reduced by more than some 10 percent—within the estimated experimental error—after applying Eqs. (13)–(17). These laborious calculations were not carried out therefore. The corrected values of Table III show then that the recombination rate constants of the normal and deuterated methyl radicals are either identical, or that the former is greater by not more than some 30 percent.

The absolute rate theory predicts[11] a maximum value of $5\times10^{13}$ cc/mole sec (correcting for the electronic multiplicity factor) for the recombination rate constant of normal methyls. The presently observed value, of about $3.7\times10^{13}$, agrees well with this prediction. The theory also requires that in order for the rate constant to be near the maximum value, the radicals must form a very loosely bound critical complex. In this case the ratio of the rate constants for the ordinary and the deuterated methyls must equal the square root of the inverse ratio of the masses of the radicals, i.d. $(6/5)^{\frac{1}{2}}=1.1$. The present experimental data are in excellent accord with this value; they show, therefore, very little hindrance of rotations of the methyl radicals in the critical complex.

For the elucidation of the pressure dependence, runs were made with steady illumination at temperatures near 180° and 240°. The observed rate constant ratios $k_2/k_3^2$ were normalized to these temperatures by

[11] Glasstone, Laidler, and Eyring, *The Theory of Rate Processes* (McGraw-Hill Book Company, Inc., New York, 1941).

using the activation energy differences reported by Trotman-Dickenson and Steacie,[8] $E_3-\frac{1}{2}E_2=9.7$ kcal for $CH_3$ and 10.3 kcal for $CD_3$. The experimental results are recorded in Table IV, which shows decided dependence of the ratio $k_2/k_3^2$ upon acetone pressure. Plots of the inverse $k_3^2/k_2$ against the inverse of the concentration of acetone give very satisfactory straight lines, as is shown in Fig. 3. The experimental results are therefore consistent with Eq. (10). The parameters of this equation for the three experimental conditions investigated are shown in Table V.

The experimental error in the values of $k_3^2/k_a$, which are equal to $k_3^2/k_2$ at high acetone pressures, is estimated at 10 percent, whereas there is an uncertainty of 30 percent in the ratios $k_b/k_c$, which are equal to those concentrations or pressures of acetone at which the recombination rate constant $k_2$ has fallen to one-half the limiting high-pressure value.

In the tenfold pressure range studied in these experiments, the recombination rate constant is reduced by a factor of 3 to 4. This pressure effect is shown to be independent of the absorbed light intensity (runs 62 and 63), even under conditions when the rate of methane production exceeds that of ethane. Further, the pressure effect is independent of the size of the reaction vessel (runs 66 to 70). This indicates that the heterogeneous recombination of the radicals is unimportant.

The runs with $CO_2$ added to the reaction mixture show a relatively small effect of $CO_2$ on the recombination rate constant. Even with approximately 40 mm of $CO_2$ added to 1 mm of acetone, the recombination rate constant is increased to a value characteristic of only 2-mm pressure of acetone. Carbon dioxide has apparently no effect on the rate of decomposition of acetone, as evidenced by unchanged rate of production of carbon monoxide. Hence its small effect on the ethane/methane ratio is due either to its low efficiency as the third body, or to a highly improbable cancellation of two opposing effects. One is the retardation of the diffusion of the radicals to the walls, and hence of the hypothetical heterogeneous recombination, the other is the accelerating third-body effect on the homogeneous recombination.

It is rather unlikely that the observed reduction of the recombination rate at low pressures is due to the onset of competing reactions. One of them might be the formation of ethylene and hydrogen by the energy-rich ethane molecules. But Lossing and Tickner[4] observed no ethylene mass spectrometrically, under conditions even more extreme than those encountered in the present research. A disproportionation reaction $2CH_3 \rightarrow CH_4+CH_2$ has been reported by Bawn and Tipper,[12] but Bawn and Dunning[13] found no evidence of it and former authors estimate its activation energy as 8 kcal. This makes it unimportant in any case at the temperatures employed in the present experiments.

TABLE V. The pressure dependence parameters of the recombination rate constants.

| Radical | Temp. | $\frac{k_3^2}{k_a}$ cc/mole sec | $\frac{k_b}{k_c}$ mole/cc | $\frac{k_b}{k_c}$ mm |
|---|---|---|---|---|
| $CH_3$ | 180 | 1.8 | $1.6\times10^{-7}$ | 4.5 |
| $CH_3$ | 240 | 27 | 0.83 | 2.7 |
| $CD_3$ | 240 | 2.4 | 0.88 | 2.8 |

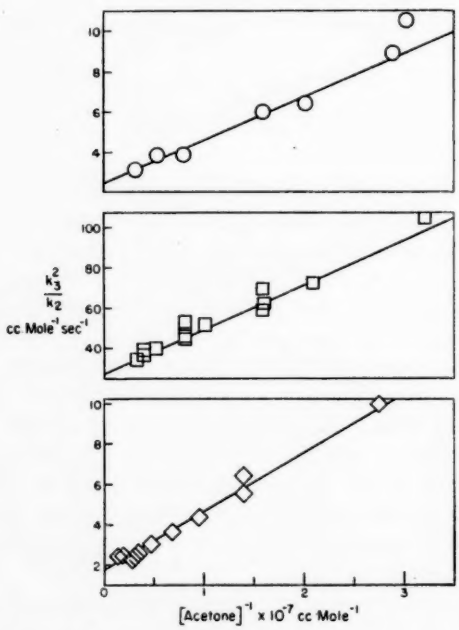


FIG. 3. Plots of the ratio $k_3^2/k_2$ against the inverse of acetone concentration. Circles are for $CD_3$ at 240°; squares for $CH_3$ at 240°; diamonds for $CH_3$ at 180°C.

Thus, there are strong reasons for believing that the observed change in the $k_3^2/k_2$ ratio is due to the third-body effect on the homogeneous recombination of methyl radicals. The magnitude of the observed effect—a change in the recombination rate constant by a factor of about four—is well outside the experimental errors. It may be noted that the earlier data of Trotman-Dickenson and Steacie,[8] obtained over the range of 4 to 100 mm at 150°, agree well with the presently observed pressure effect.

The pressure range in which the recombination rate constant becomes pressure dependent is consistent with Marcus'[14] theoretical treatment for the case of a loosely bound critical complex. But the presently observed ratio of the recombination constants for the normal and the deuterated radicals does establish a loosely bound complex. Thus, the data are consistent with Marcus' treatment, although we cannot agree with his conclusion that the experimental data favor a tightly bound critical complex.

[12] C. E. H. Bawn and C. F. H. Tipper, Disc. Faraday Soc. **2**, 104 (1947).

[13] C. E. H. Bawn and W. J. Dunning, Trans. Faraday Soc. **35**, 898 (1939).

[14] R. A. Marcus, J. Chem. Phys. **20**, 359, 364 (1952).

Slater's[15] classical treatment of the pressure dependence is interesting in that it predicts substantially identical behavior of the rate constants of the normal and the deuterated radicals—which is in accord with the present findings. Benson's[16] treatment of the pressure dependence suffers, we believe, from an oversimplification of the model. In conjunction with the present findings it leads to the conclusion that only three to four internal degrees of freedom participate in the distribution of energy in the energy-rich ethane molecules.

In conclusion a few comments on the apparent discrepancies in the absolute values of the recombination rate constants as obtained by several groups of workers. Gomer's results,[1] obtained by the same method, do not differ significantly from the present data and hence need no further comment. To make the work of Durham and Steacie[3] and Miller and Steacie[2] comparable with this research, one must apply corrections for the pressure effects on the recombination of methyl radicals and their reaction with nitric oxide. If the pressure dependence of the $CH_3+NO$ reaction is the same as presently observed for the recombination rate, the collision efficiency for the recombination reaction, as calculated by Durham and Steacie, would have to be increased by a factor of about two hundred. The present discrepancy is only a factor of thirty and hence a lesser pressure dependence of the $CH_3+NO$ reaction would bring these data into complete agreement. A discrepancy of about a factor of three between the low-temperature data of Ingold and Lossing[6] and the present measurements may be easily due to the low third-body efficiency of the inert gas (helium) which they used in addition to very low pressures of organic vapors. Such low efficiency is certainly not in conflict with the present observations on the effect of carbon dioxide. The rather strong negative temperature coefficient of the recombination rate, observed by Ingold and Lossing, is not consistent with the prediction of the absolute rate theory for the rate of formation of the critical complex. But the present interpretation of the low absolute magnitude of their recombination rate makes the stabilization of the energy-rich ethane molecules by collisions into the rate determining step. The Rice-Kassel theory of unimolecular reactions predicts a decrease in the lifetime of energy-rich molecules with rising temperature because of their rising energy content. It may well be that the temperature coefficient observed by Ingold and Lossing is due to this cause. If that is indeed true, it would appear that all the modern data on the recombination of methyl radicals are in substantial agreement among themselves and bear out very well most of the theoretical predictions.

[15] N. B. Slater, Proc. Roy. Soc. (London) **194A**, 112 (1948).
[16] S. W. Benson, J. Chem. Phys. **20**, 1064 (1952).

THE JOURNAL OF CHEMICAL PHYSICS VOLUME 21, NUMBER 10 OCTOBER, 1953

# Absorption Coefficients of Gases in the Vacuum Ultraviolet. Part II. Nitrous Oxide

MURRAY ZELIKOFF, K. WATANABE, AND EDWARD C. Y. INN
*Geophysics Research Directorate, Air Force Cambridge Research Center, Air Research and Development Command, Cambridge, Massachusetts*

(Received April 7, 1953)

Absorption coefficients of $N_2O$ in the region 1080–2100A have been measured. Four continua were observed with maxima at 1820, 1450, 1285, and 1080A having $f$ values of 0.0015, 0.0211, 0.367, and 0.1, respectively. The strongest absorption band in the ultraviolet lies at 1178A with an absorption coefficient of 3010 $cm^{-1}$ at its maximum. A number of new bands were observed, and some of them classified. Some of the continua have been interpreted in terms of possible dissociation processes, and a potential energy diagram is presented.

SEVERAL investigators have studied the absorption spectrum of nitrous oxide in the vacuum ultraviolet. Leifson[1] observed two continuous bands, the first covering the region 2000–1680A and the second extending from 1550A to the transmission limit of fluorite. However, he did not observe any discrete bands. Sen-Gupta[2] also observed two continua in roughly the same regions. The most thorough and detailed work is that of Duncan[3] who studied the region 850–2200A. The near ultraviolet absorption spectrum of $N_2O$ has been studied by a number of investigators.[4–6]

Absorption coefficients of $N_2O$ in the region 1390–2200A were recently measured by Romand and Mayence[7] who studied the two continua mentioned above. They found the maxima to lie at 1450A and 1840A. There appear to be no other measurements of absorption coefficients in the vacuum ultraviolet. This paper will describe some absorption measurements made by a technique somewhat different from that of previous

[1] S. W. Leifson, Astrophys. J. **63**, 73 (1926).
[2] P. K. Sen-Gupta, Nature **136**, 513 (1935).
[3] A. B. F. Duncan, J. Chem. Phys. **4**, 638 (1936).
[4] A. K. Dutta, Proc. Roy. Soc. (London) **A138**, 84 (1932).
[5] O. R. Wulf and E. H. Melvin, Phys. Rev. **39**, 180 (1932).
[6] L. Henry, Nature **134**, 498 (1934).
[7] J. Romand and J. Mayence, Compt. rend. **228**, 998 (1949).

workers. Absorption coefficients were measured here from 1080–2100A. All the bands found by Duncan in this region were found here, as well as many others not previously detected.

## EXPERIMENTAL

The nitrous oxide was purified from tank gas by drying over $P_2O_5$ and ten successive fractional distillations with liquid nitrogen, retaining the middle fraction each time. The final product was analyzed with a Consolidated Engineering Corporation Analytical Mass Spectrometer. No detectable impurities were found, indicating that the total impurities could not exceed ~0.05 percent.

The absorption measurements were made in a manner exactly like that described in a previous paper from this laboratory.[8] Briefly, the dispersing instrument was a Baird one-meter vacuum monochromator. Entrance and exit slits were each 0.05 mm, giving a band width of 0.85A. The spectra were scanned at 20A per minute. A hydrogen discharge light source was used and the nitrous oxide was contained in a cell having cleaved LiF windows at each end. The cell was 47 mm long and the $N_2O$ pressures were varied from about 0.01 to 200 mm Hg, depending on the extent of absorption in a given wavelength region. In all regions Beer's law was found to hold over a five- to tenfold pressure range.

Corrections were made for scattered light and fluorescence of the LiF windows. The absorption was measured at a few hundred wavelengths, one to five angstroms apart. The absorption coefficient, $k$ in $cm^{-1}$ is defined by $I/I_0=\exp(-kx)$ where $x$ is the layer thickness of the absorbing gas in cm reduced to NTP.

Previous work[8] has shown that the intensity of light leaving the exit slit was at least three orders of magnitude too small to produce any measurable photolysis of $N_2O$. A further check was made by re-running the absorption spectrum repeatedly and finding no change.

## RESULT AND DISCUSSION

For convenience of discussion, the absorption spectrum of nitrous oxide will be divided into four regions each of which will be designated by the terminology of Duncan.[3] Region E–F will cover the range from 1080 to 1215A, region D from 1215A to 1380A, region C from 1380A to 1600A, and region B from 1600A to 2100A.

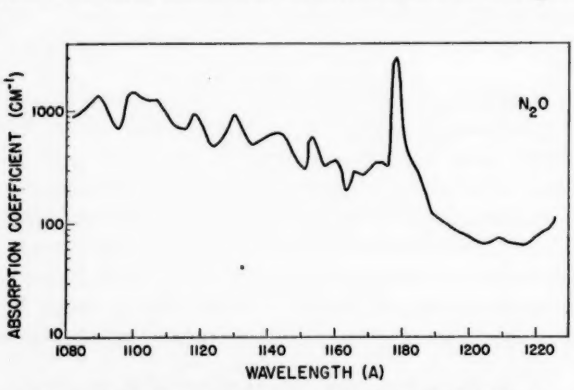


FIG. 1. Absorption coefficients of $N_2O$ from 1080–1220A.

[8] Watanabe, Inn, and Zelikoff, J. Chem. Phys. 21 1026 (1953).

## REGION *E–F*

Figure 1 is a semilog plot of $k$ *vs* $\lambda$ from 1080–1215A. Wavelengths below this region could not be studied in this work, since the transparency of LiF extends only to 1050A. Rather diffuse bands were found at 85 350, 85 800, 86 250, 86 800, 87 500, 88 500, 89 500, 90 400, 91 000, and 91 800 $cm^{-1}$. The wave numbers of these bands agree quite well with those of Duncan except for the band at 91 000 $cm^{-1}$ for which Duncan gives the value 91 200 $cm^{-1}$. Following Duncan, this band is a member ($n=4$) of a Rydberg series represented by

$$\nu=102\,567-R/(n-0.92)^2 \quad \text{where} \quad n=3, 4, 5, \cdots. \quad (1)$$

The calculated wave number for $n=4$ is 90 999 $cm^{-1}$ in close agreement with our value 91 000 $cm^{-1}$. However,

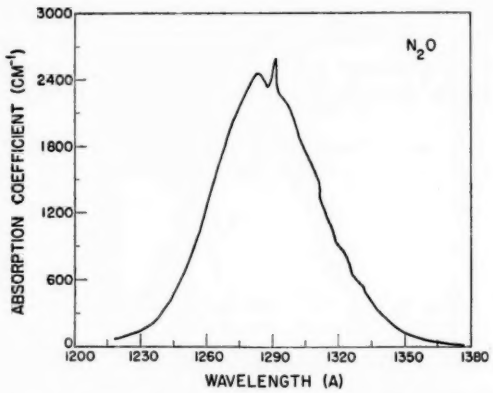


FIG. 2. Absorption coefficients of $N_2O$ from 1220–1380A.

it must be admitted that these wave-number measurements are at best only approximate, owing to the diffuse nature of the bands. Therefore, it was not possible to classify them. They may be due to one or more electronic transitions. Superimposed on these bands there appears to be a strong continuum which may be due to another electronic transition to an upper repulsive state. Most of the absorption intensity in this region may be attributed to this continuum. Its maximum cannot be established from Fig. 1. However, Duncan's photograph shows a relatively transparent region at about 1060A. Thus, the shape of the absorption curve for the continuum is inferred to be quite asymmetric. The maximum is probably near 1080A. On this basis the $f$ value of the continuum (excluding the bands) was estimated to be about 0.1 which indicates an allowed transition.

In this region there is another band at 84 900 $cm^{-1}$ which is the strongest ultraviolet absorption band observed for $N_2O$. Its $k$ value at the maximum is 3010

$cm^{-1}$. Duncan suggests that it is a member of a Rydberg series converging to an ionization potential at a wavelength below our limit of observation.

### REGION *D*

Figure 2 is a linear plot of $k$ *vs* $\lambda$ from 1215–1380A. Whereas Duncan has reported this region to contain a perfectly smooth continuum having no structure, the present study has located several weak diffuse bands on its long wavelength slope and one sharp band at 77 400 $cm^{-1}$ which may be a member of the Rydberg series described by Eq. (1). Duncan chose the maximum absorption of the continuum at 77 900 $cm^{-1}$ as his Rydberg member ($n=3$). The band at 77 400 $cm^{-1}$ fits the Rydberg series much more closely than does the continuum maximum at 77 900 $cm^{-1}$, the calculated value being 77 202 $cm^{-1}$. It is possible that this band is very strong and that the continuum is actually somewhat weaker, with its maximum value appearing to be high because of poor resolution of the sharp band. The

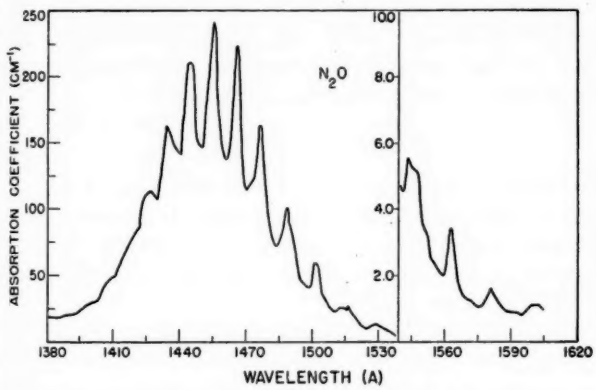


FIG. 3. Absorption coefficients of $N_2O$ from 1380–1605A.

absorption of the Rydberg band probably contributes to the maximum value of the continuum ($k=2465$ $cm^{-1}$). Diffuse bands are found at 77 100, 76 250, 75 600, and 75 100 $cm^{-1}$. The wave numbers given here are probably not very accurate, owing to the diffuse nature of these bands. It is possible that region *D* consists of more than one electronic transition with the upper state of one being repulsive. In addition, the sharp, strong band is tentatively taken as a Rydberg series member. Neglecting the Rydberg band and the possibility that the continuum may be somewhat weaker than it appears to be, the $f$ value of the continuum is calculated to be 0.367. The limits of integration are $\nu=82\,250$ $cm^{-1}$ and $\nu=73\,000$ $cm^{-1}$. The high $f$ value suggests an allowed transition.

### REGION *C*

Figure 3 is a linear plot of $k$ *vs* $\lambda$ for this region. This region is composed of a continuum on which about twenty diffuse bands are superimposed. Duncan[3] reported nine bands which fit the formula

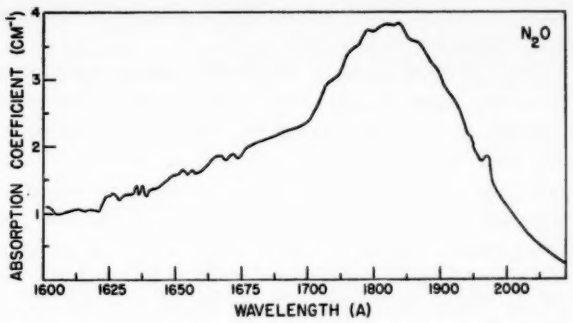


FIG. 4. Absorption coefficients of $N_2O$ from 1605–2100A.

$$\nu=65\,939+621.2v'-11.54v'^2 \quad (v'=0, 1, 2, \cdots). \quad (2)$$

He was not able to relate the frequency 621 $cm^{-1}$ to the fundamentals (589, 1285 $cm^{-1}$) observed in the infrared and suggested that the value he obtained was probably: (1) the lowering of 1285 due to anharmonicity or (2) a modification of 589. Sponer and Teller[9] suggested another possibility (3) namely, that the observed bands may represent two systems each with $621\times2$ $cm^{-1}$ spacing.

The present work has detected many more bands in this region (see Table I) which approximately fit the formula

$$\nu=59\,590+1005v'-30.0v'^2+0.53v'^3$$
$$\text{where } v'=0, 1, 2, \cdots. \quad (3)$$

Some of the bands which fit (3) are in Region B.

The value 1005 $cm^{-1}$ would tend to support the first case. The discrepancies between calculated and observed frequencies are not surprising, in view of the

TABLE I. Bands of electronic transition *C*.

| $N$ | Calc | Obs | Calc-obs | Relative intensity |
|---|---|---|---|---|
| 0 | 59 590 $cm^{-1}$ | 59 520 $cm^{-1}$ | 70 $cm^{-1}$ | 0.06 |
| 1 | 60 565 | 60 510 | 55 | 0.08 |
| 2 | 61 484 | 61 580 | −96 | 0.18 |
| 3 | 62 349 | 62 460 | −111 | 0.20 |
| 4 | 63 164 | 63 250 | −86 | 0.68 |
| 5 | 63 931 | 64 020 | −89 | 1.68 |
| 6 | 64 654 | 64 720 | −66 | 1.60 |
| 7 | 65 337 | 65 360 | −23 | 5.0 |
| 8 | 65 981 | 65 980 | 1 | 8.0 |
| 9 | 66 591 | 66 580 | 11 | 24 |
| 10 | 67 170 | 67 160 | 10 | 43 |
| 11 | 67 720 | 67 700 | 20 | 70 |
| 12 | 68 246 | 68 210 | 36 | 102 |
| 13 | 68 749 | 68 730 | 19 | 102 |
| 14 | 69 234 | 69 230 | 4 | 69 |
| 15 | 69 703 | 69 710 | −7 | 44 |
| 16 | 70 160 | 70 180 | −20 | 17 |
| 17 | 70 609 | 70 650 | −41 | 1 |
| 18 | 71 050 | 71 100 | −50 | 1 |
| 19 | 71 490 | 71 530 | −40 | 1 |
| 20 | 71 930 | 71 940 | −10 | 1 |

[9] H. Sponer and E. Teller, Revs. Modern Phys. **13**, 75 (1941).

diffuse nature of these bands. The strongest absorption lies at the band 68 730 $cm^{-1}$.

There appears to be a relatively strong continuum underlying these bands with a maximum absorption coefficient of 147 $cm^{-1}$ at 68 940. This value compares fairly well with that of Romand and Mayence[7] who found the value 118 $cm^{-1}$. The discrepancy might be attributed to the difference between photographic and photoelectric detection. The continuum is quite symmetrical and both ends can be extrapolated to zero without much difficulty. The $f$ value was measured as 0.0211, suggesting a fairly allowable transition. The limits of integration were $\nu=73\,000$ $cm^{-1}$ and $\nu=64\,250$ $cm^{-1}$.

## REGION *B*

Figure 4 is a linear plot of $k$ *vs* $\lambda$ for this region. This region is one of weak continuous absorption with a maximum $k$ value of 3.82 $cm^{-1}$ at 1820A. Romand and Mayence[7] found a maximum at 1840A with $k=3.13$ $cm^{-1}$. Here, as above, the discrepancy is probably due to the difference in method of detection. Once again, superimposed on this continuum are weak, very diffuse bands. Because of their diffuse nature, the wavelengths could not be measured accurately, and no attempt was made to classify them. The $f$ value (0.0015) of the continuum was measured as in the previous section with integration limits $\nu=65\,000$ $cm^{-1}$ and $\nu=46\,000$ $cm^{-1}$. The limits are probably not accurate, particularly the long wave limit. Various authors have found different results for this limit. The weak character of the absorption suggests that the transition is forbidden. It is difficult to say whether there are one or two electronic transitions involved here, although there seem to be two, with the upper state of one being repulsive and the upper state of the other having a minimum.

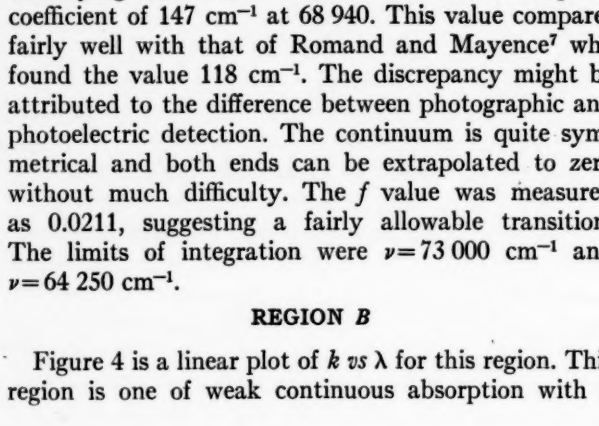


FIG. 5. Potential energy diagram for $N_2O$.

## POTENTIAL ENERGY DIAGRAM

The various absorption continua described above can be interpreted on the basis of an energy level diagram. However, such an interpretation would not be complete without taking into account the near ultraviolet data. Sponer and Bonner[10] have attempted to interpret their data in the near ultraviolet in terms of dissociation processes of $N_2O$. Using a 33 meter light path and $1\frac{1}{2}-5$ atmospheres pressure they measured $N_2O$ absorption up to 3065A and ascribed this long wave limit to the possible transition from the ground state to a state described by (4),

$$N_2O(^3\Pi \text{ or } ^3\Sigma)\rightarrow N_2(^1\Sigma)+O(^3P), \quad (4)$$

with a required energy of 1.71 ev.

The value 1.71 ev originates from thermochemical data.[11] Thus, in this transition, dissociation should become theoretically possible at 7200A. Reasoning from (4) the transition from the ground state to state (5)

$$N_2O(^1\Sigma, ^1\Pi \text{ or } ^1\Delta)\rightarrow N_2(^1\Sigma)+O(^1D) \quad (5)$$

should require 3.68 ev and have a long wave limit at 3370A. However, Sponer and Bonner, do not ascribe any of their observed continua to (5). Furthermore, the transition from the ground state to

$$N_2O(^1\Sigma)\rightarrow N_2(^1\Sigma)+O(^1S) \quad (6)$$

requiring 5.9 ev should have a long wave limit at 2100A but Sponer and Bonner, using their data and that of Dutta[4] place this long wave limit at 2600A. Finally, Sponer and Bonner postulate the transition from the ground state to

$$N_2O(^3\Pi)\rightarrow NO(^2\Pi)+N(^4S) \quad (7)$$

to explain the long wave limit of a continuous absorption from 2820A to below their limit of observation. A careful examination of their Fig. 1 (microphotometer tracing of $N_2O$ absorption) suggests that the extrapolation to 2820A might be in error, since in this region two continua are superimposed on each other. It is possible that this weak absorption extends to a considerably longer wavelength, possibly ~3300A. Indeed, in order to make the transition to (7) energetically consistent with other suggested transitions, Sponer and Bonner assign to it a required energy equal to 3.77 ev or 3300A.

In order to clear up these inconsistencies and to reconcile them with the data of the present work, the following is an attempt to present a unified picture of some of the electronic levels of $N_2O$. It should be noted at the outset that the explanation is highly tentative in nature, particularly so since extrapolation to obtain long wave limits of continua superimposed on each other is an uncertain procedure.

[10] H. Sponer and L. G. Bonner, J. Chem. Phys. 8, 33 (1940).

[11] F. R. Bichowsky and F. D. Rossini, *Thermochemistry of Chemical Substances* (Reinhold Publishing Corporation, New York, 1936).

Figure 5 is a two-dimensional plot of potential energy *vs* internuclear distance. The abscissa scale is qualitative. The dissociation products are at the right and the electronic levels of $N_2O$ are indicated with arrows pointing to the corresponding curve. The transition to the lowest excited level is taken as that corresponding to dissociation into products in the normal states. It is suggested that the continuous absorption corresponding to this transition is too weak to be observed even at the long path length and high pressure of Sponer and Bonner. The long wave limit 3065A of the latter might be extrapolated preferably to ~3370A corresponding to the transition to (5). If the Wigner-Witmer[12] rules are extended to $N_2O$, the products $N_2(^1\Sigma)$ and $O(^1D)$ should originate from a singlet state. The transition from the normal state $^1\Sigma$ to a singlet upper state seems too probable not to appear in absorption at all.

The transition to (4) would be to a $^3\Sigma$ or $^3\Pi$ and hence, forbidden, which might account for the apparent absence of absorption. The curve representing the second excited level ($^1\Sigma$, $^1\Pi$, $^1\Delta$ or $^3\Pi$) should actually be two curves corresponding to the different possible dissociation products listed. For the sake of clarity, only one curve is drawn. If, as appears to be shown by the results of Sponer and Bonner, there is a continuum between ~2100A and ~3300A with a maximum at 2730, transition to (7) might account for it.

Having thus described the three lowest electronic levels of $N_2O$ in a manner which can account for the near ultraviolet data, it becomes possible to add the data obtained in the present work. The continuum of region B above converging to about ~2100A can be accounted for by the transition to an upper repulsive state

$$N_2O(^1\Sigma)\rightarrow N_2(^1\Sigma)+O(^1S). \qquad (8)$$

It is difficult to explain the low $f$ value (0.0015) of this $^1\Sigma\rightarrow{}^1\Sigma$ transition. Still it can be pointed out that the continua at longer wavelengths are much weaker and are probably due to forbidden transitions. It is also possible that the selection rules for diatomic molecules do not exactly apply here. Energetically, the observed long wavelength limit corresponds well with the 5.9 ev required for this transition.

The transition from the normal state to the upper stable state

$$N_2O(^3\Sigma, {}^3\Pi \text{ or } {}^3\Delta)\rightarrow N_2(a\,{}^1\Pi)+O(^3P)$$
$$\text{or}\rightarrow N_2(A\,{}^3\Sigma^+)+O(^1D) \qquad (9)$$

is postulated to account for the band progression of region C represented by Eq. (2). For this progression the area under a plot of $\Delta\nu$ *vs* $n$ gives a dissociation energy of ~2.4 ev for this state. The lowest member (probably the (0, 0) band) of this progression lies at 59 520 $cm^{-1}$ or 7.4 ev; hence, the level converges to 9.8 ev which energetically can correspond to the dissociation products of (9). The designation of this level as a $^3\Sigma$, $^3\Pi$ or $^3\Delta$ raises the question of violation of a selection rule while the absorption is rather strong. No explanation is suggested for this apparent anomaly. Still the application of the Wigner-Witmer rules in choosing the electronic state may not be strictly correct.

There remain only the continua of regions C and D to be accounted for. Energetically, the transition from the ground state to

$$N_2O(^{1,3,5}\Sigma \text{ or } {}^{1,3,5}\Pi)\rightarrow N_2(A\,{}^3\Sigma^+)+O(^3P) \qquad (10)$$

should require ~8 ev. The long wave limit of the continuum of region C is about 64 250 $cm^{-1}$ or ~8 ev in very good agreement with energetic requirements.

Finally, the highest excited state shown can be represented by

$$N_2O(^{1,3}\Sigma, {}^{1,3}\Pi \text{ or } {}^{1,3}\Delta)\rightarrow N_2(B\,{}^3\Pi)+O(^3P)$$
$$\text{or}\rightarrow NO(^2\Sigma)+N(^4S). \qquad (11)$$

Here, as in a previous case, there should be two curves corresponding to the two sets of possible dissociation products, but only one is shown for the sake of clarity. For these transitions, the energy requirement is about 9.2 ev. The observed long wave limit is ~73 000 $cm^{-1}$ or ~9.1 ev in very good agreement.

[12] E. Wigner and E. E. Witmer, Z. Physik **51**, 859 (1928).

# Absorption Coefficients of Gases in the Vacuum Ultraviolet. Part III. $CO_2$

EDWARD C. Y. INN, K. WATANABE, AND MURRAY ZELIKOFF
*Geophysics Research Directorate, Air Force Cambridge Research Center, Air Research and Development Command, Cambridge, Massachusetts*
(Received April 7, 1953)

Quantitative absorption coefficient measurements have been made for $CO_2$ in the region 1050–1800A using a 1-meter vacuum monochromator with a phosphor-coated photomultiplier tube as detector. The absorption spectra obtained consisted of three continua ($\lambda_{max}$ at 1121, 1332, 1475A) and possibly a fourth, all being superposed by many bands. For each continuum $f$ values have been calculated. The results have been compared with some theoretical formulations by Mulliken. Upper limits of dissociation energies of the excited states of $CO_2$ are estimated.

## INTRODUCTION

THE absorption spectrum of $CO_2$ in the vacuum ultraviolet has been previously reported in the literature by a number of investigators.[1] However, for the absorption coefficient of $CO_2$ there appears to be only the measurements of Wilkinson and Johnston[2] in the region of about 1440–1670A and Preston[3] at Lyman alpha (1216A). Considerable attention has been focused on the electronic structure and configuration of the $CO_2$ molecule, especially the theoretical formulations of Mulliken.[4–6]

The importance of molecular absorption cross sections of the various atmospheric constituents has been emphasized in Part I[7] of this series in the light of such photochemical and collision processes that take place in the atmosphere. Furthermore, absorption coefficient measurements should provide much needed information in theoretical studies on the electronic structure of such molecules. It is, therefore, the intention here to report quantitative absorption coefficient measurements of $CO_2$ in the region from about 1060–1800A.

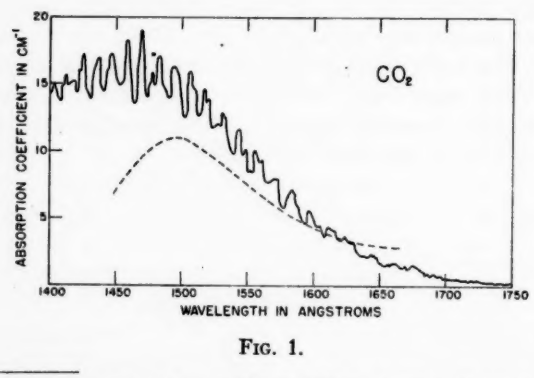


FIG. 1.

## EXPERIMENTAL

The experimental arrangement and technique have already been described in Part I[7] although, for convenience, a brief description will be given here. A windowless hydrogen discharge tube was used as the source, the light from which was dispersed with a 1-meter grating vacuum monochromator. The dispersed radiation (band width about 0.85A) was then allowed to pass through an absorption cell (with LiF windows) 47 mm in length and the transmitted radiation detected with a 1P21 photomultiplier tube coated with sodium salicylate. The photomultiplier current was then amplified and recorded on a Speedomax recorder. The spectrum was thus scanned automatically at a rate of 20A per minute.

Pure $CO_2$ was prepared by repeated sublimation of tank $CO_2$, retaining only the middle fraction in each sublimation. The purity of the $CO_2$ gas thus prepared was determined with a Consolidated mass spectrometer and the analysis showed that the $CO_2$ sample contained impurities in amounts less than 1 part in 2000.

In the actual absorption measurements, pressures of $CO_2$ ranging from about 0.002 to 100 mm Hg were used. Thus, the calculated coefficients were averaged for several different pressures. It should be noted here that two different gratings were used in these measurements, one grating giving somewhat higher resolution than the other. Despite this difference, the absorption coefficients obtained using these two gratings over the same wavelength region agreed to within experimental error.

## RESULTS AND DISCUSSION

Figures 1–3 show the absorption coefficients of $CO_2$ over the spectral region covered from about 1060–1800A. It can be seen that over this region there are three absorption continua with maxima at about 1475, 1332, and 1121A and possibly a fourth below 1100A, all continua being superposed by bands, which appear to be diffuse.

The weak absorption continuum first observed by Lyman[1] is clearly evident in Fig. 1. The absorption coefficient, $k$, was calculated from

$$I = I_0 \exp(-kx),$$

where $I_0$ is the incident and $I$ the transmitted intensity

[1] T. Lyman, Astrophys. J. **27**, 87 (1908); S. W. Leifson, Astrophys. J. **63**, 73 (1926); H. S. Henning, Ann. Physik **13**, 599 (1932); G. Rathenau, Z. Physik **87**, 32 (1934); W. C. Price and D. M. Simpson, Proc. Roy. Soc. (London) **A169**, 501 (1938).
[2] P. G. Wilkinson and H. L. Johnston, J. Chem. Phys. **18**, 190 (1950).
[3] W. M. Preston, Phys. Rev. **57**, 887 (1940).
[4] R. S. Mulliken, Phys. Rev. **40**, 60 (1932).
[5] R. S. Mulliken, J. Chem. Phys. **3**, 720 (1935).
[6] R. S. Mulliken, Revs. Modern Phys. **14**, 204 (1942).
[7] Watanabe, Inn, and Zelikoff, J. Chem. Phys. **21**, 1026 (1953).

and $x$ the layer thickness of the gas reduced to NTP. For comparison, Wilkinson and Johnston's[2] curve is plotted as the dashed curve in Fig. 1, where their values of $k$ refer to 30°C and atmospheric pressure (at NTP their values should be increased by about 10 percent). The discrepancy between our results and those of Wilkinson and Johnston may well be due to the inherent difficulties[7] in the photographic method used by the latter. They also report the maximum of the continuum to be at 1495A as compared to our value of 1475A, which agrees with Fuch's result of 1480A for the resonance wavelength calculated from dispersion data.[8] By symmetrical extrapolation of the curve for the continuum the $f$ value (see Part I[7] for the formula used in this calculation) was calculated to be 0.0043, which surprisingly agrees with the value 0.004 obtained by Wilkinson and Johnston. This agreement is probably fortuitous in that the lower $k$ values at the shorter wavelengths in their curve apparently compensated for the larger values at the longer wavelengths. At any rate, the small $f$ value indicates a forbidden electronic transition, as Mulliken[5,6] already suggested. Thus, the

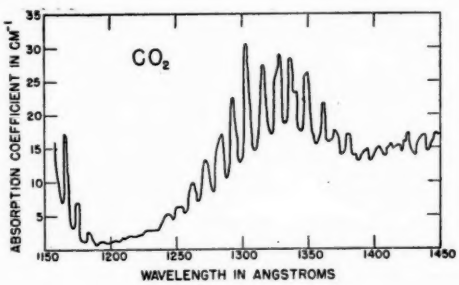


FIG. 2.

suggested transition is

$$^1\Sigma_g^+ \rightarrow (\pi_g)^{-1}\sigma_g,\ ^1\Pi_g.$$

Mulliken has also suggested the possibility that such forbidden transition may occur weakly if the upper state of the equilibrium form of the $CO_2$ molecule is triangular.

It is possible to estimate an upper limit of the energy necessary to dissociate $CO_2$ from the extrapolated long wavelength limit of the continuum. This value is approximately 6.8 ev (1818A).

The bands overlying the long-wavelength end of the 1475A continuum appear to be weak and diffuse making it difficult to single out any vibrational progression for the classification of these bands. It is interesting to note that we have observed many more bands in this region than reported by both Wilkinson and Johnston[2] and Leifson.[1] Although Price and Simpson[1] did not list the wavelengths of the bands they observed in this region, it is evident that some of these bands appear clearly on their photographic plate.

[8] O. Fuchs, Z. Physik 46, 519 (1927).

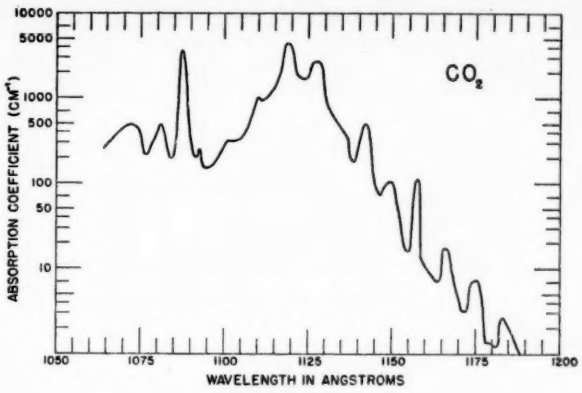


FIG. 3.

The continuum ($\lambda_{max}$ at 1332A) shown in Fig. 2 is a little more intense than the 1475A continuum. The bands are also more intense but somewhat less diffuse. The relative intensities of these two continua do not seem to agree with Price and Simpson's[1] results. In their photographic plate of the absorption spectra of $CO_2$ at very low pressures (~0.01 mm) the 1332A continuum is not present while the 1475A continuum still appears. However, at pressure of a few tenths of a mm their photograph shows the shorter-wavelength continuum to be more intense than those at the longer wavelength, which corresponds more closely to our observations. The discrepancy in their results may well be due to possible changes in the background intensity of the Lyman continuum they used.

The $f$ value for the 1332A continuum was calculated in the same way as described above. It is to be noted that since the two continua overlap, the extrapolation must take this into account. The $f$ value thus obtained is 0.0053, which is slightly larger than that of the 1475A continuum. This low value may again be indicative of a forbidden transition to a second-excited electronic state.

Again, it is difficult to analyze the diffuse bands superposed on the 1332A continuum. Price and Simpson,[1] who also observed these bands though did not list them, suggest that these bands may consist of two progressions starting from 1380A and 1368A, respectively, each with frequency intervals of about 1225 $cm^{-1}$ corresponding to the symmetrical vibration frequency of the ground state. However, attempting to follow this suggestion we find that the intervals are too irregular to assign any frequency for the assumed progressions. Furthermore, since the heads of the bands are not apparent, it is difficult to identify the proper wave number associated with each band.

It is interesting to note that at the short-wavelength tail of the 1332A continuum, the absorption coefficient is quite low and at Lyman alpha (1216A) $k = 1.97$ $cm^{-1}$. This compares very favorably with Preston's[3] value of 2.01 $cm^{-1}$.

Extremely high absorption coefficients were obtained

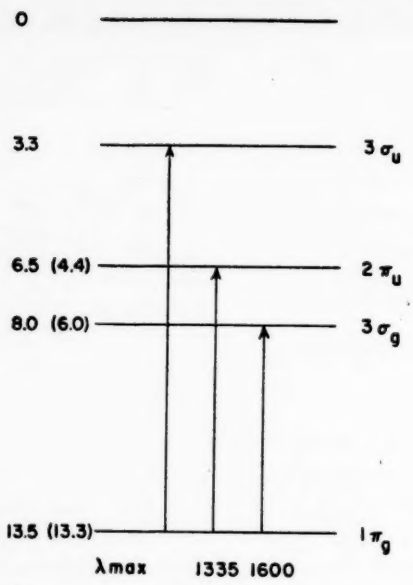


FIG. 4.

for wavelengths below 1200 as shown in Fig. 3. The highest $k$ value was about 4350 $cm^{-1}$ for the band at approximately 1119A. The continuum with its maximum at about 1121A is roughly 100 times more intense than the two longer-wavelength continua discussed above. The $f$ value calculated from this continuum was 0.12, which is indicative of an allowed electronic transition.

The strong bands overlying the 1121A continuum have been previously reported by Rathenau[1] and by Price and Simpson[1] but have not been classified by them. From our results the progression seems to have a frequency interval of about 630 $cm^{-1}$ which would correspond to the bending vibration in the ground state. The strong bands at about 1119 and 1129A have been shown by Price and Simpson[1] (they give 1120 and 1130A) to contain the second members of a Rydberg series, which converges to a limit of 13.73 ev, the first ionization potential of $CO_2$.

It is possible to make some comparisons of our results of the absorption spectra of $CO_2$ with certain theoretically predicted electronic transitions suggested by Mulliken.[6] A portion of the energy level diagram shown in Fig. 6 of Mulliken's paper is reproduced in Fig. 4 showing only the outermost occupied level of $CO_2$ and three unoccupied ones. The column on the right designates the molecular orbital and the column on the left gives the ionization energy in electron volts (averaged for $CO_2$ and $CS_2$) corresponding to each orbital. The values in parenthesis refer to the ionization energies for the $CO_2$ molecule, which Mulliken gives for the vertical processes corresponding to the absorption maxima at 1600 and 1335A (from Price and Simpson's results). Referring to our results for the $3\sigma_g \leftarrow 1\pi_g$ transition we obtained 8.4 ev (1475A) or the corresponding ionization energy of 13.7−8.4=5.3 ev. For the $2\pi_u \leftarrow 1\pi_g$ transition our results are substantially the same as Mulliken's since our value of the wavelength of the absorption maximum of 1332A compares with the 1335A he used. We suggest that the absorption maximum at 1121A corresponds to the transition $3\sigma_u \leftarrow 1\pi_g$ since there is fair agreement energetically with our results. Thus, we obtain for the energy corresponding to the latter transition 11.1 ev (1121A), which compares with Mulliken's value of about 10.2 ev. This would then give for the ionization energy of the $3\sigma_u$ orbital for $CO_2$ a value of about 13.7−11.1=2.6 ev.

Although it is difficult to obtain accurate values of dissociation energies for the various excited electronic states of the $CO_2$ molecule, it is possible to obtain from the extrapolated long-wavelength limits of the three continua upper limits of the energy necessary for the process $CO_2 \rightarrow CO+O$. Admittedly, the values of the long-wavelength limits are only approximate; however, the extrapolation is not difficult in view of the shape of the absorption coefficient curve. We, thus, obtain for the 1475A continuum a value of 6.8 ev (1818A); for the 1332A continuum 7.7 ev (1600A); and for the 1121A continuum 10.3 ev (1205A). One can compare these values with those given by Weeks[9] for the various combination of dissociation products in Table I.

TABLE I.

| States | Above $CO_2(^1\Sigma)$ ev | Observed values ev |
|---|---|---|
| $CO(^1\Sigma)+O(^3P)$ | 5.4 | 6.8 |
| $CO(^1\Sigma)+O(^1D)$ | 7.4 | 7.7 |
| $CO(^1\Sigma)+O(^1S)$ | 9.7 | 10.3 |
| $CO(a\ ^3\Pi)+O(^3P)$ | 11.4 | |
| $CO(d\ ^3\Pi i)+O(^3P)$ | 13.1 | |

Our observed values, which are upper limits, appear to correspond with the products $CO(^1\Sigma)+O(^1D)$ and $CO(^1\Sigma)+O(^1S)$. It is interesting to note that this agreement indicates that the dissociation products arising from two as yet unidentified excited electronic states of the $CO_2$ molecule yield CO in its ground state ($^1\Sigma$) with the O atom excited. The value of 6.8 ev which we observed does not agree with Week's value of 5.4 ev too well if we assume that our value corresponds to the products $CO(^1\Sigma)+O(^3P)$. This could be explained on the basis that, assuming the absorption continuum to arise from a repulsive state, a relatively steep repulsive curve for $CO(^1\Sigma)+O(^3P)$ would tend to give somewhat high upper limits of the dissociation energy in the extrapolation method used above. In fact Weeks[9] shows such a repulsive curve for this state.

We wish to acknowledge the interesting and helpful discussions with Dr. Y. Tanaka.

[9] I. F. Weeks, *Third Symposium on Combustion and Flame and Explosion Phenomena* (The Williams and Wilkins Company, Baltimore, Maryland, 1949).

# Absorption Coefficients of Gases in the Vacuum Ultraviolet. Part IV. Ozone

YOSHIO TANAKA, EDWARD C. Y. INN, AND K. WATANABE
*Geophysics Research Directorate, Air Force Cambridge Research Center, Air Research and Development Command*
(Received April 7, 1953)

Absorption coefficients of ozone gas (purity 90–95 percent) were obtained in the region 1050–2200A by a method described previously. Several strong continua, as well as weak bands, were observed. The curve for absorption intensity shows a minimum (8 $cm^{-1}$) at about 2015A. Below this wavelength, the absorption coefficient increases gradually to a weak maximum (23 $cm^{-1}$) at about 1725A and then rapidly to a strong maximum (420 $cm^{-1}$) at about 1330A. In the region 1050–1450A, the absorption intensity does not fall below the value 130 $cm^{-1}$. The results were compared with Mulliken's treatment of the electronic spectrum of ozone.

## INTRODUCTION

MANY investigators have studied the ozone molecule by optical methods to determine its molecular structure and to obtain quantitative data on its absorption spectrum, particularly in connection with the study of atmospheric ozone. As a result, a number of bands and continua have been found in the ultraviolet, visible, and infrared regions; and although ozone is somewhat unstable, a rather large amount of reliable data on absorption coefficients and effects of temperature and pressure is now available. These, however, will not be reviewed here.

In the vacuum ultraviolet region, the only experimental investigation appears to be that made by Price and Simpson.[1] According to them, the result was "disappointing," since the photographic plates showed no strong absorption in the region 2300—1600A. In the region below 1600A, a strong continuum appears in the reproduction of their photographic plate. However, they stated that in this region, the absorption of $O_2$ resulting from photodissociation of ozone prevents further investigation.

Recently developed techniques in the use of photomultiplier detectors and vacuum monochromators have made it possible to minimize photodissociation during absorption measurements by placing the absorption cell between the exit slit and detector. Using this method, it was possible to make absorption measurements of ozone from 2200 to 1050A.

## EXPERIMENTAL

Liquid ozone was prepared by a method similar to that used by Jenkins and Birdsall.[2] If nitrogen is present in tank oxygen, the ozonizer would produce nitrogen oxides which would condense with ozone. Since these oxides have strong absorption in the Schumann region, their presence could not be tolerated. Accordingly, the ozone samples were obtained by several fractional distillations of the liquid, retaining only the middle portion each time.

To fill the absorption cell, liquid ozone was transferred to the gas-filling system. The transfer was accomplished without any explosions by keeping the ozone cooled in liquid nitrogen until just prior to the absorption measurements. The liquid was allowed to evaporate slowly into the cell, and the pressure measured with a U-type $H_2SO_4$ manometer. For pressure measurements below 1 mm Hg, an expansion method was used. The vapor pressure of $H_2SO_4$ at room temperature did not produce any noticeable absorption as was shown by a blank run. The experimental technique for absorption measurements has been described[3] in Part I of this series. Since ozone decomposes at an appreciable rate, the duration of each run was limited to five minutes during which time a range of 100A could be covered. For each wavelength region four or five different pressures from 0.2 to 25 mm Hg in the absorption cell (length 4.7 cm) were used to cover the absorption intensities.

During the filling of the absorption cell (previously evacuated to $\sim 10^{-5}$ mm Hg) an interesting phenomenon was observed. As the liquid ozone evaporated into the cell, a sudden increase in photomultiplier current, reaching a maximum value in a few seconds, was observed. The current then decayed to its original value. Upon pumping out the ozone, the photomultiplier current again increased and decreased, although, in this case, the rate of current change was slower and the maximum was much less. This phenomena occurred both with the light source on and off, and may be due to chemiluminescence on the inside of the cell. No doubt, some ozone decomposed in this process giving rise to oxygen impurity, but the amount was small as determined subsequently from the absorption data.

The purity of the ozone sample was determined by a combination of three methods. First, the vaporized ozone was allowed to react with aqueous KI and the liberated $I_2$ titrated with standard $Na_2S_2O_3$. Here the ozone was found to be 90–95 percent pure for all samples taken from the purification system and from the gas filling system.[4] To determine the amount of nitrogen oxides, a Consolidated Engineering Corporation analyti-

[1] W. C. Price and D. M. Simpson, Trans. Faraday Soc. **37**, 106 (1941).
[2] A. C. Jenkins and C. M. Birdsall, J. Chem. Phys. **20**, 1158 (1952).
[3] Watanabe, Inn, and Zelikoff, J. Chem. Phys. **21**, 1026 (1953).
[4] See reference 3, Fig. 1.

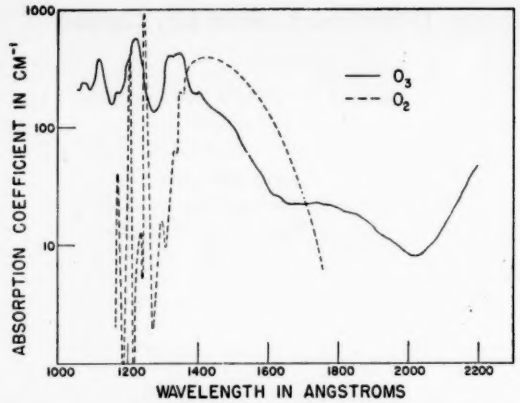


FIG. 1. Absorption coefficients of ozone (solid curve) in the spectral region 1050–2200A. The absorption coefficients of oxygen (dashed curve) are shown for comparison.

cal mass spectrometer was used. The analysis showed no detectable amount of nitrogen oxides in the ozone sample, indicating the nitrogen oxide content was less than 0.05 percent. For this analysis, the sample was allowed to stand several days to convert the ozone to oxygen, since ozone may attack the metal parts of the mass spectrometer. Under this condition, the analysis for CO, $CO_2$, $H_2O$, and hydrocarbons would result in high values, for their formation by the action of ozone on stopcock grease would be exaggerated by the length of the exposure time, and therefore, an analysis of these gases was not made. The absorption measurement itself served as the third method for estimating the amount of impurities. This was made possible by the data for a number of gases obtained previously with the same absorption apparatus. $CO_2$ has three strong peaks at 1088, 1119, and 1129A with $k$ values 3600, 4400, and 2600 $cm^{-1}$, respectively, and these appeared on the uncorrected absorption curve of $O_3$. The data showed that the amount of $CO_2$ was between one and two percent. Similarly, from a strong oxygen peak ($k$=960 $cm^{-1}$) at 1243A, the amount of $O_2$ in the absorption cell was found to be about 7 percent. The presence of CO was indicated by five weak but sharp peaks which corresponded to the heads of the CO fourth positive bands from (0–0) to (4–0). The amount of CO was estimated to be a few percent.

Although the chemical method showed that the total amount of impurities was less than 10 percent, the absorption data indicated that the value was somewhat higher, at least in the absorption cell. This is quite possible, since the reaction described above can provide the additional impurities. In general, the absorption data showed that when relatively high ozone pressures were used, the percentage of impurity was low, more nearly agreeing with the chemical determination. Therefore, to obtain the corrected absorption intensity curve for ozone, only the data obtained with the highest pressures were used. In view of all these uncertainties, it is estimated that the combined experimental error would be as high as 10 percent.

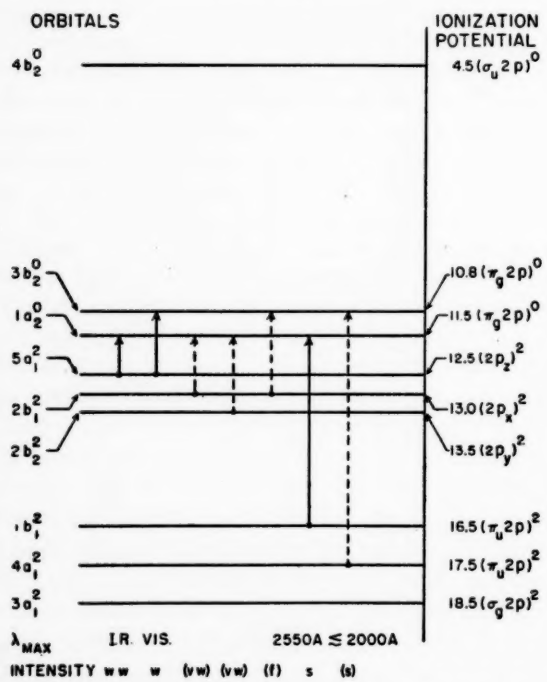


FIG. 2. Electronic transitions of ozone according to Mulliken. Solid arrows indicate observed transitions and dashed arrows are other predicted transitions.

## RESULTS AND DISCUSSIONS

The solid curve in Fig. 1 represents the absorption curve of $O_3$. This curve was obtained after corrections for $O_2$, CO, and $CO_2$ were applied to the original data. It cannot be an absorption curve of an unknown impurity with very high absorption coefficients (order of $10^4$ $cm^{-1}$) since the result was reproducible in spite of the fact that the various observed impurities varied considerably for different runs. The absorption curve (dashed) for $O_2$, the main impurity, is included for comparison.

For convenience of discussion, the regions above and below about 1300A will be considered separately. Above 1300A there appear to be continua with maxima at 1725, 1450, and 1330A. The 1725A continuum merges at about 2000A with the known strong continuum which has a maximum at 2550A. The results of Vassy[5] and Ny Tsi-Ze and Choong Shin Piaw,[6] who measured down to 2020 and 2135A, respectively, are somewhat higher than the present data. The difference was about 10 percent at 2200A and about 40 percent at 2020A as compared to the data reported by Vassy. The discrepancies are greater than can be explained by ordinary experimental errors, and might be due to their use of ozonized oxygen and photographic detection as opposed to the use of purer ozone and photoelectric detection. It is also possible that too small a correction

[5] A. Vassy, Ann. Phys. **16**, 145 (1941).
[6] Ny Tsi-Ze and Choong Shin Piaw, Compt. rend. **195**, 916 (1933).

was applied to our data and this may be responsible for about 10 percent.

Mulliken[7] has proposed an electronic configuration for ozone,

| $(\sigma_g 2s)^2(2s)^2(\sigma_u 2s)^2(\sigma_g 2p)^2(\pi_u 2p)^2(\pi_u 2p)^2(2p_y)^2(2p_x)^2(2p_z)^2(\pi_g 2p)^0(\pi_g 2p)^0(\sigma_u 2p)^0$ | | | | | | | | | | | |
|---|---|---|---|---|---|---|---|---|---|---|---|
| $1a_1^2$ | $2a_1^2$ | $1b_2^2$ | $3a_1^2$ | $4a_1^2$ | $1b_1^2$ | $2b_2^2$ | $2b_1^2$ | $5a_1^2$ | $1a_2^0$ | $3b_2^0$ | $4b_2^0$ |
| | | | 18.5 | 17.5 | 16.5 | 13.5 | 13 | 12.5 | 11.5 | 10.8 | 4.5. |

Figure 2 shows his results schematically, all notations being his. The solid arrows indicate observed transitions and dashed arrows indicate other predicted transitions. The strong band, $4a_1^2-3b_2^0$ predicted in the region just below 2000A was not observed in the present study. The 1725A continuum seems to correspond energetically with it, but is much weaker than predicted. Our results agree with those of Price and Simpson[1] who reported no bands in the region 2300–1600A. Our absorption coefficient at 1600A is 35 $cm^{-1}$, gradually decreasing to a minimum at about 2000A. Energetically, the $3a_1^2-3b_2^0$ and $5a_1^2-4b_2^0$ transitions correspond very roughly to the observed 1725 and 1450A continua, respectively, although the transition probabilities are not known. It might also be noted that the successive energy differences of the three strong continua at 1330, 1215, and 1120A correspond fairly well to the energy differences among the orbitals $1b_1^2$, $4a_1^2$, and $3a_1^2$.

An element of uncertainty is introduced into these theoretical considerations since Mulliken adopted a model of acute apex angle (39°) for $O_3$. Recent infrared[8–11] and electron-diffraction[12] studies, however, seem to support an obtuse apex angle (127°). Therefore, we have attempted to find in Mulliken's paper[13] such transitions which correspond to our observed results. Without taking account of intensity relationships, the following transitions for the case of obtuse angle appear to correspond energetically with the observed continua:

| Continuum maximum | | Attempted transition |
|---|---|---|
| 1725A | (7.2 ev) | $3a_1 \rightarrow 2b_1$ |
| 1450A | (8.6 ev) | $2b_2 \rightarrow 5a_1$? |
| 1330A | (9.3 ev) | $2b_2 \rightarrow 5a_1$? |
| 1215A | (10.2 ev) | $1a_2 \rightarrow 4b_2$ |
| | | or $1b_1 \rightarrow 5a_1$ |
| 1120A | (11.1 ev) | ? |

To these attempted transitions there may be added transitions to excited states higher than those discussed by Mulliken.

Figure 3 shows on an enlarged scale the ozone absorption spectrum from 1350–1060A. A number of bands appear in this region but, due to weakness, and overlapping of the bands by the strong continuum, it is difficult to determine progressions. However, there may exist some progressions which have separations of ~600 and ~800 $cm^{-1}$. The continua having maxima at 1215 and 1120A (more clearly seen in Fig. 1) are similar in shape and intensity to that at 1330A. It is possible that there are two other continua at 1165 and 1070A but the former does not have a prominent peak and the latter approaches the transparency limit of the LiF window, making it difficult to classify with certainty.

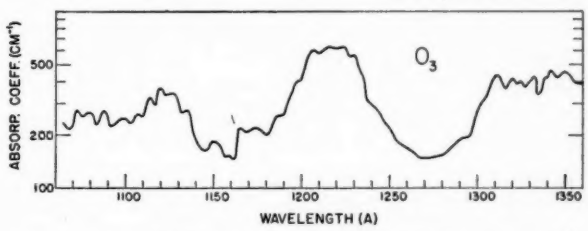


FIG. 3. Absorption spectrum of ozone in the spectral region 1060–1350A, showing a number of bands.

In conclusion, it is interesting to note that ozone has a high absorption coefficient at Lyman alpha where most of the gases reported present in the upper atmosphere have comparatively low-absorption coefficients, oxygen and nitrogen in particular. Water vapor is an exception to this with a $k$ value of 387 $cm^{-1}$. In the region of the Schumann-Runge continuum, ozone has almost as strong absorption as oxygen. Furthermore, the intensity of the $S-R$ continuum decreases rapidly on the long wavelength side, whereas, for ozone the decrease is gradual, particularly above 1600A. The absorption curves cross at about 1700A ($k=20$ $cm^{-1}$).

## ACKNOWLEDGMENT

We are happy to acknowledge our indebtedness to Dr. L. Miller for his help in the chemical analysis of the ozone samples, and to Dr. M. Zelikoff for making mass spectrometer analysis.

[7] R. S. Mulliken, Revs. Modern Phys. **14**, 204 (1942).
[8] G. B. B. M. Sutherland and W. G. Penny, Proc. Roy. Soc. (London), **156**, 678 (1936).
[9] M. K. Wilson and R. M. Badger, J. Chem. Phys. **16**, 741 (1948); R. M. Badger and M. K. Wilson, J. Chem. Phys. **18**, 998 (1950).
[10] D. M. Simpson, J. Chem. Phys. **15**, 846 (1947).
[11] Klein, Cleveland, and Meister, J. Chem. Phys. **19**, 1068 (1951).
[12] W. Shand and R. A. Spurr, J. Am. Chem. Soc. **65**, 179 (1943).
[13] See reference 7, Fig. 6.

# Studies on the Photovoltaic Effect. III*

IRVIN LEVIN,† JOSEPH R. WIEBUSH, MARTIN B. BUSH, AND CHARLES E. WHITE
*Department of Chemistry, University of Maryland, College Park, Maryland*

(Received January 30, 1953)

Further studies in the ultraviolet region between 4000 and 2500A indicate that the magnitude of the photopotential derived from a photoactive substance in solution is dependent on the absorption of the solution. Aliphatic and aromatic alcohols, hydroxy acids and phenols produce practically no photopotentials between 3000 and 8000A. The photovoltaic behavior of 38 organic halides has been studied. Methyl iodide produced the highest photopotential of any of the compounds used. The normal halides other than the iodides were inactive. In general the iso, secondary, and tertiary halides were more active than the corresponding normal halides. Results on 89 compounds other than halides are listed.

## INTRODUCTION

IN the two previous papers,[1,2] results were described on experiments which were designed to determine the cause of the photovoltaic effect. The method of experimentation and description of the apparatus were also given in detail. The photopotential, the potential difference between the irradiated volume and the remaining unirradiated solution, appears to be positive when a carbonyl-like unsaturated group is present next to an activating group which can activate this carbonyl-like structure. The photopotential is negative when an electron-saturated coordinated atom is loosely attached to another atom as in the peroxide structure. Usually, the photopotential is distinctly positive or negative depending on the above-mentioned structure types. However, a positive and a negative photopotential may occur in the same solution. This is illustrated by the previously described transient "photoinductive" effect in which the photopotential displays a definite positive or negative behavior during the first moments of irradiation and then assumes an opposite polarity to the original. This reversal of polarity is probably indicative of the mechanism by which the consecutive reactions or the presence of intermediates might occur during a photochemical process.

TABLE I. Effect of equal intensities of two wavelengths of light on the photopotential of various compounds in 95 percent ethyl alcohol.

| Compound | 2537A Galv. units[a] | 2537A Log$\epsilon$[b] | 3650A Galv. units | 3650A Log$\epsilon$ |
|---|---|---|---|---|
| Anthraquinone (0.0024 *M*) | 41.2 | >4 | about 1 | 3.4 |
| Benzaldehyde (0.094 *M*) | 162 | 3.8 | 15.4 | <1 |
| Benzil (0.044 *M*) | 70.8 | 4.3 | 12.0 | 1.8 |
| Benzoin (0.047 *M*) | 969 | 4.1 | 198 | 1.7 |
| Benzophenone (0.055 *M*) | 61.4 | 4.2 | 20.3 | 1.6 |

[a] The galvanometer units in Table I indicate the relative photopotentials.
[b] Log$\epsilon$ is the common logarithm of the extinction coefficient.

* This work was sponsored by the Office of Naval Research under Contract N8Onr-76500.

† Present address: Department of Biophysical Instrumentation, Walter Reed Army Medical Center, Washington 12, D. C.

[1] I. Levin and C. E. White, J. Chem. Phys. 18, 417 (1950).
[2] I. Levin and C. E. White, J. Chem. Phys. 19, 1079 (1951).

The present paper describes continued basic work on the effect of light absorption on the photopotential. Additional organic compounds which have been studied for their photoactivity in solution are listed. Finally, a theory on the production of the photopotential is given.

## A. THE EFFECT OF LIGHT ABSORPTION ON THE PHOTOPOTENTIAL

### Experimental

Further studies were made to determine how light absorption affects the photopotential of a substance in solution. The solvent in all of these studies was ethyl alcohol. Alcohol was selected as a solvent because it dissolves many organic compounds and does not produce a photopotential under the conditions employed in these experiments. The results summarized in Table I were obtained using 95 percent ethyl alcohol as a solvent. However, commercial absolute alcohol was used in the remainder of the experiments, and the only water present was that absorbed from the air. Since the cells were open to the air it must be assumed that some oxygen was also present in the system. A high-pressure mercury-vapor lamp (General Electric Type AH-4) was used as a source of the 3650A region of the spectrum. The light from this was filtered through a Corning glass filter No. 5860, and a 1 cm thickness of copper sulfate solution containing 125 grams of the pentahydrate in 1 liter of solution. A low-pressure mercury-vapor lamp (Fluoro-Light Model 41) in conjunction with 3 cm of chlorine gas at atmospheric pressure, in a quartz-sided container, was used for the 2537A region. Light absorption properties of most organic compounds is considerably different at these two wavelengths. By the use of equal intensities, it is believed that an indication of the relative effectiveness of these two regions of the spectrum to produce photopotentials can be obtained. Equal intensities of the 3650 and 2537A lines were obtained by placing the lamps at proper distances from the cell. The position of the lamps was determined by using a photoelectric photometer and correcting for the relative sensitivities of the photometer at these two wavelengths. It was found that where the photopotential is large, light absorption is high. This is shown in Table I.

TABLE II. Photopotentials of organic halides in absolute ethyl alcohol at a concentration of approximately 1 percent. Incident light between 3000 and 8000A.

| Compound | Photopot. of pure compound | 1 percent solution in ethanol |
|---|---|---|
| $CH_3I$ | (See Fig. 1) | 18 |
| $C_2H_5Br$ | inactive | 10 |
| $C_2H_5I$ | 720 | 38 |
| $n$-$C_3H_7Br$ | inactive | 15 |
| $n$-$C_3H_7I$ | 763→−1000 | 40→3 |
| iso-$C_3H_7Br$ | 107 | 59 |
| iso-$C_3H_7I$ | 1550→750 | indefinite |
| $n$-$C_4H_9Cl$ | inactive | inactive |
| $n$-$C_4H_9Br$ | inactive | 18 |
| $n$-$C_4H_9I$ | 272 | 18 |
| sec-$C_4H_9Br$ | 48 | 19 |
| sec-$C_4H_9I$ | 1930→1380 | 60→55 |
| iso-$C_4H_9Cl$ | 180 | 14 |
| iso-$C_4H_9Br$ | 55 | 30 |
| iso-$C_4H_9I$ | 1150→800 | inactive |
| tert-$C_4H_9Cl$ | 30 | 97 |
| tert-$C_4H_9Br$ | 114 | 101 |
| $n$-$C_5H_{11}Br$ | 115 | 12 |
| $n$-$C_6H_{13}Br$ | 72 | 56 |
| $CHBr_3$ | inactive | 80 |
| $CHI_3$ | −123 | −165→−33 |
| $CH_2=CHCH_2Br$ | 34 | 14 |
| Fluorobenzene | inactive | inactive |
| Chlorobenzene | inactive | inactive |
| Bromobenzene | 111 | 5 |
| Iodobenzene | indefinite | indefinite |
| Benzyl chloride | indefinite | 12 |
| ortho-dichlorobenzene | 35 | 9 |
| para-dichlorobenzene | (solid) | 12 |
| para-dibromobenzene | ··· | 12 |
| para-di-iodobenzene | ··· | 20 |
| ortho-chloro-nitrobenzene | ··· | 37 |
| meta-chloro-nitrobenzene | ··· | 203 |
| para-chloro-nitrobenzene | ··· | 216 |
| ortho-bromo-nitrobenzene | ··· | 37 |
| meta-bromo-nitrobenzene | ··· | 210 |
| para-bromo-nitrobenzene | ··· | 273 |
| ortho-chloro-benzaldehyde | ··· | 230 |

## Discussion

The data show that in all cases the photopotential for a given solution is higher with the more highly absorbed 2537A line than with the lesser absorbed 3650A line. For a continuous photopotential spectrum to be obtained similar to light absorption curves, a continuous and fairly intense band spectrum in the ultraviolet region to at least 2400A is required. The hydrogen discharge spectrum, high-voltage sparks using tungsten, molybdenum, aluminum, brass, etc., and other continuous ultraviolet sources are too weak or not suitable for practical use for this purpose. Further work on this phase of the problem has therefore been postponed.

### B. THE PHOTOPOTENTIALS OF ORGANIC COMPOUNDS

Alcohols were found to be generally inactive under the radiation from 3000 to 8000A as given by the unfiltered high-pressure mercury-vapor lamp. The following alcohols were tested and found to give no photopotential: methyl, ethyl, $n$-propyl, isopropyl, $n$-butyl, sec-butyl, isobutyl, tert-butyl, $n$-amyl, isoamyl, pentanol-3, $n$-hexyl, 2-ethyl, butanol, 2-methyl pentanol-4, heptanol-2, $n$-octanol-1, methyl-$n$-hexyl-carbinol, 2-ethyl hexyl, decyl, undecanol, lauryl, cetyl, allyl, glycerol, benzyl, beta-phenyl ethyl, gamma-phenyl-$n$-propyl. Under these same conditions the following compounds were also inactive: lactic, malic (very slightly active), tartaric and citric acids, phenol, benzhydrol, hydroquinone, pyrogallol, and borneol. In all of the above cases approximately 1 percent solutions in absolute ethyl alcohol were used for the experiment. A 1.0 percent solution of benzoin was frequently used to check the apparatus during these experiments. The benzoin consistently produced a photopotential slightly greater than 1000 galvanometer units. The compounds are grouped together here because of their inactivity, but in the actual experiments they were interspersed with those listed below which show considerable activity. It is recognized that the aliphatic alcohols and acids have low absorption

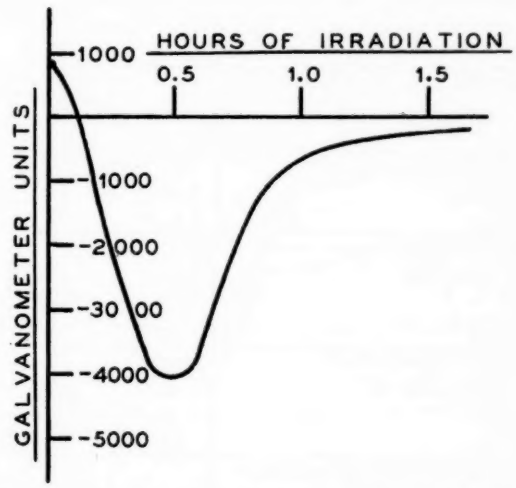


FIG. 1. Photovoltaic behavior of pure methyl iodide using 3650A.

in the region from 3000 to 8000A, and this may account for their failure to produce a potential. The aromatic compounds listed, however, show high-energy absorption in this region and still fail to produce a photopotential. In the same region of excitation 1 percent solutions (unless otherwise stated) of the following compounds gave the photopotentials indicated: picric acid −77; mandelic acid (10 percent) 9; methoxy derivative of mandelic acid (10 percent) 5; alpha naphthol 17; beta naphthol 27; 8-hydroxyquinoline 12; quinoline 6; quinoline (100 percent) 96; 8-hydroxyquinoline sulfate 2; 7-iodo-8-hydroxyquinoline-5-sulfonic acid 36; quinone −25 to +80 (transient).

The presence of one or more hydroxyl radicals with one or more carboxyl groups appeared to be ineffective in producing photoactivity in open chain formations, but developed small photopotential values when attached to an aromatic ring. One, two, or three hydroxyl groups on an aromatic ring showed no photopotential activity. On the other hand, quinone, with its greater

TABLE III. Relative photopotentials of various organic compounds in ethyl alcohol at 0.06 M unless otherwise specified using 2537A. Lamp (fluorolight) 20 cm from cell.

| Compound | Structure | Photopotential |
|---|---|---|
| | | |
| Acetaldehyde | 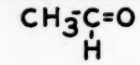 | 251 |
| Acetamide | 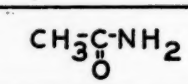 | 180 |
| Acetic Acid | 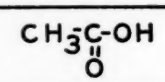 | 17 |
| Acetone | 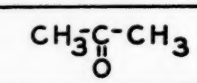 | 214 |
| Acetonitrile | 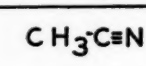 | 154 |
| Acetonyl acetone | 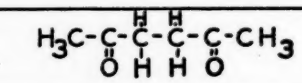 | 464 |
| Acetophenone | 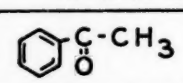 | 1486 |
| Acetophenone Oxime | 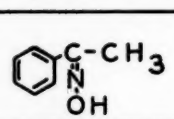 | inactive |
| Anthraquinone (0.025 M) | 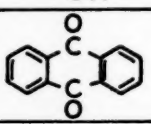 | 41 |
| Benzalacetophenone | 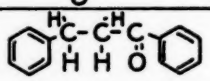 | inactive |
| Benzaldehyde | 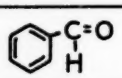 | 58 |
| Benzene | | 31 |
| Benzil | 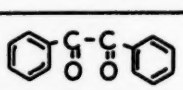 | 526 |
| Benzoic acid | 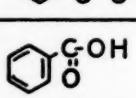 | 209 |
| Benzoin | 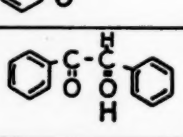 | 1725 |

possibility of electron shifts to and from the oxygen atoms, produced a transient negative potential which quickly changed to a positive value of 80 units.[1] A hydroxyl radical attached to a more complicated but saturated ring structure, as in borneol, was found to be photoinactive. No electronic resonance could be expected in this type of compound.

Further deductions on the effect of groups or atoms in

an organic molecule on the photopotential can be made by an examination of the above results. For example, a hydroxyl group on a naphthyl fused ring yielded a positive photopotential in the beta position. Beta-naphthol was slightly more photoactive than alpha-naphthol. Substitution of a nitrogen atom for a ring carbon atom,

TABLE III.—*Continued.*

| Compound | Structure | Photopotential |
|---|---|---|
| Benzoin oxime | 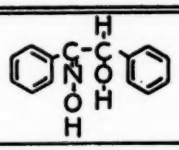 | inactive |
| Benzonitrile | | 184 |
| Benzophenone | 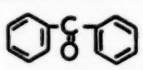 | 478 |
| Butyraldehyde | 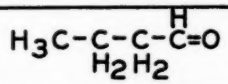 | 242 |
| Butyroin | 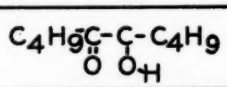 | 271 |
| Cinnamaldehyde | 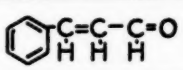 | inactive |
| Crotonaldehyde | 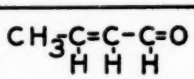 | inactive |
| Cyclohexanone | | 80 |
| Desoxybenzoin | 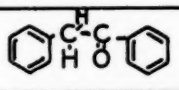 | 158 |
| Diacetone alcohol | 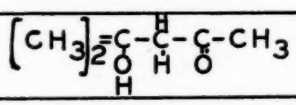 | inactive |
| Diacetyl | 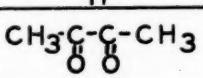 | 128 |
| Dibenzalacetone | 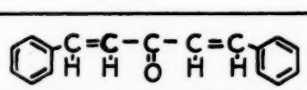 | inactive |
| Dibenzoylmethane | 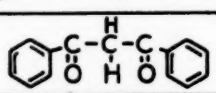 | 15 |
| Dibenzyl ketone | 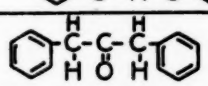 | 1868 |
| Dibenzyl ketoxime | 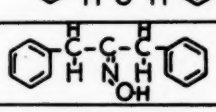 | 1448 |
| Dimethylglyoxime | 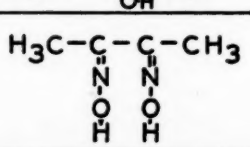 | inactive |

TABLE III.—*Continued.*

| Compound | Structure | Photopotential |
|---|---|---|
| Ethyl acetate | 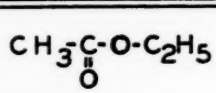 | 136 |
| Ethyl benzoate | 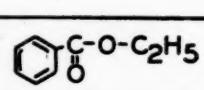 | 294 |
| Fufural | 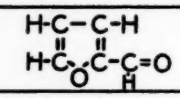 | 43 |
| Glyoxal | 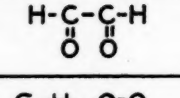 | 57 |
| Heptaldehyde | 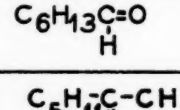 | 245 |
| Heptanone-2 | 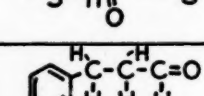 | 226 |
| Hydrocinnamaldehyde | 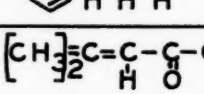 | 788 |
| Mesityl oxide | 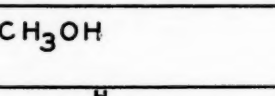 | inactive |
| Methanol | 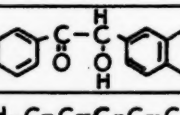 | 24 |
| Naphthoin (0.02 M) | 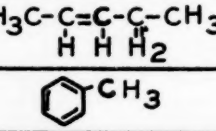 | 38 |
| Pentene-2 | 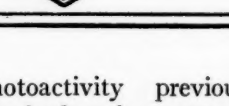 | 7 |
| Toluene | 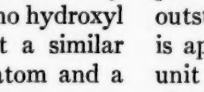 | 53 |

as in 8-hydroxyquinoline, reduced the photoactivity slightly. Quinoline, having the nitrogen but no hydroxyl group, registered a slight photoactivity at a similar concentration. The addition of an iodine atom and a sulfonic acid radical to the hydroxyquinoline structure increased the photopotential markedly over 8-hydroxyquinoline, as found with 7-iodo-8-hydroxyquinoline-5-sulfonic acid.

Table II summarizes the results with organic halides. Methyl iodide was the most striking in photopotential activity and probably illustrates how other light-unstable organic halides might behave if given sufficient time. Figure 1 illustrates that pure methyl iodide before any photochemical decomposition can occur is photopositive, but as soon as free iodine is liberated by the light, a negative potential is produced as described previously.[2] This photonegative potential reached the outstanding value of −4100 galvanometer units which is approximately −0.45 volt; since one galvanometer unit equals about 0.11 millivolt; this is the largest ever obtained during the entire work. The potential after reaching this maximum slowly decreased because of the absorption of light by the iodine which is continually being liberated. The purpose of using the 1 percent solution in ethanol as indicated in Table II was to determine any change in the polarity of the photopotential due to dilution. Such a case of change of polarity of the photopotential with dilution was found with benzaldehyde[2] and was attributed to the presence of peroxides. Table II also indicates that with the organic halides studied no distinct changes in polarity occurred on dilution as with benzaldehyde and *o*-chlorobenzaldehyde,

and that the organic halides tend to be initially photopositive.

The homologous iodides with molecules up to four carbons registered higher readings than the compounds with longer structures or with other halogen atoms in the molecule. Bromoform equimolar with ethyl alcohol on continued irradiation directly with the 100-watt high-pressure mercury-vapor lamp eventually produced 1000 galvanometer units positive, the highest value of any bromide studied. The increase of the photopotential of bromoform from +200 to +1000 in equimolar ethanolic solution may be explained by the fact that halogens yield positive values in chloroform, as described previously.[2] The alkyl chlorides, simpler aryl chlorides, and fluorobenzene were found to be in general the least photoactive. A chlorine atom appears to be more photoactive than a bromine atom when meta or para to a nitro group on a benzenoid ring. Chlorobenzaldehyde showed the highest value of all the chlorides studied.

The length of the carbon chain apparently influences the photopotential of organic halides to some extent; the photopotential decreases as the length of the chain increases. In general, the iso, secondary, and tertiary halides produce greater photopotentials than the normal halides. Aromatic halides are relatively less photoactive than aliphatic halides. Resonating structures tend to develop higher photopotential values than saturated and nonresonating forms. As a rule, iodides are more photoactive than bromides or chlorides, and bromides more photoactive than chlorides. The hydroxyl group has no effect with straight-chain or single-ring compounds unless a more strongly negative structure is also present. Two or three hydroxyl groups on the same ring fail to produce a photopotential. One hydroxyl group attached to a double ring does cause photoactivity varying with the relative position in the molecule. Salt formation decreases the photopotential considerably, probably because of ionization. Length of exposure varies the photopotential if a photochemical reaction is induced, the magnitude and polarity depending upon the halide, which acts as a solvent for the liberated halogen.

Light absorption affects the photopotential, but there is no direct relationship applicable to all compounds since absorbed light may be converted into several other effects. Alcohols do not absorb the energy of the wavelengths employed, hence they produced no photopotential. Hydroquinone and fluorobenzene absorb the wavelengths utilized but show no photopotential. Methyl iodide and bromobenzene absorb only slightly at 3000–3670A but develop appreciable photopotentials. Methyl iodide, however, absorbs more strongly in the 2537A region, and under the influence of the shorter wavelength produces much higher photopotentials.

Methyl iodide exhibits more absorption, a greater photopotential, and a greater degree of photodecomposition with 2537A light than with 3650A light. This conclusion was verified by means of titrations with thiosulfate. This shows a direct relationship between these properties. The fact that the photopotential of methyl iodide varies with length of exposure indicates that the photopotential may be a measure of photodecomposition.

Table III shows the effect of the presence of unsaturated bonds on the photopotential using 2537A and ethyl alcohol. Apparently, wherever the photopotential of the unsaturated compound is small, the light absorption is low, and the unsaturated carbonyl linkage is conjugate to other unsaturated linkages, or a nitrogen atom is involved having a lone pair of electrons which are photoinert. Wherever the photopotential is large, the light absorption is relatively high, a carbonyl group is involved, and electronic displacement within the structure seems to be hampered. These factors may cause some enhanced association with the solvent molecules during irradiation, and the solute may behave as a sink to photoelectrons drawn from the alcoholic solvent. Also, wherever a large number of electrons from a solute molecule are projected into the alcoholic solvent, as with the peroxide linkage or with free halogen dissolved in alcohol,[2] a photonegative potential is obtained probably due to enhanced association. In this photonegative case, the solute may act as a source of photoelectrons.

## CONCLUSION

The seat of the photopotential has not been definitely determined; it appears that the structure of the solute molecule in true solution is the controlling factor in the production of the photopotential due to some electronic disturbance in the molecule. The requirement that the solvent be polar seems to be of secondary importance because the potential difference between the irradiated and the dark volumes of the solution is apparently a difference in the extent of electronic excitation within the photoactive solute molecule.

As mentioned in the previous papers,[1,2] the irradiated volume of photoactive solute molecules can be considered as having a space charge differing from that of the unirradiated volume of solute molecules, and the following functional relation can be derived for this condition:

$$V = m \log I + b.$$

$V$ is the photopotential or the energy required to bring a photoactive molecule from the dark condition to the charge it has when irradiated; $m$ and $b$ are constants for a given molecule, wavelength, temperature, etc.; and $I$ is the intensity of the monochromatic light beam. This equation also indicates that the photopotential is not only related to the concentration of the photoactive solute in solution but also can be expressed in absolute voltage or energy units which are independent of the apparatus. This will be indicated in a subsequent paper.

# The Specific Heat of Graphite from 13° to 300°K*

W. DeSorbo and W. W. Tyler
*General Electric Research Laboratory, The Knolls, Schenectady, New York*
(Received March 2, 1953)

The specific heat of high-purity Acheson graphite prepared by the National Carbon Company has been measured from 13° to 300°K. In the region 13° to 54°K the $C_p$ data follows a $T^2$ dependence quite accurately in agreement with previous experimental work and recent theoretical investigations of specific heat in strongly anisotropic solids.

On the basis of some recent studies for other highly anisotropic solids, it is suggested that the specific heat of graphite will eventually follow a $T^3$ dependence at still lower temperatures.

The derived thermodynamic functions, entropy, enthalpy, and free energy, have been determined by graphical integration and tabulated at integral values of temperature up to 300°K. The entropy of graphite at 298.16°K is 1.372±0.005 cal/g-åtom deg, of which 0.004 is extrapolated from 13° to 0°K assuming the third law and the $T^2$ dependence.

## INTRODUCTION

MEASUREMENTS on the specific heat of graphite commenced with those of Weber[1] in 1875, and Zakrzewiski[2] in 1891. The room temperature values deviated considerably from the predictions of the classical Dulong and Petit law. Nernst's[3] investigation represents the first real attempt to measure the specific heat of graphite below ordinary temperatures (25.8° to 92.6°K). These measurements were followed by those of Magnus,[4] who measured the specific heat of graphite over a large temperature range (44.1° to 1100°K), and the work of Jacobs and Parks,[5] whose measurements

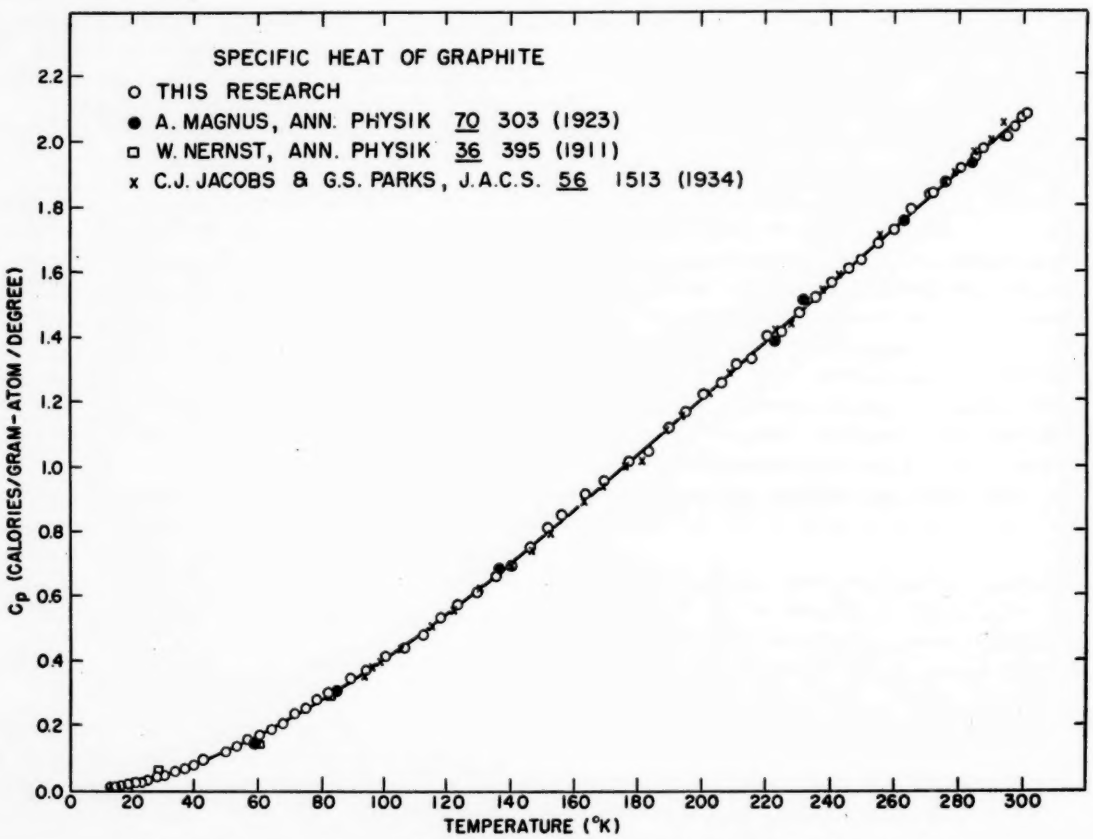


FIG. 1. Low-temperature specific heat of graphite compared with previous investigations.

* Presented in part before the Proceedings of the American Physical Society Meeting, Schenectady, New York, June 14–16, 1951; Phys. Rev. 83, 878 (1951).

[1] H. F. Weber, Ann. Physik (2) 154, 367–423, 552–82 (1875). Phil. Mag. (5) 49, 161–83, 276–302 (1875).
[2] I. Zakrzewiski, Bull. Internatl. Acad. Sci. Cracovie, 141–8 (1891).
[3] W. Nernst, Ann. Physik 36, 395 (1911).
[4] A. Magnus, Ann. Physik 70, 303 (1923).
[5] C. J. Jacobs and G. S. Parks, J. Am. Chem. Soc. 56, 1513 (1934).

extended from 93.3° to 293.5°K. More recently, this property of graphite has been determined by Estermann and Kirkland,[6] as yet unpublished but referred to in a recent publication by Gurney.[7]

It was the purpose of this investigation to extend the measurements on the specific heat of high-purity Acheson graphite to temperatures lower than those reported earlier; and to provide more detailed information concerning its temperature dependence. This study represents a part of a general program of determining the thermodynamic properties of various modifications of carbon.[8] Graphite was considered of particular interest because of anomalous specific heat variation with temperature which has been attributed to the high anisotropy of the lattice.

Graphite has a layer-like structure. Each carbon atom is bonded to three other carbon atoms forming a framework of planar hexagonal rings. The distance between carbon atoms in a plane is 1.42A. The planes are loosely coupled together, being separated by about 3.4A.[9] In a given plane, the atomic displacements perpendicular to the plane have restoring forces which are much weaker than for similar displacements in the plane. Because of this anisotropy the standard Debye theory should not apply and one expects an anomalous specific heat variation. As early as 1911, while comparing his specific heat data of graphite with the Einstein theory, Nernst[3] suggested that it is necessary to use two "Einstein temperatures" to describe the data instead of a single characteristic temperature of an isotropic lattice. One of these characteristic temperatures was considered to refer to the "soft" low-temperature modes and the other to the "hard" high-temperature modes. Magnus[4] interpreted his data in terms of two Debye expressions, with characteristic temperatures of 760°K and 2280°K. Tarassov[10] first discussed the applicability of a two-dimensional frequency-distribution function to the low-temperature specific heat of graphite. Although his treatment led to a $T^2$ dependence, Tarassov did not distinguish between "soft" and "hard" modes, attempting to describe the data in terms of one characteristic temperature.

Gurney[7] has also pointed out that a two-dimensional frequency spectrum will predict a $T^2$ dependence of the specific heat. His theory is based on particle size effects and thus the $T^2$ dependence is not intrinsic to the graphite structure. Komatsu and Nagamiya[11] have developed a theory of the specific heat of graphite based on the assumption that the graphite structure may be considered equivalent to a stack of thin elastic plates weakly coupled together. Again a $T^2$ dependence is derived and characteristic temperatures obtained for the stretching and bending modes of the plates. Recently, Krumhansl and Brooks[12] have extended the Debye theory of specific heat to elastically anisotropic solids and have shown that a $T^2$ dependence of specific heat is an intrinsic property of the graphite type lattice.

## EXPERIMENTAL

The high-purity Acheson graphite sample used in this study was obtained from the National Carbon Company, and designated as grade CS graphite. Eighty-one grams (6.775 gram-atoms) were placed in the calorimeter. No analysis has been made on the hydrogen content. The granule size of the sample ranged +100, −10 mesh. Analysis of the specimen by x-ray showed the sample to be pure graphite and gave a three-dimensional diffraction pattern. There was slight broadening of the 00.L maxima corresponding to a crystallite size in the C direction of about 230A.†

TABLE I. Specific heat of graphite.

| Mean temp(°K) | $\Delta T$ | $C_p$ cal/g-atom deg | Mean temp(°K) | $\Delta T$ | $C_p$ cal/g-atom deg |
|---|---|---|---|---|---|
| 12.92 | 1.744 | 0.0076 | 158.23 | 5.770 | 0.841 |
| 13.77 | 1.190 | 0.0091 | 163.93 | 5.450 | 0.906 |
| 15.15 | 1.361 | 0.0121 | 169.40 | 5.388 | 0.946 |
| 16.06 | 3.186 | 0.0122 | 177.55 | 6.102 | 1.004 |
| 16.20 | 1.359 | 0.0142 | 183.68 | 5.956 | 1.035 |
| 17.88 | 1.596 | 0.0159 | 189.63 | 5.709 | 1.110 |
| 18.73 | 2.130 | 0.0181 | 195.24 | 5.547 | 1.157 |
| 19.93 | 2.071 | 0.0198 | 200.81 | 5.367 | 1.207 |
| 20.77 | 1.882 | 0.0204 | 206.11 | 4.762 | 1.243 |
| 22.67 | 1.895 | 0.0253 | 211.10 | 5.221 | 1.304 |
| 24.47 | 1.807 | 0.0283 | 215.80 | 4.670 | 1.319 |
| 26.29 | 1.727 | 0.0338 | 220.40 | 4.545 | 1.388 |
| 30.56 | 2.327 | 0.0443 | 225.30 | 5.200 | 1.398 |
| 33.57 | 2.578 | 0.0583 | 230.44 | 5.075 | 1.456 |
| 36.33 | 2.900 | 0.0655 | 235.55 | 4.944 | 1.503 |
| 39.36 | 3.351 | 0.0767 | 240.48 | 4.824 | 1.549 |
| 42.48 | 3.204 | 0.0920 | 245.20 | 4.753 | 1.587 |
| 49.44 | 3.505 | 0.116 | 249.33 | 4.640 | 1.618 |
| 52.95 | 3.544 | 0.132 | 254.34 | 5.315 | 1.666 |
| 56.48 | 3.650 | 0.153 | 259.69 | 5.188 | 1.705 |
| 60.20 | 3.811 | 0.165 | 264.92 | 5.037 | 1.768 |
| 64.16 | 3.836 | 0.186 | 269.89 | 4.924 | 1.809 |
| 67.90 | 3.585 | 0.205 | 271.49 | 4.381 | 1.816 |
| 71.49 | 3.799 | 0.231 | 275.53 | 4.301 | 1.847 |
| 75.17 | 3.580 | 0.251 | 279.94 | 4.222 | 1.886 |
| 78.80 | 3.673 | 0.278 | 282.37 | 3.881 | 1.907 |
| 82.39 | 3.506 | 0.295 | 284.07 | 4.139 | 1.923 |
| 89.52 | 5.693 | 0.340 | 286.99 | 4.074 | 1.950 |
| 94.23 | 6.320 | 0.368 | 291.21 | 4.286 | 1.991 |
| 100.39 | 6.370 | 0.412 | 293.22 | 3.690 | 1.982 |
| 106.59 | 6.103 | 0.433 | 294.71 | 4.275 | 1.984 |
| 112.49 | 5.822 | 0.473 | 296.95 | 3.621 | 2.021 |
| 118.14 | 5.525 | 0.528 | 299.02 | 4.148 | 2.043 |
| 123.88 | 5.257 | 0.567 | 300.57 | 3.562 | 2.057 |
| 129.43 | 5.855 | 0.607 | | | |
| 135.19 | 5.641 | 0.654 | | | |
| 140.57 | 5.445 | 0.690 | | | |
| 146.37 | 6.187 | 0.742 | | | |
| 152.42 | 5.947 | 0.802 | | | |

[6] I. Estermann and G. I. Kirkland (unpublished).
[7] R. W. Gurney, Phys. Rev. **88**, 465 (1952).
[8] W. DeSorbo, J. Am. Chem. Soc. **75**, 1825 (1953).
[9] J. P. Howe, J. Am. Ceramic Soc. **35**, 275 (1952). (contains bibliography on structure of graphite).
[10] V. V. Tarassov, Compt. rend. (U.R.S.S.) **46**, 110 (1945).
[11] K. Komatsu and T. Nagamiya, J. Phys. Soc. (Japan) **6**, No. 6, 438 (1951).
[12] J. A. Krumhansl and H. Brooks, J. Chem. Phys. **21**, 1663 (1953).

† We are indebted to Dr. W. L. Roth of our laboratory for this work.

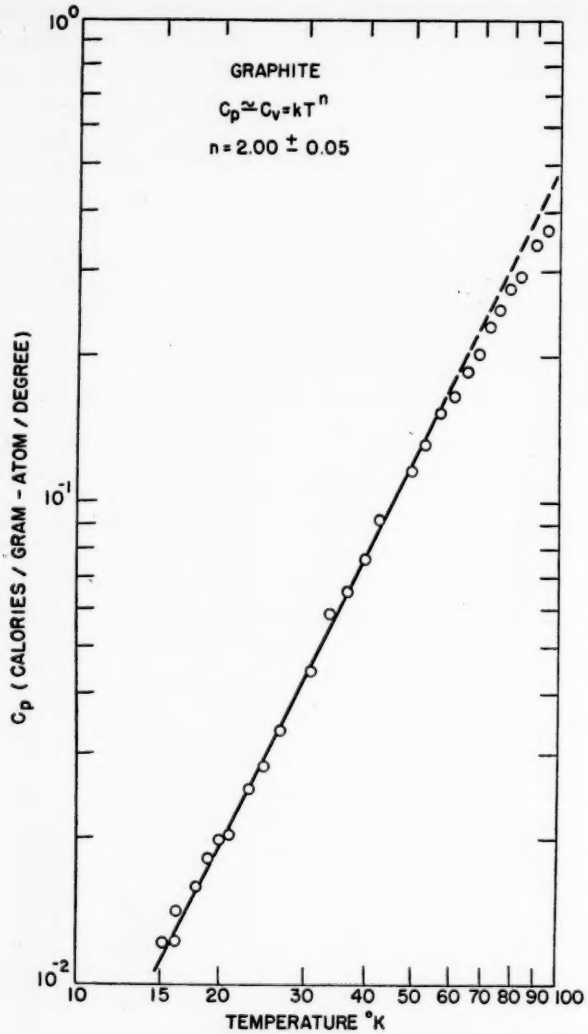


FIG. 2. Log $C_v$ as a function of log $T$ for graphite at low temperatures.

The cryostat, copper calorimeter, and accessory apparatus used in this investigation have been used previously and are described elsewhere.[8] The accuracy of the measurements is about 0.1 percent above the liquid hydrogen temperatures and below the ice point. In the hydrogen region, the accuracy may be about 2–3 percent.

## RESULTS

The data obtained in this investigation have been tabulated and are presented in Table I. A plot of these results and those of previous investigations are presented in the graph of Fig. 1. In Table II are listed the values of the thermodynamic functions obtained from a smooth curve of large plots of specific heats *vs* $T$ and of specific heats *vs* log $T$ with the aid of Simpson's rule. These functions have been evaluated at convenient intervals of temperatures up to 300°K. The entropy of graphite, having the crystallite size reported, has a value of 1.372±0.005 cal/g-atom deg at 298.16°K.

## DISCUSSION OF THE RESULTS

In Fig. 2 the data are presented as a plot of log $C_v$ *vs* log $T$ for the temperature region below 100°K. The specific heat $C_v$ is equal to $C_p$ at these temperatures within the limits of the experimental errors.‡ The $T^2$ dependence of the specific heat of graphite is verified in the temperature region 13° to 54°K.

For the purpose of extrapolating entropy to absolute zero the $T^2$ dependence of the specific heat of graphite has been used to evaluate the entropy increment between 0° and 13°K. This increment amounts to 0.004 cal/g-atom deg. In Table III the entropy values of graphite obtained in this research and that obtained earlier by Jacobs and Parks are summarized. In the earlier work the entropy increment between 0° and 90°K had been obtained by using a combination of Nernst's specific heat values and the Debye $T^3$ law.

The various theories all attempting to rationalize this $T^2$ dependence are mentioned in the introduction, and discussed in more detail by Krumhansl and Brooks.[12] Characteristic temperatures deduced from our data depend on which of the theories is chosen. Krumhansl and Brooks have fit the experimental data for graphite in the temperature range from 15° to 1000°K by considering the lattice vibrations as being of two kinds (a) displacements normal to the layer planes (bending) with a Debye temperature of 950° and (b)

TABLE II. Thermodynamic functions of graphite based on the smooth curve of specific heat.

| $T$°K | $C_p$ cal/g-atom deg | $H^0-H_0^0$ cal/g-atom | $\frac{H^0-H_0^0}{T}$ cal/g-atom deg | $S^0$ cal/g-atom deg | $-\left(\frac{F^0-H_0^0}{T}\right)$ cal/g-atom |
|---|---|---|---|---|---|
| 13 | 0.0080 | 0.0421 | 0.0032 | 0.0041 | 0.0009 |
| 15 | 0.0102 | 0.0592 | 0.0039 | 0.0056 | 0.0017 |
| 25 | 0.0300 | 0.2478 | 0.0099 | 0.0154 | 0.0055 |
| 50. | 0.1210 | 2.0226 | 0.0404 | 0.0629 | 0.0225 |
| 75 | 0.2501 | 6.5963 | 0.0879 | 0.1346 | 0.0467 |
| 100 | 0.3963 | 14.674 | 0.1468 | 0.2275 | 0.0807 |
| 125 | 0.5723 | 26.714 | 0.2137 | 0.3346 | 0.1209 |
| 150 | 0.7718 | 43.456 | 0.2897 | 0.4563 | 0.1666 |
| 175 | 0.9804 | 65.339 | 0.3733 | 0.5925 | 0.2192 |
| 200 | 1.180 | 92.460 | 0.4623 | 0.7384 | 0.2761 |
| 225 | 1.461 | 124.895 | 0.5551 | 0.8916 | 0.3365 |
| 250 | 1.629 | 162.846 | 0.6514 | 1.0510 | 0.3995 |
| 275 | 1.843 | 206.232 | 0.7500 | 1.2157 | 0.4658 |
| 298.16 | 2.038 | 251.183 | 0.8424 | 1.3718 | 0.5294 |
| 300 | 2.053 | 254.946 | 0.8498 | 1.3846 | 0.5348 |

TABLE III. Entropy of graphite at 298.16°K (cal/g-atom deg).

| Jacobs and Parks | This research |
|---|---|
| 0–90°K (Extrapolated) = 0.182 | 0–13°K (Extrapolated) = 0.004 |
| 90–298.1°K (Graphical) = 1.182 | 13–298.16°K (Graphical) = 1.368 |
| $S^\circ_{298.16} = 1.36 \pm 0.02$ | $S^\circ_{268.16} = 1.372 \pm 0.005$ |

‡ Using formula $C_p - C_v = AC_p^2T$, $A = a^2V/C_p^2K$, where $a = 2.2 \times 10^{-5}$/deg (see reference 11).

displacements in the planes (stretching) with a Debye temperature of 2500°K.

The Krumhansl-Brooks theory indicates that the $T^2$ dependence may be an intrinsic property of the graphite lattice and predicts that at sufficiently low temperatures the specific heat should vary as $T^3$. Gurney's theory, based on a particle size effect, predicts that the specific heat should vary as $T^2$ down to absolute zero. Our data does not extend to low enough temperatures to decide this point. Recent studies [13–16] on the specific heat of selenium, tellurium, and antimony indicate that other highly anisotropic solids which depart from a Debye theory at higher temperatures approach a $T^3$ dependence at the lowest temperatures. Whether the specific heat in graphite eventually goes to a $T^3$ dependency must await experimental results in the liquid helium range.

[13] W. DeSorbo, "Low temperature specific heats of chain and layer structures," Eighth Conference on Cryogenics, General Electric Company, Schenectady, New York, October 6–7, 1952.
[14] W. DeSorbo, "The specific heat of crystalline selenium at low temperatures" (to be published in J. Chem. Phys.).
[15] W. DeSorbo, J. Chem. Phys. 21, 764 (1953).
[16] W. DeSorbo, "The low temperature specific heat of antimony" (to be published in Acta Metall.).


### ACKNOWLEDGMENTS

We wish to thank A. J. Peat and A. C. Wilson for their assistance in the experimental work as well as for their help in the data computation. Computational assistance was also rendered by Mrs. E. L. Fontanella and Mrs. M. V. Doyle.

The authors are grateful to Dr. M. H. Hebb and Dr. D. Turnbull for their continued interest in this work and for their criticism of the manuscript.


THE JOURNAL OF CHEMICAL PHYSICS VOLUME 21, NUMBER 10 OCTOBER, 1953

# The Lattice Vibration Specific Heat of Graphite

J. KRUMHANSL,* *Department of Physics, Cornell University, Ithaca, New York*

AND

H. BROOKS, *Division of Applied Science, Harvard University, Cambridge, Massachusetts*

(Received March 4, 1953)

Recent experiments have shown that the specific heat of graphite varies as $T^2$ instead of $T^3$ between 15°K and 80°K. In this paper such a behavior is shown to be a consequence of the elastic anisotropy of graphite, and therefore an intrinsic property, rather than a particle size effect as suggested by Gurney, or a plate-like behavior as suggested by Komatsu and Nagamiya. The Gurney treatment is shown to be in error both as to the enumeration of modes, and as to the temperature range over which the particle size effect might be of significance. The Komatsu and Nagamiya treatment is shown to be inconsistent with elasticity theory. The present treatment employs a semirigorous analysis of the normal mode problem for the transverse vibrations, approximated for long wavelengths. It is found that experimental data from 15–1000°K can be well fitted by dividing the lattice vibrations into two types: (a) modes with atom displacements normal to the layer planes with a Debye temperature of 900°K, and (b) modes with atom displacements in the planes with a Debye temperature of 2500°K.

## I.

WE wish to discuss the normal modes of vibration of the graphite lattice. Graphite is assumed to have the Bernal structure shown in Fig. 1. The primitive translation vectors are chosen as

$$\tau_1=\sqrt{3}/2a,\quad a/2,\quad 0,$$
$$\tau_2=0,\quad -a,\quad 0,$$
$$\tau_3=0,\quad 0,\quad c.$$

The unit cell contains four atoms whose positions may be chosen, with some degree of arbitrariness, as

$$A=0,\quad 0,\quad 0,$$
$$B=-a/\sqrt{3},\quad 0,\quad 0,$$
$$C=0,\quad 0,\quad c/2,$$
$$D=a/\sqrt{3},\quad 0,\quad c/2.$$

It is to be noted that $A$ and $C$ atoms have nearest neighbors in planes immediately above and below, whereas $B$ and $D$ atoms do not. On the other hand, whereas $A$ and $C$ atoms have three next nearest neighbors in adjacent planes $B$ and $D$ atoms have six.

In a normal mode of vibration of the lattice the displacement $\boldsymbol{\delta}$ of a lattice atom is given by

$$\boldsymbol{\delta}_\alpha(\mathbf{r}_i,\boldsymbol{\sigma})=\mathbf{G}_\alpha(\boldsymbol{\sigma},\mathbf{r}_i)e^{i[\boldsymbol{\sigma}\cdot(\mathbf{r}_i+\mathbf{R})-\omega t]},$$

where $\mathbf{G}_\alpha$ is the "polarization" vector $\alpha=1,2,3$; $\boldsymbol{\sigma}$ is the wave vector; $\mathbf{r}_i$ is the position of the $i$th atom in a unit cell; $\mathbf{R}$ is the position of the origin in a cell; and $\omega$ is angular frequency of vibration.

In the isotropic case the polarization vectors take three directions, one longitudinal and two transverse with respect to the wave vector $\boldsymbol{\sigma}$. However in the present case, since there are relatively strong restoring forces for $x$ and $y$ displacements in the planes (stretching) but only weak forces for $z$ displacements (bending),

* The author is grateful to the Knolls Atomic Power Laboratory for the opportunity to spend the summer of 1951 there, during which period most of this work was completed.

we shall start with the reasonable approximation[1] that at low temperatures where the lowest frequency modes are important the polarization vector $\mathbf{G}_\alpha$ is a unit vector either in the $z$ direction (bending) or in the $xy$ plane (stretching), and that the coupling between these two types of displacements can be neglected. We proceed to discuss the bending vibrations. The following spring constants are defined for $z$ displacements and coupling between the specified atoms:

$S_0/3$ = constant between $A$ and $B$ atoms (nearest neighbors in planes), (1.3a)

$S_1$ = constant between $A$ and $C$ atoms (nearest neighbors in adjacent planes), (1.3b)

$S_2/3$ = constant between $B$ and $C$ atoms (next nearest neighbors in adjacent planes). (1.3c)

It is reasonable to assume that $S_2<S_1\ll S_0$.

The frequencies $\omega$ are determined from the characteristic determinant

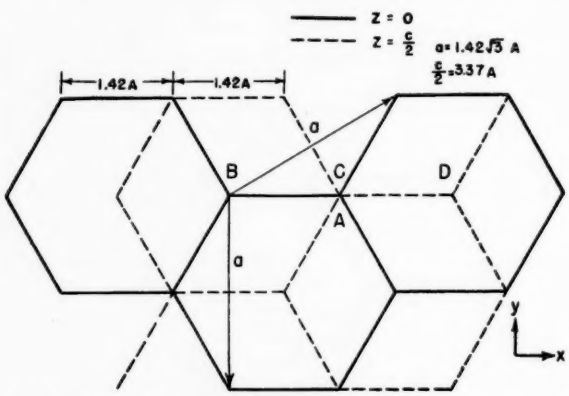


FIG. 1. The lattice structure of graphite. Solid lines indicate one plane, dotted lines indicate a neighboring plane.

$$|F_{ij}-m\omega^2\delta_{ij}|=0, \tag{1.4}$$

where $\delta_{ij}$ is the Kronecker delta and

$$\begin{aligned}&F_{11}=F_{33}=S_0+2S_1+2S_2,\\&F_{12}=F_{21}{}^*=F_{34}{}^*=F_{43}=-S_0\Gamma,\\&F_{22}=F_{44}=S_0+4S_2.\end{aligned} \tag{1.5}$$

$$F_{14}=F_{23}=F_{24}{}^*=F_{41}{}^*=F_{32}{}^*=F_{42}=-2S_2\Gamma^*\cos\sigma_z c/2$$

$$F_{13}=-2S_1\cos\sigma_z c/2$$

with

$$\Gamma=\frac{1}{3}\left[\exp\left(-i\sigma_x\frac{a}{\sqrt{3}}\right)+2\exp\left(i\sigma_x\frac{a}{2\sqrt{3}}\right)\cos\sigma_y\frac{a}{2}\right],$$

$$|\Gamma^2|=\frac{1}{9}\left(1+4\cos^2\frac{\sigma_y a}{2}+4\cos\frac{\sigma_y a}{2}\cos\frac{\sqrt{3}}{2}\sigma_x a\right). \tag{1.5a}$$

In general the solutions of (1.4) are periodic in a Brillouin zone ($BZ$) of $\boldsymbol{\sigma}$ space defined by planes normal to the vectors

$$\boldsymbol{\sigma}=\pm\pi\mathbf{b}_i,$$

where

$$\begin{aligned}&\mathbf{b}_1=2/a\sqrt{3},\quad 0,\quad 0,\\&\mathbf{b}_2=1/a\sqrt{3},\quad -1/a,\quad 0,\\&\mathbf{b}_3=1/a\sqrt{3},\quad 1/a,\quad 0,\\&\mathbf{b}_4=0,\quad 0,\quad 1/c.\end{aligned} \tag{1.6}$$

On the plane $\sigma_z=\pm\pi/c$ the roots of (1.4) are doubly degenerate for all $\sigma_x$ and $\sigma_y$; thus $\omega$ is a continuous function of $\sigma_z$ across this plane and it is appropriate to double the height of the $BZ$ in $\sigma$ space and bound it by $\sigma_z=\pm 2\pi/c$. This zone is shown in Fig. 2. For a general point in $\boldsymbol{\sigma}$ space, the solution of (1.4) requires the roots of a quartic equation in $\lambda=m\omega^2$. We have not obtained the solution of this equation for the general case. If we neglect next nearest neighbor interactions then the roots are found to be

$$\begin{aligned}m\omega^2=S_0+S_1\left(1\mp\cos\sigma_z\frac{c}{2}\right)\\-\left[S_1^2\left(1\mp\cos\sigma_z\frac{c}{2}\right)^2+S_0^2|\Gamma|^2\right]^{\frac{1}{2}}\\m\omega^2=S_0+S_1\left(1\mp\cos\sigma_z\frac{c}{2}\right)\\+\left[S_1^2\left(1\mp\cos\sigma_z\frac{c}{2}\right)^2+S_0^2|\Gamma|^2\right]^{\frac{1}{2}},\end{aligned} \tag{1.7}$$

where the equations refer to "acoustic" and "optical" modes, respectively. For the lowest-frequency acoustic modes, $\sigma_x$, $\sigma_y$ are small and

$$\omega^2\simeq\frac{S_0a^2}{12m}(\sigma_x^2+\sigma_y^2)+\frac{S_1}{m}\left(1-\cos\sigma_z\frac{c}{2}\right). \tag{1.8}$$

The surfaces of constant $\omega$ are surfaces of revolution about the $\sigma_z$ axis in $\sigma$ space. For small enough frequency they are prolate ellipsoids with major to minor axis ratio $[(2/3)(S_0/S_1)(a^2/c^2)]^{\frac{1}{2}}$. As frequency increases the constant frequency surfaces remain ellipsoidal near the center of the $BZ$, but they become crowded near the top and bottom of the $BZ$, so that they approach truncated ellipsoids. For frequencies less than

$$\omega_1=\left(\frac{2S_1}{m}\right)^{\frac{1}{2}}=2\pi\nu_1, \tag{1.9}$$

the surfaces are complete. For $\nu>\nu_1$ the surfaces are truncated by the planes $\sigma_z=\pm 2\pi/c$ as shown in Fig. 2. Thus, for $\nu>\nu_1$ the number of allowed modes in a frequency range $d\nu$ is less than the number going with the entire prolate ellipsoid. This occurs ($S_1\ll S_0$) for

[1] K. Lonsdale, Proc. Phys. Soc. (London) **54**, 314 (1942).

much lower frequencies than those for which the surface $\omega=$ const. approaches the sides of the zone, resulting in a calculated density of modes per unit frequency range $d\nu$ which varies approximately as $\nu^2$ (the normal Debye result for solids) for $\nu<\nu_1$, but as $\nu$ (the result for a two-dimensional system) when $\nu>\nu_1$.

The total number of modes $N(\nu)$ in a volume $\Omega$ of the crystal with frequency less than $\nu$ is given by

$$\Omega/(2\pi)^3\int_{-\sigma_m}^{\sigma_m}\sigma_{xy}^2 d\sigma_z=N(\nu), \tag{1.10}$$

where

$$\sigma_{xy}^2=\sigma_x^2+\sigma_y^2,$$
$$m\omega^2=S_1[1-\cos\sigma_z(c/2)], \quad \nu<\nu_1,$$
$$2\pi/c=\sigma_m, \quad \nu>\nu_1. \tag{1.10a}$$

The result is that

$$N(\nu)=\Omega\frac{24m\pi}{S_0a^2c}\left[\left(\nu^2-\frac{\nu_1^2}{2}\right)\frac{2}{\pi}\sin^{-1}\frac{\nu}{\nu_1}+\frac{\nu^2}{\pi}\left(\frac{\nu_1^2}{\nu^2}-1\right)^{\frac{1}{2}}\right], \quad \nu<\nu_1$$

$$N(\nu)=\Omega\frac{24m\pi}{S_0a^2c}\left[\nu^2-\frac{\nu_1^2}{2}\right], \quad \nu>\nu_1. \tag{1.11}$$

By differentiation the density of modes per unit frequency range $\rho(\nu)$ is

$$\rho(\nu)=\Omega\frac{48m\pi\nu_1}{S_0a^2c}\frac{2}{\pi}\frac{\nu}{\nu_1}\sin^{-1}\frac{\nu}{\nu_1}, \quad \nu<\nu_1$$

$$\rho(\nu)=\Omega\frac{48m\pi\nu_1}{S_0a^2c}\frac{\nu}{\nu_1}, \quad \nu>\nu_1. \tag{1.12}$$

For $\nu\ll\nu_1$ we can approximate (1.12)

$$\rho(\nu)=\Omega\frac{48m\pi\nu_1}{S_0a^2c}\frac{2}{\pi}\frac{\nu^2}{\nu_1^2}. \tag{1.12a}$$

The form of $\rho(\nu)$ *vs* $\nu$ is shown (solid curve) in Fig. 3. In using these results for specific heat formulas the exact expressions (1.12) are impractical. We have approximated $\rho(\nu)$ as follows:

$$\rho(\nu)=\Omega\frac{48m\pi\nu_1}{S_0a^2c}\frac{2}{\pi}\frac{\nu^2}{\nu_1^2}=\Omega b_1\nu^2, \quad \nu<\nu_0$$

$$\rho(\nu)=\Omega\frac{48m\pi\nu_1}{S_0a^2c}\frac{\nu}{\nu_1}=\Omega b_2\nu, \quad \nu>\nu_0. \tag{1.13}$$

Here $\nu_0$ is a frequency chosen so that $N_1=N(\nu_1)$ agrees with the exact (1.11) for $\nu=\nu_1$; this approximate form is shown also (dotted curve) in Fig. 3. Numerical calculation gives $\nu_0=0.9\nu_1$.

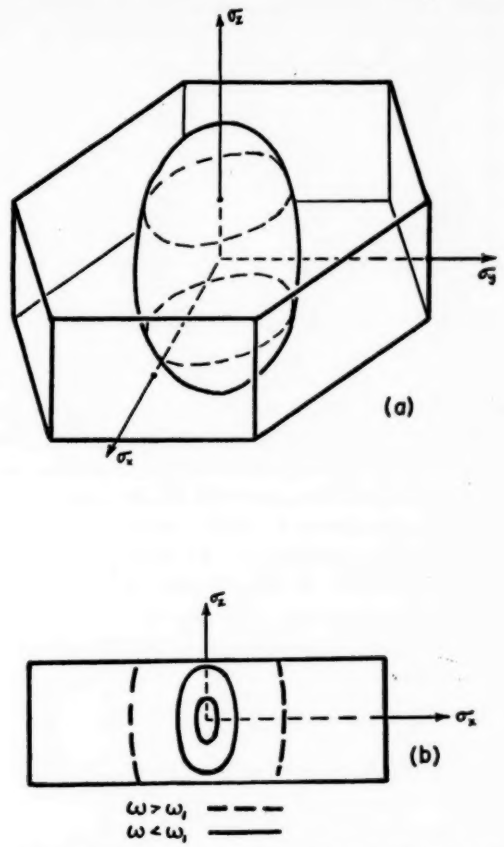


FIG. 2. The Brillouin zone for the graphite lattice. The ellipsoid in (a) is a surface of constant frequency; (b) shows in cross section how for $\omega>\omega_1$ these ellipsoids are truncated by the surfaces $\sigma_z=\pm 2\pi/c$.

The total volume in $\sigma$ space of the *BZ* in Fig. 2 is $32\pi^3/a^2c\sqrt{3}$. Taking both optical and acoustic modes doubles this. The number of modes per unit volume of $\sigma$ space is $\Omega/(2\pi)^3$. The total number of modes $N$ (optical plus acoustic) is then

$$N=\frac{\Omega}{(2\pi)^3}\frac{64\pi^3}{a^2c\sqrt{3}}=\frac{8}{a^2c\sqrt{3}}\Omega. \tag{1.14}$$

The volume of the unit cell is $(a^2c\sqrt{3}/2)$ and there are

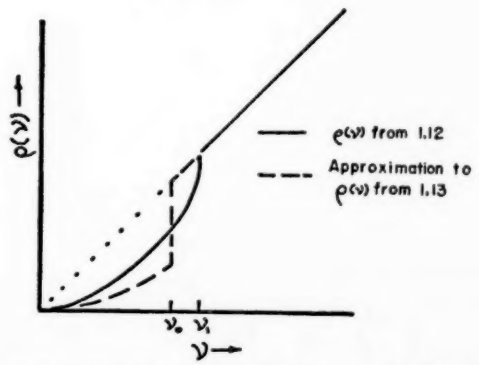


FIG. 3. The mode density for low frequencies showing the nature of approximation (1.13).

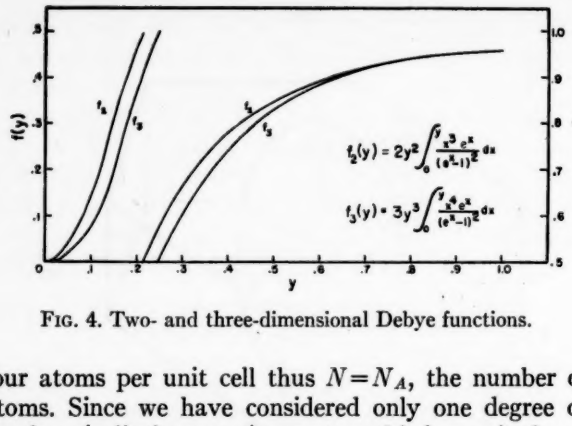


FIG. 4. Two- and three-dimensional Debye functions.

four atoms per unit cell thus $N=N_A$, the number of atoms. Since we have considered only one degree of freedom ($z$ displacement) per atom this is required.

The expressions (1.11), (1.13) are not exact for the higher-frequency modes, particularly the optical modes.[2] This is only significant at high temperatures, but the specific heat is not sensitive to the exact form of $\rho(\nu)$ at higher temperatures, so we will use the approximation (1.13) (two-dimensional Debye like) to replace an exact calculation up through the optical modes. For $\nu>\nu_1$ we have

$$N(\nu)=b_2(\nu^2/2-\nu_1^2/2)+N_1, \tag{1.15}$$

where from (1.11)

$$N_1=\Omega\frac{24m\pi}{S_0a^2c}\frac{\nu_1^2}{2}=\Omega b_2\frac{\nu_1^2}{4}. \tag{1.16}$$

It follows that we may choose an "upper" Debye frequency $\nu_m$ such that

$$N_A=b_2(\nu_m^2/2-\nu_1^2/2)+N_1. \tag{1.17}$$

From (1.16),

$$\frac{N_A+N_1}{2N_1}=\frac{\nu_m^2}{\nu_1^2}. \tag{1.18}$$

Certain relations between the quantities discussed in this section are useful and these are summarized now (the approximation (1.13) has been used):

$$\begin{aligned}
&\rho(\nu)=\Omega b_1\nu^2=\frac{8N_1}{\pi\nu_1^3}\nu^2; \quad \nu<\nu_0\\
&\rho(\nu)=\Omega b_2\nu=\frac{4N_1}{\nu_1^2}\nu=\frac{2(N_A+N_1)}{\nu_m^2}\nu; \quad \nu>\nu_0\\
&N_1=\frac{12m}{S_0a^2c}\nu_1^2;\\
&\nu_1^2=\frac{S_1}{2m\pi^2},
\end{aligned} \tag{1.19}$$

and $\nu_0$ is found from

$$\frac{8}{3\pi}\left(\frac{\nu_0}{\nu_1}\right)^3-2\left(\frac{\nu_0}{\nu_1}\right)^2+1=0; \quad \frac{\nu_0}{\nu_1}=0.90.$$

[2] J. P. Hobson and E. Nierenberg, Phys. Rev. 89, 662 (1953).

A physical description of these results is that the density of lattice vibrations per unit frequency range is like that of a three-dimensional system for frequencies less than $\nu_0$ but becomes that appropriate to a two-dimensional system for higher frequencies. The frequency $\nu_0$ is approximately that for which each plane is a rigid sheet but neighboring planes vibrate in the $z$ direction in opposite sense.

## II. THE SPECIFIC HEAT

The specific heat at constant volume of a system of oscillators is

$$c_v=k\int_0^{x_m}\frac{x^2e^x}{(e^x-1)^2}\rho(\nu)d\nu, \tag{2.1}$$

where $k$ is Boltzmann's constant $x=h\nu/kT$, and $\rho(\nu)$ is the number of oscillators in the frequency range $d\nu$. Using the results of the preceding section as summarized in (1.19) this becomes (for the bending modes only),

$$\begin{aligned}
c_v=k\Bigg[&\frac{8N_1}{\pi x_1^3}\int_0^{x_0}\frac{x^4e^xdx}{(e^x-1)^2}+\frac{2}{x_m^2}(N_A+N_1)\\
&\times\int_{x_0}^{x_m}\frac{x^3e^xdx}{(e^x-1)^2}\Bigg]
\end{aligned}$$

$$x_0=\frac{h\nu_0}{kT}, \quad x_1=\frac{h\nu_1}{kT}, \quad x_m=\frac{h\nu_m}{kT} \tag{2.2}$$

and corresponding characteristic temperatures $\theta_0, \theta_1, \theta_m$.

To discuss the variation of $c_v$ with temperature we divide the temperature range into three parts.

(a) The very low-temperature range $T<\theta_0$ for which asymptotic expansion of (2.2) yields

$$c_v=N_1k\frac{8}{3\pi}\frac{12\pi^4}{15}\left(\frac{T}{\theta_1}\right)^3, \tag{2.3}$$

the usual Debye result but with only approximately $N_1$ atoms rather than all $N_A$ being effective.

(b) The very high-temperature range $T>\theta_m\gg\theta_0$ for which it is readily found that

$$c_v=N_Ak, \tag{2.4}$$

which is the expected high-temperature specific heat of $N_A$ atoms with one degree of freedom.

(c) The intermediate region defined by

$$\begin{aligned}
&x_0\ll1\ll x_m\\
&\theta_0\ll T\ll\theta_m.
\end{aligned}$$

Using (1.19), we find

$$\begin{aligned}
c_v=k\Bigg[&\frac{8}{3\pi}N_1\frac{\nu_0^3}{\nu_1^3}+14.4(N_A+N_1)\left(\frac{T}{\theta_m}\right)^2\\
&-(N_A+N_1)\frac{\nu_0^2}{\nu_m^2}\Bigg],
\end{aligned} \tag{2.5}$$

using

$$\int_0^\infty \frac{x^3e^x}{(e^x-1)^2}dx=7.212. \tag{2.6}$$

The first term of (2.5) is the contribution of the saturated very low-temperature modes; the second term would be the low-temperature specific heat for a two-dimensional system (i.e., the individual planes), and the third term corrects the second because the system is not like a two-dimensional one below $\theta_0$.

Further reduction of (2.5) yields

$$c_v=\left[14.4(N_A+N_1)\left(\frac{T}{\theta_m}\right)^2-N_1\right]k. \tag{2.7}$$

Using (1.18), $N_1\simeq\frac{1}{2}\nu_1^2/\nu_m^2N_A$; in the next section we estimate $\nu_1/\nu_m\simeq0.1$ corresponding to $N_1$ being only 0.5 percent of the total number of atoms $N_A$.

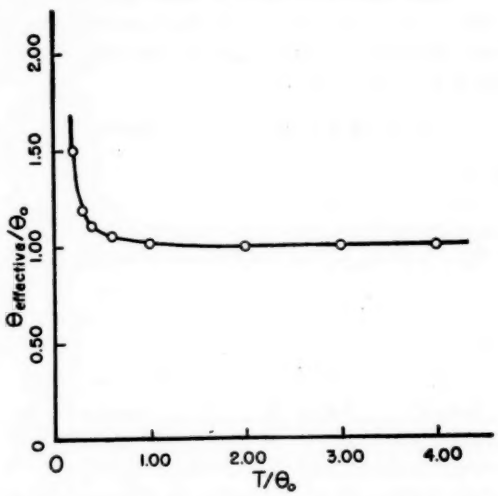


FIG. 5. Apparent Debye temperature (theoretical) if a purely two-dimensional model Eq. (2.10a) is used instead of the three-dimensional Eq. (2.10).

(d) For general values of $T$ and for $T\lesssim\theta_0$ no closed form is available. The two-dimensional "Debye" integral

$$f_2(y)=\frac{2}{y^2}\int_0^y \frac{x^3e^x}{(e^x-1)^2}dx \tag{2.8}$$

has therefore been computed graphically and is compared in Fig. 4 with the standard integral in specific heat theory, i.e.,

$$f_3(y)=\frac{3}{y^3}\int_0^y \frac{x^4e^x}{(e^x-1)^2}dx. \tag{2.9}$$

Approximation (a) predicts a $T^3$ dependence of $c_v$ at very low temperatures, while (c) predicts that in an intermediate range one should observe a $T^2$ dependence. One naturally asks whether there is a well-defined transition from the $T^3$ to $T^2$ variation. This would occur for $T\simeq\theta_0$. Assuming $\theta_0\ll\theta_m$ the expression (2.2) can be rewritten as approximately

$$c_v=N_1k\left[\left(\frac{2\nu_0^2}{\nu_1^2}-1\right)f_3\left(\frac{\theta_0}{T}\right)-2\left(\frac{\nu_0^2}{\nu_1^2}\right)f_2\left(\frac{\theta_0}{T}\right)+28.8\left(\frac{T^2}{\theta_1^2}\right)\right] \tag{2.10}$$

for $T\leq\theta_0$. When (2.10) is evaluated it is found that the approximation

$$c_v=14.4N_Ak(T/\theta_m)^2 \tag{2.10a}$$

is reasonably good down to $T\simeq0.3\theta_0$. A more quantitative way of describing this behavior is to calculate the apparent Debye temperature which would be used in (2.10a) in order to give the value of $c_v$ found from (2.10). This is shown in Fig. 5.

## III. COMPARISON WITH EXPERIMENT

Measurements of the specific heat of graphite in the temperature range 15–1000°K are available.[3] The observed $c_p$ can be corrected to give $c_v$ but at low temperatures, the difference $(c_p-c_v)$ can be neglected. The experimental value of $c_v$ at 1000°K is about $2.5N_Ak$. Using $z$ displacement modes only the maximum possible value is $N_Ak$. It is clear, then, that we must introduce $x$, $y$ displacements as well. We have assumed that these can be treated in similar fashion to the $z$ modes, but with different characteristic temperatures. In order to fit experimental data we then write

$$c_v=c_v(T;\theta_{0z},\theta_{mz})+2c_v(T;\theta_{0xy},\theta_{mxy}) \tag{3.1}$$

and approximate by

$$c_v=N_Ak\left[f_2\left(\frac{\theta mz}{T}\right)+2f_2\left(\frac{\theta mxy}{T}\right)\right].$$

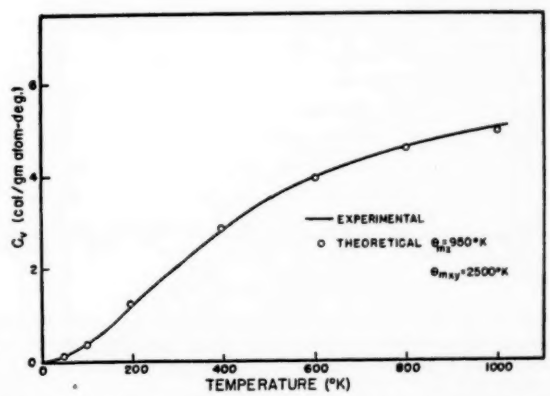


FIG. 6. Experimental and theoretical specific heat of graphite. Details of the fit of theory to experiment at very low temperatures are also given in Fig. 7.

[3] W. DeSorbo and W. W. Tyler, Phys. Rev. 83, 878 (1951), J. Chem. Phys. 21, 1660 (1953).

The best fit of the data over the range 20–1000°K is found using $\theta_{mz}=950°$, $\theta_{mxy}=2500°$. The comparison with experiment is given in Fig. 6 and Table I the experimental data being a combination of that in reference[1] and those listed in Table I.[4]

A very sensitive description of the applicability of the theory can be obtained by using the experimental data to calculate $\theta_{mz}$. Taking $c_{vxy}=2f_2(\theta_{mxy}/T)$ and $\theta_{mxy}=2500°$ (to fit the high-temperature data) we can subtract from $c_{v\,\mathrm{exp}}$ the contribution of the $xy$ modes. The remainder is assigned to the $z$ modes, and assuming these contribute $N_A k f_2(\theta_{mz}/T)$ we may calculate $\theta_{mz}$ *versus* temperature. The result is presented in Fig. 7.

It will be noted that the apparent Debye temperature $\theta_{mz}$ shows a minimum at about 40° but is rising rapidly at the lowest temperatures for which data is available. The latter would be consistent with our theory [see discussion of (2.10), (2.10a) and Fig. 5], but the minimum of $\theta_{mz}$ at 40° followed by the gradual rise toward higher temperatures is indicative of a peak in the mode density of the type found in more rigorous treatments of the lattice vibration spectrum.[5] A purely two-dimensional calculation (for the $z$ displacement modes only) used by Hobson and Nierenberg[2] shows that such peaks are present; these must almost certainly be present in a three-dimensional treatment, not only for the $z$ modes, but for the $xy$ modes as well. Unquestionably such considerations must be added to our discussion before the theory is complete in detail.

On the other hand, to explain the lack of a pronounced low-temperature increase in $\theta_{mz}$ until $T$ becomes as low as 15°K, we must postulate that $\theta_{mz}\leq$approximately 60°. We thought we might justify this by calculating $\theta_{0z}$ from data on compressibility of graphite,[6] on which both theoretical and experimental information is available. Because of the high stiffness in the planes it is justifiable to assign volume change to $c$ axis change. This allows an estimate of the spring constant $S_1$ which enters into $\theta_{0z}$, (1.9) and (1.19). The various compressibility data give $\theta_{0z}$ ranging from 85° to 150°, the latter being that derived from the experimental compressibility. Objections can be raised to the use of experimental data taken on polycrystalline samples at high pressures to give very quantitative estimates of $S_1$, so that the lower value of $\theta_{0z}$ obtained from the highest theoretical estimate of compressibility might in fact be closer to the truth. We feel, however, that we cannot press the point on the basis of the data available but must rather be content with getting the right order of magnitude. Results of $c_v$ measurements down to liquid helium temperatures are needed to decide whether a $T^3$ dependence is finally reached. At very low temperatures a linear term due to electronic heat might obscure this; over the temperature range discussed here an estimate based on the Wallace theory[7] showed this to be negligible.

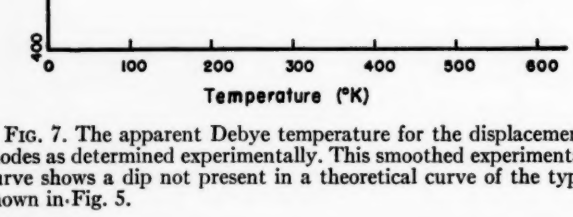


FIG. 7. The apparent Debye temperature for the displacement modes as determined experimentally. This smoothed experimental curve shows a dip not present in a theoretical curve of the type shown in Fig. 5.

## IV. SUMMARY AND DISCUSSION

The treatment of the lattice vibrations given in Sec. I shows that because of the elastic anisotropy of graphite the contours of constant frequency are "cigars" in the wave vector $\sigma$ space. The surfaces are entirely within the $BZ$ for very low frequencies. For higher frequencies they are truncated by the top and bottom of the $BZ$. For very low frequencies the mode density varies with $\nu^2$ as in the normal Debye theory, but for larger $\nu$ the mode density is linear in $\nu$. The theoretical specific heat varies (Sec. II) as $T^3$ and $T^2$, respectively (for low temperatures), the latter being applicable in the range 15°–50°K. We have fitted the experimental data by assuming that a similar analysis applies to $z$ and $xy$ displacements; approximately 80 percent of $c_v$ comes from the former at low temperatures. The Debye temperatures are $\theta_{mz}\simeq 950°$, $\theta_{mxy}\simeq 2500°$. For sufficiently low temperatures ($<10$°K?) we expect a $T^3$ dependence of $c_v$ unless the temperature is so low that the linear electronic specific heat becomes important.

During the preparation of the present manuscript the paper by Komatsu and Nagamiya[8] came to our attention. They treat the $xy$ displacements from a continuum approach and the Debye temperature 2440° which they assign to these degrees of freedom compares reasonably with our $\theta_{mxy}=2500°$. The value of $c_v$ in the low-temperature range is not very sensitive to this choice. On the other hand their treatment of the $z$ displacements assumes an array of thin elastic plates (the layer planes) coupled to each other. The individual planes are treated

[4] A. Magnus, Ann. Physik **70**, 303 (1923). W. Nernst, Ann. Physik **36**, 395 (1911). C. J. Jacobs and G. S. Parks, J. Am. Chem. Soc. **56**, 1913 (1934).

[5] E. Katz, J. Chem. Phys. **19**, 488 (1951), particularly reference 1 of his paper to work by M. Blackman, E. W. Montroll, W. V. Houston, and R. B. Leighton.

[6] P. W. Bridgman, Proc. Am. Acad. Arts Sci. **76**, 9 (1945). J. Basset, Compt. rend. **213**, 829 (1941). R. O. Brennan, J. Chem. Phys. **20**, 40 (1952).

[7] P. R. Wallace, Phys. Rev. **71**, 622 (1947).

[8] K. Komatsu and T. Nagamiya, J. Phys. Soc. Japan **6**, 438 (1951).

by continuum elasticity theory and coupling between planes as for a one-dimensional system. With these assumptions they arrive at the frequency relation

$$\omega^2 = A(\sigma_x^2+\sigma_y^2)^2 + B\left(1-\cos\sigma_z\frac{c}{2}\right) \qquad (4.1)$$

to be compared with our (1.8). The resulting density of modes $\rho(\nu)$ is quite different, varying with $\nu$ for low frequencies and being constant at high frequencies. This frequency expression is a direct result of approximating the bending of the layer planes by the flexural bending equation of an elastic plate, i.e.,

$$m(\partial^2\delta/\partial t^2) = -D\nabla_{xy}{}^4\delta, \qquad (4.2)$$

where $D$ is flexural rigidity, $\delta$ is $z$ displacement.

The usual derivation of this equation specifically assumes a layer of finite thickness and neglects pure shear modes (which is equivalent to neglecting the transverse stiffness $S_0$ of the trigonal carbon bonds). This model leads to the following physical inconsistencies:

(a) The strain energy is a quadratic function of the strain components if we regard graphite as a homogeneous anisotropic elastic solid. It follows that for long wavelengths $\omega^2$ must be a quadratic function of $\sigma_x$, $\sigma_y$, $\sigma_z$ in agreement with (1.8) but not (4.1).

(b) For small $\sigma$ the phase velocity of waves along the planes vanishes if one uses (4.1); this result is physically absurd.

(c) Their treatment can only apply to a crystalline plate of many atomic plane thickness, in which case the specific heat should be sensitive to this thickness.

For these reasons we do not believe their model to be a suitable idealization of the physical situation.

We would also like to comment on the approach used by R. W. Gurney.[9] Certain criticisms of his treatment were brought to the authors' attention by W. W. Tyler and W. DeSorbo at the time the present work was initiated. We summarize these:

(a) Gurney finally includes only "transverse" waves along the layer planes so the problem is equivalent to a two-dimensional lattice with one degree of freedom per atom. It follows that the total number of modes associated with displacements normal to the plane must be equal to the total number of atoms in the plane.

[9] R. W. Gurney, Phys. Rev. 88, 465 (1952).

TABLE I.

| $T°$ Kelvin | $c_v$ theoretical cal/g atom deg | $c_v$ experimental cal/g atom deg |
|---|---|---|
| 25 | 0.0226 | 0.295 |
| 50 | 0.102 | 0.121 |
| 100 | 0.40 | 0.40 |
| 200 | 1.28 | 1.19 |
| 300 | 2.16 | 2.05 |
| 400 | 2.90 | 2.84 |
| 600 | 4.00 | 3.96 |
| 800 | 4.62 | 4.66 |
| 1000 | 5.02 | 5.04 |

Despite the fact that he considers only one plane of atoms, the assumption of (1) of his paper automatically implies three degrees of freedom per atom, thus his (2) should be equated to $3N$ rather than $2N$. Dividing by three to include only the waves with displacements transverse to the planes yields instead of his (4), $c_v = 14.4RT^2/\theta^2$ which is to be compared to (2.7) of our paper. At high temperatures the vibrations transverse to the planes contribute only $c_v = 2/3(Nk)$, if his expression (4) is used; clearly this should be $Nk$.

(b) A further objection is a quantitative one. Using the spring constant $S_1$ which we have calculated in III we may estimate the temperature at which $kT = h\nu$ for the lowest mode of oscillation for "longitudinal waves" perpendicular to the planes (Gurney's $b$ waves). For crystals 15 layers thick, this frequency would correspond to a temperature $\theta_{0z}/15$ (approximately) which from (3.5) would correspond to $T \simeq 10°K$. Above this temperature the "size effect" would not be a significant factor. The temperature range for which he calculates $c_v$ is well above 10°K, so that there should be no difficulty in exciting the modes of his type (b). Thus his neglect of these modes is not justified. Actually the estimate of 15 layers thick is low by an order of magnitude for the samples used by DeSorbo and Tyler,[1] which are nearly 100 layers in thickness; for these the upper limit of applicability of Gurney's theory should be closer to a few degrees absolute. We know of no experimental work in which a pronounced particle thickness effect has been observed in the low-temperature range.

In concluding, the authors' would like to express their appreciation to many members of the staff of the Knolls Atomic Power Laboratory and the General Electric Research Laboratory, particularly to Dr. J. P. Howe, Dr. W. DeSorbo, and Dr. W. W. Tyler, for their continued interest in this work.

# Energy Exchange in Molecular Collisions

BENJAMIN WIDOM* AND S. H. BAUER
*Department of Chemistry, Cornell University, Ithaca, New York*
(Received January 6, 1953)

A theory was developed for computing the probability of transition, upon molecular collision, between vibrational states, involving corresponding conversion of translational energy. A spherically symmetric Lennard-Jones 6–12 potential for interaction between the colliding molecules was introduced; their relative translational motion was described classically. Further, the theory was symmetrized to permit inclusion of collisions with nonzero impact parameters. As an example, the theory was applied to the $CO_2-H_2O$ system. The effective collision diameter for an inelastic event was found to be of the observed order of magnitude, demonstrating not only the selective relaxation effect of water, but also its somewhat unusual temperature dependence.

Zener's solution of the problem for a head-on collision was generalized to three-dimensional collisions, assuming a spherically symmetric interaction potential; but the complete solution of this model, including a quantum-mechanical description of the relative translational motion, was not obtained. However, for such a potential it was possible to demonstrate that the semiclassical theory is an adequate approximation to the quantum theory result, whenever the relative translational energies are much greater than the energy of exchange.

## I. INTRODUCTION

IT has been found from measurements of the absorption and dispersion of ultrasonic waves in gases[1] that it is not uncommon for several tens of thousands of collisions to be required for the de-excitation of certain vibrational modes from their first excited states to their ground states. This de-excitation probability depends not only on the nature of the excited mode (its frequency and amplitude of vibration, etc.[2]) but also quite strongly on the chemical nature of *both* molecules which are involved in the collision. For example, if the interaction between the excited molecule $A$ and another molecule $B$ is of a nature similar to that which leads to chemical reactions, then $A$–$B$ collisions will be much more effective in de-exciting $A$ than will $A$–$C$ collisions, where $C$ is some species (perhaps another $A$) "chemically inert" to $A$. In addition to the consequent relatively large inelastic collision cross sections, "chemical reactivity" also gives rise to a temperature-dependence of these cross sections which is entirely different from that found in the case of collisions between nonreactive components.[3]

One of the most interesting examples of the effect of reactivity is found in the case of de-excitation of the bending mode of $CO_2$ by collisions with $H_2O$. At room temperature, about 100 such collisions suffice to produce the transition from the first excited state to the ground state. When, however, $H_2O$ is replaced by another $CO_2$ molecule, about 50 000 collisions are required. Furthermore, whereas this collision number decreases steadily with increasing temperature in the case of $CO_2-CO_2$ collisions, it shows a minimum at about 350° in the case of $CO_2-H_2O$ collisions. Pielemeier[4] *et al.*, have suggested that this might be due to the increasing importance of the symmetrical and unsymmetrical valence vibrations of $CO_2$ at the higher temperatures, i.e., they consider it possible that at the higher temperatures, the measured vibrational relaxation time contains unresolved effects of other modes besides that of bending.

In Secs. II, III, and IV the general theory of vibrational relaxation will be discussed, and in the light of the principles developed there, the $CO_2-H_2O$ system will be treated in the fifth section. The question of the temperature dependence of the de-excitation probability will receive particular attention, and it will be shown that the existence of a minimum in the collision number is entirely to be expected, and is a consequence of the mutual reactivity of $CO_2$ and $H_2O$. If, then, the experimental effect is a real one, i.e., if Pielemeier's objection does not invalidate the original interpretation of the data, the analysis presented in Sec. V constitutes a likely explanation of the phenomenon. In any case, it shows that "anomalous" behavior with temperature is to be expected whenever the interaction potential of the colliding molecules has an appreciable minimum at roughly a valence bond separation.

## II. QUANTUM-MECHANICAL AND SEMICLASSICAL THEORIES

Using the method of distorted waves,[5] Zener[6] derived the following formula† for the probability of the interchange of translational and internal energy during

* Present address: Department of Chemistry, University of North Carolina.

[1] This method is discussed in a recent paper by R. A. Walker, J. Chem. Phys. **19**, 494 (1951).

[2] H. A. Bethe and E. Teller, "Deviations from thermal equilibrium in shock waves," Ballistic Research Labs. Report X-117, 1941, p. 28.

[3] A. Eucken and L. Küchler, Physik. Z. **39**, 831 (1938).

[4] Pielemeier, Saxton, and Telfair, J. Chem. Phys. **8**, 106 (1940); W. H. Pielemeier and W. H. Byers, J. Acoust. Soc. Am. **15**, 17 (1943).

[5] N. F. Mott and H. S. W. Massey, *The Theory of Atomic Collisions* (Oxford University Press, London, 1949), 2nd ed., p. 144.

[6] C. Zener, Phys. Rev. **37**, 556 (1931).

† Except for a factor of 4, which Zener missed due to an oversight. This error was discovered and corrected by J. M. Jackson and N. F. Mott, Proc. Roy. Soc. (London) **A137**, 703 (1932).

a head-on collision:

$$p_{0\nu}(\epsilon_0)=1(\epsilon_\nu)(8\mu/\hbar^2)(\epsilon_\nu\epsilon_0)^{-\frac{1}{2}} \times\left|\int_0^\infty \mathfrak{R}^*(\epsilon_\nu, R)V_{\nu 0}(R)\mathfrak{R}(\epsilon_0, R)dR\right|^2. \quad (1)$$

$\epsilon_\nu$ and $\epsilon_0$ are the final and initial relative translational energies, respectively; $\mu$ is the reduced mass of the colliding molecules. If $\xi$ is symbolic for the totality of internal (vibration-rotation) coordinates of both molecules, and $R$ is the separation of the two molecular centers of mass, then $V_{\nu 0}(R)$ is the matrix element of the interaction potential, $V(\xi, R)$, taken between the system's 0th and $\nu$th internal states. $1(\epsilon_\nu)$ is the unit step function; zero for $\epsilon_\nu<0$ and unity for $\epsilon_\nu>0$. $\mathfrak{R}(\epsilon_n, R)$ is that solution of

$$d^2\mathfrak{R}/dR^2+(2\mu/\hbar^2)[\epsilon_n-V_{nn}(R)]\mathfrak{R}=0 \quad (2)$$

which satisfies

$$\lim_{R\to 0}\frac{\mathfrak{R}}{R} \quad \text{exists} \quad (3)$$

and

$$\mathfrak{R}\sim\sin[(2\mu\epsilon_n)^{\frac{1}{2}}R/\hbar+\delta_{\epsilon_n}] \quad (\text{large } R) \quad (4)$$

where $\delta_{\epsilon_n}$ is a real number (phase shift). $p_{0\nu}(\epsilon_0)$ is then the probability that in a head-on collision characterized by an initial relative translational energy $\epsilon_0$, the internal state of the system will change from the 0th to the $\nu$th. If $E_0$, $E_\nu$ are the corresponding energy levels, then

$$\epsilon_0+E_0=\epsilon_\nu+E_\nu. \quad (5)$$

If it is desired to generalize (1) to three-dimensional collisions, the quantity $V_{nn}$, which appears in (2), will depend on $\mathbf{R}$, the vector separation of the two centers of mass. Solving (2) with any degree of exactness would then be virtually impossible, unless $V_{nn}(\mathbf{R})$ were replaced by some sort of average potential, $w(R)$, which depended on the magnitude, but not on the direction, of $\mathbf{R}$. A function $w(R)$, which can be expected to possess the most important qualitative and quantitative features of $V_{nn}(\mathbf{R})$, can be obtained by averaging $V_{nn}(\mathbf{R})$ over all states degenerate with the $n$th. That the resulting function is spherically symmetric is proved in the appendix.

In addition to assuming the spherical symmetry of these potentials, in any practical application we shall make no distinction between two $V_{nn}$'s that belong to different states. The relative translational motion will be taken as determined by a single potential $w(R)$, the same for any internal state with which it happens to be associated.

With these modifications, the extension of (1) to three-dimensional collisions is

$$p_{0\nu}(\epsilon_0, l_0)=1(\epsilon_\nu)\{8\mu/[\hbar^2(\epsilon_\nu\epsilon_0)^{\frac{1}{2}}(2l_0+1)]\} \times\sum_{m_0=-l_0}^{l_0}\sum_{l_\nu=0}^{\infty}\sum_{m_\nu=-l_\nu}^{l_\nu}|\mathcal{V}^{\nu 0}{}_{l_\nu m_\nu, l_0 m_0}|^2 \quad (6)$$

where

$$\mathcal{V}^{\nu 0}{}_{l_\nu m_\nu, l_0 m_0}=\int_0^\infty\int_0^\pi\int_0^{2\pi} \times Y^*{}_{l_\nu m_\nu}(\theta, \varphi)\mathfrak{R}^*{}_{l_\nu}(\epsilon_\nu, R)V_{\nu 0}(R, \theta, \varphi) \times Y_{l_0 m_0}(\theta, \varphi)\mathfrak{R}_{l_0}(\epsilon_0, R)\sin\theta d\varphi d\theta dR. \quad (7)$$

$p_{0\nu}(\epsilon_0, l_0)$ is the probability that the transition $0\to\nu(\neq 0)$ will take place in a collision characterized by initial relative energy $\epsilon_0$ and initial relative angular momentum of magnitude $[l_0(l_0+1)]^{\frac{1}{2}}\hbar$; $R$, $\theta$, $\varphi$ are the spherical coordinates of $\mathbf{R}$; $V_{\nu 0}$ is the matrix element of the interaction potential $V(\xi, \mathbf{R})$; $Y_{l_n m_n}$ is the spherical harmonic normalized so that

$$\int_0^\pi\int_0^{2\pi} Y^*{}_{l_n m_n}(\theta, \varphi)Y_{l_n m_n}(\theta, \varphi)\sin\theta d\varphi d\theta=1. \quad (8)$$

$\mathfrak{R}_{l_n}(\epsilon_n, R)$ is that solution of

$$d^2\mathfrak{R}/dR^2+(2\mu/\hbar^2)[\epsilon_n-w(R) -\hbar^2 l_n(l_n+1)/2\mu R^2]\mathfrak{R}=0 \quad (9)$$

which satisfies (3) and (4), except that in (4), $\delta$ may depend on $l_n$ as well as on $\epsilon_n$.

From (6) and (7),

$$\sum_{l_\nu}(2l_\nu+1)p_{\nu 0}(\epsilon_\nu, l_\nu)=\sum_{l_0}(2l_0+1)p_{0\nu}(\epsilon_0, l_0) \quad (10)$$

because $V_{0\nu}=V_{\nu 0}{}^*$. The probability, $\prod$, associated with the production of a single final relative angular momentum state ($l_\nu$, say) is given by an expression such as (6), but without the summation over $l_\nu$. This probability satisfies

$$(2l_\nu+1)\prod_{l_\nu, l_0}^{\nu, 0}(\epsilon_\nu)=(2l_0+1)\prod_{l_0, l_\nu}^{0, \nu}(\epsilon_0). \quad (11)$$

In (10) and (11) it is assumed that $\epsilon_\nu$, the translational energy associated with the internal state $\nu$, and $\epsilon_0$, the translational energy associated with the internal state 0, are both positive and are related by (5). Equations (10) and (11) are statements of the principle of detailed balance, given here for the probabilities per collision of a process and its inverse. Analogous equations relate the cross sections of a process and its inverse.[7]

A large number of the difficulties which are encountered in the quantum-mechanical problem are eliminated if one is willing to consider a purely classical description of the relative translational motion of the colliding molecules. This led Zener[8] to propose a semiclassical theory of inelastic molecular collision processes, the essential result of which was obtained independently a number of years later by Landau and Teller.[9] The

[7] H. A. Bethe, *Elementary Nuclear Theory* (John Wiley and Sons, Inc., New York, 1947), p. 61.

[8] C. Zener, Phys. Rev. **38**, 277 (1931).

[9] L. Landau and E. Teller, Physik. Z. Sowjetunion **10**, 34 (1936).

vector $\mathbf{R}$, which gives the separation of the centers of mass of the two particles, is taken to be an explicit function of the time, $\mathbf{R}(t)$, as given by classical dynamics. The interaction potential $V(\xi, \mathbf{R})$ is then a known function of the time, and its effect on the internal states of the system can be found immediately by a straightforward application of the first-order time-dependent perturbation theory:

$$p_{0,\nu\neq 0}(E, b)=(1/\hbar^2)\left|\int_{-\infty}^{\infty} V_{\nu 0}[\mathbf{R}(t)]\exp(i\omega_s t)dt\right|^2. \quad (12)$$

This is the probability per collision of producing the transition $0\rightarrow\nu$ in collisions characterized by initial relative translational energy $E$ and impact parameter $b$; $\omega_s$ is given by

$$\hbar\omega_s=E_\nu-E_0. \quad (13)$$

In deriving results of the time-dependent perturbation theory one requires that in the zeroth order of approximation, the state of the system remain unchanged in time. This can introduce a lack of symmetry in the way the initial and final states of the system enter the final expressions for the transition probability. Lack of symmetry between initial and final states is more often an accidental defect of a theory, than an essential physical property of the system. The considerations that lead to (12) would seem to demand that for all $t$, $\mathbf{R}(t)$ should correspond to motion in a potential $V_{00}(\mathbf{R})$, with translational energy $E$ and impact parameter $b$. Since this lack of symmetry appears to be artificial rather than essential, Zener[8] proposed that the theory be symmetrized‡ by specifying that $\mathbf{R}(t)$ be calculated as though, for all $t$, the potential were

$$\tfrac{1}{2}[V_{00}(\mathbf{R})+V_{\nu\nu}(\mathbf{R})]$$

and the total translational energy were

$$\tfrac{1}{2}[E+(E-\hbar\omega_s)].$$

Zener made no mention of using a symmetrized impact parameter, but this should also be done; it is especially simple if the symmetrized potential, $w$, and the matrix element $V_{\nu 0}$, are spherically symmetric, i.e., functions of $R$ alone. For then the collision conserves the relative angular momentum of the colliding particles, and, if $E$, $b$ are the initial energy and impact parameter, and $E'$, $b'$ are the final ones,

$$E'=E-\hbar\omega_s$$
$$E'b'^2=Eb^2.$$

Thus, the symmetrized impact parameter can be taken to be

$$\tfrac{1}{2}b\{1+[E/(E-\hbar\omega_s)]^{\frac{1}{2}}\}.$$

‡ After collision, the molecules recede. If, at some time during this recession, the velocities of both molecules were reversed in direction, they would collide again, the collision being, in some sense, the inverse of the original one. $E'$ and $b'$ are the energy and impact parameter of this inverse collision.

In all the work which follows it will, in fact, be assumed that $w$ and $V_{\nu 0}$ are spherically symmetric. Now define the origin of time, $t=0$, to be the time at which the molecules reach $\bar{R}$, the distance of closest approach:

$$R(0)=\bar{R}. \quad (14)$$

Then $R(t)$ and $V_{\nu 0}[R(t)]$ are symmetric functions of $t$, and (12) can be written

$$p_{0,\nu\neq 0}(E, b)=(1/\hbar^2)\left|\int_{-\infty}^{\infty} V_{\nu 0}[R(t)]\exp(i\omega t)dt\right|^2, \quad (15)$$

where

$$\hbar\omega=|E_\nu-E_0|. \quad (16)$$

$R(t)$ in (15) is the classical trajectory corresponding to motion in the potential $w(R)$ with total translational energy given by the symmetrized energy $\epsilon_0$, and impact parameter equal to the symmetrized impact parameter $b_0$. From the preceding discussion of symmetrization, the initial energy $E$ and initial impact parameter $b$ are related to $\epsilon_0$ and $b_0$ by

$$E=\epsilon_0\pm\tfrac{1}{2}\hbar\omega \quad (17)$$

$$2b_0/b=1+[(\epsilon_0\pm\tfrac{1}{2}\hbar\omega)/(\epsilon_0\mp\tfrac{1}{2}\hbar\omega)]^{\frac{1}{4}}, \quad (18)$$

where the top sign is used for excitation ($E_\nu>E_0$) and the bottom sign for de-excitation ($E_\nu<E_0$).

Rosen and Zener,[10] and later Landau and Teller,[9] have asserted that the semiclassical theory is expected to be an adequate approximation to the quantum-mechanical theory whenever the relative translational energies which are involved are much greater than the energy exchange, $\hbar\omega$. It will be shown here explicitly, for the case of spherically symmetric potentials, that when the translational energies are very large the two theories do, in fact, become identical.

The effective radial potential [$w(R)$+centrifugal potential] must be such that its slope becomes infinite as $R\rightarrow 0$. Now consider the function

$$\mathfrak{R}(E, R)=\begin{cases}0, & R<\bar{R}\\ \sin[(1/\hbar)(2\mu E)^{\frac{1}{2}}(R-\bar{R})], & R>\bar{R}\end{cases} \quad (19)$$

where $\bar{R}$ is the classical turning point of the radial motion, and $E$ is the initial translational energy. For sufficiently large $E$, this function will be a good approximation to the solution of (9), except in the immediate neighborhood of $\bar{R}$; and this region where it is not a close approximation will be, for sufficiently large $E$, negligibly small compared to the total range of effective interaction, i.e., compared to the total interval over which $V_{\nu 0}(R)$ is considerable. Similarly, for all $R$ except for an insignificantly small interval,

$$\mathfrak{R}(E-\hbar\omega, R)=\begin{cases}0, & R<\bar{R}\\ \sin[(1/\hbar)(2\mu)^{\frac{1}{2}}(E-\hbar\omega)^{\frac{1}{2}}(R-\bar{R})], & R>\bar{R}\end{cases} \quad (20)$$

[10] N. Rosen and C. Zener, Phys. Rev. **40**, 502 (1932).

and, since $E \gg \hbar\omega$, it is the same $\bar{R}$ which appears in both (19) and (20). The spherical symmetry of $V_{\nu 0}$ implies, from (7), that only transitions with $l_\nu = l_0$ and $m_\nu = m_0$ can occur, and therefore the wave functions of (19) and (20) both refer to the same value of $l$. From (7),

$$\mathcal{U}^{\nu 0} = \int_{\bar{R}}^{\infty} \sin[k_0(R-\bar{R})] \sin[k(R-\bar{R})] V_{\nu 0}(R) dR \quad (21)$$

where $k_0 = (2\mu E)^{\frac{1}{2}}/\hbar$ and $k = (2\mu)^{\frac{1}{2}}(E-\hbar\omega)^{\frac{1}{2}}/\hbar$. This integral can be written as the sum of two integrals by making use of the identity

$$\sin[k_0(R-\bar{R})] \sin[k(R-\bar{R})] = \tfrac{1}{2}\{\cos[(k_0-k)(R-\bar{R})] - \cos[(k_0+k)(R-\bar{R})]\}.$$

Since $E$ is large, and, in particular, much larger than $\hbar\omega$, the quantity $\cos[(k_0+k)(R-\bar{R})]$ will oscillate many more times over the region of effective interaction than will the quantity $\cos[(k_0-k)(R-\bar{R})]$, and therefore the integral which contains the first of these will be negligible compared to that which contains the second. Then, since $E \gg \hbar\omega$ implies $(k_0-k) \sim (\mu/2E)^{\frac{1}{2}}\omega$, (21) becomes

$$\mathcal{U}^{\nu 0} = \tfrac{1}{2} \int_{\bar{R}}^{\infty} \cos[(\mu/2E)^{\frac{1}{2}}\omega(R-\bar{R})] V_{\nu 0}(R) dR. \quad (22)$$

Now define a new variable of integration, $t$,

$$R = \bar{R} + (2E/\mu)^{\frac{1}{2}} t \quad (23)$$

and note that, for sufficiently large $E$, (23) happens to be the solution of

$$t = \int_{\bar{R}}^{R(t)} (\mu/2)^{\frac{1}{2}} \{E - [w(r) + \text{centrifugal potential}]\}^{-\frac{1}{2}} dr \quad (24)$$

everywhere except in a negligibly small neighborhood of $\bar{R}$. Thus, for large $E$, (23) defines the classical time, with $t=0$ at $R=\bar{R}$. From (22), (23), and (24),

$$\mathcal{U}^{\nu 0} = \tfrac{1}{2}(2E/\mu)^{\frac{1}{2}} \int_0^{\infty} (\cos\omega t) V_{\nu 0}[R(t)] dt. \quad (25)$$

From (6),

$$p_{0\nu} = (8\mu/\hbar^2)[E(E-\hbar\omega)]^{-\frac{1}{2}} |\mathcal{U}^{\nu 0}|^2.$$

Substituting (25) into this, and remembering that $E \gg \hbar\omega$, it becomes

$$p_{0\nu} = (4/\hbar^2) \left| \int_0^{\infty} V_{\nu 0}[R(t)] \cos\omega t dt \right|^2.$$

But it was seen above that $t$ can be considered the classical time, with $t=0$ at $R=\bar{R}$. Therefore, because of the assumption of spherical symmetry, $R(t)$ and $V_{\nu 0}[R(t)]$ are even functions of the time. Hence, the last equation becomes

$$p_{0\nu} = (1/\hbar^2) \left| \int_{-\infty}^{\infty} V_{\nu 0}[R(t)] \exp(i\omega t) dt \right|^2,$$

which is precisely (15).

It is not to be concluded that at each step of this derivation one arrives at a poorer approximation than the previous one, and that the semiclassical result is the poorest of all. Actually, what has been shown is that with energies which are so high that the classical motion is close to that of two colliding billiard balls, and the wave functions close to undistorted plane waves (Born approximation with a cutoff at the classical turning point), the two methods give identical results. The poorest approximation is Eq. (22). The quantum-mechanical theory allows for the effect of the potential on the relative translational motion by including $w(R)$ in the equation which determines $\mathfrak{R}$; and the semiclassical theory does it by requiring that $w(R)$ be included in the determination of $R(t)$. Since (22) contains no allowance for the effect of $w(R)$, in the successive steps beyond (22) the expressions become more, rather than less, exact. Inelastic molecular collision probabilities prove to be quite sensitive to some of the details of the translational motion, and this is why, in any kind of perturbation theory of these processes, the effect of $w(R)$ must be included in zeroth order.

The relationship between the quantum-mechanical and semiclassical theories can be shown most clearly by considering some simple special cases. Of particular historical importance is the case in which all translational motion is confined to a line (head-on collision), with

$$w(R) = A \exp(-aR)$$

and with $V_{\nu 0}(R)$ proportional to $w(R)$, say

$$V_{\nu 0}(R) = v_{\nu 0} A \exp(-aR)$$

where $v_{\nu 0}$ is some dimensionless constant. This problem has been treated quantum-mechanically by Zener[6] and by Jackson and Mott,[11] and semiclassically by Zener[8] and by Landau and Teller.[9] In the treatment of Jackson and Mott, it is necessary to assume (as they do implicitly) that $A$ is much greater than the translational energies involved; if this is true, then in the boundary condition (3), the origin can be replaced by $R=-\infty$, and in the integral which appears in (1), the range of integration can be extended to $-\infty$. Furthermore, the quantity $\delta_{\epsilon_n}$ which appears in (4) can, in this case, easily be found and seen to be real. Then adapting the Jackson and Mott solution to (1),

$$p^{0\nu} = (1/4\pi^2)|v_{\nu 0}|^2 (x_\nu^2 - x_0^2)^2 \times \sinh x_\nu \sinh x_0/(\cosh x_\nu - \cosh x_0)^2,$$

where

$$x_\nu = 2\pi(2\mu\epsilon_\nu)^{\frac{1}{2}}/\hbar a, \quad x_0 = 2\pi(2\mu\epsilon_0)^{\frac{1}{2}}/\hbar a.$$

[11] J. M. Jackson and N. F. Mott, Proc. Roy. Soc. (London) **A137**, 703 (1932).

For the particular case of excitation ($\epsilon_\nu<\epsilon_0$, $E_\nu>E_0$), with $\hbar\omega=E_\nu-E_0$, this becomes

$$p_{QM}{}^{0\nu}=(1/4\pi^2)|v_{\nu 0}|^2 y_0{}^4 \sinh x_0 \sinh(x_0{}^2-y_0{}^2)^{\frac{1}{2}}/ [\cosh x_0-\cosh(x_0{}^2-y_0{}^2)^{\frac{1}{2}}]^2, \quad (26)$$

where

$$y_0=2\pi(2\mu\hbar\omega)^{\frac{1}{2}}/\hbar a.$$

The subscript $QM$ indicates that this is the expression given by the quantum-mechanical theory. The condition $\epsilon_0\gg\hbar\omega$ becomes, in this notation, $x_0\gg y_0$, and under this condition (26) becomes

$$p_{QM}{}^{0\nu}=(1/\pi^2)|v_{\nu 0}|^2 x_0{}^2. \quad (27)$$

The corresponding semiclassical expression, $p_{SC}{}^{0\nu}$, will be found without making use of symmetrization, in order to keep the notation simple. The effect of symmetrization will become apparent later when some numerical results are presented. $R(t)$ is then calculated assuming that for all $t$, the total relative translational energy is $\epsilon_0$. All the operations which are implied in (15) are performed in a straightforward manner, and the Fourier transform which appears can be found in the tables of Campbell and Foster.[12] The final result is

$$p_{SC}{}^{0\nu}=(1/16\pi^2)|v_{\nu 0}|^2 y_0{}^4 \operatorname{csch}^2(y_0{}^2/4x_0). \quad (28)$$

The case considered by Zener and by Landau and Teller is that in which $y_0{}^2\gg 4x_0$, for which (28) gives the usual exponential of an inverse power of $\epsilon_0$. When $x_0\gg y_0$, however, (28) reduces to (27), thus verifying that the quantum-mechanical and semiclassical theories give identical results when $\epsilon_0\gg\hbar\omega$.

Another special case which is of some interest is that in which the potentials are spherically symmetric, and given by

$$w(R)=-A/R^2 \quad (A>0)$$
$$V_{\nu 0}(R)=-v_{\nu 0}A/R^2.$$

Attention will here be restricted to those angular momentum states for which

$$[l(l+1)-2\mu A/\hbar^2]>0,$$

that is, for which the effective radial potential becomes $+\infty$ at the origin, rather than $-\infty$. This is done to secure the convergence of the semiclassical formulas, but it is not a necessary assumption for the quantum-mechanical solution of the problem. The solution of (9) which satisfies the boundary conditions is then

$$\mathfrak{R}=-(\pi k_\nu R/2)^{\frac{1}{2}}J_p(k_\nu R),$$

where

$$k_\nu=(2\mu\epsilon_\nu)^{\frac{1}{2}}/\hbar, \quad p=(\lambda+\tfrac{1}{4})^{\frac{1}{2}},$$
$$\lambda=[l(l+1)-2\mu A/\hbar^2]>0.$$

[12] G. A. Campbell and R. M. Foster, "Fourier integrals for practical applications," Bell Telephone System, Tech. Pub., Monograph B-584 (1942).

Now,[13]

$$\int_0^\infty (1/R)J_p(k_\nu R)J_p(k_0 R)dR=\frac{1}{2p}\begin{cases}(k_\nu/k_0)^p, & k_\nu\leqslant k_0\\ (k_0/k_\nu)^p, & k_\nu\geqslant k_0.\end{cases}$$

Then from (6), for the case of excitation,

$$p_{QM}{}^{0\nu}=(\pi^2\mu^2A^2|v_{\nu 0}|^2/\hbar^4p^2)(1-\hbar\omega/\epsilon_0)^p.$$

Defining

$$B=(l+\tfrac{1}{2})/k_0, \quad k_0=(2\mu\epsilon_0)^{\frac{1}{2}}/\hbar,$$

this can be written

$$p_{QM}{}^{0\nu}=[(\pi^2\mu A^2|v_{\nu 0}|^2)/2\hbar^2(B^2\epsilon_0-A)] \times\exp\{[(2\mu)^{\frac{1}{2}}/\hbar](B^2\epsilon_0-A)^{\frac{1}{2}}\log(1-\hbar\omega/\epsilon_0)\}. \quad (29)$$

In the semiclassical calculation, only those impact parameters $b$ which satisfy

$$b^2>A/\epsilon_0$$

will lead to convergent results, and this is the classical analog of the assumption made above that $l(l+1)>2\mu A/\hbar^2$. Assuming this condition holds, and again neglecting symmetrization for the moment, $R(t)$ is easily found to be

$$R(t)=[(2\epsilon_0/\mu)t^2+b^2-A/\epsilon_0]^{\frac{1}{2}}.$$

The integral in (15), for the potential being used here, is in the tables of Campbell and Foster[12]; the result is

$$p_{SC}{}^{0\nu}=[(\pi^2\mu A^2|v_{\nu 0}|^2)/2\hbar^2(b^2\epsilon_0-A)] \times\exp\{-[(2\mu)^{\frac{1}{2}}/\hbar](b^2\epsilon_0-A)^{\frac{1}{2}}\hbar\omega/\epsilon_0\}. \quad (30)$$

A comparison of (29) and (30) shows that the quantity $B$, defined as $(l+\frac{1}{2})/k_0$, is the quantum-mechanical analog of the classical impact parameter. In turn, this shows that $(l+\frac{1}{2})\hbar$, not $[l(l+1)]^{\frac{1}{2}}\hbar$, is the analog of the classical angular momentum. This appears to be quite general, and was verified in several different connections, for the same $1/R^2$ potential as was used here, by Shortley.[14] It follows immediately from (29) and (30) that, when $\epsilon_0\gg\hbar\omega$, $p_{QM}{}^{0\nu}$ and $p_{SC}{}^{0\nu}$ become identical, again verifying the general conclusions concerning the relation of the two theories.

A numerical comparison of the two theories for the two special cases which have been discussed proves of interest. For the case of the exponential potential, the following values have been assumed: $\mu=10^{-23}$, $\omega=10^{14}$, $a=4\times10^8$. For the case of the inverse square potential, the values chosen were: $b=10^{-8}$, $A=10^{-29}$, $\hbar\omega=10^{-13}$, $(2\mu)^{\frac{1}{2}}/\hbar=5\times10^{15}$. The ratio $p_{QM}{}^{0\nu}/p_{SC}{}^{0\nu}$ was then calculated as a function of $\epsilon_0/\hbar\omega$ from (26), (28), (29), and (30). The results are summarized in Table I. It is seen from this table that even at relatively low energies the semiclassical theory agrees with the quantum-mechanical theory as to order of magnitude, but that exact agreement is obtained only at very high energies.

[13] G. N. Watson, *Theory of Bessel Functions* (Cambridge University Press, Cambridge, 1945), second edition, p. 405.

[14] G. H. Shortley, Phys. Rev. **38**, 120 (1931).

TABLE I.

| $\epsilon_0/\hbar\omega$ | 1 | 2 | 3 | 4 | 5 | 6 | 7 | 8 | 9 | 10 | 11 | 12 | 13 | 14 | 15 | 16 |
|---|---|---|---|---|---|---|---|---|---|---|---|---|---|---|---|---|
| $p_{QM}{}^{0v}/p_{SC}{}^{0v}$ (exponential potential) | 0 | | | 0.69 | | | | | 0.91 | | | | | | | 0.95 |
| $p_{QM}{}^{0v}/p_{SC}{}^{0v}$ (inverse square potential) | 0 | 0.05 | 0.21 | 0.36 | 0.48 | 0.57 | 0.64 | 0.72 | 0.75 | 0.77 | | | | | | |

After dividing out common factors, $p_{QM}{}^{0v}/p_{SC}{}^{0v}$ is of the form $q_{QM}{}^{0v}/q_{SC}{}^{0v}$, where now $q_{SC}{}^{0v}$, for either potential, and over the energy range considered, is an increasing function of the energy; for the $1/R^2$ potential it is, in addition, a decreasing function of $b$. If symmetrization had been used in the semiclassical calculations, the results would have been improved, i.e., the ratio $p_{QM}{}^{0v}/p_{SC}{}^{0v}$ would have risen much more quickly to its asymptotic value of unity, and the semiclassical theory would then have been a valid approximation over a larger range of energies. These considerations were restricted to the case of excitation, in which $\hbar\omega$ is the threshold value of $\epsilon_0$, but qualitatively similar results are to be expected for de-excitation, where the threshold value of $\epsilon_0$ is 0. Another aspect which should be noted is that for the two cases considered here (though this appears to be quite general), the semiclassical theory fails to give zero probability at the threshold;[15] only a purely quantum-mechanical theory can give correct results for energies in the neighborhood of the threshold. Furthermore, this low-energy failure of the semiclassical theory is not affected by symmetrization.

## III. STATISTICS OF SEMICLASSICAL COLLISIONS

Experimental measurements of intermolecular energy exchange only provide information regarding a mean value of $p_{0v}$, where the average is over all energies and impact parameters, with the appropriate statistical weighting factors. Expressions for these statistical averages will now be derived for the semiclassical probabilities.

Since the semiclassical theory is based on the assumption of purely classical center-of-mass motion, the appropriate statistics will be that of the kinetic theory of gases. The number of collisions suffered per second by a single hard spherical molecule of type $A$, with hard spherical molecules of type $B$, in which the relative translational energy lies between $E$ and $E+dE$, is[16]

$$\delta N=8\pi^2 C_B(\mu/2\pi kT)^{\frac{1}{2}}(1/\mu^2)\exp(-E/kT)b^2 E dE \quad (31)$$

where $C_B$ is the concentration of $B$-type molecules (in molecules/cm$^3$), $\mu$ is the reduced mass of the $A$–$B$ system, and $b$ is the collision diameter for $A$–$B$ collisions. But this expression can be interpreted, equivalently, as the number of collisions suffered per second by any single molecule $A$ (hard sphere or not) with molecules of type $B$ (hard sphere or not), in which the relative translational energy lies between $E$ and $E+dE$ and in which the impact parameter is $\leqslant b$. The analogous expression for the case in which the impact parameter lies between $b$ and $b+db$ is then obtained by differentiation:

$$d\delta N=8\pi^2 C_B(\mu/2\pi kT)^{\frac{1}{2}}(2/\mu^2)\times\exp(-E/kT)Eb\,dEdb. \quad (32)$$

Consideration will now be restricted to the case of de-excitation, for definiteness, and the corresponding semiclassical probability will be called $p_{10}(E,b)$, since in a later application of these results interest will lie in a transition from the first excited state of a certain vibrational mode, to its ground state. The notation is, then, a little different from that used previously, since here the subscript 0 indicates the state of lower energy, whereas before it represented the initial state, regardless of its energy. The average probability per second that the transition $1\rightarrow 0$ will take place in collisions between an $A$ molecule and molecules of type $B$ is

$$P_{10}=Q\int_0^\infty\int_0^\infty p_{10}(E,b)\exp(-E/kT)Eb\,dEdb \quad (33)$$

where

$$Q=4[2\pi/\mu(kT)^3]^{\frac{1}{2}}C_B. \quad (34)$$

Similarly,

$$P_{01}=Q\int_0^\infty\int_{\hbar\omega}^\infty p_{01}(E,b)\exp(-E/kT)Eb\,dEdb. \quad (35)$$

The "state" represented by a subscript 1 or 0 may actually be a collection of states each of which has very nearly the same energy. For example, it may be convenient to consider all the rotational states associated with a single vibrational state as one "state," represented by a single subscript; or the "state" may actually be a collection of truly degenerate states. In any case, let $g_1$ and $g_0$ (which can be thought of as degeneracies) be the actual number of states represented by the subscripts 1 and 0, respectively. Then if $\alpha$ is the average probability associated with the production of one of the $g_0$ states in state 0, $g_0\alpha$ will be the probability associated with the production of the whole conglomerate state 0, and this $g_0\alpha$ is to be identified with $p_{10}$. Now, (15) can be seen to lead to a principle of detailed balance very similar to (11), and this principle can now be written explicitly as

$$g_1 p_{10}(E,b)=g_0 p_{01}(E',b') \quad (36)$$

[15] O. Oldenberg, J. Chem. Phys. **13**, 196 (1945).
[16] R. H. Fowler, *Statistical Mechanics* (Cambridge University Press, Cambridge, 1929), p. 423.

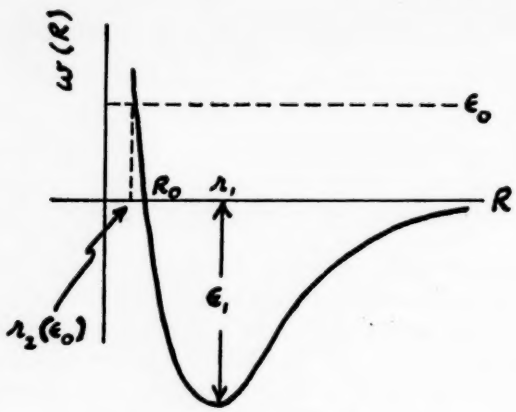


FIG. 1. The potential for the translational motion.

where $E'$, $b'$ are the energy and impact parameter that result from an inelastic $1\rightarrow 0$ collision which started with energy $E$ and impact parameter $b$. By the conservation of energy and angular momentum,

$$\begin{aligned} E' &= E+\hbar\omega \\ E'b'^2 &= Eb^2. \end{aligned} \tag{37}$$

Equation (36) would not have followed from (15) if the theory had not been symmetrized by (17) and (18). This is another argument in favor of symmetrization.

From (33), (36), and (37),

$$P_{10}=Q(g_0/g_1)\int_0^\infty\int_0^\infty \times p_{01}\{E+\hbar\omega,\, b[E/(E+\hbar\omega)]^{\frac{1}{2}}\} \times\exp(-E/kT)Eb\,dEdb \tag{38}$$

$$=Q(g_0/g_1)\exp(\hbar\omega/kT)\int_0^\infty\int_\omega^\infty \times p_{01}(x,y)\exp(-x/kT)xy\,dxdy$$

$$=(g_0/g_1)\exp(\hbar\omega/kT)P_{01} \tag{39}$$

where the last line follows from the previous one by virtue of (35). Equation (39) can be considered the statement of the statistical principle of detailed balance. It is a well-known consequence of (39) that the relaxation time, $\tau$, for the process is given by[1]

$$\tau=1/(P_{01}+P_{10}). \tag{40}$$

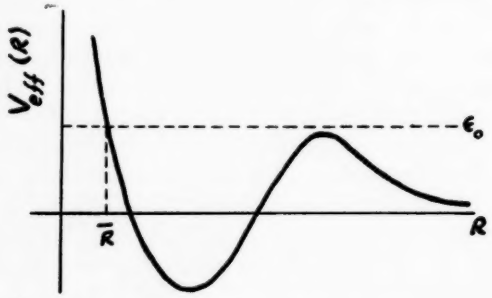


FIG. 2. The effective radial potential.

An effective collision diameter for the process can be defined as that distance $\delta$ which is such that the total number of collisions of impact parameter $\leqslant\delta$ made by a single $A$ molecule with molecules of type $B$, during the time $\tau$, is 1. From this definition and from (31),

$$\begin{aligned} 1&=\tau 8\pi^2 C_B(\mu/2\pi kT)^{\frac{1}{2}}(\delta^2/\mu^2)\int_0^\infty \exp(-E/kT)EdE \\ &=2\tau C_B\delta^2(2\pi kT/\mu)^{\frac{1}{2}}. \end{aligned} \tag{41}$$

Let $P_B$ be the partial pressure of the $B$ gas. Then

$$C_B=P_B/kT$$

and

$$1=2\tau P_B\delta^2(2\pi/\mu kT)^{\frac{1}{2}}.$$

If $\beta_{AB}$ is the relaxation time when $P_B$ is one atmosphere, then

$$\delta=(\mu kT/2\pi)^{\frac{1}{4}}(2P_0\beta_{AB})^{-\frac{1}{2}}, \tag{42}$$

where

$$P_0=1 \text{ atmos.}$$

Let

$$\tau_{10}=\int_0^\infty\int_0^\infty p_{10}(E,b)\exp(-E/kT)Eb\,dEdb. \tag{43}$$

Then from (33), (34), (39), (40), and (41),

$$\delta=[(2\tau_{10})^{\frac{1}{2}}/kT][1+(g_1/g_0)\exp(-\hbar\omega/kT)]^{\frac{1}{2}}. \tag{44}$$

If $\hbar\omega$ is greater than $kT$, as is usually the case, (44) can be written, to a good approximation,

$$\delta=(2\tau_{10})^{\frac{1}{2}}/kT. \tag{45}$$

The quantity $\pi\delta^2$ is a certain average cross section for the de-excitation process.

## IV. CLASSICAL MOTION IN A SPHERICALLY SYMMETRIC INTERMOLECULAR POTENTIAL

The trajectory $R(t)$, and therefore the probability $p_{10}(E,b)$, is fairly sensitive to the structure of the potential $w(R)$. It will be the purpose of the present discussion to investigate the details of the classical motion in a typical intermolecular potential, with particular reference to the way in which the important quantity $\bar{R}$ (the distance of closest approach) varies with the collision parameters $\epsilon_0$ (total relative translational energy) and $b_0$ (impact parameter).

A typical intermolecular potential is shown in Fig. 1. The *effective* radial potential contains the centrifugal potential, and is therefore given by $w(R)+\epsilon_0 b_0^2/R^2$. Since $w(R)$ invariably goes to 0 faster than $1/R^2$ as $R$ becomes large, the effective radial potential will (when $\epsilon_0\neq 0$ and $b_0\neq 0$) approach 0 from the positive side of the $R$-axis as $R$ becomes large. A possible situation is illustrated in Fig. 2. If $\epsilon_0$ or $b_0$ were so large as to obliterate the last trace of the minimum in $w(R)$, then $V_{\text{eff}}(R)$

might have a horizontal inflection point, or no stationary points at all, becoming, in the latter case, a monotonically decreasing function of $R$.

$\bar{R}$ is given by the abscissa of the intersection of the horizontal line at height $\epsilon_0$, with the curve $V_{\text{eff}}(R)$ *vs* $R$. Suppose that $\epsilon_0$ were smaller than the maximum in this curve. In such a case, there would be three intersections. $\bar{R}$ would have to be taken as the abscissa of the one which occurred at the largest value of $R$, corresponding to the fact that the particles, approaching from infinite separation, will bounce apart at the first encounter with the effective radial potential wall, regardless of the nature of the potential at smaller values of $R$. Now suppose that $\epsilon_0$ were not smaller than, but just slightly greater than, the maximum in $V_{\text{eff}}(R)$. This maximum could now be raised above $\epsilon_0$ without changing the latter, simply by increasing $b_0$ slightly. The corresponding $\bar{R}$ would then jump to a much higher value than it had before the small increase in $b_0$. Thus, when $V_{\text{eff}}(R)$ has a maximum, $\bar{R}$ is a discontinuous function of $b_0$, the discontinuity occurring at some value $b_c(\epsilon_0)$ which depends on $\epsilon_0$.

For the analytic presentation of these ideas, it is more convenient to deal with the function

$$g(R)=R^2[1-w(R)/\epsilon_0]$$

than with $V_{\text{eff}}(R)$ itself. $g(R)$ is illustrated in Fig. 3. $\bar{R}$ is then given by the largest of the abscissas of the intersections of a horizontal line at $b_0^2$ with the curve $g(R)$ *vs* $R$. The presence of two extrema in $g(R)$ corresponds to the case in which $V_{\text{eff}}(R)$ has a maximum. In such a case (see Fig. 3), $\bar{R}$ jumps discontinuously between $\rho_1(\epsilon_0)$ and $\rho_2(\epsilon_0)$, as $b_0^2$ passes through the critical value $b_c^2(\epsilon_0)$. No value of $\bar{R}$ can lie between $\rho_1$ and $\rho_2$. The quantity $r_2(\epsilon_0)$ is the zero of $g(R)$, i.e., it is such that $\epsilon_0=w(r_2)$; thus, $r_2(\epsilon_0)$ is the distance of closest approach in a head-on collision ($b_0=0$) with energy $\epsilon_0$. As $b_0$ increases from 0 to $b_c(\epsilon_0)$, $\bar{R}$ increases monotonically from $r_2(\epsilon_0)$ to $\rho_1(\epsilon_0)$; as $b_0$ increases from $b_c(\epsilon_0)$ to $\infty$, $\bar{R}$ increases monotonically from $\rho_2(\epsilon_0)$ to $\infty$.

Let $R_0$ be the zero of $w(R)$. Then $w(R)>0$ when $R<R_0$ and $w(R)<0$ when $R>R_0$. $\bar{R}$ satisfies the condition $\epsilon_0(1-b_0^2/\bar{R}^2)=w(\bar{R})$. Then the following facts are readily established: $\bar{R}<R_0$ and $\bar{R}>b_0$, whenever $b_0<R_0$; $\bar{R}>R_0$ and $\bar{R}<b_0$, whenever $b_0>R_0$; $\bar{R}=R_0$ whenever $b_0=R_0$; $\bar{R}\sim b_0$ for large $b_0$. These properties, together with the discussion in the preceding paragraph, afford a complete qualitative description of the course of a curve of $\bar{R}$ *vs* $b_0$. This is illustrated for the case in which a discontinuity occurs, in Fig. 4.

That the minimum in $g(R)$, when it occurs, must correspond to a positive value of the function, can be seen as follows: The curve can cross the axis only when $w(R)=\epsilon_0>0$, and this equation (see Fig. 1) can have only one solution. Thus, both extrema of $g(R)$ must lie on the same side of the $R$ axis. The maximum in $g(R)=R^2[1-w(R)/\epsilon_0]$ must occur at a larger value of

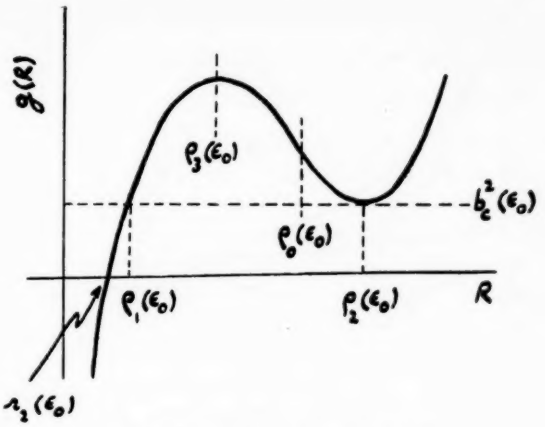


FIG. 3. The auxiliary function $g(R)$.

$R$ than does the maximum in $[1-w(R)/\epsilon_0]$, i.e., at a larger value of $R$ than does the minimum in $w(R)$. But $r_2(\epsilon_0)$, which is the only zero of $g(R)$, must occur at a smaller value of $R$ than does the minimum of $w(R)$ (see Fig. 1). Hence, the only zero of $g(R)$ lies to the left of its maximum. Therefore, $g(R)$ is positive at its maximum, and since both extrema were shown to lie on the same side of the $R$ axis, it is also positive at its minimum.

This establishes the nature of the function $g(R)$ when it happens to have two extrema, and the conditions for the existence of these extrema will now be found. $g(R)$ always goes to $-\infty$, with infinite slope, as $R\to 0$; and it goes to $+\infty$, with infinite slope, as $R\to\infty$. Hence, $g(R)$ always has a point of inflection. Let $\rho_0(\epsilon_0)$ be the abscissa of this point of inflection. Then it is clear that if the slope of $g(R)$ at $\rho_0$ is positive, $g(R)$ will have no extrema; that if the slope of $g(R)$ at $\rho_0$ is negative, $g(R)$ will be as depicted in Fig. 3; and that the transition case occurs when the inflection in $g(R)$ is a horizontal one. Thus, the condition for the existence of extrema in

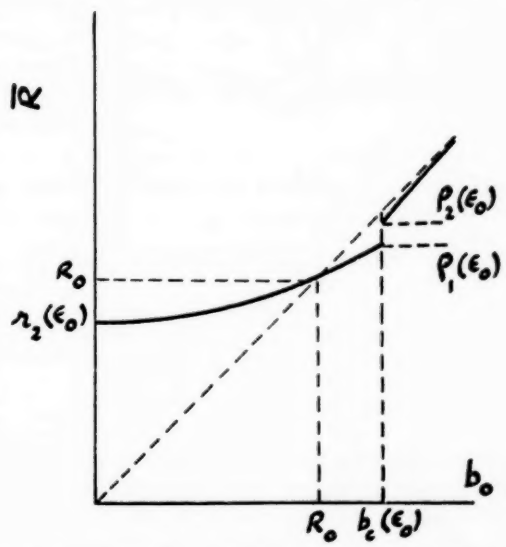


FIG. 4. The distance of closest approach as a function of impact parameter, showing the characteristic discontinuity.

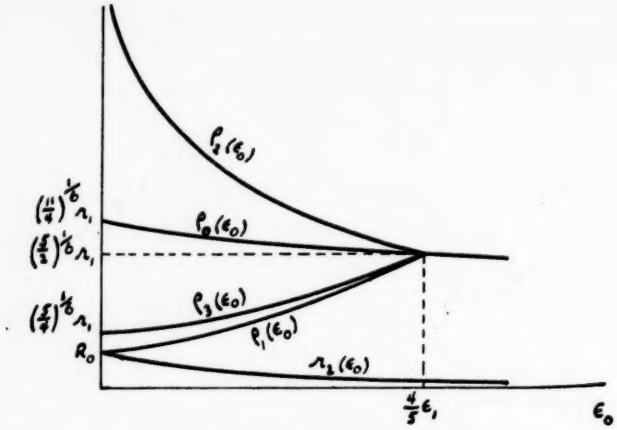

FIG. 5. The characteristic distances, as a function of incident energy, for the 6–12 potential.

$g(R)$, i.e., the condition for a discontinuity in $\bar{R}$ *vs* $b_0$, is

$$g'(\rho_0)<0,$$

where $\rho_0(\epsilon_0)$ is given by

$$g''(\rho_0)=0.$$

It will now be shown that $d\rho_2(\epsilon_0)/d\epsilon_0<0$ and $d\rho_1(\epsilon_0)/d\epsilon_0>0$; in other words, as $\epsilon_0$ increases, $\rho_2$ moves to the left and $\rho_1$ to the right. Eventually, in fact, at a certain critical value of $\epsilon_0$, $\rho_1$, and $\rho_2$ will coalesce with $\rho_0$, and this will mark the transition case in which $g(R)$ has a horizontal inflection; at still higher values of $\epsilon_0$, there will no longer be any real solution for $\rho_1$ and $\rho_2$, the slope of $g(R)$ at $\rho_0$ will be positive, and $\bar{R}$ will have ceased to be a discontinuous function of $b_0$.

By definition of $\rho_2(\epsilon_0)$, it must satisfy $g'(\rho_2)=0$. Hence,

$$2[\epsilon_0-w(\rho_2)]=\rho_2 w'(\rho_2).$$

Then differentiating with respect to $\epsilon_0$, and rearranging terms,

$$-2=(\epsilon_0/\rho_2)(d\rho_2/d\epsilon_0)\left\{\left[\frac{d^2}{dR^2}(R^2[1-w(R)/\epsilon_0])\right]_{R=\rho_2}+[\rho_2 w'(\rho_2)/\epsilon_0]-2[1-w(\rho_2)/\epsilon_0]\right\}$$

and therefore, combining these two equations,

$$-2=(\epsilon_0/\rho_2)(d\rho_2/d\epsilon_0)\left\{\frac{d^2}{dR^2}[R^2(1-w(R)/\epsilon_0)]\right\}_{R=\rho_2}$$

$$=(\epsilon_0/\rho_2)(d\rho_2/d\epsilon_0)g''(\rho_2),$$

the last line following from the definition of $g(R)$. Now, by the definition of $\rho_2$,

$$g''(\rho_2)>0.$$

Hence,

$$d\rho_2/d\epsilon_0<0.$$

By definition of $\rho_1(\epsilon_0)$, $g(\rho_1)=g(\rho_2)$. Therefore

$$\rho_1^2[\epsilon_0-w(\rho_1)]=\rho_2^2[\epsilon_0-w(\rho_2)].$$

Differentiating this with respect to $\epsilon_0$, and then rearranging terms,

$$\epsilon_0(d\rho_1/d\epsilon_0)\left\{\frac{d}{dR}[R^2(1-w(R)/\epsilon_0)]\right\}_{R=\rho_1}+\rho_1^2$$

$$=\epsilon_0(d\rho_2/d\epsilon_0)\left\{\frac{d}{dR}[R^2(1-w(R)/\epsilon_0)]\right\}_{R=\rho_2}+\rho_2^2$$

or, more simply,

$$\epsilon_0(d\rho_1/d\epsilon_0)g'(\rho_1)+\rho_1^2=\epsilon_0(d\rho_2/d\epsilon_0)g'(\rho_2)+\rho_2^2.$$

But $g'(\rho_2)=0$, $\rho_2>\rho_1$, and $g'(\rho_1)>0$. Hence,

$$d\rho_1/d\epsilon_0>0.$$

A typical intermolecular potential is illustrated by the Lennard-Jones 6–12 potential:

$$w(R)=\epsilon_1[(r_1/R)^{12}-2(r_1/R)^6].$$

The notation corresponds to that of Fig. 1. Most of the quantities which have so far been used in this discussion can be found explicitly when $w(R)$ has this form. They are presented schematically in Fig. 5. Reference can be made to Figs. 1 and 3 to find the definitions of the quantities which are diagrammed in Fig. 5. For the Lennard-Jones potential, $\bar{R}$ is a discontinuous function of $b_0$ whenever the translational energy is less than $\frac{4}{5}$ of the depth of the minimum in $w(R)$, and it is a continuous function of $b_0$ for energies which are greater than this.

From the analysis which was presented here, it is seen that $b_c(\epsilon_0)$, the critical value of $b_0$ at which the discontinuity occurs (when it does occur) can be found from

$$b_c(\epsilon_0)=\rho_2[1-w(\rho_2)/\epsilon_0]^{\frac{1}{2}} \tag{46}$$

where, for the 6–12 Lennard-Jones potential, $\rho_2(\epsilon_0)$ is given explicitly by

$$\rho_2(\epsilon_0)=r_1(2/5)^{-1/6}[1-(1-5\epsilon_0/4\epsilon_1)^{\frac{1}{2}}]^{-1/6}. \tag{47}$$

The rôle of $\epsilon_0$ thus far has been only to determine whether $\bar{R}$ will have a discontinuity with respect to $b_0$; now the direct behavior of $\bar{R}$ as a function of $\epsilon_0$ (for fixed $b_0$) will be deduced.

$\bar{R}$ is a solution of the equation

$$\epsilon_0=w(\bar{R})+\epsilon_0 b_0^2/\bar{R}^2.$$

Differentiating with respect to $\epsilon_0$,

$$1-b_0^2/\bar{R}^2=(\partial\bar{R}/\partial\epsilon_0)[w'(\bar{R})-2\epsilon_0 b_0^2/\bar{R}^3]$$

$$=(\partial\bar{R}/\partial\epsilon_0)V_{\text{eff}}'(\bar{R}).$$

$V_{\text{eff}}'(R)$ is the negative of the effective radial force, and this force must be repulsive (i.e., positive) at the distance of closest approach, $\bar{R}$. Hence,

$$V_{\text{eff}}'(\bar{R})<0$$

and, therefore,

$$\partial\bar{R}/\partial\epsilon_0<0 \quad \text{when} \quad \bar{R}>b_0,$$
$$\partial\bar{R}/\partial\epsilon_0>0 \quad \text{when} \quad \bar{R}<b_0.$$

But it was seen before that $\bar{R}>b_0$ when $b_0<R_0$, and $\bar{R}<b_0$ when $b_0>R_0$. Therefore,

$$\partial\bar{R}/\partial\epsilon_0<0 \quad \text{when} \quad b_0<R_0,$$
$$\partial\bar{R}/\partial\epsilon_0>0 \quad \text{when} \quad b_0>R_0.$$

These conclusions demonstrate that the effect of an increase in energy is always to straighten out the trajectory. When $b_0<R_0$, the potential $w(R)$ will be mainly repulsive and will try to push the particles apart (increase $\bar{R}$); but when $\epsilon_0$ is increased, this bouncing apart of the particles is resisted, the trajectory is made more nearly linear, and $\bar{R}$ decreases. Similarly, for $b_0>R_0$, an increase in $\epsilon_0$ increases $\bar{R}$, by counteracting the tendency of the attractive part of $w(R)$ to drag the particles more closely together, out of their original lines of motion.

## V. SEMICLASSICAL THEORY OF THE SYSTEM $CO_2-H_2O$

The effect of "chemical reactivity" on the magnitude of the de-excitation probability is not difficult to understand on physical grounds,[17] but the temperature dependence to which reactivity gives rise has never been adequately explained. It is the purpose of this section to show that both the quantitative and qualitative aspects of the probability *vs* temperature curve for $CO_2-H_2O$ can be understood in terms of the principles already discussed. In particular, the semiclassical theory leads directly to a probability which decreases with increasing temperature. Such an effect must always be looked for in collisions between components which may react chemically. Its physical basis will be discussed now in order to make it apparent where the effect will manifest itself in the calculations which are presented later.

In Sec. IV it was seen that with impact parameter $b<R_0$, the distance of closest approach, $\bar{R}$, decreases with increasing relative translational energy $E$ (corresponding to greater intermolecular penetration) but that in collisions with $b>R_0$, $\bar{R}$ increases with increasing $E$. It is clear that the probability of a collision being inelastic will increase as $\bar{R}$ decreases, and therefore

$p_{10}(E, b)$ increases with increasing $E$ when $b<R_0$,

$p_{10}(E, b)$ decreases with increasing $E$ when $b>R_0$.

The ultimate behavior of $P_{10}(T)$ with $T$ will then depend upon the relative importance of low-$b$ and high-$b$ collisions. The fact that low-$b$ collisions lead to the smallest $\bar{R}$, and therefore to the highest $p_{10}$, tends to make them more strongly represented in the final average $P_{10}$; the fact that most collisions, however, are high-$b$ collisions (see (31)) has exactly the opposite effect. The second of these considerations proves to be of greater importance than the first for the system $CO_2-H_2O$, so the ultimate result is that the de-excitation probability decreases with increasing relative translational energy.

To calculate this effect in detail it is necessary to have some knowledge of the interaction potential between $CO_2$ and $H_2O$, and the important features of this potential can best be inferred from the chemistry of the reaction

$$\underset{(g)}{CO_2} + \underset{(l)}{H_2O} \rightarrow \underset{(soln)}{HOCOOH} \quad \text{(carbonic acid)}.$$

It is known that in the $CO_2$ molecule the valence electrons are strongly concentrated in the neighborhood of the O atoms, and that the distribution is, in fact, so extreme[18] that a large contribution to the ground state is made by the structure

$$^{-}O \overset{++++}{C} O^{-}.$$

Furthermore, in the $H_2O$ molecule, those electrons of atomic oxygen which do not take part to any significant extent in the HOH bonding are found in orbitals which are, in the main, directed almost perpendicularly to the HOH plane, and centered at the O atom.[19] These lone-pair hybrids provide well-localized, well-directed concentrations of negative charge which are inherently suited for the formation of donor-acceptor bonds whenever $H_2O$ interacts with a molecule which possesses a well-localized center of electron deficiency.

These considerations make it probable that the reaction referred to above is of the Lewis acid-base type, and takes place in stages somewhat as follows:

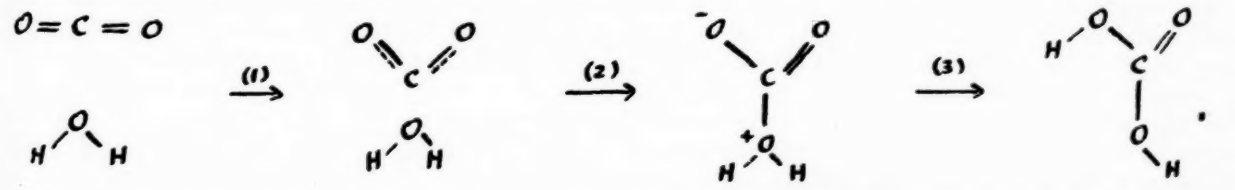


Since $H_2O$ and $CO_2$ do not produce a stable product in the gas phase, for most collisions their interaction probably goes only as far as some point intermediate between the second and third of these stages. It will be assumed that this extreme point is that at which the

[17] Reference 2, p. 32.

[18] J. E. Lennard-Jones, J. Chem. Phys. **20**, 1024 (1952).

[19] C. A. Coulson, *Valence* (Oxford University Press, London, 1952), pp. 209–210.

three O atoms and the C atom, in the $H_2O-CO_2$ system, are related to each other energetically as they are in $CO_3^=$, and the known energetics of this ion will then be used to determine the interaction potential. Clearly, the approach to the $CO_3^=$ configuration involves the bending of the $CO_2$ molecule, and, as was pointed out by Eucken and Küchler,[3] this is the probable explanation of the great effect that $H_2O$ has on the bending vibration of $CO_2$.

The above considerations, of course, apply only to very special mutual orientations of the two molecules, *viz.*, those in which the $CO_2$ line is parallel to the $H_2O$ plane, with the line between the C of $CO_2$ and the O of $H_2O$ almost perpendicular to the $H_2O$ plane. This will be referred to as "the most favorable orientation." The problem will be solved assuming that the interaction potential is spherically symmetric and corresponds to that of interaction in the most favorable orientation; the resulting expressions for probabilities per collision will then be multiplied by an "orientation factor" $\theta<1$, to correct for the fact that only in relatively few collisions will the molecules be found in orientations close to the most favorable one. The assumption of spherical symmetry, modified by the factor $\theta$, is a device to eliminate the necessity of considering molecular rotation and noncentral forces, as these would make the problem totally intractable. Any tendency of the noncentral forces to drag the molecules into some special orientation during the course of the collision is being ignored.

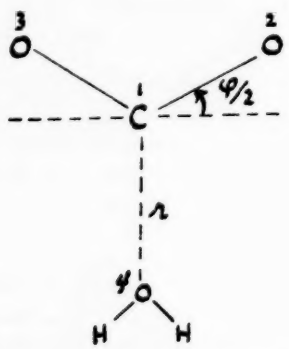


FIG. 6. Coordinates in the $CO_2-H_2O$ interaction.

During the course of the numerical work which is described later, it was found that a typical collision time (time of effective interaction) is $10^{-14}$ sec, and it is so small because the potential curve for chemically reactive components is very steep in the neighborhood of the point of closest approach. At all temperatures of interest ($<700°$K) only an insignificantly small fraction of the total number of collisions will take place between molecules whose rotational states are such as to give rotation times as small as $10^{-14}$ sec. Thus, it is meaningful to speak of *the* orientation at collision, and $\theta$ is essentially temperature-independent.

The nature of the approximation being made here is this: It is assumed that the probabilities one wishes to calculate, as a function of the relative orientation of the molecules at collision, have strong maxima in the neighborhood of the most favorable orientation, so that one can consider a certain region in relative-orientation-space which contains the most favorable orientation and which is such that for orientations within this region the probabilities can be considered the same as those associated with the most favorable orientation itself, and for orientations outside this region the probabilities are effectively zero. $\theta$ is then the fraction of the total volume of relative-orientation-space which is occupied by this "effective" region.§ It is felt on geometrical and physical grounds that $\theta$ should be about 1/1000, and this is the value that will be used. It is to be considered uncertain by a factor of about 10.

The potential is now to be constructed on the assumption that, as $CO_2$ and $H_2O$ approach in the most favorable orientation, the system will tend to take on the configuration of $CO_3^=$. For large values of $r$ (Fig. 6) the potential as a function of $\varphi$ is that which it would be in unperturbed $CO_2$,[20] *viz.* $(0.57\times10^5/2)l^2_{CO_2}\varphi^2$, where $l_{CO_2}$ is the equilibrium CO distance in $CO_2$, 1.15A.[21] The equilibrium CO distance in $CO_3^=$ is reached when $r=r_1\equiv1.31$A,[22] and here the equilibrium value of $\varphi$ is $\pi/3$. If $\delta_{23}$, $\delta_{24}$, $\delta_{34}$ are the changes in the angles $\sphericalangle213$, $\sphericalangle214$, $\sphericalangle314$, respectively, then the potential for planar bending is [23]

$$(0.51/2)\times10^5r_1^2(\delta_{23}^2+\delta_{24}^2+\delta_{34}^2)$$
$$=(0.51/2)\times10^5r_1^2[(\varphi-\pi/3)^2+(1/4)(\varphi-\pi/3)^2$$
$$+(1/4)(\varphi-\pi/3)^2]=(3/4)(0.51\times10^5)r_1^2(\varphi-\pi/3)^2.$$

The potential energy, as a function of $\varphi$, for the two extreme cases is then

$$3.77\times10^{-12}\varphi^2 \qquad (r=\infty)$$
$$6.555\times10^{-12}(\varphi-\pi/3)^2 \qquad (r=r_1).$$

For general values of $r$, the equilibrium value of $\varphi$ should vary smoothly from 0 to $\pi/3$ as $r$ varies from $\infty$ to $r_1$; also, the value of the factor which multiplies the square of the difference between $\varphi$ and its equilibrium value should vary smoothly from $3.77\times10^{-12}$ erg to $6.555\times10^{-12}$ erg as $r$ varies from $\infty$ to $r_1$. From our general knowledge of the electronic structure of molecules and of intermolecular interactions, it seems safe to assume that the function which describes these variations with $r$ is

$$\exp[(r_1-r)/a_0]$$

§ $\theta$ is then conceptually similar to the steric factor of chemical kinetics. It must not, however, without much more detailed knowledge of these systems and processes, be identified with it.

[20] G. Herzberg, *Infrared and Raman Spectra of Polyatomic Molecules* (D. Van Nostrand Company, Inc., New York, 1945), p. 173.

[21] L. Pauling, *The Nature of the Chemical Bond* (Cornell University Press, Ithaca, 1945), 2nd ed., p. 195–196.

[22] Reference 21, pp. 208–209.

[23] Reference 20, p. 178.

where $a_0$ is of the order of magnitude of the Bohr radius; for lack of more specific information $a_0$ will be taken to be exactly 0.53A. Then the potential energy, as a function of $\varphi$, will be

$$\{3.77+(6.555-3.77)\exp[(r_1-r)/a_0]\}\times\{\varphi-(\pi/3)\exp[(r_1-r)/a_0]\}^2 10^{-12}$$
$$=\{v_1+v_2\exp[(r_1-r)/a_0]\}\times\{\varphi-(\pi/3)\exp[(r_1-r)/a_0]\}^2$$

where $v_1=3.8\times10^{-12}$ erg and $v_2=2.8\times10^{-12}$ erg. This is only that part of the total potential which involves the $CO_2$-bending variable $\varphi$. It includes the effect of the

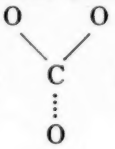

formation of the bond on the bending of the

bonds, but does not include the bond energies themselves. These bond energies will add a potential $f(r)$ which is a function of $r$ alone, as yet unspecified except that it must go to 0 for large $r$. The total potential, as a function of $r$ and $\varphi$, is then

$$f(r)+\{v_1+v_2\exp[(r_1-r)/a_0]\}\times\{\varphi-(\pi/3)\exp[(r_1-r)/a_0]\}^2.$$

But part of this potential, *viz.*, $v_1\varphi^2$, was present in the unperturbed $CO_2$ molecule. Subtracting this from the total potential, one obtains the perturbation as a function of $r$ and $\varphi$; $r$ is the distance between the C atom and the O of $H_2O$, but because of the small mass of the H atoms, $r$ can be replaced by $R$, the distance between the centers of mass of the two molecules. The perturbation is then

$$V=f(R)+\{v_1+v_2\exp[(r_1-R)/a_0]\}\times\{(\pi^2/9)\exp[2(r_1-R)/a_0]-(2\pi/3)\exp[(r_1-R)/a_0]\varphi\}+v_2\exp[(r_1-R)/a_0]\varphi^2. \quad (48)$$

For large $R$, of course, this quantity vanishes.

To proceed with the semiclassical calculation it is necessary to know the matrix elements $V_{10}(R)$ and $w(R)=\frac{1}{2}[V_{00}(R)+V_{11}(R)]$. $V_{10}$ can be found without knowing $f(R)$ because the term involving this quantity will vanish by virtue of the orthogonality of the two different vibrational states. To find $w$, on the other hand, it would in principle be necessary to know $f$. In this case, however, one has a much better estimate of the nature of $w$ than of $f$, so $w$ will be specified, not calculated. $f(R)$ can then be considered to be that function of $R$ which would make $\frac{1}{2}[V_{00}(R)+V_{11}(R)]$ equal to the "known" function $w(R)$.

$w(R)$ is the potential which determines the relative translational motion of $CO_2-H_2O$ in the most favorable orientation, and judging from the properties of known chemical bonds, it will be of the form given in Fig. 1. With the assumption that in the most favorable orientation the system tends toward the $CO_3^=$ configuration, one concludes that the potential minimum occurs at $r_1=1.31$A, the equilibrium CO distance in $CO_3^=$. The depth of the minimum, $\epsilon_1$, can be guessed at as follows: In the case of strong chemical bonds, typical potential minima are about 3–10 ev deep; van der Waals minima are about 0.001–0.02 ev deep. It is then not unreasonable to assume that the depth of the minimum corresponding to a weak chemical bond will be a few tenths of an ev. $\epsilon_1$ will be taken to be about $\frac{1}{3}$ev (8 kcal/mole). If $\epsilon_1$ were significantly greater than this, it would be difficult to understand the inherent instability of the $H_2CO_3$ molecule and the failure of $H_2O$ and $CO_2$ to react in the gas phase; if it were significantly less, the reaction in the liquid phase would be hard to explain. The assumed value of $\epsilon_1$ is perhaps uncertain by 4 kcal/mole (50 percent). $w(R)$ will now be taken to be a 6–12 Lennard-Jones potential with the assigned values of $r_1$ and $\epsilon_1$:

$$w(R)=\epsilon_1[(r_1/R)^{12}-2(r_1/R)^6]. \quad (49)$$

The matrix element $V_{10}$ can be found as follows: The kinetic energy associated with the $CO_2$ bending is

$$\tfrac{1}{2}\mu_{CO_2}l^2\dot{\varphi}^2$$

where

$$\mu_{CO_2}=(1/2)m_Om_C/(2m_O+m_C)$$
($m_O$, $m_C$ = masses of O, C atoms, respectively).

The potential energy is

$$(1/2)(0.57\times10^5)l^2\varphi^2.$$

Since the wave function falls off rapidly for large $\varphi$, one can take $(-\infty, \infty)$ as the range of the variable. Thus, if $u_n(x)$ is the normalized wave function for the $n$th state of a simple harmonic oscillator of mass $\mu_{CO_2}$, force constant $0.57\times10^5$, and variable coordinate $x$, then the wave function for $CO_2$ bending, normalized with respect to $\varphi$ in the interval $(-\infty, \infty)$, is

$$\Psi_n(\varphi)=l^{\frac{1}{2}}u_n(l\varphi), \quad (50)$$

and the energy levels are given by $E_n=(n+\frac{1}{2})h\omega$, with

$$\omega=[0.57\times10^5/\mu_{CO_2}]^{\frac{1}{2}}.$$

Then from (48) and (50),

$$V_{10}(R)=-\Lambda\exp[(r_1-R)/a_0]\times\{v_1+v_2\exp[(r_1-R)/a_0]\} \quad (51)$$

where

$$\Lambda=(2^{\frac{1}{2}}\pi/3l)(0.57\times10^5\mu_{CO_2}/h^2)^{-\frac{1}{2}}$$
$$=0.1953.$$

For a collision involving symmetrized incident relative energy $\epsilon_0$ and symmetrized impact parameter $b_0$, the effective radial potential is

$$V_{eff}(R)=w(R)+\epsilon_0b_0^2/R^2. \quad (52)$$

The distance of closest approach, $\bar{R}$, is given by the largest solution of

$$V_{\text{eff}}(\bar{R})=\epsilon_0. \tag{53}$$

Let

$$\phi_0=-V_{\text{eff}}'(\bar{R}) \quad \text{(effective radial force at } R=\bar{R}) \tag{54}$$

and

$$\psi_0=V_{\text{eff}}''(\bar{R}). \tag{55}$$

Then the expression

$$\epsilon_0-(\phi_0^2/\psi_0)\{1-\exp[(\bar{R}-R)\psi_0/\phi_0]\}$$

is a monotonically decreasing function of $R$ which approaches a definite lower limit asymptotically, and which, at $R=\bar{R}$, has the same value, the same 1st derivative, and the same 2nd derivative, as the function $V_{\text{eff}}(R)$. It was found numerically that in a typical collision the interval near $\bar{R}$ over which interaction is effective is so small, that over this entire interval

TABLE II.

| | $b$ in A | 0 | 1 | 2 | 3 | 4 | 5.55 |
|---|---|---|---|---|---|---|---|
| $E=0$ | $p_{10}$ | 0.169 | 0.166 | 0.155 | 0.141 | 0.118 | 0.080 |
| | $b$ in A | 0 | 0.689 | 1.38 | 2.07 | 2.75 | 3.58 |
| $E=0.03375\times10^{-12}$ | $p_{10}$ | 0.177 | 0.175 | 0.157 | 0.137 | 0.102 | 0.055 |
| | $b$ in A | 0 | 0.616 | 1.23 | 1.85 | 2.47 | 3.01 |
| $E=0.08375\times10^{-12}$ | $p_{10}$ | 0.185 | 0.187 | 0.163 | 0.132 | 0.085 | 0.025 |
| | $b$ in A | 0 | 0.585 | 1.17 | 1.76 | 2.34 | 2.73 |
| $E=0.13375\times10^{-12}$ | $p_{10}$ | 0.199 | 0.193 | 0.170 | 0.125 | 0.057 | 0.010 |

$V_{\text{eff}}(R)$ and the expression above are completely indistinguishable.|| Hence, to a very good approximation,

$$V_{\text{eff}}(R)\approx\epsilon_0-(\phi_0^2/\psi_0)\{1-\exp[(\bar{R}-R)\psi_0/\phi_0]\}.$$

The classical trajectory for all the important values of $t$ is then given by

$$R(t)=\bar{R}+(2\phi_0/\psi_0)\log\{\cosh(\psi_0/2\mu)^{\frac{1}{2}}t\} \tag{56}$$

where $\mu$ is the reduced mass of the $CO_2-H_2O$ system. The probability of de-excitation in a collision of energy $E$ and impact parameter $b$, of which the symmetrized values are $\epsilon_0$ and $b_0$, is

$$p_{10}(E,b)=\theta|I|^2/\hbar^2$$

where, from (51) and (56), and from the table of Campbell and Foster,[12]

$$I=\int_{-\infty}^{\infty}V_{10}[R(t)]\exp(i\omega t)dt$$

$$=-\Lambda\exp[(r_1-\bar{R})/a_0](2^\beta/4\pi\gamma)\{v_1|\Gamma(z_1)|^2/\Gamma(\beta)$$

$$+v_2 2^\beta\exp[(r_1-\bar{R})/a_0]|\Gamma(z_2)|^2/\Gamma(2\beta)\}$$

with

$$\beta=2\phi_0/a_0\psi_0, \quad \gamma=(1/2\pi)(\psi_0/2\mu)^{\frac{1}{2}}, \quad z_1=\beta/2+i\omega/4\pi\gamma,$$

$$z_2=\beta+i\omega/4\pi\gamma.$$

The quantities $\bar{R}$, $\phi_0$, $\psi_0$ are functions of $\epsilon_0$ and $b_0$ (and therefore of $E$, $b$) and are given through the Eqs. (49), (52), (53), (54), (55). The values of the constants which appear have been collected below:

$r_1=1.3\times10^{-8}$ cm $\quad (2/\mu)^{\frac{1}{2}}=3.06\times10^{11}$ g$^{-\frac{1}{2}}$

$\epsilon_1=0.5\times10^{-12}$ erg $\quad \Lambda=0.1953$

$v_1=3.8\times10^{-12}$ erg $\quad a_0=0.53\times10^{-8}$ cm

$v_2=2.8\times10^{-12}$ erg $\quad \omega=1.258\times10^{14}$ sec$^{-1}$.

$\theta=0.001$

Values of the $\Gamma$ function for real and complex arguments are found in Davis' tables.[24]

$\bar{R}$ was found graphically from (53) for several values of $\epsilon_0$ and $b_0$; the other quantities, once $\bar{R}$ was known, were found directly from their defining equations. This gave $p_{10}$ as a function of $\epsilon_0$ and $b_0$, and it was then found as a function of $E$ and $b$ by applying (17) and (18). The results are given in Table II. In Sec. IV it was seen that if $\epsilon_0<(4/5)\epsilon_1$ then $\bar{R}$ has a discontinuity with respect to $b_0$. Now, $\frac{4}{5}\epsilon_1=4\times10^{-13}$ erg, so that if one considers only temperatures below 700°K, all the significant values of $E$ will be such that the corresponding values of $\epsilon_0$ are less than $(4/5)\epsilon_1$. All the values of $E$ used in Table II satisfy this condition; hence, for each $E$ in the table, $\bar{R}$ is a discontinuous function of $b_0$, and therefore of $b$. For a given $E$, the largest value of $b$ entered in the table is this critical value, i.e., the value of $b$ at which $\bar{R}$ has a discontinuity. These critical $b$ values were obtained by the symmetrization equations from the critical $b_0$ values, and these, in turn, were obtained from formulas (46) and (47).

For all the entries in the table, the $\bar{R}$ values lie within 0.13A of each other, in spite of the relatively large range of $b_0$ values. The reason for this is that the intermolecular potential, either by repulsion when $b_0<R_0$ or by attraction when $b_0>R_0$, prevents $\bar{R}$ from deviating very much from $R_0$. $p_{10}$, as can be seen from Table II, is nevertheless a fairly rapidly decreasing function of $b$, showing then that $p_{10}$ must indeed be an extraordinarily rapidly decreasing function of $\bar{R}$. Now, when $\bar{R}$ makes its discontinuous jump at the critical value of $b$, it

|| For example, when $\epsilon_0=0.05\times10^{-12}$ erg and $b_0=0.5$A, the approximate expression for $V_{\text{eff}}(R)$ is extremely accurate in the range $\bar{R}<R<1.2$A, i.e., in the time range $0<|t|<0.05\times10^{-13}$ sec. Furthermore, the contribution to the total integral $I$ (defined below) which comes from $\infty>|t|>0.05\times10^{-13}$ is completely negligible.

[24] H. T. Davis, *Tables of the Higher Mathematical Functions* (Principia, Bloomington, 1933), vol. 1.

changes by about an angstrom unit or more, rather than by tenths of an angstrom unit. Consequently, when $b$ increases beyond the critical value, $p_{10}$ becomes totally negligible.

To find the average effective collision diameter for the de-excitation process, it is seen from (45) that one needs the value of the integral

$$\mathcal{T}_{10}=\int_0^\infty\int_0^\infty p_{10}(E,b)\exp(-E/kT)Eb\,dEdb.$$

From the preceding discussion it is known that for $T<700°$ this can, with great accuracy, be replaced by

$$\mathcal{T}_{10}=\int_0^\infty\int_0^{b_c(E)} p_{10}(E,b)\exp(-E/kT)Eb\,dbdE$$

where $b_c(E)$ is the critical value of $b$ at energy $E$. If one lets $\sigma=b^2$, then

$$\mathcal{T}_{10}=\tfrac{1}{2}\int_0^\infty\int_0^{b_c^2(E)} p_{10}\exp(-E/kT)Ed\sigma dE.$$

Now, for each $E$ in Table II, it was found that $p_{10}$ is almost exactly a linear function of $\sigma$ over the entire range $0\leqq\sigma<b_c^2(E)$. This linearity permits immediate integration over $\sigma$, and one obtains for $J(E)$, where

$$J(E)=\int_0^{b_c^2(E)} p_{10}d\sigma,$$

the values in Table III. One next observes that for the range of $E$ in this table, $J^{-2}$ is very nearly a linear function of $E$. For $T<700°$, one can just as well assume that this linear relation holds over the entire infinite range of $E$, and then the integral

$$\mathcal{T}_{10}=\tfrac{1}{2}\int_0^\infty J(E)\exp(-E/kT)EdE$$

can be evaluated. The final expression for the effective collision diameter is then obtained from (45) and is

$$\delta=1.944\times10^{-8}D^{\frac{1}{3}}(p) \tag{57}$$

where

$$p^2=44.1/T \tag{58}$$

and

$$D(p)=p^2+(\pi^{\frac{1}{2}}/2)\,(\exp p^2)(p-2p^3)(1-\operatorname{erf}p). \tag{59}$$

The expression (57) is indeed a monotonically decreasing function of $T$, as was anticipated in the introduction to this section.

Experimental values of $\delta$ for the system considered here are obtained immediately by applying (42) to the relaxation-time data of Eucken and Nümann.[25] In Table IV, these are compared with the values predicted by (57). The first column of the table gives the temperature; the second column gives the total number of measurements, $N$, made at that temperature; the third gives the total spread of the experimental results, and this, together with $N$, is a measure of the experimental precision; and the fourth and fifth columns give the experimental (average) and theoretical $\delta$ values, respectively.

TABLE III.

| $E$ | 0 | $0.03375\times10^{-12}$ | $0.08375\times10^{-12}$ | $0.13375\times10^{-12}$ |
|---|---|---|---|---|
| $J(E)$ | $3.79\times10^{-16}$ | $1.49\times10^{-16}$ | $0.99\times10^{-16}$ | $0.78\times10^{-16}$ |

The most striking, though entirely expected, feature of these results is the failure of the theoretical $\delta$ values to fall at low $T$. This is but another instance of the low-energy failure of the semiclassical theory, two examples of which were seen in Sec. II. This failure is in no way eliminated by symmetrization. By the microscopic principle of detailed balance, the de-excitation probability in a collision must be proportional to the excitation probability in the inverse collision. Since by energy conservation and by continuity, molecular excitation probabilities must be 0 at the threshold,[15] it follows that de-excitation probabilities must be 0 for zero relative energy of the colliding particles. A complete quantum-mechanical theory would then have given a $\delta$ which increased from 0 at $T=0$, and, as the semiclassical results indicate, this $\delta$ would again have fallen as one approached energies in the range of validity of the semiclassical theory. The observed maximum occurs at about 350°K, and this corresponds to an average energy of $0.5\times10^{-13}$, or about $(1/3)\hbar\omega$. Thus, the observed maximum does indeed lie in the transition interval between that region in which the semiclassical theory is expected to be correct ($E\gg\hbar\omega$) and that in which it is known to fail ($E\ll\hbar\omega$).

In order to see the extent to which these results depend on some of the assumptions which have been made, the calculations were repeated with several changes, as tabulated below. The quantities $a_0$, $\epsilon_1$, and $r_1$ were taken as the parameters to be varied. The curves of Fig. 7

TABLE IV.

| $T$ in °K | $N$ | $\Delta\delta_{\text{exp}}$ in A | $\delta_{\text{exp}}$ in A | $\delta_{\text{th}}$ in A |
|---|---|---|---|---|
| 200 | | | | 1.18 |
| 294 | 7 | 0.05 | 0.43 | 1.08 |
| 352 | 3 | 0.04 | 0.52 | 1.04 |
| 492 | 1 | | 0.40 | 0.97 |
| 688 | 5 | 0.15 | 0.26 | 0.91 |

[25] A. Eucken and E. Nümann, Z. physik. Chem. **B36**, 163 (1937).

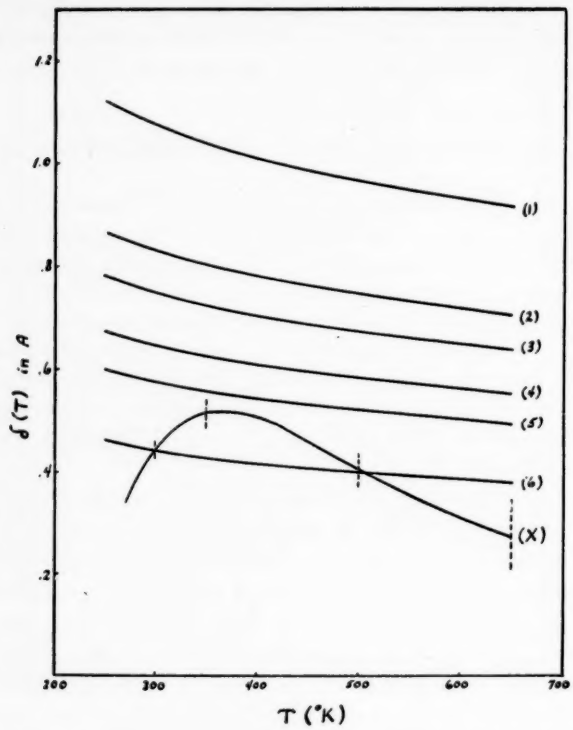


FIG. 7. The effective collision diameter. Curves (1) to (5) are for various values of the parameters; curve (6) is the modified calculation (see text); (X) is experimental.

correspond to the cases

(1) $a_0=0.53$A, $\epsilon_1=0.5\times10^{-12}$ erg, $r_1=1.3$A

(2) $a_0=0.70$A, $\epsilon_1=0.5\times10^{-12}$ erg, $r_1=1.3$A

(3) $a_0=1.00$A, $\epsilon_1=0.75\times10^{-12}$ erg, $r_1=1.3$A

(4) $a_0=1.00$A, $\epsilon_1=0.5\times10^{-12}$ erg, $r_1=1.45$A

(5) $a_0=1.00$A, $\epsilon_1=0.5\times10^{-12}$ erg, $r_1=1.3$A

(X) experimental, with estimated error given by dashed vertical segments.

The curve (6) was obtained as follows: The total potential, as a function of $r$ and $\varphi$, had been taken as

$$f(r)+\{v_1+v_2\exp[(r_1-r)/a_0]\}\times\{\varphi-(\pi/3)\exp[(r_1-r)/a_0]\}^2,$$

and this led to (51). The leading term in $V_{10}(R)$ at small $R$ was then proportional to $\exp[2(r_1-R)/a_0]$ instead of to $\exp[(r_1-R)/a_0]$. It can be argued that it would then have been more appropriate to use some average constant, $v_3$, in place of $\{v_1+v_2\exp[(r_1-r)/a_0]\}$. The most reasonable value for $v_3$ is $5.16\times10^{-12}$, this being the average of $6.555\times10^{-12}$ and $3.77\times10^{-12}$. In this scheme, then, the calculation is the same as before, only the term in $v_2$ is discarded, and $v_1$ is replaced by $v_3$. If, in addition, one chooses $a_0=0.70$A, $\epsilon_1=0.5\times10^{-12}$ erg, $r_1=1.3$A, then the curve (6) is obtained.

## VI. CONCLUDING REMARKS

In the model we have chosen to investigate for the $CO_2-H_2O$ system all collisions which may occur in a classical kinetic theory gas were considered. To make the problem tractable we were forced to postulate a spherically symmetric interaction potential, and consequently had to introduce the arbitrary parameter $\theta$, which is qualitatively a "steric factor." The magnitude of $10^{-3}$ assigned to it is reasonable for an acid-base gas reaction. The behavior with $\theta$ and with the $v$'s can be seen quite easily. Let $S$ be the slope of the curve (Fig. 7) at any point. $\delta$ and $S$ are proportional to $\theta^{\frac{1}{3}}$. They are almost proportional to $v_2$ and almost independent of $v_1$, since the term in $v_2$ is the leading term. In the one-term approximation, as illustrated by curve (6), $\delta$ and $S$ are proportional to $v_3$.

Between 350° and 700°, the indicated variations of the parameters changed the magnitude and slope by a factor of about 3. The experimental curve lies at the bottom of the range in magnitude. Its slope may be somewhat greater, although one could force a match within the experimental error by judiciously selecting extremes for the probable values of the data.

The nature of the results is determined by the potential energy functions $w(R)$ and $V_{10}(R)$, and separate and distinct approximations can be used to obtain each one. For example, a different value of $r_1$ can be chosen for each. $\delta$ is very sensitive to the values and slopes of these functions at the point $\bar{R}$. Much larger variations could then have been achieved by varying the parameters in such a way as to change these four quantities (values and slopes of the two functions at $\bar{R}$) one at a time.

For purposes of comparison we wish to call attention to an extension of Zener's one-dimensional model which appeared recently.[26] This study accounts for the high de-excitation probabilities induced by some impurities either because of their low masses or by "near resonance" energy transfers. However, the effects observed in gas mixtures for which the interaction potential between the components has a deep minimum at a "bonding" distance, cannot be treated by the method of Schwartz, Slawsky, and Herzfeld, since a sufficiently simple solution of the Schrödinger equation for the motion of a massive particle in such a potential is not available.

## APPENDIX

Let $\xi$ be symbolic for the totality of vibrational and rotational coordinates of both molecules, and let $d\xi$ be the element of volume in this vibration-rotation space.

Let $\{\psi_M(\xi)\}$, $M=1,\cdots,G$, be the $G$ orthonormal, degenerate wave functions belonging to a given vibration-rotation energy of the pair of molecules.

Let $V(\xi,\mathbf{R})$ be the interaction potential between the

[26] Schwartz, Slawsky, and Herzfeld, J. Chem. Phys. **20**, 1591 (1952).

two molecules, where **R** is the separation of their centers of mass.

Consider

$$V_{MM}(\mathbf{R})=\int \psi_M^*(\xi)V(\xi,\mathbf{R})\psi_M(\xi)d\xi$$

and

$$w=(1/G)\sum_{M=1}^{G} V_{MM}(\mathbf{R}).$$

It will be shown that $w$ is independent of the direction of **R**.

The rotation variables of the system are measured with respect to a certain space-fixed set of axes, **I**, **J**, **K**. Let $\alpha$, $\beta$ be the polar and azimuthal angles of **R** in this coordinate system.

Now consider a second set of coordinates axes, **I'**, **J'**, **K'**, which is rotated with respect to the first, and in which **J'** lies along **R**. Let $\xi'$ be symbolic for the vibration-rotation coordinates of the molecules in this system of axes. The coordinates $\xi$ are functions of $\xi'$ and of $\alpha$ and $\beta$. In the above, integral which defines $V_{MM}(\mathbf{R})$, change the variables of integration from $\xi$ to $\xi'$. Then

$$d\xi=d\xi'$$

because the one set of variables is derived from the other by a rotation of the coordinate system. Furthermore, writing **R** explicitly as $R$, $\alpha$, $\beta$,

$$V(\xi,R,\alpha,\beta)=V(\xi',R,\pi/2,\pi/2)$$

since $V$ is invariant to a change of coordinates, and **J'** was defined to lie along **R**. Then

$$V_{MM}(\mathbf{R})=\int \psi_M^*(\xi)V(\xi',R,\pi/2,\pi/2)\psi_M(\xi)d\xi',$$

with the limits of the integration the same as when $\xi$ was the integration variable.

Now, the rotation ($S$, say) which takes **I'**, **J'**, **K'** into **I**, **J**, **K** must be a member of the group of the Schrödinger equation for $\psi_M(\xi')$, since $S$ is merely an external rotation of axes. Therefore,[27]

$$\psi_M(\xi)=\sum_{\mu=1}^{G} D_{\mu M}(S)\psi_\mu(\xi').$$

The rotation $S$ depends on $\alpha$ and $\beta$, and so does the matrix $D(S)$. $D(S)$ is unitary[28] since $S$ is an orthogonal transformation and the eigenfunctions $\psi_\mu(\xi')$, for different $\mu$, were specified to be orthogonal.

[27] E. Wigner, *Gruppentheorie* (Vieweg, Braunschweig, 1931), p. 116.

[28] Reference 27, p. 119.

Substituting this last expression into the equation for $V_{MM}(\mathbf{R})$,

$$V_{MM}(\mathbf{R})=\sum_\mu\sum_{\mu'} D_{\mu M}^*(S)D_{\mu' M}(S)\times\int\psi_\mu^*(\xi')V(\xi',R,\pi/2,\pi/2)\psi_{\mu'}(\xi')d\xi'$$

$$=\sum_\mu\sum_{\mu'} D_{\mu M}^*(S)D_{\mu' M}(S)v_{\mu\mu'}(R)$$

where the matrix $v(R)$ is defined by

$$v_{\mu\mu'}(R)=\int\psi_\mu^*(\xi)V(\xi,R,\pi/2,\pi/2)\psi_{\mu'}(\xi)d\xi.$$

Thus, the dependence of $V_{MM}(\mathbf{R})$ on the angles $\alpha$, $\beta$ has been removed from $V$ itself and put, instead, into the elements of the transformation matrix $D(S)$.

Now, since $D(S)$ is unitary,

$$D_{\mu M}^*(S)=D_{M\mu}^{-1}(S)$$

and therefore

$$V_{MM}(\mathbf{R})=\sum_\mu\sum_{\mu'} D_{M\mu}^{-1}(S)D_{\mu' M}(S)v_{\mu\mu'}(R)=[D^{-1}(S)v(R)D(S)]_{MM}.$$

Then

$$w=(1/G)\sum_M V_{MM}(\mathbf{R})=(1/G)\ \text{trace}\,[D^{-1}(S)v(R)D(S)]=(1/G)\ \text{trace}\ v(R).$$

Thus, $w=w(R)$ is independent of $\alpha$ and $\beta$, as was to be shown.

This result can be readily interpreted physically. Imagine the case in which there is no coupling between the vibrational and rotational motions of the molecules, and in which the degeneracy arises only from the spatial degeneracy of the rotational states. $V_{MM}(\mathbf{R})$ is the expectation value, over all $\xi$, of the potential $V(\xi,\mathbf{R})$. The latter quantity depends only on the relative orientation of the two molecules, and every possible relative orientation is reached as $\xi$ (for any fixed **R**) varies over the entire space to which it has access. Hence, if in the averaging process that defines $V_{MM}(\mathbf{R})$, equal weight were given to every region of $\xi$ space, the average would certainly be independent of the direction of **R**. But since the rotational states are degenerate, the weighting function $\psi_M^*(\xi)\psi_M(\xi)$ gives preference to a certain unique orientation of the molecules, this unique orientation depending on the direction of **R**. When the average over $M$ is taken, in defining $w$, this uniqueness is destroyed, all orientations are again given equal weight, and the average is again independent of the direction of **R**.

# The Preparation of Chromium-51 of High Specific Activity*

GARMAN HARBOTTLE, *Chemistry Department, Brookhaven National Laboratory, Upton, Long Island, New York*

AND

ALFRED G. MADDOCK, *Radiochemical Laboratory, Department of Chemistry, Pembroke Street, Cambridge, England*

(Received July 1, 1953)

A procedure is given whereby chromium-51 of high specific activity may be separated from pile-bombarded potassium chromate.

## INTRODUCTION

IN this paper we wish to describe a method for the preparation of chromium-51 of high specific activity. Chromium-51 is a $K$-capturing isotope of 26 days half-life. It emits vanadium $K$ x-rays (energy about 5 kev) and gamma rays, the latter occurring in about 8 percent of the transitions and having an energy of 325 kev. It is formed by radiative neutron capture in chromium-50 with an isotopic cross section of 16 barns. However, $Cr^{50}$ is present in natural chromium to the extent of only 4.4 percent.[1]

The method which we employed utilizes the Szilard-Chalmers reaction[2] in potassium chromate, and the active chromium is separated in the trivalent form. Reagent grade material was used without further purification, and contained about 5 parts per million of trivalent chromium, determined on blank samples treated in the same way as the active material. The salt, wrapped in aluminum foil, was bombarded in the Brookhaven nuclear reactor in the water-cooled irradiation hole. At the bombardment site the thermal neutron flux was $3.5\times10^{12}$ neutrons per square centimeter per second, and the temperature $32\pm3$°C. Preliminary bombardments, which demonstrated the feasibility of the method and established some of the factors governing the yield, were carried out in the Harwell Reactor of the Atomic Energy Research Establishment of England. These bombardments were made at a flux of about $3.5\times10^{11}$ neutrons/cm$^2$ sec and 37°C, and the salt was sealed in silica ampoules in vacuum.

## PROCEDURE FOR THE SEPARATION OF ENRICHED CHROMIUM-51

The 12.4-hour potassium-42 activity in the bombarded salt was allowed to decay for about a week, and then the irradiated material was dissolved in approximately one normal sulfuric acid; 100 ml of acid was used per 10 grams of salt. Twenty milligrams of aluminum carrier was added (as aluminum nitrate). Aluminum hydroxide, which carries trivalent chromium, was precipitated by the addition of concentrated ammonium hydroxide, centrifuged down and washed four times by centrifugation with water containing a trace of ammonia. The aluminum hydroxide was then dissolved in about 10 ml of $2N$ sulfuric acid, the solution diluted three times, and the aluminum hydroxide reprecipitated with ammonia and washed once with water. This cycle of reprecipitation was repeated a total of four times and served to free the precipitate completely of hexavalent chromium. An additional ten milligrams of aluminum was added after the second reprecipitation.

Finally, the aluminum hydroxide was dissolved in a caustic solution prepared by the addition of five or six pellets of sodium hydroxide to ten milliliters of water and the solution oxidized by the addition of about 100 mg of sodium peroxide. The peroxide was destroyed by warming on a hot water bath. The solution now contained only aluminum, chromium (as chromate), and sodium hydroxide, and the chromium was estimated colorimetrically by the use of the absorption band shown by chromate in basic solution at 366 m$\mu$ (molar extinction coefficient $\epsilon=4670$). Aluminum does not interfere in this determination. If it is desired to obtain the chromium free of aluminum, the solution may be adjusted to $p$H 2.5 and lead chromate precipitated and centrifuged out.

## DETERMINATION OF ABSOLUTE DISINTEGRATION RATE OF CHROMIUM-51

Aliquot portions of solutions containing the enriched $Cr^{51}$ were evaporated on foils, and the emitted x-rays were counted in a proportional counter of known geometry. The counter was filled with two atmospheres of argon and 0.2 atmosphere of methane, and was operated at 2900 volts. The counter tube was of such dimensions that all x-rays passing the window were absorbed. The pulses from the counter were amplified and analyzed by a sliding-channel pulse-height analyzer of Oak Ridge design, constructed by the Brookhaven Electronics Division. The x-ray counting rate was obtained by numerically summing the area under the x-ray peak, and this figure was corrected for geometry,

* A portion of this work was performed under the auspices of the U. S. Atomic Energy Commission.

[1] (a) "Nuclear Data" published by National Bureau of Standards (1950). (b) W. S. Lyon, Phys. Rev. 87, 1126 (1952).

[2] (a) The Szilard-Chalmers method and its applications are reviewed by G. Friedlander and J. W. Kennedy, *Introduction to Radiochemistry* (John Wiley and Sons, Inc., New York, 1949), p. 252, and *Radioactivity Applied to Chemistry*, edited by A. C. Wahl and N. A. Bonner (John Wiley and Sons, Inc., New York, 1951), p. 245 ff. (b) A method similar to ours has been described by Kahn, Freedman, and Bryant, AECU 2329, Nuclear Science Abstracts 7, 1089 (February, 1953). (c) A. G. Maddock and J. Green, Nature 164, 788 (1949).

absorption by air, and absorption by the beryllium window of the counter. The disintegration rate was obtained by an additional correction for the fluorescence yield.[3]

## EXPERIMENTAL RESULTS

Two bombardments were made in which the above procedure was followed. The treatment of the samples differed only in that for the first bombardment nitric acid replaced sulfuric acid throughout. Subsequent experiments showed that, in artificial mixtures of trivalent chromium with potassium chromate, the former was completely recovered with either acid. Detailed experimental results are shown in Table I.

## FACTORS INFLUENCING THE YIELD AND SPECIFIC ACTIVITY

It was observed in the series of bombardments carried out at Harwell that the percentage of activity separable decreased with increasing bombardment time. It is thus apparent that there is an optimum bombardment time and that for long times the specific activity will be reduced both by increasing decomposition of the sample and by the radiation backreaction or recombination.[4] Bombardments of one to three days at a flux of $3.5\times10^{12}$ neutrons/cm$^2$ sec are satisfactory, and longer bombardments could probably be made at lower fluxes.

It had been noticed earlier by Maddock and Green[2c] that a thermal recombination resulting in decreasing yield begins to take place at approximately 100°C.[5] In one of our experiments, a sample of potassium chromate was bombarded in the Brookhaven reactor for one day at a flux of $3\times10^{12}$ neutrons/cm$^2$ sec and temperature 180°C, and only 0.8 percent of the activity was recoverable. Thus the temperature of the bombardment site is important, and should be maintained below 50–60° Celsius.

Other experiments in the Harwell series indicated that the percentage recovery is fairly independent of the *p*H of the solution in which the irradiated salt is dissolved. The temperature of the solution is likewise unimportant.

TABLE I. Szilard-Chalmers separation in potassium chromate.

| | Sample number 1 | Sample number 2 |
|---|---|---|
| Weight of $K_2CrO_4$ bombarded, grams | 15.4 | 10 |
| Activity recovered,[a] millicuries | 17 | 17 |
| Wt. of $Cr^{+++}$ recovered, milligrams | 0.43 | 0.42 |
| Specific activity,[a] millicuries/mg | 39 | 40 |
| Total $Cr^{51}$ produced,[b] millicuries | 115 | 160 |
| Enrichment[c] | 1400 | 680 |
| Over-all recovery of activity, percent | 14.8 | 10.6 |
| Bombardment time, hours | 31 | 66.5 |
| Temperature, centigrade | 32° | 32° |
| Flux, neutrons/cm$^2$ sec | $3.5\times10^{12}$ | $3.5\times10^{12}$ |
| Decomposition rate, parts per million/hour | 2.8 | 2.1 |
| Acid used in separation process | $HNO_3$ | $H_2SO_4$ |

[a] Corrected to the time of removal from the pile.
[b] Approximate value calculated from capture cross section, flux, and time of irradiation.
[c] Defined as ratio of specific activity of enriched fraction to that of over-all material.

## DISCUSSION

The results presented in Table I indicate that potassium chromate has an exceptional resistance to radiation decomposition in the pile. It is also interesting to note that our enriched chromium having a specific activity of around 40 millicuries/mg contains about 2500 inactive atoms to one radioactive.

## ACKNOWLEDGMENT

One of the authors (G.H.) wishes to thank the Oak Ridge Institute for Nuclear Studies for the grant of an Atomic Energy Commission Postdoctoral Fellowship, which permitted many of the foregoing experiments to be carried out.

[3] Broyles, Thomas, and Haynes, Phys. Rev. **89**, 715 (1953).

[4] The radiation-recombination effect has been noted in other systems by (a) Boyd, Cobble, and Wexler, J. Am. Chem. Soc. **74**, 237 (1952); (b) J. W. Cobble and G. Boyd, ORNL 1117 (March 17, 1952); (c) R. R. Williams, J. Phys. and Colloid Chem. **52**, 603 (1948); (d) Cleary, Hamill, and Williams, J. Am. Chem. Soc. **74**, 4675 (1952).

[5] For other systems in which thermal recombination has been observed, see references 4(b) and 4(d). Thermal recombination has also been noted in the following systems: Potassium permanganate, A. H. W. Aten, Jr., and J. B. M. Van Berkum, J. Am. Chem. Soc. **72**, 3273 (1950) and Rieder, Broda, and Erber, Monatsh. Chemie. **81**, 657 (1950). Cobaltic trisethylenediamine nitrate, A. Zuber (private communication).

# Dissociation, Chemical Exchange, and the Proton Magnetic Resonance in Some Aqueous Electrolytes*

H. S. GUTOWSKY AND A. SAIKA
*Noyes Chemical Laboratory, University of Illinois, Urbana, Illinois*
(Received February 26, 1953)

The position of the proton magnetic resonance is concentration dependent in aqueous solutions of electrolytes yielding hydrogen containing ions. Chemical exchange averages the chemical shifts in the proton resonance position over the different chemical species. The averaged shifts observed are correlated with dissociation of the solute, and evidence is obtained in very concentrated solutions for the incomplete dissociation of $HNO_3$, $HClO_4$, and $H_2SO_4$ and for the formation of ion pairs of $Na^+OH^-$. A theoretical analysis of the relation between the magnetic absorption line shape and the chemical exchange frequency suggests that rather short chemical lifetimes can be measured; at least one can infer from the appearance of a single or complex resonance that the average lifetime is greater or less, respectively, than a determinable value in a range about $10^{-2}$ to $10^{-4}$ sec.

## INTRODUCTION

A VARIETY of experimental[1,2] and theoretical papers[3,4] has appeared recently describing the dependence of nuclear magnetic resonance frequencies upon the electronic environment of the nucleus. In ethanol Arnold and Packard[1] found the position of the proton resonance of the hydroxyl group to be temperature and concentration dependent. An interesting and suggestive analysis of their data was made by Liddel and Ramsey[4] in terms of association of the hydroxyl groups by hydrogen bonding. We have found the proton resonance to be concentration dependent in aqueous solutions of some typical acids and other electrolytes and obtained results which may be correlated with the dissociation of the electrolyte.

In these solutions the proton resonance was found to be single. This endorses the existence of fast exchange of the protons among the water molecules, undissociated solute molecules, and proton containing ions. Otherwise individual proton resonance lines would appear at positions corresponding to the different electronic environment of each chemical species.[5] The transition region from a complex to a single resonance line depends upon the frequency separation of the components in the complex line, the lifetimes of the different chemical states and indirectly upon the lifetimes of the nuclear spin states.[6] The position of the single line is a number average of the resonance frequencies of the nuclei in the absence of the chemical exchange. Slichter[7] has discussed analogous spin relaxation effects in the structure of the multiplet resonances which arise from coupling of nuclear spins by the valence electrons. The analysis is extended to determine the critical frequency of chemical exchange, which is the frequency separation of the resonance lines in the absence of the exchange, the order of $10^2$ to $10^3$ $sec^{-1}$ for the solutions under our experimental conditions. The possibility of determining fast chemical exchange rates in this manner is considered. At least an upper or lower bound can be assigned readily, depending upon whether a single or multiple resonance is found.

## EXPERIMENTAL

The apparatus and procedures have been described in detail elsewhere.[8] The chemical shifts were measured as $\delta = 10^5(H_{H_2O} - H_{sample})/H_{H_2O}$, where $H_{H_2O}$ and $H_{sample}$ are the applied magnetic fields required for resonance, at fixed frequency, of protons in pure water and in the solutions, respectively. A permanent magnet with a field of about 4180 gauss adjustable over a small range was used. In these experiments the maximum experimental error in $\delta$ was about $\pm 0.02$, corresponding to errors of $\pm 0.8$ milligauss; this error was introduced mainly by the interchange of samples in the rf coils, in spite of precautions taken to prevent changes in position.

The acids on which the proton shift measurements were made included hydrochloric, nitric, perchloric, and sulfuric, all strong acids and acetic acid as an example of a weak acid. The solutions of various concentration were obtained by diluting the cp acids of the highest concentrations commercially obtainable. Sodium and potassium hydroxide were chosen as typical strong bases; their solutions and those of several salts were prepared from the cp solids. The samples were sealed in thin-walled capillary tubing, of about 1-mm bore. The measurements were made at room temperature.

## ANALYSIS OF EXPERIMENTAL DATA

### Acetic Acid

The results obtained with acetic acid are the simplest to interpret. The proton resonances in the solutions

* This work was assisted by the U. S. Office of Naval Research.
[1] J. T. Arnold and M. E. Packard, J. Chem. Phys. **19**, 1608 (1951).
[2] L. H. Meyer and H. S. Gutowsky, J. Phys. Chem. **57**, 481 (1953), and prior work cited there.
[3] N. F. Ramsey, Phys. Rev. **78**, 699 (1950); **86**, 243 (1952).
[4] U. Liddel and N. F. Ramsey, J. Chem. Phys. **19**, 1608 (1951).
[5] Many such complex lines have been found in covalent compounds with non-equivalent sites in the same molecule where chemical exchange is slow. For examples see Gutowsky, McCall, McGarvey, and Meyer, J. Am. Chem. Soc. **74**, 4809 (1952).
[6] Bloembergen, Purcell, and Pound, Phys. Rev. **73**, 679 (1948).
[7] Gutowsky, McCall, and Slichter, J. Chem. Phys. **21**, 279 (1953).
[8] Gutowsky, Meyer, and McClure, Rev. Sci. Instr. 24, 644–652 (1953).

were double. One of the lines showed no concentration dependence within experimental error; it was assigned to the protons in the methyl group according to the 3:1 intensity ratio in the glacial acid. We refer here only to the protons in the carboxylic acid group and the water, which produced the concentration dependent line. The equilibrium dissociation of the acetic acid is negligible over the concentration range in these experiments; however, the dissociation provides a mechanism for the rapid exchange of protons between the HAc and the $H_2O$. Thus, the concentration dependence of the resonance can result from an average of the absorption over the two chemical states. That is, the chemical shift will be given by

$$\delta = p_1\delta_{HAc} + p_2\delta_{H_2O}, \tag{1}$$

where $p_1$ and $p_2$ are the fractions of protons in the acid and the water, and $\delta_{HAc}$ and $\delta_{H_2O}$ are the proton

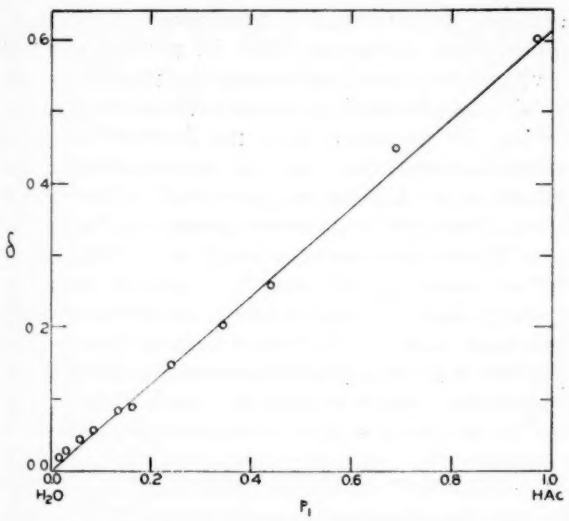


FIG. 1. The concentration dependence of the chemical shift of the proton magnetic resonance in aqueous solutions of acetic acid. $p_1$ is the fraction of protons in HAc.

resonance shifts in pure HAc and $H_2O$, respectively. The measured shifts are referred to water, or $\delta_{H_2O}\equiv 0$, so

$$\delta_{obs} = p_1\delta_{HAc}. \tag{2}$$

If $N_1$ and $N_2$ are the mole fractions of acetic acid and water, respectively, in the solutions, $p_1$ is computed simply as

$$p_1 = \frac{N_1}{N_1+2N_2} = \frac{N_1}{2-N_1}. \tag{3}$$

In Fig. 1, the observed values of $\delta$ are plotted against $p_1$. The relationship is linear, as predicted by Eq. (2) with $\delta_{HAc}=0.61$.

### Hydrochloric, Nitric, and Perchloric Acids

The equilibria in aqueous solutions of these acids may be written schematically as

$$\begin{array}{ccccccc} HA & + & H_2O & \rightleftarrows & H_3O^+ & + & A^- \\ N_1(1-\alpha) & & N_2-\alpha N_1 & & \alpha N_1 & & \alpha N_1, \end{array} \tag{4}$$

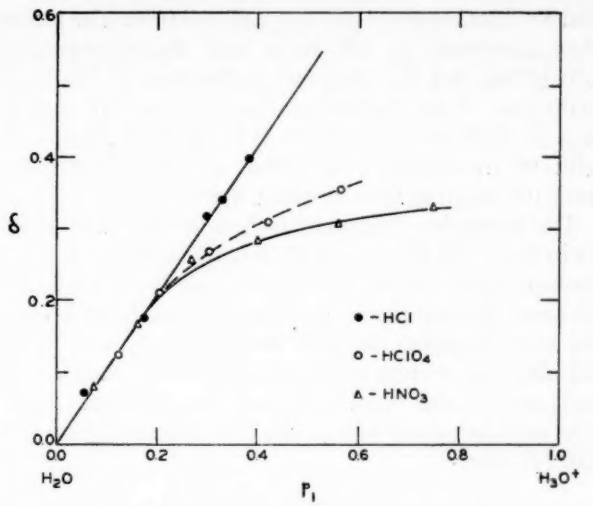


FIG. 2. The concentration dependence of the proton chemical shift in aqueous solutions of some strong, monobasic acids. $p_1$ is the fraction of protons present in $H_3O^+$, assuming complete conversion of the acid proton to $H_3O^+$.

where $N_1$ and $N_2$ are the stoichiometric mole fractions of acid and water, respectively, and $\alpha$ is an *apparent* degree of dissociation. If complete dissociation is *assumed*, then with $N_1<N_2$ the position of the proton resonance is determined by averaging $\delta$ over the hydronium ions and water molecules. This gives a result similar to Eq. (1),

$$\delta = p_1\delta_{H_3O^+} + p_2\delta_{H_2O}, \tag{5}$$

and as before, $\delta_{H_2O}\equiv 0$, so as a final representation for complete dissociation, we have

$$\delta_{obs} = p_1\delta_{H_3O^+}. \tag{6}$$

The fraction $p_1$ of protons in hydronium ions is obtained as

$$p_1 = \frac{3N_1}{2(N_2-N_1)+3N_1} = \frac{3N_1}{2-N_1}, \tag{7}$$

for $N_1 \leqslant \frac{1}{2}$.

The $\delta$'s observed for the three acids are plotted against $p_1$ in Fig. 2. For $p_1$ up to about 0.2 (7 normal acid), the data fall along a single straight line. The $\delta$'s for HCl continue to be linear to the maximum concentration investigated, $p_1=0.38$. If the straight line portion of the data is extrapolated to $p_1=1$, then by Eq. (6) one obtains the chemical shift of the hydronium ion, $\delta_{H_3O^+}=1.05\pm 0.05$. This value is of interest in connection with the nature of the hydronium ion. Combining theoretical calculations[3] for $H_2$ gas with experimental observations[9] of the chemical shifts in $H_2O$ and $H_2$, and defining $\delta_{H_2O}\equiv 0$, then $\delta_{H^+}=2.70$, where $H^+$ represents the bare proton. If the acid solutions consisted of bare protons (unsolvated) which exchanged rapidly with the hydrogen atoms in the water molecules, then for a solution of stoichiometric composition $H_3O^+$, we would

[9] H. S. Gutowsky and C. J. Hoffman, J. Chem. Phys. **19**, 1259 (1951).

find $\delta=(2\delta_{H_2O}+\delta_{H^+})/(2+1)=2.70/3=0.90$. The rather close agreement of this value with the experimental $1.05\pm0.05$, and the observed equivalence of the three hydrogens of the hydronium ion in crystals[10] suggest that in $H_3O^+$ each of the O−H bonds is about $\frac{1}{3}$ ionic with the remaining $\frac{2}{3}$ character relatively unchanged from the bonding type in water itself.

The increasing deviations from a straight line of the $\delta$'s in Fig. 2 for $HNO_3$ and $HClO_4$ at the higher concentrations result no doubt from some variety of interaction between the acid anions and the protons. If we assume the over-simplified model of incomplete dissociation to calculate the average proton chemical shift, then a term representing the contribution of the "undissociated" acid must be added to Eq. (6). Using the equilibrium of Eq. (4) gives

$$\delta_{obs}=\alpha p_1\delta_{H_3O^+}+(1/3)(1-\alpha)p_1\delta_{HA}, \qquad (8)$$

where $\delta_{HA}$ is the proton shift in the undissociated acid, and $p_1$ is still defined by Eq. (7). Strictly speaking, Eq. (8) should be applied to the whole range of concentration. However, $\alpha$ must be the order of 0.85 or less before deviations from Eq. (6) are outside of experimental error, and this occurs only at high acid concentrations.

TABLE I. Apparent degrees of dissociation of $HNO_3$.

| $p_1$ | Normality | $\delta_{obs}$ | $\alpha$ | $K\beta$ [a] |
|---|---|---|---|---|
| 0.27 | 8.3 | 0.25 | 0.84 | 230 |
| 0.40 | 11.1 | 0.28 | 0.59 | 265 |
| 0.56 | 13.4 | 0.31 | 0.42 | 415 |
| 0.75 | 15.7 | 0.33 | 0.29 | 705 |

[a] Computed as in reference 11. As $N\to0$, $\beta\to1$, the limiting value of $K\beta$ is a thermodynamic dissociation constant.

The instability of pure $HClO_4$ has discouraged the measurement of its $\delta_{HA}$. However, the $\delta$ of fuming $HNO_3$ (Sp. gr. 1.59) was observed to be 0.56. Taking this value to be $\delta_{HA}$, Eq. (8) can be used with $\delta_{H_3O^+}=1.05$ to evaluate the apparent degrees of dissociation $\alpha$ from the $\delta$'s observed at intermediate concentrations. Values computed in this manner are listed in Table I.

The results compare qualitatively with conclusions drawn from the Raman line intensities of the nitrate ion in the concentrated acids.[11] If our values of $\alpha$ are used in the same manner to estimate dissociation constants, the $K\beta$ values in Table I are obtained, the logs of which extrapolate at infinite dilution to a very approximate value of $K$, about $2\times10^2$, a thermodynamic dissociation constant, for which the Raman determined value is $K=21$. The approximations and assumptions in our calculation are severe, including: (a) The evaluation of $\delta_{H_3O^+}$ indirectly and by a long extrapolation, (b) The sensitivity of the values of $\alpha$ to even relatively small errors in $\delta$, (c) The use of $\delta=0.56$ from fuming $HNO_3$ as that of "molecular" nitric acid, (d) Another long extrapolation, from 8 normal to dilute acid, to obtain K. Even so, there is a significant difference between these results and other evidence on the existence of undissociated acid molecules in concentrated solutions.[12] For instance, the Raman data on $HNO_3$ show[11] detectable deviations from complete ionization at concentrations as low as 3 normal, while the $\delta$ values for $HNO_3$ do not diverge from linearity till about 6 normal. Also, in HCl at concentrations greater than 9 normal, a diffuse Raman line appears[12] at 2630 $cm^{-1}$ characteristic of molecular HCl, while the $\delta$ values for HCl remain linear to our most concentrated solution, 12 normal.

The uncertainties inherent in the terms ionized and undissociated have been clearly pointed out.[11,12] The Raman data and the chemical shifts offer independent operational definitions of "dissociation," so it is not surprising that the results differ for the two methods. The vibrational period, which is the limiting lifetime of a *molecule* in the Raman experiment is the order of $10^{-12}$ to $10^{-14}$ sec. On the other hand, the limiting lifetime of a *molecule* in the nuclear magnetic resonance experiment is related to the Larmor frequency and is the order of $10^{-6}$ sec. Therefore, what would appear as a "molecule" to the Raman spectroscopist could be a "sticky collision" or something else equally vague in the radio-frequency sense. The importance of the different results would seem to lie less in their difference than in their similarity; both experiments demonstrate the existence of significant concentrations of "undissociated molecules" of the strong acids in concentrated solutions.

## Sulfuric Acid

In this case, the situation is more complicated than in the previous cases, because sulfuric acid is dibasic. The second dissociation is considered to be the order of a few percent[13] in the concentration range investigated here, so one might attempt an analysis taking into account only the first equilibrium. Defining $\alpha$ as the apparent degree of the first dissociation, and with $H_2SO_4$ and $H_2O$ stoichiometric mole fractions of $N_1$ and $N_2$, there will be the following equilibrium concentrations:

$$\begin{array}{ccccc} H_2SO_4 & + & H_2O & \rightleftarrows & H_3O^+ + HSO_4^- \\ N_1(1-\alpha) & & N_2-N_1\alpha & & N_1\alpha \quad N_1\alpha. \end{array} \qquad (9)$$

The average proton resonance shift, referred to water is given as

$$\delta_{obs}=N_1(1-\alpha)\delta_{H_2SO_4}+(3/2)N_1\alpha\delta_{H_3O^+}+(1/2)N_1\alpha\delta_{HSO_4^-}. \qquad (10)$$

[10] Kakiuchi, Shono, Komatsu, and Kigoshi, J. Chem. Phys. **19**, 1069 (1951); J. Phys. Soc. Japan **7**, 102 (1952).

[11] O. Redlich and J. Bigeleisen, J. Am. Chem. Soc. **65**, 1883 (1943).

[12] O. Redlich, Chem. Revs. **39**, 333 (1946) gives an interesting review and a good bibliography.

[13] H. S. Harned and B. B. Owen, *The Physical Chemistry of Electrolytic Solutions* (Reinhold Publishing Company, New York, 1950), second edition, p. 609, summarize the evidence for undissociated molecules of strong electrolytes, including $H_2SO_4$. See also T. F. Young, Record Chem. Progr. (Kresge-Hooker Sci. Lib. **12**, 81 (1951)).

In order to analyze the data and calculate $\alpha$, both $\delta_{H_2SO_4}$ and $\delta_{HSO_4^-}$ are required. The proton shifts were measured for fuming sulfuric acid containing 30 percent and 15 percent excess $SO_3$, and both solutions were found to have $\delta=0.61$, indicating that the $SO_3$ doesn't affect the $\delta$ value of the $H_2SO_4$ and favoring the plausibility of assigning $\delta_{H_2SO_4}$ the value of the fuming acid. An estimate of $\delta_{HSO_4^-}$ can be attempted from the $\delta$ values observed in the more dilute solutions, where $\alpha$ might be considered unity. In this region, it would be predicted that

$$\delta_{obs}=N_1[(3/2)\delta_{H_3O^+}+(1/2)\delta_{HSO_4^-}]. \quad (11)$$

The experimental values of $\delta$ are plotted against $N_1$ in Fig. 3. At low concentrations, the data are linear as predicted by Eq. (11). However, the slope, $d\delta/dN_1 \leqq 3.30$, in conjunction with $\delta_{H_3O^+}=1.05$, gives a value from Eq. (11) for $\delta_{HSO_4^-}$ of 3.45. This large a value is physically unreasonable; the bare proton has the largest known value 2.70, and even though larger values seem theoretically possible[3] the range of other experimental results herein suggests a figure between 0.5 and 1.5.

If the acid in the less concentrated range dissociated to $SO_4^=$ and $H_3O^+$, the proton shift would be $\delta_{obs}=3N_1\delta_{H_3O^+}$. On this basis the observed slope gives $\delta_{H_3O^+}=1.10$, in good agreement with the $1.05\pm0.05$ obtained from the monobasic acids. But the straight line section extends to concentrations as high as 4 to 5 normal, while the Raman data[13] suggest materially incomplete $HSO_4^-$ dissociation at concentrations half as great. Also, if $\delta_{HSO_4^-}$ is assumed to be about 1.5, and $\delta_{H_2SO_4}$ is taken as 0.61, application of Eq. (10) to compute $\alpha$ gives values considerably larger than those from the Raman experiments. In the absence of a better value for $\delta_{HSO_4^-}$ little more can be said[14] regarding the results except that the proton shift "degrees of dissociation" are larger than those from the Raman data,[13] as was found for the monobasic strong acids.

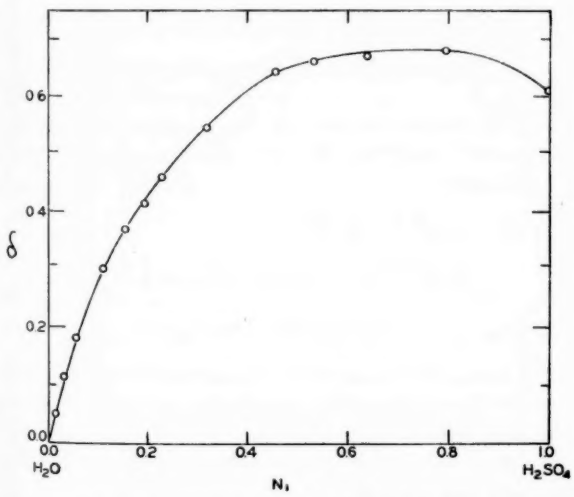


FIG. 3. The dependence of the proton chemical shift upon the mole fraction $N_1$ of sulfuric acid in aqueous solution.

[14] The proton shift was observed in a saturated solution of $NaHSO_4$; the result is compatible with $\delta_{HSO_4^-}\sim 1$, but dissociation again prevents determining an accurate value.

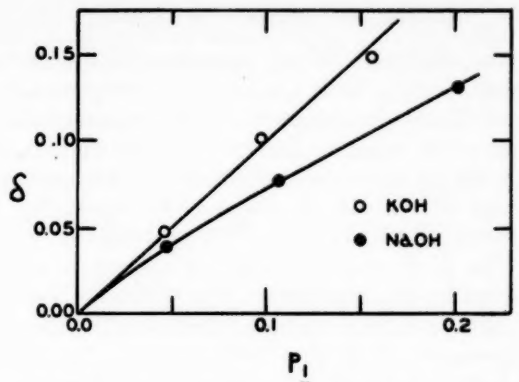


FIG. 4. The concentration dependence of the proton chemical shift in aqueous solutions of sodium and of potassium hydroxide. $p_1$ is the fraction of protons present in $OH^-$, assuming complete dissociation of the base.

## Sodium and Potassium Hydroxide

The proton shifts observed in NaOH and KOH solutions are given in Fig. 4. The range of observation was limited by the solubility and the shifts are rather small. However, the shifts do fall along *separate*, fairly smooth lines, plotted against $p_1$, the fraction of protons in $OH^-$. The limiting slopes in dilute solutions are the same within experimental error for NaOH and KOH, giving an extrapolated value for $\delta_{OH^-}$ of about 1.0. At higher concentrations, the $\delta$ values for the NaOH solutions fall significantly below those of KOH, implying the formation of $Na^+OH^-$ ion pairs. The smaller size of $Na^+$ compared to $K^+$ would lead to larger interionic forces in the NaOH solutions than in the KOH, in qualitative agreement with experiment.

## Other Solutions

We measured the positions of the proton resonances in saturated solutions of sodium chloride, potassium chloride, potassium nitrate, and potassium sulfate but observed no shifts from pure water. This substantiates the assumption implicit in the discussion above that the hydration of ions or molecules does not measurably affect the resonance position of the protons involved. In fact, the formation of an hydronium ion may be regarded as an extreme case of hydration, and there the deviation ascribable to hydration is 0.15, a rather small effect.[15] The proton resonances in solutions of ammonium hydroxide and ammonium chloride were found to be single and concentration dependent, showing the existence of exchange between all of the various protons.

[15] The formation of acids from anhydrides by adding $H_2O$, e.g., $N_2O_5+H_2O\rightarrow 2HNO_3$, is a chemical reaction rather than a simple hydration, and such reactions produce relatively large changes in $\delta$.

## CHEMICAL EXCHANGE EFFECTS

In the discussion of the experimental results it is assumed that a "fast exchange" of protons among different chemical states gives a single resonance line, an average of the separate lines there would be if the exchange did not occur. A detailed analysis of the chemical exchange effects can be obtained by modifying the treatment[7] of the spin multiplet splittings to fit this case. The Bloch equations[16] for the nuclear magnetization describe the appearance of a resonance line. The effect of the chemical exchange is obtained by including the chemical shift in the Bloch equations and seeing what happens when the chemical exchange occurs.

### Two Chemical Species

Suppose two chemical species A and B have proton resonances shifted by $\delta_{obs}$. Choosing their average resonance field $H_0$ as a reference, the chemical shift in angular frequency becomes $\delta\omega=\gamma H_0\delta_{obs}$, where $\gamma$ is the nuclear gyromagnetic ratio. Inclusion of the chemical shift in the Bloch equations gives the same modification as before, Eq. (34) in reference 7. The proton magnetization in the $x-y$ plane of species A and B is given as $M_A\equiv u_A+iv_A$ and $M_B\equiv u_B+iv_B$. From Eq. (34), $M_A$ and $M_B$ satisfy the equations

$$\frac{dM_A}{dt}+\left[\frac{1}{T_2}-i\left(\Delta\omega+\frac{\delta\omega}{2}\right)\right]M_A=-i\omega_1M_0,$$

and (12)

$$\frac{dM_B}{dt}+\left[\frac{1}{T_2}-i\left(\Delta\omega-\frac{\delta\omega}{2}\right)\right]M_B=-i\omega_1M_0,$$

where $\omega_1=\gamma H_1$, $H_1$ is the strength of the applied rf magnetic field of frequency $\omega$, and $\Delta\omega=\gamma H_0-\omega$. $T_2$ is the inverse line-width parameter, assumed to be the same in A and B. As chemical exchange occurs, a given proton obeying initially the equation in $M_B$ will change over to that in $M_A$, and the problem is that of obtaining the proper average of the magnetization over the exchange.

Defining $\alpha_A=(1/T_2)-i(\Delta\omega+\delta\omega/2)$ and $\alpha_B=(1/T_2)-i(\Delta\omega-\delta\omega/2)$ for brevity, integration of Eq. (12) gives the time dependence of $M_A$ and $M_B$, excluding the effect of chemical exchange:

$$M_A(t)=-\frac{i\omega_1M_0}{\alpha_A}(1-e^{-\alpha_At})+M_A{}^0e^{-\alpha_At}, \quad (13)$$

where $M_A{}^0$ is the value of $M_A$ for a single proton entering the chemical state HA at $t=0$, and there is a similar equation in $M_B$. There will be a given number of these protons whose magnetization was $M_A{}^0$ at $t=0$. The chemical exchange causes the population of this group to decay exponentially in time. Assuming the protons in HA to be labeled, the kinetic expressions are

$$\mathrm{H^*A+HB\rightleftarrows HA+HB}$$

$$\frac{d(\mathrm{H^*A})}{dt}=-k_2(\mathrm{H^*A})(\mathrm{HB}), \quad (14)$$

and since (HB) is constant in time, the labeled H*A have an average life $\tau_A=1/k_2(\mathrm{HB})$. The exchange of HB is similar, with the average life depending upon the number of HA molecules (HA), $\tau_B=1/k_2(\mathrm{HA})$. Or, expressing the concentrations in proton fractions

$$\tau_A=\tau/p_B,$$
$$\tau_B=\tau/p_A, \quad (15)$$

where $\tau=1/\{k_2(\mathrm{HA+HB})\}$. The influence of self-exchange upon the magnetization is incorporated in the $T_2$ values. The probability that a given proton will have stayed in HA a time between $t$ and $t+dt$ is $(1/\tau_A)e^{-t/\tau_A}dt$. This result can be combined with Eq. (13) to compute $\langle M_A\rangle$, an average over the exchange of the magnetization of those protons with $M_A=M_A{}^0$ at $t=0$:

$$\langle M_A\rangle=\int_0^\infty\frac{e^{-t/\tau_A}}{\tau_A}M_A(t)dt=\frac{M_A{}^0}{1+\alpha_A\tau_A}-\frac{i\omega_1M_0\tau_A}{1+\alpha_A\tau_A}. \quad (16)$$

However, protons enter the HA state at different times with various initial values of $M$. Therefore, we need $\langle M_A{}^0\rangle$, the average of $M_A{}^0$ over all initial states, to find $\langle\bar{M}_A\rangle=\langle\langle M_A\rangle\rangle$, the value of $M_A$ averaged over the exchange *and* the initial states. Now the solution for $M_A$ joins continuously with that of $M_B$ as the exchange occurs, therefore the average initial value of $M_A{}^0$, i.e., $\langle M_A{}^0\rangle$ is simply the "completely averaged" value of $M_B$, i.e., $\langle\bar{M}_B\rangle$. Substituting these terms in Eq. (16) and writing the equivalent equation for state B, we have

$$\langle\bar{M}_A\rangle=(\langle\bar{M}_B\rangle-i\omega_1M_0\tau_A)/(1+\alpha_A\tau_A),$$
$$\langle\bar{M}_B\rangle=(\langle\bar{M}_A\rangle-i\omega_1M_0\tau_B)/(1+\alpha_B\tau_B). \quad (17)$$

The total magnetization $M$ is the sum of the two states, each weighted by the fraction of protons it contains; thus

$$M=p_A\langle\bar{M}_A\rangle+p_B\langle\bar{M}_B\rangle$$
$$=\frac{i\omega_1M_0[(\tau_A+\tau_B)+\tau_A\tau_B(\alpha_Ap_B+\alpha_Bp_A)]}{(1+\alpha_A\tau_A)(1+\alpha_B\tau_B)-1}. \quad (18)$$

In the resonance absorption experiments $v$ is observed where $v$ comes from the imaginary component of the total magnetization $M=u+iv$.

We shall consider the two extreme cases of very slow and very fast exchange:

*i. Very slow exchange* ($\tau_A$, $\tau_B\gg1/\delta\omega$).—In this case, Eq. (18) becomes

$$M=-i\omega_1M_0\left(\frac{p_A}{\alpha_A}+\frac{p_B}{\alpha_B}\right), \quad (19)$$

[16] F. Bloch, Phys. Rev. **70**, 460 (1946).

from which

$$v=-\frac{\omega_1 M_0}{T_2}\frac{p_A}{(1/T_2)^2+[\Delta\omega+(\delta\omega/2)]^2}+\frac{p_B}{(1/T_2)^2+[\Delta\omega-(\delta\omega/2)]^2}. \quad (20)$$

This gives two resonances with relative intensities of $p_A$ and $p_B$ at $\Delta\omega=-\delta\omega/2$ and $\Delta\omega=+\delta\omega/2$, as is observed in many organic compounds where the exchange is known to be slow.

*ii. Very fast exchange* ($\tau_A$, $\tau_B \ll 1/\delta\omega$).—In this case, Eq. (18) becomes

$$M=\frac{-i\omega_1 M_0}{\alpha_A p_A+\alpha_B p_B}, \quad (21)$$

from which

$$v=\frac{-\omega_1 M_0/T_2}{(1/T_2)^2+\Delta\omega-(\delta\omega/2)(p_B-p_A)^2}. \quad (22)$$

This corresponds to a single resonance, of unit intensity at $\Delta\omega=(\delta\omega/2)$. Or changing the point of reference to the resonance of A at $-\delta\omega/2$, the resonance will appear at $\Delta\omega=p_B\delta\omega$, as we assumed in the analysis of the experimental results.

The critical transition region for the average lifetimes of the chemical species may be found from Eq. (18). The simplest case is when $p_A=p_B$, in which event $\tau_A=\tau_B=2\tau$, the equation simplifies to Eq. (41)[17] of reference 7, and the transition occurs at $2\tau\delta\omega$ between 1 and 10. The shape of the resonance changes fairly sharply with $\tau$ in the transition region. This may be seen from Fig. 5 in which computed line shapes are given for $2\tau\delta\omega=1/100$, 1, 10, and 100.

### Three Chemical Species

Several of the systems investigated involved exchange among three different chemical species, e.g., $H_2O$, $H_3O^+$, and $HNO_3$. Calling the states A, B, and C, three equations analogous to Eq. (12) are obtained. The kinetic expressions include the exchange of each species with two other species. Thus, for labeled HA,

$$H^*A+HB+HC \rightleftarrows HA+HB+HC \quad (23)$$

$$\frac{d(H^*A)}{dt}=-k_{AB}(H^*A)(HB)-k_{AC}(H^*A)(HC)$$

$$=-\{k_{AB}(HB)+k_{AC}(HC)\}(H^*A), \quad (24)$$

and

$$\tau_A=1/\{k_{AB}(HB)+k_{AC}(HC)\}\equiv 1/(r_{12}+r_{13}) \quad (25)$$

with similar expressions for HB and HC. The boundary conditions applied in averaging the magnetization of each species over the initial states upon exchange must incorporate the relative amounts of the given species exchanging as well as the completely averaged values of the magnetization in the other two species. Thus, we find

$$\langle M_A{}^0\rangle=\frac{k_{AB}(HA)(HB)\langle\bar{M}_B\rangle+k_{AC}(HA)(HC)\langle\bar{M}_C\rangle}{k_{AB}(HA)(HB)+k_{AC}(HA)(HC)}$$

$$=\tau_A(r_{12}\langle\bar{M}_B\rangle+r_{13}\langle\bar{M}_C\rangle). \quad (26)$$

The rest of the analysis proceeds along the same lines as the two species case. The final equation for the total magnetization is rather cumbersome and will not be reproduced here. However, the limiting and transition results are similar to the two species system: a single resonance at a position $\Delta\omega=p_A\delta\omega_A+p_B\delta\omega_B+p_C\delta\omega_C$ if the exchange among all three species is fast; a triple resonance at positions $\Delta\omega=\delta\omega_A$, $\delta\omega_B$, and $\delta\omega_C$ with relative intensities $p_A$, $p_B$, and $p_C$, if the exchange is slow; and the critical frequency of chemical exchange is of the same order as the frequency separation of the resonance components without the exchange.

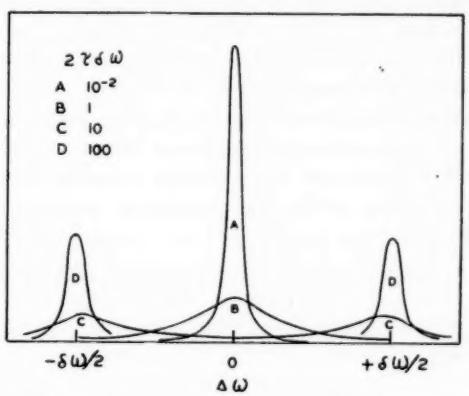


FIG. 5. Theoretical magnetic resonance line shapes in a chemically exchanging two species system with equal lifetimes and equal atomic fractions, computed for different chemical lifetimes $\tau$.

$T_2$.—The influence of $T_2$ upon the nature of the resonances is indirect. If $T_2$ is short, the resonance is naturally broad, which might obscure closely spaced chemically shifted components. If $T_2$ is long compared to the inverse frequency separation of the chemically shifted components, the analysis presented graphically in Fig. 5 applies. In Fig. 5, it is seen that chemical exchange in the transition range gives a broad line even though $T_2$ is long. The $T_2$ values should be related directly to the chemical exchange.[6] If the exchange is very effective as a relaxation mechanism, then when the exchange is fast enough to give a single, concentration dependent line, the natural width would become the order of the chemical shift, giving still an unusually broad line for a liquid phase. In brief, observation of an exceptionally broad line in a liquid phase, with exchange possible, does not prove the exchange frequency is in the critical region. Very broad resonances have been noted

[17] The right-hand side of Eqs. (41) and (42) should be multiplied by $-i$.

for fluorine[18] in $IF_7$ and for phosphorus[7] in $FPO(OH)_2$, both as liquids; the broadening mechanisms might very well be those suggested here. In chemically exchanging or reacting systems $T_2$ should be concentration dependent because self-exchange would likely be more or less effective in relaxation than is cross exchange.

## DISCUSSION

Some qualitative conclusions of interest can be drawn from the analysis and data given above. For instance, it was reported earlier[7] that $PF_5$ did not have chemically shifted fluorine resonance components even though the accepted trigonal bipyramid structure would predict two lines, and complex lines with large chemical shifts were found in $IF_5$ and $BrF_5$. However, collisions provide a mechanism for exchanging the fluorines among the apex and trigonal positions and averaging the chemical shift. The single, concentration dependent resonance lines discussed above demonstrate the existence of fast exchange in a number of cases, some expected and some perhaps not. The $H_2O-OH^-$ exchange is illustrative. The estimated value for $\delta_{OH^-}$ is 1.0 or about 200 $sec^{-1}$ at 4200 gauss. If allowance is made for the concentration dependence, the average lifetime of $OH^-$ ions in concentrated aqueous solution at room temperature is the order of $10^{-4}$ sec or less. Similar conclusions can be drawn for the acids and ammonia compounds investigated.

[18] H. S. Gutowsky and C. J. Hoffman, J. Chem. Phys. **19**, 1259 (1951).

The potential applications of these methods to other systems and nuclei appear promising. The investigation of ionic interactions and of degrees of dissociation seem straightforward, at least in qualitative terms. The determination of exchange rates or, in the general case, of reaction rates is a bit more complex. The chemical shifts, in frequency, are proportional to the applied magnetic field, and a fivefold range or so of frequency could be explored by changing the field. The average relative lifetimes depend upon concentration, and a several-fold range has been observed in these experiments. Also, the exchange rates are temperature dependent, and a wider range of exchange could be searched by changing the temperature than by changing the magnetic field, with a low temperature limit determined by the magnetic dipole broadening of the resonance lines. In case of heavier nuclei such as fluorine, the exchange rates should be smaller, and the chemical shifts are larger, so that instances of systems in the transition stage should be found more readily. A combination of temperature and magnetic field changes in the transition region would permit evaluation of the activation energy for the exchange.

## ACKNOWLEDGMENT

We wish to express our thanks to Dr. C. P. Slichter for several helpful discussions of the chemical exchange analysis. Equipment was provided mainly by a grant from the Research Corporation.

# Proton Magnetic Resonance of the $CH_3$ Group.* I. Investigation of Six Tetrasubstituted Methanes

J. G. POWLES AND H. S. GUTOWSKY
*Noyes Chemical Laboratory, University of Illinois, Urbana, Illinois*
(Received March 27, 1953)

Measurements have been made of the proton magnetic resonance absorption in methyl chloroform, 2,2-dinitropropane, 2-chloro-2-nitropropane, *t*-butyl chloride, *t*-butyl bromide, and neopentane, in the solid state. In all the materials at −196°C, except neopentane, the absorption corresponds to $CH_3$ groups effectively fixed in the lattice. The narrowing of the absorption lines with rising temperature in methyl chloroform, 2,2-dinitropropane, and 2-chloro-2-nitropropane is attributable to the increasing rate of motion of the $CH_3$ groups about their $C_3$ symmetry axis. In methyl chloroform at higher temperatures, and in *t*-butyl chloride, *t*-butyl bromide, and neopentane an additional motion of the $CH_3$ groups is required to explain the observed absorption, and possible motions are suggested. In all the polar materials the line becomes very narrow at the thermal transition at which the dielectric constant rises to a high value, marking the onset of over-all molecular rotation. In neopentane the line is narrower than expected for the rigid lattice at −196°C. With rising temperature, the line narrows to a very small value between the thermal transition and melting points. Theoretical analyses are given of the effects of external broadening upon the line shapes of fixed and rotating $CH_3$ systems, and the results are used in interpreting the experimental data.

## 1. INTRODUCTION

MEASUREMENTS have been made of the proton magnetic resonance absorption in methyl chloroform, 2,2-dinitropropane, 2-chloro-2-nitropropane, *t*-butyl chloride, *t*-butyl bromide, and neopentane in the temperature range from −196°C to room temperature. These molecules have a similar structure in which a central carbon atom is surrounded by four groups at least one of which is the $CH_3$ group and the remainder may be Cl, Br, or $NO_2$. The molecules are roughly spherical in shape, because of the comparable size of the groups and their tetrahedral arrangement, and this leads to the occurrence of "rotator" phases at temperatures below the melting point.[1] These phases have a high dielectric constant (except, of course, the nonpolar neopentane) which is undoubtedly due to movement of the molecule as a whole. At lower temperatures movement of the whole molecule is unlikely, but parts of it may still be in motion and it is the object of this paper to investigate the motions, particularly of the $CH_3$ groups, by observation of the proton magnetic resonance lines and their dependence on temperature.[2,3]

## 2. EXPERIMENTAL ARRANGEMENT

The experimental arrangement used for the observation of broad proton lines in solids has been described in detail.[4] The large magnetic field was provided by a permanent magnet having a field of some 6365 gauss so that the proton magnetic resonance was centered at about 27 mc. The resonance was observed with the aid of an oscillating detector, the output of which was a 30 cps signal proportional to the derivative (*versus* field) of the nuclear magnetic absorption, when the main magnet field was modulated by a coil carrying 30 cps current. The modulation amplitude, in all cases, was small enough to assure that the curves obtained were not affected to any significant extent by modulation broadening.[5] The 30 cps signal was fed to a lock-in amplifier and finally to a recording potentiometer, the chart of which moved in synchronization with a device regulating the large magnetic field. In this manner, an automatic record was obtained of the derivative of the absorption lines extending over a range in magnetic field adequate for the observation of the line shapes due to the $CH_3$ group.

The materials were obtained commercially. Those which were liquids at room temperature were purified by washing with calcium carbonate and distilled water; they were then dried over calcium chloride, and fractionally distilled in a 5-ft column. The purified materials were used as far as possible on the same day that they were distilled since it was found that some decomposition had taken place upon standing only 24 hours [see Sec. 3(a)]. The 2-chloro-2-nitropropane was only available in a quantity insufficient for distillation and showed evidence of a small proportion of proton containing impurity which, however, was not considered sufficient to invalidate our results. The 2,2-dinitropropane had been purified by twice recrystallizing from alcohol and drying under vacuum. The 2-chloro-2-nitropropane and the 2,2-dinitropropane were kindly lent by Professor C. P. Smyth. The neopentane was given by the Phillips Petroleum Company to whom we express our thanks. It was guaranteed 99.86 percent molar pure and was used without further treatment.

The specimens were contained in a thin-walled glass

* Supported by the U. S. Office of Naval Research.
[1] R. W. Crowe and C. P. Smyth, J. Am. Chem. Soc. **72**, 4009 (1950).
[2] Gutowsky, Kistiakowsky, Pake, and Purcell, J. Chem. Phys. **17**, 972 (1949).
[3] H. S. Gutowsky and G. E. Pake, J. Chem. Phys. **18**, 162 (1950).
[4] Gutowsky, Meyer, and McClure, Rev. Sci. Instr. **24**, 644 (1953).
[5] M. M. Perlman and M. Bloom, Phys. Rev. **88**, 1290 (1952).

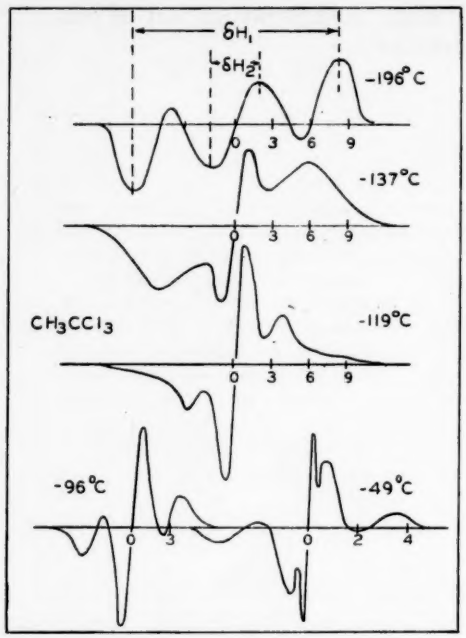


FIG. 1. Experimental absorption line derivatives for methyl chloroform at various temperatures. Abscissas are in gauss; ordinates are in arbitrary units.

tube having a volume of about $\frac{1}{2}$ cm$^3$, which was inserted in the coil of the oscillating detector. The neopentane, which is a gas at room temperature, was condensed directly from the storage tank into the tube *in situ*. The appearance of the specimen when solid was in all cases that of a white, opaque mass apparently composed of small crystals.

The lowest temperature, −196°C, was obtained by use of liquid nitrogen in an earlier form of a cryostat which has been described elsewhere.[4] This temperature was sufficiently low to allow the observation of the rigid lattice line except in neopentane. The temperature was measured by means of a copper-constantan thermocouple of which one junction was frozen in the specimen itself at a point very near to the coil of the oscillating detector. The temperature measured in this way was correct to about 1°C. Some hysteresis occurred at the thermal transitions similar to that observed in the dielectric measurements,[1] so all the measurements reported here were obtained for rising temperature. The specimen was cooled to liquid nitrogen temperature in about one hour and measurements were made at suitable intermediate temperatures, rising until the line narrowed to the order of 0.1 gauss.

### 3. EXPERIMENTAL RESULTS

It is convenient to consider several aspects of the absorption lines, namely, the actual line *shape*, the line width, the utility and significance of which depends somewhat on the line shape obtained, and the second moment of the absorption line, as well as the variation of these quantities with temperature. The most detailed line shapes and the ones most susceptible to theoretical interpretation were obtained for methyl chloroform and these are treated in some detail. The experimental results are presented in this section for all of the compounds, and the interpretations and analyses are given in the following part, Section 4.

#### (a) Methyl Chloroform

In Fig. 1 there is reproduced the observed and somewhat smoothed line shape for methyl chloroform at −196°C; the ordinate is proportional to $df(H)/dH$, where $f(H)$ is the absorption. The values of $df(H)/dH$ shown in Fig. 1 are in arbitrary units. The line shape at −137°C in Fig. 1 is where the line has begun to narrow, that at −119°C shows further narrowing, and that at −96°C is a line shape for which a particularly simple theoretical interpretation is possible. The line continued to narrow slightly with increasing temperature until at −49°C the width fell to a small value such that the observed line width was determined by the resolving power of the equipment. At −49°C there is a phase transition[6] with an entropy increase of 7.9 eu/mole and the dielectric constant rises to a high value.[1] A rather less important transition at −68°C, which is indicated by an entropy increase of 0.25 eu/mole and a small rise in dielectric constant, appears to have little effect on the line shape.

The line shape in Fig. 1 for −49°C was obtained when the specimen was partly transformed and is evidently a superposition of broad and narrow lines. The transition in line shape occurred in a temperature range of less than $\frac{1}{4}$°C.

A line shape similar in form to that for −49°C in Fig. 1, but with the "spike" rather less pronounced was

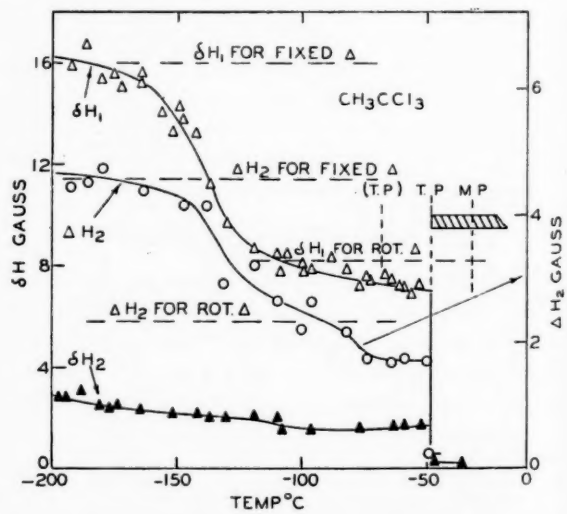


FIG. 2. Experimental line widths and root second moments for methyl chloroform as a function of temperature. The cross-hatching indicates the region of temperature in which the dielectric constant is high.

[6] Rubin, Levedahl, and Yost, J. Am. Chem. Soc. **66**, 279 (1944)

obtained at −59°C, i.e., 10° below the transition, for a specimen of methyl chloroform which had been distilled 24 hours previously. In a specimen measured immediately after distillation, the central "spike" was *entirely absent* below the transition temperature. It is evident therefore that the former specimen contained a proton bearing impurity possessing sufficient freedom of motion below the transition temperature of methyl chloroform to give a narrow line. The intensity of a narrow line is much greater than that of a broad line from the same number of nuclei, so these measurements are particularly sensitive to this type of impurity. Similar but less striking evidence of the rapid decomposition of methyl chloroform has been observed in dielectric constant measurements.[7] Had we not observed that the spike disappeared upon purification of the sample, it might have been ascribed to a pretransition phenomenon in which a number of molecules had sufficient freedom of motion below the transition temperature to give a narrow line superimposed on the broad line due to the other molecules. It is clear that precautions must be taken to guard against the effects of small amounts of proton bearing impurities.[8]

In these compounds the line shapes are complex and it is convenient to define the line width as the separation between the pairs of peaks in the observed derivative of the absorption line. For a simple absorption curve the derivative has only one pair of peaks. For the more complicated line shapes we can measure two or more line widths, $\delta H_1$, $\delta H_2$, etc. which are the separation of the outer, next inner, etc. pairs of peaks of the derivative curve. In this sense methyl chloroform has two line widths $\delta H_1$ and $\delta H_2$ as illustrated in Fig. 1 and these values are given as a function of temperature in Fig. 2. The cross-hatched region of temperature in Fig. 2 and succeeding figures is that in which the dielectric constant has a high value[1] and the transition and melting points are shown by T. P. and M. P.

In earlier measurements of the line widths for methyl chloroform, the outer peaks were not observed at temperatures above the transition at about −120°C; the line width *versus* temperature curve reported previously[3] is a composite of $\delta H_1$ and $\delta H_2$ in Fig. 2, joining at the line width transition. The earlier, incomplete data probably resulted from broadening of the outer peaks by the greater magnetic field inhomogeneities, and from the manual method of measuring the line widths without plotting the whole line shape. The results in the low temperature region agree very well. Also in Fig. 2, the values of the root second moment, $\Delta H_2$, are given for methyl chloroform at different temperatures. The

[7] Powles, Williams, and Smyth, J. Chem. Phys. **21**, 136 (1953).
[8] A similar case is described by F. A. Rushworth, J. Chem. Phys. **20**, 920 (1952); and E. R. Andrew, J. Chem. Phys. **18**, 607 (1950).

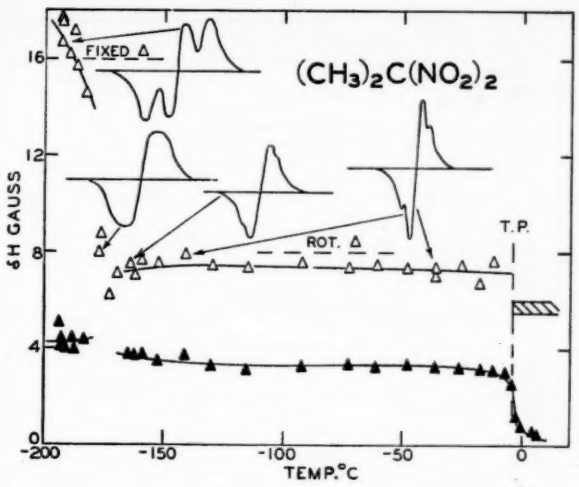


FIG. 3. Experimental line widths and absorption line derivatives for 2,2-dinitropropane *versus* temperature.

second moment of an absorption line,[9] is defined as

$$\Delta H_2^2 = \int_{-\infty}^{\infty} f(H)(H-H_0)^2 dH \Big/ \int_{-\infty}^{\infty} f(H) dH,$$

where $H$ is the applied magnetic field, and $H_0$ is the field at the center of the line. The second moments were calculated from the observed line shapes after numerical integration to obtain $f(H)$. The root second moments, $\Delta H_2$, are plotted for graphical convenience. The scatter of the points for $\Delta H_2$ about the smooth curve drawn through them is rather greater than for $\delta H$ because $\Delta H_2$ is sensitive to the exact line shape in the outer regions. For the other materials a simpler line shape is observed and the values of $\Delta H_2$ show a correspondingly smaller scatter.

### (b) 2,2-Dinitropropane

The results for line shape and line width for 2,2-dinitropropane as a function of temperature are shown in Fig. 3. The values of the root second moment are given in Fig. 4. The narrowing of the line at the thermal transition at −5°C is less abrupt than in the case of methyl chloroform. A similar effect is observed in the dielectric measurements.[1,7] The line shape at −194°C is similar to that for methyl chloroform, but in the line width transition region and above there are significant differences and similarities. It is noteworthy that the line does not change in any respect between −140 and −5°C.

### (c) 2-Chloro-2-Nitropropane, *t*-Butyl Chloride, and *t*-Butyl Bromide

The results for these materials are given in Figs. 4–8. In all three cases the line shape at the higher temperatures shows no evidence of the outer peaks observed for

[9] J. H. Van Vleck, Phys. Rev. **74**, 1168 (1948).

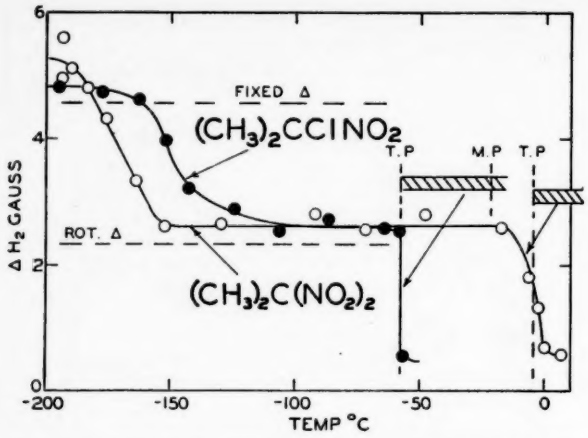


FIG. 4. Root second moments for 2,2-dinitropropane and 2-chloro-2-nitropropane *versus* temperature.

methyl chloroform and 2,2-dinitropropane. The line narrows at the transition at which the dielectric constant rises. This effect is particularly interesting in the cases of *t*-butyl chloride and *t*-butyl bromide both of which have two thermal transitions,[10] below the melting point, of almost equal importance. In *t*-butyl chloride the dielectric constant rises at the upper transition and in *t*-butyl bromide at the lower.[10] The narrowing of the nuclear resonance line also occurs at these points in striking confirmation of the dielectric measurements. For 2-chloro-2-nitropropane the line shape at −196°C is similar to that for the materials already discussed. Those for *t*-butyl bromide and *t*-butyl chloride have forms which also may be simply interpreted.

### (d) Neopentane

Neopentane (Fig. 9) is exceptional in that the line is comparatively narrow even at −195°C, as has been previously observed,[3] however, there is an indication of the onset of broadening in the slight rise in the $\Delta H_2$ curve at the lowest temperature. No change was observed in the absorption obtained on passing through the thermal transition temperature at −133°C, where the entropy increase is 4.39 eu/mole.[11] This agrees with the earlier results.[3] Starting at −80°C the line narrows gradually with temperature to a limiting value, but there is no anomaly in the specific heat. This very different behavior of neopentane undoubtedly reflects the very symmetrical form of the molecule, which may be compared with methane for which the line width transition occurs below 20°K.[12] The apparent line widths reported earlier for neopentane at temperatures above −80°C are somewhat larger, because of greater magnetic field inhomogeneities, than are the present results. We have now measured 2,2-dichloropropane and find that its behavior is very similar to that of methyl chloroform. Detailed results will be published later.

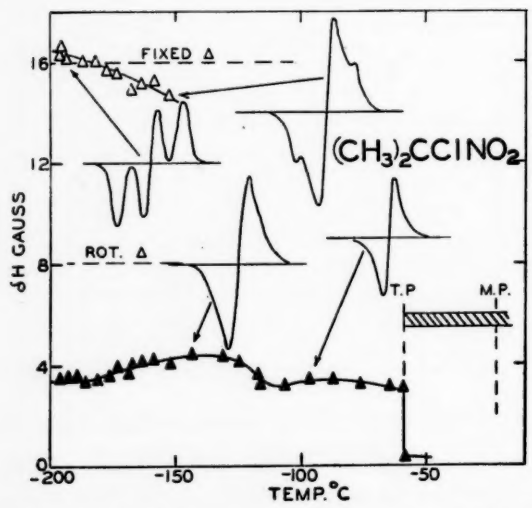


FIG. 5. Experimental absorption line derivatives and widths for 2-chloro-2-nitropropane *versus* temperature.

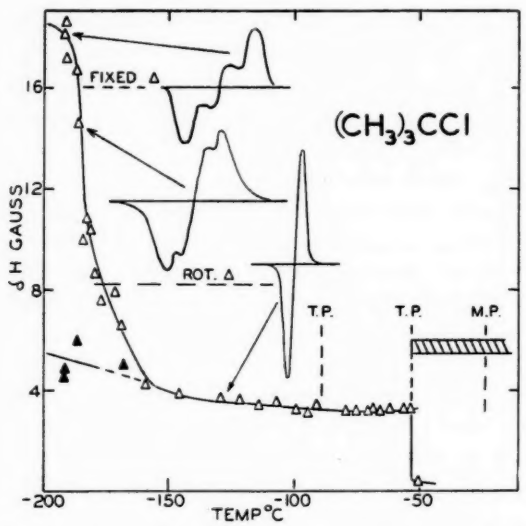


FIG. 6. Experimental absorption line derivatives and widths for *t*-butyl chloride *versus* temperature.

## 4. INTERPRETATION OF RESULTS

### (a) Rigid Lattice Lines

The observed broadening of the absorption lines is due to the magnetic dipolar interactions of the protons in these materials. For the case in which the magnetic nuclei are effectively stationary, the second moment has been given by Van Vleck,[9] and for protons this is

$$\Delta H_2^2=\frac{9}{2}\cdot\mu^2\cdot\frac{1}{N}\sum_{i>k}(3\cos^2\theta_{jk}-1)^2/r_{jk}^6.$$

$\mu$ is the proton magnetic moment; $N$ is the number of nuclei considered to interact; $\theta_{jk}$ is the angle between the

[10] Kushner, Crowe, and Smyth, J. Am. Chem. Soc. **72**, 1091 (1950).

[11] J. G. Aston and G. H. Messerly, J. Am. Chem. Soc. **58**, 2354 (1936).

[12] N. L. Alpert, Phys. Rev. **75**, 398 (1949).

large magnetic field and the line joining nuclei $j$ and $k$; and $r_{jk}$ is the internuclear distance. The contribution to $\Delta H_2^2$ due to nuclei other than protons is negligible in these materials. In compounds where all the protons are in $CH_3$ groups, the largest contribution to $\Delta H_2^2$ for a given proton is that of its two neighbors in the $CH_3$ group. For an *isolated* trio of protons arranged in an equilateral triangle of side $R$, one obtains

$$\Delta H_2^2 = \tfrac{2}{3}\alpha^2 \sum_{j>k} (3\cos^2\theta_{jk} - 1)^2,$$

where $\alpha = (3/2)\mu/R^3$.

If the normal to the triangle is randomly oriented with respect to the large magnetic field, as it is in the crystalline powders investigated, one finds

$$\Delta H_{2\ \text{fixed, powder}} = 2(2/5)^{\frac{1}{2}} \cdot \alpha.$$

$\Delta H_2$ is independent of the orientation of the triangle about its $C_3$ symmetry axis.[13] Taking the $H-H$ distance

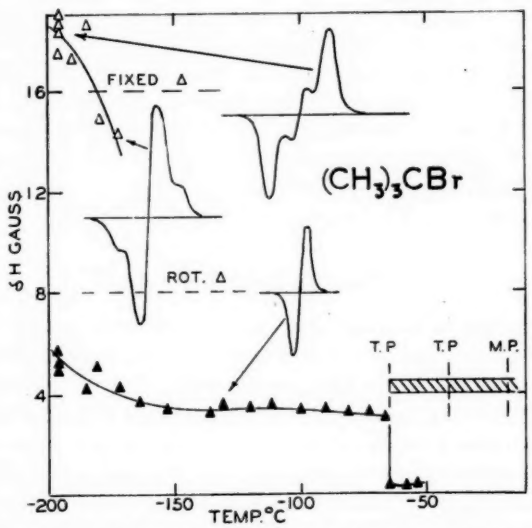


FIG. 7. Experimental absorption line derivatives and widths for $t$-butyl bromide *versus* temperature.

in the $CH_3$ groups to be 1.79A, the numerical result is $\Delta H_2 = 4.66$ gauss. This value is marked on the curves of $\Delta H_2$ *versus* temperature as the fixed triangle value.

The effect of the protons in neighboring $CH_3$ groups gives an additional broadening. Provided certain conditions are satisfied the effect may be represented by a Gaussian broadening factor $\exp(-H^2/2\beta^2)$ as shown by Pake.[14] In the materials investigated here, $\beta^2$ has a value of several units of gauss.[2] With this broadening the root second moment for a crystalline powder containing fixed $CH_3$ groups becomes

$$\Delta H_2 = [(8/5)\alpha^2 + \beta^2]^{\frac{1}{2}}.$$

The actual line shape for an equilateral three spin system has been derived by Andrew and Bersohn,[13] and

[13] E. R. Andrew and R. Bersohn, J. Chem. Phys. **18**, 159 (1950).
[14] G. E. Pake, J. Chem. Phys. **16**, 327 (1948).

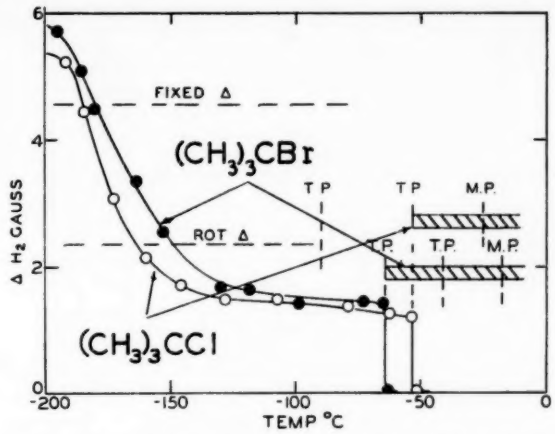


FIG. 8. Root second moments for $t$-butyl chloride and $t$-butyl bromide *versus* temperature.

for such systems, isolated and randomly oriented as in a crystalline powder, the line shape is extremely complex. However, in all practical cases the effect of nuclei external to the given trio is to simplify the line shape. The theory for fixed $CH_3$ groups has been compared[13] with experimental[3] results using an external broadening corresponding to $\beta^2 = 2$ gauss.[2] The comparison was made of the theoretical and graphically integrated experimental derivative absorption lines. However, since we observe the derivative of the absorption line we shall obtain in the following the theoretical derivative curve directly, without recourse to the absorption line. The comparison of the derivatives is in fact a more sensitive test of the theory. The case of the triangular group rotating about its $C_3$ axis is also derived by Andrew and Bersohn[13] and this matter is taken up again below.

It is instructive to calculate the derivative curves for a number of different values of the external broadening for the fixed triangle case. The results are shown in Fig. 10 for $\beta^2 = 8$, 6, 4, and 2 gauss$^2$. It may be noted that the separation of the outer peaks is hardly affected by the external broadening in this range, being somewhat

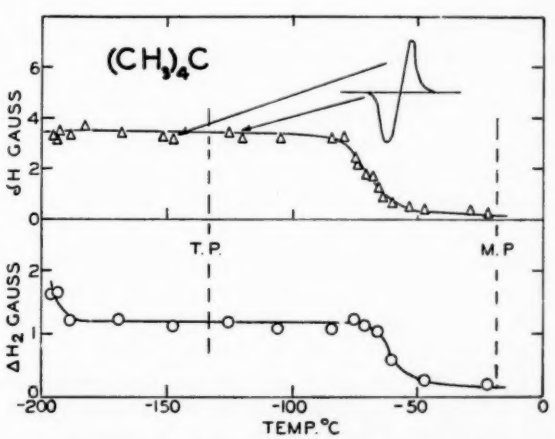


FIG. 9. Absorption line derivatives, widths, and root second moments for neopentane *versus* temperature.

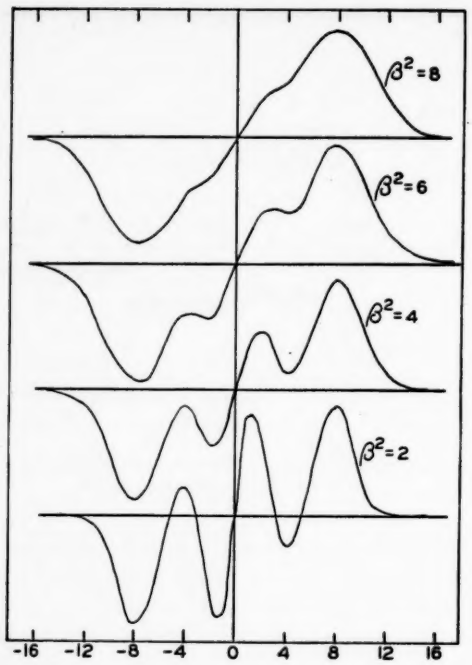


FIG. 10. Theoretical absorption line derivatives for fixed $CH_3$ groups with various degrees of external broadening. $\beta^2$ is the contribution in gauss$^2$ of the external broadening to the second moment of the absorption line. Abscissas are in gauss; ordinates are in arbitrary units.

larger, the larger the broadening. The inner peaks are due in large measure to the central component of the primitive line shape (reference 13, Fig. 2(a)) and their separation is roughly proportional to $\beta$. The relative amplitudes of the two peaks depends very much on the broadening and for $\beta^2 \gtrsim 6$ gauss$^2$ the inner peaks are no longer resolved.

A comparison of the line shapes of Fig. 10 with the experimental line shape for methyl chloroform at $-196$°C shows that it and the theoretical curve for $\beta^2=2$ are almost identical and this is, of course, confirmed by the values of $\delta H_1$ and $\delta H_2$ given in Fig. 2. Moreover, we calculate for $\beta^2=2$ that $\Delta H_2=4.80$ and this is in good agreement with experiment. Indeed it has been estimated[2] that for a reasonable arrangement of the molecules in the methyl chloroform crystal, the external broadening corresponds to a value $\beta^2=2$ gauss$^2$. The experimental results therefore correspond very closely with theory for methyl chloroform at low temperatures when it is assumed that the $CH_3$ groups remain fixed or at least that any motion such as zero point torsional oscillation which may occur does not affect the measurement significantly.[3,13] This means that any other motion of the $CH_3$ groups as a whole takes place with an effective frequency of less than about $10^4$ cps.[15]

For 2,2-dinitropropane at $-194$°C the agreement is again very good in all respects for $\beta^2=5$ gauss$^2$. The increase in external broadening may be ascribed to the fact that there are now two $CH_3$ groups per molecule thus increasing the probability of interaction between the different groups.

For 2-chloro-2-nitropropane at $-195$°C agreement is found for $\beta^2 \simeq 3$ gauss$^2$, that is, the external interaction is rather smaller than in 2,2-dinitropropane in spite of it also having two $CH_3$ groups per molecule. It is possible that in the latter molecule the two $CH_3$ groups are forced closer together by the large $NO_2$ groups than is the case in the molecule containing Cl and $NO_2$ substituents. Again, the large $NO_2$ groups are likely to increase the distance between individual molecules and hence should reduce the intermolecular broadening. Both factors suggest that the external broadening in these two compounds is due rather to interactions between the $CH_3$ groups in the same molecule than with those in adjacent molecules.

The lowest temperature line shapes for *t*-butyl chloride and *t*-butyl bromide correspond fairly well to $\beta^2=5$ and 7 gauss$^2$, respectively. These large values of $\beta^2$ reflect the high concentration of $CH_3$ groups. One might suggest that the higher value of $\beta^2$ in *t*-butyl bromide is due to a closer approach of the $CH_3$ groups in this molecule occasioned by the larger bromine atom. For such large broadening it is probable that its representation as a Gaussian function is no longer valid. Nevertheless, the line shape is still a recognizable perturbation of that of an isolated equilateral three spin system.

### (b) Rotating Triangle Case

Motion of the nuclei, or rather of the line joining any two interacting nuclei with respect to the large magnetic field, changes the line shape from that of the rigid lattice.[15,13] It has already been noted that a narrowing of the nuclear magnetic resonance line occurs when the dielectric constant rises at the thermal transitions. These effects are associated with a considerable increase in freedom of motion of the whole molecule. The linewidth transition at lower temperatures is connected with motion of parts of the molecule, in this case the $CH_3$ groups. This is likely to occur at a lower temperature than motion of the whole molecule, and will not lead to any substantial change in dielectric constant.

The value of the second moment for a triangular group of nuclei rotating about its $C_3$ symmetry axis is found to be for protons and for a crystalline powder

$$\Delta H_{2\ \text{rot. powder}} = (2/5)^{\frac{1}{2}} \cdot \alpha,$$

i.e., $\Delta H_2$ falls to one-half the rigid lattice value. The detailed line shape for the rotating triangle has been obtained by Andrew and Bersohn.[13] We have calculated the theoretical derivative line shape for external broadening corresponding to $\beta^2=2$, 1, 5 and $\frac{1}{5}$ gauss$^2$, and these are shown in Fig. 11. Lower values of external broadening are of course appropriate in this case. The reduction in external broadening is discussed by Andrew[8] for certain types of motion. A similar analysis of the

[15] Bloembergen, Purcell, and Pound, Phys. Rev. 73, 679 (1948).

broadening encountered in this investigation suggests that the effect of rotational motion of the $CH_3$ groups is to reduce $\beta^2$ by a factor of about four. A reduction of this order is observed.

The general effect of external broadening on the line shape is similar to that observed in the fixed triangle case. The outer peak separation is almost independent of $\beta$ at a value of 8.2 gauss; the inner peak separation is proportional to $\beta$ and the relative amplitude of the two peaks varies strongly with the broadening as shown in Fig. 12. The ordinates in Fig. 11 are in arbitrary units both absolutely and with respect to the different diagrams. For $\beta^2 \gtrsim 2$ the *outer* peaks are not resolved.

The experimental line shape for methyl chloroform at −96°C is in good agreement in all respects with the theoretical line shape for the rotating triangle for $\beta^2=\frac{1}{2}$ gauss$^2$. The interactions external to the $CH_3$ groups are reduced as a result of the motion by a factor of about 4 in $\beta^2$. It is evident therefore that the change in line shape in methyl chloroform between −196 and −96°C is due to increasingly effective motion of the $CH_3$ groups about their symmetry axes. The further narrowing which takes place above −96°C is due to some additional motion and this is discussed in Section 4(c).

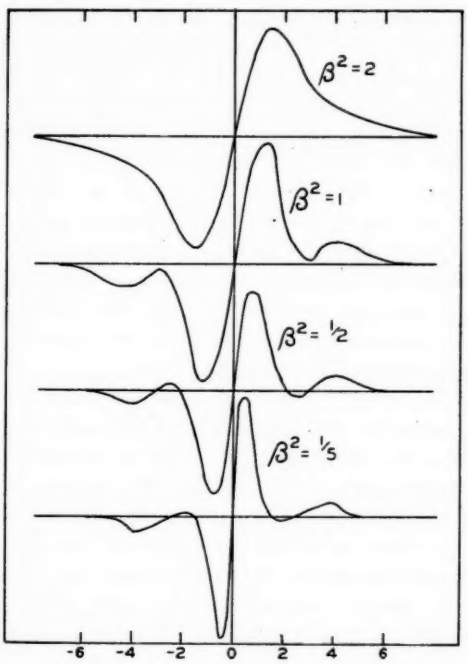


FIG. 11. Theoretical absorption line derivatives for $CH_3$ groups rotating about the $C_3$ symmetry axis. Various degrees of external broadening are indicated by $\beta^2$, the contribution in gauss$^2$ to the second moment of the absorption line. Abscissas are in gauss; ordinates are in arbitrary units.

In 2,2-dinitropropane the value of $\Delta H_2$ above −130°C is appropriate to the rotating triangle with an external broadening of $1\frac{1}{2}$ gauss$^2$, however, the agreement between the theoretical and experimental line shapes is not as good as for methyl chloroform. The deviation is not sufficient, however, to invalidate the conclusion that the line narrowing is due primarily to motion of the $CH_3$ groups about their $C_3$ axes.

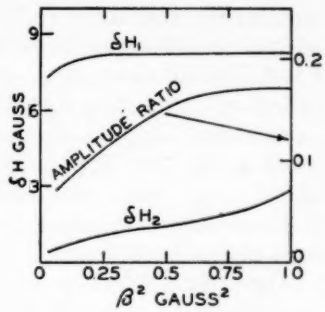


FIG. 12. The line widths, $\delta H_1$ and $\delta H_2$, and the amplitude ratio of the outer peak to inner peak as a function of the external broadening in gauss$^2$ for rotating $CH_3$ groups.

For 2-chloro-2-nitropropane the $\Delta H_2$ value above the line width transition also levels off at a value corresponding to the rotating triangle with $1\frac{1}{2}$ gauss$^2$ external broadening. However, in this case the outer peaks in the line shape were not observed. On the assumption that the external broadening is a Gaussian function this would indicate a value of $\beta^2>2$ gauss$^2$. The external broadening may be such that it invalidates this simple procedure, but the motion responsible for the line narrowing is still the rotational motion of the $CH_3$ groups.

In both *t*-butyl chloride and *t*-butyl bromide the line narrows to a value such that both $\Delta H_2$ and the line width fall well below the values appropriate for the rotating $CH_3$ groups. The outer peaks are not observed but this could be ascribed to the large external broadening. But in order to obtain the low value of $\Delta H_2$, it must be assumed that there is some more extensive motion of the molecule in the crystal. Possible motions are investigated in Section 4(c).

The results for neopentane also cannot be explained without involving a motion in addition to rotation of the $CH_3$ groups and this is also considered in Section 4(c).

### (c) Second Moments for Composite Motions

The compounds containing $CH_3$, Cl, and Br have absorption lines which are narrower below the thermal transitions than explainable by rotation of the $CH_3$ groups alone. These compounds are very nearly spherical in shape because of the comparable size[16] and tetrahedral arrangement of the groups, so reorientations of the whole molecule may occur quite easily. For instance, in methyl chloroform the internal barrier to rotation of the $CH_3$ group in the free molecule is approximately 2.7 kcal/mole,[6] and the onset of rotation or of quantum-mechanical tunneling of the $CH_3$ group might or might not involve rotation of the $CCl_3$ group about the C−C bond. Rotation of the $CCl_3$ group would have only a small effect on the proton resonance, but might be detected by measurement of the chlorine pure

[16] L. Pauling, *Nature of the Chemical Bond* (Cornell University Press, Ithaca, New York, 1948), second edition, p. 189.

quadrupole resonance.[17] A motion which is more effective in narrowing the proton resonance is rotation of $Cl-CCl_2CH_3$ about the C—Cl bond or what may be called a $C_3'$ axis. This is equivalent to a rotation of the axis of the $CH_3$ group about an axis making with it an angle $\psi$, of $(180-109\frac{1}{2})°$. Or the molecule may rotate about a $C_2'$ axis corresponding to $\psi=109\frac{1}{2}/2°$. The latter motion would seem, however, to be less probable on steric grounds.

The value of $\Delta H_2$ depends on $\psi$ and on whether or not the $CH_3$ groups are assumed to rotate about their $C_3$ axes in addition. The expected values of $\Delta H_2$ are shown for the two cases in Fig. 13. The details of this analysis will be given in a later paper. It has been assumed in the lower curve that the two motions may be averaged over separately. It is also assumed that the rotations are uniform although the same result would be obtained for a rotational motion in an $n$-nodal potential with $n \geqslant 3$.[3] It is likely therefore that the simple calculation is valid for nonuniform rotation about $C_3'$ but possibly not for $C_2'$ where we may have $n=2$.

The simplest explanation of the slight narrowing of the resonance in methyl chloroform above −96°C is

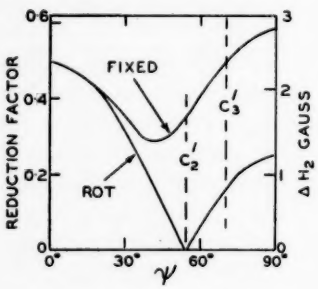


FIG. 13. Root second moments for $CH_3$ groups in which the $C_3$ symmetry axis is rotating about another axis at an angle of $\psi°$. In the lower curve, the $CH_3$ group is assumed to rotate also about its $C_3$ axis. The $C_2'$ and $C_3'$ refer to specific modes of motion discussed in the text.

motion about the $C_3'$ axes. This motion, if sufficiently rapid, is seen from Fig. 13 to reduce $\Delta H_2$ to 0.8 gauss, when it is assumed that the $CH_3$ groups are also rotating. The contribution to $\Delta H_2$ due to external broadening should be quite small. The fact that $\Delta H_2$ is larger than 0.8 gauss at these temperatures could result from the additional motion not being rapid enough. The thermal transition at −49°C intervenes before the maximum narrowing obtains.

Motion of the molecule about the $C_3'$ axis involves motion of the dipole moment of the molecule and so may give an increment in the dielectric constant. The square of the effective dipole moment, on which the increment of the dielectric constant depends, is given by $\mu^2\cos^2(180-109\frac{1}{2})°=0.11\mu^2$ where $\mu$ is the molecular dipole moment. On this basis one expects an increase in dielectric constant of only about one-tenth of that occurring at the thermal transition. There are other factors such as the crystal anisotropy and the relative potential energy of the alternative positions which could reduce this increment in dielectric constant compared with that in the rotator phase. On the simple theory of Bloembergen *et al.*[15] and assuming the correlation times for the magnetic resonance and dielectric relaxation processes to be the same, the measurements of dielectric constant reported at 500 cps[1] should be below the critical frequency for this contribution to the dielectric constant. We conclude therefore, that a rather small change in dielectric constant should occur at about −80°C and Crowe and Smyth[1] do find a small increase in dielectric constant at −70°C. However, more complicated motions than that discussed could also lead to similar effects on the dielectric constant and the nuclear magnetic resonance absorption.

For 2,2-dinitropropane and 2-chloro-2-nitropropane motion of the molecule as a whole is much less probable, or at least takes place at a much lower effective frequency. This may be ascribed to the comparatively large size and irregular shape of the $NO_2$ group and the resulting larger energy barriers to motion.[7] As already shown, the onset of rotational motion of the $CH_3$ groups is a satisfactory explanation of the low temperature transition. In these two substances there is the possibility that one of the $CH_3$ groups in the molecule rotates and not the other. The observed value of $\Delta H_2$ above the line-width transition region shows that both $CH_3$ groups in the molecule are effectively in motion and that any coupling between them or with $CH_3$ groups in adjacent molecules does not affect the observed nuclear magnetic resonance greatly.

In both *t*-butyl chloride and *t*-butyl bromide the low temperature line-width transition occurs without passing through a distinct stage which may be associated with a simple rotational motion of the $CH_3$ groups. The $\Delta H_2$ values above the transition are about 1.5 gauss, which is in the range predicted for combined rotation of the whole molecule about the C—X bond and rotation of the $CH_3$ groups about their $C_3$ axes. But a large, inaccurately known fraction of the observed $\Delta H_2$ must come from inter $CH_3$ group interactions, and this prevents any firm conclusions about the details of the restricted, overall molecular motions which must occur. Measurements were made on solutions of *t*-butyl chloride in carbon tetrachloride to obtain more detailed information by reducing the intermolecular magnetic interactions. The results will be discussed in the second paper of this series; it is found that neighboring molecules affect the freedom of motion of the $CH_3$ groups as well as interacting magnetically.

Neopentane has a low $\Delta H_2$ value of 1.2 gauss in the temperature range from −185° to −75°C. Over-all rotation of the molecule, combined with rotation of the methyl groups would reduce the intramolecular broadening to zero. However, the intermolecular broadening would still be the order of 1 to 2 gauss[2], as observed. This model appears reasonable in view of the very symmetrical form of the neopentane molecule. The change in line width near −70°C could then be assigned

[17] Measurements with this object in view are in progress in this laboratory.

to self-diffusion which, if fast enough, would reduce the intermolecular broadening to zero. An effective frequency of self-diffusion of about $10^4$ cps is required. A narrow line in solid cyclohexane a few degrees below its melting point has been interpreted in this manner by Andrew and Eades.[18] Applying their analysis to neopentane at $-60°C$, the activation energy of self-diffusion is estimated to be about 8 kcal/mole. The postulated self-diffusion is consistent with x-ray studies,[19] which reveal a large degree of disorder in the neopentane crystal at $-50°C$.

The sharp line-width transitions at higher temperatures to very narrow lines in the other five compounds coincide with either thermal or dielectric constant transitions or both. These transitions unquestionably arise from a relatively cooperative change in the over-all molecular rotation and mobility.

[18] E. R. Andrew and R. G. Eades, Proc. Roy. Soc. (London) **A216**, 398 (1953).
[19] A. H. Mones and B. Post, J. Chem. Phys. **20**, 755 (1952).

### (d) The Line-Width Transitions

In the original work on methyl chloroform[3] an empirical formula was used to derive from the variation of line width with temperature an activation energy for the motion leading to the line narrowing. However, our present results used in this formula give a curved line rather than a straight one from which an activation energy could be derived. If, however, the best straight line is drawn through the experimental points it would correspond to an activation energy of about 2 kcal/mole which is rather closer to the barrier restricting internal rotation in the free molecule, 2.7 kcal/mole,[6] than to the previous result of 6 kcal/mole.

The interpretation of the intermediate line shapes in the line-width transition regions in terms of the motions of the molecules or groups in the crystal will be treated in Paper III of this series.

#### ACKNOWLEDGMENT

Most of the equipment was provided by a grant-in-aid from the Research Corporation.

# Proton Magnetic Resonance of the $CH_3$ Group. II. Solid Solutions of *t*-Butyl Chloride in Carbon Tetrachloride*

J. G. Powles and H. S. Gutowsky
*Noyes Chemical Laboratory, University of Illinois, Urbana, Illinois*

(Received June 29, 1953)

Measurements of the proton magnetic resonance absorption in solid solutions of *t*-butyl chloride in carbon tetrachloride are reported for temperatures above −195°C. The results confirm, in general, the phase diagram established previously by thermal and dielectric measurements. In addition, information is obtained on the $CH_3$ group and molecular motions in the various phases. Rotation of the $CH_3$ groups at −195°C depends on the composition. In solutions between 34.9 and 70.6 mole percent *t*-butyl chloride there is effective rotation of the $CH_3$ groups about their $C_3$ axes whereas in pure *t*-butyl chloride the $CH_3$ groups are fixed at this temperature. For some compositions two separate phases are formed at low temperatures and the observed absorption agrees with that predicted from the properties and relative proportions of the protons in the two phases. Somewhat anomalous results were obtained for the more dilute solutions. For all compositions at temperatures above −150°C the resonance line narrows to about the same value, 3 gauss, and this is shown to be due to rotation of the molecule about the C−Cl bond in addition to rotation of the $CH_3$ groups about their $C_3$ axes. Other possible motions are discussed, and the second moment of the absorption line is calculated theoretically for complex motions of the $CH_3$ group. The differences in the freedom of motion of the $CH_3$ groups in the different phases are attributed to interactions both within a molecule and with neighboring molecules.

## 1. INTRODUCTION

THE proton magnetic resonance absorption and its temperature dependence in pure, solid *t*-butyl chloride were included in an earlier paper.[1] It was found that $CH_3$ group and molecular rotation occur in the solid. The chloride atom and the $CH_3$ group are of comparable size so a *t*-butyl chloride molecule can be replaced by a carbon tetrachloride molecule without much distortion of the lattice, and solid solutions of these two compounds exist. The thermal[2,3] and dielectric[3] properties of the solutions provide a fairly complete phase diagram[3] for the system and also give information about the molecular rotation in the various phases. In this paper observations of the proton magnetic resonance are reported for the solutions. An analysis of the results determines the motions of the $CH_3$ groups, confirms the nature of the molecular motions and of the solid phases, and also establishes the dependence of the various types of motion upon the concentration and temperature of the solid.

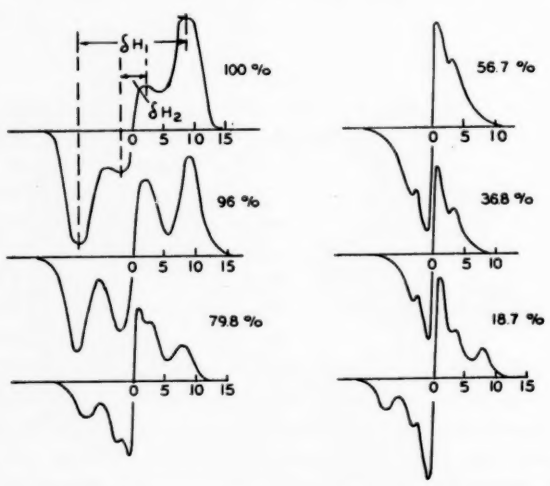


FIG. 1. Experimental derivative absorption line shapes at −195°C for various mole percentages of *t*-butyl chloride in carbon tetrachloride. The abscissas are in gauss and the ordinates are in arbitrary units.

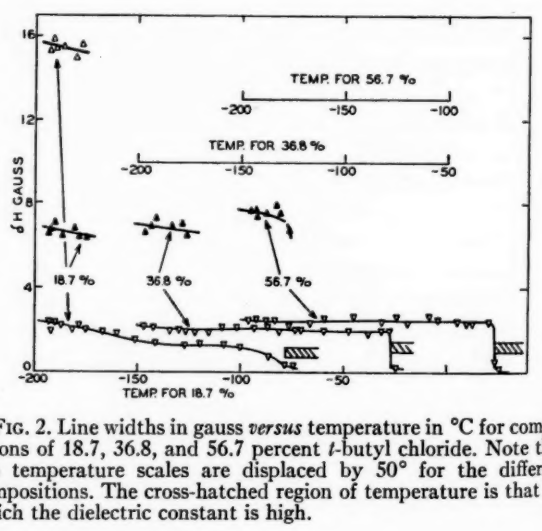


FIG. 2. Line widths in gauss *versus* temperature in °C for compositions of 18.7, 36.8, and 56.7 percent *t*-butyl chloride. Note that the temperature scales are displaced by 50° for the different compositions. The cross-hatched region of temperature is that for which the dielectric constant is high.

## 2. EXPERIMENTAL DETAILS AND RESULTS

The equipment has been described elsewhere[4] and the particular experimental procedures are given in I. The derivative of the absorption line with respect to the magnetic field was plotted automatically against the magnetic field, at different temperatures. Conner and Smyth[3] found more complex behavior of the solutions for falling than for rising temperature, so our measurements were made with rising temperature. The sample was cooled to the temperature of liquid nitrogen in about an hour, and the proton absorption was then

* Supported in part by the U. S. Office of Naval Research.

[1] J. G. Powles and H. S. Gutowsky, J. Chem. Phys. **21**, 1695 (1953), afterwards referred to as I.

[2] A. Turkevich and C. P. Smyth, J. Am. Chem. Soc. **62**, 2468 (1940).

[3] W. P. Conner and C. P. Smyth, J. Am. Chem. Soc. **63**, 3424 (1941).

[4] Gutowsky, Meyer, and McClure, Rev. Sci. Instr. **24**, 644 (1953).

recorded at increasing temperatures until the resonance line became narrower than about 0.3 gauss. Ordinarily, a run took eight hours; the agreement of line width and dielectric constant transition temperatures indicates phase equilibrium was maintained, at least in most cases.

In Fig. 1 the derivative line shapes observed at −195°C are shown for several mole percentages of *t*-butyl chloride in carbon tetrachloride. The absorption intensities in the different curves were chosen arbitrarily for graphical convenience. For some concentrations and temperatures three pairs of peaks are distinguishable in the derivative curves. In all cases, a simple line shape with only one pair of peaks was observed at temperatures above −140°C. The separation between a given pair of peaks is defined as a line-width $\delta H$, as indicated in Fig. 1.

The line widths are given in Figs. 2 and 3 as a function of temperature for the various concentrations. Two line-

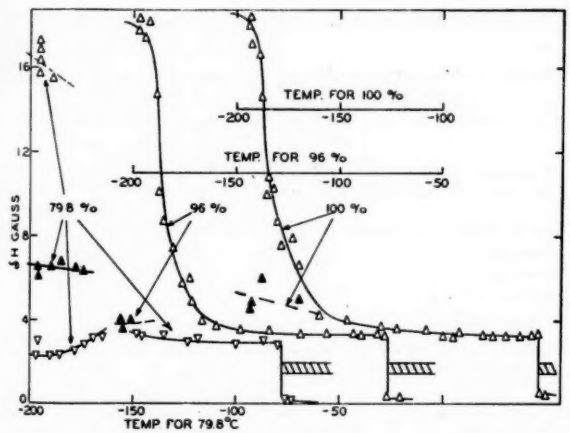


FIG. 3. Line widths in gauss *versus* temperature in °C for compositions of 79.8, 96, and 100 percent *t*-butyl chloride. Note that the temperature scales are displaced by 50° for the different compositions. The cross-hatched region of temperature is that for which the dielectric constant is high.

width transitions occur in all cases. A large, gradual reduction in line width, with increasing temperature, starts at about −185°C and in 10 to 30° the line reaches a limiting width of about 3 gauss which persists for 75° or more. A sharp transition then occurs at a temperature correspondlng to the thermal and/or dielectric constant transition, T.P. At temperatures above this transition the line-width is less than 0.3 gauss, the lower limit measured. In the figures, the cross-hatched regions of temperature are those for which the dielectric constant is large.[3]

The second moments $\Delta H_2$[2] of the absorption lines are useful in analyzing the motions responsible for the line narrowing.[1] Second moments have been calculated from the observed absorption, and in Fig. 4 the root second moments, $\Delta H_2$, are plotted against temperature for the different concentrations. The $\Delta H_2$ values at −195°C are considerably smaller in the dilute than in

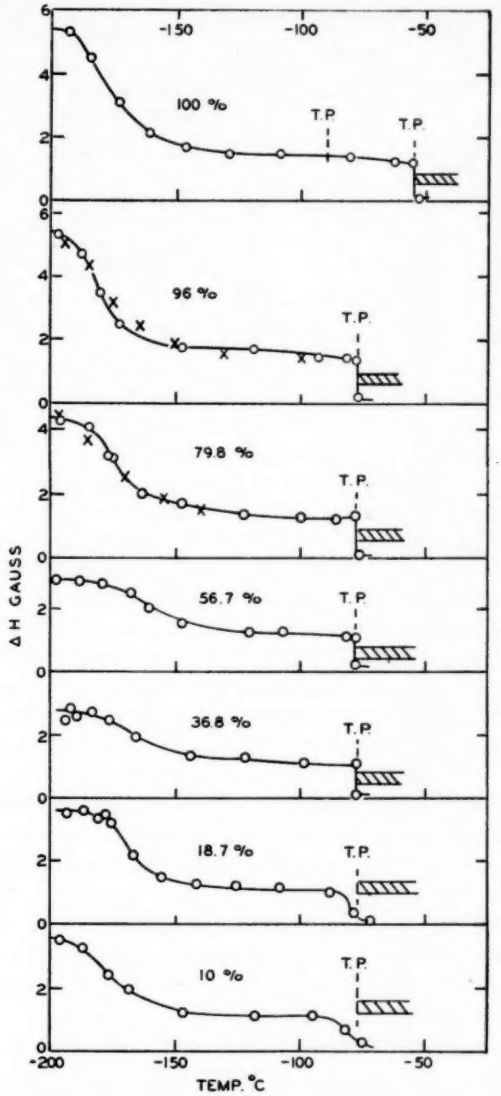


FIG. 4. Root second moments *versus* temperature in °C for the various systems. The T.P's indicate the thermal and/or dielectric constant transition points. The crosses for the 79.8 and 96 percent systems are values computed in a manner described in the text, Sec. 3b.

the concentrated solutions. At higher temperatures there are two transitions in $\Delta H_2$, paralleling those in the line widths. At temperatures just below the high-temperature transition, the values of $\Delta H_2$ are much the same for all concentrations. The low concentration of protons in the 10 percent solution gave weak absorption; the resulting less accurate data are not included in Figs. 1–3.

### 3. INTERPRETATION OF THE RESULTS

#### (a) Introduction

In Fig. 5 there is shown the equilibrium phase diagram proposed by Conner and Smyth[3] for the *t*-butyl chloride-carbon tetrachloride solid system. A single phase is found for all compositions for temperatures

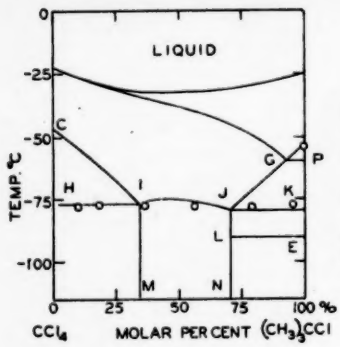


FIG. 5. The equilibrium phase diagram proposed by Conner and Smyth for the *t*-butyl chloride—carbon tetrachloride system. The circles represent the high-temperature magnetic resonance line-width transitions found in this research.

above *CIJGP*. High dielectric constants, indicating rotation of some or all of the *t*-butyl chloride molecules, are observed at temperatures above *HIJK* (−75 to −80°C). A single phase is found for all temperatures only for concentrations of *t*-butyl chloride between 34.9 and 70.6 mole percent (*M* and *N*); and the curve *IJ* gives the transition temperatures for rotation of the *t*-butyl chloride in this concentration range. For bulk compositions between zero and *M*, there is complete miscibility at temperatures above the line *CI*. At lower temperatures, carbon tetrachloride separates out until at −77°C there is a mixture of carbon tetrachloride and a solution of concentration *M*. Similarly, for bulk compositions between *N*, 70.6, and 100 mole percent *t*-butyl chloride, *t*-butyl chloride begins to separate out at temperatures along the curve *JGP* until there is a mixture of *t*-butyl chloride and a solution of concentration *N* at −80°C. The main transition in the dielectric constant of pure *t*-butyl chloride is at −53°C; the line *LE* marks a further small change in the pure *t*-butyl chloride at −90°C, the effect of which is not observable in the proton resonance.

In I, it was concluded from the broad proton resonance in pure *t*-butyl chloride that at −195°C the over-all molecular motions and also $CH_3$ group rotations are effectively frozen out. The absorption line starts narrowing with increasing temperature at −190°C, and over a range of about 30° arrives at an intermediate value corresponding to rotation of the $CH_3$ groups as well as a restricted motion of the whole molecule. At −54°C another sharp transition occurs and the line becomes very narrow, marking the onset of over-all molecular tumbling, in agreement with the sudden rise in dielectric constant.

### (b) Results at −195°C

The data on the 36.8 and 56.7 percent solutions are considered first since there is only one phase at all temperatures. The results for the two solutions are nearly identical. $\Delta H_2$ is 2.9 gauss at the lowest temperatures. This value is much lower than the 5.3 gauss found in pure *t*-butyl chloride, proving there are motions in the solutions which do not occur at the same temperature in the pure compound. The most likely motion is rotation of the $CH_3$ groups, as found in methyl chloroform.[1] In an isolated *t*-butyl chloride molecule, steric repulsions permit one or two but not all three of the $CH_3$ groups to rotate at a given instant. The resonance absorption is additive in a sample, so for nuclei in two states of motion,

$$\Delta H_2^2=\kappa\Delta_1 H_2^2+(1-\kappa)\Delta_2 H_2^2, \quad (1)$$

where $\Delta_1 H_2^2$ and $\Delta_2 H_2^2$ are the second moments for the two states and $\kappa$ is the fraction of nuclei in state 1. The $\Delta H_2$ values calculated for rotation of one, two, or three $CH_3$ groups per molecule are given in the first line of Table I, neglecting broadening external to each $CH_3$ group.

If allowance is made for broadening of the resonance by magnetic interactions between different groups, the theoretical value of 2.33 gauss for all $CH_3$ groups in effective rotation about their $C_3$ axes compares favorably with the experimental value of 2.9 gauss. This is not incompatible with the probable rotation of only two groups per molecule at a time, since lattice and molecular vibrations as well as coupling of rotating $CH_3$ groups in adjacent molecules could average the rotation among all three groups. The line shapes observed in the two solutions are in less satisfactory agreement with the theoretical line shapes given in I for rotating $CH_3$ groups. Similar discrepancies are discussed in I; they probably arise from using overly simple broadening functions to compute "actual" line shapes from the shape for an isolated, rotating $CH_3$ group.

TABLE I. Root second moment values for various $CH_3$ group and molecular rotations in *t*-butyl chloride.[a]

| Molecular motion | Motion of $CH_3$ groups: 3 $CH_3$ fixed | 2 $CH_3$ fixed, 1 $CH_3$ rotating | 1 $CH_3$ fixed, 2 $CH_3$ rotating | 3 $CH_3$ rotating |
|---|---|---|---|---|
| Molecule fixed | 4.66 gauss | 4.03 gauss | 3.30 gauss | 2.33 gauss |
| $C_3$ rotation | 2.4 | 2.0 | 1.5 | 0.8 |
| $C_3'$ rotation[b] | 2.4[c] | 2.1[c] | 1.8[c] | 1.5 |
| $C_2'$ rotation[b] | 1.7 | 1.4 | 1.0 | 0.0 |

[a] The computations do not include broadening of the absorption by the magnetic interactions external to each $CH_3$ group.
[b] These terms are defined in Sec. 3c.
[c] These $\Delta H_2$ values depend on whether the $CH_3$ group on the $C_3'$ axis is one of the rotating groups. The values given are averages over the possible states of motion.

In the samples with over-all compositions of 79.8 and 96 percent *t*-butyl chloride below −80°C there are two phases, one of *t*-butyl chloride and the other a solid solution of concentration *N*, 70.6 percent. The observed line shapes and second moments in the two-phase system should be an average of the absorption in the separate phases, each phase weighted according to the fraction of the total protons it contains. The data for pure *t*-butyl chloride are in Figs. 1 to 4, as are the data for the 56.7 percent solution, which can be used for concentration *N* because the results for concentrations in the *M* to *N* range are nearly identical. The calculated fractions, obtained from the equilibrium diagram, of *t*-butyl chloride in the solution phase of the two phase

system are 0.61 and 0.10 for bulk compositions of 79.8 and 96 percent, respectively. Inserting these fractions in Eq. (1), values for $\Delta H_2$ have been computed at various temperatures and are plotted as crosses in Fig. 4; the calculated results are substantially the same as the observed. The agreement at temperatures above $-130°C$ is trivial since the $\Delta H_2$ values for the two different phases are there about the same. However, below $-130°C$ the agreement is good evidence for the formation of two phases.

The line shapes observed for the 79.8 and 96 percent compositions should also be a weighted average of those observed for the two phases. The line shapes of the two phases differ most at low temperatures, and Figs. 6 (a) and (b) give calculated line shapes for $-195°C$, assuming the two phases. The agreement with the experimental line shapes in Fig. 1 is very striking, particularly for the 79.8 percent composition.

In samples with less than 34.9 percent *t*-butyl chloride, composition *M*, at temperatures below $-77°C$ one would expect to find the absorption characteristic of the solution of concentration *M*, since all of the *t*-butyl chloride should be in this phase. However, at $-195°C$ in the samples of over-all composition 10 and 18.7 percent, the absorption lines have outer peaks which are not found for the 36.8 percent solution; and the $\Delta H_2$ values are higher. The separation of these outer peaks is close to that characteristic of fixed $CH_3$ groups, suggesting that some of the $CH_3$ groups are not rotating. Either some of the *t*-butyl chloride molecules have all of their methyl groups effectively nonrotating or else a fraction of the molecules have one or two of their methyl groups nonrotating. We have not been able to distinguish between these alternates nor is it clear just why these dilute systems behave as they do.

The $\Delta H_2$ value for the 18.7 percent composition is 3.6 gauss at $-195°C$. From this, the fraction of methyl groups which are not rotating can be estimated with Eq. (1) and is found to be 0.3. The line-shape predicted on this basis is given in Fig. 6(c), and compares favorably with the observed shape shown in Fig. 1. Essentially the same shape results whether it is assumed one $CH_3$ group per molecule is fixed or whether 0.3 of the molecules are fixed. The 10 percent composition gave results very similar to the 18.7 percent, but less accurate because of the low concentration of protons in the sample. From these results one might infer that only two of the methyl groups in each molecule are effectively rotating in the phase of concentration *M*. However, a check was made of the absorption by a sample with 30.5 percent *t*-butyl chloride. In this case at $-195°C$ the resonance did not have the outer peaks but was similar to that of the 36.8 percent composition, and the $\Delta H_2$ values in both systems were about 2.3 gauss. This suggests for over-all concentrations below 34.9 percent the coexistence with *M* of a dilute solution (less than 10 percent) of *t*-butyl chloride in carbon tetrachloride instead of pure carbon tetrachloride as assumed in the phase diagram. At compositions only slightly less than *M* the fraction of protons in the more dilute solution would be small and their absorption would be obscured by that of phase *M*. This dilute solution would not need to be stable, but could be a nonequilibrium trapping of some of the *t*-butyl chloride molecules in the carbon tetrachloride lattice. The main requirement is that some of the $CH_3$ groups be restrained from rotating. Also, it is to be noted that the absorption line-width transitions at $-75°C$ in the zero-to-*M* concentration range are relatively gradual compared to those found in the more concentrated systems.

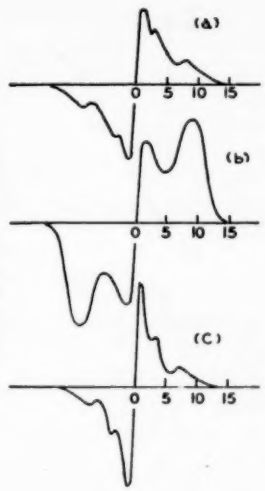


FIG. 6. Line-shapes for two phase systems calculated by adding the line-shapes for each phase. (a) Bulk composition 79.8 percent *t*-butyl chloride at $-195°C$; 0.10 of the protons are in the *t*-butyl chloride phase, 0.90 are in the 70.6 percent *t*-butyl chloride solution. (b) Bulk composition 96 percent *t*-butyl chloride at $-195°C$; 0.61 of the protons are in the *t*-butyl chloride phase, 0.39 are in the 70.6 percent *t*-butyl chloride solution. (c) The line-shape for a sample in which 0.30 of the $CH_3$ groups are rotating and 0.70 are not.

### (c) Low-Temperature Line-Width Transitions

For all compositions, upon warming, the line widths undergo gradual changes within the range of $-190°C$ to $-150°C$ to simple lines about 2 to 3 gauss wide. The line widths then remain constant for 75° or more. The $\Delta H_2$ values are also constant, lying between 1.2 to 1.5 gauss for the various compositions. This is well below the 2.33 gauss for isolated, rotating $CH_3$ groups and proves the presence of some over-all, but restricted, molecular motions.

The simplest motion is rotation of the $C_3C-Cl$ skeleton about the C—Cl bond, that is, $C_3$ rotation of the whole molecule. Other motions are rotation of $ClC_2C-C$ about a C—C bond, which we call $C_3'$ rotation, and rotation of $ClC-C-C_2$ about an intermediate axis, $C_2'$ rotation. These molecular motions might occur with or without rotation of the $CH_3$ groups. The $\Delta H_2$ values for the various combinations of $CH_3$ group and the above molecular motions have been computed and are included in Table I. Some description of the calculations is given in I, while the details of the analysis are given in the Appendix.

Comparison of the observed $\Delta H_2$ values with the computed values in Table I is complicated by the unknown broadening from magnetic interactions external to each $CH_3$ group. The similarity of the line widths and -shapes and $\Delta H_2$ values for all concentrations

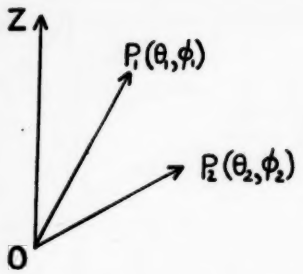


FIG. 7. Diagram for Eq. (A.2).

at temperatures above the line-width transition suggests the *t*-butyl chloride molecules are in the same state of motion in the different systems. The decrease in $\Delta H_2^2$ from 1.9 gauss$^2$ in pure *t*-butyl chloride to 1.4 gauss$^2$ in the 35.8 percent solution would then be a decrease of 0.5 gauss$^2$ in intermolecular broadening. Inter-$CH_3$ group-broadening within a given molecule would be much the same in the different systems.

It was concluded in Sec. 3b that all of the $CH_3$ groups are rotating in the 36.8 and 56.7 percent solutions at −195°C. So, at higher temperatures, any molecular motion occurs in addition to rotation of the three $CH_3$ groups. The appropriate theoretical $\Delta H_2$ values in Table I are 0.8, 1.5, and 0 gauss, respectively, for $C_3$, $C_3'$, and $C_2'$ molecular rotation. The experimental values are about 1.3 gauss, so $C_3$ molecular rotation appears most likely. This would require external broadening of about 0.9 gauss$^2$, which is reasonable.

If some of the $CH_3$ groups were not rotating, none of the $\Delta H_2$ values for the composite motions considered in Table I agrees with experiment, except possibly $\Delta H_2 = 1.0$ gauss for $C_2'$ rotation of a molecule with only two $CH_3$ groups rotating. However, $C_2'$ molecular rotation involves motion of the molecular dipole moment, and there is no indication of this in the dielectric constant measurements.[3] It is concluded that in all the systems over the temperature range indicated there is effective $C_3$ rotation of the whole molecule and also rotation of the three $CH_3$ groups.

### (d) High-Temperature Line-Width Transitions

In all of the samples at temperatures between −75° and −80°C, the line widths undergo transitions with rising temperature to lines narrower than 0.3 gauss, the lower limit measured. These line-width transition temperatures are plotted as circles in Fig. 5 where they are seen to coincide with changes in the dielectric constant. Over-all rotation of the *t*-butyl chloride molecules and the probable resulting increase in translational mobility account for both transitions. For the 79.8 and 96 percent compositions between −80° and −53°C there should still be a broad line from molecules which are restricted to $C_3$ rotation in the *t*-butyl chloride phase. However, the *t*-butyl chloride molecules in the phase of composition *N* give a very narrow, intense line above −80°C, and account for the transitions observed.

### (e) Concluding Summary

The results outlined above provide a coherent physical picture of the molecular interactions and motions in the solids. In pure *t*-butyl chloride at low temperatures, once the $CH_3$ groups have enough thermal energy to start rotating, all of the molecules as well start rotating about their C−Cl bonds. This results probably from the cog-wheel shape of the $CH_3$ group and a steric type of intermolecular coupling.[5] In the *M* to *N* composition range the symmetrical carbon tetrachloride molecules in the lattice reduce the intermolecular $CH_3$ group coupling and permit the $CH_3$ groups to rotate at −195°C although the molecules do not. But there is still enough coupling so that the $CH_3$ rotational energy is effectively interchanged among all three $CH_3$ groups in a molecule, even if only two can rotate at once. The easier rotation of the $CH_3$ groups in the *M* to *N* solutions is consistent with the easier over-all molecular rotation. The rotational transition is at about −80°C in the solutions while in pure *t*-butyl chloride it is 27° higher, at −53°C.

## APPENDIX

*The effect of rotational motion about two axes upon $\Delta H_2^2$ for the three-spin system:*

The second moment for the resonance absorption of three protons fixed at the vertices of an equilateral triangle of side *R* is

$$\Delta H_2^2 = (2/3)\alpha^2 \sum_{n=1}^{3} (3\cos^2\theta_n - 1), \qquad (A.1)$$

where $\alpha = (3/2)\mu R^{-3}$ and $\theta_n$ is the angle between the *n*th side of the triangle and the direction of the main magnetic field.

The rotational averages are simplified by using the following theorem. Consider as in Fig. 7 two lines $\mathbf{OP}_1$ and $\mathbf{OP}_2$ with polar coordinates $\theta_1$, $\phi_1$; $\theta_2$, $\phi_2$. If either line rotates about the polar axis **OZ**, then

$$(3\cos^2\theta_{12} - 1) = (1/2)(3\cos^2\theta_1 - 1)\cdot(3\cos^2\theta_2 - 1), \qquad (A.2)$$

a result which follows at once from the spherical harmonic addition theorem.

Consider first the rotation of the triangular group about a fixed axis **OA**. The lines $\mathbf{OP}_1$, $\mathbf{OP}_2$, and **OZ** will correspond to the magnetic field direction, a side of the triangle, and the axis of rotation, respectively. In this case $\theta_1$, $\theta_2$ will be $\theta''$, $\gamma_n$, the polar angles with respect to the axis of rotation. Then

$$\langle (3\cos^2\theta_n - 1)\rangle_{\substack{\text{rotation}\\ \text{about fixed axis}}} = (1/2)(3\cos^2\theta'' - 1)(3\cos^2\gamma_n - 1). \qquad (A.3)$$

If the $C_3$ axis of the triangle makes an angle $\psi$ with the

[5] E. R. Andrew [J. Chem. Phys. **18**, 607 (1950)] gives an interesting detailed analysis along these lines of the molecular rotations in long chain solid hydrocarbons.

axis of rotation $OA$ and if the azimuthal orientation of the triangle is $\phi$, then for the $n$th side

$$\cos\gamma_n=\sin\psi\cdot\sin[\phi+(n-1)2\pi/3]. \quad \text{(A.4)}$$

Combining Eqs. (A.1)–(A.3) gives

$$\Delta H_2^2=(1/6)\alpha^2(3\cos^2\theta''-1)^2 \times\sum_{n=1}^{3}[3\sin^2\psi\cdot\sin^2\{\phi+(n-1)2\pi/3\}-1]^2. \quad \text{(A.5)}$$

It can be shown that

$$\sum_{n=1}^{3}\sin^4\{\phi+(n-1)2\pi/3\}=(9/8)$$

and

$$\sum_{n=1}^{3}\sin^2\{\phi+(n-1)2\pi/3\}=(3/2),$$

that is, $\Delta H_2^2$ is independent of $\phi$. Substituting these values in Eq. (A.4), there results

$$\Delta H_2^2=(1/2)\alpha^2(3\cos^2\theta''-1)^2[(27/8)\sin^4\psi-3\sin^2\psi+1].$$

If the sample is a crystalline powder all directions of the axis of rotation are equally probable, so a spatial average over $\theta''$ must be taken, giving finally

$$\Delta H_2^2=(2/5)\alpha^2[(27/8)\sin^4\psi-3\sin^2\psi+1]. \quad \text{(A.6)}$$

Consider next the case in which the triangular group rotates about its $C_3$ axis in addition to rotating about the axis $OA$. If the two motions are independent it is legitimate to average over each separately. The above theorem is used again but now the lines $\mathbf{OP_1}$, $\mathbf{OP_2}$, and $\mathbf{OZ}$ correspond to a side of the triangle, the rotation axis $\mathbf{OA}$, and the $C_3$ axis. The polar angles $\theta_1, \theta_2$, are now $\pi/2, \psi$ and substituting in (A.2) one finds

$$\langle(3\cos^2\gamma_n-1)\rangle_{\substack{\text{rotation about}\\ C_3\text{ axis}}} =(1/2)(-1)(3\cos^2\psi-1). \quad \text{(A.7)}$$

Substituting (A.7) into (A.3) gives the result

$$\langle\langle(3\cos^2\theta_n-1)\rangle_{\substack{\text{rotation about}\\ \text{fixed axis OA}}}\rangle_{\substack{\text{rotation}\\ \text{about } C_3\text{ axis}}} =-(1/4)(3\cos^2\theta''-1)(3\cos^2\psi-1). \quad \text{(A.8)}$$

Substituting this in Eq. (A.1) and taking a spatial average over $\theta''$ gives the final result for a crystal powder

$$\Delta H_2^2=(\alpha^2/10)(3\cos^2\psi-1)^2. \quad \text{(A.9)}$$

Equations (A.6) and (A.9) can be checked by taking $\psi=0$, which corresponds to rotation about the $C_3$ axis and reduces the second moment by a factor of $(1/4)$.[6] Values of $\Delta H_2$ as a function of $\psi$ have been given graphically in Fig. 13 of I.

Equation (A.8) may be generalized as follows. Suppose a proton-proton line makes an angle $\theta$ with respect to the main field $H$ and $\theta_1$ with respect to an axis of rotation which we designate the 1st axis of rotation. If the $n$th axis of rotation makes an angle of $\theta_n$ with respect to the $(n-1)$th axis and so on, and $\theta^{(n)}$ is the angle between $H$ and the $n$th axis, then

$$\langle\cdots\langle(3\cos^2\theta-1)\rangle\cdots\rangle_{\substack{n\text{ axes of}\\ \text{rotation}}} =\{(3/2)\cos^2\theta_1-\tfrac{1}{2}\}\cdots\{(3/2)\cos^2\theta_n-\tfrac{1}{2}\} \times\{3\cos^2\theta^{(n)}-1\}. \quad \text{(A.10)}$$

Because $|\{(3/2)\cos^2\theta_k-\tfrac{1}{2}\}|\leq 1$ the introduction of additional rotations, particularly if these are about axes the directions of which are uncorrelated, rapidly reduces the magnitude of the average on the left of Eq. (A.10), and hence of $\Delta H_2^2$.

We wish to thank Dr. R. Bersohn for several cogent suggestions incorporated in the Appendix.

---

[6] H. S. Gutowsky and G. E. Pake, J. Chem. Phys. **18**, 162 (1950).

# Microwave Spectra and Molecular Structures of $HSiCl_3$, $CH_3SiCl_3$, and $(CH_3)_3SiCl$†

RICHARD C. MOCKLER,* JEP H. BAILEY, AND WALTER GORDY
*Department of Physics, Duke University, Durham, North Carolina*

(Received June 18, 1953)

From measurements of pure rotational transitions in the microwave region, the following molecular constants have been obtained. The $B_0$ values are in Mc/sec, 2472.45±0.04 for $HSi^{28}Cl_3^{35}$; 2346.07±0.04 for $HSi^{28}Cl_3^{37}$; 1769.84±0.03 for $C^{12}H_3SI^{28}Cl_3^{35}$; 1699.79±0.03 for $C^{12}H_3Si^{28}Cl_3^{37}$; 2197.44±0.04 for $(C^{12}H_3)_3Si^{28}Cl^{35}$; and 2147.88±0.03 for $(C^{12}H_3)_3Si^{28}Cl^{37}$. With $d_{SiH}=1.47$A (assumed), it is found for $SiHCl_3$ that $d_{SiCl}=2.021$A and $\angle ClSiCl=109°22'$. With the $CH_3$ configuration assumed as in methane and $\angle ClSiCl$ as in $SiHCl_3$ it is found for $CH_3SiCl_3$ that $d_{SiC}=1.876$A and $d_{SiCl}=2.021$A. With all bond angles assumed to be tetrahedral and the CH distance to be that in methane, it is found for $(CH_3)_3SiCl$ that $d_{SiC}=1.87$A and $d_{SiCl}=2.03$A.

PREVIOUS microwave investigations of $CHCl_3$ and $CH_3CCl_3$ in this laboratory[1] have shown that moments of inertia can be obtained and structural parameters calculated from the microwave rotational spectra of trichloro compounds without resolution and analysis of the complicated hyperfine structure caused by the Cl nuclear quadrupole interactions. This is done by the measurement of rotational transitions of medium or high $J$ values. Because the nuclear quadrupole splitting, like the Stark or Zeeman splitting, decreases rapidly with increasing $J$, it becomes relatively insignificant in Cl compounds ($eQq\approx 70$ Mc) for $J$ greater than about 5. Even for bromoform[2] ($eQq\approx 500$ Mc) it has proved possible to obtain accurate moments of inertia without analysis of the hyperfine structure by measurements of high rotational transitions ($J>10$). The present paper describes similar investigations of $HSiCl_3$ and $CH_3SiCl_3$. Partial and approximate structural determinations of these molecules have previously been made from electron diffraction.[3] Although more accurate determinations have been made in the present study, the structural information on these molecules is still incomplete. In particular, the CH and SiH distances and HCH angles are yet to be evaluated.

It has been shown that the tertiary butyl halides[4] have microwave rotational spectra characteristic of symmetric-top molecules. Furthermore, the carbon halogen distances in these molecules are essentially the same as those for the methyl halides. The present report deals also with the microwave spectrum and molecular dimensions of the structurally similar molecule $(CH_3)_3SiCl$.

## EXPERIMENTAL METHOD

The spectra were observed with a Stark modulation spectrometer. A 100-kc square-wave modulation was employed with the receiver tuned to the fundamental frequency. In most instances the frequency sweep method was employed, and the lines were displayed on a cathode-ray scope. In this type of observation a National HRO receiver was employed to amplify the signal. The lines of the weaker isotopic combinations were observed with an automatic pen-and-ink recorder (Esterline-Angus), so that a phase-sensitive detector and narrow-banded amplifier could be used.

The absorption cell was made of a 20-foot section of X-band wave guide with the center electrode supported with Teflon in the manner described by McAfee, Hughes, and Wilson.[5]

Line frequencies were measured in the usual manner with a frequency standard monitored by comparison of the lowest frequency in the multiplier chain, 5 Mc, with the standard 5-Mc frequency broadcast by station WWV.

All chemicals used were obtained from Anderson Laboratories.

## SPECTRAL CONSTANTS

Table I gives the observed frequencies. Where the error limits are 0.5 Mc or less, the lines were measured with standard frequency markers. Other lines were measured with a cavity wave meter only. For those lines measured with the frequency standard, the limiting factor in the accuracy is the broadness of the lines caused by the unresolved $K$ components and by hyperfine structure.

The species having mixed Cl isotopes are actually asymmetric tops, although they may be considered symmetric tops in the first approximation. The mixed species were treated as symmetric tops in assignment of the frequencies for Table I. The frequencies given in these cases are the wave-meter readings taken with the wave-meter pip set at the center of a group of partially resolved lines. The asymmetry here splits the transition into several components which, however, are too closely spaced for advantageous use in the

† This research was supported in part by The U. S. Air Force under Contract No. AF18(600)-497 monitored by the Office of Scientific Research, Air Research and Development Command, and by a grant from The Research Corporation.

* Part of this work was done while this author held a Frederick Gardner Cottrell Fellowship and part while he held a Texas Company Fellowship. It was submitted by him as part of a thesis required for the Ph. D. degree at Duke University.

[1] Ghosh, Trambarulo, and Gordy, J. Chem. Phys. **20**, 605 (1952).

[2] Williams, Cox, and Gordy, J. Chem. Phys. **20**, 1505 (1952).

[3] P. W. Allen and L. E. Sutton, Acta Cryst. **3**, 46 (1950).

[4] J. Q. Williams and W. Gordy, J. Chem. Phys. **18**, 994 (1950).

[5] McAfee, Hughes, and Wilson, Rev. Sci. Instr. **20**, 821 (1949).

TABLE I. Frequencies of observed transitions.

| Molecule | Transition | Frequency (Mc/sec) |
|---|---|---|
| $H\text{-}Si^{28}Cl_3^{35}$ | $J=5\rightarrow6$ | 29 669.87±0.5 |
| | 6→7 | 34 614.34±0.5 |
| | 7→8 | 39 560±10[a] |
| | 8→9 | 44 500±10[a] |
| $H\text{-}Si^{28}Cl_2^{35}Cl^{37}$ | 5→6 | 29 140±20[a] |
| | 6→7 | 34 000±20[a] |
| | 7→8 | 38 834±1 |
| | 8→9 | 43 690±10[a] |
| $H\text{-}Si^{28}Cl^{35}Cl_2^{37}$ | 7→8 | 38 180±10[a] |
| $H\text{-}Si^{28}Cl_3^{37}$ | 5→6 | 28 152.85±0.5 |
| | 6→7 | 32 845.02±0.5 |
| $CH_3\text{-}Si^{28}Cl_3^{35}$ | 8→9 | 31 840±20[a] |
| | 9→10 | 35 396.71±0.5 |
| | 10→11 | 38 950±20[a] |
| | 11→12 | 42 500±25[a] |
| $CH_3\text{-}Si^{28}Cl_2^{35}Cl^{37}$ | 8→9 | 31 410±10[a] |
| | 9→10 | 34 902.3±0.5 |
| | 10→11 | 38 400±10[a] |
| | 11→12 | 41 900±20[a] |
| $CH_3\text{-}Si\text{-}Cl^{35}Cl_2^{37}$ | 8→9 | 30 980±20[a] |
| | 9→10 | 34 400±20[a] |
| | 10→11 | 37 900±20[a] |
| | 11→12 | 41 310±20[a] |
| $CH_3\text{-}Si\text{-}Cl_3^{37}$ | 8→9 | 30 596.09±0.5 |
| | 9→10 | 33 995.81±0.5 |
| $(CH_3)_3\text{-}Si\text{-}Cl^{35}$ | 4→5 | 21 974.00±0.3[b] |
| | 6→7 | 30 762.89±0.2[b] |
| | 7→8 | 35 107.16±0.3<br>35 133.71±0.3<br>35 157.01±0.3[b]<br>35 198.47±0.3<br>35 219.92±0.3 |
| | 8→9 | 39 524.50±0.3<br>39 550.89±0.3<br>39 597.95±0.3<br>39 622.21±0.3 |
| $(CH_3)_3\text{-}Si\text{-}Cl^{37}$ | 7→8 | 34 317.44±0.5<br>34 343.20±0.5<br>34 366.12±0.5[b]<br>34 406.36±0.5<br>34 426.86±0.5 |
| | 8→9 | 38 607.26±0.5<br>38 636.09±0.5<br>38 662.28±0.5<br>38 707.44±0.5<br>38 731.09±0.5 |

[a] Frequencies measured with cavity type wave meter.
[b] Ground vibrational state. Frequencies unmarked by a or b are presumed to belong to higher vibrational states in the case of $(CH_3)_3Si\text{-}Cl$.

structural determinations. Hence, no effort was made to measure each component.

Table II gives the $B_0$ values and moments of inertia for the symmetric-top species measured. They were determined from the equation

$$\nu=2B_0(J+1)-4D_J(J+1)^3-2D_{JK}(J+1)K^2,$$

in which $D_J$ and $D_{JK}$ are assumed to be zero. Actually, these constants are not zero but are evidently negligible here, since their effects on the spectra could not be observed for the transitions measured. The moments of inertia are obtained from the $B_0$'s by $I=h/8\pi^2B_0$.

The composite line widths measured between half-power points were in all cases less than 10 Mc. For molecules with large moments of inertia about the symmetry axes, as these have, there is little decrease in the population of the states with decreasing $K$ up to the highest $K$'s involved in the present measurement. If nuclear statistics are neglected, the line intensity should decrease with $K$ approximately as $(1-K^2/(J+1)^2$. This factor, which results from the dipole matrix elements, indicates that the lines for $K=6$ of the $J=8\rightarrow9$ transition would be approximately half as strong as the $K=0$ line. From the slope and width of the observed lines it is apparent that the $K=6$ components of $SiHCl_3$ must be within 5 Mc of the $K=0$ component. This requires that $D_{JK}<10$ kc. From considerations similar to those described for $HSiCl_3$ it can be shown that $D_{JK}<10$ kc also for $CH_3SiCl_3$.

In $CH_3SiCl_3$ there are two symmetrical groups, $CH_3$ and $SiCl_3$, and if these groups could rotate independently the quantum number $K$ for rotation about the symmetry axes would consist of two parts, $K=|K_1+K_2|$, where $K_1$ and $K_2$ are integers or zero. Because of the interaction between the $CH_3$ and $SiCl_3$ groups, the internal rotation is restricted, and it is more correct in the present consideration to treat the relative movement of $CH_3$ and $SiCl_3$ as torsional oscillation rather than as free internal rotation. Theoretically, it should be possible to obtain a value for the frequency of the torsional oscillation and the height of the restricting barrier from a comparison of the intensities of the rotational lines in the ground and excited torsional oscillation states. Such has been done[6] for $CH_3SiF_3$ and the restricting barrier found to be 1200 $cm^{-1}$ in this molecule. Because of the broadness and complexity of its lines caused by the Cl nuclear coupling, no similar intensity measurements were undertaken for $CH_3SiCl_3$.

The rotational lines of $(CH_3)_3SiCl$ were found to fall closely in a harmonic series characteristic of a symmetric-top rotor. Several lines were observed for each transition. These lines are too widely spaced to be either Cl quad-

TABLE II. Rotational constants.

| Molecule | $B_0$(Mc/sec) | $I_B$($\times10^{40}$gcm$^2$) |
|---|---|---|
| $H\text{-}Si\text{-}Cl_3^{35}$ | 2472.489±0.041 | 338.291 |
| $H\text{-}Si\text{-}Cl_3^{37}$ | 2346.071±0.042 | 357.573 |
| $CH_3\text{-}Si\text{-}Cl_3^{35}$ | 1769.836±0.025 | 473.995 |
| $CH_3\text{-}Si\text{-}Cl_3^{37}$ | 1699.791±0.025 | 493.527 |
| $(CH_3)_3\text{-}Si\text{-}Cl^{35}$ | 2197.441±0.038 | 381.178 |
| $(CH_3)_3\text{-}Si\text{-}Cl^{37}$ | 2147.883±0.031 | 390.567 |

[6] (a) H. Minden and B. P. Dailey, Phys. Rev. **82**, 338 (1951); (b) J. Sheridan and W. Gordy, J. Chem. Phys. **10**, 965 (1951).

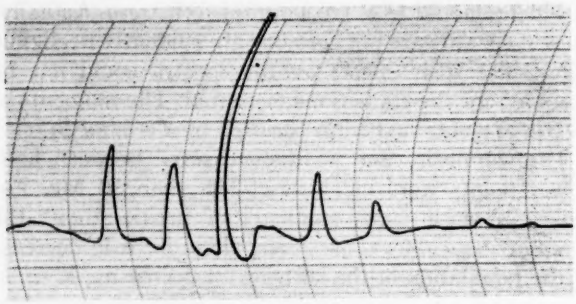

FIG. 1. Recording tracing of the 7→8 transition of $(CH_3)_3SiCl^{35}$.

rupole hyperfine structure or $K$ components separated by centrifugal distortion. Nor do they have the proper pattern to represent either of these types of structure. They are believed to arise from molecules in different vibrational levels. The strongest line observed for each transition was taken to represent the lowest vibrational level and was used for the calculation of the molecular dimensions. Measurements of relative intensities at different temperatures tend to confirm this choice. Had another of the group been chosen for this purpose the results would have been essentially the same, provided that the corresponding line in the different isotopic species had been used. The corresponding line in the different transitions yields the same value within the limits of experimental error for $B_0$. This is the feature which proves the symmetric-top structure.

A recorder tracing of one of the transitions of $(CH_3)_3Si^{28}Cl^{35}$ is shown in Fig. 1. Note that the tallest line is also the sharpest. Indeed, the degree of its sharpness is surprising. Its width measured between half-power points is only 3 Mc. This small width requires that the centrifugal stretching constant $D_{JK}$ be of the order of 3 kc or less. The width of this line is of the magnitude expected from the unresolvable hyperfine structure caused by the $Cl^{35}$ nuclear quadrupole coupling alone, with $D_{JK}=0$.

Of interest is the fact that all other lines are significantly wider (about two times wider) than the tallest one. This difference in width is too great to be attributed to differences in quadrupole coupling in different vibrational states. It must arise from a closely spaced sublevel structure of the over-all vibrational state in which the molecules reside when making the rotational transition which is observed. Indeed, this is just what is expected if the vibrational states represent torsional oscillations of the $CH_3$ groups. The complicated problem of the internal rotation or torsional oscillation of three mutually interacting groups of this kind has not to our knowledge been attacked theoretically. However, in the simpler problem of a single particle oscillating in a potential field of several equal minima separated by potential barriers of equal height, it is known that the vibrational levels, even the ground vibrational levels, are all split into sublevels. The effect of this sublevel structure on the rotational levels of $CH_3SiF_3$, in excited torsional oscillation states has been resolved.[6b] The sublevel splitting is greater the less the barrier height is above the particular excited level.

While it seems highly probable that the unusual structure exhibited in Fig. 1 results in the main from the torsional oscillation of the three $CH_3$ groups and their interaction with rotation and with other vibrational modes, we have not yet been able to account quantitatively for the observed features. Further experimental work is planned on this and similar trimethyl molecules in the hope that the theoretical approach will thereby be made simpler. If the lines toward higher frequencies from the most intense line are considered to represent molecules in excited states of the same mode, the fundamental frequencies of the mode can be estimated from the relative intensities to be roughly 100 to 150 $cm^{-1}$.

TABLE III. Molecular structures.

| Molecule | Structure |
|---|---|
| $SiHCl_3$ | $\angle ClSiCl = 109°22' \pm 15'$<br>$d_{SiCl} = 2.021 \pm 0.002$A<br>($d_{SiH} = 1.47$A assumed) |
| $CH_3SiCl_3$ | $d_{SiC} = 1.876$A<br>$d_{SiCl} = 2.021$A<br>(Assumptions: $CH_3$ configuration as in methane and $\angle ClSiCl$ as in $HSiCl_3$) |
| $(CH_3)_3SiCl$ | $d_{SiC} = 1.87$A<br>$d_{SiCl} = 2.03$A<br>(Assumptions: $d_{CH} = 1.093$ and all angles tetrahedral.) |

TABLE IV. Comparison of observed and calculated bond lengths.

| Molecule | Bond | Observed length in $A$: This study | Observed length in $A$: Electron diffraction[a] | Calculated length in $A$[b] |
|---|---|---|---|---|
| $HSiCl_3$ | SiCl | 2.021 | 1.98−2.05(±0.03) | 2.08 |
| $CH_3SiCl_3$ | | 2.021 | 2.01(±0.02) | |
| $(CH_3)_3SiCl$ | | 2.03 | 2.09(±0.03) | |
| $CH_3SiCl_3$ | SiC | 1.876 | | 1.89 |
| $(CH_3)_3SiCl$ | | 1.87 | 1.89(±0.03) | |

[a] From review by P. W. Allen and L. E. Sutton, Acta Cryst. 3, 46 (1950).
[b] Calculated with $d_{AB} = r_A + r_B - 0.06\,|x_A - x_B|$.

## MOLECULAR STRUCTURES

Since only two symmetric-top species were measured and since there are three unknown parameters, it is necessary to assume one of the parameters in $SiHCl_3$ in order to calculate the other two. The SiH distance was chosen as the one to be assumed, because the probable errors in the guessing of this distance causes little error in the other two parameters. Because of the light mass of the $H$, small variations in $d_{SiH}$ change the moments

of inertia but little. Furthermore, Gordy, Smith, and Trambarulo[7] have shown that the lengths of a large number of bonds formed by hydrogen with different elements $A$ fit the rule,

$$d_{AH}=r_A+0.32-.06|x_A-2.1|$$

within $\pm 0.02$. Here $r_A$ and $x_A$ are the covalent radius and electronegativity, respectively, of the atom $A$. For Si, $r_A$ is 1.17A, $x_A$ is 1.8, and the calculated $d_{SiH}$ is 1.47A. This value is assumed in the calculation of the $d_{SiCl}$ and $\angle$ ClSiCl listed in Table III.

In calculating the structure of $CH_3SiCl_3$ it was necessary to assume not only the $CH_3$ configuration but also one other parameter. Therefore, the calculated parameters have less significance than those for $HSiCl_3$. We assumed the $CH_3$ configuration as in methane and the $\angle$ ClCCl found for $HSiCl_3$.

For $(CH_3)_3SiCl$ we have assumed all bond angles to be tetrahedral and the CH distance to be that in methane, 1.093A. With these assumptions reasonable values were obtained for the CSi and SiCl distances. These values are close to those of the same bonds in $CH_3SiCl_3$.

The bond distances obtained are compared in Table IV with those calculated from the revised[7] Schomaker-Stevenson rule and with those obtained from electron diffraction. It will be noted that the observed SiCl distances are 0.06A shorter than the calculated values. This extra shortening is in addition to that attributed to ionic resonance and already taken into account in the calculated values. It can be attributed to double-bond character in the SiCl bonds. It has been shown[6a,7] that the second-row elements, particularly Si, show a special tendency to use the $3d$ orbitals to augment their valency. A reasonable representation of the electronic ground state of these molecules would be a resonant hybrid with the forms

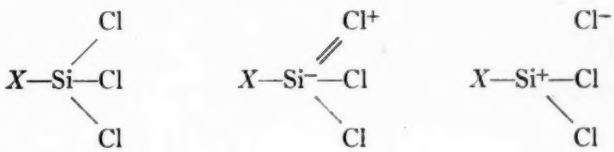


being the principal contributing ones.

[7] Gordy, Trambarulo, and Smith, *Microwave Spectroscopy* (John Wiley and Sons, Inc., New York, 1953), Chap. 8.

THE JOURNAL OF CHEMICAL PHYSICS VOLUME 21, NUMBER 10 OCTOBER, 1953

# Microwave Spectrum and Molecular Structure of Trichloro Germane*

PUTCHA VENKATESWARLU, RICHARD C. MOCKLER,† AND WALTER GORDY
*Department of Physics, Duke University, Durham, North Carolina*

(Received June 18, 1953)

From measurements of the pure rotational transitions in trichloro germane, the rotational constants $B_0$ (in megacycles/sec) for the various isotopic modifications of the molecule were found to be: 2172.75 for $HGe^{70}Cl_3^{35}$, 2169.26 for $HGe^{72}Cl_3^{35}$, 2165.84 for $HGe^{74}Cl_3^{35}$, 2063.74 for $HGe^{70}Cl_3^{37}$, 2060.43 for $HGe^{72}Cl_3^{37}$, and 2057.20 for $HGe^{74}Cl_3^{37}$. The calculated structure from the above data for the molecule in the ground state is: $d_{GeH}=1.55\pm0.04$A, $d_{GeCl}=2.1139\pm0.0010$A, and $\angle$ ClGeCl $=108°17'\pm12'$. Rotational lines for the molecule when it is in the two excited $GeCl_3$ deformation vibrations are also measured and the corresponding molecular structures calculated.

## INTRODUCTION

THE structures of but few germanium molecules are known. The symmetric-top molecules $GeCl_4$, $GeBr_4$, $GeI_4$, and $Ge_2H_6$ have been investigated by electron diffraction,[1] $GeH_4$ by infrared[2] spectroscopy, and the halides $GeH_3Cl$, $GeH_3Br$, and $GeF_3Cl$ by microwave spectroscopy.[3] No previous structural investigations, so far as we know, have been made on trichloro germane $GeHCl_3$ which is the subject of the present investigation.

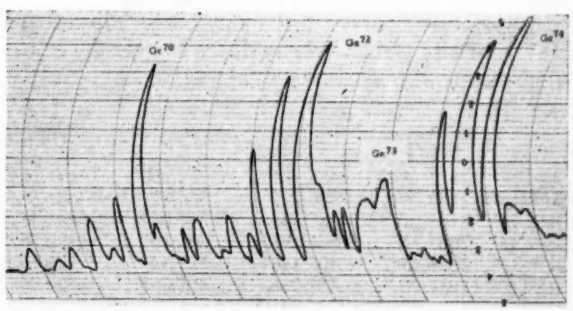


FIG. 1. Recording tracing of the $J=8\rightarrow9$ transition of $HGeCl_3^{35}$ for various Ge isotopes. The strongest line of each set corresponds to the ground vibrational state; the two to the left of each of these correspond to the $GeCl_3$ deformation vibrations.

* This research was supported by the United States Air Force under Contract No. AF18(600)-497 monitored by the Office of Scientific Research, Air Research and Development Command.

† Texas Company Fellow, now at University of Kentucky.

[1] P. W. Allen and L. E. Sutton, Acta Cryst. 3, 46 (1950).

[2] G. Herzberg, *Infrared and Raman Spectra of Polyatomic Molecules* (D. Van Nostrand Company, Inc., New York, 1945).

[3] Dailey, Mays, and Townes, Phys. Rev. 76, 137 (1949); Sharbaugh, Pritchard, Thomas, Mays, and Dailey, Phys. Rev. 79, 189 (1950); Anderson, Sheridan, and Gordy, Phys. Rev. 81, 819 (1951).

TABLE I. Observed rotational frequencies of $HGeCl_3$ in the ground state.

| Species | Transition $J''\rightarrow J'$ | Frequency[a] Mc/sec | $B=\nu/2J'$ |
|---|---|---|---|
| $HGe^{70}Cl_3^{35}$ | 4→5 | 21 728.34[b] | 2172.83 |
| | 5→6 | 26 073.24 | 2172.77 |
| | 6→7 | 30 418.73 | 2172.77 |
| | 7→8 | 34 763.48 | 2172.72 |
| | 8→9 | 39 109.31 | 2172.74 |
| $HGe^{72}Cl_3^{35}$ | 4→5 | 21 693.05[b] | 2169.31 |
| | 5→6 | 26 031.05 | 2169.25 |
| | 6→7 | 30 370.06 | 2169.29 |
| | 7→8 | 34 707.67 | 2169.23 |
| | 8→9 | 39 047.07 | 2169.28 |
| $HGe^{74}Cl_3^{35}$ | 4→5 | 21 659.15[b] | 2165.92 |
| | 5→6 | 25 990.93 | 2165.91 |
| | 6→7 | 30 321.85 | 2165.85 |
| | 7→8 | 34 652.66 | 2165.79 |
| | 8→9 | 38 984.86 | 2165.83 |
| $HGe^{70}Cl_3^{37}$ | 8→9 | 37 147.40 | 2063.74 |
| $HGe^{72}Cl_3^{37}$ | 7→8 | 32 967.08 | 2060.44 |
| | 8→9 | 37 087.62 | 2060.42 |
| | 9→10 | 41 208.73 | 2060.44 |
| $HGe^{74}Cl_3^{37}$ | 7→8 | 32 915.41 | 2057.21 |
| | 8→9 | 37 029.43 | 2057.19 |
| | 9→10 | 41 144.02 | 2057.20 |

[a] The absolute frequencies are probably accurate to ±0.7 Mc but the isotopic frequency differences are more accurate.
[b] These lines are not well separated from the nearby lines corresponding to the excited vibrational states.

The method of investigation is the same as that described in the accompanying paper[4] on $HSiCl_3$ and $CH_3SiCl_3$. The sample of $GeHCl_3$ used was obtained from Anderson Laboratories. It was found to be relatively unstable at room temperatures and was kept at liquid air temperatures when not in use. Nevertheless, it was found necessary to repurify the sample at frequent intervals by fractional distillation.

## SPECTRAL FREQUENCIES AND CONSTANTS

As in $HSiCl_3$ it was found possible to ignore the Cl quadrupole hyperfine structure in the spectrum. Fortunately also the $D_{JK}$ in this molecule is sufficiently small that the separation of the lines of different $K$ are not resolved even at pressures of the order of $10^{-2}$ mm of Hg. These facts not only simplified the analysis of the spectrum but also made it possible to detect rotational lines of isotopic species of low abundance. Even without the complications of hyperfine structure and separation of $K$ components, the rotational spectrum of $HGeCl_3$ is fairly cluttered with lines of different isotopic species (germanium has 3 relatively abundant isotopes and Cl has two) and with lines of molecules in excited vibrational states. By careful examination and precise measurement of the different lines of several rotational transitions, it was possible to correctly assign the different lines observed to different molecular species.

Figure 1 is an automatic recording of the rotational lines of the molecules $HGe^{70}Cl_3^{35}$, $HGe^{72}Cl_3^{35}$, $HGe^{73}Cl_3^{35}$, and $HGe^{74}Cl_3^{35}$ corresponding to the transition $J=8\rightarrow9$. The lines are only about 4 Mc in breadth. This sets an upper limit of 4 kc for $D_{JK}$.

TABLE II. Molecular constants of $HGeCl_3$ in the ground state.

| | $B_0$ Mc/sec | $I_B$(observed)[a] (g cm²×10⁻⁴⁰) | $I_B$(calculated)[b] (g cm²×10⁻⁴⁰) | $I_A$(calculated)[b] (g cm²×10⁻⁴⁰) |
|---|---|---|---|---|
| $HGe^{70}Cl_3^{35}$ | 2172.75 | 386.101 | 386.099 | 681.551 |
| $HGe^{72}Cl_3^{35}$ | 2169.26 | 386.722 | 386.722 | 681.551 |
| $HGe^{74}Cl_3^{35}$ | 2165.84 | 387.333 | 387.331 | 681.551 |
| $HGe^{70}Cl_3^{37}$ | 2063.74 | 406.496 | 406.497 | 720.502 |
| $HGe^{72}Cl_3^{37}$ | 2060.43 | 407.149 | 407.149 | 720.502 |
| $HGe^{74}Cl_3^{37}$ | 2057.20 | 407.788 | 407.788 | 720.502 |

[a] Obtained from the observed $B_0$ values using $h=6.6237\times10^{-27}$ erg sec.
[b] Calculated from the molecular structure given in Table V.

[4] Mockler, Bailey, and Gordy, J. Chem. Phys. 21, 1710 (1953).

TABLE III. Observed rotational frequencies of $HGeCl_3$ molecules in the lowest excited vibrational state.

| Species | Transition $J''\rightarrow J'$ | Frequency Mc/sec | $B=\nu/2J'$ | $B_v$ average | $I_{B_v}$ (g cm² ×10⁻⁴⁰) |
|---|---|---|---|---|---|
| $HGe^{70}Cl_3^{35}$ | 4→5 | 21 733.38[a] | 2173.34 | | |
| | 5→6 | 26 080.10 | 2173.34 | | |
| | 6→7 | 30 426.84 | 2173.35 | | |
| | 7→8 | 34 771.98 | 2173.25 | | |
| | 8→9 | 39 118.91 | 2173.27 | 2173.30 | 386.004 |
| $HGe^{72}Cl_3^{35}$ | 4→5 | 21 696.76[a] | 2169.68 | | |
| | 5→6 | 26 035.67 | 2169.64 | | |
| | 6→7 | 30 376.20 | 2169.73 | | |
| | 7→8 | 34 715.29 | 2169.71 | | |
| | 8→9 | 39 055.31 | 2169.74 | 2169.70 | 386.644 |
| $HGe^{74}Cl_3^{35}$ | 4→5 | 21 662.45[a] | 2166.25 | | |
| | 5→6 | 25 995.03 | 2166.25 | | |
| | 6→7 | 30 327.36 | 2166.24 | | |
| | 7→8 | 34 659.03 | 2166.19 | | |
| | 8→9 | 38 992.19 | 2166.23 | 2166.23 | 387.263 |

[a] The lines indicated by [a] are not well separated from the nearby lines corresponding to the ground state.

The line frequencies for the ground vibrational state are given in Table I. Spectral constants obtained from these are listed in Table II with those calculated from the molecular dimensions which were assigned. In calculating the spectral constant $B_0$ with the equation,[2]

$$\nu=2B_0(J+1)-4D_J(J+1)^3-2D_{JK}(J+1)K^2$$

the terms in $D_J$ and $D_{JK}$ were neglected. The accuracy and resolution obtained did not allow an evaluation of these extremely small stretching constants $D_J$ and $D_{JK}$ in this molecule. However, the results do set the upper limit for $D_{JK}<4$ kc and for $D_J<2$ kc.

## MOLECULES IN THE EXCITED VIBRATIONAL STATE

The molecule $HGeCl_3$ belongs to the point group $C_{3v}$ and will have six fundamentals of which three belong to the species $A_1$ (totally symmetric), and the other

three to the species $E$ (doubly degenerate). All the six fundamentals are both Raman and infrared active. Volkringer, Tchakirian, and Freymann[5] investigated the Raman spectrum of $HGeCl_3$ in HCl solution and obtained four lines at 131, 162, 251, and 315 $cm^{-1}$, of which the first two probably correspond to the two $GeCl_3$ deformations. The low values of these frequencies indicate that there would be appreciable number of molecules in these excited vibrational states at the room temperature and also at lower temperatures.

Figure 1 shows clearly the rotational lines when the molecule is in two different excited states besides the main lines corresponding to the molecule in the ground state. The excited states presumably correspond to the $GeCl_3$ deformation vibrations [$\nu_3(a_1)$ and $\nu_6(e)$]. The frequencies of the rotational lines corresponding to the more populated vibrational state (which probably corresponds to the lower-frequency $GeCl_3$ deformation vibration) of the $Cl^{35}$ species are given in Table III. A few of the rotational lines corresponding probably to the higher-frequency $GeCl_3$ deformation vibration are also measured and their frequencies given in Table IV. The corresponding $B_v$ and $I_{B_v}$ values are also included in Table III and IV.

TABLE IV. Observed rotational frequencies of $HGeCl_3$ molecules in the second-lowest excited vibrational state.

| Species | Transition $J''\rightarrow J'$ | Frequency Mc/sec | $B_v$ | $I_{B_v}$ (g cm² $\times 10^{-40}$) |
|---|---|---|---|---|
| $HGe^{70}Cl_3^{35}$ | 7→8 | 34 777.01 | 2173.56 | 385.957 |
| $HGe^{72}Cl_3^{35}$ | 7→8 | 34 719.42 | 2169.96 | 386.598 |
| $HGe^{74}Cl_3^{35}$ | 6→7 | 30 332.33 | 2166.59 | |
| | 7→8 | 34 664.83 | 2166.55 | 387.206 |

## MOLECULAR STRUCTURE

The molecule $GeHCl_3$ has only three independent structural parameters whereas six isotopic species were measured (Tables I and II). More than enough information is therefore available to obtain a complete structural determination of the molecule. The calculated dimensions are given in Table V in which the structure of $ClGeH_3$ is also included for comparison. As a check on the internal consistency, these values were used to calculate $I_B$ values for all six isotopic species. These are compared with the measured values in Table II. This comparison was useful in the assignment of probable errors in the structural dimensions obtained.

[5] Volkringer, Tchakirian, and Freymann, Compt. rend., **199**, 292 (1934).

TABLE V. Structure of $HGeCl_3$[a] and $ClGeH_3$.

| Molecule $XGeY_3$ | $d_{GeCl}$ | $d_{GeH}$ | $\angle$YGeY |
|---|---|---|---|
| $HGeCl_3$ in the ground state | 2.1139±0.0010 | 1.55±0.04 | 108°17′±12′ |
| $HGeCl_3$ in the low frequency $GeCl_3$ deformation vibration | 2.1141±0.0010 | 1.55 (assumed) | 108°3′±12′ |
| $HGeCl_3$ in the high frequency $GeCl_3$ deformation vibration | 2.1138±0.0010 | 1.55 (assumed) | 108°8′±12′ |

[a] The following values were used for the various constants involved for the determination of the structure of $HGeCl_3$: $M_{Ge_{74}}=73.9426$, $M_{Ge_{72}}=71.9430$, $M_{Ge_{70}}=69.9447$, $M_H=1.00813$, $M_{Cl_{35}}=34.97867$, $M_{Cl_{37}}=36.9777$ all in a.m.u. and Avogodro's number $N=6.0250\times10^{23}$.

The errors in the calculated structural dimensions will probably not be more than ±0.001A for $d_{GeCl}$, ±0.04A for $d_{GeH}$, and ±12′ for $\angle$ClGeCl. The large error assigned to $d_{GeH}$ results from the small effects on the moments of inertia of the variation in this parameter and probably also from the large zero-point vibration energy of the light H.

It is of interest that the GeCl distance is within 0.02A of that calculated with the revised Schomaker-Stevenson rule[6]

$$d_{AB}=r_A+r_B-0.06|x_A-x_B|\ddagger$$

and that the GeH distance is within the limits of error of the value 1.52A calculated with this rule if the revised value 0.032 of the H radius is employed. The fact that the observed GeCl distance is only slightly greater than the calculated value suggests that there is only a small amount of double-bond character in the GeCl bond. Contrast this with the SiCl bond in $HSiCl_3$ discussed in the accompanying paper.

It is of interest to compare the structural dimensions of the molecule in the excited deformation vibrational states with those in the ground state. Assuming $d_{GeH}$ to be the same as in the ground state (this is a good approximation as the vibrations correspond to $GeCl_3$ deformations), we obtain from the observed spectral constants the values for $d_{GeCl}$ and $\angle$ClGeCl. These values for the two lowest excited states are listed in Table V. The differences in the $\angle$ClGeCl for the different states concerned, though small, are more pronounced than the differences in $d_{GeCl}$ values. This, of course, is understandable as the vibrations of the excited states correspond to the $GeCl_3$ deformations.

[6] Gordy, Smith, and Trambarulo, *Microwave Spectroscopy* (John Wiley and Sons, Inc., New York, 1953).

‡ $|x_A-x_B|$ represents the electronegativity difference of the bonded atoms, and $r_A$ and $r_B$ their respective radii.

# Excluded Volume in Polymer Chains

B. H. ZIMM, *General Electric Research Laboratory, The Knolls, Schenectady, New York*

AND

W. H. STOCKMAYER AND M. FIXMAN,* *Department of Chemistry, Massachusetts Institute of Technology, Cambridge, Massachusetts*

(Received March 4, 1953)

This discussion is concerned with the excluded volume effect in polymer chains, i.e., the mathematical problem of random flights with correlations between the flights, which is of importance in relating the mean size of a chain to its structure. A general formulation of the problem is set up and compared with the theory of Markoff processes. It is shown that although an integral equation of the Markoff form for the distribution function exists, it contains a complicated function whose exact evaluation is difficult. Since the same function occurs in the problem of the osmotic second virial coefficient, it is natural to relate the excluded volume effect to the second virial coefficient. The results of preliminary numerical calculations for the relation between the mean square radius of the chain and the second virial coefficient, in good agreement with experiment, are given. It is concluded that the volume effect is certainly not negligible for real chains, except when the second virial coefficient is zero, and that the effect increases with increasing chain length.

## 1. INTRODUCTION

IN recent years many attacks have been made on the problem of the so-called excluded volume effect in a polymer chain, and in this paper we report some of our efforts in this direction. The effect arises when consideration of the actual volume of chain elements is introduced into the classical random-flights problem. In complete form, the solution to the problem would specify the probability distribution of all configurations of the chain in such fashion that various average quantities of physical interest could be readily found. However, most of the published work has been confined to a more limited problem, that of the mean square distance $\langle L^2\rangle$ between the ends of a chain of $N$ links, and the asymptotic behavior of $\langle L^2\rangle/N$ for large $N$ has been of particular interest.

The problem is to find the effect on the chain dimensions of interactions between nonbonded pairs of chain atoms. For a true random-flight chain of $N$ links, without interactions, the well-known result for large $N$ is

$$\langle L^2\rangle = Na^2, \tag{1.1}$$

where $a$ is the length of a link. We shall term "short-range" all interactions, such as fixed valence angles and hindered rotation about bonds, between atoms that are near neighbors. These do not change the form of Eq. (1.1), but do change the value of the constant $a$, which then becomes different from the actual length of a link.[1,2] Tchen[3] has shown that all interactions between pairs of atoms separated by only a finite number of links cannot change the asymptotic proportionality of $\langle L^2\rangle$ to $N$ as $N$ approaches infinity. In such cases the constant $a$ becomes the "statistical chain element" of Kuhn.[4]

In contrast to the situation with respect to short-range effects, little agreement exists about the long-range effects caused by the general van der Waals interactions among nonbonded chain atoms. Three distinctly different conclusions have been reached by various workers.

(a) The effect is negligible, so that $\langle L^2\rangle$ retains exactly the value it would have if long-range interactions were absent.[5–7]

(b) The effect increases $\langle L^2\rangle$ but does not alter its proportionality to $N$; i.e., it behaves just like the "short-range" effects discussed above.[8–10]

(c) The effect causes $\langle L^2\rangle$ to become asymptotically proportional to a power of $N$ higher than the first;[4,11,12] or at least $\langle L^2\rangle/N$ does not approach a finite limit as $N$ increases without limit.

Of these, the first point of view is surely incorrect. Two of the papers in this group[5,6] have already been adequately criticized elsewhere,[9] while that of Grimley[7] is rendered invalid at the start by his choice of partition function, in which a set of interdependent probabilities is treated as though they were independent. Very recently Rubin,[13] in a discussion with very much the same point of departure as our own treatment, has definitely rejected the alternative (a).

It is more difficult to decide between the other alternatives (b) and (c). The studies[8–10] leading to (b) all treated the problem as that of a Markoff process, a maneuver that can easily lead to errors,[14] as we shall also show. On the other hand, the present theories indicating

* This work was supported in part by the Office of Ordnance Research under contract with the Massachusetts Institute of Technology.

[1] W. J. Taylor, J. Chem. Phys. **15**, 412 (1947).
[2] H. Benoit, J. Polymer Sci. **3**, 376 (1948).
[3] C. M. Tchen, J. Chem. Phys. **20**, 214 (1952).
[4] W. Kuhn, Kolloid-Z. **68**, 2 (1934).
[5] J. J. Hermans, Rec. trav. chim. **69**, 220 (1950).
[6] H. Hadwiger, Makromol. Chem **5**, 148 (1950).
[7] T. B. Grimley, Proc. Roy. Soc. (London) **A212**, 339 (1952).
[8] E. W. Montroll, J. Chem. Phys. **18**, 734 (1950).
[9] Hermans, Klamkin, and Ullman, J. Chem. Phys. **20**, 1360 (1952).
[10] P. Debye and R. J. Rubin, Phys. Rev. **87**, 214 (1952).
[11] P. J. Flory, J. Chem. Phys. **17**, 303 (1949).
[12] M. Yamamoto, Busseiron Kenkyû **44**, 36 (1951); Chem. Abstracts **46**, 1844 (1952).
[13] R. J. Rubin, J. Chem. Phys. **20**, 1940 (1952).
[14] K. Suzuki, J. Chem. Phys. **19**, 385 (1952).

(c) also involve many approximations. On the whole, we are inclined, on the basis of existing experiments[15] as well as theory, to favor view (c), although no definite proof is offered herein. Both (b) and (c) are possible according to the recent analysis of Rubin[13] already quoted.

Actually, $\langle L^2\rangle$ is not the quantity of greatest practical interest. Light scattering, for example, measures the mean square radius $R^2$, defined by

$$R^2=\Sigma_i\langle R_i^2\rangle/N=\Sigma_p\Sigma_t\langle r_{pt}^2\rangle/2N^2, \tag{1.2}$$

where $\langle R_i^2\rangle$ is the mean square distance of the $i$th element from the molecular center of mass, and $\langle r_{pt}^2\rangle$ is the mean-square distance between the $p$th and $t$th elements. The several "hydrodynamic radii" inferred from such kinetic properties as intrinsic viscosity or friction constant may be expected to depend on still other averages.

The volume effect depends markedly on the nature of the polymer-solvent interactions, which usually are judged experimentally by the value of the osmotic second virial coefficient.[7,11,15] A useful theory of the volume effect should therefore consider the solvent explicitly and relate the quantities $R^2$ and the virial coefficient $A_2$ as directly as possible. This has been recognized by several authors,[7,11] and is in part the object of the present work. Such a relation would be much easier to test experimentally than one concerned with the asymptotic behavior of $R^2/N$.

In what follows, we consider the general distribution function of a single chain molecule in the same form that has been previously used to treat the second virial coefficient,[16] and later derive a differential equation which is suitable for approximate calculations of $\langle r_{pt}^2\rangle$. The relation of these results to the theory of Markoff processes, which has been applied to the polymer problem by several writers[5,6,8–10] is also examined. The close relationship between the excluded-volume problem and that of the second virial coefficient is explicitly demonstrated. Finally, some preliminary calculations relating $R$ and $A_2$ are briefly described and discussed. No attempt is made to treat the problem in relation to intrinsic viscosity or other kinetic properties, as rigorous theories in applicable form are lacking.

## 2. THE DISTRIBUTION FUNCTION

Let $f_N(p, t)$ be the pair distribution function for elements $p$ and $t$ of a chain of $N$ elements; that is, $f_N(p, t)d(p)d(t)$ measures the probability that the elements $p$ and $t$ have their coordinates at specified values in the range $d(p)$ and $d(t)$. To derive the properties of $f_N(p, t)$ we must consider more general distribution functions. For a chain of $N$ elements, we denote by $F_{\nu N}\{\nu\}$ the probability function governing the positions of a set of $\nu(\leqslant N)$ specified chain elements, as a function of the coordinates $\{\nu\}$ of all the members of this set. The most detailed of these functions is $F_{NN}\{N\}$, in which the distribution of all the coordinates $\{N\}$ of the entire chain is explicitly formulated. From the definitions, it is clear that

$$F_{\nu N}\{\nu\}=\int\cdots\int F_{NN}\{N\}d\{N\}/d\{\nu\}, \tag{2.1}$$

in which the symbol $d\{N\}/d\{\nu\}$ indicates that the integration† goes over all coordinates except those of the specified $\nu$ elements. Instances of the above relation, of special importance later, are

$$F_{3N}(p, t, t+1)=\int\cdots\int F_{NN}\{N\}d\{N\}/d(p, t, t+1); \tag{2.2}$$

$$f_N(p, t)\equiv F_{2N}(p, t)=\int F_{3N}(p, t, t+1)d(t+1); \tag{2.3a}$$

$$f_N(p, t+1)=\int F_{3N}(p, t, t+1)d(t). \tag{2.3b}$$

In these expressions $p$, $t$, $t+1$ designate particular chain elements, their coordinates being indicated by symbols in parentheses.

A definite form must now be adopted for the basic function $F_{NN}\{N\}$, and we take

$$F_{NN}\{N\}=Q_N^{-1}\prod_{i=1}^{N-1}\psi(i, i+1)\prod_{1\leqslant i<j\leqslant N}\phi(i, j), \tag{2.4}$$

where the indices $i$ and $j$ denumerate the chain elements. Here $Q_N^{-1}$ is a normalizing factor to be discussed below. The quantity $\psi(i, i+1)$ may be called the bond probability; it exists only for adjacent elements in the chain. Since this bond function necessarily has a short range (i.e., it rapidly goes to zero if the distance between the two bonded elements involved strays appreciably from the normal bond length), the details of its analytical form are unimportant, and it is sufficient to use a delta function. If we write $\mathbf{s}$ for the vector distance between elements $i$ and $i+1$, and $a$ for the normal bond length, and further agree to normalize $\psi$ to unity, we have

$$\psi(i, i+1)=\psi(\mathbf{s})=(4\pi a^2)^{-1}\delta(|\mathbf{s}|-a) \tag{2.5a}$$

with

$$\int\psi(i, i+1)d(i)=1=\int\psi(i, i+1)d(i+1). \tag{2.5b}$$

The functions $\phi(i, j)$ give contributions to the distribution function from all pairs of elements. Since interactions between any two bonded elements are already

[15] Outer, Carr, and Zimm, J. Chem. Phys. **18**, 830 (1950).
[16] B. H. Zimm, J. Chem. Phys. **14**, 164 (1946).

† In all the integrals of this section, integration is to be understood as extending over all values of each of the coordinates involved. In general the limits are not explicitly given.

described by the $\psi$ functions, it is convenient to set $\phi(i, i+1)$ at unity. For nonbonded pairs of atoms, the nature of the function $\phi(i, j)$ has been discussed previously.[16] We recall that it can be related to the potential of mean force $u(i, j)$ between the elements $i$ and $j$ when in the chosen solvent

$$u(i, j) \equiv -kT \ln \phi(i, j), \tag{2.6}$$

and to a short-range function

$$\chi(i, j) \equiv \phi(i, j) - 1, \tag{2.7}$$

which vanishes unless $i$ and $j$ are quite close to each other. It can be seen from Eq. (2.4) that if $\chi$ were zero for all pairs of elements, the distribution function would reduce to that for the problem of random flights.

Several objections could be raised to the form of Eq. (2.4), but these do not seem relevant to the problem of interest.

(a) There is explicit provision neither for constancy of valence angles (which would require a bond probability depending on the coordinates of three adjacent chain elements), nor for restricted rotation about chain bonds (which would require the bond probability to depend on the coordinates of at least four chain elements). However, these are still essentially short-range effects, and it has been repeatedly shown that they do not alter the Gaussian asymptotic form of the pair distribution function when interactions between distant elements are ignored. It is therefore adequate to follow Kuhn,[4] to the extent that we treat a chain of $N$ elements linked by universally jointed bonds of length $a$ in place of a more detailed physical model of the chain.‡

(b) According to Eq. (2.4), the potentials of average force $u(i, j)$ between nonbonded elements are additive; this is the "superposition" principle,[17] which is known to be inexact. This assumption would surely force itself on any present attempt at explicit calculation. It causes trouble only if three or more nonbonded elements are simultaneously close to each other, and since the actual average density of chain elements within typical polymer molecules is low, we may expect little error for the important configurations of the chain. In a recent paper, Rubin[13] has used essentially the same function as (2.4), with special choices of $\psi$ and $\phi$.

It is convenient to normalize the distribution functions so that

$$\int \cdots \int F_{NN}\{N\} d\{N\} = V, \tag{2.8a}$$

where $V$ is the arbitrarily large volume of solution in which the chain molecule moves. This amounts to defining the normalizing factor $Q_N$ of the chain as

$$Q_N = V^{-1} \int \cdots \int \prod_{i=1}^{N-1} \psi(i, i+1) \times \prod_{1 \leqslant i < j \leqslant N} \phi(i, j) d\{N\} \tag{2.8b}$$

and further has the convenient consequence that the pair distribution function is normalized to unity,

$$\int f_N(p, t) d(t) = 1 = \int f_N(p, t) d(p). \tag{2.8c}$$

Without loss of generality, we can therefore fix the position of element $p$ at the origin of the coordinate system, and this will be implicit in all relations to follow.

An examination of Eq. (2.4) reveals that the complete distribution function may be factored as follows:

$$F_{NN}\{N\} = Q_N^{-1} \psi(t, t+1) Q_t F_{tt}(1, 2, \cdots, t) \times Q_k F_{kk}(t+1, \cdots, N)[1 + H_{tk}], \tag{2.9}$$

where we have put $k = N - t$ and the last factor is defined by

$$1 + H_{tk} \equiv \prod_{\substack{1 \leqslant i \leqslant t \\ t+1 \leqslant j \leqslant N}} \phi(i, j). \tag{2.10}$$

This factorization is the basis of the several useful results, and provides a means of relating the intramolecular long-range effects on the $t$th link in a chain of $N$ elements to the interactions between the two parts of the chain on either side of the specified link.

### 3. EXCLUDED VOLUME AND MARKOFF CHAINS

We may define a new function $\Phi_N(p, t, t+1)$ by the equation

$$F_{2N}(p, t, t+1) / f_N(p, t) \equiv \Phi_N(p, t, t+1). \tag{3.1}$$

Clearly $\Phi_N$ is the conditional probability for the $(t+1)$st element when the elements $p$ and $t$ are at specified positions. By Eq. (2.3b), we then have

$$f_N(p, t+1) = \int f_N(p, t) \Phi_N(p, t, t+1) d(t), \tag{3.2}$$

which is the integral equation for a Markoff process, with $\Phi_N$ playing the role of the transition probability.[18] Moreover, Eq. (3.1) with Eq. (2.3a) shows this probability to be normalized, in the sense that

$$\int \Phi_N(p, t, t+1) d(t+1) = 1, \tag{3.3}$$

but this is not true with respect to integration over the coordinates of element $t$. It should however be noted that $\Phi_N$ depends not only on the position of element $t+1$

‡ Alternatively, one could modify the functions $\phi(i, j)$ between second and third neighbors along the chain to take account of local hindrances, but this would seem needlessly complicated.

[17] J. G. Kirkwood, J. Chem. Phys. 3, 300 (1935).

[18] S. Chandrasekhar, Revs. Modern Phys. 15, 1 (1943), Eq. (218).

relative to that of $t$, but also on their positions with respect to element $p$. The formal resemblance to a true Markoff chain is therefore limited, and in any case is useful only if a physically plausible form for $\Phi_N$ can be guessed or derived from an appropriate model.

Our distribution function (2.4) allows us to display the physical nature of $\Phi_N$ quite readily. From Eqs. (2.2) and (2.9) we may write

$$f_{3N}(p, t, t+1)=Q_tQ_kQ_N^{-1}\psi(t, t+1)$$

$$\times\int\cdots\int F_{tt}F_{kk}(1+H_{tk})d\{N\}/d(p, t, t+1), \quad (3.4)$$

where for brevity the explicit coordinates of $F_{tt}$ and $F_{kk}$ have been suppressed. Also, Eq. (2.3a) yields

$$f_N(p, t)=Q_tQ_kQ_N^{-1}\int\cdots\int\psi(t, t+1)$$

$$\times F_{tt}F_{kk}(1+H_{tk})d\{N\}/d(p, t), \quad (3.5)$$

so that the conditional probability may be expressed as

$$\Phi_N(p, t, t+1)=\gamma(p, t)\psi(t, t+1)$$

$$\times\int\cdots\int F_{tt}F_{kk}(1+H_{tk})d\{N\}/d(p, t, t+1), \quad (3.6)$$

where $\gamma(p, t)$ is a normalizing function to be determined from (3.3).

It will be helpful to express $\Phi_N$ in yet another form. The integral of Eq. (3.6) is the sum of two terms, the first of which is easily split into a product of two independent factors,

$$\int\cdots\int F_{tt}F_{kk}d\{N\}/d(p, t, t+1)$$

$$=\left[\int\cdots\int F_{tt}d\{t\}/d(p, t)\right]$$

$$\cdot\left[\int\cdots\int F_{kk}d\{k\}/d(t+1)=f_t(p, t)\cdot 1. \quad (3.7)\right.$$

The second term cannot be simply reduced, and will be of special interest. Designating it by $J_N$, we have

$$J_N(p, t, t+1)$$

$$\equiv\int\cdots\int F_{tt}F_{kk}H_{tk}d\{N\}/d(p, t, t+1). \quad (3.8)$$

With these relations, the conditional probability may be written

$$\Phi_N(p, t, t+1)=\gamma'(p, t)\psi(t, t+1)$$

$$\times\{1+[J_N(p, t, t+1)/f_t(p, t)]\}, \quad (3.9)$$

where $\gamma'$ is a new normalizing function of $(p, t)$.

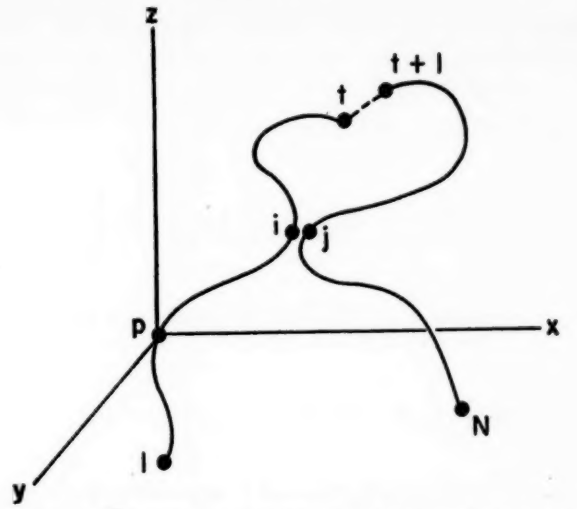


FIG. 1. Configurations of a chain involving a single contact between elements $i$ and $j$; other chain elements of special interest in various equations are designated.

From Eq. (2.10) the function $H_{tk}$ is seen to involve interaction terms $\phi(i, j)$ between all the elements in the first part of the chain (i.e. the first $t$ elements) with all of those in the other part. The nature of the integral $J_N$ may perhaps be better understood by referring to Fig. 1. The integration goes over all the coordinates except those of elements $p, t, t+1$ and the term $H_{tk}$ in the integrand will be zero unless one or more elements of the first part of the chain is close to one or more elements in the second part.

Other forms for $\Phi_N$ have been employed[6,9] which amount to considering only the interaction of the $(t+1)$st element with the others. Since our deductions are straightforward consequences of the distribution function (2.4), it would appear that such special assumptions about $\Phi_N$, or the related diffusion equation,[10] cannot be expected to yield trustworthy conclusions regarding the volume effect.

It may at first appear surprising that the complete set of interactions between the two parts of the chain should play a first-order role in the transition probability for the $(t+1)$st element. However, all these elements are coupled into a single chain by valence bonds, so that an interaction anywhere may result in an average force at any specified link. Only if the valence links were all severed could the fate of the element $(t+1)$ be discussed entirely in terms of its own direct interactions ($\phi$ functions) with the other elements.

## 4. DIFFERENTIAL FORMS

To bring the result of the previous section into a form suitable for calculation, it is expedient to follow

Hermans, Klamkin, and Ullman[9] by going over to a differential equation. From Eqs. (3.5) to (3.8) we have

$$f_N(p,t)=Q_tQ_kQ_N^{-1}\Big[f_t(p,t)+\int\psi(t,t+1)J_N(p,t,t+1)d(t+1)\Big]$$

$$=\frac{f_t(p,t)+\int\psi(t,t+1)J_N(p,t,t+1)d(t+1)}{1+\int\int\psi(t,t+1)J_N(p,t,t+1)d(t,t+1)},\quad(4.1)$$

where the second form follows by normalizing the first to unity. Similarly, with the aid of (3.2) we obtain

$$f_N(p,t+1)=\int\psi(t,t+1)f_t(p,t)d(t)+\int\psi(t,t+1)J_N(p,t,t+1)d(t)$$

$$\Big/\,1+\int\int\psi(t,t+1)J_N(p,t,t+1)d(t,t+1).\quad(4.2)$$

To obtain a differential equation,[18] we now regard $f_N(p,t)$ as a continuous function $f_N(\mathbf{r},t)$, where $\mathbf{r}$ represents the coordinate (relative to that of element $p$ at the origin) of element $t$ of the chain, and set

$$\partial f_N/\partial t=f_N(p,t+1)-f_N(p,t).\quad(4.3)$$

The right-hand member, from Eqs. (4.1) and (4.2) is then expanded in terms of the displacement $\mathbf{s}$ from the $t$th to the $(t+1)$st element, and terms of third or higher order in $\mathbf{s}$ are dropped. This procedure leads in straightforward fashion to the result

$$\frac{6}{a^2}\frac{\partial f_N}{\partial t}=\frac{\nabla^2f_t+(\nabla_t^2J_N-\nabla_{t+1}^2J_N)\mathbf{r},\mathbf{r}+\cdots}{1+\int J_N(\mathbf{r},\mathbf{r})d\mathbf{r}+\cdots},\quad(4.4)$$

where in the denominator only the leading term of the expansion is explicitly written. The symbols $\nabla_t^2$ and $\nabla_{t+1}^2$ denote Laplacian operators with respect to the coordinates of elements $t$ and $t+1$, respectively,§ and the notation $\mathbf{r},\mathbf{r}$ means that the values of the functions so designated are to be taken when the coordinates of both these elements are at $\mathbf{r}$.

We shall not deal further with the distribution function itself, but turn our attention to the mean-square distance $\langle r_{pt}^2\rangle=\langle\mathbf{r}\cdot\mathbf{r}\rangle$ between elements $p$ and $t$. We multiply both sides of Eq. (4.4) by $r^2\cdot4\pi r^2dr$ and integrate, noting that

$$\int_0^\infty(\nabla^2f_t)r^2\cdot4\pi r^2dr=6\int_0^\infty f_t\cdot4\pi r^2dr=6,\quad(4.5)$$

and thus obtain

$$\frac{d\langle r_{pt}^2\rangle}{a^2dt}=\frac{1+(2\pi/3)\int_0^\infty(\nabla_t^2J_N-\nabla_{t+1}^2J_N)_{r,r}r^4dr+\cdots}{1+4\pi\int_0^\infty J_N(\mathbf{r},\mathbf{r})r^2dr+\cdots}.\quad(4.6)$$

The successful use of this formal relation in obtaining the excluded volume effect on $\langle r_{pt}^2\rangle$ obviously depends on the choice of a function to represent $J_N$. Exact evaluation based on Eq. (3.8) seems remote of attainment, but the physical sense of (3.8), as earlier discussed, should be kept in mind when selecting a trial function. Before considering this choice further, we make another important digression.

## 5. RELATION TO SECOND VIRIAL COEFFICIENT

The function $J_N$, which has been related to the deviations of a single chain from random-flight behavior, is also closely connected to the problem of the second virial coefficient. The osmotic pressure of a solution containing chains of various lengths can be expressed by the familiar expansion

$$\pi/RT=\Sigma_iC_iM_i^{-1}+\Sigma_i\Sigma_jA_{ij}C_iC_j+\cdots,\quad(5.1)$$

where $M_i$ is molecular weight and $C_i$ is concentration (in weight per unit volume) of the species $i$. Setting $B_{ij}=M_iM_jA_{ij}$, we have[16] the following expression for the second virial coefficient for chains composed of $l$ elements interacting with chains of $N-l=k$ elements:

$$B_{lk}=-(N_0/2V)\int\cdots\int F_{ll}F_{kk}H_{lk}d\{N\},\quad(5.2)$$

where $N_0$ is Avogadro's number and the other symbols retain their earlier meanings. If we introduce $J_N$ from its definition (3.8) and recall that integration over the coordinates of the last element simply gives a factor $V$, we get

$$-2B_{lk}/N_0=\int\int J_N(p,t,t+1)d(t,t+1).\quad(5.3)$$

The close connection between the excluded-volume problem and the virial-coefficient problem, though

§ It will be recalled that $J_N(p,t,t+1)$ depends on the coordinates of the two movable links $t$ and $t+1$. In the leading term of the numerator the Laplacian has been simply written $\nabla^2$ since $f_t$ does not depend on the coordinates of element $t+1$.

obvious enough from a physical point of view, thus stands very clearly revealed mathematically in terms of $J_N$. The similarities and differences may perhaps be made clearer by reference to Fig. 1. In the problem of the second virial coefficient, nothing directly restricts the relative motion of elements $t$ and $t+1$, and these can move quite far apart before all interactions between the two chains are reduced to negligible values. In the problem of the single chain, however, these elements are of course bonded together, and mathematically the occurrence of the bond function $\psi(t, t+1)$ in the integrals restricts our attention to those configurations in which these elements are separated by small distances.

From Fig. 1 we can also infer the nature of the average force on the $t$ to $t+1$ link resulting from the interaction function $J_N$ of Eq. (3.9). When the van der Waals interactions between the segments $i<t$ and $j>t+1$ are repulsive, the "tail" of the molecule (segments between $t+1$ and $N$) will be pushed out of the region between $p$ and $t$ so that the link between $t$ and $t+1$ will be pulled away from $p$.

The above result gives further weight, if it be needed, to our remarks in Sec. 3 concerning the transition probability $\Phi_N$. Since the virial coefficient clearly demands consideration of interactions between all parts of the two chains concerned, it is clear from Eq. (3.9) that the excluded-volume problem does so also.

Although Eq. (5.3) sheds no direct light on the asymptotic excluded-volume problem, it does inspire some optimism in the more practical sense indicated in the introductory section. As in some other physical theories, it is not unlikely that an approximate construction of $J_N$, though perhaps too inexact for an absolute evaluation of either volume effect or virial coefficient, could nevertheless lead to a nearly correct correlation between them. Thus, for example, we might choose $J_N$ in conformity with the "single contact" approximation;[16] or we might start with the mean density of chain elements and ignore fluctuations, as did Flory and Krigbaum[19] in their treatment of the virial coefficient. A detailed account of our attempts in this direction with various choices of $J_N$ will not be given in the present paper. However, in succeeding paragraphs we discuss preliminary results with the single contact approximation.

## 6. PRELIMINARY CALCULATIONS AND DISCUSSION

In the single-contact approximation, only those configurations are considered in which a single pair of elements is interacting (i.e., only one of the $\phi$ functions differs appreciably from unity). Such a configuration has been depicted in Fig. 1, where $i$ and $j$ denote the interacting pair. If only these configurations are counted, Eq. (2.10) reduces to

$$H_{tk}=\sum_{i\leqslant t,\, j\geqslant t+1}\sum \chi(i, j). \tag{6.1}$$

[19] P. J. Flory and W. J. Krigbaum, J. Chem. Phys. **18**, 1086 (1950).

We also assume that the functions $F_{tt}$, $F_{kk}$ may be approximated by their random-flight values, which we shall designate with a superscript zero. Equation (3.8) then yields

$$J_N(p, t, t+1)$$

$$=\Sigma_i\Sigma_j\int\int\chi(i, j)F_{3t}{}^0(p, i, t)f_k{}^0(t+1, j)d(i, j). \tag{6.2}$$

Next, the short-range nature of the $\chi$ function can be invoked. Following an argument already given,[16] we find

$$J_N=-\beta\Sigma_i\Sigma_j\int F_{3t}{}^0(p, t, \varrho)f_k{}^0(t+1, \varrho)d\varrho, \tag{6.3}$$

where we mean that both elements $i$ and $j$ are at the same position $\varrho$, and

$$\beta=-\int\chi(i, j)d(j)$$

$$=\int[1-\exp(-u(i, j)/kT)]d(j). \tag{6.4}$$

The quantity $\beta$ is already familiar and has been amply discussed elsewhere;[7,16] if the chain elements are represented as hard spheres, it becomes the volume excluded to one element by another, which Hermans and coworkers[9] denoted by $v$. In most polymer solutions $\beta$ will be positive, since for appreciably negative values the polymer becomes insoluble. In general, $\beta$ depends on temperature, pressure and nature of solvent.

Since the functions $f_k{}^0$ and $F_{3t}{}^0$ in Eq. (6.3) are simply gaussian forms (the latter bivariate), the integral offers no major difficulty, and the result can be used in Eq. (4.6). We omit further details, and give for illustration merely the special case obtained when element $p$ is at one end of the chain:

$$\frac{d\langle r_1t^2\rangle}{a^2dt}=1+\frac{8z}{3}[2q^{\frac{1}{2}}+(1-q)^{\frac{1}{2}}-1-q]+\cdots$$

$$q=t/N;\quad z=N^{\frac{1}{2}}\beta(3/2\pi a^2)^{\frac{3}{2}}. \tag{6.5}$$

In this result, terms of order $N^{-\frac{1}{2}}$ only have been retained.

Integration now yields

$$L^2/Na^2=\langle r_{1N}{}^2\rangle/Na^2=1+(4z/3)+\cdots. \tag{6.6}$$

Just this result, except for a small constant term, has been reported for the case of hard-sphere interaction, by Yamamoto,[12] and also very recently by Grimley.[20]

The approximation of expanding the fraction in Eq. (4.6) in series to obtain Eq. (6.5) requires comment. This device is formally valid since the denominator, as a normalization coefficient, is necessarily positive; hence

[20] T. B. Grimley, J. Chem. Phys. **21**, 185 (1953).

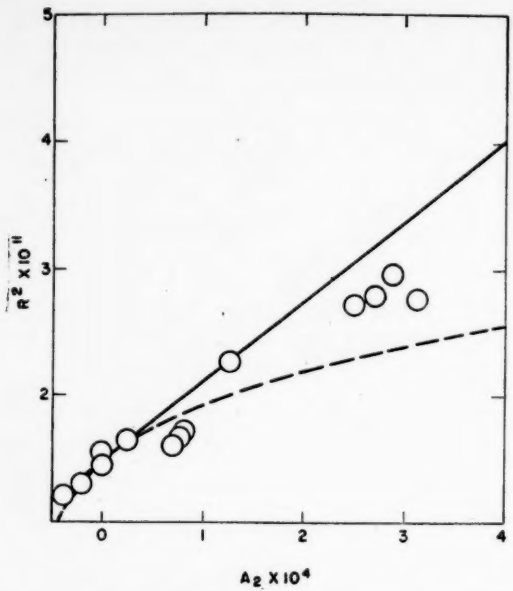


FIG. 2. Mean-square radius $R^2$ *vs* virial coefficient $A_2$. Data from Outer, Carr, and Zimm (reference 15), with omission of measurements for mixtures of dichlorethane and cyclohexane, for which the radii deduced from light scattering and intrinsic viscosity are not in agreement. Solid line is Eq. (6.11), dashed line Eq. (6.13).

its second term is less than the first in the usual case where the second term is negative. However, if the single contact approximation were introduced before expansion, the denominator might become zero or negative. The effect of the approximation is much less serious, therefore, if it is introduced after expansion of the fraction.

To obtain the mean-square radius, $\langle r_{pt}^2 \rangle$ must be similarly found and then summed by Eq. (1.2), the result‖ being

$$6R^2/Na^2 = 1 + (134z/105) + \cdots. \tag{6.7}$$

The results of Eqs. (6.6) and (6.7) indicate a volume effect which is an increasing function of molecular weight; however, it is certain that the single-contact approximation is inadequate at high molecular weights. But it can be shown that if all configurations can be neglected in which three or more elements from different parts of the chain are all simultaneously close to each other (which seems like a very good approximation), then the more general result will be of the form

$$6R^2/Na^2 = f(z), \tag{6.8}$$

where $f(z)$ starts at unity for $z=0$, increases linearly for small $z$, but has unknown asymptotic behavior. The single-contact approximation gives correctly the linear part of $f(z)$.

In the single-contact approximation the molar second virial coefficient, from Eqs. (5.3) and (6.3), is just

$$B_{tk} = tk\beta N_0/2, \tag{6.9a}$$

as has been shown earlier,[16] and correspondingly

$$A_2 = N_0\beta/2M_0^2, \tag{6.9b}$$

where $M_0$ is the molecular weight of a chain element. Again, this result is wrong for high molecular weights, and the more general result will be of the form

$$A_2 = (N_0\beta/2M_0^2)h(z), \tag{6.10}$$

where $h(z)$ is unity for small $z$ and is known from both theory[16] and experiment[15] to be a slowly decreasing function of $z$ for large $z$.

We now demonstrate that, in at least one experimental case, even the single-contact results give a good value for the effect on the mean-square radius of changing the solvent. If Eq. (6.9b) is substituted in (6.7) and the definition of $z$ from (6.5) is used, we find

$$R^2 = R_0^2 + 0.0572A_2M^2/N_0R_0 + \cdots, \tag{6.11}$$

where $R_0^2 = Na^2/6$ and $M$ is the molecular weight of the polymer. The light-scattering results of Outer, Carr, and Zimm[15] on a polystyrene fraction $(B-2)$ of molecular weight $1.6\times10^6$ in various solvents can be used to test this equation. They give their results for the molecular size in terms of the root-mean-square end-to-end distance $L$, calculated on the random flight assumption, but these can be transformed to values of $R$ simply through division by $6^{\frac{1}{2}}$. If we plot $R^2$ against $A_2$ and choose $R_0^2$ to be $1.5\times10^{-11}$ cm$^2$ (to fit the values at $A_2=0$), we obtain from Eq. (6.11) the straight line¶ shown in Fig. 2.

The excellent agreement suggests that the single-contact approximation, although very far from correct in itself for large $z$, nevertheless can be used effectively to correlate the volume effect with the virial coefficient. It must be clearly recognized that in this correlation $\beta$ plays the role of a parameter, and one should not take its physical interpretation as an excluded volume too literally except for very small $z$.

Further, instead of introducing in Eq. (6.2) the random-flights approximation for $F_{kk}$ and $F_{tt}$, we might make use of the above result as a better approximation. This would have the effect of changing $a$ in the factor $z$ to $\alpha a$, where $\alpha$, given by

$$\alpha^2 = L^2/Na^2, \tag{6.12}$$

is Flory's factor.[11] As a result, we would get an equation of Flory's form from Eq. (6.6),

$$\alpha^5 - \alpha^3 = \frac{4}{3}\left(\frac{3}{2\pi a^2}\right)^{\frac{3}{2}}\beta N^{\frac{1}{2}}. \tag{6.13}$$

‖ One of us (M.F.) has developed an alternative method which is more convenient for obtaining higher approximations. The derivation of the above result will be reserved for the discussion of this method.

¶ In the paper of Outer, Carr and Zimm, $R$ itself was plotted against $A_2$, but the results do not warrant a choice between such a plot and that of Fig. 2. It may also be objected that the appropriate value of $A_2$ to use would correspond to a smaller molecular weight (less than half of the chain). This is true, but $A_2$ changes only slowly with $M$ as the agreement would scarcely be altered.

This result, which differs from Flory's[11] only in the constant is clearly one of a series of equations that would result from more and more rigorous treatment of the distribution functions $F_{kk}$ and $F_{tt}$. We hope to discuss these further in a later paper with the aid of the simplified derivation referred to above.

In conclusion, we now venture an opinion about the asymptotic problem. If Eq. (6.8) is accepted, it is seen that the effects of molecular weight and of solvent are both contained in the variable $z$, which is proportional to $N^{\frac{1}{2}}\beta$. Consequently, if the volume effect is to become asymptotically independent of molecular weight, it must also become independent of solvent. Existing light-scattering and hydrodynamic data on long-chain polymers, such as those of Fig. 2, show unequivocally that the solvent effect is by no means absent for the highest polymers experimentally accessible, and indeed appears to increase as molecular weight increases. We are, therefore, led to believe that $f(z)$ does not asymptotically become constant.

Finally, we remark that our discussion fundamentally requires that when the second virial coefficient vanishes, as it does in certain experimentally studied cases, the volume effect must vanish also.

### ACKNOWLEDGMENT

One of us (W.H.S.) is grateful to the General Electric Company for the privilege of being a guest in their Research Laboratory during the summer of 1951, when a large part of this work was accomplished. The later support of the Office of Ordnance Research is acknowledged with thanks.

THE JOURNAL OF CHEMICAL PHYSICS VOLUME 21, NUMBER 10 OCTOBER, 1953

# The Photolysis of Mercury Dimethyl in the Presence of Hydrocarbons*

RICHARD E. REBBERT † AND E. W. R. STEACIE
*Division of Pure Chemistry, National Research Council, Ottawa, Canada*

(Received June 8, 1953)

Mercury dimethyl was photolyzed in the presence of various hydrocarbons between 28°C and 251°C. The activation energies in kcal per mole for reactions of the type

$$CH_3+RH\rightarrow CH_4+R$$

are: 2-methyl propane-7.4; 2,3-dimethyl butane-6.8; *n*-butane-8.6; cylcohexane-8.3; 2,2-dimethyl propane-10.4; and toluene-7.3, where it is assumed that the activation energy for the reaction

$$2CH_3\rightarrow C_2H_6$$

is zero. The collision theory steric factors are less than $10^{-3}$ for all these reactions.

The agreement of the above results with those obtained from the photolysis of acetone is noted.

## INTRODUCTION

In a previous paper[1] experiments on the photolysis of mercury dimethyl were described, which were necessary before it could be used as a source of methyl radicals in the study of reactions as

$$CH_3+RH\rightarrow CH_4+R. \quad (1)$$

In the present paper experiments are reported on six hydrocarbons. This work was undertaken as a check on the work done with acetone as the source of methyl radicals.[2] The agreement between the two sources is excellent. Such an agreement seems to rule out any "hot" radical effect under the conditions of temperature and pressure used.

## EXPERIMENTAL

### Apparatus

The apparatus was essentially the same as that used for the photolysis of mercury dimethyl alone. A Hanovia S-500 medium pressure mercury arc was the light source used. This beam was collimated by a system of two quartz lenses and two stops. The quartz reaction cell was 10 cm long and 5 cm in diameter with a volume of 179.5 cc. This was the volume used in all calculations. The cell was placed in an aluminum block furnace, and the temperature was controlled manually to better than ±1.0°C.

In the runs with 2-methyl propane, a chlorine gas filter and a Corning 986 filter were used, but for the other hydrocarbons no filters were used. The products were analyzed by means of two LeRoy[3] stills in conjunction with a small mercury diffusion pump and a combination Toepler pump and gas buret. It was found necessary to use two LeRoy stills as the small amounts

* National Research Council Contribution No. 3075.
† National Research Council of Canada Post-Doctorate Fellow, 1951–1953.
[1] R. E. Rebbert and E. W. R. Steacie, Can. J. Chem. **31**, 631 (1953).
[2] A. F. Trotman-Dickenson and E. W. R. Steacie, J. Chem. Phys. **19**, 163 (1951); **19**, 329 (1951).
[3] D. J. LeRoy, Can. J. Research **B.28**, 492 (1950).

TABLE I. The reaction of methyl radicals with hydrocarbons

| Temp. (°K) | Mercury dimethyl pressure (mm) | Hydrocarbon pressure (mm) | Time (sec) | Products (Micromoles) $CH_4$ | $C_2H_6$ | $k_1/k_2^{\frac{1}{2}}\times10^{13}$ |
|---|---|---|---|---|---|---|
| | | | 2 Methyl propane[a] | | | |
| 366 | 36.0 | 32.0 | 14 400 | 1.92 | 5.76 | 4.3 |
| 386 | 38.6 | 34.3 | 14 400 | 3.32 | 5.67 | 7.2 |
| 402 | 40.6 | 38.7 | 12 600 | 4.38 | 4.44 | 10.5 |
| 421 | 41.9 | 34.1 | 9000 | 4.23 | 3.20 | 15.8 |
| 440 | 44.9 | 41.0 | 9000 | 6.09 | 2.53 | 21.9 |
| 460 | 46.2 | 40.7 | 7200 | 6.65 | 1.95 | 30.9 |
| 482 | 48.5 | 25.1 | 7200 | 6.48 | 1.66 | 47.9 |
| 506 | 49.7 | 46.3 | 7200 | 7.38 | 0.41 | 69.2 |
| 376 | 38.1 | 37.2 | 9000 | 2.11 | 5.43 | 5.4 |
| 493 | 50.0 | 20.7 | 7200 | 8.07 | 2.30 | 56.2 |
| | | | 2,3 Dimethyl butane | | | |
| 301 | 33.1 | 35.3 | 3600 | 0.46 | 11.42 | 1.1 |
| 325 | 33.0 | 34.5 | 2700 | 0.64 | 9.20 | 2.3 |
| 347 | 35.9 | 34.0 | 2100 | 0.97 | 7.68 | 4.6 |
| 375 | 37.8 | 35.1 | 1800 | 1.79 | 7.46 | 9.8 |
| 398 | 39.3 | 38.1 | 1800 | 3.00 | 6.48 | 16.6 |
| 425 | 43.0 | 39.2 | 1800 | 5.10 | 6.05 | 29.5 |
| 448 | 45.3 | 44.6 | 1200 | 5.19 | 3.71 | 42.7 |
| 473 | 48.9 | 37.8 | 900 | 5.04 | 2.83 | 64.6 |
| 493 | 49.2 | 27.0 | 900 | 5.87 | 3.19 | 95.5 |
| | | | Cyclohexane | | | |
| 354 | 35.5 | 57.5 | 2700 | 1.12 | 9.66 | 2.5 |
| 375 | 37.1 | 38.1 | 2400 | 1.40 | 9.37 | 5.2 |
| 401 | 40.6 | 39.5 | 2400 | 3.06 | 9.55 | 11.2 |
| 424 | 43.1 | 41.3 | 1800 | 3.77 | 6.72 | 19.1 |
| 448 | 46.1 | 43.8 | 1200 | 4.13 | 4.18 | 30.9 |
| 472 | 47.7 | 42.8 | 1200 | 5.71 | 3.55 | 49.0 |
| 493 | 49.1 | 25.1 | 900 | 4.91 | 3.19 | 81.3 |
| | | | *n*-Butane | | | |
| 365 | 36.9 | 63.8 | 2700 | 0.81 | 9.61 | 1.6 |
| 373 | 37.1 | 40.6 | 2400 | 0.74 | 9.74 | 2.3 |
| 398 | 39.3 | 41.9 | 1800 | 1.11 | 7.21 | 4.8 |
| 399 | 40.6 | 42.0 | 3600 | 2.23 | 16.33 | 4.3 |
| 425 | 42.7 | 43.4 | 1800 | 2.29 | 7.70 | 9.1 |
| 449 | 44.4 | 45.6 | 1800 | 3.97 | 7.13 | 16.2 |
| 462 | 46.6 | 46.6 | 1200 | 3.42 | 4.70 | 20.4 |
| 473 | 47.4 | 49.1 | 1200 | 4.27 | 4.27 | 26.3 |
| 496 | 49.2 | 42.5 | 1200 | 5.97 | 4.86 | 37.2 |
| | | | Neopentane | | | |
| 404 | 40.0 | 81.0 | 2700 | 0.92 | 12.44 | 0.91 |
| 413 | 41.1 | 89.0 | 2400 | 1.10 | 11.50 | 1.1 |
| 424 | 42.4 | 84.0 | 2100 | 1.25 | 10.33 | 1.4 |
| 444 | 44.8 | 89.2 | 1800 | 1.96 | 9.14 | 2.5 |
| 463 | 46.4 | 96.1 | 1800 | 3.22 | 8.96 | 4.1 |
| 483 | 48.7 | 86.3 | 1200 | 3.19 | 6.07 | 6.3 |
| 504 | 50.6 | 98.7 | 900 | 4.01 | 4.35 | 10.5 |
| 524 | 52.6 | 101.2 | 900 | 5.95 | 4.24 | 16.2 |
| | | | Toluene | | | |
| 422 | 22.7 | 13.8 | 2400 | 1.02 | 7.09 | 10.7 |
| 442 | 24.0 | 14.7 | 1800 | 1.16 | 5.54 | 14.8 |
| 464 | 24.6 | 14.9 | 1800 | 1.93 | 6.49 | 21.9 |
| 483 | 25.6 | 15.7 | 1800 | 2.85 | 6.43 | 30.9 |
| 503 | 26.5 | 16.5 | 1800 | 3.91 | 6.08 | 40.7 |
| 523 | 28.2 | 17.3 | 900 | 2.69 | 2.85 | 53.7 |

[a] A chlorine gas filter and a Corning 986 filter were used for 2-methyl propane.

of methane and ethane were detained by the excess hydrocarbon added. The first still was maintained at such a temperature as to allow the methane and ethane to pass but to retain most of the undecomposed mercury dimethyl and hydrocarbon. Mixing of the mercury dimethyl and hydrocarbon before photolysis was obtained by raising and lowering mercury in a bulb of 300-cc capacity.

## Materials

The mercury dimethyl was obtained from the Delta Chemical Works and then distilled to remove ether. Its vapor pressure was 17.7 mm at 0°C. The literature value is 17.4 mm at 0°C.[4]

The 2-methyl propane, *n*-butane, cyclohexane, and toluene were Phillips Research Grade products and were stated to be better than 99.7 mole percent pure. The 2,2-dimethyl propane and the 2,3-dimethyl butane were standard samples from the National Bureau of Standards. These were reported to have 0.04 ±0.02 and 0.11±0.06 mole percent impurity, respectively.

## RESULTS

In Table I are given the results on the experiments with mercury dimethyl in the presence of six different hydrocarbons. These results are plotted in Figs. 1, 2 and 3 along with the results obtained from acetone.[2] At the highest temperature, there is a slight deviation from a straight line for 2,3 dimethyl butane and cyclohexane, and also at the lowest temperature for cylcohexane. These deviations may be accounted for by a slight dependency on concentration, as the concentration was changed in these experiments in an attempt to get a more favorable ratio of methane and ethane. The slight deviations at the low temperatures for 2,3 dimethyl butane, 2,2 dimethyl propane and toluene is probably due to experimental error, since the amount of methane formed is too small to be measured accurately.

The activation energies $E_1-\frac{1}{2}E_2$ are given in Table II, along with the rate constants $k_1/k_2^{\frac{1}{2}}$ at 182°C and the steric factors $P_1/P_2^{\frac{1}{2}}$. The results from acetone are also given. The agreement in activation energy and in rate constant is excellent. The rate constants are expressed in molecules, cc, and seconds. No allowance has been made for the temperature coefficient of the collision

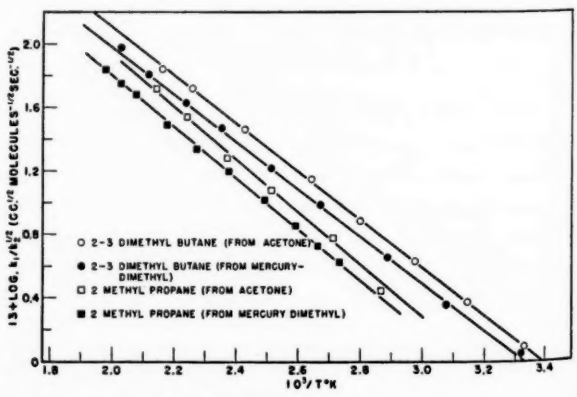


FIG. 1. Methyl radical plus 2,3-dimethyl butane and 2-methyl propane.

[4] F. Ratman, J. Appl. Chem. (U.S.S.R.) **9**, 593 (1936).

rate in determining the activation energies. However, an allowance was made in the calculations of the steric factors.

## METHOD

The photolysis of mercury dimethyl gives methane and ethane by the following reactions:

$$2CH_3 \rightarrow C_2H_6 \quad (2)$$

and

$$CH_3 + Hg(CH_3)_2 \rightarrow CH_4 + CH_3HgCH_2. \quad (3)$$

When another substance containing hydrogen is added, methane is also formed by the reaction

$$CH_3 + RH \rightarrow CH_4 + R. \quad (1)$$

The rate of formation of methane and ethane for

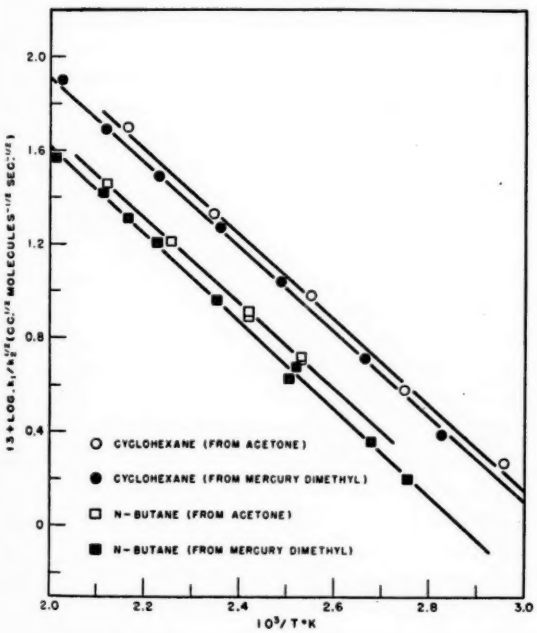


FIG. 2. Methyl radical plus cyclohexane and *n*-butane.

mercury dimethyl alone is given by the expressions

$$R_{CH_4} = k_3[CH_3][Hg(CH_3)_2]$$

and

$$R_{C_2H_6} = k_2[CH_3]^2.$$

Thus, we have

$$\frac{k_3}{k_2^{\frac{1}{2}}} = \frac{R_{CH_4}}{R_{C_2H_6}^{\frac{1}{2}}[Hg(CH_3)_2]}.$$

If we now add a substance containing hydrogen, we have

$$R_{CH_4} = k_3[CH_3][Hg(CH_3)_2] + k_1[CH_3][RH]$$

and

$$R_{C_2H_6} = k_2[CH_3]^2.$$

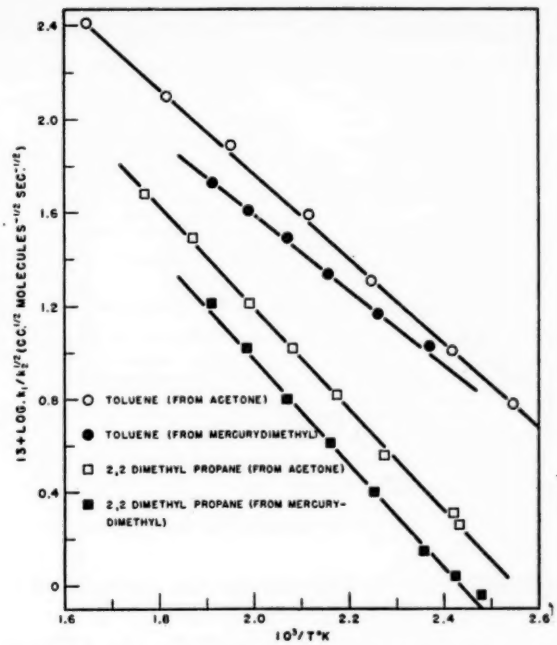


FIG. 3. Methyl radical plus toluene and 2,2-dimethyl propane.

Thus,

$$\frac{R_{CH_4}}{R_{C_2H_6}^{\frac{1}{2}}} = \frac{k_3[Hg(CH_3)_2]}{k_2^{\frac{1}{2}}} + \frac{k_1[RH]}{k_2^{\frac{1}{2}}}.$$

In a previous paper[1] $k_3/k_2^{\frac{1}{2}}$ was determined, and since we know $[Hg(CH_3)_2]$, [RH], $R_{CH_4}$ and $R_{C_2H_6}$, we can find $k_1/k_2^{\frac{1}{2}}$ for reaction (1), where RH in our case is any one of the six hydrocarbons.

## DISCUSSION

The results indicate that in a molecule with secondary and primary hydrogen atoms, the main reaction is the abstraction of a secondary hydrogen atom by a methyl radical in preference to a primary hydrogen atom. However, if a tertiary hydrogen atom is present in the molecule, then the main reaction is with the tertiary hydrogen atom.

The agreement of the present results with those obtained from acetone is excellent. The slight deviations in the activation energies can easily be assigned to experimental error. The largest difference observed between the two sources is 1.0 kcal/mole in the case of toluene. This difference may be an inherent error due to the two different methods used in calculating the rate constants for this one compound. When acteone was the source of methyl radicals for toluene, deuterated acetone was used, and the ratio $CD_3H/CD_4$ was measured directly by the mass spectrometer. A similar difference is found by Whittle and Steacie[6] between these two methods of calculating the rate constants even for the

[6] E. Whittle and E. W. R. Steacie, J. Chem. Phys. (to be published).

TABLE II. The abstraction of hydrogen atoms by methyl radicals.

| Compound | Results from mercury dimethyl $E_1-\frac{1}{2}E_2$ (kcal/mole) | Results from mercury dimethyl $\frac{k_1}{k_2^{\frac{1}{2}}}\times10^{13}$ (at 182°C) | Results from mercury dimethyl $P_1/P_2^{\frac{1}{2}}\times10^4$ | Results from acetone $E_1-\frac{1}{2}E_2$ (kcal/mole) | Results from acetone $\frac{k_1}{k_2^{\frac{1}{2}}}\times10^{13}$ (at 182°C) | Results from acetone $P_1/P_2^{\frac{1}{2}}\times10^4$ | Collision[b] diameter (in A) |
|---|---|---|---|---|---|---|---|
| 2, methyl propane | 7.4 | 30 | 2 | 7.6 | 42 | 3 | 5.9 |
| 2,3 dimethyl butane | 6.8 | 48 | 1.5 | 6.9 | 68 | 2 | 6.5 |
| *n*-butane | 8.6 | 18 | 4 | 8.3 | 21 | 3 | 5.8 |
| cyclohexane | 8.3 | 36 | 6 | 8.3 | 42 | 8 | 6.0 |
| 2,2 dimethyl propane | 10.4 | 3.3 | 9 | 10.0 | 6.3 | 6 | 6.0 |
| Toluene | 7.3 | 19 | 1 | 8.3[a] | 26 | 5 | 5.9 |
| Mercury dimethyl | 10.8 | 5.5 | 16 | | | | 6.0 |

[a] This result is for the reaction $CD_3+C_6H_5CH_3\rightarrow CD_3H+C_6H_5CH_2$.
[b] The collision diameter of the methyl radical was taken as 3.5A.

same reactions. In studying the reactions

$$CH_3+D_2\rightarrow CH_3D+D$$

and

$$CD_3+H_2\rightarrow CD_3H+H,$$

they found that in each case the gas analysis results gave an activation energy about 1.0 kcal/mole less than the results from the mass spectrometer. This difference in the results implies that, if the highest possible accuracy is needed, the data obtained on the rate of abstraction of a hydrogen atom by a methyl radical from mercury dimethyl or from acetone when either one is photolyzed alone are not strictly correct if other substances are present. It is known that the ratio $k_3/k_2^{\frac{1}{2}}$ varies slightly with pressure for both mercury dimethyl and for acetone, and thus is probably the explanation of the discrepancy.

Agreement of the present results with sources other than acetone may also be mentioned. Jones and Steacie[6] studied the reaction of methyl radicals with 2-methyl propane and *n*-butane using the photolysis of azomethane as a source of methyl radicals. They reported 6.7±0.8 kcal/mole and 9.0±1.0 kcal/mole for 2-methyl propane and *n*-butane, respectively. Also for *n*-butane, Gomer[7] who used mercury dimethyl as a source of methyl radicals, obtained an activation energy of 8.4 kcal/mole which is in very good agreement with the present result. However, he calculated this activation energy in a somewhat different way. A recalculation according to our method gives 9.5 kcal/mole for this reaction. In any case, the discrepancy is not large.

The deviations in the absolute values of $k_1/k_2^{\frac{1}{2}}$ from the two sources (i.e., mercury dimethyl and acetone) are also actually very small when we consider the fact that these results were obtained by two different experimenters, working with different apparatus and using different sources of methyl radicals. However, the persistence of the higher ratio $k_1/k_2^{\frac{1}{2}}$ from mercury dimethyl as compared with that from acetone suggests that part of the difference may be due to some other cause than experimental error. It would seem that the most probable reason for this difference is the error involved in taking the cell volume as the effective reaction volume. This would be correct only if methyl radicals were produced uniformly throughout the reaction cell. Acutally, the effective reaction volume is somewhat less than the cell volume and depends to a very large extent on the extinction coefficient of the compound photolyzed. Since the extinction coefficient for mercury dimethyl is probably somewhat higher than that for acetone, the ratio of the effective reaction volume to cell volume should be less for mercury dimethyl than for acetone and consequently the values of $k_1/k_2^{\frac{1}{2}}$, based on cell volume, will be a little lower for mercury dimethyl. Another contributing cause of these differences in $k_1/k_2^{\frac{1}{2}}$ is the slight pressure dependency of this ratio for both acetone and mercury dimethyl.

The most important conclusion to be drawn from this work is the relative unimportance of any "hot" radical effect in the photolysis of mercury dimethyl or acetone. If there were a "hot" radical effect in one and not in the other, we would expect quite different values for the activation energies. Even if there were a "hot" radical effect in both substances, we would still expect different values for the activation energies, as mercury dimethyl requires much less energy for dissociation than acetone, and consequently there is more excess energy available for the methyl radicals.

[6] M. H. Jones and E. W. R. Steacie, Can. J. Chem. **31**, 505 (1953).
[7] R. Gomer, J. Am. Chem. Soc. **72**, 201 (1950).

# Vibrational Spectra of Fluorinated Aromatics. VII. 1,2,4-Trifluorobenzene*

E. E. Ferguson, R. L. Hudson,† and J. Rud Nielsen, *Department of Physics, University of Oklahoma, Norman, Oklahoma*

AND

D. C. Smith,‡ *Naval Research Laboratory, Washington, D. C.*

(Received June 8, 1953)

The infrared absorption spectrum of liquid 1,2,4-trifluorobenzene has been obtained in the region 2–38$\mu$ with the aid of LiF, NaCl, KBr, and KRS-5 prisms. The Raman spectrum of the liquidh as been photographed with a three-prism glass spectrograph of linear dispersion 15A/mm at 4358A, and depolarization ratios have been measured for the stronger Raman bands. A complete assignment of fundamental vibration frequencies is given, and the spectra are interpreted in detail.

## INTRODUCTION

In previous papers of this series[1–6] the infrared and Raman spectra of 1,3,5-trifluoro-, 1,4-difluoro-, 1,2,4,5-tetrafluoro-, 1,3-difluoro-, and fluorobenzene have been reported. No previous work appears to have been done on 1,2,4-trifluorobenzene. In the present paper spectral data, assignments of fundamentals, and detailed interpretations of the spectra will be presented for this compound.

## EXPERIMENTAL

The sample of 1,2,4-trifluorobenzene was kindly supplied by Dr. G. C. Finger of the Illinois State Geological Survey. No information was available as to its purity. The infrared absorption spectrum of the liquid phase was measured from 2 to 38$\mu$, the Raman spectrum was obtained at room temperature, and quantitative polarization measurements were made in the manner previously described.[1]

## RESULTS

The infrared absorption of liquid 1,2,4-trifluorobenzene from 2 to 22$\mu$ is shown in Fig. 1. The wave numbers of the observed absorption maxima are listed in the first column of Table I. The relative intensities of the bands are indicated by means of the previously used abbreviations. The observed Raman shifts for liquid 1,2,4-trifluorobenzene, along with relative intensities and depolarization ratios of the stronger Raman bands, also are given in Table I.

## INTERPRETATION

The 1,2,4-trifluorobenzene molecule has the symmetry $C_s$, and the 30 vibrational modes divide into 21 planar vibrations of species $a'$ and 9 nonplanar vibrations of species $a''$. The species $a'$ vibrations give rise to polarized Raman bands and the $a''$ to depolarized Raman bands. Since there are such a large number of fundamentals of each species, only those whose assignment seems uncertain will be discussed in detail.

### Species a′

Bands that occur with high intensity in either the infrared or the Raman spectrum, or both, and that are polarized in the Raman effect are interpreted as $a'$ fundamentals. The uncertain $a'$ assignments are the following: the weak Raman band at 288 cm$^{-1}$ with a medium intensity counterpart in the infrared and the weak Raman band at 341 cm$^{-1}$ that corresponds to a strong infrared band both lie near very strong Raman bands, and hence their measured depolarization ratios, 0.77 and 0.86, respectively, are somewhat uncertain. However, both bands have the rather sharp appearance characteristic of polarized Raman bands.

The assignment of the very weak, polarized Raman band observed at 835 cm$^{-1}$ as an $a'$ fundamental is uncertain, since it can be explained as either of the binary combinations $377+456=833\,A'$ or $238+602=840\,A'$. Also the frequency 1376 cm$^{-1}$, which is weak in both spectra and is assigned here as an $a'$ fundamental, may be the overtone of the $a''$ fundamental at 688 cm$^{-1}$.

### Species a″

The nine nonplanar fundamental vibrations are mixtures of three hydrogen bending modes, three fluorine bendings, and three ring bendings. There are two assignments which must be considered uncertain in the species $a''$. One of these is the strong infrared band at 602 cm$^{-1}$ with a weak counterpart in the Raman spectrum. The measured depolarization ratio, somewhat uncertain because of the low intensity, has the low value 0.75. The remaining uncertainty is in the assignment of the medium intensity infrared band at 932 cm$^{-1}$ as an $a''$

* This work has been supported in part under contract with the U. S. Atomic Energy Commission and the U. S. Office of Naval Research.

† Present address: Ethyl Corporation, Baton Rouge, Louisiana.

‡ Present address: Phillips Petroleum Company, Bartlesville, Oklahoma.

[1] Nielsen, Liang, and Smith, Discussions Faraday Soc. **9**, 177 (1950).

[2] Eldon Ferguson, J. Chem. Phys. **21**, 886 (1953).

[3] Ferguson, Hudson, Nielsen, and Smith, J. Chem. Phys. **21**, 1457 (1953).

[4] Ferguson, Hudson, Nielsen, and Smith, J. Chem. Phys. **21**, 1464 (1953).

[5] Ferguson, Collins, Nielsen, and Smith, J. Chem. Phys. **21**, 1470 (1953).

[6] Smith, Ferguson, Hudson, and Nielsen, J. Chem. Phys. **21**, 1475 (1953).

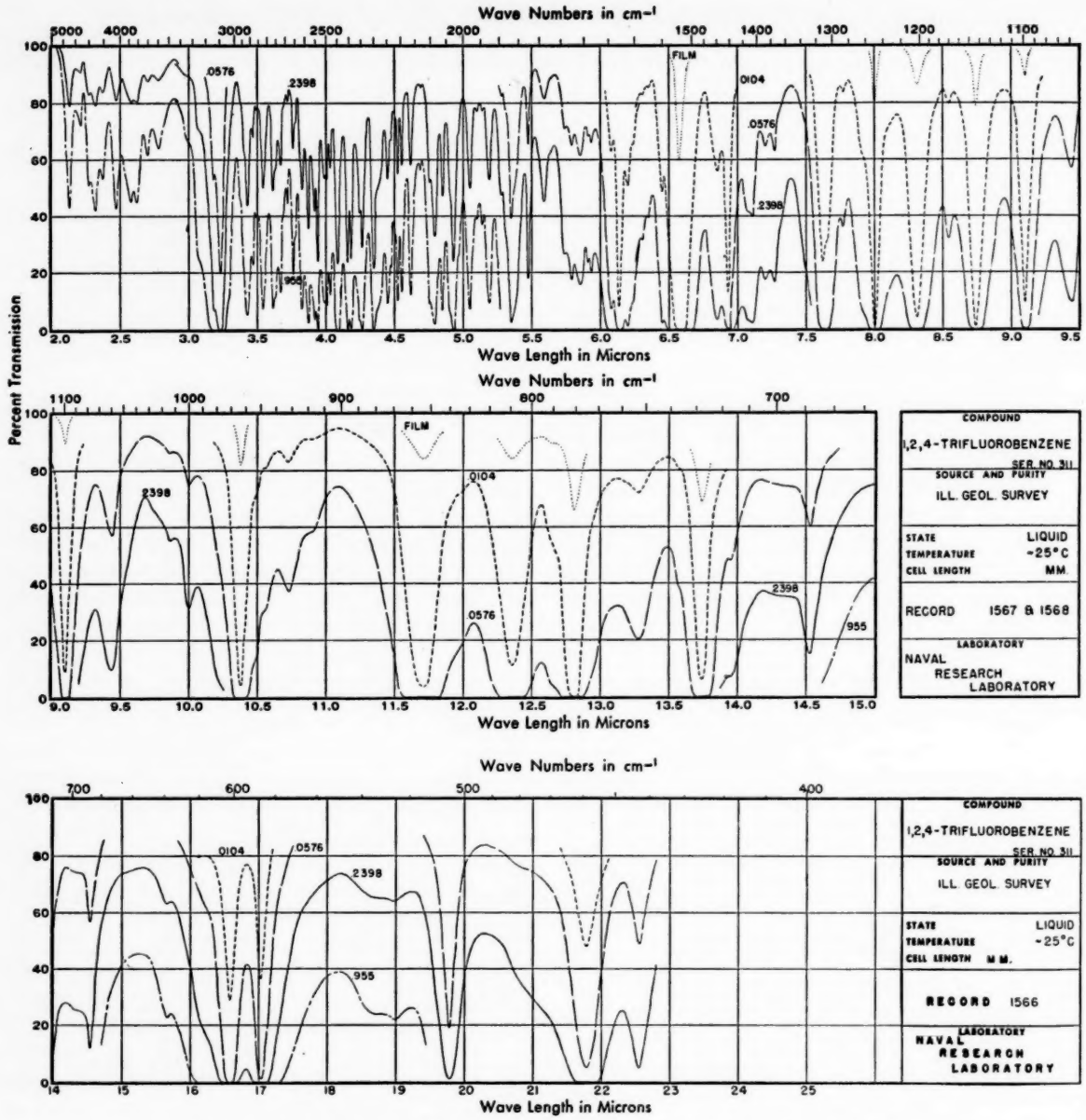


FIG. 1. Infrared spectrum of liquid 1,2,4-trifluorobenzene (KRS-5 region not included).

fundamental. An empirical sum rule has been found to fit the nonplanar fundamentals of five previously studied fluorinated benzenes quite well,[5] and the choice of 932 $cm^{-1}$ makes the sum of nonplanar frequencies equal to the similar sum for 1,3,5-trifluorobenzene within 0.1 percent. The only other reasonable choice would be the medium infrared band at 753 $cm^{-1}$. Either band can be explained as a combination band.

## DISCUSSION

The assigned fundamentals are listed in Table II. The 39 observed Raman shifts and the 98 observed infrared absorption maxima are all interpreted as fundamentals or binary sums with this assignment, and many of the bands can be interpreted in more than one way because of the large number of coincidences arising from 30 fundamentals. The interpretations are given in the last column of Table I.

The $a'$ fundamentals which may most accurately be ascribed to fluorine stretching are those at 1204 and 1250 $cm^{-1}$, which are very strong in the infrared spectrum and only of medium intensity in the Raman effect, and probably the band at 1308 $cm^{-1}$, which is strong in both spectra. This latter band appears to be double in both spectra, presumably due to a resonance with $586+728=1314\,A'$, or $456+856=1312\,A'$. The average of these three "CF stretching" frequencies, 1251 $cm^{-1}$, is intermediate between the similar average for the two difluorobenzenes studied, 1218.5 $cm^{-1}$ and that for 1,2,4,5-tetrafluorobenzene, 1257.5 $cm^{-1}$.

TABLE I. Infrared and Raman spectra of 1,2,4-trifluorobenzene (liquid).

| Infrared | | Raman | | | |
|---|---|---|---|---|---|
| Wave number | Description | Wave number | Description | Depolarization | Interpretation |
| | | 161 | m, d | 0.79 | $a''$ fundamental |
| | | 238 | s, d | 0.84 | $a''$ fundamental |
| 286 | m | 288 | w, sh | 0.77 | $a'$ fundamental |
| 340 | s | 341 | w, sh | 0.86 | $a'$ fundamental |
| 377 | w | 377 | vs | 0.86 | $a''$ fundamental |
| 400 | w | 401 | w | | $161+238=399\ A'$ |
| 441 | m | 441.6 | s, sh | 0.46 | $a'$ fundamental; $161+288=449\ A''$ |
| 455 | s | 457 | vw | 0.9? | $a''$ fundamental |
| 503 | s | 503.5 | s, sh | 0.24 | $a'$ fundamental |
| ~527 | w | | | | $238+288=526\ A''$ |
| 587 | s | 585.6 | s, sh | 0.50 | $a'$ fundamental |
| 603 | s | 601 | w | 0.75 | $a''$ fundamental |
| | | | | | $161+441=602\ A''$ |
| | | 618 | vvw | | $238+377=615\ A'$; $161+456=617\ A'$ |
| 639 | vw | | | | $288+341=629\ A'$ |
| 688 | m | 688 | w | 0.9 | $a''$ fundamental |
| 717 | w | | | | $341+377=718\ A''$ |
| 728 | vs | 727.8 | vs, sh | 0.08 | $a'$ fundamental |
| 753 | m | | | | $2\times377=754\ A'$; $161+586=747\ A''$ |
| 781 | vs | 780.6 | vvs | 0.08 | $a'$ fundamental |
| 809 | vs | 808 | vw | dp? | $a''$ fundamental |
| | | 835 | vw | 0.3 | $a'$ fundamental; $377+456=833\ A'$; $238+602=840\ A'$ |
| ~854 | vs | 859 | vvw | dp | $a''$ fundamental |
| | | 908 | vw | | $441+456=897\ A''$ |
| | | 916 | vw | | $2\times456=912\ A'$ |
| 932 | m | | | | $a''$ fundamental; $341+586=927\ A'$; $238+688=926\ A'$ |
| 963 | vs | 963.7 | vs, sh | 0.07 | $a'$ fundamental |
| 1000 | m | 1003 | vvw | | $2\times503=1006\ A'$; $161+835=996\ A''$ |
| 1014 | vw | | | | $288+728=1016\ A'$; $238+781=1019\ A''$; $161+856=1017\ A'$ |
| 1059 | m | 1064 | vw | | $377+688=1065\ A'$; $456+602=1058\ A'$ |
| 1099 | vs | 1098.2 | m, sh | 0.83 | $a'$ fundamental |
| 1144 | vs | 1142.6 | w | 0.1 | $a'$ fundamental |
| 1171 | m | | | | $2\times586=1172\ A'$; $441+728=1169\ A'$ |
| 1203 | vs | 1205 | w | | $a'$ fundamental |
| | | 1232 | vw | | $503+728=1231\ A'$; $377+856=1233\ A'$ |
| 1250 | vs | 1250 | w | 0.7 | $a'$ fundamental |
| 1287 | m | 1287 | vw | | $503+781=1284\ A'$; $602+688=1290\ A'$ |
| 1312 | s | 1308[a] | s | 0.01 | $a'$ fundamental; $586+728=1314\ A'$; $456+856=1312\ A'$ |
| 1376 | w | 1375.5 | vw | 0.27 | $a'$ fundamental; $2\times688=1376\ A'$ |
| 1389 | w | | | | $288+1098=1386\ A'$; $586+808=1394\ A''$ |
| 1406 | m | | | | $441+964=1405\ A'$; $602+808=1410\ A'$ |
| 1443 | s | 1441.3 | w | 0.23 | $a'$ fundamental |
| 1460 | m | 1455 | vvw | | $2\times728=1456\ A'$; $602+856=1458\ A'$; $161+1308=1469\ A''$ |
| 1522 | vs | 1518 | w | 0.83 | $a'$ fundamental |
| 1550 | m | | | | $238+1308=1546\ A''$; $341+1204=1545\ A'$ |
| 1575 | vw | | | | $2\times781=1562\ A'$; $602+964=1566\ A''$ |
| 1585 | vw | | | | $441+1143=1584\ A'$; $856+728=1584\ A''$ |
| 1613 | vw | | | | $2\times808=1616\ A'$; $781+835=1616\ A'$ |
| 1629 | s | 1628 | m | 0.86 | $a'$ fundamental |
| 1645 | vw | | | | $341+1308=1649\ A'$; $688+964=1652\ A''$ |
| 1685 | vw | | | | $377+1308=1685\ A''$; $586+1098=1684\ A'$ |
| 1691 | vw | | | | $728+964=1692\ A'$; $835+856=1691\ A''$ |
| 1709 | vw | 1708 | vvw | | $503+1204=1707\ A'$; $2\times856=1712\ A'$ |
| 1727 | vw | | | | $288+1441=1729\ A'$; $586+1143=1729\ A'$ |
| 1743 | vw | | | | $602+1143=1745\ A''$; $781+964=1745\ A'$ |
| 1788 | w | | | | $161+1628=1789\ A''$; $586+1204=1790\ A'$ |
| 1826 | w | | | | $728+1098=1826\ A'$; $856+964=1820\ A''$ |
| | | 1859 | vvw | | $341+1518=1859\ A'$ |
| 1868 | m | | | | $238+1628=1866\ A''$; $728+1143=1871\ A'$ |
| 1893 | vw | | | | $586+1308=1894\ A'$; $688+1204=1892\ A''$ |
| 1926 | vw | | | | $2\times964=1928\ A'$; $781+1143=1924\ A'$ |
| 1945 | vw | | | | $503+1441=1944\ A'$; $808+1143=1951\ A''$ |
| 1961 | vw | | | | $441+1518=1959\ A'$; $856+1098=1954\ A''$ |
| 1980 | w | | | | $781+1204=1985\ A'$; $835+1143=1978\ A'$ |
| 2028 | w | | | | $586+1441=2027\ A'$; $503+1518=2021\ A'$ |
| 2061 | w | | | | $964+1098=2062\ A'$; $856+1204=2060\ A''$ |
| 2086 | w | | | | $781+1308=2089\ A'$; $456+1628=2084\ A''$ |
| 2102 | w | | | | $586+1518=2104\ A'$; $688+1308=1996\ A''$ |
| 2132 | w | | | | $503+1628=2131\ A'$; $688+1441=2129\ A''$ |
| 2165 | w | | | | $964+1204=2168\ A'$; $856+1308=2164\ A''$ |
| 2196 | w | | | | $2\times1098=2196\ A'$ |
| 2211 | w | | | | $586+1628=2214\ A'$ |
| 2235 | w | | | | $602+1628=2230\ A''$ |
| 2246 | w | | | | $728+1518=2246\ A'$; $808+1441=2249\ A''$ |
| 2300 | m | | | | $781+1518=2299\ A'$; $856+1441=2297\ A''$ |
| 2345 | m | | | | $1143+1204=2347\ A'$ |
| 2356 | vw | | | | $728+1628=2356\ A'$; $835+1518=2353\ A'$ |
| 2390 | m | | | | $1143+1250=2393\ A'$ |
| 2404 | m | | | | $2\times1204=2408\ A'$; $964+1441=2405\ A'$ |
| 2447 | m | | | | $1143+1308=2451\ A'$ |
| 2480 | w | | | | $964+1518=2482\ A'$ |
| 2497 | w | | | | $2\times1250=2500\ A'$ |
| 2506 | w | | | | $1204+1308=2512\ A'$ |
| 2537 | w | | | | $1098+1441=2539\ A'$ |
| 2551 | w | | | | $1250+1308=2558\ A'$ |
| 2581 | w | | | | $1143+1441=2584\ A'$ |
| 2615 | w | | | | $2\times1308=2616\ A'$; $1098+1518=2616\ A'$ |
| 2658 | w | | | | $1143+1518=2661\ A'$ |
| 2690 | w | | | | $1250+1441=2691\ A'$; $1308+1376=2684\ A'$ |
| 2726 | w | | | | $1098+1628=2726\ A'$ |
| 2765 | w | | | | $1143+1628=2771\ A'$; $1250+1518=2768\ A'$ |

TABLE I—*Continued.*

| Infrared Wave number | Infrared Description | Raman Wave number | Raman Description | Raman Depolarization | Interpretation |
|---|---|---|---|---|---|
| 2822 | w | | | | 1308+1518=2826 $A'$; 1376+1441=2817 $A'$ |
| 2859 | w | | | | 1250+1628=2878 $A'$ |
| 2882 | w | | | | 2×1441=2882 $A'$ |
| 2914 | w | | | | 1308+1628=1336 $A'$; 1376+1518=2894 $A'$ |
| | | 3062 | vw | | $a'$ fundamental |
| 3098 | s | 3094 | vs | 0.02 | $2a'$ fundamentals |
| 3142 | w | | | | 1518+1628=3146 $A'$ |
| 3600 | w | | | | 503+3094=3597 $A'$ |
| 3700 | w | | | | 602+3094=3696 $A''$ |
| 3820 | w | | | | 728+3094=3822 $A'$ |
| 3880 | w | | | | 781+3094=3875 $A'$ |
| 4050 | w | | | | 964+3094=4058 $A'$ |
| 4220 | w | | | | 1143+3094=4237 $A'$ |
| 4310 | w | | | | 1205+3094=4299 $A'$; 1250+3062=4312 $A'$ |
| 4410 | w | | | | 1308+3094=4402 $A'$ |
| 4520 | w | | | | 1441+3094=4535 $A'$ |
| 4690 | w | | | | 1628+3062=4690 $A'$ |

[a] Appears double.

TABLE II. Fundamental vibrational frequencies for 1,2,4-trifluorobenzene (liquid).

| Species $a'$ | Species $a''$ |
|---|---|
| 288 | 161 |
| 341 | 238 |
| 441 | 377 |
| 503 | 456 |
| 586 | 602 |
| 728 | 688 |
| 781 | 808 |
| 835 | 856 |
| 964 | 932 |
| 1098 | |
| 1143 | |
| 1204 | |
| 1250 | |
| 1308 | |
| 1376 | |
| 1441 | |
| 1518 | |
| 1628 | |
| 3062 | |
| 3094 | |
| 3094 | |

The $a''$ fundamentals at 808 and 856 $cm^{-1}$, which involve largely nonplanar hydrogen bending, are very strong in the infrared spectrum and very weak in the Raman spectrum, in accord with the finding for all of the fluorinated benzenes previously studied. The $a''$ fundamental at 932 $cm^{-1}$, also involving largely hydrogen bending, is observed only in the infrared with with medium intensity.

The planar fundamentals seem to lie somewhat lower than one would expect from the compounds previously studied. The reason for this is not known. However, it may be remarked that no empirical sum rule has been found to apply well to the planar fundamentals of the previously observed fluorinated benzenes.

## ACKNOWLEDGMENT

The writers wish to acknowledge their indebtedness to Dr. G. C. Finger for the gift of the sample.

# Vibrational Spectra of Fluorinated Aromatics. VIII. 1,4-Bis(trifluoromethyl)benzene*

E. E. FERGUSON, LOUIS MIKKELSEN,† AND J. RUD NIELSEN, *Department of Physics, University of Oklahoma, Norman, Oklahoma*

AND

D. C. SMITH,‡ *Naval Research Laboratory, Washington, D. C.*

(Received June 8, 1953)

The infrared absorption of liquid 1,4-bis(trifluoromethyl) benzene has been obtained in the region 2–22$\mu$ with the aid of LiF, NaCl, and KBr prisms. The Raman spectrum has been photographed with a three-prism glass spectrograph of linear dispersion 15A/mm at 4358A. A nearly complete assignment of fundamental vibration frequencies is given, and the spectra are interpreted in detail.

## INTRODUCTION

IN previous papers of this series[1–7] the infrared and Raman spectra of 1,3,5-trifluoro-, 1,4-difluoro-, 1,2,4,5-tetrafluoro-, 1,3-difluoro-, fluoro-, and 1,2,4-trifluorobenzene have been reported. Cooper and Noegel[8] have investigated the near ultraviolet spectrum of 1,4-bis(trifluoromethyl) benzene. In the present paper, infrared and Raman spectral data for this compound in the liquid state, assignments of fundamentals, and detailed interpretations of the spectra are presented.

## EXPERIMENTAL

The sample of 1,4-bis(trifluoromethyl) benzene was kindly supplied by Professor J. H. Saylor of Duke University. The infrared absorption spectrum of the liquid phase was measured from 2 to 22$\mu$ in the manner previously described.[1] The Raman spectrum was obtained at room temperature, and quantitative polarization measurements were made.

## RESULTS

The infrared absorption of liquid 1,4-bis(trifluoromethyl) benzene from 2 to 22$\mu$ is shown in Fig. 1. The observed absorption maxima are listed in Table I along with relative intensities of the bands. The observed Raman shifts and the depolarization ratios of the stronger bands are included in Table I.

## INTERPRETATION

It is a useful aid in the interpretation of these spectra to assign "skeletal" fundamental frequencies based on a model of symmetry $V_h$, according to which the $CF_3$ groups are assumed to be points, and add to these the fundamentals involving distortion, rocking, or torsion of the $CF_3$ groups. This method was used by Pitzer and Scott[9] in their analysis of the *p*-xylene spectra. The approximation is undoubtedly worse in the case of 1,4-bis(trifluoromethyl) benzene, since the restricting potential for free rotation is probably larger for $CF_3$ than for $CH_3$ groups, and because C—F stretching may interact strongly with carbon ring vibrations and hydrogen bending vibrations, while C—H stretchings in *p*-xylene are not coupled greatly with other motions of the molecule.

The spectra show no coincidences of strong infrared and Raman bands. The four medium Raman bands that coincide with medium or strong infrared absorptions can all be ascribed to deformations of the $CF_3$ groups. This indicates that the assumption of an approximate center of symmetry for this molecule is valid. The $g$ vibrations are Raman active, those of species $a_g$ giving rise to polarized Raman bands and the others to depolarized bands, and all of the $u$ vibrations are infrared active, except the two of species $a_u$. The assignments of the "skeletal" frequencies will be discussed first, and then the $CF_3$ group vibrations.

## SKELETAL VIBRATIONS

### Species $a_g$

The very strong polarized Raman bands at 236, 1063, and 3092 cm$^{-1}$ are readily identified as three of the six totally-symmetric "skeletal" fundamentals. The first two assignments are confirmed by the ultraviolet investigation of Cooper and Noegel.[8] The fundamental at 3092 cm$^{-1}$ involves largely C—H stretching. The strong polarized Raman bands at 1334 and 1628 cm$^{-1}$ are also interpreted as $a_g$ fundamentals. A strong polarized doublet occurring in the Raman spectrum at 790 and 803 cm$^{-1}$ is assumed to be an $a_g$ fundamental in

* Part of this work has been supported by the U. S. Atomic Energy Commission under Contract No. AT-(40-1)-1074.

† Present address: Petroleum Experiment Station, U. S. Bureau of Mines, Bartlesville, Oklahoma.

‡ Present address: Phillips Petroleum Company, Bartlesville, Oklahoma.

[1] Nielsen, Liang, and Smith, Faraday Soc. Disc. **9**, 177 (1950).

[2] Eldon Ferguson, J. Chem. Phys. **21**, 886 (1953).

[3] Ferguson, Hudson, Nielsen, and Smith, J. Chem. Phys. **21**, 1457 (1953).

[4] Ferguson, Hudson, Nielsen, and Smith, J. Chem. Phys. **21**, 1464 (1953).

[5] Ferguson, Collins, Nielsen, and Smith, J. Chem. Phys. **21**, 1470 (1953).

[6] Smith, Ferguson, Hudson, and Nielsen, J. Chem. Phys. **21**, 1475 (1953).

[7] Ferguson, Hudson, Nielsen, and Smith, J. Chem. Phys. **21**, 1727 (1953).

[8] C. D. Cooper and F. W. Noegel, J. Chem. Phys. **20**, 1903 (1952).

[9] K. S. Pitzer and D. W. Scott, J. Am. Chem. Soc. **65**, 803 (1943).

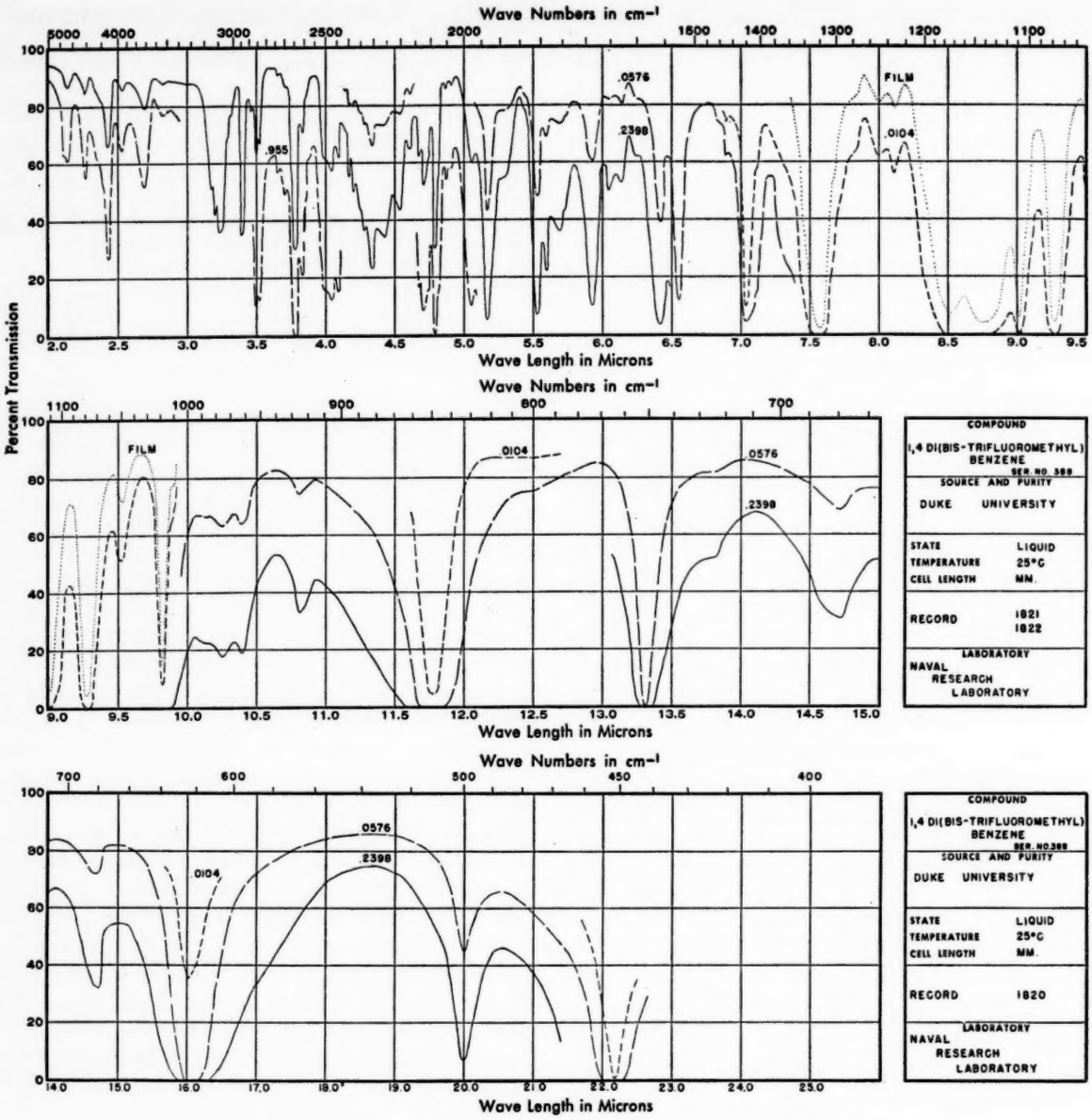


FIG. 1. Infrared spectrum of liquid 1,4-bis (trifluoromethyl) benzene.

Fermi resonance with the overtone of the weak Raman band at 401 $cm^{-1}$, assigned as a $b_{2g}$ fundamental.

### Species $b_{1g}$

The single fundamental vibration of species $b_{1g}$ is a nonplanar hydrogen bending corresponding to those occurring at 850 $cm^{-1}$ in benzene and at 800 $cm^{-1}$ in 1,4-difluorobenzene. It is identified with the weak Raman band at 841 $cm^{-1}$. Its low intensity is in accord with the fact that nonplanar hydrogen bendings have been found to give rise to weak Raman bands in all the fluorinated benzenes so far studied.[2-7]

### Species $b_{2g}$

The $b_{2g}$ fundamental involving largely C—H stretching is identified with the strong Raman band at 3079 $cm^{-1}$. The weak diffuse Raman band observed at 296 $cm^{-1}$ is assumed with some certainty to be the lowest $b_{2g}$ fundamental. The medium depolarized Raman band at 1596 $cm^{-1}$ is also assigned as a $b_{2g}$ fundamental. One of the Raman bands at 401, 422, or 429 $cm^{-1}$ is undoubtedly a $b_{2g}$ fundamental involving largely C—$CF_3$ bending. The weak band at 401 $cm^{-1}$ has been chosen rather arbitrarily. The remaining $b_{2g}$ fundamental is identified with the medium Raman band at 1194 $cm^{-1}$, although the measured depolarization ratio of 0.51 is quite low. The measured depolarization ratios seem too low in general. This may be caused by a systematic error or by the fact that the molecule has lower symmetry than assumed.

TABLE I. Infrared and Raman spectra of 1,4-bis(trifluoromethyl) benzene (liquid).

| Raman | | Infrared | Interpretation |
|---|---|---|---|
| 170 vs, sh | 0.72 | | $b_{3g}$ fundamental |
| 236 vvs, sh | 0.26 | | $a_g$ fundamental |
| 296 w, d | | | $b_{2g}$ fundamental |
| 401 w, b | | | $b_{2g}$ fundamental; $170+236=406\ B_{3g}$ |
| 422 m, d | 0.50 | | $g$ $CF_3$ rocking fundamental |
| 429 m, d | p | | $b_{3g}$ fundamental |
| | | 451 vs | $b_{2u}$ fundamental |
| 497 vvw | | ~500 s | $b_{3u}$ fundamental |
| 572 w, d | | | $170+401=571\ B_{1g}$ |
| 584 w, d | | | $(130)+451=581\ A_g$; $170+422=592$; $2\times296=592\ A_g$ |
| | | 624 vs | $b_{1u}$ fundamental; $u$ asym $\delta(CF_3)$ fundamental? |
| 635 s, sh | 0.80 | | $g$ asym $\delta(CF_3)$ fundamental; $236+401=637\ B_{2g}$ |
| 679 m, sh | dp | ~678 m | $u+g$ asym $\delta(CF_3)$ fundamentals; $236+451=687\ B_{2u}$ |
| 705 vvvw | | | $296+401=697\ A_g$ |
| | | 726 vvw | $236+497=733\ B_{3u}$ |
| 753 m, sh | p | 751 vs | $u+g$ sym $\delta(CF_3)$ fundamentals |
| 790 s, sh | 0.06 | | $2\times401=802\ A_g$; $170+635=805$ |
| 803 s, sh | 0.06 | 800 vvw | $a_g$ fundamental; $296+497=793\ B_{1u}$; $170+624=794\ B_{2u}$ |
| 841 w | | | $b_{1g}$ fundamental; $2\times422=844\ A_g$ |
| | | ~849 vs | $b_{2u}$ fundamental |
| 871 vvw | | | $b_{3g}$ fundamental |
| 900 vvw | | | $2\times451=902\ A_g$ |
| 910 vvw | | | $236+679=915$ |
| | | ~925 m | $a_u$ fundamental?; $422+497=919$; $296+624=920\ B_{3u}$ |
| | | 962 w | $(130)+841=971\ B_{3u}$ |
| | | 976 w | $236+751=987$; $296+678=974$ |
| 1019 vvw | | 1018 vvs | $b_{1u}$ fundamental; $401+624=1025\ B_{3u}$ |
| | | 1049 s | $b_{3u}$ fundamental; $429+624=1053\ B_{2u}$; $422+624=1046$ |
| 1063 s, sh | 0.16 | | $a_g$ fundamental |
| | | 1078 vvs | $b_{1u}$ fundamental |
| | | 1110 vvs | $b_{3u}$ fundamental |
| 1137 m, b | 0.65 | ~1140 vvs, b | $u+g$ asym $\nu(CF_3)$ fundamentals |
| 1180 vw | | ~1175 vvs | $u+g$ asym $\nu(CF_3)$ fundamentals; $422+752=1174$ |
| 1194 m | 0.51 | | $b_{2g}$ fundamental; $401+803=1204\ B_{2g}$ |
| | | 1233 m | $296+925=1221\ B_{2u}$; $170+1078=1248\ B_{2u}$ |
| | | 1250 m | $236+1018=1254\ B_{1u}$; $451+803=1254\ B_{2u}$; $497+752=1249$ |
| 1269 vvw | | | $401+871=1272\ B_{1g}$ |
| 1308 w | | | $451+849=1300\ A_g$ |
| 1320 m | p | ~1321 vvs, b | $u+g$ sym $\nu(CF_3)$ fundamentals |
| 1334 s, sh | 0.10 | | $a_g$ fundamental |
| 1373 vw, d | | | $170+1194=1364\ B_{1g}$ |
| 1420 vw, d | | 1422 vs | $b_{3u}$ fundamental; $624+803=1427\ B_{1u}$ |
| | | 1451 | $429+1018=1447\ B_{2u}$; $401+1049=1450\ B_{1u}$ |
| 1504 w, d | | | $451+1049=1500\ B_{1g}$; $2\times752=1504\ A_g$ |
| 1519 w, d | | | $497+1018=1515\ B_{2g}$; $679+841=1520$ |
| | | 1527 s | $b_{1u}$ fundamental |
| | | 1558 s | $497+1063=1560\ B_{3u}$ |
| 1574 vw | | | $497+1078=1575\ B_{2g}$ |
| 1596 m, d | dp | | $b_{2g}$ fundamental; $2\times803=1606\ A_g$; $752+841=1593$ |
| 1628 s, sh | 0.69 | ~1629 w | $a_g$ fundamental |
| | | 1653 w | $236+1422=1658\ B_{3u}$ |
| | | 1686 s | $624+1063=1687\ B_{1u}$; $679+1018=1697$ |
| | | ~1754 w | $679+1078=1757$ |
| | | 1786 m | $679+1110=1789$ |
| | | 1808 s | $803+1018=1821\ B_{1u}$; $752+1049=1801$ |
| 1926 vvvw | | 1934 s | $401+1527=1928\ B_{3u}$; $849+1078=1927\ B_{3g}$ |
| 1944 vvvw | | | $871+1063=1934\ B_{3g}$; $925+1018=1943\ B_{1g}$ |
| | | 1976 w | $841+1140=1981$ |
| | | 2037 vw | $849+1180=2029$; $871+1175=2046$ |
| | | 2053 vw | $751+1320=2071$; $635+1422=2057$ |
| | | 2088 m | $1018+1063=2081\ B_{1u}$; $451+1628=2079\ B_{2u}$ |
| | | 2123 m | $1049+1063=2112\ B_{3u}$; $497+1628=2125\ B_{3u}$ |
| | | 2137 w | $1063+1078=2141\ B_{1u}$ |
| 2158 vvvw | | | $2\times1078=2156\ A_g$; $1049+1110=2159\ A_g$; $841+1320=2161$ |
| | | 2169 w | $1063+1110=2173\ B_{3u}$; $849+1320=2169$ |
| | | 2203 w | $1063+1140=2203$ |
| | | 2257 w | $624+1628=2252\ B_{1u}$ |
| | | 2304 m | $1110+1194=2304\ B_{1u}$ |
| | | 2336 w | $1140+1194=2334$ |
| | | 2381 w | $1049+1334=2383\ B_{3u}$ |
| | | 2398 w | $1078+1334=2412\ B_{1u}$; $871+1527=2398\ B_{2u}$; $803+1628=2431\ A_g$ |
| 2436 vvw, d | | | |
| | | 2445 w | $1110+1334=2444\ B_{3u}$ |
| | | 2475 w | $849+1628=2477\ B_{2u}$ |
| | | 2611 w | $1194+1422=2616\ B_{1u}$ |
| | | 2646 m | $1018+1628=2646\ B_{1u}$ |
| | | 2703 w | $1078+1628=2706\ B_{1u}$; $1137+1596=2733$ |
| 2718 vvw | | | |
| | | 2740 w | $1110+1628=2738\ B_{3u}$ |
| 2842 vvw | | 2841 m | $2\times1422=2844\ A_g$; $1320+1527=2847$ |
| | | 2857 m | $1334+1527=2861\ B_{1u}$ |
| | | 2890 w | $1321+1596=2917$ |
| 2937 vw, d | | | $1422+1527=2949\ B_{2g}$ |
| | | 2950 m | $1321+1628=2949$ |
| 2965 vvw | | | $1334+1628=2962\ A_g$ |
| 3079 s, d | 0.31 | | $b_{2g}$ fundamental |
| 3092 vs, d | | | $a_g$ fundamental |
| | | ~3096 m | $b_{1u}$ fundamental |
| | | 3125 m | $b_{3u}$ fundamental?; $1527+1596=3123\ B_{3u}$ |
| | | 3155 w | $1527+1628=3155\ B_{1u}$ |
| 3182 vw, b | | | $2\times1596=3192\ A_g$ |
| 3255 m, sh | | | $2\times1628=3256\ A_g$; $170+3092=3262\ B_{3g}$ |
| | | 3546 w | $451+3092=3543\ B_{2u}$ |
| | | 3717 w | $624+3092=3716\ B_{1u}$ |
| | | 3953 w | $871+3096=3967\ B_{2u}$ |
| | | 4115 m | $1018+3092=4110\ B_{1u}$ |
| | | 4673 w | $1596+3096=4692\ B_{3u}$ |

### Species $b_{3g}$

The very strong Raman band at 170 $cm^{-1}$ is assigned as the lowest $b_{3g}$ fundamental. The very weak Raman band at 871 $cm^{-1}$ is assigned as a $b_{3g}$ hydrogen bending fundamental with considerable certainty. The intermediate $b_{3g}$ fundamental is identified with the medium Raman band at 429 $cm^{-1}$.

### Species $b_{1u}$

The medium infrared band at 3096 $cm^{-1}$ is assumed to represent the single fundamental of species $b_{1u}$ involving C—H stretching. The very strong infrared band at 624 $cm^{-1}$ is interpreted as a $b_{1u}$ fundamental involving C—$CF_3$ stretching. The remaining $b_{1u}$ fundamentals are identified with the extremely strong infrared bands at 1018 and 1078 $cm^{-1}$ and the strong infrared band at 1527 $cm^{-1}$. Any one of these bands may actually represent a $b_{3u}$ fundamental, since there is no experimental basis for determining these species, and since three $b_{3u}$ fundamentals occur in the same spectral region.

TABLE II. Fundamental vibration frequencies for 1,4-bis(trifluoromethyl) benzene (liquid).

| Approximate motion | Skeletal vibrations | | | | | | | |
|---|---|---|---|---|---|---|---|---|
| | $a_g$ | $b_{1g}$ | $b_{2g}$ | $b_{3g}$ | $a_u$ | $b_{1u}$ | $b_{2u}$ | $b_{3u}$ |
| C—H stretching | 3092 | | 3079 | | | ~3096 | | 3125 |
| C—$CF_3$ stretching | 803 | | | | | 624 | | |
| C—C stretching | 1628 | | 1596 | | | 1527 | | 1422 |
| C—C breathing | 1063 | | | | | 1018 | | 1110 |
| C—H bending | 1334 | 841 | 1194 | 871 | ~925 | 1078 | ~849 | 1049 |
| C—$CF_3$ bending | | | 401 | 429 | | | 451 | 497 |
| C—C—C bending | 236 | | 296 | 170 | ? | | ~(130) | |
| | $CF_3$ vibrations | | | | | | | |
| | $g$ | $g$ | | | | $u$ | $u$ | |
| Symmetric C—F | 1320 | | | | | ~1321 | | |
| Asymmetric C—F | 1137 | 1180 | | | | ~1140 | ~1175 | |
| Symmetric $\delta(CF_3)$ | 753 | | | | | 751 | | |
| Asymmetric $\delta(CF_3)$ | 679 | 635 | | | | ~678 | ~624? | |
| $CF_3$ rocking | 422 | ? | | | | ? | ? | |
| $CF_3$ torsion | ? | | | | | ? | | |

### Species $b_{2u}$

The highest $b_{2u}$ fundamental, involving largely nonplanar hydrogen bending, is undoubtedly represented by the intense infrared band at 849 $cm^{-1}$. The very strong infrared band at 451 $cm^{-1}$, which is the lowest infrared band observed, is probably the intermediate $b_{2u}$ fundamental, which may be characterized roughly as C—$CF_3$ bending. The lowest $b_{2u}$ fundamental is assumed to lie around 130 $cm^{-1}$, since the corresponding fundamental in benzotrifluoride has been observed at 139 $cm^{-1}$.

### Species $b_{3u}$

The highest $b_{3u}$ fundamental is identified with the medium infrared band at 3125 $cm^{-1}$. The $b_{1u}$ and $b_{3u}$ C—H stretching frequencies may well be interchanged. The strong infrared band at 497 $cm^{-1}$ is assumed to be the lowest $b_{3u}$ fundamental. The remaining three $b_{3u}$ fundamentals are identified with the strong infrared bands at 1049, 1110, and 1422 $cm^{-1}$, any of which may be interchanged with a fundamental assigned to $b_{1u}$, as mentioned above.

### Species $a_u$

The two inactive $a_u$ fundamentals may be characterized roughly as a nonplanar ring bending and a nonplanar hydrogen bending. A medium infrared band at 925 $cm^{-1}$ is assumed to represent the latter, the selection rules being assumed relaxed for the liquid state. The other $a_u$ fundamental, which may be expected to lie around 200 $cm^{-1}$, is not observed.

### $CF_3$ Vibrations

The two $CF_3$ groups will give rise to 18 additional normal vibrations which may be characterized roughly as follows: two symmetric and four asymmetric CF stretchings, two symmetric and four asymmetric $CF_3$ deformations, four $CF_3$ rockings and two torsions. Symmetry and asymmetry here refer to a $CF_3$ group alone. Further, these vibrations may be approximately divided into half $g$ and half $u$ vibrations. The $g$ vibrations are expected to be stronger in the Raman effect, and the $u$ vibrations stronger in infrared absorption.

The medium polarized Raman band at 1320 $cm^{-1}$ is identified with the symmetric $g$ CF stretching and the extremely intense broad infrared band at 1321 $cm^{-1}$ with the symmetric $u$ CF stretching fundamental. Since the $CF_3$ groups are so widely separated, it seems quite reasonable that symmetric $g$ and $u$ fundamentals would have nearly the same frequency. The medium diffuse Raman band at 1137 $cm^{-1}$ and the intense broad infrared band at 1140 $cm^{-1}$ are interpreted as asymmetric $g$ and $u$ CF stretching fundamentals, respectively, as are the weak Raman band at 1180 $cm^{-1}$ and the intense infrared band at 1175 $cm^{-1}$. The medium infrared bands at 1233 and 1250 $cm^{-1}$, and the weak Raman bands at 1269 and 1308 $cm^{-1}$, are interpreted as combination bands. It does not seem likely that any of these are CF stretching fundamentals, since the spread from 1137 to 1180 $cm^{-1}$ is as large as one might expect for the four asymmetric vibrations.

A fundamental involving a symmetric $g$ $CF_3$ deformation is identified with the medium polarized Raman band at 753 $cm^{-1}$, and the corresponding fundamental involving symmetric $u$ $CF_3$ deformation is identified with the very strong infrared band at 751 $cm^{-1}$. The medium depolarized Raman band at 679 $cm^{-1}$ and the medium infrared band at 678 $cm^{-1}$ are assumed to represent $g$ and $u$ asymmetric $CF_3$ deformations, respectively. The remaining $g$ $CF_3$ deformation fundamental is identified with the strong depolarized Raman band at 635 $cm^{-1}$. The remaining $u$ fundamental is quite uncertain. The only infrared band observed that could be so interpreted is a very weak band at 726 $cm^{-1}$. It seems more reasonable to assume that this funda-

mental is masked by the very strong $b_{1u}$ fundamental at 624 $cm^{-1}$.

The medium diffuse Raman band at 422 $cm^{-1}$ is interpreted as a $g$ $CF_3$ rocking fundamental. No evidence is found for the remaining $CF_3$ rocking fundamentals. The two $u$ fundamentals lie too low to be observed in this investigation.

The two torsional frequencies would be expected to lie very low, roughly in the neighborhood of 150 $cm^{-1}$, and to be essentially inactive. No evidence is found for these frequencies.

## DISCUSSION

The assumption of (approximate) $V_h$ symmetry appears quite adequate for the interpretation of the observed spectra. The 62 infrared absorption maxima and the 47 Raman shifts observed for the liquid state are all satisfactorily interpreted as fundamentals or as binary sum bands. The assigned fundamentals are listed in Table II, and the complete interpretation of the spectra is included in Table I. Because of the large number of fundamentals, many coincidences occur, and many of the bands may be interpreted in several ways.

Due to the complexity of this molecule, a number of uncertainties in the assignment of fundamentals exist. Several inactive and low-lying infrared-active fundamentals are not observed. Some of the species assignments may be reversed, particularly of the fundamentals assigned to species $b_{1u}$ and $b_{3u}$ and of the three Raman-active fundamentals at 401, 422, and 429 $cm^{-1}$. Some of the uncertainty as to species of the strong infrared bands could be resolved by an examination of the infrared spectrum of the gaseous phase.

## ACKNOWLEDGMENT

The writers wish to acknowledge their indebtedness to Professor J. H. Saylor for the gift of the sample.

# Vibrational Spectra of Fluorinated Aromatics. IX. *p*-Fluorotoluene*

E. E. FERGUSON, R. L. HUDSON,† AND J. RUD NIELSEN, *Department of Physics, University of Oklahoma, Norman, Oklahoma*

AND

D. C. SMITH,‡ *Naval Research Laboratory, Washington, D. C.*

(Received June 8, 1953)

The infrared absorption spectrum of liquid *p*-fluorotoluene has been obtained in the region 2–38$\mu$ with the aid of LiF, NaCl, KBr, and KRS-5 prisms. The stronger bands of the gas phase have been scanned with NaCl and KBr prisms. The Raman spectrum of the liquid has been photographed with a three-prism glass spectrograph of linear dispersion 15A/mm at 4358A. A complete assignment of fundamental vibration frequencies is given, and the spectra are interpreted in detail.

## INTRODUCTION

IN previous papers of this series[1–8] the infrared and Raman spectra of fluoro-, 1,3- and 1,4-difluoro-, 1,2,4- and 1,3,5-trifluoro-, and 1,2,4,5-tetrafluorobenzene, and also 1,4-bis(trifluoromethyl) benzene, have been reported. Some Raman data and partial assignments of fundamentals for *p*-fluorotoluene are given in Landolt-Börnstein,[9] and infrared contours of some of the stronger bands for the gaseous state have been reported by Thompson and Temple.[10]

New spectral data, assignments of fundamentals, and detailed interpretations of the spectra, will be presented in the present paper.

## EXPERIMENTAL PROCEDURE

The sample of *p*-fluorotoluene was kindly supplied by Dr. G. C. Finger of the Illinois State Geological Survey. No information is available as to its purity. The infrared absorption spectrum of the liquid phase from 2 to 38$\mu$ was obtained in the manner previously described.[1] The infrared absorption band contours in the gaseous state were observed in the NaCl and KBr regions in an attempt to determine band types. The Raman spectrum was photographed at room temperature, and quantitative polarization measurements were made as previously described.[1]

## RESULTS

The infrared absorption of liquid *p*-fluorotoluene between 2 and 22$\mu$ is shown in Fig. 1. The wave numbers of the observed absorption maxima are listed in the first column of Table I. The relative intensities of the bands are indicated in column 2 by means of the previously used abbreviations and the contours for the gas phase are given in the third column where observed. The observed Raman data for liquid *p*-fluorotoluene are given in the next three columns of Table I, the polarization ratios being taken from Landolt-Börnstein.[9]

## INTERPRETATION

The *p*-fluorotoluene molecule has the same symmetry as toluene. The spectra of toluene have been satisfactorily interpreted by Pitzer and Scott[11] assuming the molecular symmetry $C_{2v}$. However, fundamental vibrational assignments for *p*-difluorobenzene[3] and *p*-xylene[11] have previously been based on the symmetry $V_h$, and in order to best utilize these results, it is here assumed that the *p*-fluorotoluene molecule also has approximately the symmetry $V_h$. This is a reasonable assumption, since the mass of a methyl group is not greatly different from that of a fluorine atom. Sheline and Pitzer[12] have suggested that in order to consider the methyl group as a point mass in studying the vibrational spectra of tetramethylmethane, one should use an "effective mass" of 16.67 for stretching vibrations and 18.16 for bending vibrations. Thus, it is possible that the "effective mass" of the methyl group is even closer to that of the fluorine atom than one might offhand expect.

The fundamental frequency assignments of *p*-difluorobenzene and *p*-xylene lie very close together, as shown in Table II, and one would therefore expect the fundamentals of *p*-fluorotoluene to correlate closely

* Part of this work has been supported under contract with the U. S. Atomic Energy Commission and the U. S. Office of Naval Research.

† Present address: Ethyl Corporation, Baton Rouge, Louisiana.

‡ Present address: Phillips Petroleum Company, Bartlesville, Oklahoma.

[1] Nielsen, Liang, and Smith, Disc. Faraday Soc. **9**, 177 (1950).

[2] Eldon Ferguson, J. Chem. Phys. **21**, 886 (1953).

[3] Ferguson, Hudson, Nielsen, and Smith, J. Chem. Phys. **21**, 1457 (1953).

[4] Ferguson, Hudson, Nielsen, and Smith, J. Chem. Phys. **21**, 1464 (1953).

[5] Ferguson, Collins, Nielsen, and Smith, J. Chem. Phys. **21**, 1470 (1953).

[6] Smith, Ferguson, Hudson, and Nielsen, J. Chem. Phys. **21**, 1475 (1953).

[7] Ferguson, Hudson, Nielsen, and Smith, J. Chem. Phys. **21**, 1727 (1953).

[8] Ferguson, Mikkelsen, Nielsen, and Smith, J. Chem. Phys. **21**, 1731 (1953).

[9] Landolt-Börnstein, *Zahlenwerte und Funktionen* (Springer Verlag, Berlin-Göttingen-Heidelberg, 1951), sixth edition, Vol. 1, Part 2, pp. 308, 324.

[10] H. W. Thompson and R. B. Temple, J. Chem. Soc. **151**, 1432 (1948).

[11] K. S. Pitzer and D. W. Scott, J. Am. Chem. Soc. **65**, 803 (1943).

[12] R. K. Sheline and K. S. Pitzer, J. Chem. Phys. **18**, 595 (1950).

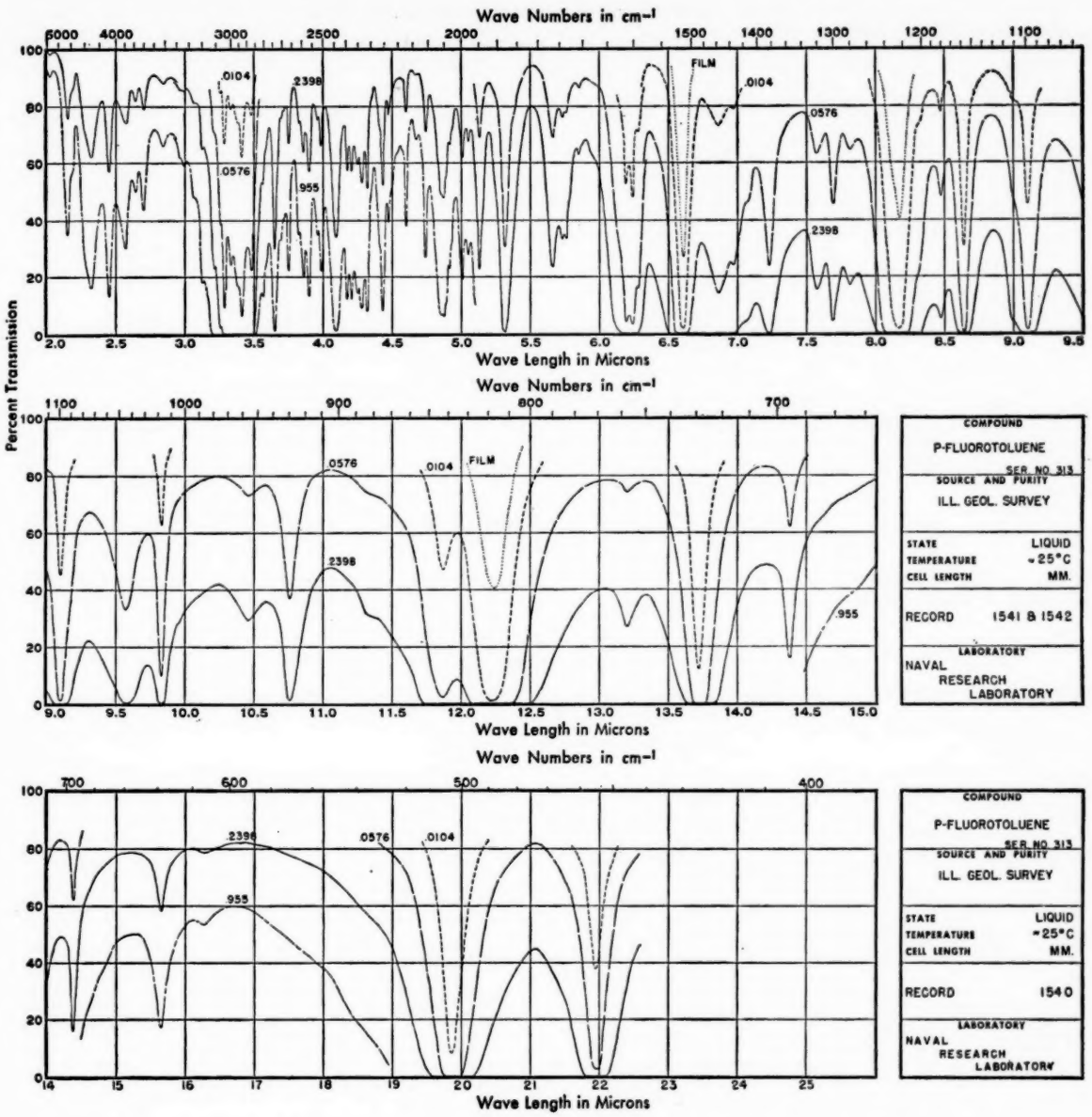


FIG. 1. Infrared spectrum of liquid $p$-fluorotoluene (KRS-5 region not included).

with those of these two molecules. This is indeed found to be the case.

It will be assumed that the $p$-fluorotoluene molecule has approximately the symmetry $V_h$. The skeletal vibrations then divide themselves into symmetry species in the following manner: $6a_g+1b_{1g}+5b_{2g}+3b_{3g}+2a_u+5b_{1u}+3b_{2u}+5b_{3u}$.

The $a_g$ vibrations yield polarized, the $b_g$ vibrations depolarized Raman bands. The $b_{1u}$, $b_{3u}$, and $b_{2u}$ vibrations yield infrared bands with type $A$, $B$, and $C$ contours, respectively. The $a_u$ vibrations are inactive in both spectra. The selection rules will of course not conform strictly to a $V_h$ model, and some coincidences of strong Raman and infrared bands are to be expected.

Since several Raman and infrared coincidences do occur, the selection rules for symmetry $C_{2v}$ should be kept in mind. For this symmetry, the species $a_g$ and $b_{1u}$ combine to give species $a_1$, yielding polarized Raman bands and type $A$ infrared bands. The species $b_{2g}$ and $b_{3u}$ form species $b_1$ which has depolarized Raman bands and type $B$ infrared bands. Species $b_{3g}$ and $b_{2u}$ combine to give species $b_2$ having depolarized Raman bands and type $C$ infrared bands, and $a_u$ and $b_{1g}$ form species $a_2$ with depolarized Raman bands.

In addition to the skeletal vibrations, there will be vibrations of the methyl group.

### Species $a_g$

The four strong polarized Raman bands at 454, 825, 842, and 1214 cm$^{-1}$ are readily assigned as species $a_g$

TABLE I. Infrared and Raman spectra of *p*-fluorotoluene.

| Infrared Liquid $cm^{-1}$ | Infrared Gas contour | Raman Liquid $cm^{-1}$ | Raman Polarization[a] | Interpretation |
|---|---|---|---|---|
| | | 152 m, d | | $b_{2u}$ fundamental |
| 313 m | | 312 m | | $b_{2g}$ fundamental |
| 341 s | | 341 vs, d | dp | $b_{3g}$ fundamental |
| 422 s | | 425 vw, d | | $b_{3u}$ fundamental |
| 456 s | | 454 vs, sh | p′ [b] | $a_g$ fundamental |
| 503 s | C? | 502 w | | $b_{2u}$ fundamental |
| ~615 vvw | | | | 152+455=607 $B_{2u}$ |
| 639 m | | 638 s, sh | dp | $b_{2g}$ fundamental |
| 695 m | | 695 m, sh | p′ | $b_{3g}$ fundamental |
| 729 s | A | 728 m, sh | | $b_{1u}$ fundamental |
| | | 740 vvw | | 313+422=735 $B_{1u}$? |
| 758 w | | | | 313+455=768 $B_{2g}$? |
| 817 s | C | | | $b_{2u}$ fundamental |
| | | 825 vs | p | $a_g$ fundamental |
| 842 m | | 842 vs | p | $a_g$ fundamental |
| | | 908 vvw | | 2×455=910 $A_g$ |
| 929 m | | 929 vw, d | | $b_{3g}$ fundamental; |
| | | | | 422+503=925 $B_{1g}$ |
| 956 w | | | | $a_u$ fundamental?; |
| | | | | 455+503=958 $B_{2u}$ |
| | | 1003 w | | 2×503=1006 $A_g$; |
| | | | | 313+695=1008 $B_{1g}$ |
| 1017 s | A | 1017 w, sh | | $b_{1u}$ fundamental |
| 1045 s | B? | 1040 vvw | | $b_{3u}$ fundamental; |
| | | | | 313+728=1041 $B_{3u}$; |
| | | | | 341+695=1036 $A_g$ |
| | | 1061 vvw | | 341+728=1069 $B_{2u}$?; |
| | | | | 422+638=1060 $B_{1u}$? |
| 1099 s, sh | B | 1099 w | | $b_{3u}$ fundamental; |
| | | | | 455+638=1093 $B_{2g}$ |
| 1157 s, sh | A | 1157 s, sh | p′ | $b_{1u}$ fundamental; |
| | | | | 455+695=1150 $B_{3g}$ |
| 1181 w | | 1178 w | | $CH_3$ rocking fundamental?; |
| | | | | 341+842=1183 $B_{3g}$ |
| | | 1214 vs | p | $a_g$ fundamental |
| 1224 s | | 1221 vs | | $b_{2g}$ fundamental?; |
| | | | | 503+728=1231 $B_{3g}$ |
| 1280 vw | | 1278 w | | 2×638=1276 $A_g$; |
| | | | | 455+825=1280 $A_g$ |
| 1300 w | | 1299 m | p′ | $b_{2g}$ fundamental; |
| | | | | 455+842=1297 $A_g$ |
| 1321 w | | | | 503+825=1328 $B_{2u}$; |
| | | | | 152+1178=1330 |
| | | 1351 vvw | | 638+695=1333 $B_{1g}$ |
| 1383 m | | 1382 s, sh | p′ | sym $\delta$ ($CH_3$) fundamental |
| | | 1404 w | | 2×695=1390 $A_g$ |
| 1435 vvw | | 1433 vvw | | 422+1017=1439 $B_{2g}$ |
| 1498 w | | 1455 w, d | | two asym $\delta(CH_3)$ fundamentals; |
| | | | | 2×728=1456 $A_g$ |
| | | 1495 w | | 638+842=1480 $B_{2g}$; |
| | | | | 455+1044=1499 $B_{3u}$ |
| 1513 s | | 1508 w | | $b_{1u}$ fundamental; |
| | | | | 695+817=1512 $B_{1u}$ |
| 1603 s | | 1601 s, sh | | $a_g$ fundamental; |
| | | | | 503+1099=1602 $B_{1g}$ |
| 1615 s | | 1614 m, d | p′ | $b_{3u}$ fundamental; |
| | | | | 455+1157=1612 $B_{1u}$ |
| 1709 vvw | | | | 695+1017=1712 $B_{2u}$; |
| | | | | 503+1214=1717 $B_{2u}$ |
| 1736 w | | | | 638+1099=1737 $B_{1u}$ |
| 1746 w | | | | 817+929=1746 $B_{1u}$ |
| 1766 w | | | | 152+1602=1754 $B_{2u}$ |
| | | 1858 vvw | | 2×929=1858 $A_g$; |
| | | | | 638+1222=1860 $A_g$; |
| | | | | 817+1044=1861 $B_{1g}$ |
| 1882 m | | | | 892+1044=1886 $B_{3u}$ |
| | | 1906 vvw | | 695+1214=1909 $B_{3g}$; |
| | | | | 2×956=1912 $A_g$ |
| 1949 w | | 1940 vw | | 422+1512=1934 $B_{2g}$; |
| | | | | 728+1222=1950 $B_{3u}$ |
| 1981 vw | | | | 825+1157=1982 $B_{1u}$ |
| 2034 vvw | | | | 817+1214=2031 $B_{2u}$ |
| 2054 w | | | | 455+1614=2069 $B_{3u}$ |
| 2109 w | | | | 503+1602=2105 $B_{2u}$ |
| ~2140 vvw | | | | 638+1512=2150 $B_{3u}$ |
| 2173 w | | | | 956+1222=2178 $B_{2u}$ |
| 2236 vvw | | | | 638+1614=2252 $B_{1u}$ |
| 2256 w | | | | 1044+1214=2258 $B_{3u}$ |
| 2316 vvw | | | | 1099+1214=2313 $B_{3u}$ |
| 2335 vvw | | | | 825+1512=2337 $B_{1u}$; |
| | | | | 728+1602=2330 $B_{1u}$ |
| 2354 vvw | | | | 842+1512=2354 $B_{1u}$ |
| 2379 vvw | | 2385 vvw | | 1157+1222=2379 $B_{3u}$; |
| | | | | 929+1455=2384 |
| 2395 w | | | | 1099+1299=2498 $B_{1u}$ |
| | | 2416 vvw | | 2×1214=2428 $A_g$ |
| 2442 vw | | | | 825+1614=2439 $B_{2u}$ |
| | | 2454 vvw | | 2×1222=2444 $A_g$; |
| | | | | 842+1602=2444 $A_g$ |
| 2510 vw | | | | 1044+1455=2499 |
| 2525 vw | | | | 1157+1382=2539 |
| 2563 vw | | | | 1099+1455=2554 |
| 2592 vw | | | | 1214+1382=2596 |
| 2614 vw | | | | 1017+1602=2619 $B_{1u}$ |
| 2665 vw | | | | 1044+1602=2646 $B_{3u}$ |
| 2706 vw | | | | 1099+1602=2701 $B_{3u}$ |
| 2741 w | | 2740 w | | 1222+1512=2734 $B_{3u}$ |
| 2866 vvw | | | | 1382+1455=2387? |
| 2874 vw | | 2871 w | | 1382+1512=2894; |
| | | | | 2×1455=2910 $A_g$ |
| 2931 s | | 2928 s | p | three $\nu(CH_3)$ fundamentals |
| 3001 m | | | | 1382+1614=2996 |
| 3043 m | | | | $b_{1u}$ fundamental |
| 3069 vw | | 3071 vs | p′ | $a_g+b_{2g}+b_{3u}$ fundamentals |
| 3111 vw | | | | 1512+1602=3114 $B_{1u}$ |
| 3201 vw | | | | 1602+1614=3216 $B_{3u}$ |
| 3340 vw | | | | 313+3043=3356 $B_{3u}$ |
| 3520 vw | | | | 455+3069=3524 $B_{3u}$ |
| 3700 vw | | | | 638+3069=3707 $B_{1u}$ |
| 3790 vw | | | | 728+3071=3799 $B_{1u}$ |
| 3890 w | | | | 842+3043=3885 $B_{1u}$; |
| | | | | 817+3071=3888 $B_{2u}$ |
| 4080 w | | | | 1017+3071=4088 $B_{1u}$ |
| 4310 w | | | | 1222+3069=4291 $B_{1u}$; |
| | | | | 1382+2929=4311 |
| 4650 w | | | | 1602+3043=4645 $B_{1u}$ |
| 4950 vvw | | | | |

[a] Taken from Landolt-Börnstein (reference 9).
[b] p′ probably polarized Raman band.

fundamentals. The sharp component of the doublet near 1601 $cm^{-1}$ and the strong Raman band at 3071 $cm^{-1}$ are assumed to represent the remaining two $a_g$ fundamentals. There is strong infrared absorption at 456 and 1603 $cm^{-1}$ and medium absorption at 842 $cm^{-1}$.

### Species $b_{1g}$

The single vibration of species $b_{1g}$ belongs to a nonplanar hydrogen bending, and corresponds to a vibration having the frequency 850 $cm^{-1}$ in benzene, 811 $cm^{-1}$

in *p*-xylene, and 800 cm$^{-1}$ in *p*-difluorobenzene. It is fairly certain, therefore, that this vibration has a frequency in the range 800–850 cm$^{-1}$. No spectral evidence for it is found. However, since nonplanar aromatic hydrogen bendings generally give rise to weak Raman bands, the intense $a_g$ fundamentals at 825 and 842 cm$^{-1}$ might well mask such a band.

### Species $b_{2g}$

The medium Raman bands at 312 and 1299 cm$^{-1}$, and the strong Raman bands at 638 and 1221 cm$^{-1}$, are assumed to represent $b_{2g}$ fundamentals, partly on the basis of correlation with the spectral assignments for related compounds and partly because these are the most intense Raman bands available for the assignments. Medium infrared absorption occurs at 313 and 639 cm$^{-1}$, strong absorption at 1224 cm$^{-1}$ and weak absorption at 1300 cm$^{-1}$. The highest $b_{2g}$ fundamental, involving CH stretching, is assumed to be overlapped in the Raman spectrum by the very intense $a_g$ fundamental at 3071 cm$^{-1}$.

### Species $b_{3g}$

The lowest $b_{3g}$ fundamental is identified with the very strong depolarized Raman band at 341 cm$^{-1}$ with a strong infrared counterpart. The band at 312 cm$^{-1}$, assigned as a $b_{2g}$ fundamental, might have been chosen for this assignment except that the lowest nonplanar fundamental has been found to give rise to quite intense Raman bands in the fluorinated aromatics previously studied.[1–8]

The medium infrared and Raman bands at 695 cm$^{-1}$ are assigned as the intermediate $b_{3g}$ fundamental. The highest $b_{3g}$ fundamental involving largely hydrogen bending is probably represented by one of the faint Raman bands at 908 and 929 cm$^{-1}$. The slightly more intense band at 929 cm$^{-1}$ is chosen.

### Species $b_{1u}$

The three strong infrared bands at 729, 1017, and 1157 cm$^{-1}$ all have definite type *A* contours and hence are assigned as species $b_{1u}$ fundamentals. There are sharp Raman counterparts to each of these frequencies, as would be expected on the basis of $C_{2v}$ symmetry. The strong infrared band at 1513 cm$^{-1}$ of uncertain contour is also assumed to be a $b_{1u}$ fundamental, corresponding to the fundamental at 1511 cm$^{-1}$ in *p*-difluorobenzene and 1525 cm$^{-1}$ in *p*-xylene. The medium infrared band at 3043 cm$^{-1}$ is assumed to be the highest $b_{1u}$ fundamental.

### Species $b_{2u}$

The medium Raman band at 152 cm$^{-1}$ is assumed to represent the lowest $b_{2u}$ fundamental, corresponding to that observed at 170 cm$^{-1}$ in *p*-xylene. The strong infrared band at 817 cm$^{-1}$ has a type *C* contour and is therefore assigned as a $b_{2u}$ fundamental. The strong infrared band at 503 cm$^{-1}$, which shows slight indication of a type *C* contour, is assumed to be the remaining $b_{2u}$ fundamental.

TABLE II. Correlation of fundamental assignments of *p*-xylene, *p*-fluorotoluene, and *p*-difluorobenzene.

| *p*-xylene[b] | Species $a_g$ *p*-fluorotoluene | *p*-difluorobenzene[c] | *p*-xylene[b] | Species $b_{1u}$ *p*-fluorotoluene | *p*-difluorobenzene[c] |
|---|---|---|---|---|---|
| 460 | 455 | 451 | 720 | 728 | 737 |
| 826 | 825 | 840 | 1030 | 1017 | 1012 |
| 1182 | 842 | 858.5 | 1200 | 1157 | 1183 |
| 1204 | 1214 | 1245 | 1525 | 1512 | 1511 |
| 1616 | 1602 | 1617 | (3046) | 3043 | 3028 |
| (3062) | 3071 | 3084 | | | |
| | | | | Species $b_{2u}$ | |
| | Species $b_{1g}$ | | 170 | 152 | (186) |
| 811 | (810) | 800 | 389 | 503 | 509 |
| | | | 800 | 817 | 833 |
| | Species $b_{2g}$ | | | | |
| 313 | 313 | 507 | | Species $b_{3u}$ | |
| 644 | 638 | 635 | (232) | 422 | 350 |
| ~1200? | 1222 | 1142 | 1100 | 1044 | 1085 |
| 1575 | 1299 | 1285 | 1450 | 1099 | 1212 |
| (3047) | (3071) | ~3080 | 1640[a] | 1614 | 1437 |
| | | | (3080) | (3069) | 3088 |
| | Species $b_{3g}$ | | | | |
| ~313? | 341 | 375 | | Species $a_u$ | |
| 697 | 695 | 692 | (400) | (390) | (370) |
| 959 | 929 | 887 | 971 | 956? | (935) |

[a] Correlated to $b_{2u}$ vibration in benzene believed to be at 1648 cm$^{-1}$ but since shown to be at 1310 cm$^{-1}$.
[b] See reference 11.
[c] See reference 3.

### Species $b_{3u}$

The strong infrared band at 1099 cm$^{-1}$ definitely has a type *B* contour, and hence is assigned as a $b_{3u}$ fundamental. The strong infrared band at 1045 cm$^{-1}$, which shows slight evidence of a type *B* contour, is also assigned as a $b_{3u}$ fundamental. The lowest fundamental of this species is identified with the strong infrared band, observed in the liquid only, at 422 cm$^{-1}$. The assignment of the CH stretching fundamental of species $b_{3u}$ is uncertain because of the poor resolution in this region but it is tentatively identified with the weak infrared band at 3069 cm$^{-1}$. The strong infrared band at 1615 cm$^{-1}$ of uncertain contour and its medium counterpart in the Raman spectrum are assumed to represent the remaining $b_{3u}$ fundamental.

### Species $a_u$

The two inactive $a_u$ fundamentals might be expected to appear in the Raman spectrum, since the molecule strictly has $C_{2v}$ or lower symmetry. The lower $a_u$ fundamental probably lies around 390 cm$^{-1}$. No evidence was found for it. However, it may possibly be masked by the very intense Raman band at 341 cm$^{-1}$. The highest $a_u$ fundamental is tentatively identified with the weak infrared band at 956 cm$^{-1}$.

### $CH_3$ Vibrations

The medium sharp Raman band and the medium infrared band at 1382 cm$^{-1}$ must be assigned as a funda-

TABLE III. Fundamental vibrational frequencies for *p*-fluorotoluene (liquid).

| Species $a_g$ | | | Species $b_{1u}$ | | | |
|---|---|---|---|---|---|---|
| Raman | Polarization[a] | Infrared | Raman | Polarization[a] | Infrared | Band contour |
| 454 vs, sh | p′ | 456 s | 728 m, sh | | 729 s | A |
| 825 vs | p | | 1017 w, sh | | 1017 s | A |
| 842 vs | p | 842 m | 1157 s, sh | p′ | 1157 s, sh | A |
| 1214 vs | p | | 1508 w | | 1513 s | |
| 1601 s, sh | | 1603 s | | | 3043 m | |
| 3071 vs | p′ | 3069 vw | | | | |
| Species $b_{1g}$ | | | Species $b_{2u}$ | | | |
| | | | 152 m, d | | | |
| (810) not observed | | | 502 w | | 503 s | C? |
| | | | | | 817 s | C |
| Species $b_{2g}$ | | | Species $b_{3u}$ | | | |
| 312 m | | 313 m | | | | |
| 638 s, sh | dp | 639 m | 425 vw, d | | 422 s | |
| 1221 vs | | 1224 s | 1040 vvw | | 1045 s | B? |
| 1299 m | p′ | 1300 w | 1099 w | | 1099 s, sh | B |
| (3071) vs | p′ | 3069 vw | 1614 m, d | p′ | 1615 s | |
| | | | | | 3069 vw | ? |
| Species $b_{3g}$ | | | | | | |
| 341 vs, d | dp | 341 s | $\delta(CH_3)$ | | | |
| 695 m, sh | p′ | 695 m | 1382 s, sh | p′ | 1383 m | |
| 929 vw, d | | 929 m | 1455 w, d | | 1458 w | |
| Species $a_u$ | | | $\nu(CH_3)$ | | | |
| ~(390) not observed | | | 2928 s | p | 2931 s | |
| | | 956 w? | $CH_3$ rocking | | | |
| | | | 1178 w | | 1181 w | |

[a] See reference 9.

mental involving symmetric methyl deformation, in accord with the fact that Pitzer and Scott[11] have found this type of vibration to have a wave number very close to 1380 $cm^{-1}$ in several methyl-substituted benzenes. They find unsymmetrical methyl deformations to lie close to 1450 $cm^{-1}$ for all such compounds, the two components being generally unresolved. Accordingly, the weak depolarized Raman band and the weak infrared band at 1455 $cm^{-1}$ are interpreted as the two fundamentals involving largely this type of motion.

The strong polarized Raman band at 2928 $cm^{-1}$ and the strong infrared band at 2931 $cm^{-1}$ are interpreted as the three fundamentals associated with CH stretching in the methyl group. Such vibrations have been found to lie in this region and to be generally unresolved.[11]

The frequencies to be assigned to the two fundamentals involving rocking of the whole methyl group are uncertain. The weak infrared and Raman bands near 1180 $cm^{-1}$ may represent one of these fundamentals. No evidence is found for the frequency of the vibration involving methyl torsion which would be essentially inactive.

## DISCUSSION

The assumption of (approximate) $V_h$ symmetry appears quite adequate for the interpretation of the main features of the observed spectra. The fundamental vibration frequencies for the liquid state are listed in Table III. The 74 infrared absorption maxima and the 44 Raman shifts observed for the liquid state are all satisfactorily interpreted as fundamentals or as binary sum bands in Table I. Many bands can be interpreted in several ways due to the large number of coincidences.

The assigned fundamentals of *p*-fluorotoluene are compared to those of *p*-difluorobenzene and *p*-xylene in Table II. The close correlation of the fundamentals of these three molecules is remarkable.

The greatest uncertainty is the frequency of the unobserved $CH_3$ torsional vibration which is expected to lie in the neighborhood of 200 $cm^{-1}$. The frequencies of the unobserved $CH_3$ rocking vibration, the $b_{1g}$ fundamental vibration, the lowest $a_u$ fundamental and the uncertain highest $a_u$ fundamental can be estimated within rather narrow limits. Some uncertainty exists in the species assignment. Thus, the two highest fundamentals assigned to species $b_{1u}$ and $b_{2u}$ may be interchanged.

## ACKNOWLEDGMENT

The writers wish to acknowledge their indebtedness to Dr. G. C. Finger for the gift of the sample.

# The Microwave Spectrum of Phosgene*

G. WILSE ROBINSON†
*Department of Chemistry and Chemical Engineering, State University of Iowa, Iowa City, Iowa*
(Received June 30, 1953)

The microwave spectra of $C^{12}O^{16}Cl^{35}Cl^{35}$ and $C^{12}O^{16}Cl^{35}Cl^{37}$ have been investigated in the region 23 000–28 000 Mc/sec. The analyses of the rotational spectra yield for the phosgene molecule: C–O distance = 1.166 ±0.002A; C–Cl distance = 1.746±0.004A; and Cl–C–Cl angle = 111.3±0.1°. An analysis of the quadrupole hyperfine structure was made for both isotopic species and the quadrupole coupling constants were obtained for $C^{12}O^{16}Cl^{35}Cl^{35}$. An attempt is made to explain the large observed value of the field dyadic asymmetry parameter $\eta$.

## INTRODUCTION

THE investigation of microwave spectra of molecules containing more than one nucleus with quadrupole moment has been limited almost entirely to linear or symmetric top molecules. Furthermore, in only one instance[1] has the quadrupole hyperfine structure been analyzed for a molecule containing two identical quadrupole nuclei. Since certain quantities derived from the interaction of the nuclear quadrupole moments with rotational angular momentum are so closely related to chemical bonding,[2,3] it is important that such molecules be given adequate attention. To this end a previous paper[4] dealt with numerical calculations necessary for the analysis of the quadrupole hyperfine structure of molecules containing two nuclei having spin $\frac{3}{2}$. The present paper uses the results of the first to study the microwave spectra of two isotopic modifications of phosgene, $C^{12}O^{16}Cl^{35}Cl^{35}$ and $C^{12}O^{16}Cl^{35}Cl^{37}$.

## EXPERIMENTAL

The phosgene was prepared by direct combination of carbon monoxide and excess chlorine in the presence of heat and light. Powdered charcoal was used as a catalyst and the excess chlorine was removed with powdered antimony. The crude phosgene was collected at dry ice temperature and was purified in vacuum by three distillations to liquid nitrogen, only the middle fraction being retained in each stage. One-half cubic centimeter of liquid phosgene proved a more than ample supply for the entire experiment.

The spectrograph used for this work is essentially modeled after the one described by McAfee, Hughes, and Wilson,[5] the details being somewhat different. The Stark modulation was obtained by means of a square-wave generator built at the State University of Iowa. This unit had a continuous amplitude range from 0–1000 volts. The source of the microwave energy was a set of Raytheon klystron oscillators which, with some adjustment, would cover the range 23 000 to 28 000 Mc/sec.

The absorption cell consisted of twelve feet of copper *K*-band wave guide, vacuum sealed at each end by means of mica held in place with bee's wax. Since most of the measurements were made at dry ice temperature, the components of the absorption cell had to be strong and yet flexible to withstand thermal expansion and contraction of parts. Inside the wave guide, a steel connecting lead for the Stark voltage was insulated from the absorption cell by means of heavy glass beads and silver soldered to the edge of the Stark electrode. To facilitate repairs this lead was introduced through a Stupekoff type Kovar fitting soldered into the face of a brass disk which in turn was vacuum-sealed to the absorption cell by means of a Linear "O-ring." The Stark electrode was insulated from the walls of the wave guide with grooved Kel-F tape.

Both oscilloscope and recorder techniques were used to obtain the phosgene spectrum. In each case, after passing through the wave guide, the microwave energy was rectified by a 1N26 crystal detector. For oscilloscope work the output of this crystal was amplified and placed on the vertical plates of an oscilloscope. Since the sensitivity of this scheme proved far too low at the low gas pressure and low crystal current necessary for adequate resolution of the many closely spaced spectral lines, this method was abandoned except for exploratory work or for the study of the stronger lines in the spectrum.

Very much higher sensitivity may be secured by using a recorder technique since very narrow band widths may be employed. The output of the 1N26 crystal, after being amplified and fed through a phase-sensitive detector, is used to drive an Esterline-Angus 0–1-ma recording milliammeter. The phase-sensitive detector distinguishes the zero-field absorption lines from their Stark components. Mechanical frequency drive for the klystron was obtained from a synchronous 4-rph motor geared down to half-speed so that on an average about

* This paper is based in part on a thesis submitted by G. Wilse Robinson in partial fulfillment of the requirements for the degree Doctor of Philosophy at the State University of Iowa, Iowa City, Iowa. The work was made possible by the support extended to the State University of Iowa by the U. S. Office of Naval Research under contract N8-onr-79400.

† Present address: Department of Chemistry, University of Rochester, Rochester, New York.

[1] R. J. Myers and W. D. Gwinn, J. Chem. Phys. **20**, 1420 (1952).
[2] C. H. Townes and B. P. Dailey, J. Chem. Phys. **17**, 782 (1949).
[3] C. H. Townes and B. P. Dailey, J. Chem. Phys. **20**, 35 (1952).
[4] G. Wilse Robinson and C. D. Cornwell, J. Chem. Phys. **21**, 1436 (1953).
[5] McAfee, Hughes, and Wilson, Rev. Sci. Instr. **20**, 821 (1949).

TABLE I. Rotational parameters and coupling constants of $C^{12}O^{16}Cl^{35}Cl^{35}$ and $C^{12}O^{16}Cl^{35}Cl^{37}$.

| | $C^{12}O^{16}Cl^{35}Cl^{35}$ | | $C^{12}O^{16}Cl^{35}Cl^{37}$ | |
|---|---|---|---|---|
| $(a-c)/2$ | 2.75325 | ±0.00002 kMc/sec | 2.75314 | ±0.00002 kMc/sec |
| $(a+c)/2$ | 5.16550 | ±0.00002 | 5.11462 | ±0.00004 |
| $\kappa$ | −0.61401 | ±0.00002 | −0.63007 | ±0.00002 |
| $I_a$[a] | 63.8249 | ±0.0005 amu-A² | 64.2385 | ±0.0007 amu-A² |
| $I_b$[a] | 145.443 | ±0.003 | 149.533 | ±0.004 |
| $I_c$[a] | 209.519 | ±0.004 | 214.024 | ±0.006 |
| $I_c-I_b-I_a$ | 0.251 | ±0.008 | 0.253 | ±0.011 |
| $eQV_{aa}$ | −37.20 | ±0.05 Mc/sec | | b |
| $eQV_{bb}$ | 10.13 | ±0.05 | | b |
| $eQV_{cc}$ | 27.07 | ±0.10 | 24.20 | ±0.10 |

[a] The moments of inertia were obtained from the reciprocals of $a$, $b$, and $c$ multiplied by the constant 505.413.
[b] $eQV_{aa}$ and $eQV_{bb}$ for $C^{12}O^{16}Cl^{35}Cl^{37}$ are $\vartheta$ dependent and, therefore, cannot be included in the table.

one-half to one Mc/sec of frequency was swept over every second. For rapid scanning of an extended frequency range a faster motor was employed.

Using the above techniques, low gas pressures, and low crystal current, it was possible in many instances at least partially to resolve pairs of absorption lines two- or three-tenths of a Mc/sec apart. Further work on molecules containing two chlorine nuclei should probably not be attempted unless a resolving power at least this good can be attained.

Frequency measurements were made by use of interpolation receivers in conjunction with a harmonic generator whose fundamental frequency of five Mc/sec was tuned to WWV. For oscilloscope work, a single interpolation receiver was tuned so that a frequency marker on the screen was brought directly upon the absorption line to be measured. For recorder work, two interpolation receivers were set so that a marker was introduced on the trace every 1.25 Mc/sec. In the latter case, the frequency of an absorption line was found by linear interpolation between adjacent markers. Nonlinearity and "backlash" in the klystron as well as erratic frequency drifts could not be completely avoided, so errors increase as the frequency separation of the markers increases. Some error is also introduced because of the varied width of the markers and the inability of the electronic circuit to compensate for this. An idea of the errors involved may be obtained from the fact that the recorder frequencies did not agree with the oscilloscope frequencies to as much as one-tenth of a Mc/sec in some cases. To obtain a continuous set of good markers over a range of even a few Mc/sec was very difficult since unfortunately the power output of the harmonic generator was low. Spurious markers from external disturbances were frequent, because, in order to record weak markers, the gain of the interpolation receivers had to be high. This fact made it necessary to carefully watch a recording so that the spurious markers could be deleted as they occurred. Many weak markers could never be obtained and for this reason some of the absorption lines were not measured with the normal accuracy of the instrument. Also, a few of the weaker transitions at the higher frequencies (e.g., $1_{11}-2_{20}$), although observed on the traces, could not be analyzed because of poor or missing markers. For rapid exploratory work or to identify markers, a single set of markers could be introduced every 30, 90, or 270 Mc/sec as desired.

## THE PHOSGENE SPECTRUM

The phosgene molecule is an asymmetric rotor whose dipole moment lies along or very near to the intermediate axis of inertia. From naturally occuring chlorine it is primarily an isotopic mixture of $C^{12}O^{16}Cl^{35}Cl^{35}$, $C^{12}O^{16}Cl^{35}Cl^{37}$, and $C^{12}O^{16}Cl^{37}Cl^{37}$ in the approximate ratio of 9:6:1. These isotopic modifications will hereinafter be referred to as 35,35, 35,37, and 37,37, respectively. The microwave spectrum at room temperature is composed of the nuclear electric quadrupole components of rotational transitions in the low-lying vibrational states[6] of all three isotopic modifications. To simplify this spectrum to a point where an analysis was possible, all data were recorded at dry ice temperature. The intensities of the low-$J$ rotational transitions in the ground vibrational state are thus increased at the expense of transitions originating in the higher levels.

TABLE II. The structural parameters of phosgene.

| | Microwave | Electron diffraction[a] |
|---|---|---|
| C−O | 1.166±0.002A | 1.18±0.03A |
| Cl−O | 2.589±0.001 | 2.59±0.03 |
| Cl−Cl | 2.884±0.001 | 2.90±0.04 |
| C−Cl | 1.746±0.004 | 1.74±0.02 |
| ∠Cl−C−Cl | 111.3 ±0.1° | 112.5 ±1.5° |

[a] See reference 7.

Furthermore, at this low temperature, resolution is significantly increased because of decreased line breadth.

In a molecule such as phosgene, where the asymmetry is large, the electron diffraction structure at best can only be relied upon to predict rotational frequencies to within a thousand Mc/sec or so. The existing electron diffraction data[7] along with probable errors, however, were helpful as a means of obtaining an idea of which rotational transitions might be expected to lie in the region of interest.

Also the electron diffraction Cl−C−Cl angle was useful as a means of obtaining approximate values of the quadrupole coupling constants $eQV_{aa}$ and $eQV_{bb}$. For this calculation it was assumed that the electronic field is cylindrically symmetric with respect to the C−Cl internuclear axes and that the bonding of the chlorine atoms is similar to that in methyl chloride for which the coupling constant is known.[8] From the approximate values of the coupling constants, a rough idea of $X^{+9}$ for

[6] Nielsen, Burke, Woltz, and Jones, J. Chem. Phys. **20**, 596 (1952).
[7] P. W. Allen and L. E. Sutton, Acta Cryst. **3**, Part I, 46 (1950). This is a review of electron diffraction work prior to 1950.
[8] Gordy, Simmons, and Smith, Phys. Rev. **74**, 243 (1948).
[9] See reference 4 for definition of symbols.

all rotational levels of interest was obtained. The approximate hyperfine structure was then computed using the results of reference 4, and the patterns were used to identify rotational transitions in the spectrum. Initially, however, no attempt was made to use this procedure with $P$ and $R$ transitions since, in these cases, the hyperfine patterns are far too sensitive to errors in coupling constants and structure.

An examination of recordings made at rapid sweep revealed a large number of what seemed to be the expected types of patterns; that is, the unsymmetrical groups and the symmetrical triplets.[4] One symmetrical triplet was discovered for which the splitting was large enough to belong to a low-$J$ $Q$ transition. The uncertainty in the electron diffraction structure made it impossible to decide upon one of a number of possible assignments for this group, but, with the help of approximate isotopic shift calculations and the approximate fine structure patterns for 35,37, the analogous transition for 35,37 was eventually found and identified as $3_{22}-3_{31}$. The assignment of one $Q$ transition fixes $a-c$ as a function of $\kappa$, and the $Q$-branch assignment was readily completed for the two most abundant isotopic modifications. An assignment was not attempted of the weak 37,37 spectrum for lack of an isotopically enriched sample.

The $Q$ branch assignment yielded accurate values of $a-c$, $\kappa$ and the quadrupole coupling constants. Furthermore, to a first approximation the phosgene molecule is planar and $a+c$ can be written as a function of $a-c$ and $\kappa$. The $P$ and $R$ transitions were found on this basis when some revision was allowed because of possible "aplanarity." In both isotopic modifications studied, $I_c-I_a-I_b$ turned out to be about 0.25 amu-A$^2$ corresponding to a frequency shift of about $3.3(J+1)$ Mc/sec.

## DISCUSSION OF DATA

Table I lists the values of the rotational parameters and coupling constants obtained from the study while the structural parameters are compared with the recent electron diffraction work of Schomaker[7] in Table II. Since there are three independent structural parameters, a complete structural determination involves the use of data from at least two isotopic species. Accordingly the bond angles and distances were obtained from a best fit of nine $J\leqslant 5$ transitions belonging to 35,35 and eight $J\leqslant 5$ transitions belonging to 35,37. Since only a limited number of higher $J$ transitions were studied, no attempt was made to apply a centrifugal distortion correction to the results. Thus the structure can be thought of as an average over $J\leqslant 5$ and the limits of error are given with this fact in mind. It is seen that the structure is essentially equivalent to that obtained from the electron diffraction study.

In Table III are listed observed and calculated frequencies for all $J\leqslant 10$ rotational transitions studied. The *calculated frequencies* were computed by the method

TABLE III. Observed *vs* calculated rotational frequencies for phosgene.

| Rotational transition | $C^{12}O^{16}Cl^{35}Cl^{35}$ Obs[a] Mc/sec | $C^{12}O^{16}Cl^{35}Cl^{35}$ Calc Mc/sec | $C^{12}O^{16}Cl^{35}Cl^{37}$ Obs[a] Mc/sec | $C^{12}O^{16}Cl^{35}Cl^{37}$ Calc Mc/sec |
|---|---|---|---|---|
| $1_{10}-2_{21}$ | 26 168.72 | 26 168.49 | 25 964.8 | 25 964.8 |
| $3_{03}-4_{14}$ | 23 637.1 | 23 637.2 | 23 261.0 | 23 261.0 |
| $4_{04}-5_{15}$ | 27 764.0 | 27 764.3 | 27 285.5 | 27 285.8 |
| $4_{14}-5_{05}$ | 25 304.87 | 25 305.46 | 24 653.6 | 24 654.7 |
| $6_{34}-7_{25}$ | 25 719.8 | 25 719.5 | 24 132.7 | 24 132.3 |
| $3_{22}-3_{31}$ | 24 973.78 | 24 973.91 | 25 075.68 | 25 075.44 |
| $3_{21}-3_{30}$ | 24 173.32 | 24 173.25 | 24 340.3 | 24 340.0 |
| $4_{22}-4_{31}$ | 23 218.36 | 23 218.13 | 23 449.9 | 23 449.6 |
| $4_{23}-4_{32}$ | 25 398.70 | 25 398.64 | 25 466.8 | 25 465.7 |
| $5_{15}-5_{24}$ | 23 364.80 | 23 364.46 | 23 066.28 | 23 065.93 |
| $5_{24}-5_{33}$ | 26 196.98 | 26 197.12 | 26 201.9 | 26 202.1 |
| $6_{16}-6_{25}$ | 26 765.1 | 26 764.9 | 26 328.5 | 26 327.9 |
| $6_{25}-6_{34}$ | 27 476.1 | 27 476.4 | 27 387.0 | 27 387.8 |
| $7_{07}-7_{16}$ | | | 26 146.5 | 26 145.3 |
| $9_{18}-9_{27}$ | 26 375.1 | 26 376.6 | 25 297.0 | 25 299 |
| $9_{36}-9_{45}$ | 27 977.6 | 27 976.1 | | |
| $10_{37}-10_{46}$ | 25 998.02 | 25 997.5 | 26 557.5 | 26 557 |

[a] The limits of error are indicated by the number of significant figures carried—seven significant figures, ±0.1 Mc/sec; six significant figures, ±0.3 Mc/sec.

of continued fractions.[10] The effect of centrifugal distortion on some higher-$J$ transitions is noticeable.

The quadrupole coupling constants belonging to 35,35 were obtained from a least-squares fit of the prominent components of the $1_{10}-2_{21}$ group. These values reproduce the quadrupole hyperfine structure within experimental error of the majority of the 35,35 transitions studied. The observed and calculated hyperfine splittings for a few of the transitions are listed in Table IV. It is interesting to note the presence of some components belonging to the $1_{10}-2_{21}$ transition for which $\Delta\epsilon=\pm 2$.§

In the case of 35,37 nuclear quadrupole energy levels are functions not only of $eQV_{aa}$ and $eQV_{bb}$ for both chlorine nuclei, but also of the rotationally dependent quantity $R$.[9] Actually in the case of a planar molecule it can be seen[11] that to a very good approximation only one other parameter besides those already determined from other sources define $R$ and $X^+$ and, therefore, the nuclear quadrupole energy levels. This parameter $\vartheta$ is the angle between the principal axis system of the field dyadic and its respective C−Cl internuclear axis system. The above statement follows if the assumptions are made that, (a) the electronic charge distribution forming the C−Cl$^{35}$ bonds in 35,35 as well as the ones forming the C−Cl$^{35}$ and C−Cl$^{37}$ bonds in 35,37 are all equivalent; and (b) the ratio $Q^{37}/Q^{35}$ of the quadrupole moments is the same in phosgene as in other chlorine containing compounds.[12] Both of these assumptions should be valid to a high degree of accuracy and should enable one to obtain

[10] King, Hainer, and Cross, J. Chem. Phys. **11**, 27 (1943).

§ $\epsilon$ is the pseudospin quantum number referred to in reference 4. It has been implied previously (see reference 1) that these transition probabilities are zero.

[11] C. D. Cornwell (private discussion).

[12] R. Livingston, Phys. Rev. **82**, 289 (1951).

TABLE IV. Observed *vs* calculated quadrupole hyperfine structure patterns for phosgene.

| $\epsilon$ $F$ | $\epsilon'$ $F'$[a] | $I$[b] | Obs[c] Mc/sec | Calc[d] |
|---|---|---|---|---|
| | | $1_{10}-2_{21}$ (35,35) | | |
| 3 3 | 1 3 | 5 | −10.70 | −10.78 |
| 3 3 | 3 2 | 3 | −8.0 | −8.13 |
| 3 2 | 1 3 | 6 | −6.99 | −7.12 |
| 1 1 | 1 2 | 8 | −5.48 | −5.22 |
| 3 2 | 3 2 | 5 | −4.62 | −4.46 |
| 1 0 | 1 1 | 5 | −3.2 | −3.19 |
| 1 2 | 3 1 | 7 | | −3.09 |
| 3 4 | 3 5 | 33 | −2.77 | −2.62 |
| 1 2 | 1 2 | 6 | −1.00 | −0.76 |
| 3 3 | 3 4 | 17 | −0.22 | −0.16 |
| 3 3 | 3 3 | 9 | +2.38 | +2.50 |
| 1 1 | 3 2 | 3 | +5.4 | +5.41 |
| 3 2 | 3 3 | 12 | +6.09 | +6.17 |
| 1 2 | 1 3 | 9 | +7.38 | +7.21 |
| 1 2 | 3 2 | 3 | +9.9 | +9.86 |
| 3 4 | 3 4 | 11 | +10.72 | +10.67 |
| | | $3_{22}-3_{21}$ (35,35) | | |
| 2 3 | 2 3 | 8 | −12.30 | −12.09 |
| 2 5 | 2 5 | 15 | 0 | 0 |
| 2 4 | 2 4 | 9 | | 0 |
| 2 2 | 2 2 | 4 | | 0 |
| 2 1 | 2 1 | 3 | | 0 |
| 0 3 | 0 3 | 8 | +12.05 | +12.09 |
| | | $3_{21}-3_{30}$ (35,35) | | |
| 3 1 | 3 2 | 3 | −13.7 | −13.73 |
| 1 3 | 1 3 | 8 | −11.90 | −11.53 |
| 3 2 | 3 3 | 3 | −7.50 | −7.66 |
| 3 6 | 3 6 | 18 | | −7.36 |
| 3 2 | 3 1 | 3 | −6.4 | −6.48 |
| 1 4 | 1 4 | 11 | −1.62 | −1.62 |
| 3 3 | 3 4 | 3 | +5.43 | +5.15 |
| 3 3 | 3 3 | 3 | | +5.64 |
| 3 3 | 3 2 | 3 | +6.6 | +6.42 |
| 3 5 | 3 5 | 11 | +7.31 | +7.36 |
| 1 2 | 1 2 | 7 | +7.96 | +7.98 |
| 3 4 | 3 4 | 8 | +13.33 | +13.39 |
| | | $1_{10}-2_{21}$ (35,37) | | |
| 3 2 | 1 3 | 2 | ··· | −6.61 |
| 1 1 | 1 2 | 3 | ··· | −5.66 |
| 1 2 | 3 1 | 3 | −2.7 | −2.96 |
| 3 4 | 3 5 | 11 | −2.3 | −2.36 |
| 2 3 | 2 4 | 9 | −0.16 | −0.18 |
| 2 3 | 2 3 | 3 | +0.10 | +0.05 |
| 3 3 | 3 4 | 6 | | +0.09 |
| 2 2 | 2 3 | 5 | | +0.11 |
| 0 1 | 0 2 | 3 | +1.24 | +1.36 |
| 3 3 | 3 3 | 3 | +2.2 | +2.33 |
| 3 2 | 3 3 | 4 | +5.5 | +5.50 |
| 1 2 | 1 3 | 3 | ··· | +6.40 |
| 3 4 | 3 4 | 4 | ··· | +9.89 |
| | | $3_{22}-3_{21}$ (35,37) | | |
| 1 3 | 1 3 | 3 | −11.92 | −11.81 |
| 2 3 | 2 3 | 3 | −11.0 | −10.12 |
| 3 6 | 3 6 | 6 | −7.02 | −7.02 |
| 1 4 | 1 4 | 4 | −2.00 | −2.03 |
| 2 5 | 2 5 | 5 | −0.47 | −0.38 |
| 2 4 | 2 4 | 3 | | +0.46 |
| 3 3 | 3 3 | 1 | +5.0 | +5.32 |
| 3 5 | 3 5 | 4 | +6.70 | +7.40 |
| 0 3 | 0 3 | 3 | +10.25 | +10.99 |
| 3 4 | 3 4 | 3 | +12.45 | +12.81 |
| | | $4_{23}-4_{32}$ (35,35) | | |
| 1 4 | 1 4 | 13 | −7.46 | −7.40 |
| 3 7 | 3 7 | 30 | −5.35 | −5.27 |
| 3 3 | 3 3 | 6 | −2.22 | −2.23 |
| 1 5 | 1 5 | 19 | −0.72 | −0.68 |
| 3 6 | 3 6 | 19 | +3.97 | +3.95 |
| 3 4 | 3 4 | 8 | +5.20 | +5.15 |
| 1 3 | 1 3 | 11 | | +5.24 |
| 3 5 | 3 5 | 13 | +8.83 | +8.76 |
| | | $5_{15}-5_{24}$ (35,35) | | |
| 2 5 | 2 5 | 17 | −5.18 | −5.11 |
| 2 7 | 2 7 | 25 | 0 | 0 |
| 2 6 | 2 6 | 19 | | 0 |
| 2 4 | 2 4 | 13 | | 0 |
| 2 3 | 2 3 | 11 | | 0 |
| 0 5 | 0 5 | 17 | +5.13 | +5.11 |

[a] The primes indicate the final state.
[b] $I$ is a theoretical relative intensity of the line inclusive of rotational and isotopic abundance parts but not of the Boltzmann factor. The lower limit of observation was $I\sim3$.
[c] The frequencies refer to the distance from the rotational center of the group. Weak lines not observed are omitted while the stronger lines not observed because of interference are indicated by a dots.
[d] Calculated from $eQV_{aa}$ and $eQV_{bb}$ in Table I. For 35,37 $\vartheta$ was assumed to be zero. Bracketed frequencies indicate a group of unresolved lines.

much of the quadrupole coupling information about 35,37 from 35,35 for which relatively accurate data were obtained.

According to assumption (a), $\vartheta$ would be the same for all C−Cl bonds in phosgene and can be determined if the cross derivatives of the field dyadic along any given axis are known. Thus far no information of this type exists. However, if it were possible to measure the quadrupole coupling constants $eQV_{aa}$ and $eQV_{bb}$ under a rotation of the axis system, then $\vartheta$ could be determined. Although rather small in most molecules, it was thought that the effect in phosgene would be measurable because of the relatively large rotation ($\sim1°$) of the *abc* principal inertial axis system in 35,37. Unfortunately, no transition was found in which $R$ changed enough to permit this determination. It was found that to produce a 0.2-Mc/sec shift in the energy levels, $R^2$ had to vary about 100 percent. Table V assumes different reasonable values of $\vartheta$ as determined by the resulting values of $eQ^{35}V_{zz}$ and gives the variation of $X^+$ and $R^2$ for the $2_{21}$ level of 35,37. Here $z$ is that principal axis of the field dyadic which most nearly coincides with the C−Cl internuclear axis. It can be seen that there is little variation of $X^+$ $(2_{21})$ for a 2° variation of $\vartheta$. This is typical since changes in contributions from $eQV_{aa}$ and $eQV_{bb}$ approximately cancel for small $\vartheta$. Also the variation of $R^2$ $(2_{21})$ is seen to be so small that an evaluation of $\vartheta$ would lie outside the scope of our spectrograph. Since the energy levels are so insensitive to $\vartheta$ and for lack of a better value, the calculated hyperfine structure of 35,37 in Table IV was computed on the assumption that $\vartheta=0$. Obviously this is not equivalent to the assumption that the energy levels for 35,37 differ from those for 35,35 only by the scale factor $Q^{35}+Q^{37}/2Q^{35}$ (i.e., $R=0$), and rather large errors may be introduced in some low-$J$ cases if this assumption is made. It might be noticed in Table IV that in the case of the two isotopic $3_{22}-3_{31}$ transitions, the quadrupole satellites are shifted noticeably from the calculated frequencies. This deviation is probably due to a second-order quadrupole effect caused by the near degeneracy of the $3_{31}$ and $3_{30}$ rotational levels. To some extent deviations were also found in the $3_{21}-3_{30}$ and $5_{24}-5_{33}$ transitions. Data concerning this fact are so meager and relatively rough that it does not warrant a determination of $eQV_{ab}$ at this time.

TABLE V. The effect of variations of $\vartheta$ on some nuclear quadrupole coupling parameters.

| $\vartheta$ | $eQ^{35}V_{zz}$[a] | $\eta$ | $X^+(2_{21})$[a] | $R^2(2_{21})$ |
|---|---|---|---|---|
| +4° | −61.89 | 0.125 | −9.54 | 0.022 |
| +3° | −65.12 | 0.169 | −9.55 | 0.024 |
| +2° | −68.91 | 0.214 | −9.55 | 0.026 |
| +1° | −73.37 | 0.262 | −9.56 | 0.028 |
| 0° | −78.68 | 0.312 | −9.56 | 0.030 |
| −1° | −85.14 | 0.364 | −9.57 | 0.032 |
| −2° | −93.11 | 0.419 | −9.58 | 0.034 |

[a] Mc/sec.

It is also interesting to note from Table V the large variation of $eQ^{35}V_{zz}$ with $\vartheta$. Since there is no reason to believe that $z$ coincides with the internuclear axis in a molecule except in special cases because of symmetry, values of $eQV_{zz}$ obtained for molecules without a knowledge of $\vartheta$ must be looked upon with caution. Conversely, since $eQV_{zz}$ is so sensitive to changes in $\vartheta$, it would be possible to arrive at a good value of $\vartheta$ from even a rather crude theoretically determined value of $eQV_{zz}$.

Perhaps the most striking piece of information gained from the work is the large value of the dyadic asymmetry parameter $\eta$,[3] where

$$\eta=\left|\frac{eQV_{xx}-eQV_{yy}}{eQV_{zz}}\right|.$$

Since this quantity is $\vartheta$ dependent, it has been included in Table V where an idea of its magnitude can be

obtained. Townes and Dailey[3] attribute the rather large value of $\eta$ (0.15) in solid $I_2$ to a contribution from two weaker covalent bonds in the crystal lattice. In the case of phosgene, $\eta$ seems certainly as large as in solid $I_2$ depending upon $\vartheta$, but here the effect cannot be attributed to intermolecular bonding. To account for $eQV_{xx}>eQV_{yy}$, where $y$ is perpendicular to the plane of the molecule, the electronic distribution, instead of being cylindrically symmetric about the $z$ axis, must extend to a greater degree out of the plane of the molecule. This phenomenon might be due to one or more of the following effects: (a) a considerable amount of $\pi$-type (double) bonding in the C—Cl bond; (b) a distortion of the closed shells of each chlorine atom; and (c) a distortion of the charge distribution of the C—Cl bonds, presumably by mutual repulsion. Of these, perhaps the first is the most important. Besides the three trigonal ($sp^2$) bonding orbitals of carbon, there exists a $2p\pi$ orbital perpendicular to the plane of the molecule. Overlap of this orbital with the $3p\pi$ orbital of chlorine would form a bond with the required characteristics. Because of the rather large electronegativity of chlorine, evidently enough of the charge distribution is sufficiently near to the chlorine nucleus to give the large observed effect. The observed bond angle of 111.3° being much smaller than the theoretical 120° trigonal angle should not affect these qualitative arguments. If the contribution of the $\pi$ bond to the dyadic is added to that of the $sp^2\sigma$ bond, $|(eQV_{zz})_{\text{obs}}|$ should be smaller than if only the pure $\sigma$ bond were considered. For example, roughly assuming cylindrical symmetry of the $\pi$ bond along the $y$ axis and of the $\sigma$ bond along the $z$ axis, a value of, say, −75.13 Mc/sec for $(eQ^{35}V_{zz})\sigma$ requires that $(eQ^{35}V_{zz})_{\text{obs}}=-69.88$ Mc/sec. If the rather crude postulate were now made that the $\sigma$ bond contributes to the components of the dyadic an amount equivalent to $eQ^{35}V_{zz}$ for the $sp^3$ hybrid bond in methyl chloride ($eQ^{35}V_{zz}=-75.13$ Mc/sec),[8] then, barring other contributions, $(eQ^{35}V_{zz})_{\text{obs}}\sim-69.88$ Mc/sec for for phosgene. This would correspond to a value of $\vartheta$ slightly less than +2°.

The $\pi$-bonding effect should not be present in tetrahedral molecules such as methyl chloride and methylene chloride, or in digonal ($sp$) molecules such as cyanogen chloride because of the absence of a lone carbon $2p\pi$ orbital. In the former case the superposition of the two mutually perpendicular $3p\pi$ orbitals of chlorine leads to cylindrical symmetry about the bond axis. In the latter case, two mutually perpendicular $\pi$ bonds are formed and the cylindrical symmetry about the bond axis also is preserved. $\eta$ would be expected to be zero in each instance. The amount of $\pi$ bonding as well as the value of $eQV_{zz}$, however, depends on so many different variables that any of these arguments can be only very qualitative. For example, the fact that $\pi$ bonding is not present in methyl chloride or methylene chloride might be experimentally established by their comparatively high values of $eQ^{35}V_{yy}$, ∼37.7 Mc/sec[8] and 39.2 Mc/sec[1], respectively. Compared with these, $eQ^{35}V_{yy}$ for phosgene is strikingly small. The C—Cl internuclear distances in these molecules (1.78A and 1.77A, respectively) are also larger than in phosgene. On the other hand, in cyanogen chloride[13,14] ($sp$ hybridization) the C—Cl distance is 1.62A while $eQ^{35}V_{yy}=41.6$ Mc/sec. It might be that here the $sp$ orbitals penetrate towards the chlorine nucleus to a greater extent than they do in $sp^3$ and $sp^2$ hybridization. Since the magnitudes of the components of the dyadic are dependent on $1/r^3$, this could account partially for the large observed values of $eQV_{zz}$, $eQV_{yy}$, and $|eQV_{zz}|$ in $sp$-type molecules.[15] A study of vinyl chloride,[16] for which $\pi$ contributions also would be expected, yielded 31.2 Mc/sec for $eQV_{yy}$. This is comparable to the phosgene value. The asymmetry parameter $\eta$, however, does not appear to be nearly as large in this molecule, while the C—Cl internuclear distance (1.70A) is much smaller.

Effects (b) and (c) above would be enhanced by an accumulation of charge in the C—Cl bond. A distortion to any great extent of the closed shells could be indicated by a low value of $|eQV_{zz}|$ and $eQV_{yy}$. A distortion of the bonds, on the other hand, might also yield a low value of $eQV_{yy}$, assuming the charge distribution is pushed out of the plane of the molecule. Without an accurately determined value of $eQV_{zz}$, however, an evaluation of any of these effects cannot be made with too much confidence. But it would seem that the mutual repulsion of the bonds is not large considering the long range over which the forces must act. A distortion of the closed shells could contribute a large amount to the dyadic if enough charge accumulated near the chlorine atom. Townes and Dailey[2,3] however, have stated that such effects might be expected to be secondary.

I wish to express my appreciation of the interest and assistance of Professor George Glockler, director of the microwave project at the State University of Iowa. I also wish to thank Dr. C. D. Cornwell for many valuable discussions and for his tireless labors with the spectrograph. Without this help the problem could not have been solved. The technical assistance of Mr. Jack Althouse and Mr. Randolph Phillips is also greatly appreciated.

[13] Smith, Ring, Smith, and Gordy, Phys. Rev. **74**, 370 (1948).
[14] Townes, Holden, and Merritt, Phys. Rev. **74**, 1113 (1948).
[15] See also Westenberg, Goldstein, and Wilson, Phys. Rev. **76**, 472 (1949), where $eQ^{35}V_{zz}=-79.67$ Mc/sec and C—Cl = 1.63A for chloroacetylene.
[16] J. H. Goldstein and J. K. Bragg, Phys. Rev. **75**, 1453 (1949).

# Investigation of Pyrolyses of Benzyl Benzoate, Acetate, and Formate

M. SZWARC, *State University of New York, College of Forestry, Syracuse, New York*

AND

J. WATSON TAYLOR, *Chemistry Department, The University, Manchester, England*

(Received May 22, 1953)

The pyrolysis of benzyl benzoate, benzyl acetate, and benzyl formate has been studied by means of "toluene carrier gas" technique. It has been shown that benzyl-benzoate decomposes according to the equation

$$Ph\cdot CH_2\cdot O\cdot CO\cdot Ph \rightarrow Ph\cdot CH_2\cdot + Ph\cdot COO.$$

The $Ph\cdot CH_2-O\cdot CO\cdot Ph$ bond dissociation energies have been estimated as less than 69 kcal/mole. Decompositions of benzyl acetate and of benzyl formate are more complicated; the dissociation into radicals is accompanied by some decompositions into smaller molecules.

Our data enable us to determine the relative rates of reactions,

$$Ph\cdot + C_6H_5\cdot CH_3 \rightarrow Ph\cdot H + C_6H_5\cdot CH_2\cdot$$

and

$$Ph\cdot + C_6H_5\cdot CH_2\cdot O\cdot CO\cdot C_6H_5 \rightarrow Ph\cdot H_4 + C_6H_5\cdot CH\cdot O\cdot CO\cdot C_6H_5\cdot.$$

the latter reaction appears to be twice as rapid the former.

IN this communication we report the results of our studies of pyrolyses of benzyl-benzoate, benzyl-acetate, and benzyl-formate. Our intention was to determine the

$$Ph\cdot CH_2-O\cdot CO\cdot X$$

bond dissociation energies (X stands for H, $CH_3$, or Ph) and thus to pave the way for calculation of heats of formation of benzoate, acetate, and formate radicals. We investigated these decompositions by using the "toluene carrier gas" technique, which has been shown to be useful for such studies.[1] The method uses a flow system in which the compound investigated is decomposed in the presence of an excess of toluene. The latter reacts with radicals produced in primary reactions, and consequently inhibits chain decompositions. Moreover, the reaction between these radicals and toluene yields benzyl radicals, and the formation of the latter can be inferred from the presence of dibenzyl amongst the reaction products. Hence, the detection of dibenzyl in the products of pyrolysis is indicative of the decomposition of the compound investigated into radicals.

TABLE I.[a]

| Run | T°K | Benzyl benzoate $CO_2$ / $Ph\cdot COO\cdot CH_2\cdot Ph$ | Dibenzyl / $CO_2$ |
|---|---|---|---|
| 10 | 935 | 0.322 | 0.97 |
| 9 | 947 | 0.448 | 0.91 |
| 14 | 960 | 0.293 | 1.16 |
| 13 | 964 | 0.323 | 0.99 |
| 17 | 970 | 0.423 | 0.96 |
| 12 | 971 | 0.404 | 0.97 |
| 15 | 972 | 0.430 | 1.00 |
| 16 | 973 | 0.399 | 1.06 |
| 11 | 977 | 0.481 | 1.00 |

[a] Technical difficulties prevented us from making similar determinations at lower fractions of decomposition.

Our studies have shown that the esters investigated decompose initially according to the equation

$$Ph\cdot CH_2\cdot O\cdot CO\cdot X \rightarrow Ph\cdot CH_2\cdot + X\cdot COO.$$

However, the decomposition of benzyl acetate and of benzyl formate is accompanied by some other primary reactions, occurrence of which makes the over-all process too intricate and consequently not suitable for determination of bond dissociation energies. Hence, we confine our report to discussing the results of pyrolysis of benzyl-benzoate, these decompositions being less affected by the undesirable reactions, and in the end we give a very brief summary of results obtained in the investigation of the pyrolyses of benzyl acetate and benzyl formate.

## MECHANISM OF THE DECOMPOSITION OF BENZYL-BENZOATE

Assuming that the $C_6H_5\cdot COO-CH_2\cdot C_6H_5$ bond is the weakest one in the benzyl-benzoate molecule, we anticipate that reaction (1)

$$Ph\cdot COO\cdot CH_2\cdot Ph \rightarrow Ph\cdot COO\cdot + \cdot CH_2\cdot Ph \quad (1)$$

would be the initial step of the decomposition. It is very probable that thermally unstable benzoate radicals, produced in reaction (1), would decompose rapidly according to Eq. (2)

$$Ph\cdot COO\cdot \rightarrow Ph\cdot + CO_2. \quad (2)$$

If the reaction is carried out in the presence of excess of toluene then phenyl radicals are expected to be removed by reaction (3)[2]

$$Ph\cdot + C_6H_5\cdot CH_3 \rightarrow C_6H_5\cdot CH_2\cdot + C_6H_6. \quad (3)$$

[1] M. Szwarc, Chem. Revs. 47, 75 (1950).

[2] Szwarc, Ghosh, and Sehon, J. Chem. Phys. 18, 1142 (1950).

Finally, under the conditions prevailing in our experiments benzyl radicals are expected to dimerize.

According to this mechanism each mole of benzyl-benzoate decomposed should lead to the formation of one mole of carbon dioxide, one mole of benzene, and one mole of dibenzyl. Since reaction (1) is expected to be the rate-determining one, its rate would be measured by the rate of formation of any of the products, e.g., carbon dioxide.

## EXPERIMENTAL

The thermal decomposition of benzyl benzoate has been studied over the temperature range 900°–1000°K. Carbon dioxide and dibenzyl in an approximately 1:1 ratio (see Table I) have been identified as products of the decomposition, and the formation of dibenzyl is considered as a proof of the radical character of the reaction. Dibenzyl and the undecomposed benzyl benzoate were condensed together in a U trap following the reaction vessel and kept at −10°C. The dibenzyl was estimated by transferring the contents of the trap to a chromatographic alumina column, eluting with 60–80° petroleum ether into a weighed flask, and weighing the flask after vacuum distilling the solvent in the cold. The accuracy of the method was checked by blank experiments. Closer examination of the samples of isolated dibenzyl showed that they contained about 25 percent of diphenyl methane. The presence of the latter compound is considered as an additional evidence of the formation of phenyl radicals.

TABLE II.

| Run | Benzyl benzoate $P_{Ph\cdot COO\cdot CH_2Ph}$ mm Hg | $k_{960°K}$ sec$^{-1}$ | CO / $CO_2$ |
|---|---|---|---|
| | Time of contact about 0.8 sec. | | |
| 12 | 0.2 | 0.47 | 0.05 |
| 18 | 0.2 | 0.43 | 0.04 |
| 19 | 0.2 | 0.44 | 0.04 |
| 11 | 0.3 | 0.44 | 0.06 |
| 14 | 0.4 | 0.43 | 0.08 |
| 15 | 0.5 | 0.45 | 0.09 |
| 13 | 0.6 | 0.41 | 0.07 |
| | Time of contact about 2.4 secs | | |
| 6 | 0.5 | 0.41 | 0.11 |
| 9 | 0.5 | 0.38 | 0.11 |
| 5 | 0.6 | 0.44 | 0.13 |
| 7 | 0.6 | 0.41 | 0.12 |
| 10 | 0.8 | 0.41 | 0.16 |
| 8 | 1.0 | 0.42 | 0.20 |
| | Variation of partial pressure of toluene | | |
| | $P_{toluene}$ mm Hg | | |
| 17 | 6.4 | 0.43 | 0.07 |
| 11 | 9.7 | 0.44 | 0.06 |
| 12 | 10.8 | 0.47 | 0.05 |
| 16 | 17.0 | 0.44 | 0.05 |
| | Effect of packing the reaction vessel (surface increased ×7.5) | | |
| 31*P* | 0.5 | 0.44 | ... |
| 32*P* | 0.4 | 0.42 | ... |

TABLE III.

| Run | Benzyl benzoate $T$°K | % decomposition | $k$·sec$^{-1}$ |
|---|---|---|---|
| 24 | 908 | 5.0 | 0.060 |
| 25 | 908 | 4.7 | 0.057 |
| 10 | 935 | 32.2 | 0.153 |
| 9 | 947 | 44.8 | 0.230 |
| 5 | 949 | 48.2 | 0.292 |
| 6 | 950 | 48.8 | 0.278 |
| 7 | 951 | 49.6 | 0.293 |
| 8 | 951 | 51.7 | 0.301 |
| 14 | 960 | 29.3 | 0.433 |
| 13 | 964 | 32.3 | 0.482 |
| 17 | 970 | 42.3 | 0.622 |
| 12 | 971 | 40.4 | 0.711 |
| 15 | 972 | 43.0 | 0.706 |
| 19 | 972 | 42.2 | 0.684 |
| 16 | 973 | 39.9 | 0.717 |
| 18 | 973 | 42.7 | 0.690 |
| 11 | 977 | 48.1 | 0.824 |
| 26 | 987 | 64.3 | 1.32 |
| 22 | 993 | 69.3 | 1.49 |
| 20 | 999 | 77.2 | 1.91 |
| 21 | 1001 | 78.0 | 1.97 |

The rate of formation of carbon dioxide has been found proportional to the partial pressure of benzyl benzoate suggesting that it was produced by the unimolecular decomposition of the ester. In view of these facts we assumed that the rate of formation of $CO_2$ is equal to the rate of the initial decomposition of benzyl benzoate into benzyl and benzoate radicals and the first-order rate constants listed in Table II were calculated on this basis. The data of Table II give further confirmation of the first-order character of the reaction by showing that the observed rate constants are independent of the partial pressure of benzyl benzoate, the partial pressure of toluene, and of the time of contact, and proving that the pyrolysis is a homogeneous gas reaction. Table III gives the temperature dependence of the rate constants and the plot of log$k$ against $1/T$ is given in Fig. 1. The straight line thus obtained corresponds to an activation energy of 69 kcal/mole and a frequency factor of $2\times10^{13}$ sec$^{-1}$.

In addition to carbon dioxide, the pyrolysis produced smaller quantities of permanent gases which would not be expected from the simple scheme given above. Combustion analysis of these gases showed them to contain over 50 percent hydrogen with smaller quantities of methane and carbon monoxide (see Table IV). No "$C_2$" hydrocarbons were detected amongst the products of reaction.

The formation of hydrogen and at least of a part of the methane can be attributed to the partial decomposition of dibenzyl. This phenomenon has been observed in other pyrolytic studies and it is discussed elsewhere.[2] The decomposition of dibenzyl should be favored by a longer time of contact, and it is significant that the amount of permanent gases produced increases with increasing time of contact. The measured amount of hydrogen and methane corresponds to about 25 percent of the carbon dioxide produced showing that

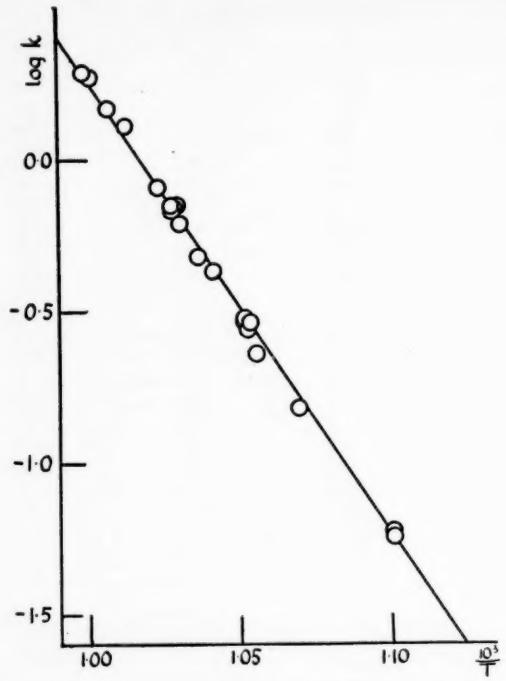


FIG. 1. Benzyl benzoate. Rate constants based on $d(CO_2)/dt$.

the reaction producing these gases is only a minor side reaction.

We paid considerable attention to the problem of carbon monoxide formation. Carbon monoxide could be produced either by the reduction of the carbon dioxide which was initially formed in the pyrolysis or by some reaction (or series of reactions) which lead directly to its formation. We tested the first alternative by carrying out experiments in which a mixture of toluene and carbon dioxide was pyrolyzed under the conditions prevailing in our normal runs. These experiments showed conclusively that carbon dioxide is not reduced under these conditions. We inquired whether the radicals present in our system might cause the reduction of carbon dioxide. To test this possibility we carried out experiments in which a mixture of toluene, ethylbenzene, and carbon dioxide were pyrolyzed. From previous investigations we know that under our experimental conditions ethyl benzene decomposes into benzyl and methyl radicals and, at higher partial pressures of ethyl benzene, hydrogen molecules and atoms might be also produced.[3] However, even under these drastic conditions no carbon monoxide was detected. We conclude, therefore, that the carbon monoxide observed in our experiments does not arise from the reduction of carbon dioxide. Closer examination of the data shows that the relative amount of carbon monoxide produced is independent of the time of contact and of temperature, but it is approximately proportional to the ratio of benzyl-benzoate/toluene. This is shown in Fig. 2 in which the ratio of $CO/CO_2$ is plotted against the ratio of benzyl-benzoate/toluene. This observation suggests that toluene and benzyl-benzoate compete for phenyl radicals produced in the initial decomposition, namely,

$$Ph\cdot + CH_3\cdot Ph \rightarrow Ph\cdot H + Ph\cdot CH_2\cdot, \quad (3)$$

$$Ph\cdot + Ph\cdot COO\cdot CH_2\cdot Ph \rightarrow Ph\cdot H + Ph\cdot COO\cdot \dot{C}H\cdot Ph. \quad (4)$$

The latter reaction being followed by the rapid decomposition of the $Ph\cdot COO\cdot \dot{C}H\cdot Ph$ radical,

$$Ph\cdot CO\cdot O\dot{C}H\cdot Ph \rightarrow Ph\cdot + CO + Ph\cdot CH\cdot O. \quad (5)$$

To test this suggestion we analyzed the products of the pyrolysis for benzaldehyde, and we found that benzaldehyde is indeed formed in the reaction, semiquantitative determinations showing that its amount is roughly proportional to the amount of carbon monoxide formed. Hence, if our suggestion is correct, the slope of the straight line given in Fig. 2 yields the ratio $k_4/k_3$. Since the $CO/CO_2$ ratio is independent of temperature, it appears that reactions (3) and (4) proceed with approximately equal activation energies.*

TABLE IV.

| Run | T°K | Benzyl benzoate Permanent gases $CO_2$ | Permanent gases % $H_2$ | $CH_4$ | CO |
|---|---|---|---|---|---|
| 25 | 908 | 0.30 | 52 | 17 | 31 |
| 10 | 935 | 0.42 | 45 | 16 | 39 |
| 9 | 947 | 0.39 | 52 | 19 | 29 |
| 5 | 949 | 0.40 | 50 | 18 | 32 |
| 6 | 950 | 0.38 | 52 | 18 | 30 |
| 7 | 951 | 0.41 | 51 | 19 | 30 |
| 8 | 951 | 0.48 | 46 | 13 | 41 |
| 14 | 960 | 0.29 | 53 | 20 | 27 |
| 13 | 964 | 0.29 | 55 | 19 | 26 |
| 17 | 970 | 0.30 | 57 | 19 | 24 |
| 12 | 971 | 0.27 | 56 | 24 | 20 |
| 15 | 972 | 0.32 | 55 | 17 | 28 |
| 19 | 972 | 0.28 | 60 | 25 | 15 |
| 16 | 973 | 0.30 | 56 | 26 | 18 |
| 18 | 973 | 0.28 | 59 | 26 | 15 |
| 11 | 977 | 0.29 | 59 | 20 | 21 |
| 26 | 987 | 0.28 | 60 | 23 | 17 |
| 22 | 993 | 0.28 | 64 | 22 | 14 |
| 20 | 999 | 0.28 | 66 | 20 | 14 |
| 21 | 1001 | 0.29 | 65 | 22 | 13 |

## BOND DISSOCIATION ENERGIES

Discussion of our experimental results leads to the conclusion that the observed over-all activation energy corresponds to the $Ph\cdot CH_2-O\cdot CO\cdot Ph$ bond dissociation energy, i.e.,

$$D(Ph\cdot CH_2-O\cdot CO\cdot Ph) = 69 \text{ kcal/mole}.$$

[3] M. Szwarc, J. Chem. Phys. **17**, 431 (1949).

* Both $E_4$ and $E_3$ are expected to be small and thus the suggestion $E_3 \sim E_4$ is very plausible.

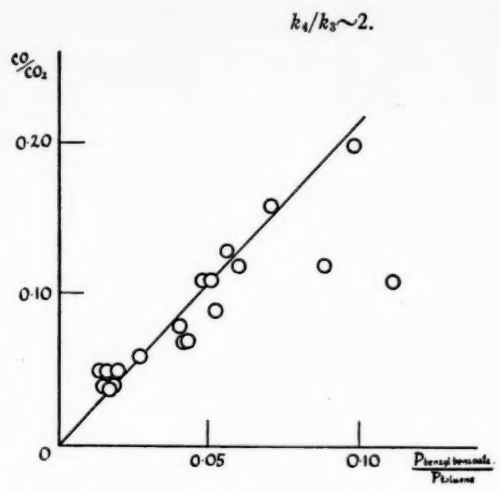


FIG. 2. Benzyl benzoate. Relative rates of reactions (3) and (4).

However, there are reasons to doubt the correctness of this estimate.

1. The frequency factor, calculated from our data, seems to be high, namely, $2 \cdot 10^{15}$ sec$^{-1}$.

2. It is our feeling that $D(\mathrm{Ph \cdot CH_2 - O \cdot CO \cdot Ph})$ should be rather less than 69 kcal/mole, since a lower value would be more consistent with the available data on somewhat similar bond dissociation energies.

There are some remarks concerned with point 1. It appears that values of the order $10^{13}$ sec$^{-1}$ are characteristic to frequency factors corresponding to unimolecular dissociations of molecules into radicals and *atoms*, i.e., corresponding to a process $\mathrm{R \cdot X \rightarrow R + X}$, X being an atom.[4] On the other hand, there is evidence that unimolecular dissociation processes which lead to a rupture of molecules into two big fragments correspond to higher-frequency factors. If these observations are correct, then they might point to the freedom of rotation of fragments in the transition state.† Of course, no gain in entropy is accrued in the case of dissociation into a radical and an *atom*, in agreement with many observations. The gain in entropy of rotation leads to the increase in heat of activation, thus the observed activation energies are *greater* than the corresponding dissociation energy.

Although it is premature to reach any definite conclusions on this subject, since more experimental data are required, we would like nevertheless to suggest that

$$D(\mathrm{Ph \cdot CH_2 - O \cdot CO \cdot Ph \cdot}) < 69 \text{ kcal/mole}.$$

[4] M. Szwarc and D. Williams, Nature **170**, 290 (1952).

† See, e.g., Faraday Society Discussions on the Reactivity of Free Radicals (Toronto, 1952).

TABLE V.

| Run | $T$°K | Benzyl acetate $CO_2$ / $CH_3 \cdot COO \cdot CH_2 \cdot Ph$ | Dibenzyl / $CO_2$ | Dibenzyl / $CH_4$ |
|---|---|---|---|---|
| 78 | 971 | 0.406 | 0.53 | 0.94 |
| 76 | 973 | 0.434 | 0.53 | 0.93 |
| 77 | 973 | 0.436 | 0.51 | 0.97 |
| 75 | 986 | 0.606 | 0.45 | 0.85 |

TABLE VI.

| Run | $T$°K | Benzyl formate $CO_2$ / $H \cdot COO \cdot CH_2 \cdot Ph$ | Dibenzyl / $CO_2$ | Dibenzyl / $H_2+CH_4$ |
|---|---|---|---|---|
| 61 | 973 | 0.348 | 0.56 | 0.84 |
| 62 | 977 | 0.385 | 0.51 | 0.80 |
| 63 | 983 | 0.408 | 0.52 | 0.80 |
| 60 | 988 | 0.416 | 0.58 | 0.85 |

## DECOMPOSITION OF BENZYL ACETATE AND OF BENZYL FORMATE

Decompositions of these esters have been studied very carefully. However, in spite of considerable experimental material which was accrued during this investigation, we were unable to elucidate completely the mechanism of decomposition. The difficulty arises from the occurrence of some reactions which probably result from a direct decomposition of these molecules into smaller molecules, e.g.,

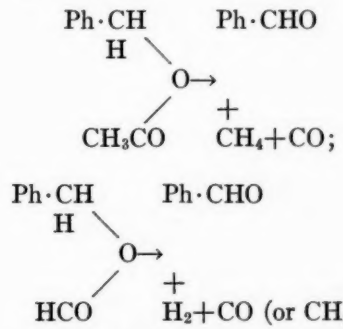


There is no doubt, however, that the decomposition of these compounds proceeds also via radical mechanism. The data collected in Tables V and VI, demonstrate that dibenzyl is formed during the reaction, and this is considered as evidence for radical formation.

In view of these complications, no great significance can be attributed to the rate constants calculated on the basis of $CO_2$ formation or of $CH_4$ formation. Nevertheless, it is worth while to mention that such calculations lead to rate constants, activation energies, and frequency factors which are close to the values obtained in the decomposition of benzyl-benzoate.

# Electronic Energy Levels of Molecular Oxygen*†

ALVIN MECKLER
*Massachusetts Institute of Technology, Cambridge, Massachusetts*‡
(Received January 12, 1953)

A configuration interaction study of the lower-lying electronic energy levels of molecular oxygen is made. With the 1*s* and 2*s* shells kept filled, the remaining eight electrons are distributed among the twelve spin-orbitals arising from the 2*p* levels on each atom. The atomic functions are represented as Gaussians, which are poor atomic functions but facile integrands in many-center integrals. The molecular orbitals are formed as symmetrical linear combinations of the atomic orbitals, simply for convenience. Inclusion of all configurations implies complete equivalence of all possible constructions of linear combinations.

Out of the 495 configurations (many-electron determinants) a group of nine states of $^3\Sigma_g^-$ character is set up and twelve of $^1\Sigma_g^+$ character. The interaction matrix of each block is computed and diagonalized (by electronic computer). The results for the ground state, which is a triplet, are very good. The binding energy is off by 2 percent, the internuclear distance is off by 1 percent, the fundamental nuclear vibration frequency is off by 4 percent. The lowest singlet state is not given as accurately.

The energies and wave functions for the lowest triplet and singlet are calculated and compared for various values of internuclear separation. Discussion is made of the validity of single configuration theory, from both the Heitler-London and Hund-Mulliken points of view.

## I. INTRODUCTION

THE modern theory of molecules, as that of atoms and solids, is based on the one-electron approximation developed along lines characterized as orbital theory. The theory recognizes the electron-nucleus interaction as the dominant potential energy term in the Hamiltonian, for without it there could be no bonded structure, and it assumes a degree of dominance sufficient to justify an independent particle description of the many-electron system. In this way models are developed wherein each electron is assigned to an individual orbital and the wave function of the entire system is constructed as a product of the individual one-electron functions. There are two ways to use this concept of orbitals; one procedure cannot be more than a one-electron approximation, the other has the theoretical possibility of converging to the true solution of the many-electron Schrödinger equation. The first procedure, which can be typified by the name of Hartree-Fock, attempts to arrive at the best possible orbitals to be used in a single product-function. The other procedure, a configuration interaction study, looks for an optimum decomposition of the molecular wave function into a set of manageable and physically understandable product-functions. This paper covers an investigation of the lower-lying electronic energy levels of molecular oxygen expressed in terms of configuration interaction. The electron orbitals are fixed functions but there are enough so that the state of the molecule can be represented as a linear combination of certain configurations.

## II. CONFIGURATION THEORY

This is the general program. We begin with a set of $N$ single-particle functions $u_i(\bar{x})$. The symbol $\bar{x}$ stands for the spatial coordinates and a spin coordinate. With a spin-free Hamiltonian, a $u_i$ can be taken as a product of a spatial function and a spin function

$$u_i(\bar{x})=\varphi_i(x)\begin{cases}\alpha\\ \beta,\end{cases}$$

where $x$ denotes the three spatial coordinates, $\alpha$ indicates that the $z$ component of spin is $+\frac{1}{2}$, and $\beta$ indicates that the $z$ component of spin is $-\frac{1}{2}$. It will be shown later that there is no loss of generality in assuming the $\varphi$'s form an orthonormal set.

The next step is the selection of $n(n\leqslant N)u_i$'s and the assignment of $n$ electrons to this subset. There are $N!/n!(N-n)!$ possible selections. Each selection defines a product wave function which is to be antisymmetrized in accordance with the exclusion principle and which can be concisely written as

$$\psi=(n!)^{-\frac{1}{2}}\det\{u_1(1)u_2(2)\cdots u_n(n)\}.$$

The $n$ tuple in the brackets is the diagonal row of the determinant; it specifies the particular configuration.

The final step is to diagonalize the Hamiltonian in the finite dimensional space spanned by the $N!/n!(N-n)!$ configurations. If $N$ were infinite and the $u_i$'s formed a complete set, this procedure would yield a rigorous solution to the wave equation. With a finite $N$, we must hope that the configurations used are the most influential ones of a complete set. This is the practical problem. Towards its solution the criterion for best one-electron orbitals should be established. This criterion will not be derived in this paper. However, it is possible to do oxygen to an extent whose complete correspondence in other molecules would be untractable. Examination of the oxygen wave functions may allow some judgment as to what types of configurations are the most important ones.

* Supported by the U. S. Office of Naval Research.
† Part of a thesis submitted in partial fulfillment of the requirements for the Ph.D. degree at the Massachusetts Institute of Technology.
‡ Now a member of the Lincoln Laboratory at M.I.T.

## III. THE ATOMIC CORRESPONDENCE

A measure of the extent of configuration interaction considered can be seen in the atomic level system at infinite separation. A classification of molecular states must become a classification of atomic states at infinite internuclear separation or, going in the other direction, a molecular state is seen to arise from a superposition and consequent interaction of atomic configurations. In orbital theory we effect this atomic correspondence by constructing molecular orbitals as linear combinations of atomic orbitals.[1] At this point, it is well to review a basic theorem.

If $u_i(\bar{x})$ $(1 \leqslant i \leqslant N)$ is a set of $N$ independent functions and $v_j(\bar{x})$ $(1 \leqslant j \leqslant N)$ is a set whose members are linear combinations of the first set,

$$v_j = \sum_i c_{ij} u_i$$

then the entire set of $N!/n!(N-n)!$ configurations formed with the $u_i$'s as elements is equivalent to the entire set of $N!/n!(N-n)!$ configurations formed with the $v_j$'s as elements. The same energy levels will be derived with either representation. Neither representation can describe the system more completely than the other.[2]

With the freedom guaranteed by the equivalence theorem, the uncombined atomic orbitals themselves may be chosen as molecular orbitals, to form what might be called the primitive set. The calculations can be simplified, usually, by orthogonalizing and symmetrizing the primitive set according to the geometry of the molecule, but it must be understood that although the new representation may be more diagonal, it cannot be more complete.

The primitive set will asymptotically describe atomic states of varying degrees of excitation and ionicity. In general one would have to neglect many high-lying atomic states in order to carry out the calculation. For oxygen we are fortunate in that the obvious selection of atomic orbitals, and all the configurations thereby implied, does not lead to an insurmountable number of configurations. By the obvious selection we mean that set indicated by the normal atomic configuration, $1s^2 2s^2 2p^4$. These twenty functions can be taken as the primitive set for the oxygen molecule,

$$1s\begin{cases}\alpha\\ \beta\end{cases} \quad 2s\begin{cases}\alpha\\ \beta\end{cases} \quad 2p_0\begin{cases}\alpha\\ \beta\end{cases} \quad 2p_+\begin{cases}\alpha\\ \beta\end{cases} \quad 2p_-\begin{cases}\alpha\\ \beta\end{cases}.$$

A set of ten for each atom.[3] At infinite separation we will recognize normal, excited, singly ionized, and doubly ionized oxygen atoms. Actually, only those configurations in which the $1s$ and $2s$ shells are filled will be considered. It is perhaps more honest to say that the primitive set consists of the twelve $2p$ orbitals into which we will assign eight electrons in 495 possible ways.

## IV. THE HEITLER-LONDON AND HUND-MULLIKEN APPROXIMATIONS

### Expectation of the Present Calculation

Before setting up the full configuration interaction, we would like to review the two standard single configuration approximations, mainly to establish a background for our results. The well-known Heitler-London and Hund-Mulliken schemes are attempts to represent a molecular state as a single configuration. Each is outfitted with an ordered set of wave functions and, starting at the bottom level, electrons are assigned until all the electrons are accounted for. The Heitler-London, sometimes expanded into the valence-bond, configuration describes each electron fixed in its aboriginal atomic state, an approximation accurate only at large separations. The Hund-Mulliken[4] method has an electron distributed equally about each nucleus in a simple type of molecular orbital patterned after the rigorous solution to the hydrogen molecule ion. A Hund-Mulliken configuration is valid for small internuclear distances. It describes strong overlapping of the atoms, and it does not separate into unmixed atomic states at infinite separation.

According to the Heitler-London picture, electrons are paired off with opposite spins. The combination of two normal oxygen atoms should yield a singlet ground state for the molecule (zero-resultant spin). This is just not so. The ground state of the oxygen molecule is a triplet state (one unit of total spin angular momentum). The Hund-Mulliken assignment takes better advantage of $p$ orbital degeneracy. There are two standard molecular orbital levels for each of the atomic $p$ levels. The lowest level is $p_0$ like and it is filled with two electrons of opposite spin. The other $p_0$ like level is not next in line; it lies above the $+$ and $-$ levels. Therefore, the next two electrons go into a $p_+$ level, the next two go into the equivalent $p_-$ level, and the remaining two have a choice of four space-spin positions on the $+$ and $-$ level. Hund's rule, used as in atomic structure, decrees that the state of highest spin should be lowest.

This is a rather sketchy outline of what happens with the two approximations. Nevertheless, disagreement exists and is stimulus for the study of the complete system of configurations. We shall extract, in significant detail, the lowest triplet state and its competing singlet state. Projection of the proper combination of configurations upon the frameworks of the two simple approximations should reveal the domain of

[1] W. Moffitt [Proc. Roy. Soc. (London) **210**, 224 (1951)] maintains that this is too drastic a step and an unnecessary one at this stage. We will return to his criticism at the conclusion of this paper.

[2] Appendix I contains a proof of this theorem.

[3] The functions will be given analytically later on. The notation of 0, +, − signifies the component of orbital angular momentum about the internuclear axis as either 0, +1, or −1.

[4] The Hund-Mulliken method is often referred to simply as "the molecular orbital method." In this article a molecular orbital is a wave function used in a molecular problem, not necessarily a symmetry orbital. Perhaps we should call the Hund-Mulliken type "standard molecular orbitals."

validity of each and the mode of accommodation of the inappropriate technique to the region belonging to the other. Such an analysis of the wave functions of paramagnetic oxygen should be useful in the study of ferromagnetic solids, for the degeneracies inherent in the oxygen problem approach those involved in the bonding of $d$-shell electrons.

We will now go on to the computation, returning to the choice of atomic functions.

## V. THE ATOMIC FUNCTIONS

A computational detail which presents a major hurdle in this type of problem is the evaluation of many-center integrals. Overlap, kinetic energy, electronic interaction integrals between numerical or simple exponential types of atomic orbitals are very difficult to carry out. At the time this work was begun very few had been explicitly calculated, although much recent work has been done.[5] A suggestion of Boys definitely relieved the situation of any element of impracticability with respect to getting integrals done.[6] Boys demonstrated the simple evaluation of many-center integrals between atomic functions which are Gaussian exponentials

$$x^l y^m z^n \exp(-ar^2).$$

In fact, denoting the various origins of the problem (i.e., positions of the nuclei) by

$$A_x A_y A_z$$
$$B_x B_y B_z, \text{ etc.}$$

and letting

$$x_A = x - A_x \qquad K = -\nabla^2$$
$$aA = \exp(-ar^2) \qquad V_c = 2/r_c$$
$$M = 2/r_{12},$$

then these integrals are given in the paper

| | |
|---|---|
| $(aA \mid bB)$ | overlap |
| $(aA \mid K \mid bB)$ | kinetic energy |
| $(aA \mid V_c \mid bB)$ | nuclear framework |
| $(aA^{(1)}bB^{(1)} \mid M \mid cC^{(2)}dD^{(2)})$ | electronic interaction. |

The advantage of the method is that integrals involving non-$s$ like functions ($z_A \exp(-ar^2)A$ is a $p$ function) can be obtained from those given in the paper by differentiation. To bring down a $z_A$ into the integrand of an integral here, differentiate with respect to $A_z$ and divide by $2a$.

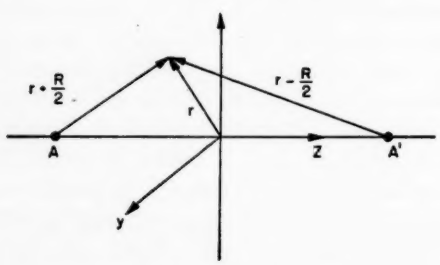


FIG. 1. Coordinate system.

The Gaussians are not the best representations of atomic functions, but that is the point. The proper adjustment of molecular levels will come about not so much from a choice of really good atomic orbitals, but rather from a full perturbation procedure applied to the great number of degenerate molecular functions.

Specifically then, the atomic functions used are

$$1s \rightarrow \exp(-ar^2)$$
$$2s \rightarrow \exp(-br^2) - \gamma \exp(-ar^2)$$
(made orthogonal to the $1s$)
$$2p \rightarrow \begin{Bmatrix} x+iy \\ z \\ x-iy \end{Bmatrix} \exp(-br^2).$$

The energy of an atomic $1s^2$ ($Z=8$) configuration was minimized to get the half-width or $a$ factor for the $1s$ function. As a check, the overlap integral between the two $1s$ functions was evaluated and compared with the corresponding integral in which the standard simple exponential was used. It was demanded that the integrals drop to half their zero separation values at the same point of internuclear separation. The $a$ factor fitted the check nicely.

The $b$ factor of the $2p$ function was determined by a correspondence between overlap integrals. The $(p_0, p_0)$ overlap integral using Gaussians was made to go through zero at the same point that the integral using the simple exponential function does. The final choices are

$$a = 20$$
$$b = 0.8.$$

## VI. THE MOLECULAR ORBITALS AS LINEAR COMBINATIONS OF ATOMIC ORBITALS

There are an infinite number of ways to orthonormalize a set of independent functions. Because of the equivalence theorem, we know that in the long run it will make no difference how we do it. The run will be all the more pleasant, however, if we design the molecular orbitals so that the symmetry properties of the determinantal functions will be either obvious or easily discernible.

The Hamiltonian and the coordinate system follow:[7]

$$H = \sum_{i=1}^{16} -\nabla_i^2 - \sum_i \frac{2Z}{|\mathbf{r}_i - \frac{1}{2}R|} - \sum_i \frac{2Z}{|\mathbf{r}_i + \frac{1}{2}R|} + \sum_{i<j} \frac{2}{r_{ij}} + \frac{2Z^2}{R}.$$

Figure 1 is meant to show that the origin is located midway between the two identical nuclei, the $z$ axis lies along the internuclear axis, the internuclear distance is $R$. Hereafter, we shall distinguish atomic orbitals located on the different nuclei by means of the prime symbol. The following is the notation for the normalized

[5] For a bibliography see C. C. J. Roothaan, J. Chem. Phys. **19**, 1445 (1951).

[6] S. F. Boys, Proc. Roy. Soc. (London) **200**, 542 (1950).

[7] The unit of distance is the Bohr radius $a_0 = 0.5293$A. The unit of energy is the hydrogen atom ionization energy $e^2/2a_0 = 13.602$ ev.

atomic functions:

$$s=(\pi/2a)^{-\frac{3}{4}}\exp[-a(r+\tfrac{1}{2}R)^2]$$
$$s'=(\pi/2a)^{-\frac{3}{4}}\exp[-a(r-\tfrac{1}{2}R)^2]$$
$$\sigma=(\pi/2b)^{-\frac{3}{4}}\exp[-b(r+\tfrac{1}{2}R)^2]$$
$$\sigma'=(\pi/2b)^{-\frac{3}{4}}\exp[-b(r-\tfrac{1}{2}R)^2]$$
$$p_0=2(b)^{\frac{1}{2}}(\pi/2b)^{-\frac{3}{4}}(z+\tfrac{1}{2}R)\exp[-b(r+\tfrac{1}{2}R)^2]$$
$$p_0'=2(b)^{\frac{1}{2}}(\pi/2b)^{-\frac{3}{4}}(z-\tfrac{1}{2}R)\exp[-b(r-\tfrac{1}{2}R)^2]$$
$$p_\pm=(2b)^{\frac{1}{2}}(\pi/2b)^{-\frac{3}{4}}(x\pm iy)\exp[-b(r+\tfrac{1}{2}R)^2]$$
$$p_\pm'=(2b)^{\frac{1}{2}}(\pi/2b)^{-\frac{3}{4}}(x\pm iy)\exp[-b(r-\tfrac{1}{2}R)^2].$$

Now there are certain dynamic and symmetry operators which commute with the Hamiltonian. Configurations can be grouped into sets which are eigenfunctions of these operators and between sets of different character there will be no matrix component of the Hamiltonian. The operators are total spin, $z$ component of total spin, $z$ component of total orbital angular momentum, inversion of all electronic coordinates through the origin, and reflection of all the electronic coordinates through a plane containing the molecular axis. We have combined the atomic orbitals into molecular orbitals of definite axial angular momentum and definite parity (inversion character). They are

$$\varphi_s=\frac{1}{\sqrt{2}}(s+s') \qquad \chi_s=\frac{1}{\sqrt{2}}(s-s')$$
$$\varphi_\sigma=\frac{N}{\sqrt{2}}\{(\sigma+\sigma')+A(s+s')\}$$
$$\chi_\sigma=\frac{P}{\sqrt{2}}\{(\sigma-\sigma')+D(s-s')\}$$
$$\varphi_0=\frac{M}{\sqrt{2}}\{(p_0-p_0')+B(\sigma+\sigma')+C(s+s')\}$$
$$\chi_0=\frac{J}{\sqrt{2}}\{(p_0+p_0')+E(\sigma-\sigma')+F(s-s')\}$$
$$\varphi_\pm=\frac{L}{\sqrt{2}}(p_\pm+p_\pm')$$
$$\chi_\pm=\frac{K}{\sqrt{2}}(p_\pm-p_\pm').$$

They can easily be shown to satisfy the following behavior tablulation:

| Under inversion | Axial reflection ($yz$ plane) |
|---|---|
| $\varphi_s\leftrightarrow\varphi_s$ | $\varphi_s\leftrightarrow\varphi_s$ |
| $\varphi_\sigma\leftrightarrow\varphi_\sigma$ | $\chi_s\leftrightarrow\chi_s$ |
| $\varphi_0\leftrightarrow\varphi_0$ | $\varphi_\sigma\leftrightarrow\varphi_\sigma$ |
| $\chi_s\leftrightarrow-\chi_s$ | $\chi_\sigma\leftrightarrow\chi_\sigma$ |
| $\chi_\sigma\leftrightarrow-\chi_\sigma$ | $\varphi_0\leftrightarrow\varphi_0$ |
| $\chi_0\leftrightarrow-\chi_0$ | $\chi_0\leftrightarrow\chi_0$ |
| $\varphi_\pm\leftrightarrow-\varphi_\pm$ | $\varphi_+\leftrightarrow-\varphi_-$ |
| $\chi_\pm\leftrightarrow\chi_\pm$ | $\chi_+\leftrightarrow-\chi_-$. (1) |

TABLE I. Molecular orbital coefficients.

| $R$ | $N^2$ | $A$ | $P^2$ | $D$ | | |
|---|---|---|---|---|---|---|
| 1.5 | 0.75316 | −0.28078 | 1.80210 | −0.19627 | | |
| 2.0 | 0.87747 | −0.24952 | 1.33989 | −0.22753 | | |
| 2.5 | 0.97632 | −0.24048 | 1.16017 | −0.23658 | | |
| 4.0 | 1.05846 | −0.23853 | 1.06220 | −0.23853 | | |
| 6.0 | 1.06033 | −0.23853 | 1.06033 | −0.23853 | | |
| 9.0 | 1.06033 | −0.23853 | 1.06033 | −0.23853 | | |
| | 1.06033 | −0.23853 | 1.06033 | −0.23853 | | |
| $R$ | $M^2$ | $B$ | $C$ | $J^2$ | $E$ | $F$ |
| 1.5 | 0.89789 | −0.38777 | −0.00014 | 5.95571 | 0.94443 | −0.07635 |
| 2.0 | 0.74952 | −0.30863 | 0.03918 | 2.57830 | 0.47239 | −0.06965 |
| 2.5 | 0.77155 | −0.17724 | 0.03424 | 1.57892 | 0.21065 | −0.04146 |
| 4.0 | 0.98082 | −0.00932 | 0.00222 | 1.02004 | 0.00631 | −0.00150 |
| 6.0 | 0.99998 | 0.00000 | 0.00000 | 1.00002 | 0.00000 | 0.00000 |
| 9.0 | 1.00000 | 0.00000 | 0.00000 | 1.00000 | 0.00000 | 0.00000 |
| | 1.00000 | 0.00000 | 0.00000 | 1.00000 | 0.00000 | 0.00000 |
| $R$ | $L^2$ | $K^2$ | | | | |
| 1.5 | 0.71095 | 1.68512 | | | | |
| 2.0 | 0.83202 | 1.25297 | | | | |
| 2.5 | 0.92414 | 1.08942 | | | | |
| 4.0 | 0.99834 | 1.00166 | | | | |
| 6.0 | 1.00000 | 1.00000 | | | | |
| 9.0 | 1.00000 | 1.00000 | | | | |
| | 1.00000 | 1.00000 | | | | |

The $\varphi$'s are already orthogonal to the $\chi$'s because of the symmetries. The coefficients are determined by the stipulation that the $\varphi$ group and the $\chi$ group each form an orthonormalized set. Because of the large value of $a$, the $1s$ functions overlap to an absolutely negligible extent $[\sim\exp(-\frac{1}{2}aR^2)]$ and so the normalization of $\varphi_s$ and $\chi_s$ is independent of $R$. Things are arranged so that the atomic correspondence is evident. In fact, at infinite separation

$$\varphi_\sigma\rightarrow\frac{1}{\sqrt{2}}\{(2s)+(2s)'\} \qquad \chi_\sigma\rightarrow\frac{1}{\sqrt{2}}\{(2s)-(2s)'\}$$
$$\varphi_\pm\rightarrow\frac{1}{\sqrt{2}}\{(2p)+(2p)'\} \qquad \chi_\pm\rightarrow\frac{1}{\sqrt{2}}\{(2p)-(2p)'\}.$$

Table I lists the values of the coefficients at various internuclear distances.

## VII. THE MOLECULAR CONFIGURATIONS

Our orbitals are now fixed and we can begin the assignment of electrons. As stated, the $1s$ and $2s$ shells will be kept filled with eight electrons. The closed shells contribute no spin angular momentum to the molecule, they have even parity, zero axial angular momentum, and are invariant under a reflection operation. We can, therefore, go on to assign the remaining eight electrons to the $2p$ orbitals and classify the molecular configurations without worrying about the inner shells.

Table II begins the cataloguing of states. Each $2p$ level can be filled with a maximum of four electrons; a spin pair can go into the $\varphi$ orbital and another spin pair can go into the $\chi$ orbital. The table exhausts all the possibilities of assignment of eight electrons to the twelve positions.

TABLE II. Possible values of $M_L$. One-electron angular momentum is denoted by $m_l$ and total axial angular momentum is denoted by $M_L$. The first three rows of the table indicate the occupation numbers for each level of $m_l$. The fourth row indicates $M_L=\Sigma_l m_l$.

| $m_l$ | Number of electrons | | | | | | | | | | | | | | |
|---|---|---|---|---|---|---|---|---|---|---|---|---|---|---|---|
| +1 | 4 | 4 | 4 | 4 | 4 | 3 | 3 | 3 | 3 | 2 | 2 | 2 | 1 | 1 | 0 |
| 0 | 4 | 3 | 2 | 1 | 0 | 4 | 3 | 2 | 1 | 4 | 3 | 2 | 4 | 3 | 4 |
| −1 | 0 | 1 | 2 | 3 | 4 | 1 | 2 | 3 | 4 | 2 | 3 | 4 | 3 | 4 | 4 |
| $M_L$ | +4 | +3 | +2 | +1 | 0 | +2 | +1 | 0 | −1 | 0 | −1 | −2 | −2 | −3 | −4 |

We shall investigate only states of zero total axial angular momentum. The next step is to take the three columns

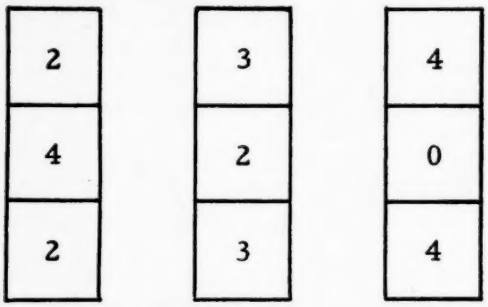


and expand their possibilities with the details of spin assignment. This has been done in Table III.

Actually, we have only listed states of even total parity, states which transform into themselves under inversion. The parity character of the determinantal function is the product of the individual parity characters. The notational pattern is this: the tabulated electron assignment

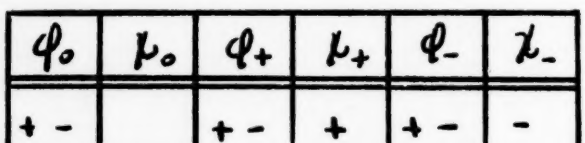


stands for the determinant

$$\frac{1}{\sqrt{16!}}\det\{\varphi_s\alpha(1)\varphi_s\beta(2)\chi_s\alpha(3)\chi_s\beta(4)$$
$$\times\varphi_\sigma\alpha(5)\varphi_\sigma\beta(6)\chi_\sigma\alpha(7)\chi_\sigma\beta(8)\varphi_0\alpha(9)\varphi_0\beta(10)$$
$$\times\varphi_+\alpha(11)\varphi_+\beta(12)\chi_+\alpha(13)\varphi_-\alpha(14)$$
$$\times\varphi_-\beta(15)\chi_-\beta(16)\}.$$

Since the closed shells contribute nothing pertinent for classification, we may use the form as a working notation for

$$\Sigma_P(-1)^pP\cdot\{\varphi_0\alpha(1)\varphi_0\beta(2)\varphi_+\alpha(3)\varphi_+\beta(4)$$
$$\times\chi_+\alpha(5)\varphi_-\alpha(6)\varphi_-\beta(7)\chi_-\beta(8)\},$$

where $P$ runs over the 8! permutations of the 8 variables and $p$ is the number of interchanges that must be made to obtain the permutation from the standard arrangement.

The interconnections of the various configurations by reflection in an axial plane are shown in the eighth column. The molecular orbital behavior table (Eqs. 1) serves as guide; we have only to account for a possible change in the standard arrangement by the proper sign.

The last column indicates the transformation of each configuration under application of the total spin operator.[8] We have recorded the behavior of only one configuration of a connected group. It is sufficient to include only states of total $z$ component of spin equal to zero.

We shall investigate the ${}^3\Sigma_g^-$ and ${}^1\Sigma_g^+$ states. The symbol ${}^3\Sigma_g^-$ denotes a wave function associated with one unit of total spin angular momentum, zero units of total axial angular momentum, an even parity ($g$) under inversion, and a change of sign (−) under a reflection through an axial plane. It turns out that the ground state of the oxygen molecule will come about from the interaction of nine ${}^3\Sigma_g^-$ states, while the interesting singlet state will be evolved out of twelve ${}^1\Sigma_g^+$ states. These states are set up from an inspection of Table III and are presented in Eqs. 2. At this point we have our set of initial molecular states, states of definite multiplicity and of definite symmetry. The matrix of the Hamiltonian must now be computed and diagonalized,

$$\psi_a=2^{-\frac{1}{2}}(I^*-I_s^*)$$
$$\psi_b=2^{-\frac{1}{2}}(III^*-III_s^*)$$
$$\psi_c=2^{-\frac{1}{2}}(I+I_s)$$
$$\psi_d=2^{-\frac{1}{2}}(II+II_s)$$
$$\psi_e=2^{-\frac{1}{2}}(IX+IX_s) \qquad {}^3\Sigma_g^-$$
$$\psi_f=2^{-\frac{1}{2}}(X+X_s)$$
$$\psi_g=\tfrac{1}{2}(III-III_s+VII-VII_s)$$
$$\psi_h=\tfrac{1}{2}(IV-IV_s+VI-VI_s)$$
$$\psi_i=\tfrac{1}{2}(V-V_s+VIII-VIII_s)$$

$$\psi_a=12^{-\frac{1}{2}}(2I^*+2I_s^*-II^*-II_s^*-III^*-III_s^*)$$
$$\psi_b=\tfrac{1}{2}(III^*+III_s^*-II^*-II_s^*)$$
$$\psi_c=IV^*$$
$$\psi_d=VII^*$$
$$\psi_e=2^{-\frac{1}{2}}(V^*+VI^*)$$
$$\psi_f=2^{-\frac{1}{2}}(I-I_s)$$
$$\psi_g=2^{-\frac{1}{2}}(II-II_s) \qquad {}^1\Sigma_g^+$$
$$\psi_h=24^{-\frac{1}{2}}(2III+2III_s-2VII-2VII_s-IV$$
$$-IV_s+VI+VI_s-V-V_s+VIII+VIII_s)$$
$$\psi_i=8^{-\frac{1}{2}}(V+V_s-VIII-VIII_s-IV-IV_s+VI+VI_s)$$
$$\psi_j=2^{-\frac{1}{2}}(IX-IX_s)$$
$$\psi_k=2^{-\frac{1}{2}}(X-X_s)$$
$$\psi_l=XI. \qquad (2)$$

[8] The spin algebra is standard and is reviewed in Appendix II.

TABLE III. Configuration tabulation.

| $\psi$ | $\varphi_0$ | $\chi_0$ | $\varphi_+$ | $\chi_+$ | $\varphi_-$ | $\chi_-$ | Refl. | $S\psi$ |
|---|---|---|---|---|---|---|---|---|
| $I^*$ | +− | +− | + | + | − | − | $I_s^*$ | $=2I^*+II^*+II_s^*+III^*+III_s^*$ |
| $I_s^*$ | +− | +− | − | − | + | + | $I^*$ | |
| $II^*$ | +− | +− | + | − | + | − | $II_s^*$ | |
| $II_s^*$ | +− | +− | − | + | − | + | $II^*$ | |
| $III^*$ | +− | +− | + | − | − | + | $III_s^*$ | |
| $III_s^*$ | +− | +− | − | + | + | − | $III^*$ | |
| $IV^*$ | +− | +− | +− | | +− | | $IV^*$ | $=0$ |
| $V^*$ | +− | +− | +− | | | +− | $V^*$ | $=0$ |
| $VI^*$ | +− | +− | | +− | +− | | $VI^*$ | $=0$ |
| $VII^*$ | +− | +− | | +− | | +− | $VII^*$ | $=0$ |
| $I$ | +− | | +− | + | +− | − | $-I_s$ | $=I+I_s$ |
| $I_s$ | +− | | +− | − | +− | + | $-I$ | |
| $II$ | +− | | + | +− | − | +− | $-II_s$ | $=II+II_s$ |
| $II_s$ | +− | | − | +− | + | +− | $-II$ | |
| $III$ | + | − | +− | + | − | +− | $-VII$ | $=2III+IV+IV_s+V+V_s$ |
| $III_s$ | − | + | +− | − | + | +− | $-VII_s$ | |
| $IV$ | + | − | +− | − | + | +− | $-VI$ | |
| $IV_s$ | − | + | +− | + | − | +− | $-VI_s$ | |
| $V$ | + | + | +− | − | − | +− | $-VIII$ | |
| $V_s$ | − | − | +− | + | + | +− | $-VIII_s$ | |
| $VI$ | + | − | + | +− | +− | − | $-IV$ | $=2VI+VII+VII_s+VIII+VIII_s$ |
| $VI_s$ | − | + | − | +− | +− | + | $-IV_s$ | |
| $VII$ | + | − | − | +− | +− | + | $-III$ | |
| $VII_s$ | − | + | + | +− | +− | − | $-III_s$ | |
| $VIII$ | + | + | − | +− | +− | − | $-V$ | |
| $VIII_s$ | − | − | + | +− | +− | + | $-V_s$ | |
| $IX$ | | +− | +− | + | +− | − | $-IX_s$ | $=IX+IX_s$ |
| $IX_s$ | | +− | +− | − | +− | + | $-IX$ | |
| $X$ | | +− | − | +− | + | +− | $-X_s$ | $=X+X_s$ |
| $X_s$ | | +− | + | +− | − | +− | $-X$ | |
| $XI$ | | | +− | +− | +− | +− | $XI$ | $=0$ |

## VIII. SETTING UP AND DIAGONALIZING THE MATRIX

To review the formation of the secular equation. For either of the two noninteracting blocks, ${}^3\Sigma_g^-$ or ${}^1\Sigma_g^+$, we approximate an eigenfunction by the form

$$\Psi_\mu=\sum_j a_j^\mu\psi_j,$$

where $\psi_j$ is one of the orthonormalized states in the set (Eqs. 2). For a given $\mu$, the numbers $a_j^\mu$ may be considered a vector with components along the basic set of axes $\psi_j$. We shall be asking for eigenvectors and eigenvalues by beginning with

$$H\Psi_\mu=E_\mu\Psi_\mu$$

or

$$H\sum_j a_j^\mu\psi_j=E_\mu\sum_j a_j^\mu\psi_j.$$

A necessary condition for this to hold is that

$$\sum_j a_j^\mu H_{ij}=E_\mu\sum_j a_j^\mu\delta_{ij}$$

this being the result of multiplying on both sides by $\psi_i^*$ and integrating over all the electronic coordinates, including spin. Interpreting our symbols as matrices and vectors, we may rewrite the last equation as

$$\mathbf{H}\mathbf{a}^\mu=E_\mu\mathbf{a}^\mu.$$

We are to form the matrix of our Hamiltonian between the initial set of configurations. Its eigenvalues are the electronic energy levels; the corresponding eigenvectors are the representations of the electronic wave functions in terms of the initial set of configurations.

The integrals over determinantal functions were reduced to sums of one- and two-electron integrals in the usual way.[9] In this process, one must keep track of the relations between standard arrangements. The all important question of signs depends upon the definitions of standard arrangements. A standard arrangement is a flexible thing, more or less a question of taste, but we have tempered this flexibility by connecting the configurations through symmetry operations. In arranging two configurations in an integral, correlation must be maintained with the "fundamental" standard arrangements listed in Table III.

The inner shell electrons contribute to the diagonal energies in a nontrivial way. First, there is the interaction of the $1s$ and $2s$ electrons among themselves and with the nuclear framework; this energy being the same for each diagonal element, although varying with internuclear distance. The second contribution comes from the interaction of the $2p$ electrons with the inner shell and differs from one state to the other. The $\varphi_0$ and $\chi_0$ orbitals are distinguished from the others by the core at finite separation.

Finally, as a computational aid, we mention certain inequalities useful in checking integrals. Roothaan[10] has derived some which are important from both a theoretical and a computational point of view and these are presented in Appendix III along with a new one which brings in the so-called "hybrid" integrals.

[9] J. C. Slater, *Quantum Theory of Matter* (McGraw-Hill Book Company, Inc., New York, 1951) first edition, p. 192.

[10] C. C. J. Roothaan, Revs. Modern Phys. **23**, 69 (1951).

TABLE IV. Tabulation by space orbital.

| | $^3\Sigma_g^-$ | | | | $^1\Sigma_g^+$ | | | |
|---|---|---|---|---|---|---|---|---|
| *a* | $\sigma_g^2$ | $\pi_u^2$ | $\pi_g^2$ | $\sigma_u^2$ | $\sigma_g^2$ | $\pi_u^2$ | $\pi_g^2$ | $\sigma_u^2$ |
| *b* | $\sigma_g^2$ | $\pi_u^2$ | $\pi_g^2$ | $\sigma_u^2$ | $\sigma_g^2$ | $\pi_u^2$ | $\pi_g^2$ | $\sigma_u^2$ |
| *c* | $\sigma_g^2$ | $\pi_u^4$ | $\pi_g^2$ | ··· | $\sigma_g^2$ | $\pi_u^4$ | ··· | $\sigma_u^2$ |
| *d* | $\sigma_g^2$ | $\pi_u^2$ | $\pi_g^4$ | ··· | $\sigma_g^2$ | ··· | $\pi_g^4$ | $\sigma_u^2$ |
| *e* | ··· | $\pi_u^4$ | $\pi_g^2$ | $\sigma_u^2$ | $\sigma_g^2$ | $\pi_u^2$ | $\pi_g^2$ | $\sigma_u^2$ |
| *f* | ··· | $\pi_u^2$ | $\pi_g^4$ | $\sigma_u^2$ | $\sigma_g^2$ | $\pi_u^4$ | $\pi_g^2$ | ··· |
| *g* | $\sigma_g$ | $\pi_u^3$ | $\pi_g^3$ | $\sigma_u$ | $\sigma_g^2$ | $\pi_u^2$ | $\pi_g^4$ | ··· |
| *h* | $\sigma_g$ | $\pi_u^3$ | $\pi_g^3$ | $\sigma_u$ | $\sigma_g$ | $\pi_u^3$ | $\pi_g^3$ | $\sigma_u$ |
| *i* | $\sigma_g$ | $\pi_u^3$ | $\pi_g^3$ | $\sigma_u$ | $\sigma_g$ | $\pi_u^3$ | $\pi_g^3$ | $\sigma_u$ |
| *j* | ··· | ··· | ··· | ··· | ··· | $\pi_u^4$ | $\pi_u^2$ | $\sigma_u^2$ |
| *k* | ··· | ··· | ··· | ··· | ··· | $\pi_u^2$ | $\pi_u^4$ | $\sigma_u^2$ |
| *l* | ··· | ··· | ··· | ··· | ··· | $\pi_u^4$ | $\pi_u^4$ | ··· |

Diagonalization of high accuracy was performed by Whirlwind, the M.I.T. high-speed electronic digital computer. Using an 8-decimal digit capacity, the machine guaranteed 7 digits in the eigenvalues and about 4 in the eigenvectors. Actually, it is unfair to talk so of the accuracy in the eigenvectors. One might interpret the variation theorem as the statement that an eigenvector need, possibly can, only be determined to about half the digital accuracy of the corresponding eigenvalue. In any case, we can now proceed to the presentation and discussion of results.

## IX. RESULTS

### Eigenvalues

Table III is a rather too detailed specification of the configurations. It is sufficient and perhaps less confusing to tabulate the states as in Table IV. Here, all that is specified is the space orbital assignment. In fact, only the absolute value of the orbital angular momentum is indicated. (A molecular orbital is symbolized by a Greek small script letter ($\sigma, \pi, \delta, \cdots$) to indicate the absolute value of the axial angular momentum (0, 1, 2, ···) and a subscript ($g$ or $u$) to indicate even or odd parity.) The specified character of the states dictates how spin and orbital motion directions are to be assigned and the determinants grouped.

The triplet state labeled *c* is the one that would be used in single configuration theory. It represents the Hund-Mulliken approximation described above. Similarly, the singlet state labeled *f* would be taken as the first approximation to the higher-state of the molecule. Hund's rule finds expression in the matrix where the diagonal energy of the triplet is indicated to be less than that of the singlet by twice the value of an exchange integral.[11] The exchange integral is positive and does not vanish at infinite separation. This persistent energy difference between the singlet and triplet states is one aspect of the incompleteness of single configuration theory. The problem is to maintain the order of states at molecular distances while allowing both states to decompose into two normal oxygen atoms at infinite separation.

Though single configuration theory is wrong at large distances, it is often used for calculations of the dissociation energy. Table V lists the diagonal matrix elements of state *c* and state *f* as functions of internuclear distance. The equilibrium separation of oxygen is 2.28 atomic units, and the dissociation energy is 0.3735 atomic units.[12] State *c* is a miserable representation of actuality. It might very well be argued that the use of Gaussians distorts the theory considerably. Accepting this, it is really quite heartening to see what configuration interaction will do. Table VI lists the energy levels which are the eigenvalues of the matrices which describe the configuration interaction. Before discussing the improvement in dissociation energy, let us first point out the continuity from defined atomic states of various degrees of excitation, ionicity, and degeneracy to the set of noninteracting molecular states. The lowest singlet state still lies above the lowest triplet state at large distances. Both rise coincidentally until about 4 atomic units. From here on in, the molecule takes shape; the triplet energy takes a sharp bonding fall and the singlet state lags above it.

To get a better judgment of the predicted binding energies by other than graphical means, Morse curves can be introduced. This has been done for the lowest triplet and the lowest singlet. The energy is expressed as

$$E=A+D[1-e^{-a(R-R_0)}]^2.$$

The four parameters were determined by forcing agreement with the calculated energy values at $R=1.5$, 2.0, 2.5, and 4.0.[13] For the triplet state

$$A=-0.3728$$
$$D=0.5079$$
$$a=1.649$$
$$R_0=2.255$$

and for the singlet state

$$A=-0.2109$$
$$D=0.3205$$
$$a=1.760$$
$$R_0=2.30.$$

$A$ is, of course, the depth of the energy curve which has its minimum at $R=R_0$. The binding, or dissociation,

TABLE V. Single configuration approximation energies.

| $R$ | 1.5 | 2.0 | 2.5 | 4.0 | 6.0 | 9.0 | ∞ |
|---|---|---|---|---|---|---|---|
| $^3\Sigma_g^-$ | 2.78263 | −0.11554 | −0.11205 | 0.99287 | 1.26201 | 1.37476 | 1.59798 |
| $^1\Sigma_g^+$ | 3.03784 | 0.12248 | 0.11047 | 1.19632 | 1.46401 | 1.57663 | 1.79983 |

[11] The formulas for the matrix elements and the numerical material not included in this paper will be available in a technical report of the Solid State and Molecular Theory Group of M.I.T.

[12] G. Herzberg, *Spectra of Diatomic Molecules* (D. Van Nostrand Company, New York, 1950).

[13] The *a* in the formula is not related to the *a* of the atomic orbitals.

TABLE VI. Final energy values.

| | $R$ | 1.5 | 2.0 | 2.5 | 4.0 | 6.0 | 9.0 | ∞ | Atomic multiplet |
|---|---|---|---|---|---|---|---|---|---|
| | | 2.72829 | −0.23468 | −0.31694 | 0.08042 | 0.00149 | −0.00007 | 0.00000 | $O\ O\ {}^3P{}^3P$ |
| | | 6.40877 | 1.54484 | 0.83050 | 0.27940 | 0.20262 | 0.20169 | 0.20185 | $O\ O\ {}^3P{}^1D$ |
| | | 7.76336 | 2.38823 | 1.22172 | 0.30399 | 0.20344 | 0.20179 | 0.20185 | $O\ O\ {}^3P{}^1D$ |
| | | 8.29122 | 3.01394 | 1.87352 | 0.65839 | 0.50607 | 0.50456 | 0.50463 | $O\ O\ {}^3P{}^1S$ |
| | $^3\Sigma_g^-$ | 8.78366 | 3.46764 | 1.94880 | 0.97060 | 1.0196 | 1.12510 | 1.34567 | $O^+\ O^-\ {}^4S{}^3P$ |
| | | 10.4106 | 4.00478 | 2.27794 | 1.2630 | 1.3133 | 1.42527 | 1.64844 | $O^+\ O^-\ {}^2D{}^3P$ |
| | | 10.5320 | 4.46958 | 2.53580 | 1.2724 | 1.3224 | 1.42787 | 1.64844 | $O^+\ O^-\ {}^2D{}^3P$ |
| | | 10.9300 | 4.70011 | 3.11485 | 1.5104 | 1.5160 | 1.62718 | 1.85030 | $O^+\ O^-\ {}^2P{}^3P$ |
| | | 14.4078 | 6.54955 | 4.62401 | 3.9510 | 4.5439 | 4.99493 | 5.88731 | $O^{++}O^-\ {}^3P{}^1S$ |
| | | 2.79791 | −0.05417 | −0.18362 | 0.07800 | 0.00147 | −0.00004 | 0.00000 | $O\ O\ {}^3P{}^3P$ |
| | | 2.99230 | 1.62544 | 0.96468 | 0.18686 | 0.00234 | 0.00000 | 0.00000 | $O\ O\ {}^3P{}^3P$ |
| | | 5.73553 | 1.92591 | 1.04601 | 0.45875 | 0.40500 | 0.40369 | 0.40370 | $O\ O\ {}^1D{}^1D$ |
| | | 6.73148 | 2.46215 | 1.39478 | 0.48964 | 0.40564 | 0.40370 | 0.40370 | $O\ O\ {}^1D{}^1D$ |
| | | 6.84833 | 2.67301 | 1.52243 | 0.59051 | 0.40635 | 0.40371 | 0.40370 | $O\ O\ {}^1D{}^1D$ |
| | | 8.07864 | 3.79130 | 1.73972 | 0.79866 | 0.70916 | 0.70657 | 0.70648 | $O\ O\ {}^1S{}^1D$ |
| | $^1\Sigma_g^+$ | 9.17578 | 3.85523 | 2.21663 | 1.1319 | 1.0107 | 1.00919 | 1.0093 | $O\ O\ {}^1S{}^1S$ |
| | | 10.5099 | 4.37816 | 2.62522 | 1.2745 | 1.3133 | 1.42526 | 1.64844 | $O^+\ O^-\ {}^2D{}^3P$ |
| | | 10.6910 | 4.82006 | 3.03125 | 1.4799 | 1.5159 | 1.62718 | 1.85030 | $O^+\ O^-\ {}^2P{}^3P$ |
| | | 10.7902 | 5.36583 | 3.28579 | 1.5122 | 1.5243 | 1.62972 | 1.85030 | $O^+\ O^-\ {}^2P{}^3P$ |
| | | 11.8867 | 6.75097 | 4.82246 | 4.2524 | 4.7679 | 5.20356 | 6.08917 | $O^{++}O^-\ {}^1D{}^1S$ |
| | | 14.7282 | 7.01370 | 5.09405 | 4.5536 | 5.0610 | 5.50306 | 6.39193 | $O^{++}O^-\ {}^1S{}^1S$ |

energy is calculated from $A$ by correcting for the zero-point vibrational energy of the nuclei. The use of a Morse potential leads to the formula for the dissociation energy $D_0$ as

$$D_0 = A + a(D/\mu)^{\frac{1}{2}} - (a^2/4\mu),$$

where $\mu$ is the mass of an oxygen atom, all quantities given in atomic units.[12]

Another interesting quantity that can be calculated from a Morse curve is the fundamental vibrational frequency $\omega_e$, the frequency with which the nuclei would vibrate if the vibration were a simple harmonic one

$$\omega_e = 2a(D/\mu)^{\frac{1}{2}}.$$

Table VII compares the results of this calculation with the experimental values. Figure 2 is a graph of the Morse curves.[14] The triplet state evolved out of the interaction of nine states which take account of the spin and orbital degeneracies is energetically close to the truth, the limit of truth being set by the variation theorem. Going from the single-configuration to many-configuration theory not only netted us an exceedingly good ground-state energy with correct behavior at infinity, but it also yielded a very good curvature to the energy curve. This point is revealed in the agreement in $\omega_e$. In calculations on a solid, single-configuration theory can be made to give excellent energies, but estimates of compressibility are bound to suffer the effects of the rise of the energy curve to a wrong value at large distances.[15] This is illustrated in Fig. 3 which is a plot of the diagonal energy of state $c$ alongside the true energy curve.

The singlet state does not come out so well. The error in binding energy is about 19 percent, the harmonic frequency is very bad. Moffitt's main criticism is directed at calculations on the higher states of a molecule and this investigation perhaps bears him out. The point he makes is that even the comparatively large number of configurations used in a calculation such as this is not a large enough number to yield a decent picture of the energy levels of the separated atoms. In fact, in so far as the atomic levels are concerned, there is no configuration interaction being considered. The single configuration theory, which we have seen to be very poor for the molecule, is also poor for the atom. We have an inaccurate energy scale of the separated atoms and Moffitt maintains that the excitation energies of the higher molecular states with respect to the ground state are badly in error because of this. The results of this investigation indicate that the ground

[14] The author has been warned that some confusion might arise at this point. It is to be remembered that the Morse curve is supposed to represent the results of this calculation only from about $R=4.0$ inward. From $R=4.0$ to $R=\infty$ a continuous curve is drawn which drops down to the axis as demanded by the calculated values at $R=6.0$, 9.0, and ∞. The quantity $D_0$ is, except for the zero-point correction, the energy difference of the stable molecule and the dissociated atoms. It is this quantity which is experimentally determined by analysis of band spectra. (See Herzberg, reference 12.) The energy of the dissociated atoms is zero on our energy scale. The dotted asymptotic limits of the Morse curves appear in Fig. 2 for purposes of later discussion; they do not represent the molecular dissociation. The full curve does.

TABLE VII. Molecular parameters.

| Param. | Exper. | Calc. | Percent error | |
|---|---|---|---|---|
| $R^0$ | 2.28 | 2.255 | 1.1 | |
| $D_0$ | −0.3735 | −0.3660 | 2 | $^3\Sigma_g^-$ |
| $\omega_e(\text{cm}^{-1})$ | 1580.4 | 1503 | 4.2 | |
| $R^0$ | 2.32 | 2.30 | 0.9 | |
| $D_0$ | −0.2527 | −0.2051 | 19 | $^1\Sigma_g^+$ |
| $\omega_e(\text{cm}^{-1})$ | 1432.7 | 1273 | 11 | |

[15] P. O. Löwdin, J. Chem. Phys. 19, 1579 (1951).

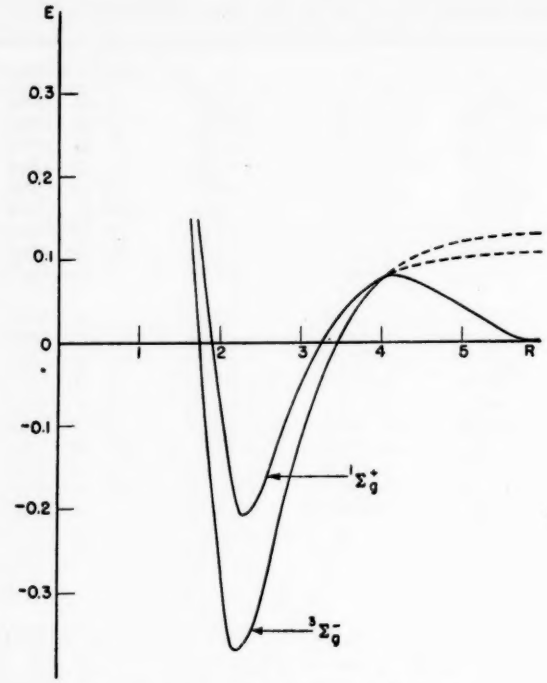


FIG. 2. Morse curve fit to electronic energy.

state itself can be very closely approached even with this inherent fault of the method. As for the higher states, a correction more in the spirit of the calculation than Moffitt's empirical adjustment might be the inclusion of configurations where the $2s$ electrons, say, were promoted into $2p$ levels. These new configurations need not be treated on equal footing with the other existing ones. That is, perturbation methods might be used to add the little more that is needed.

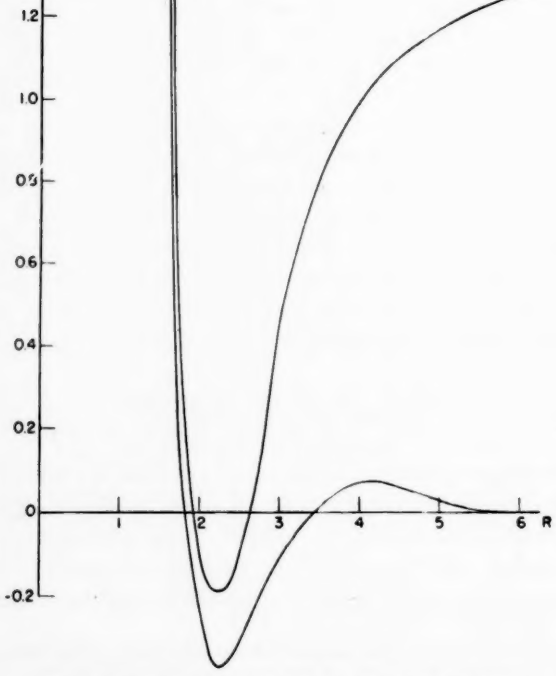


FIG. 3. Single-configuration energy *vs* true energy.

It is worth while to plot the difference in energy between the singlet and triplet states, as in Fig. 4. This curve is typical of a magnetic competition. The magnetic and nonmagnetic states start out indistinguishable from one another until the magnetic state steeply becomes preferential only to rapidly approach the other state again—perhaps to rise to the unpreferred position—as the internuclear distance decreases.

## Eigenvectors

The eigenvectors of the lowest triplet and the lowest singlet states are displayed in Table VIII. (An erratic behavior of the singlet vector at large distances is illusory. The singlet state is doubly degenerate at infinite separation; the computer was somewhat capricious in its choice of ground-state eigenvector at large distances.) From the eigenvectors also, one can see a slow change at large internuclear distance and then the very rapid component readjustment in the molecular region. From $R=4.0$ inward, state $c$ becomes the dominant axis for the triplet and state $f$ predominates for the singlet.

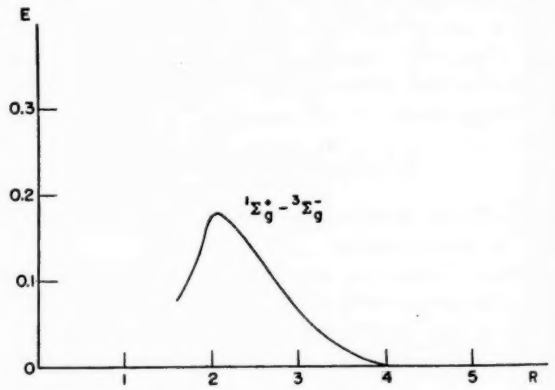


FIG. 4. Triplet-energy difference.

The lack of difference between the triplet and singlet states at large internuclear distances can be shown by transforming to an atomic rather than a molecular representation. At infinite separation we have the eigenvectors which represent the various atomic states. We can express an eigenvector at any other value of internuclear separation as a linear combination of those orthonormal vectors which asymptotically describe the atomic constituents. This has been done in Table IX for the lowest triplet and singlet states. This table would have been the initial table of eigenvectors if orthogonalized atomic functions of the Wannier type had been used instead of the symmetrical molecular orbitals.[16]

[16] For the same type of base transformation applied to the hydrogen molecule and analyzed in detail, see J. C. Slater, J. Chem. Phys. **19**, 220 (1951).

TABLE VIII. Ground-state eigenvectors.

| $R$ | 1.5 | 2.0 | 2.5 | 4.0 | 6.0 | 9.0 | ∞ |
|---|---|---|---|---|---|---|---|
| | | | $^2\Sigma_g^-$ | | | | |
| *a* | 0.0058 | 0.0117 | 0.0240 | 0.0044 | 0.0000 | 0.0000 | 0.0000 |
| *b* | 0.0055 | 0.0104 | 0.0179 | 0.0077 | 0.0000 | 0.0000 | 0.0000 |
| *c* | −0.9957 | −0.9849 | −0.9668 | −0.4361 | −0.3538 | −0.3536 | −0.3536 |
| *d* | 0.0475 | 0.1041 | 0.1548 | 0.4005 | 0.3537 | 0.3536 | 0.3536 |
| *e* | 0.0387 | 0.0646 | 0.0956 | 0.3263 | 0.3534 | 0.3536 | 0.3536 |
| *f* | −0.0047 | −0.0182 | −0.0455 | −0.3161 | −0.3534 | −0.3536 | −0.3536 |
| *g* | −0.0517 | −0.0946 | −0.1424 | −0.4785 | −0.5000 | −0.5000 | −0.5000 |
| *h* | −0.0449 | −0.0728 | −0.0924 | 0.4626 | 0.5000 | 0.5000 | 0.5000 |
| *i* | −0.0047 | −0.0124 | −0.0218 | −0.0026 | 0.0000 | 0.0000 | 0.0000 |
| | | | $^1\Sigma_g^+$ | | | | |
| *a* | 0.0166 | −0.0108 | −0.0164 | 0.0148 | 0.3093 | 0.4723 | 0.4269 |
| *b* | −0.0446 | 0.0010 | −0.0031 | −0.0004 | 0.0003 | −0.0001 | 0.0000 |
| *c* | −0.9025 | −0.0284 | −0.0515 | −0.0218 | −0.2677 | −0.4092 | −0.3697 |
| *d* | −0.0070 | 0.0018 | 0.0022 | −0.0078 | −0.2678 | −0.4092 | 0.3697 |
| *e* | −0.0846 | 0.0046 | 0.0130 | 0.0201 | 0.3790 | 0.5784 | 0.5229 |
| *f* | 0.4167 | 0.9718 | 0.9390 | 0.5035 | 0.3403 | 0.1418 | 0.2254 |
| *g* | −0.0369 | −0.1941 | −0.2848 | −0.4805 | −0.3403 | −0.1419 | −0.2254 |
| *h* | 0.0262 | 0.1018 | 0.1402 | 0.2423 | 0.1965 | 0.0819 | 0.1301 |
| *i* | 0.0104 | 0.0264 | 0.0049 | −0.4114 | −0.3402 | −0.1419 | −0.2254 |
| *j* | −0.0060 | −0.0653 | −0.1017 | −0.3844 | −0.3401 | −0.1419 | −0.2254 |
| *k* | −0.0022 | −0.0240 | −0.0569 | −0.3724 | −0.3401 | −0.1419 | −0.2254 |
| *l* | 0.0123 | 0.0331 | 0.0297 | 0.0021 | 0.0000 | 0.0000 | 0.0000 |

With orthogonal orbitals, it is the closest we can get to the projection on the Heitler-London framework promised earlier.

Table IX clearly shows that a single-configuration theory based on orthogonalized atomic functions would have been quite good for large distances. The singlet cannot be distinguished from the triplet. The picture is that of two normal oxygen atoms approaching one another, repelling one another until about 4 atomic units of separation. Excited and ionized states are now to be considered in the formation of the molecular states. At equilibrium separation, the atomic correspondence is completely smeared; any attempt at a perturbation calculation would have to start from the molecular orbital setup. Incidentally, second-order perturbation does not work here. One does not converge to anything like the right value by considering state *c* as the zeroth-order wave function and computing the energy by a formula such as

$$E=H_{cc}+\sum_k \frac{|H_{ck}|^2}{E-H_{kk}}.$$

There are many other large off-diagonal elements, indirect chains between state *c* and other states. However, it should be noted that states *c*, *d*, *e*, *f*, *g*, and *h*, which

TABLE IX. Ground-state eigenvectors atomic correspondence.

| $R$ | | 1.5 | 2.0 | 2.5 | 4.0 | 6.0 | 9.0 | ∞ |
|---|---|---|---|---|---|---|---|---|
| | | | | $^2\Sigma_g^-$ | | | | |
| *O O* | $^3P^3P$ | 0.3875 | 0.4252 | 0.4714 | 0.9934 | 1.0000 | 1.0000 | 1.0000 |
| *O O* | $^3P^1D$ | 0.2539 | 0.2719 | 0.2843 | 0.0437 | 0.0000 | 0.0000 | 0.0000 |
| *O O* | $^3P^1D$ | 0.4179 | 0.4343 | 0.4533 | 0.0333 | 0.0000 | 0.0000 | 0.0000 |
| *O O* | $^3P^1S$ | 0.2098 | 0.2091 | 0.2037 | 0.0062 | 0.0000 | 0.0000 | 0.0000 |
| $O^+$ $O^-$ | $^4S^2P$ | −0.4037 | −0.3857 | −0.3645 | −0.0202 | 0.0000 | 0.0000 | 0.0000 |
| $O^+$ $O^-$ | $^2D^2P$ | −0.0633 | −0.0411 | −0.0201 | 0.0276 | 0.0000 | 0.0000 | 0.0000 |
| $O^+$ $O^-$ | $^2D^2P$ | −0.4492 | −0.4430 | −0.4265 | −0.0698 | 0.0000 | 0.0000 | 0.0000 |
| $O^+$ $O^-$ | $^2P^2P$ | −0.3496 | −0.3483 | −0.3340 | −0.0632 | 0.0000 | 0.0000 | 0.0000 |
| $O^{++}O^{--}$ | $^3P^1S$ | 0.2749 | 0.2112 | 0.1520 | 0.0011 | 0.0000 | 0.0000 | 0.0000 |
| | | | | $^1\Sigma_g^+$ | | | | |
| *O O* | $^3P^3P$ | 0.4043 | 0.2982 | 0.3467 | 0.5443 | 0.9371 | 0.9772 | 1.0000 |
| *O O* | $^3P^3P$ | −0.0098 | 0.4720 | 0.5282 | 0.8305 | 0.3488 | −0.2120 | 0.0000 |
| *O O* | $^1D^1D$ | 0.2342 | −0.1169 | −0.1019 | −0.0018 | −0.0005 | 0.0002 | 0.0000 |
| *O O* | $^1D^1D$ | 0.3305 | 0.1275 | 0.1181 | −0.0020 | −0.0003 | 0.0002 | 0.0000 |
| *O O* | $^1D^1D$ | −0.1844 | −0.3394 | −0.3363 | −0.0227 | 0.0001 | 0.0000 | 0.0000 |
| *O O* | $^1S^1D$ | −0.1647 | −0.1001 | −0.1019 | −0.0019 | 0.0000 | 0.0000 | 0.0000 |
| *O O* | $^1S^1S$ | 0.0244 | −0.1981 | −0.1715 | −0.0026 | 0.0000 | 0.0001 | 0.0000 |
| $O^+$ $O^-$ | $^2D^2P$ | −0.6052 | −0.3958 | −0.4035 | −0.0873 | 0.0000 | 0.0000 | 0.0000 |
| $O^+$ $O^-$ | $^2P^2P$ | 0.3333 | −0.2315 | −0.2338 | −0.0651 | 0.0000 | 0.0000 | 0.0000 |
| $O^+$ $O^-$ | $^2P^2P$ | 0.0997 | 0.4977 | 0.4357 | 0.0380 | 0.0000 | 0.0000 | 0.0000 |
| $O^{++}O^{--}$ | $^1D^1S$ | −0.3367 | −0.1156 | −0.0810 | −0.0008 | 0.0000 | −0.0001 | 0.0000 |
| $O^{++}O^{--}$ | $^1S^1S$ | 0.0994 | −0.1500 | −0.0993 | −0.0008 | 0.0001 | 0.0001 | 0.0000 |

are the important ones at molecular separations, are the only ones necessary (and all are necessary) to represent two normal oxygen atoms at infinite separation. Is there some good rule of thumb here? Choose the molecular orbitals to be definitely non-atomic, clearly of a "molecular" type. Then consider the configurations necessary to represent the ground state atoms and allow only those configurations to interact. The procedure may be of help for bigger systems.

One last point: the energy curve has a hump. The usual Morse curve representation of a molecular energy curve has the axis as its asymptote; ours, in order to fit four calculated points, must approach a definitely positive value at infinity. We have tried to find some experimental evidence of this hump but there does not seem to be any clear-cut way of exhibiting it or denying it. The vibrational levels come in the right places, but they have not been observed high enough so that the hump would have any unique effect. However, it seems that other people have considered an energy curve which extrapolates to a positive height at infinite separation.

Pauling[17] has been led to the concept of the valence state of an atom, a hypothetical state which is not "one of the stationary spectroscopic states of the isolated atoms, but . . . is defined as that state in which it (the atom) has the same electronic structure as it has in the molecule." In the paper referred to, Pauling deduces the value of the energy of this state by four different methods all of which agree reasonably well with one another. One of the methods is an extrapolation of the vibrational levels, the introduction of a Morse curve which goes to 6.69 ev at infinite separation. (Ours goes to 6.91 ev.) We have not been able to do more with this concept of the valence state, but the fact that it has been introduced lends credence to the hump, or vice versa.

In conclusion, may we again emphasize the fortunate situation with oxygen, that a fairly complete treatment of configuration interaction did not exceed human endurance and machine storage capacity. Except for oxygen and a few other very simple molecules, it is ridiculous to tabulate all the configurations arising from the atomic primitive set of orbitals, as has been done here. It is necessary to have an *a priori* measure by weight of the secular determinant, to be able to say that this configuration is important, this is not. Configuration interaction is imperative if orbital theory is to be used but it must be handled in a manner that does not surge to impracticability.


## ACKNOWLEDGMENT

Mrs. Neria K. Ryder, of the Massachusetts Institute of Technology Joint Computing Section, was a most capable aid in the numerical work. The success with Whirlwind is due largely to the guidance of Dr. John W. Carr and Dr. Allan Perlis, of the Whirlwind Mathematics Group, who revealed and taught the technique of diagonalization to the author.

The Solid State and Molecular Theory Group at M.I.T. is that in which the author learned and did most of the physics in this article, receiving both stimulation and encouragement from the members of the group. The greatest debt is to Professor John C. Slater who suggested the problem and stood as a certain and revitalizing source of knowledge.


## APPENDIX I. ORBITAL EQUIVALENCE THEOREM[18]

Let $u_i$ be a set of $N$ independent one-electron functions. If there are $n(\leqslant N)$ electrons, form $n$ independent combinations of the $u_i$'s,

$$\varphi_i=\sum_j c_{ij}u_j \qquad \begin{matrix}1\leq i\leq n\\ 1\leq j\leq N,\end{matrix}$$

where the $c_{ij}$'s are as yet undetermined. Putting in the symbol for the electronic coordinates (space and spin) we get a matrix relation

$$\varphi_i(x_k)=\sum_j c_{ij}u_j(x_k),$$

or

$$\mathbf{\Phi}\quad \mathbf{CU}.$$

That is, the square matrix $\mathbf{\Phi}$ is the product of two rectangular matrices: $\mathbf{C}$ which is an $n\times N$, and $\mathbf{U}$ which is an $NXn$. The many-electron wave function is essentially the determinant of $\mathbf{\Phi}$. A determinant is definable only for a square matrix, but it is possible to express the determinant of the product of two rectangular matrices in a significant way.[19] It turns out that the determinant of the product is the sum of products of minors taken from the two rectangular matrices. Begin with the first $n$ columns of $\mathbf{C}$. Multiply the determinant of this $n\times n$ submatrix by the minor formed from the corresponding first $n$ rows of $\mathbf{U}$. The other products in the expansion are formed in the same way. A minor consisting of a selection of $n$ columns of $\mathbf{C}$ is the coefficient of the minor formed from the selection of the corresponding rows of $\mathbf{U}$. But this expansion is the starting point of configuration interaction. The many-electron wave function is a linear combination of the $N!/n!(N-n)!$ determinants formed from the $N$ $u_i$'s. The minors of $\mathbf{C}$ are the coefficients which are to be varied until the Hamiltonian is made diagonal.

This is a somewhat stilted way of getting at configuration interaction, but the equivalence theorem becomes trivial in this formalism. Let

$$v_j=\sum_i R_{ji}u_i$$

be a determined linear combination of the original set.

[17] L. Pauling, Proc. Natl. Acad. Sci. **35**, 229 (1949).

[18] A proof along similar lines was given by P. O. Löwdin in the Quart. Prog. Report of the M.I.T. Solid-State and Molecular Theory Group (January, 1952).

[19] A. G. Aitken, *Determinants and Matrices* (Oliver and Boyd, London, 1939).

Proceeding in the same way as before, we set up

$$\varphi_i(x_k)=\sum_j d_{ij}v_j(x_k)=\sum_{jl} d_{ij}R_{jl}u_l(x_k).$$

Again, there is a rectangular $n\times N$ matrix multiplied by the rectangular $N\times n$ **U** matrix. Since the minors of the former are to be varied anyway, set

$$\mathbf{C}=\mathbf{DR} \quad c_{il}=\sum_j d_{ij}R_{jl}$$

and equivalence is established. Because of the determinantal form of the many-electron wave function, the arbitrariness in the base system of one-electron space carries right through to an arbitrariness in the base system of many-electron space.

## APPENDIX II. SPIN ALGEBRA

Let **s** represent the vector operator of one-electron spin. It can be decomposed into three Cartesian components obeying the following commutation rules:

$$s^2s_x-s_xs^2=0$$
$$s_xs_y-s_ys_x=is_z$$
$$s_xs_y+s_ys_x=0$$
$$s_x^2=\tfrac{1}{4}$$
$$s^2=s_x^2+s_y^2+s_z^2=\tfrac{3}{4}.$$

The above formulas are to be completed, of course, by the cyclic substitution of $x$, $y$, and $z$.

Spin eigenfunction and spin eigenvalue are codefined by

$$s_z\alpha=\tfrac{1}{2}\alpha$$
$$s_z\beta=-\tfrac{1}{2}\beta.$$

We will also use the well-known "step-up" and "step-down" operators defined by

$$s_+\alpha=0 \quad s_-\alpha=\beta$$
$$s_+\beta=\alpha \quad s_-\beta=0,$$

or explicitly

$$s_+=s_x+is_y$$
$$s_-=s_x-is_y.$$

The combinatorial rules of a many-electron spin system are simple,

$$\mathbf{S}=\sum_i \mathbf{s}_i$$
$$S_z=\sum_i s_{iz}.$$

These lead to

$$S^2=\sum_i s_i^2+\sum_{i\neq j}\mathbf{s}_i\cdot\mathbf{s}_j$$

and

$$\mathbf{s}_i\cdot\mathbf{s}_j=s_{ix}s_{jx}+s_{iy}s_{jy}+s_{iz}s_{jz}=\tfrac{1}{2}s_{i+}s_{j-}+\tfrac{1}{2}s_{i-}s_{j+}+s_{iz}s_{jz},$$

so that

$$S^2=\sum_i s_i^2+\sum_{i\neq j}s_{i+}s_{j-}+\sum_{i\neq j}s_{iz}s_{jz}.$$

This operator is to be applied to a determinantal wave function, whose antisymmetrical nature narrows things down. The first term

$$\sum_i s_i^2$$

transforms a configuration into itself multiplied by $\frac{3}{4}n$, where $n$ is the number of electrons. The last term

$$\sum_{i\neq j}s_{iz}s_{jz}$$

also does not change the configuration. The multiplication factor is the same for all states having $S_z=0$, for

$$\sum_{i\neq j}s_{iz}s_{jz}=\sum_i{}'\, s_{iz}\sum_j{}'\, s_{jz},$$

where the prime denotes summation over all electrons except the $i$'th. If $S_z=0$, then this inner summation is effectively

$$-s_{iz},$$

and the whole double-summation effectively acts like

$$\sum_i -s_{iz}^2$$

which is equal to $-n/4$.

It is only the step-up step-down term which transforms one configuration into another. The term

$$\sum_{i\neq j}s_{i+}s_{j-}$$

says that we are to take each $+$ and $-$ couple and flip the signs. The flipping of a pair located in one spatial orbital column (Table III) can be interpreted as an interchange of two electrons in the standard arrangement; the configuration is transformed into its negative. We cannot flip only one of the spin functions of a spatial orbital pair because we would then have two electrons occupying the same space-spin orbital and subsequent antisymmetrization would yield a null determinant. The flipping of a spin pair taken from singly occupied space orbitals produces another configuration. The interconnections of the various configurations are simple and the proper combinations can be immediately ascertained.

## APPENDIX III. INEQUALITIES

The symbol $(uv|wz)$ stands for

$$\int u^*(1)v(1)\frac{2}{r_{12}}w^*(2)z(2)dx_1dx_2.$$

Roothaan's inequalities are

$$0\leq(uv|vu)\leq(uu|vv)\leq\frac{(uu|uu)+(vv|vv)}{2}.$$

The first integral is commonly called the "exchange" integral and it is positive definite. The other integrals are called "Coulomb" integrals. We have derived another inequality, a geometric mean inequality, and one that brings in the so-called "hybrid" integrals. We begin with the positive definiteness of any exchange integral.

In particular

$$[(Au+v)w|w(Au+v)]\geq 0.$$

In expanded form

$$A^2(uw|wu)+2A(uw|wv)+(vw|wv)\geq 0.$$

That is, this second-degree polynomial in $A$ can have either no real roots or one doubly degenerate real root. The following inequality among the coefficients is nesessary and sufficient:

$$(uw|wv)^2\leq (uw|wu)(vw|wv).$$

THE JOURNAL OF CHEMICAL PHYSICS VOLUME 21, NUMBER 10 OCTOBER, 1953

# The Photochemical Separation of Isotopes

BRUCE H. BILLINGS AND W. J. HITCHCOCK, *Research Laboratory, Baird Associates, Inc., Cambridge, Massachusetts*

AND

MURRAY ZELIKOFF, *Air Force Cambridge Research Center, Cambridge, Massachusetts*

(Received April 3, 1952)

A method of successfully separating mercury isotopes by a photochemical process is described. The method involves the use of a monoisotopic resonance lamp as the source of light for the photochemical reaction. In this particular case a $Hg^{198}$ lamp was used to excite only the $Hg^{198}$ atoms. The excited Hg atoms react with water vapor to produce enriched mercuric oxide. In the first experiments an enrichment factor of 1.5 was obtained.

The analysis of the isotopes was undertaken by the use of multilayer dielectric Fabry-Perot interferometers.

## I. INTRODUCTION

IN almost all the existing practical methods of separating isotopes, the separation factor of a single stage of the equipment is some function of the mass ratio. This factor is the ratio of the relative abundance of the desired isotopes in the output to the relative abundance in the input material. For typical substances with typical separation methods,[1] it runs from 1.1 to 1.006. There are a few methods which are able to achieve single-stage factors greater than unity. One such method is the mass spectrograph. This paper is concerned with another method which has the possibility of yielding a large separation factor.

### Photochemical Separation of Isotopes

This technique involves the separation of isotopes by a photochemical reaction. There have been several attempts in the literature to obtain such photochemical isotope separation, some of which seem to have had a small amount of success.[2,3]

There are three fundamental principles and conditions which must be fulfilled before an isotopic separation can be made. These are:

(1) The absorption spectra of either the isotope itself or some compound containing the isotope should be different for the two isotopes at some wavelength. For example, if the element is a gas, then the absorption spectrum of the vapor will, in general, be different for different isotopes because of the various kinds of isotope shifts. If the material is a compound, then perhaps the dissociation limit will be different for different isotopes. If the material is in a liquid or solid and sharp absorption lines occur, then these lines may be separated or in some particular cases actually absent for different isotopes.

(2) A light source must be found which is of sufficiently narrow spectral band width that it will excite only one particular isotopic species, whether it is an atom or a compound. This particular light source can, in principle, be obtained by many methods. The method which is used here, which has been extremely successful, is the use of a light source made up of only one isotope. The excited radiation emitted from this isotope is absorbed only by one isotope if the lines are sufficiently narrow.

It is also possible to use broad band sources if filters are used which will filter out the light absorbed by only one isotope. If the isotope involved is not very abundant in the naturally occurring element, it is possible to use this naturally occurring element as an absorption filter, since the isotopic constituents in high concentration will preferentially absorb the light. Other filters can be narrow band transmission or reflection filters which admit the light desired.

Occasionally, there may be certain atomic lines which will occur at just the right place to excite a molecular species containing only one isotope. Under these fortuitous circumstances a partial separation is also possible.

(3) A reaction of the excited atom or molecule must

[1] W. Walcher, Ergeb. Exakt. Naturw. p. 155 (1939).
[2] Merton, Ponder, Bowen, and Hartley, Phil. Mag. **43**, 430 (1922).
[3] K. Zuber, Helv. Phys. Acta **9**, 285 (1936).

be found in which the excited species will react and the unexcited species will not react. If the reaction is one of dissociation of a molecule into a radical, then it is relatively simple to find a reaction for that radical in which the molecule will not react. If, however, the excited species is merely an excited atom, a reaction must be found in which the excited atom not only will take part but will undergo compound formation. Presumably such reactions do exist for a large number of atoms. However, very little work has been done with excited atom reactions, and it is not always known whether the excited atom takes part in the compound formation directly. The compound formation must not be followed by decomposition of the compound. If this occurs, the isotopic atom goes into the bulk of the material and is lost for enrichment purposes. If there is only one species of isotopic atom excited, then it is possible to study a number of reactions. Then, by determining the isotope ratio in the compounds formed, it is possible to obtain a good idea of the type of elementary processes involved.

TABLE I. Distribution of Hg isotopes according to various investigators.

| Isotope | Aston | Atomic Energy Commission |
|---|---|---|
| 204 | 6.85 | 6.7 |
| 202 | 29.27 | 29.6 |
| 200 | 23.77 | 23.3 |
| 198 | 9.87 | 10.1 |
| 196 | 0.10 | 0.15 |
| 201 | 13.67 | 13.2 |
| 199 | 16.45 | 17.0 |

## The Mercury 2537A Radiation

The work reported here grew out of the study of the fine structure of the mercury radiation. Mercury itself is peculiarly adaptable for preliminary investigations. Table I shows the isotope distribution in ordinary mercury as obtained by various investigators[4] using a mass spectrometer.

Lamps composed almost exclusively of $Hg^{198}$ are available.[5] The mercury resonance line of 2537A is often used in studies of photochemical reactions, and, in particular, the photosensitized reaction with water seems to be one in which only the sensitized mercury would form a compound.

The 2537A radiation from ordinary mercury has a fine structure which differs markedly from the fine structure of the 5461 line. The sketch in Fig. 1 taken from Schuler[6] shows the wavelength separations and intensities of the various components. It is apparent from this sketch that the 198 component is quite far removed from all components with the exception of

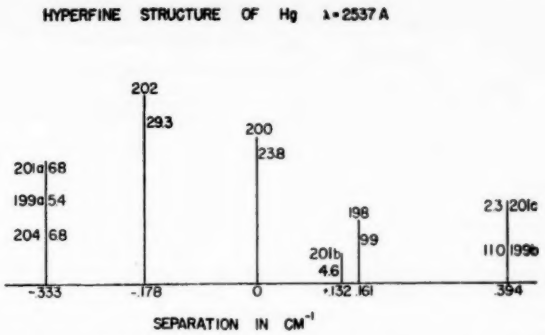


FIG. 1. Sketch of intensity and wavelength separation of the components of the mercury 2537 line.

the *b* component of 201. Accordingly, in the worst case one might expect some primary excitation of $Hg^{201}$ as well as $Hg^{198}$, if a 198 lamp is used to do the exciting.

## Previous Work on Separation of Hg Isotopes

The first attempt to separate the isotopes of mercury was made by Zuber.[3] He used the 2537A resonance line from a cold mercury arc, allowing it to pass through a Mrozowski[7] filter and then into a mercury vapor-oxygen mixture. After a period of irradiation the remaining mercury vapor was condensed out in a cold trap. Any oxide which had formed remained on the walls of the original reaction vessel. This oxide was decomposed by exposure to a hot mercury lamp and the isotopic composition measured.

Zuber reported a partial enrichment of some of the isotopic components. The amount of material involved was about $10^{-8}$ gram and was, in fact, never collected. Apparently oxygen alone was found to be unsuitable for the process, but dry air (containing $N_2$) improved the enrichment. Zuber suggests that possibly nitrogen oxides were formed in air, preventing secondary reactions which might obscure the enrichment. He recognized that in order to separate an isotope the excited mercury atom must react in the primary step to form the oxide and that the oxide must not engage in secondary reactions.

It is known that the action of excited mercury on oxygen results in ozone and mercuric oxide.[8] Because of the possibility of reaction between ozone and mercury, it was felt that the enrichment obtainable with the oxygen reaction would be small. Accordingly the experimental work was performed with a water-vapor reaction.

## II. EXPERIMENTAL WORK DONE ON Hg WATER-VAPOR REACTION

The work reported in this section was done merely as a preliminary investigation to test the method of isotope separation. Because of time limitation there was

[4] F. W. Aston, Proc. Roy. Soc. (London) **A115**, 509 (1927).
[5] This lamp is made by Baird Associates, Inc., Cambridge, Massachusetts.
[6] H. Schuler, Z. Physik **72**, 432 (1931).
[7] S. Mrozowski, Z. Physik **78**, 826 (1932).
[8] R. G. Dickinson and M. S. Sherrill, Proc. Natl. Acad. Sci. **12**, 175 (1926).

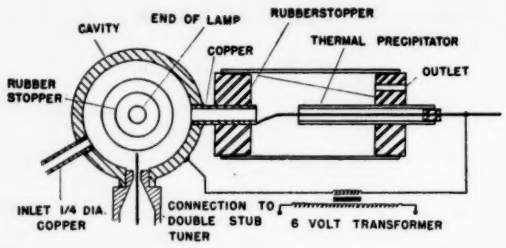


FIG. 2. Experimental arrangement for producing photochemical enrichment of mercury-198. The reaction takes place in the resonant cavity which is coupled to a magnetron oscillator through a double stub tuner.

no attempt made to make any necessary theoretical investigations or to attempt to optimize the conditions of reaction.

The experimental procedure involved four parts: (1) excitation of the mercury-198 discharge tube; (2) arrangement of the apparatus for the chemical reaction; (3) the procedure for collecting the purified separated material; (4) construction of discharge tube using purified material.

The discharge tubes were manufactured from pure mercury-198 which was obtained from gold that had been radiated in the pile at Oak Ridge. The tubes were 6 in. long and 7.7 mm o.d. and were made of Vycor glass so that a large percentage of the 2537 radiation would escape.

From work done at the National Bureau of Standards by Dr. William F. Meggers, it appears that the life of a Hg discharge tube goes up with the frequency of the electrodeless excitation. A magnetron radiating at approximately 3000 megacycles was used at the source of exciting radiation.

Several different experimental arrangements were made, and many of these gave successful runs. In the final system the lamp was held in a cavity which was coupled to the magnetron by a double stub tuner. The cavity was cylindrical, approximately 10 cm in diameter and was made of brass. The mercury vapor was obtained by bubbling nitrogen through an inch or so

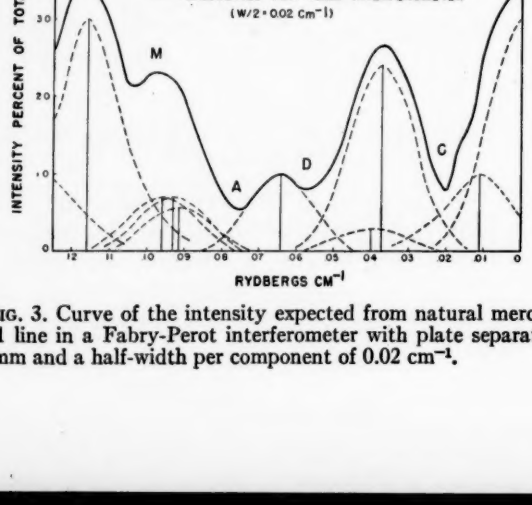


FIG. 3. Curve of the intensity expected from natural mercury 5461 line in a Fabry-Perot interferometer with plate separation 43 mm and a half-width per component of 0.02 $cm^{-1}$.

of mercury in the bottom of an Erlenmeyer flask. This was done in order to exclude oxygen from the mixture. It was felt that any ozone formed would react with the mercury to produce unenriched oxide. The stream of nitrogen was passed into the magnetron cavity which served both as the reaction chamber and as the lamp exciter. The lamp was excited through a water jacket consisting of a Vycor tube about 12 mm in diameter. From the cavity the vapor was passed through a hot wire precipitator.[9] The flow system was used so that the mercury oxide formed would not be decomposed by the 2537A line. The magnetron was run at a power level of approximately 20 watts. A sketch of the equipment is shown in Fig. 2.

When the apparatus was run, a deposit formed on the jacket of the precipitator. This deposit was washed off with nitric acid and a fine copper wire dipped into the solution. The mercury amalgamated the copper and was later distilled off into an evacuated glass tube to make an electrodeless lamp. Analysis of the enriched mercury was carried out with a Fabry-Perot interferometer. An example of this technique is shown by Walcher[10] for

TABLE II. Fabry-Perot measurement of isotope concentration ratios in an Atomic Energy Commission mercury sample. The measurement was made at the 5461A line.

| (1) Isotope | (2) Abundance as determined by the Atomic Energy Commission | (3 Relative abundance $C_x/C_{202}$ | (4) Relative intensity in Fabry-Perot 5461A line $I_x/I_{202}$ |
|---|---|---|---|
| 204 | 17.2 | 0.72 | 0.71 |
| 202 | 23.7 | 1.00 | 1.00 |
| 200 | 17.8 | 0.75 | 0.76 |
| 198 | 15.2 | 0.64 | 0.63 |

the analysis of lead isotopes in ores containing uranium. The analytical part of the work was done at the mercury green line at 5461A. This line was isolated by a combination of a multilayer interference filter and a piece of green gelatin. The excitation of the lamps made both with natural mercury and with mercury from the photochemical reaction was done at 150 mc. The suitability of the 5461A mercury line for measurement of isotope concentration was demonstrated by Sterner.[11] He manufactured a series of lamps from isotope mixtures provided by the Atomic Energy Commission. The excitation of the lamps was carried out with the same 150-mc exciter used in the analytical work associated with this paper. The results of his Fabry-Perot analysis on a typical sample are compared directly with the Atomic Energy Commission mass spectrographic analysis in Table II.

The work of Sterner[12] shows that it is possible to

[9] J. Brell and T. W. Brieve, J. Sci. Instr. (London) 28, 21 (1951).
[10] W. Walcher, Nucleonics 6, 28 (1950).
[11] J. Sterner, Ph.D. thesis, Massachusetts Institute of Technology, 1951.
[12] J. Sterner, Phys. Rev. 86, 139 (1952).

improve considerably on the Fabry-Perot interferometer as used with the customary metal films. This is by use of an all dielectric reflecting scheme which eliminates completely the absorption loss and makes possible a gain of nearly twenty-fold over the intensity of an ordinary interferometer, and, at the same time, an improvement in resolution is achieved for a given free spectral range. With these dielectric plates a spacer was selected which would leave the 198 component free from distortion by overlapping fringes of a higher order. A value of 43 mm was found for this spacer. By using the procedure outlined by McNally,[13] curves were plotted of the pattern to be expected with natural mercury. Figure 3 shows the predicted curve obtained with natural mercury using 0.02 reciprocal centimeters as the half-intensity width of the component.

A series of photographs was taken of the fringe patterns produced by this interferometer and various experimental lamps. The plates were run on a recording microdensitometer, and the resulting contour pattern followed that predicted from the calculations just described within very close limits. Figure 4 is a photographic reproduction of one of these contour patterns obtained with natural mercury.

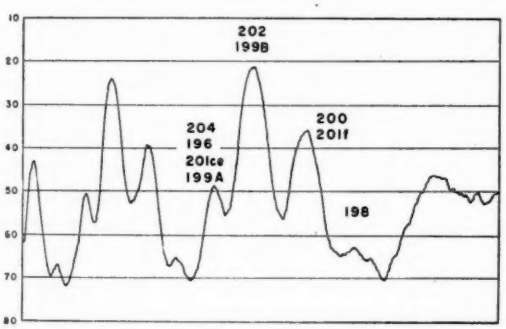


FIG. 4. Microdensitometer trace of Fabry-Perot pattern of 5461A line of natural mercury. The plate separation is 43 mm.

An interesting maximum on this pattern is the one occurring between the maximum which is due to isotope 202 and that which is due to isotope 198. This peak, which has an intensity almost two-thirds that of the main peak, is caused by the superposition of several small components.

Figure 5 is a microdensitometer tracing of the fringe pattern obtained with an irradiated material. A comparison between Fig. 4 and Fig. 5 shows quite clearly that there has been a considerable enrichment of the 198 isotope.

Because of the overlapping of the different lines, the analysis of the plates differs slightly from that performed in ordinary spectrographic procedures. A curve was plotted on semilog paper of densitometer readings at the various peaks as a function of the peak value on the predicted curve given in Fig. 3. These values lay on a straight line, which showed that the predicted curve was essentially correct. The assumption was then made that in the enriched lamp the relative concentration of the isotopes was unchanged. In the plot of the enriched lamp, 198 did not lie on the curve. The new curve was normalized so that the total intensity for the enriched lamp would be the same as the lamp with natural mercury. Table III shows that the enrichment of 198 is approximately 1.5. This crude method of calculating enrichment could not be used in any precise experiment. However, the technique was applied in such a way that it would be certain to yield results that were slightly low.

[13] J. R. McNally, J. Opt. Soc. Am. **39**, 1050 (1949).

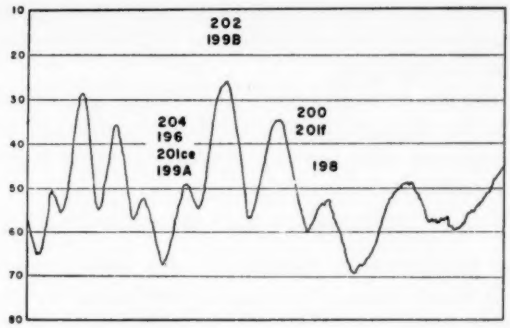


FIG. 5. Microdensitometer trace of Fabry-Perot pattern of 5461A line of mercury which has been photochemically enriched in the 198 isotope. The plate separation is 43 mm.

## The Mercury Water-Vapor Reaction

In the present enrichment study, water vapor and mercury were passed in a stream of nitrogen over a mercury-198 lamp. Here, as described previously, the excited atoms were primarily the 198 isotope. The irradiated gases were led through a thermal precipitator and the mercuric oxide deposited on its walls. This deposit was removed and analyzed. The result showed that $Hg^{198}$ was enriched by a factor 1.5. Since the purpose of this study was isotope separation, no rate studies were made, and the products were not analyzed. However, some remarks might be made on the possible mechanism of the process.

If there is to be enrichment, excited mercury atoms must react in the primary step to either form a compound which is removed from further contact with the reaction or which itself may react further, being restricted, however, in that it must not regenerate free Hg.

TABLE III.

| Isotope | Normal | Enriched |
|---|---|---|
| 196 | negligible | negligible |
| 198 | 10% | 15% |
| 199 | 16 | 15 |
| 200 | 24 | 26 |
| 201 | 14 | 12 |
| 202 | 29 | 26 |
| 204 | 7 | 6 |
| | 100% | 100% |

This requirement assists somewhat in narrowing down the number of processes which have been advanced as possible mechanisms.

Senftleben and Rehren[14] and Bates and Taylor[15] studied the Hg-photosensitized decomposition of water and suggested that the only primary process energetically possible is

$$Hg^*+H_2O\rightarrow Hg+H+OH. \quad (1)$$

The present work makes Eq. (1) highly unlikely, since it would permit no isotope enrichment. It should be noted that

$$Hg^*+H_2O\rightarrow H_2+O+Hg \quad (2)$$

is also energetically possible but must be eliminated for the same reason as Eq. (1).

The excellent work of Beutler and Rabinowitch[16] provides a primary step which might be correct,

$$Hg^*+H_2O\rightarrow HgH+OH. \quad (3)$$

The authors[14–16] who have studied the photosensitized decomposition have apparently not attempted to suggest the remaining steps of the mechanism. There are, of course, several possible reactions which might complete the process. The one which seems most attractive to the present authors is

$$HgH+OH\rightarrow HgO+H_2. \quad (4)$$

This reaction would take place with very small energy of activation, since the energy required to break up OH (~103 kcal) is supplied approximately by energy released in the formation of $H_2$ (~103 kcal).

Since the experimental methods used in this study were similar to those of Bates and Taylor, we may assume that the products contained hydrogen and oxygen. The production of $H_2$ is accounted for by Eqs. (3) and (4), but side reactions must be postulated to account for oxygen. Thus,

$$HgO+h\nu\rightarrow Hg+O, \quad (5)$$

$$O+O+M\rightarrow O_2+M, \quad (6)$$

$$OH+OH\rightarrow H_2+O_2. \quad (7)$$

This would reduce the over-all yield of product HgO and might also reduce the enrichment somewhat.

There is another possible primary process which can be considered,

$$Hg^*+H_2O\rightarrow HgO+H_2. \quad (8)$$

This is energetically possible since

$$H_2O\rightarrow H_2+O \quad (9)$$

requires ~115 kcal. The energy of excitation of Hg is 112 kcal, and the formation of HgO can supply the additional 3 kcal. If Eq. (7) is to be accepted, side reactions such as Eqs. (5) and (6) must be postulated once again to account for the production of oxygen.

## Conclusions

The most important conclusion that has been obtained from this work is that the method of photochemical separation of isotopes is quite feasible. The use of these "breeder" techniques gives results which lead to a high enrichment factor. Obviously this method can be used with other elements and other reactions if suitable materials are available.

The present knowledge concerning the reaction of sensitized atoms is rather meager. One reason for this is that, until now, it was not possible to study only the excited atoms in a mixture. By the use of these isotope absorption techniques, it is now possible to excite only one isotope. With the help of the enrichment factor, the role of the sensitized atom in the reaction may be deduced. This type of analysis was done previously in the section on the $Hg^*-O_2-H_2O$ reactions. Further work of this type should be done so that the mechanism of photosensitization might be better understood.

An incidental result of this research is the fact that a Fabry-Perot interferometer can be very useful for isotopic analyses. This is especially true if it is used in conjunction with narrow band filters and multilayer plates. In certain processes where isotopic concentration is important, these optical methods may prove to be cheaper and as reliable as mass spectrographic techniques.

[14] H. Senftleben and I. Rehren, Z. Physik **37**, 529 (1926).
[15] J. R. Bates and H. S. Taylor, J. Am. Chem. Soc. **49**, 2438 (1927).
[16] H. Beutler and E. Rabinowitch, Z. physik. Chem. **B5–6**, 403 (1930).

# Studies of Ionization Efficiency. Part III. The Detection and Interpretation of Fine Structure

J. D. MORRISON
*Chemical Physics Section, Division of Industrial Chemistry, Commonwealth Scientific and Industrial Research Organization, Melbourne, Australia*

(Received January 13, 1953)

The effect of the spread in energy of the ionizing electron beam on the resolution of structural details in ionization efficiency curves has been evaluated, and the possibility of its removal by analytical methods is discussed. It has been shown that the first and second derivatives of the ionization efficiency possess useful properties, and that, when certain assumptions are made about the shape of the ionization probability function for a single process, a new method of measuring ionization potentials can be devised.

Correlation techniques have been employed to enhance materially the signal-to-noise ratio in the output from the ion collector. Detailed measurements of the ionization efficiencies for the inert gases have been made, and the assumptions referred to are justified.

It is shown that the ionization efficiencies for some molecular ions can be correlated with their vacuum ultraviolet and near x-ray spectra. It is found that competition occurs between all possible processes of excitation and ionization at each level of energy. The higher-energy levels of molecules can be studied and, in principle, an unequivocal assignment of bond dissociation energies from mass spectrometric data is possible.

## INTRODUCTION

THE examination of the factors contributing to the shape of ionization efficiency (I.E.) curves, which was commenced in Part I,[1] is an important preliminary to the measurement of fragment-ion appearance potentials, and their interpretation to give bond dissociation energies. Only after a completely satisfactory correlation has been obtained between the mass spectrometric results and the limited amount of known spectroscopic data for the vacuum ultraviolet region can any confidence be placed in the unsupported evidence of the former. Also any attempts to place the phenomenon of ionization by electron impact on a sound theoretical basis require much more reliable data than are at present available.

One of the puzzling features of mass spectrometric I.E. curves has been the similarity of the curves for different processes, and the lack of any of the structural details which would be expected from the complexity of the processes occurring. This was discussed in Part I, where it was shown that by careful measurement some structure could be detected in the curves for a few substances. In the present paper it will be shown how, by improvement in technique, this work can be extended, and a detailed correlation of the results with spectroscopic data obtained.

## TECHNIQUE OF MEASUREMENT

A most important factor which at present limits the accuracy with which I.E. curves can be recorded using the mass spectrometer is the signal-to-noise ratio in the output from the ion collector and associated amplifier. The noise may be divided into two parts, that generated in the input resistance to the amplifier, which is short-term in nature, and long-term variations in conditions which make it difficult to reproduce I.E. curves in detail. Recent work[2] indicates that caution must be exercised in comparing the results obtained from different spectrometers.

If it is assumed that over a period of time short compared with the long-term systematic variations, all the other fluctuations are random, then it should be possible to lessen them by an integration of the signal in time. Such time-correlation will give an effective increase in signal-to-noise ratio. This has been tested by carrying out summations over groups of ten curves recorded in sequence for a given process of ionization, when it is found that a significant increase in signal-to-noise ratio is obtained, noise being taken in the broader sense as all the time-dependent factors which are superposed on the true ionization efficiency. The improvement is sufficient to allow the application of mathematical operations to the curves, and is of especial value in the detection of fine structure.

The amount of labor involved in this method of obtaining I.E. curves becomes prohibitively great when the mass spectrometer records are measured manually, so an instrument has been designed which carries out the whole operation of measuring the ionization efficiency automatically. A 2-volt range of the ionizing electron voltage is scanned repeatedly at a frequency of one cycle every two minutes by a step voltage wave form, each step being 0.05 volt. The ion peak is scanned once on each step, the peak and zero values are sampled, stored, then subtracted and the results recorded. The curves are usually summed in groups of ten. Otherwise the conditions of measurement are as described in Part I. To cover a greater range of ionizing electron energies, the curve is scanned in 2-volt sections each overlapping by one volt, and the results adjusted in scale to fit each other. A fuller description of this instrument is being published elsewhere.[3]

[1] J. D. Morrison, J. Chem. Phys. **19**, 1305 (1951).

[2] Lossing, Tickner, and Bryce, J. Chem. Phys. **19**, 1254 (1951).

[3] J. D. Morrison, Rev. Sci. Instr. (to be published).

### EFFECT OF ELECTRON ENERGY SPREAD

Factors which are time invariant, such as the thermal energy spread of the ionizing electron beam, are not removed by this technique. To obtain the true ionization efficiencies, the curves would have to be measured using a monoenergetic electron beam. This has been done by Lawrence[4] and Nottingham,[5] using electromagnetic energy filters, and as part of the present studies using an electrostatic analyzer. The ion currents obtained by these methods are extremely small, and accurate measurement is difficult. This criticism would seem to apply equally to the ingenious method used by Fox and co-workers.[6]

It is therefore of some interest to examine the extent to which details in the I.E. curves will be obscured by the ionizing electron energy spread, to discover the limits set to the resolution of fine structure by this cause, and to consider possible methods of removing the spread analytically.

It will be assumed that the ionization probability $P$ for the excitation of a molecule in its ground state to a single electronic level of the ion can be denoted by

$P=0$ for $E<E_c$ $E=$ ionizing electron energy

$P=p(E)$ for $E\geq E_c$ $E_c=$ ionization potential.

The resulting ion current produced at any nominal electron energy $V$ by an electron beam with a Maxwellian energy spread denoted by $m(U)$ is proportional to

$$i(V)=\int_{E_c}^{\infty} m(U)p(E)dE. \tag{1}$$

The total electron energy $E=U+V$, where $U$ is the thermal energy of the electrons

$$\therefore\quad i(V)=\int_{E_c}^{\infty} m(E-V)p(E)dE. \tag{2}$$

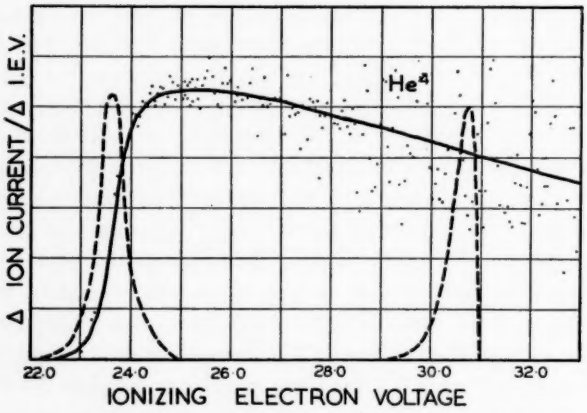


FIG. 1. The first and second derivative ionization efficiency for singly-charged helium. The Maxwellian distribution for $T=2500°K$ is superposed on the figure.

[4] E. O. Lawrence, Phys. Rev. **28**, 947 (1926).
[5] W. B. Nottingham, Phys. Rev. **55**, 203 (1939).
[6] Fox, Hickam, Kjeldaas, and Grove, Phys. Rev. **84**, 859 (1951).

The initial point of onset $E_c$ is now replaced by a region of exponential increase. For the measurement of the lowest ionization energy, the effect of the energy spread can be overcome empirically by taking the point at which the derivative of the logarithm of the I.E. attains a critical value.[7,1] This method is only suitable for measuring the point of onset of the least energetic transition, and in cases where another transition occurs at an energy not much higher than the lowest, may lead to erroneous values.[8] By making certain further restrictions on the form of $p(E)$ it is possible to derive the following relations.

Differentiating (2) with respect to the nominal energy $V$

$$\frac{di(V)}{dV}=\int_{E_c}^{\infty}\frac{\partial m(E-V)}{\partial V}p(E)dE$$

$$=-\int_{E_c}^{\infty}\frac{\partial m(E-V)}{\partial E}p(E)dE$$

since

$$\frac{\partial m(E-V)}{\partial V}=-\frac{\partial m(E-V)}{\partial E}.$$

Integrating by parts

$$\frac{di(V)}{dV}=-m(E-V)p(E)\Big|_{E_c}^{\infty}+\int_{E_c}^{\infty}m(E-V)\frac{dp(E)}{dE}dE. \tag{3}$$

If $p(E_c)=0$, the integrated term vanishes, since as $E\to\infty$ so $m(E-V)\to 0$. Provided that $p(E)$ and all its derivatives up to an including order $n-1$ vanish at $E=E_c$, the process can be repeated and leads to the formula

$$\frac{d^n i(V)}{dV^n}=\int_{E_c}^{\infty}m(E-V)\frac{d^n p(E)}{dE^n}dE. \tag{4}$$

If the first nonvanishing derivative is of order $k$, Eq. (4) holds for $n\leq k$ but for the $(k+1)$th derivative

$$\frac{d^{k+1}i(V)}{dV^{k+1}}=m(E_c-V)p_k(E_c)+\int_{E_c}^{\infty}m(E-V)\frac{d^{k+1}p(E)}{dE^{k+1}}dE,$$

where $p_k(E_c)$ is the $k$th derivative of $pE$ evaluated at $E=E_c$. If $p(E)$ is proportional to $(E-E_c)^k$, then the $(k+1)$th derivative vanishes[9] and

$$\frac{d^{k+1}i(V)}{dV^{k+1}}\propto m(E_c-V).$$

[7] R. E. Honig, J. Chem. Phys. **16**, 105 (1948).
[8] Compare agreement of mass spectrometric ionization potentials with spectroscopic data, J. D. Morrison and A. J. C. Nicholson, J. Chem. Phys. **20**, 1021 (1952).
[9] The author is indebted to the referee for his assistance in the derivation of this analytical treatment.

That is, if $p(E)$ is a polynomial of $k$th degree, the $(k+1)$th derivative of the ionization efficiency reduces to the electron energy distribution, reversed with respect to the energy scale, and with the cutoff on the high-energy side at $E_e$. The resolution of two such processes can be reduced to the problem of separating the maxima in the resultant curve produced by the addition of two Maxwellian distributions. The only limit set to the resolution of processes in actual curves is, therefore, the practical one of obtaining sufficiently accurate data for derivatives to be taken. Provided a great enough signal to noise ratio can be attained, the use of electron analysers is unnecessary.

Examining the problem from another aspect, every point on $P$ gives rise to a reversed Maxwellian distribution of amplitude proportional to it, and to a first approximation, the observed ion current curve can be considered as the sum of a series of such overlapping distributions taken at a set of small voltage intervals. The form of the energy distribution for the mass spectrometer filament can be obtained experimentally, and it is in theory possible by starting at some point on the I.E. curve or preferably its derivatives where they are linear over a range of two or more volts, to arrive at the true form of $P$ by a process of repeated subtraction. At present, however, the measured curves are not recorded with sufficient accuracy for the gain in information to be enough to make the labor of this process worth while.

## EXPERIMENTAL

From the foregoing discussion, it appears that the derivatives of the ionization efficiency should have interesting properties, and that notwithstanding the electron energy spread, it should be possible to verify the assumptions made about the form of the true ionization probability from experimental curves, and to obtain resolution of fine structure if it is present.

The instrumental technique described gives I.E. curves which are sufficiently accurate for the differential curves $\Delta i(V)/\Delta V$ to be obtained by subtraction. As $\Delta V$ is 0.05 ev, the curves are close approximations to the true derivatives. It is apparent from the measured curves shown that whilst the scatter in the values for the first derivative is small for the first volt or so, it rapidly becomes greater. This is inherent in the present method of measuring the direct curve to a constant 0.1 percent accuracy, and subsequently taking its derivative. A later instrument, to be described, measures the derivatives directly, and will hence obviate this effect, which is not caused by the limiting attainable signal-to-noise ratio.

### The Inert Gases

The ionization efficiencies of inert gases are of especial interest in that the excitation is known from spectroscopic data to be particularly simple. Helium is the only case which can be studied where the ionization

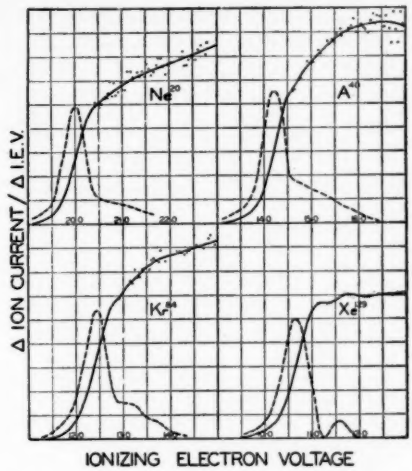


FIG. 2. The derivative ionization efficiencies for singly-charged neon, argon, krypton, and xenon. The energy scale is uncorrected.

over a range of tens of volts corresponds to the ionization probability of a single electronic transition, the second electronic level of the ion being 40.8 ev above the first. For neon, argon, krypton, and xenon, the ionization for the first ten volts above onset must be due only to the excitation of the $^2P_{1\frac{1}{2}}$ and $^2P_{\frac{1}{2}}$ lowest states of the singly-charged ions. The first and second derivative curves for these are given in Figs. 1 and 2. For comparison, the Maxwellian distribution calculated for $T=2500°K$ is superposed on Fig. 1, reversed on the energy scale. The first derivative curves vary slightly from one gas to another, but it is evident in all cases that the second derivative curves are very closely similar to the reversed Maxwellian distribution. In the case of helium it can hence be deduced that the true first derivative curve is very nearly a step function, corresponding to a linear increase in the actual probability,

$$\text{i.e.,}\quad p(E) \propto (E-E_e).$$

This is in accord with the results obtained by Fox *et al.* referred to above. In fact, it is possible that the actual ionizing electron velocity distribution does have a "tail" on the low-energy side as well, due to the imperfect electron optics of the ion chamber. In this case the first derivative for helium does become a step function, which decreases slowly at higher energies. The curves for the other inert gases are similar, but here there is a second slower increase in gradient above the first, before the curve reaches a maximum and then slowly decreases. At higher energies, the curves are structurally featureless up to the energy corresponding to the ionization potential for double ionization, when the first derivatives for the singly-charged ions from argon and krypton, the only two gases studied in this region, show a series of decreases which are paralleled by increases in the first derivative curves for the doubly-charged ions.

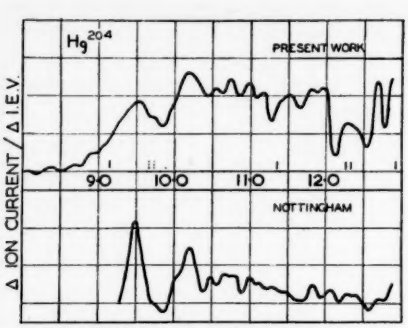


FIG. 3. Comparison of the present results for mercury with a curve obtained from data in paper by Nottingham. Relative position of energy levels of the ion are shown as solid lines, other levels as dotted lines, superposed on the figure.

### Mercury

The ionization efficiency for the production of singly-charged mercury has been studied extensively in the past by workers using instruments of ion-gauge type; the most recent being that carried out by Nottingham using a velocity-analyzed electron beam.[5] The present results are in excellent agreement with his work, practically all the details of fine structure in the curves being in coincidence (Fig. 3). As expected, the electron energy spread does not mask structural details which are more widely spaced in energy than about 0.3 ev. The small peaks at the foot of the curve, which had been also observed by earlier workers,[10] were interpreted by Nottingham as photoelectric in origin. This interpretation does not seem to be valid in the present work, as the ion collector is completely separated from the ionizing region.

### Polyatomic Molecules

The first derivative curves for the polyatomic molecular ions $N_2$, HCl, $CO_2$, and $C_6H_6$ are shown in Fig. 4. It is evident that in these cases many details of fine structure are present. Too much weight should not be attached to minor fluctuations in the curves, although even these seem to be reproducible. The second derivatives again reproduce the reversed Maxwellian distribution. It is observed that in general the first derivative I.E. curves for the heavier atoms and for molecules decrease to zero more rapidly at high energies than do those for the lighter atoms.

## DISCUSSION

### Energy Scale

Before any attempt can be made at correlation of the observed curves with spectroscopic energy levels, the energy scale must be corrected for errors due to contact potential, electron acceleration caused by the cross-field from the ion "pusher" electrodes, etc. It follows from the earlier discussion of the effect of the energy spread that the ionization potential for a process should correspond to the point on the second derivative I.E. at which the reversed Maxwellian falls to zero on the high-energy side. The peak of the Maxwellian, which is easier to distinguish, will be about 0.2 ev lower than this.

The value of the ionizing electron energy at which the second derivative curve for krypton reaches its maximum value is usually found to be about 1.53 ev below the spectroscopic ionization potential, although it varies slightly depending on the other gas present in the mass spectrometer. The relative ionization potentials for all the other inert gases except helium, found by comparing them in this way with krypton measured at the same time, are in agreement with the spectroscopic figures to within 0.05 ev. Helium cannot be measured simultaneously with krypton because of the great difference in mass.

The energy scale can be fixed, and the ionization potentials of the polyatomic molecules be determined in a similar manner.

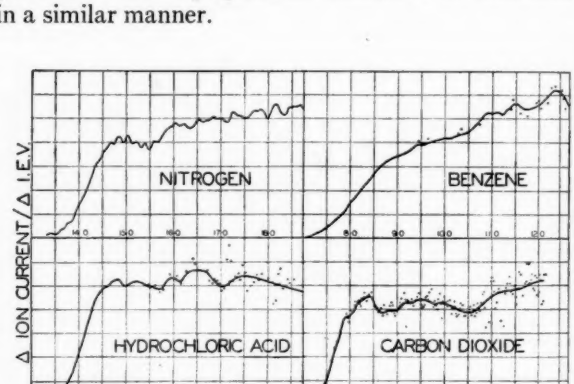


FIG. 4. The derivative ionization efficiencies for singly-charged nitrogen ($N_2$), hydrochloric acid, carbon dioxide, and benzene.

### Correlation of Results with Spectroscopic Data

It can be seen from Figs. 2–4 that when the spectroscopically-known energy levels for the ionic state in question are compared with the first derivative I.E. curve, they are found to be associated with increases in the gradient of the I.E. For the inert gases from neon to xenon, the doublet separations of $^2P_{1\frac{1}{2}}$ and $^2P_{\frac{1}{2}}$ are 0.097, 0.177, 0.666, and 1.307 ev, respectively.[11] For the first two, the spacings are too close to be resolved in the present method, but in krypton and xenon there are some indications of resolution of the higher process. The distance of the smaller peak from the larger one in the second derivative curve for xenon is about 1.0–1.1 ev, slightly less than the spectroscopic spacing, but it seems very probable that it can be interpreted as due to the second process. If the assumptions made in the

[10] P. T. Smith, Phys. Rev. **37**, 808 (1931).

[11] R. F. Bacher and S. Goudsmit, *Atomic Energy States* (McGraw-Hill Book Company, Inc., New York, 1932); also Humphreys, De Bruin, and Meggers, Phys. Rev. **37**, 106 (1931).

foregoing discussion are valid, the curves can be interpreted only by taking the probability for the excitation of the $^2P_{\frac{3}{2}}$ level as from $\frac{1}{4}$ to $\frac{1}{6}$ that for the $^2P_{1\frac{1}{2}}$.

Benzene has pronounced increases at 9.35 and 11.95 ev (scale corrected), as compared with spectroscopically measured ionization potentials of 9.24 and 11.75 ev.[12] In carbon dioxide increases occur at 13.85, 17.1, 20.6, 22.15, 31.89, and 36.39 ev, comparing with known and predicted ionization potentials at 13.79, 17.4, 18.1, 22.0, 30.0, and 30.5 ev.[13]

In addition to this structure which can be identified, there are sharp decreases in gradient in many of the curves which are not accompanied by any ionized energy levels, and which in any case cannot be accounted for if the ionization probability for all single processes is similar to that observed for helium. The curves for helium and the other inert gases would seem to indicate that the first derivative of $P$ for a single process rises very steeply on the low-energy side, and then decreases slowly to zero over a range of from 30 to 100 ev. $P$ can be approximated roughly by an expression[14] of form,

$$i(E)=\frac{E}{E_e^2}\exp-\frac{E}{E_e}.$$

That such a broad maximum should be observed is reasonable, as both the impinging electron and the electron ejected on ionization, can carry away any amount of kinetic energy after the impact.

On the other hand, it is known that the excitation of unionized levels of atoms and molecules by electron impact is in many cases a much more specific resonance process, the probability of excitation rising to a sharp maximum within 0.1 ev of the critical value and falling off again rapidly at higher energies.[15] It was observed above, in the case of the single and double ionization of argon and krypton, that competition between two completely different ionization processes can occur, increases in the gradient of the curves for the double ionization being associated with similar decreases in the curves for single ionization. A similar type of competition might be expected between processes of ionization and excitation. The presence of unionized levels of the atom or molecule above the lowest ionization potential will then be accompanied by sharp decreases in the derivative I.E. The pronounced decrease in the initial part of the mercury first derivative curve in Fig. 3 can be associated with two known levels of the atom. Similarly, some of the decreases in the curves for nitrogen and carbon dioxide can be connected with Rydberg series of levels in the neutral molecules which converge to higher ionization potentials.[16,17]

In the case of polyatomic molecules, it is to be expected that a third type of competition should occur between the process leading to the production of the molecular ion, and the other processes giving rise to the various fragment ions. A decrease does occur in the curve for the parent ion from methane at the energy at which the $CH_3$ ion is beginning to be formed.

## CONCLUSION

On the basis of the experimental evidence presented above, a number of significant conclusions can be drawn which throw considerable light on the interpretation of the results obtained from electron impact.

The ionization probability for a single process, such as that occurring in the excitation of the lowest ionized state of helium, has a broad maximum, and is distinguished only by the fact that it has a sharp point of onset. The second derivative of the ionization efficiency is a positive peak at the ionization potential, which if there were no energy spread in the ionizing electron beam, would be very sharp. The second derivative curves for the other inert gases would consist of two such peaks, corresponding in energy to the two lowest states of the singly-charged ions.

It is found that competition can occur between all the various processes possible at any given energy, whether of excitation, ionization, or dissociation. The simultaneous occurrence of other processes at each energy would be shown up by the presence of a sharp negative peak in the second derivative curve.

It would seem that the second derivative of the ionization efficiency for any given ion should consist of a set of sharp positive peaks at the energy levels of the ion itself, and a set of negative peaks at any other energy levels in the molecule which may be excited. The assignment of the energy levels for a molecule should therefore, in principle at least, be greatly simplified, because the electron energy spectrum for each radical should show up as a set of positive peaks in its own second derivative curve, and as sets of negative peaks at the same energies in the derivative ionization efficiencies of all the other ions formed from the same molecule. The second derivative curves give in effect vertical line sections through the potential energy diagram for the molecule, because all transitions have taken place from the ground state. In the case of a fragment ion produced by dissociation the energy levels of the ion will be superposed on those for the neutral fragment, and both will be displaced along the

[12] W. C. Price and R. W. Wood, J. Chem. Phys. **3**, 439 (1935).
[13] H. J. Henning, Ann. Physik (5) **13**, 599 (1932); W. C. Price and D. M. Simpson, Proc. Roy. Soc. (London) **A169**, 501 (1938); S. Mozrowski, Revs. Modern Phys. **14**, 216 (1942); Phys. Rev. **60**, 730 (1941); **62**, 270 (1942); **72**, 691 (1947); R. S. Mulliken, J. Chem. Phys. **3**, 720 (1935).
[14] A more elaborate expression is given for helium He→He$^+$ by Tate, as

$$i(Vo)=3.383(Vo/Va)^{\frac{1}{2}}[1-e^{-54Vo/Va}]^{\frac{1}{2}}[1-e^{(-Va-Vo)}/2.28Vo].$$

quoted by P. T. Smith, Phys. Rev. **36**, 1293 (1930).
[15] W. H. Brattain, Phys. Rev. **34**, 474 (1929), also compare Bates, Fundaminsky, Leach, and Massey, Trans. Roy. Soc. (London) **A243**, 93 (1950).
[16] G. Herzberg, *Spectra of Diatomic Molecules* (D. Van Nostrand Company, Inc., New York, 1950), p. 449.
[17] See Henning, reference 13.

energy scale by an amount equal to the bond dissociation energy. The presence of kinetic energy in any fragment produced by dissociation should show up as additional displacement of some of the levels.

In view of the very close resemblance between the results of the electron impact method, and the spectra of radiation spectroscopy, the present technique might by analogy be termed electron spectroscopy. In contrast to uv spectroscopy, which is restricted to the study of molecular energy levels below about 20 ev, the new methods can be extended to energies of the order of hundreds of electron volts.

ACKNOWLEDGMENTS

The author wishes to express his thanks to Dr. J. M. Cowley and Dr. A. L. G. Rees for their helpful criticism.

THE JOURNAL OF CHEMICAL PHYSICS VOLUME 21, NUMBER 10 OCTOBER, 1953

# X-Ray Scattering from a "Free-Volume" Liquid

LOUIS H. LUND
*Missouri School of Mines and Metallurgy, Rolla, Missouri*
(Received June 19, 1953)

The x-ray scattering of a monatomic liquid is calculated by averaging the intensity function over configurations of the atoms in a cellular "free-volume" configuration space corresponding to single cell occupancy. A zero-order approximation to the derived scattering equation leads to the conventional x-ray scattering equation. A slightly better approximation is also shown.

## 1. INTRODUCTION

IN a recent paper, Kirkwood[1] has shown that the free volume theory of the liquid state may be put on considerably firmer ground by approaching the problem from a fundamental statistical mechanics approach with well defined approximations. Spanning the liquid with a virtual lattice of $N$ cells with single cell occupancy, and minimizing the configuration contribution to the Helmholtz free energy, leads to an integral equation connecting the distribution function for a single molecule within its cell and its potential energy $U$ in the cell. A zeroth-order approximation to the solution of the integral equation gives essentially the earlier formulation of the cell method of Lennard-Jones and Devonshire.[2]

It is of some physical interest to calculate the x-ray scattering from such a formal free volume liquid picture. The conventional liquid scattering formula[3] is, of course, well known, but its derivation has not followed, at least in a formal way, the statistical mechanical averaging of the configurations of the atoms of the liquid. It is the purpose of this note to show that just as the zeroth-order approximation to the Kirkwood integral equation leads to the simple cell theory of the liquid state, so does the zeroth approximation to the x-ray scattering equation derived here lead to the conventional x-ray liquid scattering equation.

## 2. METHOD OF CALCULATION

Suppose the liquid of $N$ identical monatomic atoms is irradiated by a collimated monochromatic x-ray beam of wavelength $\lambda$ and that the directions of the incident and scattered beams are characterized in the usual fashion by unit vectors $\mathbf{S}_0$ and $\mathbf{S}$. The coherent part of the electric field scattered in the direction of the unit vector $\mathbf{S}$ by the $N$ atoms in a particular configuration is

$$E=f\sum_{n=1}^{N}e^{i\mathbf{k}\cdot\mathbf{r}_n}, \tag{1}$$

where $\mathbf{r}_n$ is a vector from a fixed origin to the $n$th atom; $2\theta$ the angle between $\mathbf{S}$ and $\mathbf{S}_0$, $\mathbf{K}=2\pi/\lambda(\mathbf{S}-\mathbf{S}_0)$, $f$ is the atomic structure factor, and the magnitude of $K=(4\pi/\lambda)\sin\theta$. The total scattered intensity from this particular configuration of the $N$ atoms averaged over all $\mathbf{K}=2\pi/\lambda(\mathbf{S}-\mathbf{S}_0)$ is

$$I(k)=f^2\sum_{n=1}^{N}\sum_{m=1}^{N}(\sin kr_{nm}/kr_{nm}), \tag{2}$$

where $r_{nm}=|r_n-r_m|$.

What one seeks now is an average of the foregoing over-all configurations of the $N$ atoms, and where the averaging follows at least in some approximation the methods of statistical mechanics. The formal free-volume picture of the liquid provides a convenient way for doing this.

Let us follow Kirkwood, and span the liquid by a virtual lattice of $N$ cells $\Delta_1\cdots\Delta_N$ and denote the probability density in configuration space corresponding to single cell occupancy by $P_N$. Then we will have

$$\langle I(k)\rangle_{Av}=f^2\int^{\Delta_1}\cdots\int^{\Delta_N}\prod_{s=1}^{N}\phi(r_s)\sum_{n,m}^{N}\frac{\sin kr_{nm}}{kr_{nm}}\prod_{k}dv_k, \tag{3}$$

[1] J. G. Kirkwood, J. Chem. Phys. **18**, 380 (1950).
[2] J. E. Lennard-Jones and A. F. Devonshire, Proc. Roy. Soc. (London) **163**, 53 (1937).
[3] N. S. Gingrich, Revs. Modern Phys. **15**, 90 (1943).

where we have made the same Hartree-type approximation to $P_N$ as did Kirkwood, and where $\phi(r_s)$ is the normalized probability density function of the $s$th atom and $r_s$ is measured relative to some convenient origin in the $s$th cell. We then have

$$\langle I(k)\rangle_{Av}=Nf^2\left\{1+\int^{\Delta_1}\int^{\Delta_l}\times\sum_{l=2}^{\infty}\frac{\sin k(R_{1l}+r_1-r_l)}{k(R_{1l}+r_1-r_l)}\phi(r_1)dv_1\phi(r_l)dv_l\right\},\quad(4)$$

where the summation extends from an arbitrary atom in the aggregate labeled 1 and $R_{1l}$ is the position vector of the $l$th cell relative to the first.

Now, if for a zeroth approximation, we take $\phi(r_s)=\delta(r_s)$, and if we describe the density of cell centers about the first cell by a function $\rho(R_{1l})\equiv\rho(r)$ of the continuously varying $R_{1l}\equiv r$, we are led immediately to

$$\langle I(k)\rangle_{Av}=Nf^2\left\{1+\int_0^{\infty}4\pi r^2(\rho(r)-\rho_0)(\sin kr/kr)dr\right\},\quad(5)$$

which is the usual liquid scattering equation,[4,5] in which a quasi-solid configuration of atoms vibrating about equilibrium positions is envisaged about any atom in the liquid with the function $\rho(r)$ defining the average distribution of these equilibrium positions. Thus the usual derivation of the above can be regarded as a zeroth approximation to $\langle I(k)\rangle_{Av}$ based on an averaging of $I(k)$ in a "free volume" cellular configuration space with single-cell occupancy. One can improve the situation by retaining the function $\rho(r)$ and writing $e^{-U(r)/kT}$ for the normalized probability distribution function for a molecule in a cell where $U(r)$ is the potential function for a molecule in its cell. One then has

$$\langle I(k)\rangle_{Av}=Nf^2\left\{1+\int_0^{R}4\pi r^2\rho(r)x\left\{\int^{\Delta_1}\int^{\Delta_l}\times\frac{\sin k(r+r_1-r_l)}{k(r+r_1-r_l)}e^{-U(r_1)/kT}e^{-U(r_l)/kT}dv_1dv_l\right\}dr\right\}.\quad(6)$$

The volume integrals over the cells obviously involve complicated integrations, and one can obtain a reasonably adequate answer by supposing the probability distribution function uniform over the cell volume, expanding $\sin k(r+r_1-r_l)/k(r+r_1-r_l)$ in a Taylor's series of the variables $r_1$ and $r_l$ about the cell centers, and retaining terms only through the second order.

If we integrate and simplify, we find, for a spherical cell,

$$\langle I(k)\rangle_{Av}=Nf^2\left\{1+\left\{1-\frac{9\delta^2k^2}{240}\right\}\int_0^{\infty}4\pi r^2(\rho(r)-\rho_0)\times\frac{\sin kr}{kr}dr+\frac{9\delta^2k^2}{240}\int_0^{\infty}4\pi r^2(\rho(r)-\rho_0)\Phi(kr)dr\right\},\quad(7)$$

where

$$\Phi(kr)=2[\sin kr-kr\cos kr/(kr)^3],$$

and $\delta$ is the cell radius. It is clear that the above gives the same zero-angle scattering as Eq. (5). It is also clear that for any reasonable cell radius, say 0.5A, the additional terms will be small. An explicit, although admittedly rough calculation, using the above equation can be made for the case of a very dilute diatomic gas ($\rho_0\cong 0$) with $\rho(r)=\delta(r-R_0)$,* where $R_0$ is the interatomic distance in the molecule and taken here, for simplicity, to be 3.0A.

For $\delta=0.5$A, the intensity is virtually indistinguishable from that calculated with Eq. (5). For $\delta$ as large as 1.0A the result differs from that calculated with Eq. (5) by at most $+\frac{3}{4}$ percent at $k=0.66$.

One could, of course, use a considerably more realistic and still mathematically tractable $\rho(r)$ in Eq. (7) to correspond to the actual radial density function for a liquid.[6] It does not seem likely, however, that the results of such a calculation would lead to results sensibly different from those obtained from using Eq. (5). It is of some physical interest to note, however, that for very small scattering angles (and where the additional terms are largest), the positive correction term in Eq. (7), will exceed the negative term. Thus, near the critical temperature, if one imagines the cell size to be anomalously large, the small angle scattering will be larger than that calculated with Eq. (5). Finally, in view of the results obtained, it would appear that little would be gained by relieving the restriction of single-cell occupancy and allowing multiple occupancy of the cells in the averaging over the configuration space.

[4] N. S. Gingrich, Revs. Modern Phys. **15**, 90 (1943).

[5] The conventional procedure has been followed in deriving Eqs. (5) and (7). $R$, the upper limit in the integration over $r$ (i.e., the largest linear dimension of the sample) has been replaced by infinity, and $\rho_0$, the average number of equilibrium centers per unit volume, has been introduced into the integrand with subsequent neglect of the $\rho_0$ contribution of the added compensating integral. See reference 3.

* And, of course, normalized to correspond to one nearest neighbor.

[6] N. S. Gingrich and B. E. Warren, Phys. Rev. **46**, 248 (1934).

# Absorption in the Low-Frequency Wing of the $NH_3$ Inversion Spectrum*

G. Birnbaum and A. A. Maryott
*National Bureau of Standards, Washington, D. C.*

(Received April 20, 1953)

The absorption due to the low-frequency wings of the $NH_3$ inversion lines was measured accurately at 2800 Mc for a pressure of 10-cm Hg. At this pressure, where the shift in inversion frequency has not set in, the absorption was about 40 percent larger than that calculated by summing the Van Vleck-Weisskopf expression over the rotational states using known resonance frequencies and line widths. A similar discrepancy was found in comparing the theoretical absorption with previously obtained data at 9000 Mc, while at resonance, 24 000-Mc theory and experiment were in very good agreement. To investigate various features of pressure broadening, the variation of absorption with pressure (5 to 30-cm Hg), temperature (−12 to 100°C), and frequency (1200 to 2800 Mc) was examined. These functional variations are interpretable, for the most part, by the Van Vleck-Weisskopf relation.

## 1. INTRODUCTION

ALTHOUGH the line shape equation of Van Vleck and Weisskopf[1] has successfully described many features of microwave spectra,[2] it has not yet been decided whether this equation gives the measured absorption deep in the wings of a line. Such a comparison constitutes a critical test of any line shape theory, but it is difficult to do this for a single line because of overlapping with neighboring lines. Also at frequencies removed from resonance by many line widths the absorption becomes too weak to measure with sufficient accuracy. It is preferable, therefore, to investigate the absorption arising from a band of lines.

With regard to the microwave absorption of water vapor, Van Vleck[3] showed that the calculated absorption due to the low-frequency wings of the rotational lines, which extend into the infrared region, was about four times lower than the experimental value. He pointed out that this discrepancy might have been due to the uncertainty in the line width assignments or to the Van Vleck-Weisskopf equation itself whose validity for infrared lines is questionable. For these reasons, the above comparison may not constitute a satisfactory test of the equation.

A severe test is provided by investigating the absorption arising from the widely studied lines of the $NH_3$ inversion spectrum centered about 24 000 Mc. Accordingly, careful measurements of this absorption were made at a frequency of 2800 Mc. At a pressure of 10-cm Hg, the absorption is large enough to be accurately measured while the shift of the inversion spectrum toward zero frequency reported by various investigators[4–8] has not yet set in. At this pressure, the measured value was found to be about 40 percent higher than the theoretical value obtained by numerically summing the Van Vleck-Weisskopf equation over the rotational states using known resonance frequencies and line widths. A similar discrepancy was found using data previously obtained at 9000 Mc, whereas theory and experiment were in close accord at resonance.

In an effort to understand the nature of this discrepancy as well as to investigate other features of the collision broadening phenomenon, further measurements were made at 2800 Mc for pressures up to 30-cm Hg and for temperatures from −12 to 100°C. In addition some observations were made over the frequency interval 1200 to 2800 Mc.

## 2. THEORETICAL CONSIDERATIONS

The inversion spectrum of $NH_3$ consists of many lines of different intensities and widths, the most important of which lie in the region $2\times10^4$ to $3\times10^4$ Mc. The complicated nature of the spectrum thus makes the comparison of theory and experiment considerably more intricate than for a single line.

According to the Van Vleck-Weisskopf formula specialized to the ammonia problem, the absorption $\alpha$ per cm is given by

$$\frac{\alpha}{\nu^2}=\frac{4\pi^2N}{3kT}\sum_{JK} f_{JK}|\mu_{JK}|^2 \times\left(\frac{\Delta\nu_{JK}}{\Delta\nu_{JK}^2+(\nu_{JK}-\nu)^2}+\frac{\Delta\nu_{JK}}{\Delta\nu_{JK}^2+(\nu_{JK}+\nu)^2}\right), \quad (1)$$

where $N$ is the number of molecules per cc, $f_{JK}$ is the fractional number occupying the rotational levels

* Presented in part at the Conference on Electrical Insulation, National Academy of Sciences, National Research Council, at Lennox, Massachusetts, October, 1952.

[1] J. H. Van Vleck and V. F. Weisskopf, Revs. Modern Phys. **17**, 227 (1945).

[2] See, for example, T. F. Rogers, *Factors Affecting the Width and Shape of Atmospheric Microwave Absorption Lines* (Air Force Cambridge Research Center, Cambridge, Massachusetts, October, 1951).

[3] J. H. Van Vleck, Phys. Rev. **71**, 425 (1947).

[4] B. Bleaney and R. P. Penrose, Proc. Phys. Soc. (London) **59**, 418 (1947).

[5] I. R. Weingarten, thesis, Columbia University, New York (1948).

[6] D. F. Smith, Phys. Rev. **74**, 506 (1948).

[7] B. Bleaney and J. H. N. Loubser, Proc. Phys. Soc. (London) **63A**, 483 (1950).

[8] G. Birnbaum, Phys. Rev. **77**, 144 (1950).

characterized by the quantum numbers $J$, $K$, and $|\mu_{JK}|^2=\mu^2K^2/(J^2+J)$. The permanent dipole moment $\mu$ has the value $1.47\times10^{-18}$ esu.[9] The quantities $\nu$, $\nu_{JK}$, and $\Delta\nu_{JK}$ are in $cm^{-1}$.

The resonance frequencies $\nu_{JK}$ can be calculated with an accuracy more than sufficient for our purpose from the empirical formula of Bleaney and Penrose,[10] *viz.*,

$$\nu_{JK}=0.7935-0.0050_5(J^2+J)+0.0070_4K^2 +0.63[0.0070K^2-0.0050(J^2+J)]^2. \quad (2)$$

The line-width constant $\Delta\nu_{JK}$ for a narrow line equals half the width of the line at half intensity. Bleaney and Penrose[10] determined the widths of a number of lines at a pressure of 0.05-cm Hg and found that they could be expressed by the essentially empirical formula,[4,11]

$$\nu_{JK}=1.00\times10^{-2}p_{cm}\left(\frac{288}{T}\right)\left(\frac{K^2}{J^2+J}\right)^{\frac{1}{2}}. \quad (3)$$

The extension to other pressures was made on the assumption that the line width is directly proportional to pressure. Deviations between the observed and calculated values of the line widths at 0.05-cm Hg were no greater than the experimental error, namely, 5 percent. Theoretical line-width equations have been proposed by Margenau,[12] Anderson,[13] and Mizushima.[14] Anderson's equation, in particular, fits the data about as well as Eq. (3) but is by no means as easy to use.

We have introduced into the original equation of Bleaney and Penrose a factor to allow for the variation with temperature predicted by the theories of Margenau and Anderson and verified in the case of the 3,3 line of $NH_3$ by Howard and Smith.[15] This temperature behavior, which is characteristic of pressure broadening arising from dipole-dipole interactions, is also substantiated by the data to be considered in this paper.

Equation (1), with $\nu_{JK}$ and $\Delta\nu_{JK}$ given by Eqs. (2) and (3), has been tested by Bleaney and Penrose[4] in the resonance region 0.65 to 0.90 $cm^{-1}$. At a pressure of 10-cm Hg the individual lines are sufficiently broadened to obscure the fine structure, and the absorption curve is quite smooth with a peak at 0.78 $cm^{-1}$. They obtained a theoretical curve (which fitted the experimental data within several percent) by summing Eq. (1) for all the important lines. This agreement indicates that the line widths vary linearly with pressure up to 10-cm Hg. At higher pressures Bleaney and Loubser[7] found that the line widths began to increase less rapidly with pressure and the resonance frequencies began to shift toward zero.

### 3. EXPERIMENTAL METHOD

The absorption was determined by a cavity method in which measurements were made on the cavity response curve displayed on a cathode-ray tube. Details of the experimental technique are given in a previous publication.[16] To obtain better precision than obtainable by direct observation of the pattern, the resonance curves were photographed and enlarged before scaling. Lower values of absorption were obtained from amplitude measurements by making use of the relation

$$\alpha=\frac{2\pi\nu}{Q_0}\left[\left(\frac{P_0}{P}\right)^{\frac{1}{2}}-1\right],$$

where $\alpha$ is the absorption in $cm^{-1}$, $Q_0$ is the loaded $Q$ of the empty cavity, $\nu$ is the wave number in $cm^{-1}$, and $P_0$ and $P$, respectively, are the peak amplitudes of the resonance curves of the evacuated and gas-filled cavities. Higher values of absorption were obtained from measurements of the $Q$'s of the empty and filled cavity by the formula

$$\alpha=2\pi\nu\left(\frac{1}{Q}-\frac{1}{Q_0}\right).$$

For measurements at 2800 Mc a tunable cavity operating in the $TE_{011}$ mode with a loaded $Q$ of $3.5\times10^4$ was employed. Tests with a nonabsorbing gas such as $N_2$ showed that the small distortion of the cavity with gas pressure did not change the $Q$. As the crystal detector was mounted directly adjacent to the cavity, and therefore subject to thermal changes in the oven, the response law of the crystal was determined at each temperature of observation by using a series of calibrated attenuators. Only at the two extremes of temperature, $-12$ and 100°C, was there a noticeable deviation from square law behavior,[17] and appropriate corrections to the apparent values of $Q$ and amplitude were made at these temperatures. At pressures in the neighborhood of 30-cm Hg, a cylindrical cavity operating in the $TM_{010}$ mode with a $Q$ of about $7\times10^3$ was also used.

Determinations of absorption with the two cavities and with the $Q$ and amplitude techniques generally agreed within 2 to 3 percent at pressures in the vicinity of 30-cm Hg where such intercomparisons were made. Below this pressure the reproducibility was about $5\times10^{-8}$ $cm^{-1}$ or 3 percent, whichever was greater. From an investigation of possible sources of systematic error, it is estimated that the total experimental error cannot be significantly larger than the figure given.

For measurements in the region 1200 to 2800 Mc, a tunable, hybrid mode cavity was used.[18] The $Q$ of this

[9] A. A. Maryott and F. Buckley, "Table of dielectric constants and electric dipole moments of substances in the gaseous state," Natl. Bur. Standards U. S. Circ. 537.

[10] B. Bleaney and R. P. Penrose, Proc. Roy. Soc. (London) **A189**, 358 (1947).

[11] B. Bleaney and R. P. Penrose, Proc. Phys. Soc. (London) **60**, 540 (1948).

[12] H. Margenau, Phys. Rev. **76**, 121 (1949).

[13] P. W. Anderson, Phys. Rev. **76**, 674 (1949).

[14] M. Mizushima, Phys. Rev. **83**, 94 (1951).

[15] R. Howard and W. V. Smith, Phys. Rev. **77**, 840 (1950).

[16] G. Birnbaum, S. J. Kryder, and H. Lyons, J. Appl. Phys. **22**, 95 (1951).

[17] In all cases, the initial power level at the detector was about the same, namely, several microwatts.

[18] L. Essen, Wireless Eng. **23**, 126 (1946).

TABLE I. Variation of absorption in $NH_3$ with pressure and temperature at $\nu=0.094$ cm$^{-1}$.

| $T$(°K) | $\alpha/p^2\times10^6$ [a] | $p$ range (cm Hg) | Number of points | $\alpha T^3$ ($p=10$ cm Hg) |
|---|---|---|---|---|
| 261 | 4.25±0.03 | 5–15 | 5 | 75.6 |
| 298 | 2.96±0.02 | 5–25 | 17 | 78.3 |
| 312 | 2.46±0.02 | 5–30 | 6 | 74.7 |
| 333 | 2.01±0.03 | 5–30 | 7 | 74.2 |
| 353 | 1.75±0.02 | 9–30 | 5 | 75.0 |
| 373 | 1.51±0.05 | 9–30 | 6 | 78.3 |

[a] Mean values and average deviations listed.

cavity was too low (about 3500) to permit reliable measurements of absorption at pressures much below 30-cm Hg.

## 4. RESULTS

### 4.1 Variation of Absorption with Temperature and Pressure at 0.094 cm$^{-1}$

If $\nu_{JK}$ and $\Delta\nu_{JK}/p$ are independent of the pressure, Eq. (1) reduces to

$$\alpha/\nu^2=kp^2 \tag{4}$$

for a frequency sufficiently far removed from resonance so that the inequality $\Delta\nu_{JK}{}^2\ll(\nu-\nu_{JK})^2$ is true for each line whose intensity is large enough to appreciably affect the absorption. The data are summarized in Table I. At a given temperature $\alpha/p^2$ is constant up to 30-cm Hg for all temperatures above 25°C. Individual values of $\alpha$ deviate more or less randomly from Eq. (4) by about 1 percent on the average. At the lowest temperature (−12°), the values $\alpha/p^2$ in the region 15 to 30-cm Hg are definitely higher than the value shown in Table I (about 15 percent higher at 30-cm Hg). At 25°C a slight, but hardly significant deviation in this direction was noted in the neighborhood of 30-cm Hg.

It is interesting to note that Eq. (4) holds experimentally for higher pressures than would be anticipated from Eq. (1).[19] Furthermore, the deviations noted are opposite in direction to those expected. Thus at a pressure of 30-cm Hg, $\Delta\nu_{JK}{}^2$ is no longer negligible in comparison with $(\nu-\nu_{JK})^2$ and consequently values of $\alpha/p^2$ about 10 percent lower than measured might be expected. If allowance is also made for a shift in the resonance frequencies and line breadth parameters of the order previously reported,[7] this difference is somewhat increased.

In the wings of the absorption band, the variation of the line widths with temperature may be readily determined. From Eq. (1) with $N\propto T^{-1}$ and Eq. (3) where $\Delta\nu\propto T^{-1}$, the absorption at constant pressure should be proportional to $T^{-3}$ provided the sum

$$\sum_{JK} f_{JK}|\mu_{JK}|^2\left(\frac{K^2}{J^2+J}\right)^{\frac{1}{2}}\left\{\frac{1}{(\nu_{JK}-\nu)^2}+\frac{1}{(\nu_{JK}+\nu)^2}\right\}$$

is independent of temperature. Computations at 298 and 373°K showed that this sum was virtually independent of temperature. The constancy of the product $\alpha T^3$ included in Table I for a pressure of 10-cm Hg shows that the line widths vary in the expected manner.

### 4.2 Comparison of Observed and Calculated Absorption

Observed values of $\alpha/\nu^2$ at several frequencies are compared with those calculated from Eqs. (1)–(3) for a pressure of 10-cm Hg in Table II. At $\nu=0.094$ cm$^{-1}$, a wave number roughly 9 line widths removed from the resonance wave numbers of the more intense lines, the measured absorption is approximately 1.4 times larger than the calculated value. Data previously reported at $\nu=0.31$ cm$^{-1}$ show a discrepancy of similar magnitude.

TABLE II. Observed and calculated values of $\alpha/\nu^2$ for $NH_3$ at $p=10$-cm Hg.

| $T$°K | $\nu$(cm$^{-1}$) | $\alpha/\nu^2\times10^4$ (cm$^{-1}$) obs | calc | Ratio$\left(\frac{\text{obs}}{\text{calc}}\right)$ |
|---|---|---|---|---|
| 298 | 0.094 | 3.35[a] | 2.41 | 1.39 |
| 298 | 0.31 | 5.12[b] | 3.83 | 1.34 |
| 288 | 0.78 | 80.5[c] | 83.0 | 0.97 |

[a] Present work.
[b] Reference 16.
[c] This value was computed from Bleaney and Loubser's parameters (private communication) to obtain a more accurate value than could have been read from their curves.

The summation of Eq. (1) was extended over all lines with quantum numbers up to and including $J=K=12$, and only the strongest lines up to $J=K=16$. The error in neglecting the remaining lines is small and compensated for, in part, by the error made in neglecting to account for the small number of molecules in vibrational states other than the ground state. More serious is the error which could arise from uncertainties in the values of line width. An indication that this uncertainty is quite small, probably no more than several percent, is the excellent agreement between experiment and theory at $\nu=0.78$ cm$^{-1}$, a wave number very close to the peak absorption. Thus the discrepancy noted in the low-frequency wing of the absorption band appears to be well outside of any uncertainties in the measured and computed values.

### 4.3 Measurements in the Region 0.094 to 0.041 cm$^{-1}$ (1200 to 2800 Mc)

The experimental values of $\alpha/\nu^2$ for a temperature of 25°C and a pressure of 30-cm Hg are shown in Table III.

[19] This is also true of results obtained in a previous investigation (reference 16) at 25°C and at a wave number of 0.31 cm$^{-1}$. The relation $\alpha/\nu^2=5.12\times10^{-6}p_{cm}{}^2$ fits the data obtained from 2 to 20-cm Hg by the amplitude method. The data obtained by the $Q$ method agree well with this relation if the two points at the lowest pressure (which are not accurate anyway) are excluded.

For comparison the absorption (corrected to 25°C) calculated from the parameters $\Delta\nu$ and $\nu_0$ of Bleaney and Loubser are included. These empirical parameters and the theoretical intensity of the inversion spectrum, when substituted in a single Van Vleck-Weisskopf expression, were used by Bleaney and Loubser to obtain a curve which represented their experimental data. At a pressure of 30-cm Hg, this curve which quite closely fits their data near resonance, clearly falls under their experimental points as well as ours on the low-frequency side of the resonance. Thus at this pressure the single Van Vleck-Weisskopf shape factor cannot be a good representation of the absorption band both near resonance and in the low-frequency wing.

On the assumption that $\alpha$ is proportional to $p^2$ up to 30-cm Hg, as was the case at the higher frequencies, one may obtain values of $\alpha$ extrapolated to 10-cm Hg. At this pressure and at the lowest wave number 0.041 $cm^{-1}$, the discrepancy between observed and calculated absorption is about $\frac{2}{3}$ as large as that noted at 0.094 $cm^{-1}$ and 0.31 $cm^{-1}$. However, this apparent improvement may not be significant in view of the greater uncertainty of the data in this case.

## 5. DISCUSSION

At the lower pressures the Van Vleck-Weisskopf theory of line shape is in accord with the observed variation of absorption with pressure and temperature in the low-frequency wing of the band. For that matter, however, the original Lorentz theory or a statistical theory[12] would likewise agree with these experiments. The Van Vleck-Weisskopf equation gave the observed absorption at the peak of the band but so would the Lorentz equation.

A better test of the theory was obtained by an accurate comparison of the measured and calculated absorption in the wings of the lines, specifically at 0.094 and 0.31 $cm^{-1}$. The absorption at 10-cm Hg was found to be higher than that computed from the Van Vleck-Weisskopf expression by factors of 1.39 and 1.34, respectively.[20] A discrepancy of this magnitude, to be sure, is quite small compared to those noted in line shape studies in the infrared and optical regions. However, it is definitely outside of experimental error and might be taken to indicate some defect in the theory.

TABLE III. Absorption in $NH_3$ deep in the low-frequency wing at 30-cm Hg and 25°C. The numbers in parentheses are calculated from Bleaney and Loubser's parameters (private communication).

| $\alpha/\nu^2\times10^4$ | | |
|---|---|---|
| 0.094 $cm^{-1}$ | 0.0610 $cm^{-1}$ | 0.0407 $cm^{-1}$ |
| 31.3 (22.2) | 26.5 | 26.2 (21.5) |

It should be noted, on the other hand, that the theory requires that the duration of a collision be negligible compared with the mean time between collisions. At a pressure of 10 cm Hg the fractional time that two molecules are separated by less than 13°A (the mean optical collision diameter) amounts to 0.03. While this time is small, if the molecules during the time of collision were to act as Debye nonresonant rotators,[21] it is conceivable that the absorption in the low frequency wing might be substantially increased. In this case one would expect better agreement between theory and experiment as the pressure is reduced. However, the observed proportionality between $\alpha$ and $p^2$ both at 0.094 and 0.31 $cm^{-1}$ shows that no better agreement is obtained at the lowest pressure measured, namely 5 cm Hg.

## ACKNOWLEDGMENT

The authors thank Mr. S. J. Kryder for assisting with the measurements and Dr. H. Lyons for his interest in this work.

[20] On the other hand, the measured absorption is lower by roughly a factor of 1.4 than that estimated from the sum of the Lorentz expression over the rotational states. Interestingly enough, at this pressure the single Van Vleck-Weisskopf expression used by Bleaney and Loubser (reference 7) represents well the measured absorption both at resonance and in the wings, although this result can only be fortuitious in view of the discrepancy noted above.

[21] A brief theoretical development somewhat along these lines was presented by D. F. Smith (reference 6).

# Substituted Methanes. XV. Infrared Spectral Data, Assignments, and Calculated Thermodynamic Properties for Fluorotrichloromethane

RICHARD B. BERNSTEIN, *Department of Chemistry*

AND

JAMES P. ZIETLOW* AND FORREST F. CLEVELAND, *Spectroscopy Laboratory, Department of Physics, Illinois Institute of Technology, Chicago 16, Illinois*

(Received January 29, 1953)

Infrared spectral data for gaseous $CCl_3F$ have been obtained in the region 400–3200 $cm^{-1}$, using NaCl and KBr prisms. The present data are compared with previous Raman and infrared data, and assignments and calculated wave numbers are given. The fundamentals (*=liquid) are $\nu_1(a_1)$ 1085, $\nu_2(a_1)$ 534, $\nu_3(a_1)$ 351,* $\nu_4(e)$ 846, $\nu_5(e)$ 400,* and $\nu_6(e)$ 245* $cm^{-1}$. Thermodynamic properties were calculated for 17 temperatures from 100° to 1500°K and were compared with previous calorimetric results.

## SPECTRAL DATA AND ASSIGNMENTS

INFRARED spectral data for the gas[1,2] and for the two lowest bands of the liquid,[2] as well as Raman spectral data for the liquid and the results of a normal coordinate treatment,[3] have been given previously. The present infrared data were obtained with a Perkin-Elmer Model 21 double-beam spectrophotometer (NaCl optics) and with a Beckman IR-2 single-beam spectrophotometer (KBr optics). The present and previous infrared and Raman spectral data, calculated values, and assignments are given in Table I. The transmittance curves obtained for a 10-cm gas cell with the Perkin-Elmer and Beckman instruments are shown in Figs. 1 and 2, respectively.

In general, the agreement of the present results with those of Plyler and Benedict (PB), and Thompson and Temple (TT) is good. The strong band at 1081, however, was not observed by PB, but was observed by TT. Besides this, TT found that this band was stronger than the 1085 $cm^{-1}$ band, whereas in the present work these intensities were just the reverse. The bands reported by PB at 680, 1115, and 1215 $cm^{-1}$ were not found by us; conversely, the bands at 1471, 1150, and the previously mentioned band at 1081 found in the present work were not found by PB. The 1925 $cm^{-1}$ band reported by TT was not observed by us or by PB. The two lowest frequencies, observed only by PB in the liquid state, agree well with the previous Raman values.

If the moments of inertia calculated from the electron diffraction data[4] are used in conjunction with the Gerhard-Dennison theory,[5] the spacing of the $P$ and $R$ branch maxima is expected to be about 17 $cm^{-1}$ for the parallel bands with the $Q$ branch having an intensity of 40 percent of the whole band. Complete resolution was not attained for any of the $CCl_3F$ bands. However, the $\nu_2$ band showed the resolved $Q$ and $R$ maxima at 534 and 543 $cm^{-1}$, respectively, with the $P$ branch as a shoulder near 525 $cm^{-1}$ on the $Q$ branch. Similarly, the $\nu_1$ and $\nu_4+\nu_6$ superimposed absorptions, with $Q$ branches at 1085 and 1081 $cm^{-1}$, respectively, have shoulders at 1077 ($\nu_1$, $P$), 1096 ($\nu_1$, $R$), and 1073 ($\nu_4+\nu_6$, $P$) $cm^{-1}$. Other bands also show such correlation.

If the $2\nu_1$ and $3\nu_1$ bands are used to establish the $\nu_1$ frequency, it is found that with one anharmonic constant ($x_{11}=-12.5$ $cm^{-1}$) in the potential energy expression, $\omega_1=1111$ $cm^{-1}$ and $\nu_1=1086$ $cm^{-1}$. The stronger absorption maximum is at 1085 $cm^{-1}$, and this is chosen as the fundamental.

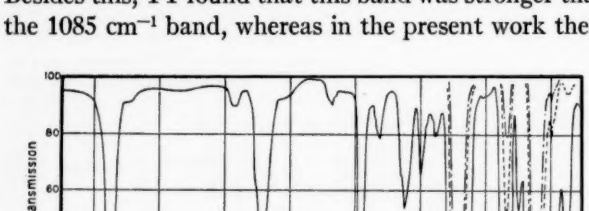


FIG. 1. Infrared absorption bands for gaseous $CCl_3F$ (sample from Kinetic Chemicals, Inc., distilled; Perkin-Elmer Model 21 double-beam, NaCl optics; 10-cm cell, 30°C).

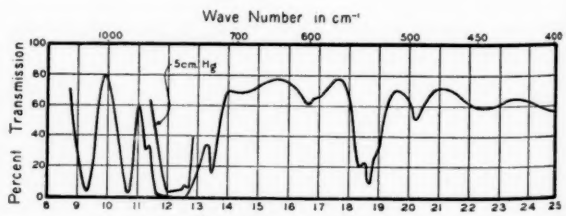


FIG. 2. Infrared absorption bands for gaseous $CCl_3F$ (sample from Kinetic Chemicals, Inc., distilled; Beckman IR-2, KBr optics; 70 cm Hg, 10-cm cell, 30°C).

* Present address: Research and Development Laboratories, The Pure Oil Company, Crystal Lake, Illinois.

[1] H. W. Thompson and R. B. Temple, J. Chem. Soc. **1948**, 1422.

[2] E. K. Plyler and W. S. Benedict, J. Research Natl. Bur. Standards **47**, 202 (1951).

[3] Zietlow, Cleveland, and Meister, J. Chem. Phys. **18**, 1076 (1950).

[4] L. O. Brockway, J. Phys. Chem. **41**, 185, 747 (1937).

[5] S. L. Gerhard and D. M. Dennison, Phys. Rev. **43**, 197 (1932).

TABLE I. Raman and infrated spectral data, calculated wave numbers, and assignments for fluorotrichloromethane ($CCl_3F$).[a]

| Raman[b] (liquid) | | Infrared (gas) Thompson, Temple[c] | | Infrared (gas) Plyler, Benedict[d] | | Present results | | Theoretical | | |
|---|---|---|---|---|---|---|---|---|---|---|
| $\Delta\nu$ | $I$ | $\nu$ | $I$ | $\nu$ | $I$ | $\nu$ | $I$ | $\nu_c$ | Assignment | Type |
| 244.6 | 25 | ... | ... | ... | ... | ... | ... | ... | $\nu_6$ | $e$ |
| 350.5 | 30 | ... | ... | 350[g] | w | ... | ... | ... | $\nu_3$ | $a_1$ |
| 397.8 | 15 | ... | ... | 401[g] | vw | ... | ... | ... | $\nu_5$ | $e$ |
| ... | ... | ... | ... | 451 | w | ... | ... | 446 | $\nu_4-\nu_5$ | $A_1+A_2+E$ |
| ... | ... | ... | ... | 495 | w | 492[e] | w | 495 | $\nu_4-\nu_3$ | $E$ |
| | | | | | | | | 490 | $2\nu_6$ | $A_1+E$ |
| 535.8 | 100 | 532[f] | w | 535 | m | 534$Q$ | m | ... | $\nu_2$ | $a_1$ |
| | | | | | | 543$R$ | | | | |
| ... | ... | ... | ... | 603 | w | 601 | vw | 601 | $\nu_4-\nu_6$ | $A_1+A_2+E$ |
| ... | ... | ... | ... | 680 | w | ... | ... | 702 | $2\nu_3$ | $A_1$ |
| ... | ... | 744 | w | 748 | w | 745 | m | 751 | $\nu_3+\nu_5$ | $E$ |
| ... | ... | ... | ... | 797 | m | 796 | m | 800 | $2\nu_5$ | $A_1+E$ |
| 835.4 | 5 | 854 | vs | 847 | vs | 846 | vs | ... | $\nu_4$ | $e$ |
| ... | ... | ... | ... | 895 | w | 891 | w | 885 | $\nu_2+\nu_3$ | $A_1$ |
| ... | ... | 930 | w | 932 | s | 931 | vs | 934 | $\nu_2+\nu_5$ | $E$ |
| | | | | | | 936 | | | | |
| 1068.1 | 1 | ... | ... | ... | ... | ... | ... | 1068 | $2\nu_2$ | $A_1$ |
| ... | ... | 1072 | vs | ... | ... | 1081 | s | 1091 | $\nu_4+\nu_6$ | $A_1+A_2+E$ |
| 1079 | ~0.7 | 1085 | s | 1085 | s | 1085 | vs | ... | $\nu_1$ | $a_1$ |
| ... | ... | ... | ... | 1115? | m | ... | ... | ... | ... | ... |
| ... | ... | ... | ... | ... | ... | 1147 | vw | 1151 | $\nu_3+2\nu_5$ | $A_1+E$ |
| | | | | | | 1153 | | | | |
| ... | ... | ... | ... | 1193 | w | 1194 | w | 1197 | $\nu_3+\nu_4$ | $E$ |
| | | | | | | | | 1200 | $3\nu_5$ | $A_1+A_2+E$ |
| ... | ... | ... | ... | 1215 | w | ... | ... | ... | ... | ... |
| ... | ... | 1234 | m | 1239 | w | 1242 | m | 1246 | $\nu_4+\nu_5$ | $A_1+A_2+E$ |
| ... | ... | 1310 | w | 1317 | w | 1320 | w | 1330 | $\nu_1+\nu_6$ | $E$ |
| ... | ... | 1377 | w | 1376 | m | 1379 | s | 1380 | $\nu_2+\nu_4$ | $E$ |
| ... | ... | ... | ... | ... | ... | 1471 | w | 1485 | $\nu_1+\nu_5$ | $E$ |
| 1645 | vw | ... | ... | ... | ... | ... | ... | ... | ... | ... |
| 1659 | vw | 1685 | w | 1678? | w | 1683$P$ | s | 1692 | $2\nu_4$ | $A_1+E$ |
| | | | | | | 1692$Q$ | | | | |
| ... | ... | ... | ... | 1775? | vw | 1771 | w | 1787 | $\nu_1+2\nu_3$ | $A_1$ |
| ... | ... | 1825 | w | ... | ... | ... | ... | ... | ... | ... |
| ... | ... | 2135 | m | 2132 | m | 2147 | s | 2170 | $2\nu_1$ | $A_1$ |
| ... | ... | ... | ... | 3195 | vw | (3183)[h] | vw | 3255 | $3\nu_1$ | $A_1$ |

[a] $\Delta\nu$ = Raman displacement in $cm^{-1}$; $I$ = relative intensity (s = strong, m = medium, w = weak, v = very); $\nu$ = wave number in $cm^{-1}$; $\nu_c$ = wave number computed from the fundamentals given in Table II.
[b] From reference 3.
[c] From reference 1.
[d] From reference 2.
[e] The region below 400 $cm^{-1}$ was not covered in the present investigation.
[f] The region below 532 $cm^{-1}$ was not investigated by Thompson and Temple.
[g] These two bands were measured in the liquid state only.
[h] Value somewhat uncertain.

Our assignment of the fundamentals is the same as that of PB, as are the assignments for many of the overtone and combination bands. The values adopted for the fundamentals are given in Table II.

## THERMODYNAMIC FUNCTIONS

Previously there have appeared two papers on the experimental determination of the calorimetric properties of $CCl_3F$. Benning *et al.*[6] gave heat capacity data for the liquid and vapor, reliable to about ±2 percent. Osborne *et al.*[7] reported values of the heat capacity and entropy for the solid and liquid. Above 25°K the stated accuracy of the heat capacity data is ±0.1 percent. These authors also list entropy values at 298.16 and 290.40°K computed from spectroscopic and molecular structure data, using the Raman values[8] of the fundamentals for the liquid. Thompson and Temple[1] also reported calculated thermodynamic properties over a limited temperature range.

The present paper lists values for the thermodynamic properties calculated from the fundamentals given in Table II. Brockway's[4] data for the structural parameters

TABLE II. The fundamentals of $CCl_3F$.

| Designation | $\nu$ ($cm^{-1}$) | Type | Degeneracy |
|---|---|---|---|
| $\nu_1$ | 1085 | $a_1$ | 1 |
| $\nu_2$ | 534 | $a_1$ | 1 |
| $\nu_3$ | 351[a] | $a_1$ | 1 |
| $\nu_4$ | 846 | $e$ | 2 |
| $\nu_5$ | 400[a] | $e$ | 2 |
| $\nu_6$ | 245[a] | $e$ | 2 |

[a] Values for the liquid state.

[6] Benning, McHarness, Markwood, and Smith, Ind. Eng. Chem. 32, 976 (1940).
[7] Osborne, Garner, Doescher, and Yost, J. Am. Chem. Soc. 63, 3496 (1941).
[8] G. Glockler and G. R. Leader, J. Chem. Phys. 7, 278 (1939).

TABLE III. Heat content, free energy, entropy, and heat capacity of $CCl_3F$ for the ideal gaseous state at 1 atmos pressure.[a]

| $T$ | $(H^0-E_0^0)/T$ | $-(F^0-E_0^0)/T$ | $S^0$ | $C_p^0$ |
|---|---|---|---|---|
| 100 | 8.52 | 49.87 | 58.39 | 10.29 |
| 200 | 10.74 | 56.43 | 67.17 | 15.35 |
| 273.16 | 12.34 | 60.02 | 72.36 | 17.91 |
| 298.16 | 12.84 | 61.13 | 73.96 | 18.62 |
| 300 | 12.87 | 61.21 | 74.08 | 18.67 |
| 400 | 14.61 | 65.15 | 79.76 | 20.81 |
| 500 | 16.00 | 68.57 | 84.57 | 22.20 |
| 600 | 17.11 | 71.59 | 88.70 | 23.11 |
| 700 | 18.02 | 74.29 | 92.31 | 23.73 |
| 800 | 18.76 | 76.75 | 95.51 | 24.17 |
| 900 | 19.38 | 79.01 | 98.39 | 24.49 |
| 1000 | 19.90 | 81.07 | 100.97 | 24.72 |
| 1100 | 20.35 | 82.98 | 103.33 | 24.90 |
| 1200 | 20.74 | 84.77 | 105.51 | 25.04 |
| 1300 | 21.07 | 86.44 | 107.51 | 25.15 |
| 1400 | 21.37 | 88.02 | 109.39 | 25.24 |
| 1500 | 21.63 | 89.50 | 111.13 | 25.32 |

[a] $T$ is in °K and the other quantities are in cal deg$^{-1}$ mole$^{-1}$.

TABLE IV. Calculated and calorimetric data for $CCl_3F$ vapor.

| | $C_p$ (cal deg$^{-1}$ mole$^{-1}$) | | | $S^0$ (cal deg$^{-1}$ mole$^{-1}$) | | | |
|---|---|---|---|---|---|---|---|
| $T$°K | Calc | Obs[a] | a.d.[b] | Calc[c] | Obs[d] | Calc[d] | Calc[c] |
| 311.01 | 18.95 | 19.16 | ±0.47 | | | | |
| 214.53 | 19.04 | 19.23 | ±0.51 | | | | |
| 358.74 | 20.04 | 20.44 | ±0.40 | | | | |
| 407.43 | 20.94 | 21.67 | ±0.82 | | | | |
| 290.40 | | | | 73.48 | 73.58[f] | 73.56 | |
| 298.16 | | | | 73.96 | 74.07[f] | 74.05 | 74.13 |

[a] Benning *et al.*, reference 6.
[b] a.d. = average deviation of the measured values.
[c] Present results.
[d] Osborne *et al.*, reference 7.
[e] Thompson and Temple, reference 1.
[f] These values are corrected for gas imperfection; to obtain values for the real gas, subtract 0.13 from the entropy of the ideal gas (see reference 7).

were used: C−Cl 1.76A, C−F 1.40, Cl−Cl 2.91, Cl−F 2.56, Cl−C−Cl 111.5°; other quantities were calculated with Birge's constants.[9] The moments of inertia were $I_{xx}=I_{yy}=210.4$ and $I_{zz}=300.3$ awu A$^2$.

Table III contains the values of the thermodynamic functions calculated with a rigid-rotator, harmonic oscillator approximation. Table IV shows a comparison between the calculated and calorimetric heat capacity and entropy values. In order to account for the difference between the entropy values calculated by Osborne *et al.*,[7] Thompson and Temple,[1] and the present ones, the translational, vibrational, and rotational contributions to the entropy at 298.16°K are tabulated separately in Table V. Three sets of fundamentals were used for the calculation of the vibrational contribution: (a) the present values, (b) the values of Glockler and Leader (used by Osborne *et al.*), and (c) the values of Thompson and Temple. The values of Plyler and Benedict are nearly identical with the present values and thus would give practically the same contribution to the entropy.

Since heat capacities for the liquid are known, it was of interest to attempt an approximate calculation of these from the gas values and the data of Benning *et al.* The equation used was[10]

$$(C_p)_l=(C_p)_g-dL/dT+[V_g-V_l-T(\partial V_g/\partial T)_p+T(\partial V_l/\partial T)_p]dP/dT,$$

where $L$ is the heat of vaporization, $g$ and $l$ refer to gas and liquid, and $P$, $V$, $T$ are pressure, volume, and absolute temperature, respectively. At 298.16°K, the contribution of the last term in this equation is 0.08 cal deg$^{-1}$ mole$^{-1}$.

TABLE V. Calculated entropy for $CCl_3F$ vapor at 298.16°K.

| Fundamentals used | Translational | Rotational | Vibrational | Total |
|---|---|---|---|---|
| Present values | 40.66 | 25.69 | 7.61 | 73.96 |
| Glockler, Leader (Osborne *et al.*) | 40.66 | 25.71 | 7.68 | 74.05 |
| Thompson, Temple | 40.66 | 25.72 | 7.75 | 74.13 |
| | | | Observed: | 74.07 |

The value of $dL/dT$ chosen from Benning *et al.* was −12.24 cal deg$^{-1}$ mole$^{-1}$ which is subject to an appreciable uncertainty.[11] The computed value for $(C_p)_l$ at 298.16°K is 30.78 cal deg$^{-1}$ mole$^{-1}$, compared with the value 29.06 from the smoothed data of Osborne *et al.* and 29.43 from Benning *et al.* The agreement is satisfactory in view of the inaccuracy in $dL/dT$.

## ACKNOWLEDGMENTS

The authors appreciate the assistance of the Office of Ordnance Research, U. S. Army; and the U. S. Atomic Energy Commission. The sample was kindly furnished by E. G. Young of the Kinetic Chemicals Division of the E. I. du Pont de Nemours and Company.

[9] R. T. Birge, Revs. Modern Phys. **13**, 233 (1941).

[10] J. C. Slater, *Introduction to Chemical Physics* (McGraw-Hill Book Company, Inc., New York, 1939), first edition, p. 177.

[11] A. F. Benning and R. C. McHarness, Ind. Eng. Chem. **31**, 912 (1939).

# Substituted Methanes. XVI. Vibrational Spectra, Potential Constants, and Calculated Thermodynamic Properties of Dibromodifluoromethane

CHARLOTTE E. DECKER,* ARNOLD G. MEISTER, AND FORREST F. CLEVELAND, *Spectroscopy Laboratory, Department of Physics*

AND

RICHARD B. BERNSTEIN, *Department of Chemistry, Illinois Institute of Technology, Chicago 16, Illinois*

(Received April 27, 1953)

Raman displacements, semiquantitative relative intensities, and quantitative depolarization factors of liquid $CBr_2F_2$, and infrared wave numbers and the percent transmission in the region 450–4000 $cm^{-1}$ for gaseous $CBr_2F_2$ have been obtained. Satisfactory assignments were made for all the observed bands. Using the Wilson *FG* matrix method, with a potential function containing all possible second-degree terms, reasonable values of the potential constants were calculated. Finally, the heat content, free energy, entropy, and heat capacity for the ideal gaseous state at 1 atmos pressure were calculated for 12 temperatures, from 100 to 1000°K, using a rigid rotator, harmonic oscillator approximation.

AT the time this investigation was begun, Raman displacements and relative intensities for liquid $CBr_2F_2$ had been reported by Glockler and Leader[1] and by Delwaulle and Francois.[2] The latter also gave five quantitative depolarization factors and qualitative estimates of the polarization state of four other lines. During the present investigation, infrared wave numbers and estimated relative intensities for many of the bands were reported by Plyler and Acquista.[3]

## SPECTRAL DATA AND ASSIGNMENTS

The sample of $CBr_2F_2$ was distilled under vacuum at low temperature, since the liquid boils at 24.5°C. The first slightly yellow fraction was discarded and the middle fraction was used in obtaining the spectra.

### Raman Data

Raman displacement spectrograms were obtained for the liquid with exposures ranging from 3 to 50 hr, using a 2-prism spectrograph constructed in this laboratory.[4] The depolarization spectrograms were obtained by a single-exposure method with the high-dispersion camera (E-614) on a Hilger E-612 spectrograph, and also with a Hilger E-518 spectrograph. The equipment and experimental techniques have been described in detail previously.[4–6] The values of the Raman displacements and depolarization factors were checked by the use of a Leeds and Northrup microphotometer.

The triplet 330, 340, 367 $cm^{-1}$ was very difficult to measure, since the central line is the strongest line of the Raman spectrum, while the outer lines are extremely weak. Their intensity was hardly above the background caused by the wings of the 340 $cm^{-1}$ band. The polarization states of the two weak lines were estimated from the microphotometer tracings. The Raman data obtained from the spectrograms, and assignments of the observed lines are given in Table I.

### Infrared Data

Infrared spectra were obtained for the gas with a Perkin-Elmer model 21 double-beam spectrophotometer (NaCl optics) and with a Beckman IR-2 spectrophotometer (KBr optics).

The sample was run on the Perkin-Elmer instrument in the region 660–4000 $cm^{-1}$, using 10-cm gas cells at pressures of 39.8 and 9.2 cm of Hg to obtain the combination and overtone bands. To resolve the fundamentals, the gas cell was evacuated to a pressure of less than 1 mm. Infrared data were secured from the records obtained with the Beckman instrument in the region below 1000 $cm^{-1}$. The infrared percent transmission curves are given in Figs. 1(a), 1(b), and 2. The infrared spectral data and assignments have been given previously.[7]

TABLE I. Raman spectral data for liquid $CBr_2F_2$.[a]

| | $\Delta\nu$ | | | $I$ | | $\rho$ | | | |
|---|---|---|---|---|---|---|---|---|---|
| *GL* | *DF* | *PR* | *PV* | *PR* | *DF* | *PR* | Pol. state | Assignment | Type |
| 165.3 | 165 | 168 | 165 | 43 | 0.4 | 0.47 | *P* | $\nu_4$ | $a_1$ |
| 282.2 | 281 | 281 | 282 | 2 | *D* | (0.51)[b] | *D*[b] | $\nu_8$ | $a_2$ |
| 330.1 | 330 | 325 | 330 | *vw* | *D* | *D* | *D* | $\nu_9$ | $b_2$ |
| 340.0 | 340 | 340 | 340 | 100 | 0.1 | 0.07 | *P* | $\nu_3$ | $a_1$ |
| 367.4 | 367 | 369 | 367 | *vw* | *D* | *D* | *D* | $\nu_7$ | $b_1$ |
| 622.9 | 623 | 624 | 623 | 8 | 0.03 | 0.13 | *P* | $\nu_2$ | $a_1$ |
| ... | ... | 659 | 659 | *vw* | ... | (0.47) | *P* | $2\nu_9$ | $A_1$ |
| 815.8 | 816 | 816 | 816 | 3 | 0.7 | 0.72 | *D* | $\nu_8$ | $b_2$ |
| 1076.7 | 1077 | 1077 | 1077 | 3 | 0.3 | 0.40 | *P* | $\nu_1$ | $a_1$ |
| 1142.0 | 1143 | 1141 | 1142 | *vw* | *D* | 0.76 | *D* | $\nu_6$ | $b_1$ |

[a] $\Delta\nu$ = Raman displacement in $cm^{-1}$; $I$ = relative intensity (*vw* = very weak); $\rho$ = depolarization factor; *GL* = Glockler and Leader, reference 1; *DF* = Delwaulle and Francois, reference 2; *PR* = present results; *PV* = probable value; Pol. = polarization; *D* = depolarized; *P* = polarized; and the parentheses enclose values that are uncertain.

[b] The low value of the depolarization factor is probably caused by overlapping of the very strong, polarized 340 $cm^{-1}$ line. The background is high on the plates on which the 282 $cm^{-1}$ line is sufficiently intense to measure. Also, the normal coordinate treatment indicates this line should be depolarized.

* Submitted in partial fulfillment of the requirements for the degree of Master of Science in Physics.

[1] G. Glockler and G. R. Leader, J. Chem. Phys. **7**, 553 (1939).

[2] M. L. Delwaulle and F. Francois, Compt. rend. **214**, 828 (1942).

[3] E. K. Plyler and N. Acquista, J. Research Natl. Bur. Standards **48**, 92 (1952).

[4] F. F. Cleveland, J. Chem. Phys. **11**, 1 (1943).

[5] F. F. Cleveland, J. Chem. Phys. **11**, 227 (1943).

[6] F. F. Cleveland, J. Chem. Phys. **13**, 101 (1945).

[7] Decker, Cleveland, and Bernstein, J. Chem. Phys. **21**, 189 (1953).

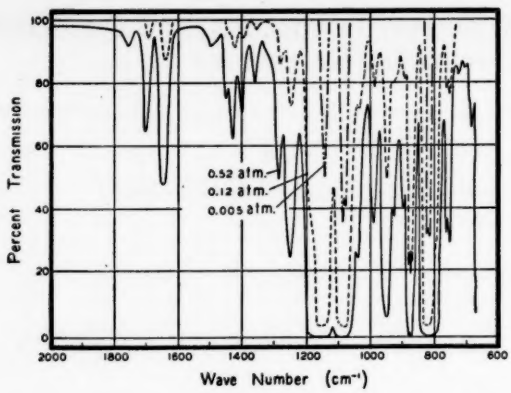


FIG. 1(a). Infrared spectrum of gaseous $CBr_2F_2$ (NaCl optics).

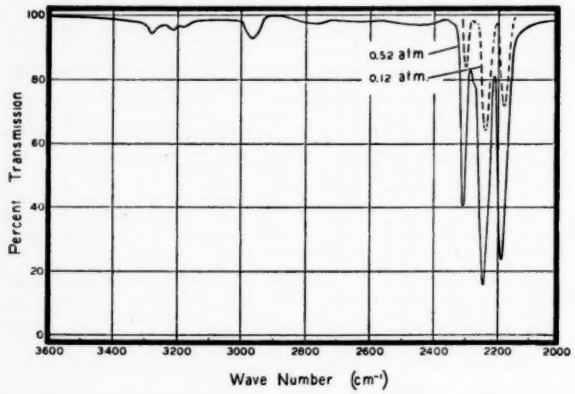


FIG. 1(b). Infrared spectrum of gaseous $CBr_2F_2$ (NaCl optics).

## Assignments

In making the assignments, the observed wave numbers were checked against the fundamental frequencies of related molecules to see if there were any bands which could be due to impurities. The strongest bands of the most probable impurities either were not observed or fell so near to the fundamentals of $CBr_2F_2$ that they would have been masked.

## NORMAL COORDINATE TREATMENT

The Wilson *FG* matrix method was used to verify the assignment of the fundamentals by transferring potential constants from $CBr_3F$[8] and $CF_3Br$[9] and calculating values of the wave numbers. The observed wave numbers were then used to find a reasonable set of potential constants for $CBr_2F_2$.

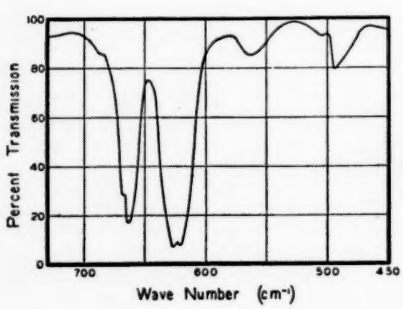


FIG. 2. Infrared spectrum of gaseous $CBr_2F_2$ (KBr optics).

The notation introduced by Davis *et al.*[10] is used for the bond distances, interbond angles, and potential constants ($f_1=C-F_1$, $f_2=C-F_2$, $b_1=C-Br_1$, $b_2=C-Br_2$, $f_1f_2=F_1-C-F_2$, etc.). Since the redundant coordinates, the symmetry coordinates, and the $F$ and $G$ matrices for the $a_2$, $b_1$, and $b_2$ vibration types were essentially the same as those obtained by Davis,[10] they will not be given here. However, for the $a_1$ vibrations it was found expedient to use a new set of symmetry coordinates in order to get $F$ matrix elements which were easier to use. The following symmetry coordinates were chosen for these:

$$R_1=2^{-\frac{1}{2}}(\Delta f_1+\Delta f_2),$$
$$R_2=2^{-\frac{1}{2}}(\Delta f_1f_2-\Delta b_1b_2),$$
$$R_3=2^{-\frac{1}{2}}(\Delta b_1+\Delta b_2),$$
$$R_4=12^{-\frac{1}{2}}[(\Delta b_1f_1+\Delta b_2f_2+\Delta b_1f_2+\Delta b_2f_1)-2(\Delta f_1f_2+\Delta b_1b_2)].$$

These led to the following new $F$ and $G$ matrix elements:

$$F_{11}=f_f+f_f{}^f,$$
$$F_{12}=f_f{}^{ff}-f_f{}^{bb},$$
$$F_{13}=2f_b{}^f,$$
$$F_{14}=2(f_f{}^{bf}+f_{f'}{}^{bf}-f_f{}^{ff}-f_f{}^{bb})6^{-\frac{1}{2}},$$
$$F_{22}=\tfrac{1}{2}(f_{ff}+f_{bb}-2f_{bb}{}^{ff}),$$
$$F_{23}=f_b{}^{ff}-f_b{}^{bb},$$
$$F_{24}=6^{-\frac{1}{2}}(f_{bb}-f_{ff}+2f_{bf}{}^{ff}-2f_{bb}{}^{bf}),$$
$$F_{33}=f_b+f_b{}^b,$$
$$F_{34}=2(f_b{}^{bf}+f_{b'}{}^{bf}-f_b{}^{ff}-f_b{}^{bb})6^{-\frac{1}{2}},$$
$$F_{44}=(f_{bb}+f_{ff}+2f_{bb}{}^{ff}+f_{bf}+f_{bf}{}^{bf'}+f_{bf}{}^{b'f}+f_{bf}{}^{b'f'}-4f_{bf}{}^{ff}-4f_{bb}{}^{bf})/3;$$
$$G_{11}=\mu_F+2\mu_C/3,$$
$$G_{12}=-2\mu_C(f^{-1}+b^{-1})2^{\frac{1}{2}}/3,$$
$$G_{13}=-2\mu_C/3,$$
$$G_{14}=2\mu_C(f^{-1}-b^{-1})/3^{\frac{1}{2}},$$
$$G_{22}=\mu_Ff^{-2}+\mu_{Br}b^{-2}+4\mu_C(f^{-1}+b^{-1})^2/3,$$
$$G_{23}=2\mu_C(f^{-1}+b^{-1})2^{\frac{1}{2}}/3,$$
$$G_{24}=3^{\frac{1}{2}}[\mu_{Br}b^{-2}-\mu_Ff^{-2}+4\mu_C(b^{-2}-f^{-2})/3]2^{-\frac{1}{2}},$$
$$G_{33}=\mu_{Br}+2\mu_C/3,$$
$$G_{34}=2\mu_C(b^{-1}-f^{-1})3^{-\frac{1}{2}},$$
$$G_{44}=3[\mu_Ff^{-2}+\mu_{Br}b^{-2}+4\mu_C(b^{-1}-f^{-1})^2/3]/2.$$

[8] Meister, Rosser, and Cleveland, J. Chem. Phys. **18**, 346 (1950).
[9] McGee, Cleveland, Meister, Decker, and Miller, J. Chem. Phys. **21**, 242 (1953).
[10] Davis, Cleveland, and Meister, J. Chem. Phys. **20**, 454 (1952).

In the above expressions, $\mu_C$, $\mu_{Br}$, and $\mu_F$ are the reciprocals of the atomic masses of the C, Br, and F atoms, respectively. The values of the masses (in awu) used in the calculations were 12.01, 79.916, and 19.00, in the same order. The equilibrium values of the C—Br and C—F bond distances were estimated from values for the same bonds in related molecules, since no microwave or electron-diffraction results were found for $CBr_2F_2$. The values assumed were $b=1.91$ and $f=1.33$A.

The calculated wave numbers are compared with the observed values in Table II, and the resulting potential constants are listed in Table III.

TABLE II. Comparison of observed and calculated fundamentals of $CBr_2F_2$.

| | $\nu_4$ | $\nu_5$ | $\nu_9$ | $\nu_3$ | $\nu_7$ | $\nu_2$ | $\nu_8$ | $\nu_1$ | $\nu_6$ |
|---|---|---|---|---|---|---|---|---|---|
| Observed | 165[a] | 282[a] | 330[a] | 340[a] | 367[a] | 623[b] | 831[b] | 1090[b] | 1153[b] |
| Calculated | 165 | 283 | 331 | 339 | 367 | 616 | 831 | 1093 | 1153 |

[a] Observed for the liquid (Reference 1).
[b] Observed for the gas (Reference 7).

TABLE III. Potential constants for $CBr_2F_2$.

| Bond-Bond (md/A) | | Type of constant Bond-Angle (md/rad) | | Angle-Angle (md A/rad²) | |
|---|---|---|---|---|---|
| $f_f$ | 6.1400 | $f_{f,f'}$ | 0.37704 | $f_{ff}$ | 1.5409 |
| $f_{f'}$ | 0.80996 | $f_{f,b}$ | 0.29605 | $f_{bf}$ | 1.1750 |
| $f_b$ | 2.9132 | $f_{b,b'}$ | 0.28016 | $f_{bb'}$ | 1.0185 |
| $f_{f'}$ | 0.66281 | $f_{b,b}$ | 0.26869 | $f_{bf,b'f}$ | 0.05514 |
| $f_{b'}$ | 0.13918 | $f_{f',b'}$ | −0.27382 | $f_{bf,b'f'}$ | 0.11594 |
| | | $f_{b,f'}$ | −0.24816 | $f_{bf,f'}$ | 0.04588 |
| | | $f_{b,b'}$ | −0.19481 | $f_{bb',f}$ | 0.07466 |
| | | $f_{f,b'}$ | −0.01254 | $f_{bf,b'f'}$ | −0.05271 |
| | | | | $f_{bb',f'}$ | −0.05031 |

## THERMODYNAMIC PROPERTIES

The heat content, free energy, entropy, and heat capacity at constant pressure were calculated for one mole of the ideal gas at 1 atmos pressure with a rigid rotator, harmonic oscillator approximation. The effect of nuclear spins and isotopic mixing was neglected. Using the values given above for the bond distances and the masses of the C, F and Br atoms, respectively, the principal moments of inertia were found to be $I_{xx}=159.0$, $I_{yy}=502.6$, and $I_{zz}=433.8$ awu A². The symmetry number is 2. The wave numbers of the fundamentals used in the calculations are given in Table II. Each is singly degenerate. Although five of the values are for the liquid state, the close agreement of the calculated values of the combination and overtone bands involving these fundamentals with the observed values for the gas[7] indicates (1) that the gas values of the low fundamentals are not appreciably different from the liquid values; and (2) that the anharmonicity is small. The calculated values of the thermodynamic properties are given in Table IV.

TABLE IV. Heat content, free energy, entropy, and heat capacity of $CBr_2F_2$ for the ideal gaseous state at 1 atmos pressure.[a]

| $T$ | $(H^0-E_0^0)/T$ | $-(F^0-E_0^0)/T$ | $S^0$ | $C_p^0$ |
|---|---|---|---|---|
| 100 | 8.78 | 53.02 | 61.80 | 10.86 |
| 200 | 11.08 | 59.81 | 70.89 | 15.51 |
| 273.16 | 12.59 | 63.49 | 76.08 | 17.76 |
| 298.16 | 13.05 | 64.61 | 77.66 | 18.40 |
| 300 | 13.08 | 64.69 | 77.77 | 18.44 |
| 400 | 14.69 | 68.68 | 83.37 | 20.46 |
| 500 | 15.99 | 72.11 | 88.10 | 21.84 |
| 600 | 17.04 | 75.11 | 92.15 | 22.79 |
| 700 | 17.92 | 77.82 | 95.74 | 23.46 |
| 800 | 18.64 | 80.26 | 98.90 | 23.94 |
| 900 | 19.25 | 82.49 | 101.74 | 24.30 |
| 1000 | 19.77 | 84.54 | 104.31 | 24.56 |

[a] $T$ is in degrees Kelvin and all thermodynamic functions are in units o cal deg$^{-1}$ mole$^{-1}$.

## ACKNOWLEDGMENTS

The sample was supplied through the courtesy of Dr. Edmond G. Young, Kinetic Chemicals Division of the E. I. DuPont de Nemours and Company. The authors are grateful to Mr. Alfons Weber for obtaining the Raman spectrograms with the Hilger E-612 spectrograph, which was obtained in part with a grant from the Research Corporation. They also appreciate the assistance of the Office of Ordnance Research, U. S. Army; the Office of Naval Research; the Atomic Energy Commission; the American Academy of Arts and Sciences; and the Society of the Sigma Xi.

# On the Use of Ultrasonic Absorption for the Determination of Very Rapid Reaction Rates at Equilibrium: Application to the Liquid Phase Association of Carboxylic Acids*†

ELI FREEDMAN‡
*Department of Chemistry, Cornell University, Ithaca, New York*
(Received October 6, 1952)

An equation is derived for the excess acoustic absorption in a liquid system due to the occurrence of a chemical reaction; the method used follows in part that used by Damköhler in the case of gases. It is shown that the gross reaction rate at equilibrium can in general be found once the frequency at which the maximum excess absorption per wavelength occurs has been found, provided thermodynamic data for the reaction are known.

The application of this method to the study of the kinetics of very rapid reactions is discussed and the effects of other causes of absorption are considered.

As another application of the results obtained the acoustic absorption of acetic and propionic acids is considered. A consistent interpretation of data in the literature is given on the assumption that the excess absorption is due to the perturbation of an equilibrium between monomeric and dimeric molecules. The mole fraction equilibrium constant $K_N$, and the heat of reaction for the dimerization are calculated. The values found for acetic acid are $K_N(293°K)=61.97$ and $\Delta H=-6.21$ kcal/mole; for propionic acid, $K_N(281.2°K)=3.040\times10^3$ and $\Delta H=-9.33$ kcal/mole. Rate constants and activation energies for the dissociation of the dimers are also calculated.

## INTRODUCTION

IN 1942 Damköhler[1] published a long detailed paper on the theory of the determination of rapid gross reaction rates[2] in an equilibrium mixture of reacting ideal gases by the measurement of sound velocity and absorption. Recently Liebermann[3] and Barthel[4] have considered (for some special cases) the role of chemical reactions as a possible cause of sound absorption in electrolytic solutions.

In this paper the excess acoustic absorption in a liquid medium due to the occurrence of a chemical reaction will be calculated under certain simplifying assumptions.[5] The results will be applied to the interpretation of the ultrasonic absorption of acetic and propionic acids, and the usefulness of ultrasonic techniques in chemical kinetics will be considered.

## THE EXCESS ABSORPTION DUE TO CHEMICAL REACTION

The acoustic absorption coefficient will be found by a method essentially like that employed by Bauer[6] in his theory of the ultrasonic absorption of unassociated liquids.

### Definitions

The reaction to be considered will be written in the form

$$\sum_{i=1}^{n} a_i A_i = 0. \tag{1}$$

Here the $A_i$ ($i=1, 2, \cdots, M$) represent the components of the reaction. The $a_i$ are the stoichiometric coefficients of the $A_i$ in the balanced chemical equation, and are either positive or negative: $a_i>0$ if $A_i$ is produced by the reaction; $a_i<0$ if $A_i$ is consumed by the reaction.

Let $n_i$ and $N_i$ be the number of moles and the mole fraction, respectively, of $A_i$. Then $N_i=n_i/n$, where $n=\sum n_j+n_S$. (In this equation and henceforth, summation limits are understood to be 1 and $M$, unless otherwise indicated.)

The heat of reaction $\Delta H$, is

$$\Delta H=\sum a_i \bar{H}_i, \tag{2}$$

where $\bar{H}_i$ is the partial molal heat content of $A_i$ in the particular medium. The solvent, if any, is assumed to be inert.

The mole fraction equilibrium constant $K_N$ is given by

$$\ln K_N=\sum a_i \ln N_i^0, \tag{3}$$

where the superscript "0" here and elsewhere refers to an equilibrium value, although for simplicity it will be omitted wherever no ambiguity will result.

The total heat content of the system is given by

$$H=\sum n_i \bar{H}_i+n_S \bar{H}_S, \tag{4}$$

where the subscript "$S$" refers to the solvent, if any.

---

* Based on a Ph.D. thesis submitted by Eli Freedman to the Graduate Faculty of Cornell University, September, 1952.

† Part of this paper was presented at the 122d National Meeting of the American Chemical Society, September, 1952.

‡ Present address: Research Analysis Group, Department of Physics, Brown University, Providence 12, Rhode Island.

[1] G. Damköhler, Z. Elektrochem. **48**, 62, 116 (1942). This paper also contains a historical review of the problem.

[2] G. Damköhler's *Bruttogeschwindigkeit*. This term should be carefully distinguished from *net reaction rate* (which is zero at equilibrium) and *specific reaction rate* (which depends on the mechanism assigned to the reaction).

[3] L. Liebermann, Phys. Rev. **76**, 1520 (1949).

[4] R. Barthel, J. Acoust. Soc. Am. **24**, 313 (1952).

[5] While this paper was being prepared, Dr. Milton Manes of the U. S. Bureau of Mines informed the author that he had arrived at similar results. See J. Chem. Phys. **21**, 1791 (1953).

[6] E. Bauer, Proc. Phys. Soc. (London) **62A**, 141 (1949).

### The Equilibrium Heat Capacity

The differentiation of Eq. (4) with respect to temperature, keeping the pressure constant, gives

$$C_P^0 \equiv \left(\frac{\partial H}{\partial T}\right)_P = \sum n_i \left(\frac{\partial \bar{H}_i}{\partial T}\right)_P + n_S \left(\frac{\partial \bar{H}_S}{\partial T}\right)_P + \sum \bar{H}_i \left(\frac{\partial n_i}{\partial T}\right)_P . \quad (5)$$

Here $C_P^0$ is the measured equilibrium heat capacity of the entire system. The first two terms on the right, which will be designated $C_P^\infty$, represent the contributions of the individual components to the total heat capacity. The third term on the right, which will be designated $C_P^r$, gives the contribution to the total heat capacity made by the occurrence of the reaction.

A new variable $\xi$ will now be introduced. It is defined by the equation

$$\delta n_i = a_i \delta \xi. \quad (6)$$

(The operator "$\delta$" has its usual meaning of a small change or variation.)

From the definition of $C_P^r$ and Eqs. (2) and (6), it is seen that

$$C_P^r = \Delta H \left(\frac{\delta \xi}{\delta T}\right)_P . \quad (7)$$

The differentiation of Eq. (3) with respect to temperature at constant pressure gives

$$\left(\frac{\partial \ln K_N}{\partial T}\right)_P = \frac{\Delta H}{RT^2} = \sum \frac{a_i}{n_i}\left(\frac{\partial n_i}{\partial T}\right)_P - \sum \frac{a_i}{n}\left(\frac{\partial n}{\partial T}\right)_P . \quad (8)$$

Combining Eqs. (6) and (8), solving for $(\partial \xi/\partial T)_P$, and then substituting the result into Eq. (7) gives

$$C_P^r = DR(\Delta H/RT)^2, \quad (9)$$

where

$$D = [\sum (a_i^2/n_i) - (\sum a_i^2)/n]^{-1}. \quad (10)$$

### Introduction of Time

These equations apply only to purely equilibrium processes. Now it is necessary to inquire into the changes that will be caused by taking into account the fact that a finite time is required for the reaction to achieve its equilibrium state again, once it has been momentarily displaced from that state by a small perturbation.

To find an expression for $\partial \xi/\partial t$, suppose that the reaction (1) is displaced from its equilibrium position to an extremely small extent, say, by the passage of a sound wave through it. The perturbation is to be taken so small that it will be a good approximation to assume that the forward and backward gross reaction rates are virtually equal to each other. Let these forward and backward rates be $U_f$ and $U_b$, respectively. Then evidently $U_f^0 = U_b^0$. This equilibrium gross reaction rate will henceforth be denoted by $U$. With these definitions it follows that near equilibrium

$$(\partial \xi/\partial t)_P = U_f - U_b. \quad (11)$$

Inasmuch as $U_f$ and $U_b$ are presumed to be so near their equilibrium value, $\ln U_f$ and $\ln U_b$ can each be expressed as the first two terms of a Taylor series expansion about $\ln U$:

$$\ln U_f = \ln U + \left(\frac{\partial \ln U_f}{\partial T}\right)_{eq} (T - T^0). \quad (12)$$

Here, "*eq*" means that the derivatives are evaluated for the equilibrium state. Rearranging Eq. (12) leads to

$$\ln(U_f/U) = \ln[1 - (U - U_f)/U] \cong (U_f - U)/U;$$

hence,

$$(U_f - U)/U = (d \ln U_f/dT)_{eq}(T - T^0). \quad (13)$$

Likewise,

$$(U_b - U)/U = (d \ln U_b/dT)_{eq}(T - T^0). \quad (14)$$

In many cases $U_f$ and $U_b$ can be represented by equations of the type

$$U_f = k_f \prod N_i^{-a_i} \cdot F, \quad (a_i < 0) \quad (15)$$

and

$$U_b = k_b \prod N_j^{a_j} \cdot F, \quad (a_j > 0), \quad (16)$$

where $F$ is some unspecified function of the concentrations and temperature.[7] Provided that only the first-order terms are retained in Eqs. (13) and (14), it will be seen that nothing need be known about the functional form of $F$. However, $F$ must be the same function in both (15) and (16) since at equilibrium it is necessary that

$$\frac{k_f}{k_b} = \frac{\prod N_j^{a_j}}{\prod N_i^{-a_i}} = K_N. \quad (17)$$

The two $k$'s introduced in Eqs. (15) and (16) are specific reaction rate constants and hence are dependent only upon the temperature.

Subtracting Eq. (14) from Eq. (13) and substituting Eqs. (15) and (16) into the resulting equation, due attention being paid to signs, gives

$$(U_f - U_b)/U = (\Delta H/RT^2)(T - T^0) - \sum (a_i/N_i)(\partial N_i/\partial T)_P (T - T^0), \quad (18)$$

where use has also been made of Eqs. (3) and (17). The derivation of Eq. (18) has followed closely the work of Damköhler.[1] Combining Eqs. (18) and (11) and expressing $(\partial N_i/\partial T)_P$ in terms of $(\partial \xi/\partial T)_P$ (as

[7] More general relationships than Eqs. (15) and (16) between the gross reaction rates and the concentrations of the components have recently been derived by Manes, Hofer, and Weller, J. Chem. Phys. **18**, 1355 (1950).

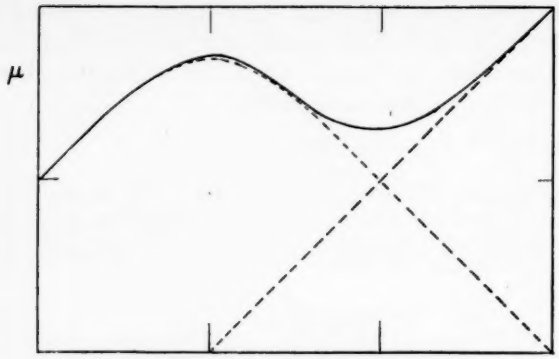


FIG. 1. Absorption due to reaction greater than absorption due to other causes: $8EB^2c/A=0.08$.

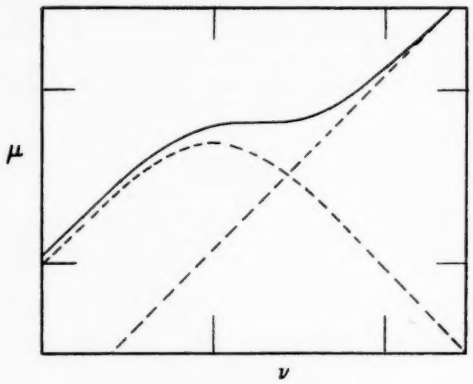


FIG. 2. Absorption due to reaction comparable to absorption due to other causes: $8EB^2c/A=1$.

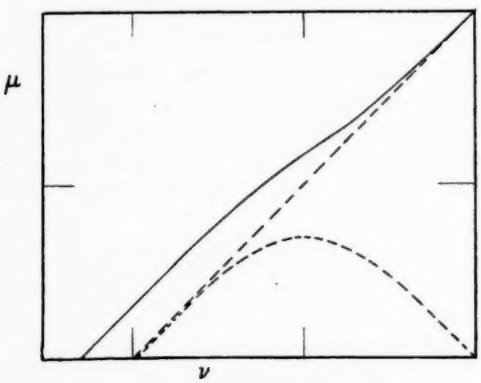


FIG. 3. Absorption due to reaction less than absorption due to other causes: $8EB^2c/A=8$.

FIGS. 1–3. Total absorption coefficient per wavelength (solid lines) plotted against frequency. The bell-shaped dashed lines show the absorption due to reaction; the dashed straight lines show the absorption due to all other causes. Horizontal and vertical scales are logarithmic in all plots. Numbers have been omitted as the graphs are purely illustrative.

above) yields

$$(1/U)(\partial\xi/\partial t)_P=(\Delta H/RT^2)(T-T^0)$$
$$-[\sum(a_i^2/n_i)-(\sum a_j)^2/n](\partial\xi/\partial T)_P(T-T^0). \quad (19)$$

For a harmonic disturbance, $T=T^0+\Delta Te^{i\omega t}$. Equation (19) can now be solved for $(\partial\xi/\partial T)_P$ since $(\partial\xi/\partial t)_P=(\partial\xi/\partial T)_P(\partial T/\partial t)$,

$$(\partial\xi/\partial T)_P=D(\Delta H/RT^2)/[1+(i\omega D/U)]. \quad (20)$$

The effective heat capacity at constant pressure for frequency $\omega$ can now be defined as

$$C_P^{\text{eff}}=C_P^{\infty}+\Delta H(\partial\xi/\partial T)_P, \quad (21)$$

in analogy with the equation used previously for $C_P^0$. The distinction is that here $(\partial\xi/\partial T)_P$ is a function of the frequency. Combining Eqs. (20) and (21) yields, with the use of Eq. (9),

$$C_P^{\text{eff}}=C_P^{\infty}+C_P^r/[1+i\omega D/U]. \quad (22)$$

Thus the effective heat capacity is a complex quantity, and consists of two components, one of them instantaneous and the other relaxational. It should be pointed out that this division is with reference to the reaction. The "instantaneous" component is not strictly that, but may itself be divided into several further components, each with a nonzero relaxation time. It is assumed here, however, that all of these relaxation times are much smaller than that of the reaction itself.[8]

By employing the internal energy $E$ instead of the heat content $H$ and by carrying out the differentiations with respect to the temperature at constant volume instead of constant pressure, an equation for $C_V^{\text{eff}}$ can be obtained in an identical manner. If it is assumed that the volume change of reaction is negligible, then this expression reduces to

$$C_V^{\text{eff}}=C_V^{\infty}+C_P^r/[1+i\omega D/U]. \quad (23)^9$$

The ratio of the effective heat capacity at constant pressure to that at constant volume is

$$\gamma^{\text{eff}}=C_P^{\text{eff}}/C_V^{\text{eff}} \quad (24)$$

and of course is also a complex quantity.

## The Absorption Coefficient

The sound absorption coefficient can now be found. Consider a plane wave,

$$u=u_0\exp[(t-x/\Gamma)]=u_0e^{-\alpha x}\exp[(t-x/c)],$$

where $\Gamma$ is the complex phase velocity of the wave; $c$, its real phase velocity; and $\alpha$, the linear amplitude absorption coefficient. It is easily shown that

$$\alpha=-(\omega c/2)Im(1/\Gamma^2). \quad (25)$$

For the present case it follows from the work of Markham, Beyer, and Lindsay[10] that $\Gamma$ is given by

$$\Gamma^2=\gamma^{\text{eff}}/\rho\beta_T. \quad (26)$$

This may be compared to the equation satisfied by $c^2$

[8] It is to be noted that if there are several relaxation processes, then $C_P^{\infty}$ will decrease with increasing frequency as successive components are "frozen" out.

[9] Note that the numerator of the second term on the right is $C_P^r$, not $C_V^r$. This is a direct consequence of the assumption that there is but a negligible volume change due to reaction.

[10] Markham, Beyer, and Lindsay, Revs. Modern Phys. 23, 353 (1951). See especially Sec. 7A.

(the velocity at very low frequencies),

$$c_0^2=\gamma_0/\rho\beta_T, \tag{27}$$

where $\rho$ is the density, $\beta_T$ is the coefficient of isothermal compressibility, and $\gamma_0$ is the ratio $C_P^0/C_V^0$. In writing Eq. (26) it is assumed that $\beta_T$ is a real number. This will be the case when, as has already been assumed, the volume change due to reaction is negligible. (Otherwise there would be the possibility of "structural absorption" of the type investigated by Hall[11] in the case of water.)

Combining Eqs. (22)–(27) there is obtained, after some algebra,

$$\alpha=\left[\frac{\gamma_0\omega c}{2c_0^2}\right]\frac{(C_P^0-C_V^0)C_P^r(\omega D/U)}{(C_P^0)^2+(C_P^\infty)^2(\omega D/U)^2}. \tag{28}$$

Use is made of the equations $C_P^0=C_P^\infty+C_P^r$ and $C_V^0=C_V^\infty+C_P^r$ in simplifying the numerator of (28).

In studying the variation of the absorption with frequency it is more useful to consider the absorption coefficient per wavelength, which is defined by

$$\mu=\alpha\lambda, \tag{29}$$

where $\lambda$ is the sound wavelength. It follows at once that

$$\mu=\pi\gamma_0\left(\frac{c}{c_0}\right)^2\frac{(C_P^0-C_V^0)C_P^r(\omega D/U)}{(C_P^0)^2+(C_P^\infty)^2(\omega D/U)^2}. \tag{30}$$

The function $\mu(\omega D/U)$ has the typical bell-shape associated with absorption due to a relaxation mechanism. It attains a maximum when

$$\omega_m/U=C_P^0/DC_P^\infty, \tag{31}$$

on the assumption that $c$ is independent of the frequency. The value of $\mu$ at the maximum is

$$\mu_m=(\pi/2)(c/c_0)^2(\gamma_0-1)C_P^r/C_P^\infty. \tag{32}$$

It is to be emphasized that $\alpha$ and $\mu$ of the preceding equations refer only to the excess absorption caused by the occurrence of the chemical reaction, and not to absorption due to any other cause. This point will be taken up below.

## APPLICATION TO CHEMICAL KINETICS

There does not exist at present a widely-applicable technique for the measurement of extremely rapid reaction rates in solutions at ordinary concentrations and temperatures. In fact it can be shown[12] by considering the diffusion of thin filaments of reactants into one another that rates of reactions having a half-time less than $10^{-4}$ second cannot be determined by the usual flow methods, for diffusion becomes the rate-controlling step instead of reaction. In order to measure the rate of such rapid reactions use must be made of some method which does not require the mixing of the reactants. Studying the rate of return of the system to equilibrium after it has been subjected to a small perturbation from an equilibrium state is one such procedure,[13] and the use of ultrasonic waves appears to be a specific means of accomplishing this. As yet, however, few such experiments have been reported.[14]

At first glance this method would appear simple and of fairly wide application: The absorption coefficient per wavelength is first measured as a function of the circular frequency $\omega$; this leads to a determination of $\omega_m$, which in turn gives $U$ directly from Eq. (31) provided $D$ can be determined.

There is, however, one important difficulty: the effect of other sources of absorption on the accuracy of the determination of $\mu_m$ and hence of $\omega_m$. Of the various possible other sources the two most important are vibrational heat capacity relaxation and viscosity, in that order. For the case in which the vibrational heat capacity relaxation frequencies are all far removed from the relaxation frequency of the reaction, $\nu_m=\omega_m/2\pi$, the linear absorption due to other causes in the neighborhood of $\nu_m$ will be proportional to the frequency squared; hence, to a first approximation the total absorption per wavelength $\mu_T$ will be given by

$$\mu_T=A\nu/(B^2+C^2\nu^2)+Ec\nu \tag{33}$$

in the neighborhood of $\nu_m$. Here $\nu$ is the sound frequency, $E$ is a constant, $c$ is the sound velocity at frequency $\nu$, and $A$, $B$, and $C$ are defined by comparison with Eq. (30). The function $\mu_T(\nu)$ has two stationary points; their locations are given by the two positive values of

$$\nu^2=\frac{A-2EcB^2\pm A[1-8EcB^2/A]^{\frac{1}{2}}}{2C^2E}.$$

If $8EcB^2/A<1$, then $\mu_T(\nu)$ has both a relative maximum and a relative minimum, the former occurring at the lower frequency. If, however, $8EcB^2/A\geqslant 1$, the maximum and minimum disappear, and $\mu_T(\nu)$ has only an inflection point. Three different cases are shown graphically in Figs. 1, 2, and 3. Whether $\nu_m$ can be calculated with any degree of accuracy in such situations will depend in general upon the accuracy with which the absorption due to other causes for a given system can be estimated. This will be difficult, as there does not yet exist an adequate theory for the acoustic absorption of solutions.

[11] L. Hall, Phys. Rev. **73**, 775 (1948).
[12] S. H. Bauer (private communication).

[13] See the paper mentioned in reference 7 for a general discussion of the theory of the determination of reaction rates by the measurement of gross reaction rates at or near equilibrium.
[14] Mention should be made, however, of early attempts to determine reaction rates in the system $N_2O-N_2O_4$ by the measurement of sound velocity; these are summarized by H. O. Kneser and O. Gauler, Physik. Z. **37**, 677 (1936). See also the discussion in Damköhler's paper (reference 1). Also: S. H. Bauer, J. Phys. Chem., April, 1953.

TABLE I. Properties of acetic acid.

| Quantity[a] | | |
|---|---|---|
| $C_P = 1.96_0 + 0.0038_9 t$ joules/gram-°C [b] | | |
| $V_t = V_0 1 + 0.001063t - 1.2636\times10^{-7}t^2 + 1.0876\times10^{-8}t^3$ [c] | | |
| $\rho_{20} = 1.049$ gram/ml [d] | | |
| $t$ | Adiabatic compressibility | Isothermal compressibility[e] |
| 20 | $75.73\times10^{-6}$ atmos$^{-1}$ | $91.98\times10^{-6}$ atmos$^{-1}$ |
| 30 | 81.55 | 98.48 |
| 40 | 87.50 | 105.10 |
| 50 | 94.10 | 112.55 |
| 60 | 101.18 | 120.66 |

[a] $t$ = temperature, °C.
[b] *International Critical Tables* **5**, 114.
[c] Lange, *Handbook of Chemistry*, sixth edition, p. 1589.
[d] Reference c, p. 331.
[e] D. Tyrer, J. Chem. Soc. **105**, 2534 (1914).

## APPLICATION TO CARBOXYLIC ACIDS

One application of the results obtained in the preceding section is to associated liquids, at least those of the types exemplified by the lower aliphatic alcohols and the carboxylic acids. (Some such restriction as this is necessary at present so that only liquids in which the association manifests itself by the formation of specific chemical entities are included.)

### Acetic Acid

Acetic acid vapor is known to be composed of an equilibrium mixture of a monomer and a dimer. The dimer is held together by hydrogen bonding between the two carboxyl groups,

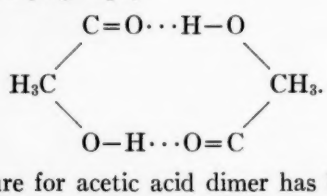

This structure for acetic acid dimer has been verified directly by electron diffraction.[15] That a similar equilibrium occurs in the liquid phase has been established for pure acetic acid by Raman spectroscopy,[16] and for solutions of acetic acid in nonpolar solvents by polarization measurements,[17,18] distribution experiments (see Moelwyn-Hughes[19]), and infrared spectroscopy.[20]

Accordingly it can be assumed that liquid acetic acid is an equilibrium mixture of a monomer and a dimer, the reaction being

$$2CH_3COOH \rightleftharpoons (CH_3COOH)_2.$$

Therefore, $a_1=-2$, $a_2=1$, $\sum a_j=-1$, and so

$$D=[4/n_1+1/n_2-1/(n+n_2)]^{-1}.$$

If $y$ is the degree of dissociation of the dimer, and if one mole of dimer was initially present (before dissociation), then by Eq. (9)

$$C_P{}^r = R(\Delta H/RT)^2(y/2)(1-y^2).$$

In this case, $C_P{}^0$ is taken as the heat capacity of 120.1 g of acetic acid.[21] The data used in the calculations are assembled in Table I. In Table II are listed various constants derived from those in Table I. The ultrasonic data are those of Lamb and Pinkerton.[22]

From Eq. (32),

$$\frac{\pi}{2}\left(\frac{c}{c_0}\right)^2(\gamma_0-1)\frac{C_P{}^r}{C_P{}^0-C_P{}^r}=\mu_m. \qquad (34)$$

Lamb and Pinkerton's data show that at no temperature does $(c_\infty/c_0)^2$ exceed 1.036, so that $(c/c_0)^2$ may be reasonably taken to be 1. Here $c$ is the velocity at frequency $\nu_m$; its exact value is unknown, but it must lie between $c_0$ and $c_\infty$.

At $T_1=293$°K, $\mu_m=0.0510$; at $T_2=323$°K, $\mu_m=0.0610$; hence it follows from (34) that

TABLE II. Some physical constants of acetic acid calculated from data in Table I.

| $T$(°K) | Coefficient of thermal expansion | Density (g/ml) | Heat cap. ($c_P{}^0$) (cal/gram-°C) | $c_P{}^0-c_V{}^0$ (cal/gram-°C) | $\frac{\pi}{2}(\gamma_0-1)$ |
|---|---|---|---|---|---|
| 293 | 0.001069 | 1.049 | 0.4875 | 0.09243 | 0.3675 |
| 303 | 0.001085 | 1.038 | 0.4968 | 0.09101 | 0.3523 |
| 313 | 0.001105 | 1.027 | 0.5061 | 0.09040 | 0.3416 |
| 323 | 0.001132 | 1.017 | 0.5154 | 0.09056 | 0.3348 |
| 333 | 0.001165 | 1.007 | 0.5247 | 0.09131 | 0.3310 |

$$\frac{C_P{}^r}{58.544-C_P{}^r}=0.13877 \text{ at } 293°\text{K},$$

and

$$\frac{C_P{}^r}{61.898-C_P{}^r}=0.18218 \text{ at } 323°\text{K}.$$

Solving each of these equations gives $C_P{}^r(293)=7.1347$ cal/mole and $C_P{}^r(323)=9.5388$ cal/mole.

Let $y$ and $z$ be the degrees of dissociation of the dimer at $T_1=293$°K and $T_2=323$°K, respectively. Then

$$R(\Delta H/RT_1)^2(y/2)(1-y^2)=7.1347 \qquad (35)$$

and

$$R(\Delta H/RT_2)^2(z/2)(1-z^2)=9.5388. \qquad (36)$$

A third equation is necessary. The mole fraction equilibrium constants at 293°K and 323°K are $K_y=(1-y^2)/$

[15] J. Karle and L. O. Brockway, J. Am. Chem. Soc. **66**, 574 (1944).
[16] P. Traynard, Bull. soc. chim. France **14**, 316 (1947). Traynard finds a value for $\Delta H$ much larger than that reported here.
[17] Hobbs, Deal, Maryott, and Gross, *Abstracts of Papers*, American Chemical Society, April 1951, p. 50 p.
[18] Pohl, Hobbs, and Gross, J. Chem. Phys. **9**, 408 (1941).
[19] E. A. Moelwyn-Hughes, *The Kinetics of Reactions in Solution* (Oxford University Press, London, 1947), second edition, p. 171 *f*.
[20] M. M. Davies and G. B. B. M. Sutherland, J. Chem. Phys. **6**, 767 (1938).
[21] In a brief communication of the results of this section, E. Freedman, J. Chem. Phys. **19**, 1318 (1951) there were unfortunately several errors. The most serious one is in the equation for $\mu(\nu)$. The correct equation can be obtained at once by substituting the expressions just given for $C_P{}^r$, $C_P{}^0$, and $D$ into Eq. (30).
[22] J. Lamb and J. M. M. Pinkerton, Proc. Roy. Soc. (London) **199A**, 114 (1949).

$4y^2$ and $K_z=(1-z^2)/4z^2$. The integrated van't Hoff equation is

$$\ln\left[\frac{K(T_2)}{K(T_1)}\right]=\frac{\Delta H}{R}\left[\frac{1}{T_1}-\frac{1}{T_2}\right],$$

provided $\Delta H$ is independent of temperature in the range taken. For $T_1=293°K$, and $T_2=323°K$, this equation becomes, upon converting to common logarithms,

$$\log\left[\frac{K(323)}{K(293)}\right]=6.9302\times10^{-5}\Delta H.$$

Substituting the expressions for $K_y$ and $K_z$ gives

$$2\log(y/z)+\log\left[\frac{1-z^2}{1-y^2}\right]=6.9302\times10^{-5}\Delta H, \quad (37)$$

the necessary third equation.

These three equations can be solved by a straightforward method of successive approximations. The results are $K(293)=61.97$, and $\Delta H=-6.21$ kcal/mole. These values can now be used to compute $\mu_m$ at all the remaining temperatures. The results are collected in Table III and are seen to be in good agreement with Lamb and Pinkerton's data.[22]

The gross reaction rate, $U$, can be calculated now from Eq. (31), since $\nu_m$ is given by Lamb and Pinkerton.[22] The result of this computation is in Table III. If now it is assumed that for the reverse reaction, $U=k_bN_2$, $k_b$ can be found immediately. The values of $k_f$ are contained in Table III. Finally the energy of activation of the reverse reaction can be found by plotting $\log k_b$ against $1/T$. It is found that the plot is linear; the slope gives $q_b=12{,}700$ cal/mol. This calculation depends on the mechanism assumed for the reverse reaction. The measurement of the ultrasonic absorption over a range of concentration of solutions of acetic acid in an inert solvent (e.g., toluene) would be a way by which this point could be investigated further.

No error has been introduced by neglecting the possible volume change of reaction, as the data of Pohl, Hobbs, and Gross[18] on the electric polarization of acetic acid show that this volume change is zero.

### Discussion of the Results for Acetic Acid

In view of the fact that there has been considerable discussion in the literature on the acoustic behavior of acetic acid and its interpretation, it seems appropriate to discuss the significance of the preceding results in a little more detail.

The dimerization of acetic acid has been studied extensively both in the vapor phase and in non-polar solvents. A recent investigation[23] of the vapor phase association gave $\Delta H=-15.3$ kcal/mole of dimer, and a recent study[17] of the association of acetic acid in benzene solution gave $\Delta H=-9.2$ kcal/mole of dimer. Moelwyn-

[23] M. D. Taylor, J. Am. Chem. Soc. **73**, 315 (1951).

TABLE III. Results of calculations for acetic acid.

| $T$(°K) | Max. abs. coefs. per wavelength Obs[a] | Calc | Gross reaction rate $U\times10^{-5}$ (mole/liter) |
|---|---|---|---|
| 293 | 0.0510 | 0.0510 | 0.969 |
| 303 | 0.0545 | 0.0540 | 1.87 |
| 313 | 0.0583 | 0.0574 | 3.53 |
| 323 | 0.0610 | 0.0610 | 6.56 |
| 333 | 0.0641 | 0.0648 | 11.7 |

| $T$(°K) | Mole fraction equil. constant $K_N$ | Specific rate const. for dissn.[b] $k_b\times10^{-5}$ (sec$^{-1}$) |
|---|---|---|
| 293 | 61.97 | 1.10 |
| 303 | 43.58 | 2.18 |
| 313 | 31.34 | 4.22 |
| 323 | 23.01 | 8.08 |
| 333 | 17.21 | 14.9 |

[a] See reference 22.
[b] Assuming first-order mechanism for the dissociation.

Hughes[24] has shown that the change in $\Delta H$ from vapor to solution can be satisfactorily accounted for by assuming that the electrostatic energy between dipolar molecules is reduced by a fraction $(D+2)/(3D)$ in a medium of dielectric constant $D$. Thus, if $D$ for benzene is taken as 2.28, the fraction is 0.627; whereas

$$\frac{\Delta H_{\text{benzene}}}{\Delta H_{\text{vapor}}}=\frac{9.2}{15.3}=0.601.$$

A similar calculation for pure acetic acid with $D$ taken as 7.1 gives the factor as 0.427. Hence the predicted value for $\Delta H$ in pure acetic acid would be

$$\frac{0.427}{0.601}(-9.2)=-6.5 \text{ kcal/mole of dimer}$$

which compares favorably with the value $-6.2$ kcal/mole of dimer found above. This calculation is, of course, based on an oversimplified model; but it serves to show that the values found by the ultrasonic method are indeed reasonable. The first attempt at a calculation of the heat of association of acetic acid from ultrasonic data was made by Lamb and Pinkerton.[22] However they employed the simple "two state" model, $A\rightleftarrows B$, and thus implicitly assumed an incorrect stoichiometry for the reaction $2CH_3COOH\rightleftarrows(CH_3COOH)_2$. (It was for this reason[25] that they were unable to obtain the correct temperature dependence of the absorption from their computation.) They arrived at a value of $\Delta H$ of $-8860$ cal/mole and speculated that the process occurring involved the formation of one hydrogen bond only. It is now seen that this is not the case.

Lamb and Pinkerton[22] found evidence of another relaxation process in acetic acid, this one near 67 mega-

[24] Reference 19, p. 206.

[25] In earlier note (see reference 21) it was stated that the reason for their failure to account for the temperature dependence was the use of an incorrect rate law. Dr. Milton Manes has pointed out in a letter that any number of rate laws would work, provided that they implied the correct 2:1 ratio of monomer to dimer.

TABLE IV. Some physical constants of propionic acid.

| $T$(°K) | $C_p$ (cal/g-°C)[a] | Sound vel. (m/s)[b] | $C_v$ (cal/g-°C) | $\frac{\pi}{2}(\gamma_0-1)$ |
|---|---|---|---|---|
| 281.2 | 0.5595 | 1236 | 0.4594 | 0.3463 |
| 294.2 | 0.5595 | 1171 | 0.4645 | 0.3252 |
| 304.2 | 0.5595 | 1121 | 0.4687 | 0.3047 |
| 314.2 | 0.5595 | 1071 | 0.4730 | 0.2875 |
| 324.2 | 0.5595 | 1021 | 0.4776 | 0.2686 |

[a] *International Critical Tables* **5**, 108.
[b] L. Bergmann, *Der Ultraschall* (Zurich, 1949), fifth edition.

cycles per second. It would not be unreasonable to surmise that a vibrational heat capacity relaxation occurs near this frequency. Or, in view of the fact that the existence of a trimer or a tetramer in acetic acid vapor has been reported by some investigators,[26] it may be that this second relaxation process is caused by the presence of an equilibrium involving a higher polymer. Again, this could be investigated by making absorption measurements on solutions of acetic acid in an inert solvent.

## Propionic Acid

Similar calculations can be carried out with the data of Lamb and Huddart[27] for the absorption of propionic acid. In order to find $C_V^0$, the equation $C_V^0=(C_P^0)^2/[C_P^0+c_0^2T\epsilon^2]$ is employed (instead of $C_P^0/C_V^0=\beta_T^0/\beta_S^0$, which was used in the case of acetic acid). Here, $C_P^0$ and $C_V^0$ are the equilibrium heat capacities at constant pressure and volume of one gram of acid; $\epsilon$ is the coefficient of thermal expansion; and $c_0$ is the velocity of sound at very low frequency. The data used are listed in Table IV. In the computations $C_P^0$ and $C_V^0$ are taken as the heat capacities of 148.2 g of acid. The remaining part of the calculation is the same as for acetic acid, and leads to the result that $K_N(281.2°)=3.040\times10^3$, and $\Delta H=-9.33$ kcal/mole. The values of $\mu_m$ calculated with the aid of these constants are compared with Lamb and Huddart's data in Table V, which also contains the values found for $U$ and $k_b$. The calculated activation energy for the dissociation is 13.2 kcal. The calculated value for $\Delta H$ of the vapor phase reaction is $-17.2$ kcal/mole if the dielectric constant of propionic acid is taken to be 3.2. This is in fair agreement with the measured value at 433°, $-15.2$ kcal/mole.[28]

TABLE V. Results of calculations for propionic acid.

| $T$(°K) | Max. abs. coef. per wavelength Obs[a] | Calc | Gross reaction rate $U\times10^{-4}$ (mole/liter) | Mole fraction equil. constant $K_N\times10^{-2}$ | Specific rate const. for dissn.[b] $k_b\times10^{-4}$ (sec$^{-1}$) |
|---|---|---|---|---|---|
| 281.2 | 0.0107 | 0.0108 | 3.03 | 30.40 | 3.08 |
| 294.2 | 0.0134 | 0.0136 | 8.67 | 14.54 | 8.90 |
| 304.2 | 0.0154 | 0.0155 | 18.1 | 8.680 | 18.7 |
| 314.2 | 0.0178 | 0.0178 | 34.8 | 5.262 | 36.4 |
| 324.2 | 0.0201 | 0.0199 | 67.2 | 3.318 | 71.0 |

[a] See reference 27.
[b] Assuming first-order mechanism for the dissociation.


### ACKNOWLEDGMENT

It is a pleasure to acknowledge the friendly aid and constructive criticisms of Professor S. H. Bauer in carrying out this work.


[26] For example, see H. L. Ritter and J. H. Simons, J. Am. Chem. Soc. **67**, 757 (1945) (tetramer); or E. W. Johnson and L. K. Nash, *ibid.* **72**, 547 (1950) (trimer).
[27] J. Lamb and J. Huddart, Trans. Faraday Soc. **46**, 540 (1950).
[28] M. D. Taylor, J. Am. Chem. Soc. **74**, 4151 (1952).

# Relationships between Kinetics and Acoustic Phenomena in Equilibrium Systems

MILTON MANES*
*Synthetic Fuels Research Branch, Fuels-Technology Division, Bureau of Mines, Region VIII, Bruceton, Pennsylvania*
(Received August 15, 1952)

In a reacting (one-phase, one-reaction) system close to equilibrium, each variable (for example, composition, volume, temperature) approaches its equilibrium value at a rate proportional to its displacement from equilibrium. All the first-order rate constants in a particular state are identical. One can therefore characterize any system at equilibrium by a single relaxation time. When the relaxation of a chemical reaction gives rise to absorption and dispersion of sound, the thermal and dilatational contributions to the relaxational compressibility are necessarily in phase with each other and with the chemical reaction. A known but hitherto limited equation for the propagation of sound has been generalized to combine all such contributions for any system, irrespective of reaction mechanism, so that the propagation of sound may be described in terms of the instantaneous compressibility, the static compressibility, and the relaxation time. The relaxation time is a rather simple function of composition, temperature, and the rate laws for the forward and reverse reactions; it can be expressed for any postulated pair of rate laws. Therefore, measurement of the relaxation time of a (single) chemical reaction at different equilibrium compositions and temperatures yields kinetic information. The relationships derived here may be applied under certain conditions to acoustic studies of very fast reactions

## I. INTRODUCTION

MEASUREMENTS of reaction rates of reversible reactions close to equilibrium yield information about the kinetics of the forward and reverse reactions and may be especially useful for investigating reactions that are too fast to be followed by conventional methods. This study, an extension of an earlier one on this subject,[1] deals with methods for measuring such reaction rates, the emphasis being on sound absorption and dispersion.

Acoustic absorption and dispersion effects resulting from relaxation of equilibrium systems are well recognized.[2] The field has been critically reviewed by Markham, Beyer, and Lindsay.[3] The specific problem of the application of acoustic methods to kinetics has been discussed by Damköhler.[2c] In addition, reaction kinetics have been taken into account by several authors[2,3] who have ascribed ultrasonic absorption maxima to the perturbation of chemical equilibria. A preliminary report on the relaxation time of equilibrium systems as related to ultrasonic absorption and reaction kinetics has been published by the present author.[2g]

A number of problems remain: (a) Choice of an equation for the propagation of sound in equilibrium systems. Several such equations have been derived from different points of view and on the basis of different approximations.[3] (b) The general case in which the kinetics do not necessarily coincide with the Guldberg-Waage mass action "law." (c) The general case in which chemical reaction leads to (isothermal) expansion as well as a thermal effect and in which absorption may not necessarily be small. (d) The validity of using "effective" values of $C_p$ and $C_v$. These problems can be solved, first by a phenomenological derivation of an equation which relates absorption and dispersion of sound to the relaxation time $\tau$ of the chemical reaction, then by relating $\tau$ to the reaction kinetics. Solution of the general case makes it possible to estimate the precision of different approximations. This paper will be limited to the effect of the chemical reaction; shear viscosity and heat capacity relaxation will not be considered.

## II. RELAXATION TIME FOR A REACTION CLOSE TO EQUILIBRIUM

This problem was treated by Liebermann[2f] who gave the equations for relaxation time for two cases but did not include a generalized formula.

It has been shown that, for small displacements from equilibrium,

$$r = x \cdot \Delta F, \tag{1}$$

where $r$ is the net (observable) rate of reaction, $\Delta F$ is the free energy difference per mole of products and reactants, and $x$ is a proportionality factor.[1] This factor is determined by the particular state of equilibrium and depends on the kinetics of the reaction, on all other factors that influence reaction rates, and on the units chosen, but it is independent of the manner of displacement from equilibrium. The factor $x$ is, therefore, characteristic of a given system.

It will now be shown that the establishment of equilibrium is a first-order process. One can write the net reaction rate $r$ in terms of the degree of advancement $\xi$ of the reaction, where the unit may be the number of moles of any key component. Substitution of $d\xi/dt$ for $r$ in Eq. (1) and multiplication of both sides by

* Now with Koppers Company, Inc., Pittsburgh, Pennsylvania.
[1] Manes, Hofer, and Weller, J. Chem. Phys. **18**, 1355 (1950).
[2] See, for example, (a) A. Einstein, Sitzber. preuss. Akad. Wiss. 380 (1920). (b) E. Bauer, Proc. Phys. Soc. (London) **62A**, 141 (1949). (c) G. Damköhler, Z. Elektrochem. **48**, 62, 116 (1942). (d) E. Freedman, J. Chem. Phys. **19**, 1318 (1951). (e) D. Tabuchi, J. Chem. Soc. Japan, Pure Chem. Sect. **71**, 329 (1950). (f) L. Liebermann, Phys. Rev. **76**, 1520 (1949). (g) M. Manes, J. Chem. Phys. **20**, 1658 (1952).
[3] Markham, Beyer, and Lindsay, Revs. Modern Phys. **23**, 353 (1951).

$d(-\Delta F)/d\xi$ yields

$$\frac{-d\ln(-\Delta F)}{dt}=x\cdot\frac{d(-\Delta F)}{d\xi}=\frac{1}{\tau}=k. \tag{2}$$

Near a given state of equilibrium both $x$ and $d(-\Delta F)/d\xi$ are constant and finite,[4] and therefore their product is a constant. For a small displacement from equilibrium, every variable of a system approaches its equilibrium value in a first-order process with the same rate constant. Let $a$ be any observable variable (for example, temperature, volume, pressure, $\xi$) that is functionally related to the position of equilibrium, and let $a^*$ be its value at equilibrium. Then $\Delta F=0$ when $(a-a^*)=0$, and, for differential displacements

$$-\Delta F=y_a(a-a^*), \tag{3}$$

where $y_a$ is a factor of proportionality for the parameter $a$. Since $y_a$ is a constant in the region under discussion,

$$-\frac{d\ln(-\Delta F)}{dt}=\frac{-d\ln(a-a^*)}{dt}=\frac{1}{\tau}. \tag{4}$$

For differential displacements from equilibrium, therefore, the approach of every displaced parameter to its equilibrium value is first order in the displacement and can be characterized by the same relaxation time $\tau$. Only the magnitude of $\tau$ depends on the kinetics of the equilibrium reaction; the first-order character of the decay process is universal for a single-reaction system.

The $a$'s may be directly observable (for example, pressure), or they may be functions of observable variables (for example, $\Delta F$). However, if $a$ is to be measured under constraint, it must be constraint of the reaction. For example, adiabatic compressibility and $C_p$ may be measured in an adiabatic system under a constant pressure constraint. However, when temperature and volume vary as a reaction proceeds, one cannot define isothermal compressibility or $C_v$ with precision; the significance of this point will become apparent later. According to Eq. (4), one may determine $\tau$ for a chemical reaction by observing, for example, relaxation of pressure in a system subjected to a sudden volume change, relaxation of volume in a system under a pressure constraint,[5] or acoustic phenomena. This type of indirect measurement of changes of composition near equilibrium is not fundamentally different from similar measurements in conventional kinetics.

### III. RELAXATION TIME AND ACOUSTIC EFFECTS

Having defined the relaxation time for the general case, one can now derive an equation for the propagation of sound in relaxing systems by extending the application of Hall's treatment.[6] He took a phenomenological approach using the dynamical, differential stress-strain equation for a relaxing system,

$$dS/dt=\frac{S_0-S}{\tau}+\beta_\infty(dP/dt); \tag{5}$$

$S(=\Delta V/V)$ is relative compression, $\beta_\infty$ instantaneous adiabatic compressibility, $\beta_0$ total or static adiabatic compressibility, and $\beta_0 P=S_0$ the equilibrium value of compression for a constant pressure $P$.

Hall[6] applied his equation to the restricted case of water at its maximum density, where the thermal expansion coefficient is zero and, consequently, where the compressibility would not be changed by the thermal effect of any shift in equilibrium. The adiabatic compressibility may be written as

$$\beta=\kappa C_v/C_p, \tag{6}$$

where $\kappa$ is the isothermal compressibility. In Hall's case, $\kappa$ is complex and $C_p/C_v$ is real. One can extend Hall's treatment of the case in which $C_p$ and $C_v$ are complex by combining all of the relaxational contributions in a single relaxational compressibility. The validity of this extension is shown by Eq. (4).[7] The effects of structural and thermal relaxation are additive because they are both determined by the relaxation of the reaction and are therefore always in phase with the reaction. When the instantaneous and static compressibilities and the relaxation time of a system are known, the stresses on an element of volume of the system can be described. This suffices to determine the propagation of sound in a medium of known density. The extension can now be made as follows: Hall's equation for a harmonic pressure wave, $P=P_0e^{i\omega\tau}$, where $\omega=2\pi\nu$ and $\nu$ is the frequency, is

$$S=\beta P=\left(\beta_\infty+\frac{\beta_0-\beta_\infty}{1+i\omega\tau}\right)P. \tag{7}$$

One may express the (complex) velocity of sound in terms of the density and (complex) compressibility in the usual manner and separate the real and imaginary parts,

$$\frac{1}{\Gamma^2}=\rho\beta=\rho\left[\frac{\beta_0+\beta_\infty\omega^2\tau^2}{1+\omega^2\tau^2}-\frac{i\omega\tau\beta_r}{1+\omega^2\tau^2}\right], \tag{8}$$

where $\beta_r=(\beta_0-\beta_\infty)$ is the relaxational compressibility, $\rho$ the density, and $\Gamma$ the (complex) velocity. For a plane wave,

$$\exp[i\omega(t-x/c)-ax]=\exp[i\omega(t-x/\Gamma)], \tag{9}$$

where $c$ is the actual velocity, $a$ the (amplitude) absorption coefficient per cm, and $x$ the distance in cm. The (amplitude) absorption coefficient per wavelength,

[4] The sign of $x$ is negative. The trivial case is neglected in which one of the components is differentially close to zero. The assumption of only one significant reaction is equivalent to the assumption that there is only one $\xi$.

[5] K. P. Coffin and S. H. Bauer, Rev. Sci. Instr. **23**, 115 (1952).

[6] L. Hall, Phys. Rev. **73**, 775 (1948).

[7] I am indebted to Dr. E. Freedman for pointing out the necessity for justifying the extension of Hall's equation.

will also be used, $\mu(=a\lambda)$. Equation (9) shows that

$$1/\Gamma=(1/c)-(ia/\omega). \tag{10}$$

Squaring both sides of Eq. (10) and introducing Eq. (8), one obtains

$$\frac{1}{\Gamma^2}=\frac{1}{c^2}-\frac{a^2}{\omega^2}-\frac{2ia}{\omega c}=\rho\left[\frac{\beta_0+\beta_\infty\omega^2\tau^2}{1+\omega^2\tau^2}-\frac{i\omega\tau(\beta_0-\beta_\infty)}{1+\omega^2\tau^2}\right]. \tag{11}$$

The imaginary components are then equated,

$$a=-\frac{\omega c}{2}Im\left(\frac{1}{\Gamma^2}\right), \tag{12}$$

or

$$\mu=-\pi c^2 Im\left(\frac{1}{\Gamma^2}\right)=\pi\rho c^2\frac{(\beta_0-\beta_\infty)\omega\tau}{1+\omega^2\tau^2}. \tag{13}$$

For small values of absorption, $c^2$ is approximately equal to $c_0^2$ or $c_\infty^2$. In this case the absorption maximum occurs at $\omega\tau=1$. However, one may solve explicitly for $c^2$. On equating the real components of Eq. (11) and using the calculated value for $a$, one finds

$$c^2=\frac{2}{R+[R^2+(Im)^2]^{\frac{1}{2}}}, \tag{14}$$

where $R\equiv R(1/\Gamma^2)$ is the real part of $(1/\Gamma^2)$ and $Im\equiv Im(1/\Gamma^2)$ is the imaginary part of $(1/\Gamma^2)$. Substitution for $c^2$ in Eq. (13) gives the desired general result.

The mechanism of the relaxation process can now be represented in a rather simple manner, and the general expression for absorption can be simplified. First, from Eq. (11),

$$\beta=\beta_\infty+\frac{\beta_r}{1+\omega^2\tau^2}(1-i\omega\tau)=\beta_\infty+\beta_r^*. \tag{15}$$

Equation (15) shows two components of compressibility, instantaneous compressibility $\beta_\infty$ and the complex contribution $\beta_r^*$ of the relaxational compressibility. The resolution of these components and the phase relationships between pressure, the reaction and its contributions, and compressibility are shown in Fig. 1. Here, 0 represents the origin and $X$ and $iY$ are the real and imaginary axes. The distance $\langle OP\rangle$ equals $\beta_\infty$ on the $X$ axis. The diameter of the circle passing through $P$ equals $\beta_r$, and its center lies on the $X$ axis. A line from $P$ at an angle $\phi$ (where $0<|\phi|<\pi/2$) intersects the circle at some point $T$. The points $O$ and $T$ are connected, and $\langle TR\rangle$ is perpendicular to the $X$ axis. If $\phi=\tan^{-1}(-\omega\tau)$, then $\langle PR\rangle=\beta_r/(1+\omega^2\tau^2)$ (the real part of $\beta_r^*$), $\langle TR\rangle=-i\omega\tau\beta_r/(1+\omega^2\tau^2)$ (the imaginary part of $\beta_r^*$), $\langle PT\rangle=\beta_r^*$, and $\langle OT\rangle=\beta$. The compressibility of the medium (and therefore the compression) lags behind the imposed pressure by the phase angle $\psi$. The contribution of the reaction (and therefore the reaction itself) lags behind the imposed pressure by the phase angle $\phi$. The dependence on $\omega\tau$ of the compressibility may be seen by moving $T$ on the circle from $P$ to $Q$. At $\omega\tau=\infty$, the reaction lags 90° behind the pressure (which is in phase with $\beta_\infty$) but is infinitesimal. At $\omega\tau=1$, the imaginary component is at a maximum and the real part of the compressibility is at a point of inflection. Finally, as $\omega\tau$ approaches 0, the compressibility approaches $\beta_0$. A similar representation for temperature would show, in general, the same phase angle $\phi$, but a different value for the analog of $\psi$. This situation has complicated attempts to apply quasi-thermodynamic methods to the case where $\psi$ is not small.[3] Figure 1 also helps to interpret the assumption of "adiabatic" compressibility, i.e., to resolve the apparent contradiction that each element of volume is in thermal isolation yet dissipates energy. Part of the heat that is liberated during compression cannot be absorbed during rarefaction because of the phase relationships. The assumption of an "adiabatic" process requires only that all of the remainder of the evolved

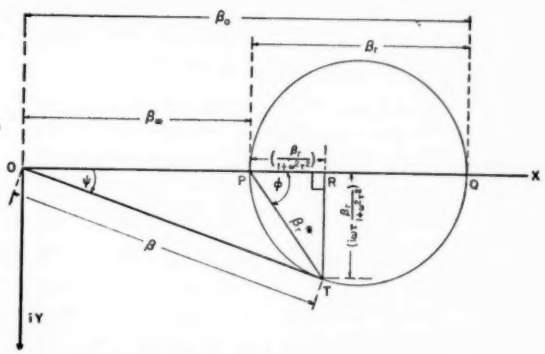


FIG. 1. Relationships between real and imaginary components of the complex compressibility. The phase angle $\phi$ represents the lag of the reaction behind the imposed pressure. The phase angle $\psi$ represents the lag of the compression $(\Delta V/V)$ behind the imposed pressure.

heat (corresponding roughly to the "real" part of the compression energy) be conserved. Figure 1 makes it possible to express Eq. (13) as

$$\mu=-\frac{2\pi\sin\psi}{1+\cos\psi}=-\pi\frac{\sin\psi}{1-\sin^2(\psi/2)}, \tag{16}$$

where the trigonometric functions of $\psi$ are given by Eq. (11).

Equation (16) holds for all values of the absorption coefficient. Moreover, it holds for all fluid systems, whether ideal or not, as long as one has a proper value for $\beta_0$ and $\beta_\infty$. The difficulty of describing such systems is reduced to the problem of determining these parameters. Furthermore, Eq. (16) allows a precise estimate to be made of the errors involved in various simplifying assumptions.

The definitions of $\beta_0$ and $\beta_\infty$ are $\beta_0=\kappa_0(C_v^0/C_p^0)$ and $\beta_\infty=\kappa_\infty(C_v^\infty/C_p^\infty)$. The equilibrium and instantaneous

values are written as

$$\kappa_\infty = -\frac{1}{V}\left(\frac{\partial V}{\partial P}\right)_{T,\xi}, \qquad \kappa_0 = \kappa_\infty - \frac{1}{V}\left[\left(\frac{\partial V}{\partial \xi}\right)_{T,p}\left(\frac{\partial \xi^0}{\partial P}\right)\right]_T \quad (17)$$

$$C_v^\infty = \left(\frac{\partial E}{\partial T}\right)_{v,\xi}, \quad C_v^0 = C_v^\infty + \left(\frac{\partial E}{\partial \xi}\right)_{T,v}\left(\frac{\partial \xi^0}{\partial T}\right)_v \quad (18)$$

$$C_p^\infty = \left(\frac{\partial H}{\partial T}\right)_{p,\xi}, \quad C_p^0 = C_p^\infty + \left(\frac{\partial H}{\partial \xi}\right)_{T,p}\left(\frac{\partial \xi^0}{\partial T}\right)_p, \quad (19)$$

where the values of $H$ and $E$ refer to the system as a whole, and the superscript on $\xi$ emphasizes that its equilibrium value is specified. In principle, at least, the instantaneous and static compressibilities can be determined for any system if the thermodynamics of the system are sufficiently well known. The partial derivatives $\partial V/\partial\xi$, $\partial E/\partial\xi$, and $\partial H/\partial\xi$ are simply $\Delta V$, $\Delta E$, and $\Delta H$ for the reaction.[8] The other partial derivatives may be determined by considering the variation of the position of equilibrium. In the general case,

$$aA+bB+\cdots \rightleftharpoons mM+nN+\cdots. \quad (20)$$

The product $\Pi$ is defined as

$$\Pi = (Q)^q(R)^r\cdots:(A)^{-a}(B)^{-b}\cdots, \quad (21)$$

and $\Pi=K$ at equilibrium, $K$ being the equilibrium constant. There are a number of ways of expressing $\Pi$, depending on the meaning one attaches to the letters in parentheses; one can use $\Pi_p$, $\Pi_c$, $\Pi_N$, or $\Pi_n$, depending on whether partial pressures, concentrations, mole fractions, or moles are used. In the simplest case, that of an ideal gas reaction,

$$\left(\frac{\partial \xi}{\partial p}\right)_T = -\frac{\Delta V}{RT}\Big/\left(\frac{\partial \ln\Pi_p}{\partial \xi}\right)_{T,p} \quad (22)$$

$$\left(\frac{\partial \xi}{\partial T}\right)_p = \frac{\Delta H}{RT^2}\Big/\left(\frac{\partial \ln\Pi_p}{\partial \xi}\right)_{T,p} \quad (23)$$

$$\left(\frac{\partial \xi}{\partial T}\right)_V = \frac{\Delta E}{RT^2}\Big/\left(\frac{\partial \ln\Pi_c}{\partial \xi}\right)_{V,T} \quad (24)$$

and

$$\left(\frac{\partial \ln\Pi_c}{\partial \xi}\right)_{V,T} = \frac{d\ln\Pi_n}{d\xi} = \left[\frac{a^2}{n_A}+\cdots+\frac{q^2}{n_Q}+\cdots\right], \quad (25)$$

$$\left(\frac{\partial \ln\Pi_p}{\partial \xi}\right)_{T,p} = \frac{d\ln\Pi_n}{d\xi} - \frac{(\Delta n)^2}{n}, \quad (26)$$

where $\Delta n=(q+r+\cdots)-(a+b+\cdots)$, and $n$ is the total number of moles in the system. For a reaction with negligible volume change, $\Pi_n$ may be replaced simply by $\Pi$.

In the following, some of the methods are considered which have been used, either explicitly or implicitly, to derive equations for the propagation of sound, and the results of these methods are compared with Eqs. (13) and (16). One approach[2b,f,9] is to start with the adiabatic compressibility,

$$\beta = \kappa C_v/C_p, \quad (6)$$

which, together with the density, determines the rate of propagation of sound. Equation (6) is correct both for "frozen" and equilibrium values of the variables, since they can be defined under both conditions. Now one defines a complex "effective" value of $\beta$, as

$$\beta^{\text{eff}} = \kappa^{\text{eff}}\frac{C_v^{\text{eff}}}{C_p^{\text{eff}}}, \quad (27)$$

where

$$C_v^{\text{eff}} = C_v^\infty + \frac{C_v^0 - C_v^\infty}{1+i\omega\tau}, \text{ etc.} \quad (28)$$

"Effective" values of $C_v$, $C_p$, and $\kappa$ may be written directly,[2f] or they may be derived on the basis of certain approximations.[2c] If $\kappa$ is assumed to have no relaxational component, one considers the relaxation only of $C_p$ and $C_v$. This sort of treatment leads to an inconsistency. If one considers $\beta$ to be complex, then the "effective" value is

$$\beta^{\text{eff}} = \beta_\infty + \frac{\beta_0 - \beta_\infty}{1+i\omega\tau}. \quad (29)$$

However, if one resolves this quantity into two factors, say $C_p$ and $C_v$, and writes "effective" values for each factor, then the result is not the same as Eqs. (27) and (28). Clearly, both ways of defining "effective" values of $\beta$ cannot be correct. The definition of $\beta$ from the equation of Hall follows logically from the differential equation and is therefore less arbitrary than breaking a complex quantity into "effective" values. Moreover, $\beta$ is the ratio between two quantities, condensation and pressure, which, in principle, are observable. There is some question, on the other hand, as to the meaning of $C_p$ and $C_v$ in a reacting system which is neither at constant pressure nor at constant volume. One may anticipate, however, that the error inherent in "effective" values is small for small values of the absorption. In case there is no volume relaxation, one gets, following the method of E. Bauer, Damköhler, or Liebermann,

$$\frac{1}{\Gamma^2} = \rho\kappa\frac{C_v^{\text{eff}}}{C_p^{\text{eff}}}. \quad (30)$$

[8] Strictly speaking, these are measured at equilibrium rather than at the standard states. However, the nonideal case will not be considered any further; therefore this point is of no further concern.

[9] E. Freedman, thesis, Cornell University, Ithaca, New York (1952). See also J. Chem. Phys., this issue.

By applying Eqs. (30), (12), and (28) and assuming further that $C_p^0-C_p^\infty=C_v^0-C_v^\infty$, one obtains

$$\mu=\pi\frac{c^2}{c_0^2}\frac{C_p^0}{C_v^0}\frac{(C_p^0-C_p^\infty)(C_p^0-C_v^0]\omega\tau}{(C_p^0)^2+(C_p^\infty\omega\tau)^2}. \quad (31)$$

The same assumptions applied to Eq. (13) yield

$$\mu=\pi\frac{c^2}{c_0^2}\frac{C_p^0}{C_v^0}\frac{(C_p^0-C_p^\infty)(C_p^0-C_v^0)\omega\tau}{C_p^0C_p^\infty(1+\omega^2\tau^2)}. \quad (32)$$

The difference between the two equations disappears as $C_p^0$ approaches $C_p^\infty$. Equation (31) is identical with the one derived independently by Freedman,[9,10] since his $\omega D/U$ is identical with $\omega\tau$. For the small values of the absorption coefficient which he observed, the difference between the approximate equation and the general one is not significant.

When the thermodynamics of a system are known, its relaxation time can be determined from the position of the absorption maximum by using Eq. (16). For small absorption coefficients, the frequency of maximum absorption immediately yields the relaxation time, even without further knowledge of the thermodynamics, since in this case $\omega\tau\approx 1$.

## IV. RELAXATION TIME AND KINETICS

One can relate relaxation time directly to reaction kinetics for a wide variety of rate laws, although not necessarily for the most general case. For the reaction

$$aA+bB+\cdots\rightleftharpoons mM+nN+\cdots,$$

the rate laws for the forward and reverse reactions are assumed to be

$$r_f=G_f[(A),\ (B),\ \cdots(M),\ (N)\cdots] \quad (33)$$

and

$$r_b=G_b[(A),\ (B),\ \cdots(M),\ (N)\cdots]. \quad (34)$$

One may assume that

$$\frac{G_f}{G_b}=\frac{k_f}{k_b}\left[\frac{(A)^a(B)^b\cdots}{(M)^m(N)^n\cdots}\right]^z, \quad \text{with} \quad \frac{k_f}{k_b}=K^z, \quad (35)$$

where $z$ has any positive value.[1,11] These assumptions cover a wide range of rate laws and do not invoke the Guldberg-Waage mass-action "law."[12] For most simple cases the rate laws are postulated so that $z$ is unity, although one cannot, in principle, determine its value except by measurements far from equilibrium. Near equilibrium, for the cases under discussion[1]

$$r=r_f-r_b=r_f(-\Delta F/RT). \quad (36)$$

Substituting $r=d\xi/dt$ into Eq. (36) gives

$$\frac{-d\ln(-\Delta F)}{dt}=z\cdot\frac{r_f}{RT}\cdot\frac{d(\Delta F)}{d\xi}=z\cdot r_f\cdot\frac{d\ln(\Pi/K)}{d\xi}, \quad (37)$$

or

$$\frac{1}{\tau}=z\cdot r_f\cdot\frac{d\ln\Pi}{d\xi}, \quad (38)$$

where $r_f$ and $\xi$ are defined consistently with each other. For example, if $r_f$ is defined in terms of concentration change per unit time, $\xi$ is defined in terms of the concentration of a key component.

One can now combine Eqs. (33) and (38) to express $\tau$ in terms of any postulated pair of rate laws. For example, for the system $A\rightleftharpoons B$, where the reaction is assumed to be first order in both directions, one obtains $\tau=(k_f+k_b)^{-1}$.[6] For the system $2A\rightleftharpoons A_2$, assuming the forward reaction to be of second order and the reverse reaction to be of first order, one obtains $\tau=[k_b+4n_Ak_f]^{-1}$.[3] One can easily express $\tau$ for more complicated systems by using Eqs. (33) and (38).

If $z$ is constant, then the relationship between $\tau$ and $r_f$ is independent of the rate law, depending rather on the thermodynamics of the reaction. For a known reaction, each determination of the relaxation time (for small absorptions, each determination of the frequency at maximum absorption) determines the corresponding value of $r_f$. Measurements of $r_f$ at different compositions and temperatures may be used to determine the rate law and the temperature dependence of the rate constants.[1] Therefore, the frequency of maximum absorption under different conditions determines the reaction kinetics except for the magnitude of $z$.

If one had some method of identifying a given absorption maximum with relaxation of a given reaction, then one would not need to know the magnitude of the absorption coefficient. However, in the absence of such a method the dependence of the intensity of maximum absorption on composition may be used to identify an absorption maximum with the corresponding reaction, provided that the equilibrium constant and the composition are known. For example, in the case of a reaction in which absorption is small, one can write, to a good approximation,

$$\frac{\beta_0-\beta_\infty}{\beta_\infty}=\frac{\kappa_0-\kappa_\infty}{\kappa_\infty}+\frac{C_p^0-C_p^\infty}{C_p^\infty}-\frac{C_v^0-C_v^\infty}{C_v^\infty}. \quad (39)$$

Each of the terms on the right side of this equation and, therefore, the relaxational compressibility are proportional to $(d\xi/d\ln\Pi)$, either exactly or nearly so. For

[10] E. Freedman first published an equation (reference 2a) which can now be considered as a special case of Eq. (31). Some time later, this writer derived Eq. (31) and attempted to apply it to Freedman's case, but did not find complete agreement. Correspondence with Dr. Freedman revealed that an error in the published equation has since been corrected, and that he had meanwhile also derived the equation for the more general case. Although the two derivations are not identical, they are equivalent.

[11] Relations between $G_f$ and $G_b$ for the general case have been worked out by Hollingsworth, J. Chem. Phys. **20**, 921 (1952).

[12] Strictly speaking, the terms in parentheses in Eq. (35) should denote activities or fugacities. If the activity coefficients are assumed to be unity, these terms may represent partial pressures or mole fractions or, only approximately, concentrations.

small absorption Eq. (13) can be reduced to the proportionality

$$\mu_m \propto \frac{d\xi}{d\ln\Pi} \propto \left[\frac{a^2}{n_A}+\frac{b^2}{n_B}+\cdots+\frac{q^2}{n_Q}+\cdots\right]^{-1}. \quad (40)$$

One can thus identify an absorption maximum with a reaction of known equilibrium constant by measuring the relative intensities of maximum absorption at judiciously chosen compositions and a fixed temperature. If, in addition, the temperature dependence of the equilibrium constant and the absolute magnitude of the absorption are known, the identification is even more positive.

The applicability of absorption measurements to the study of kinetics is limited to cases in which absorption maxima are experimentally accessible and in which $K$ is neither too large nor too small, i.e., where significant amounts of all of the components are present at equilibrium. As one component disappears, $d\xi/d\ln\Pi$ becomes vanishingly small, hence the intensity of absorption disappears. Furthermore, absorption due to other causes must not be too large. These problems are discussed in some detail by Freedman.[9] However, there are undoubtedly some reactions whose kinetics can be studied by no other method and to which the ultrasonic method may be applied with a very high degree of accuracy. For example, it should be possible to measure the kinetic effects of neutral salts on equilibria involving relatively unstable complexes.

## V. EFFECT OF TEMPERATURE ON RELAXATION TIME IN SYSTEMS OF PREDETERMINED COMPOSITION

Systems of predetermined composition are not usually met with in kinetics. However, this condition exists in associated liquids which have been investigated by means of ultrasonics. According to Eq. (38) and if $z=1$, the relaxation time may be considered to consist of two factors, the actual equilibration rate $r_f$ and the "sensitivity factor" $d\ln\Pi/d\xi$, which determines the effect on the equilibrium of a certain amount of reaction. The further the equilibrium is shifted in one direction, the larger the value of $d\ln\Pi/d\xi$. If the rate of the forward reaction is $r_f=k_f\cdot G_f[(A)\cdots(Q)\cdots]$, that is, if there is one rate constant for the forward reaction, then

$$\frac{-d\ln\tau}{d(1/T)}=\frac{d\ln k_f}{d(1/T)}+\frac{d\ln G_f}{d(1/T)}+\frac{d}{d(1/T)}\ln\left(\frac{d\ln\Pi}{d\xi}\right). \quad (41)$$

The effect of a change of temperature on relaxation time can therefore be considered as threefold: The effect on the rate constant $k_f$ (which follows the Arrhenius law), and the effect of the composition change (resulting from the shift of equilibrium) on the rate function $G_f$ and on the sensitivity factor. The effect of $G_f$ depends on the rate law and on the magnitude and temperature dependence of the equilibrium constant $K$; the effect on the sensitivity factor is, in general, a function only of the magnitude and temperature dependence of $K$. The dependence of the last two factors on $1/T$ is linear when one component is present in only small quantities (for small and large values of $K$) and nonlinear for values of $K$ of the order of unity. It follows that a plot of $\log\nu_M$ as a function of $1/T$ is linear only when $K\gg1$ or $K\ll1$. In these cases, some multiple or fraction of $\Delta H$ for the reaction must be added to or subtracted from the apparent activation energy to give the activation energy for the rate constant. For example, for a reaction that is first order in both directions, $\tau=(k_f+k_b)^{-1}$ and therefore

$$\frac{-d\ln\tau}{d(1/T)}=\frac{d\ln(k_f+k_b)}{d(1/T)}. \quad (42)$$

In this case,

$$\frac{-d\ln\tau}{d(1/T)}\cong\frac{E_f}{R} \text{ where } k_f\gg k_b,\ K\gg1 \quad (43)$$

and

$$\frac{-d\ln\tau}{d(1/T)}\cong-\frac{E_b}{R}=-E_f-\Delta H \text{ where } k_f\ll k_b,\ K\ll1. \quad (44)$$

An Arrhenius-type plot of $\nu_M$ over a large temperature range, including the temperature region where $K\cong1$, consists of two linear portions, differing in slope by $\Delta H/R$, and a transition region at $K\cong1$. Published data on the ultrasonic absorption of acetic acid[13] fit an Arrhenius-type plot very well and should therefore be characteristic of a system in which one component is present at a relatively low concentration. Freedman's analysis of their data shows this to be the case, the relative amount of dimer molecules being of the order of 95 percent. Freedman treated a problem which is inherently more difficult than those mentioned in this paper, since he determined $K$ and $\Delta H$ for a reaction which is not well known. The accuracy of his calculated values depends on the accuracy of the absolute magnitudes of the absorption coefficients. When the equilibrium data must be determined by ultrasonic measurements and when one can reach a temperature range where $K\cong1$, the transition region in the Arrhenius plot of $\nu_M$ may serve as an added check on the calculated values of $K$.

## ACKNOWLEDGMENT

Thanks are due Dr. L. J. E. Hofer for helpful discussions and encouragement.

[13] J. Lamb and J. M. M. Pinkerton, Proc. Roy. Soc. (London) **199A**, 114 (1949).

# The Reaction of Cyclobutane with Hg 6($^3P_1$) Atoms*†

D. L. KANTRO AND H. E. GUNNING
*Department of Chemistry, Illinois Institute of Technology, Chicago, Illinois*
(Received March 2, 1953)

The reaction of cyclobutane with Hg 6($^3P_1$) atoms has been studied in a static system at 30.10±0.01°C, over the pressure range from 2–250 mm. The primary products of the reaction are hydrogen, *n*-butylcyclobutane, and a saturated $C_8H_{14}$ product which is assumed, from kinetic and mass spectral evidence, to be cyclobutylcyclobutane. In addition, prolonged exposure produced a saturated $C_{12}H_{22}$ product which is probably a dicyclobutylbutane.

The quantum yields of pressure decrease ($\phi_P$) hydrogen formation ($\phi_{H_2}$) and cyclobutane consumption ($\phi_C$) all reach constant maximum values at cyclobutane pressures greater than approximately 100 mm. These values are $\phi_C=0.53$, $\phi_{H_2}=0.10$, and $\phi_P=0.16$. From the simple stoichiometry of the reaction the quantum yields of *n*-butylcyclobutane ($\phi_{BC}$) and cyclobutylcyclobutane ($\phi_{C_2}$) formation were calculated. From the data $\phi_{BC}=0.16$ and $\phi_{C_2}=0.10$.

The following mechanism was found to be consistent with the observed characteristics of the reaction:

$$\text{cyclo } C_4H_8+\text{Hg } 6(^3P_1)\rightarrow\text{cyclo } C_4H_7+H+\text{Hg } 6(^1S_0),$$
$$H+\text{cyclo } C_4H_8\rightarrow\text{cyclo } C_4H_7+H_2,$$
$$2\text{ cyclo } C_4H_7\rightarrow\text{dicyclo } C_8H_{14},$$
$$2\text{ cyclo } C_4H_7\rightarrow\text{cyclo } C_8H_{14},$$
$$H+\text{cyclo } C_8H_{14}\rightarrow\text{cyclo } C_8H_{15},$$
$$\text{cyclo } C_8H_{15}+\text{cyclo } C_4H_8\rightarrow\text{cyclo } C_4H_7+\text{cyclo } C_8H_{16},$$

where dicyclo $C_8H_{14}$ represents cyclobutylcyclobutane; cyclo $C_8H_{14}$, cyclobutylbutene; cyclo $C_8H_{15}$, cyclobutylbutyl radicals; and $C_8H_{16}$, *n*-butylcyclobutane. The cyclobutylbutene is considered as an intermediate in the formation of the stable *n*-butylcyclobutane product.

## INTRODUCTION

IN a comparative study of the relationship between structure and reactivity in the reactions of the cycloparaffins with Hg 6($^3P_1$) atoms, cyclobutane occupies a particularly significant role. Thus, in cyclopropane[1–3] the ring undergoes decomposition, with the resulting radicals stabilizing themselves by the formation of a complex polymer. On the other hand, cyclopentane,[4,5] methylcyclopentane,[6] and cyclohexane[7] are all essentially paraffinic in their reactions, in that the primary processes involve C—H bond rupture almost exclusively. Relatively little ring cleavage seems to occur either in the primary process or in subsequent secondary reactions.

The present investigation on cyclobutane was undertaken as part of a systematic study of the mercury-6($^3P_1$) photosensitized reactions of the cycloparaffins, designed to gain insight into the kinetics of cycloalkyl radical reactions in the gas phase. The details of the investigation follow.

## EXPERIMENTAL

Kinetic studies on cyclobutane are hampered by the fact that neither cyclobutane nor any of its derivative hydrocarbons is available commercially. A more serious difficulty, however, is the paucity of data on these compounds. Thus cyclobutylcyclobutane, an expected product in the present investigation, since it is the recombination product of cyclobutyl radicals, has not yet been synthesized. Consequently, the identification of the products of the reaction constituted one of the major obstacles to be surmounted.

### Synthesis of Cyclobutane

A number of syntheses of cyclobutane were attempted in the course of this investigation. For the data reported here the cyclobutane used was prepared by synthesizing cyclobutanone and reducing the ketone to the hydrocarbon. Only a brief outline of the synthesis will be given.

The cyclobutanone was prepared by the reaction of ketene with diazomethane.[8,9] Diazomethane was obtained from methylurea by standard procedures.[10] Ketene was prepared by passing acetone over an incandescent platinum filament. The ketene gas was washed by bubbling through four decalin-filled traps.

* This work was supported by the U. S. Atomic Energy Commission.

† Part of a dissertation submitted by one of the authors (D.L.K.) in partial fulfillment of the requirements for the Ph.D. degree at Illinois Institute of Technology.

[1] H. E. Gunning and E. W. R. Steacie, J. Chem. Phys. **17**, 351 (1949).

[2] R. J. Scott and H. E. Gunning, J. Phys. Chem. **56**, 156 (1952).

[3] Ford, Mori, and Gunning (unpublished work).

[4] Allen, Kantro, and Gunning, J. Am. Chem. Soc. **72**, 3588 (1950).

[5] Beck, Kniebes, and Gunning (unpublished work).

[6] M. Schlochauer and H. E. Gunning, J. Chem. Phys. **19**, 474 (1951).

[7] Beck, Kniebes, and Gunning, paper presented at the 122nd Meeting of the American Chemical Society, September, 1952.

[8] P. Lipp and R. Koester, Ber. deut. chem. Ges. **64**, 2823 (1931).

[9] Lipp, Buchkremer, and Seeles, Ann. phys. **499**, 1 (1932).

[10] A. H. Blatt (Editor), *Organic Syntheses* (John Wiley and Sons, Inc., New York, 1943), Vol. II, pp. 165–167, 461–464.

TABLE I. Rates and quantum yields of pressure decrease *vs* initial pressure of cyclobutane.

| $P_0$ mm | $-dn/dt$ moles/min $\times 10^6$ $Ia = 5.85 \times 10^{-6}$ einstein/min | $Ia = 8.58 \times 10^{-6}$ einstein/min | $\phi P$ |
|---|---|---|---|
| 2.50 | 0.54 | | $0.09_3$ |
| 10.70 | | 0.90 | 0.11 |
| 25.20 | | 1.31 | 0.15 |
| 28.55 | | 1.39 | 0.16 |
| 42.35 | 1.07 | | 0.18 |
| 51.00 | 0.95 | | 0.16 |
| 51.95 | 0.95 | | 0.16 |
| 63.05 | | 1.56 | 0.18 |
| 70.00 | 0.94 | | 0.16 |
| 95.05 | 1.06 | | 0.18 |
| 103.45 | | 1.39 | 0.16 |
| 120.85 | 0.96 | | 0.16 |
| 123.00 | 0.98 | | 0.17 |
| 133.40 | | 1.41 | 0.16 |
| 142.80 | 1.02 | | 0.17 |
| 147.65 | 1.03 | | 0.17 |
| 150.80 | | 1.35 | 0.16 |
| 160.35 | 0.91 | | 0.16 |
| 160.75 | 1.02 | | 0.17 |
| 166.60 | | 1.30 | 0.15 |
| 170.90 | | 1.39 | 0.16 |
| 184.85 | 0.92 | | 0.16 |
| 192.50 | | 1.34 | 0.16 |
| 198.60 | | 1.17 | 0.14 |
| 219.45 | | 1.33 | 0.16 |
| 235.25 | | 1.47 | 0.17 |
| 235.80 | | 1.41 | 0.16 |
| 245.60 | 0.94 | | 0.16 |

The ketene gas was fed into an ethereal solution of the diazomethane, maintained at −25°C. Upon flashing off the ether, the cyclobutanone was purified by distillation in a miniature Podbielniak Hypercal column. The purified ketone had a bp of 95.7–95.9°C at 750 mm. A semicarbazone was prepared[11] which gave a melting point of 203–204°C in agreement with reported values.[9] The purified cyclobutanone obtained represented a 65 percent yield, based on *N* nitrosomethyl urea.

The cyclobutane was prepared from the purified cyclobutanone by the method of Roberts and Sauer,[12] using hydrazine hydrate as the reducing agent. The cyclobutane gas, evolved from the reaction mixture, was passed through a condenser, three concentrated sulfuric acid bubblers, and a phosphorus pentoxide tube, before being condensed with liquid nitrogen in a trap in the vacuum system. A 70 percent yield of cyclobutane was obtained. A sample of this cyclobutane was sent to the National Bureau of Standards for mass spectrometric analysis. The analysis gave 92 percent cyclobutane, with the remainder consisting of *n*-butane, pentenes, *n*-pentane, and *n*-hexane.

[11] R. L. Shriner and R. C. Fuson, *The Systematic Identification of Organic Compounds* (John Wiley and Sons, Inc., New York, 1948), third edition, pp. 170–171, 262.

[12] J. D. Roberts and C. W. Sauer, J. Am. Chem. Soc. **71**, 3925 (1949).

The crude cyclobutane was purified by careful fractionation on the Hypercal column, modified for low-temperature distillations. The middle fraction boiling in the range 11.8–12.0°C at 748 mm was retained. A sample of the vapor in equilibrium with this liquid at −78°C was analyzed for us on a Consolidated mass spectrometer by Dr. R. B. Bernstein of this department. The analysis gave cyclobutane 97.5 percent, *n*-butane 2.5 percent. Correction for the higher volatility of *n*-butane gave cyclobutane 99 percent, *n*-butane 1 percent, for the composition of the liquid. This material was used in obtaining the data reported here.

### Synthesis of *n*-Butylcyclobutane

Since mass spectral data on the reaction products strongly suggested that *n*-butylcyclobutane might be a product of the reaction, an independent synthesis of this compound was undertaken. Since no new techniques are involved, the synthesis will only be briefly noted here. Cyclobutane-carboxyl chloride, prepared by the action of thionyl chloride on the corresponding acid, was converted to *n*-propyl cyclobutyl ketone with di-*n*-propyl cadmium, by a method analogous to the one used by Pinson and Friess[13] in the preparation of methylcyclobutyl ketone. The ketone was reduced to the desired product by the Huang-Minlon modification of the Wolff-Kishner reduction.[12,14] Dr. C. E. Boord and Dr. J. M. Derfer, Department of Chemistry, The Ohio State University, very obligingly supplied us with the infrared absorption data on pure *n*-butylcyclobutane. Since 0.6 g of the hydrocarbon was prepared only simple microdistillation was used in purification. Infrared and mass spectral data showed a minimum purity of 90 percent for our sample.

### The Reaction System

As in the previous studies in this series, the mercury-$6(^3P_1)$ photosensitized decomposition of cyclobutane was carried out at a temperature close to 30°C, in a static system. For a general description of the experimental technique, reference should be made to earlier publications.[6,15]

The cylindrical, fused-quartz reaction cell was 10 cm long and 5 cm in diameter, with flat, polished quartz windows at each end. The cell was connected to the vacuum system via a 14/35 standard taper, with Sealstix cement.

The cell was maintained at 30.10±0.01°C in a thermostatically controlled water bath, as in previous investigations. The Pearson-type differential manometer used to measure the pressure changes had an amplification factor of one hundred.

The source of 2537A radiation was a Hanovia Sc-2537

[13] R. Pinson, Jr., and S. L. Friess, J. Am. Chem. Soc. **72**, 5333 (1950).

[14] Huang-Minlon, J. Am. Chem. Soc. **68**, 2487 (1946).

[15] G. A. Allen and H. E. Gunning, J. Chem. Phys. **16**, 1146 (1948).

mercury-in-quartz resonance discharge tube, wound in the form of a 5-coil helix. The lamp was clamped broadside to the quartz window of the thermostat. The discharge was maintained with a Sola luminous tube transformer, stabilized with a Sola constant voltage transformer. The secondary of the tube transformer furnished 30 ma at 3000 volts.

The 1849A radiation from the lamp was removed by interposing a filter of Vycor No. 7910 glass between the lamp and the cell. The effect of variation in light intensity on the quantum yield was determined by placing a calibrated sulphidized copper screen in the light path. The screen was calibrated by Mr. C. C. McDonald of this laboratory at 2537A, using a collimated beam of the resonance radiation, the intensity of which was monitored with a Westinghouse WL-775 phototube coupled with a Beckman Ultrohmeter. It was found that for the screen used in this investigation the intensity was reduced to 0.324 of its original value. As in previous work, the cyclopropane reaction was used as the actinometer.[1,6]

TABLE II. Rate of hydrogen formation as a function of initial cyclobutane pressure ($P_0$).

| $P_0$ mm | $d[H_2]/dt$ moles/min $\times 10^6$ | $\phi_{H_2}$ |
|---|---|---|
| 41 | 0.38 | $0.06_5$ |
| 98 | 0.50 | $0.08_5$ |
| 145 | 0.60 | $0.10_3$ |
| 164 | 0.58 | 0.098 |
| 215 | 0.62 | $0.10_6$ |

## RESULTS

### The Variation of Pressure with Time

The reaction is pressure-decreasing, attaining a linear rate of decrease in 10 to 15 minutes of irradiation, as in cyclopentane[4] and methylcyclopentane.[6] The linear rates of pressure decrease from 2 to 245 mm, expressed in micromoles per minute, disappearing from the gas phase are given in Table I. Two independent series of runs were done at light intensities of $5.8_5\times10^{-6}$ and $8.5_8\times10^{-6}$ einsteins per minute. It will be noticed that the rate of pressure decrease becomes independent of pressure beyond approximately 35 mm. In this respect cyclobutane resembles cyclopropane.[1] In the last column of Table I the quantum yield of pressure decrease is given. A constant value of 0.16, independent of light intensity, persists throughout the entire complete quenching region. Using the calibrated screen, the intensity was reduced to $1.90\times10^{-6}$ einstein/min. At an initial pressure of 46.3 mm, $-dn/dt$ was $0.34\times10^{-6}$ mole/min; whence $\phi_P=0.18$. Hence it may be concluded that the quantum yield of pressure decrease is independent of light intensity.

### Products Noncondensable in Liquid Nitrogen

Repeated analyses of the noncondensables obtained from runs made over the entire pressure range studied showed unequivocally that the gas was at least 99 percent hydrogen. At constant cyclobutane pressure, the plot of moles of hydrogen formed *vs* time is linear, at least during the first half hour of reaction, extrapolating to the origin, as shown in Fig. 1. The rate of hydrogen formation was therefore obtained as the slope of these linear isobaric plots. The data for five pressures are given in Table II. The quantum yields of hydrogen formation $\phi_{H_2}$ are also recorded in this table.

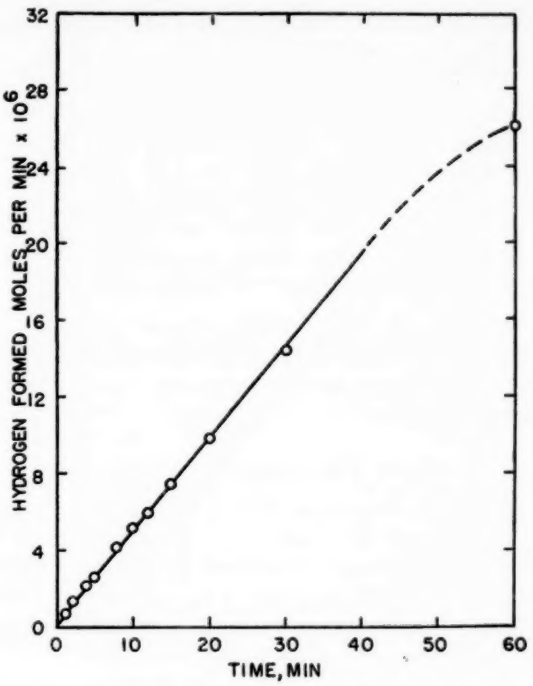


FIG. 1. Variation of hydrogen yield with time at a cyclobutane pressure of 98 mm.

It is apparent from Table II that the quantum yield of hydrogen formation ($\phi_{H_2}$) becomes constant at 0.10, within the experimental error, at least at pressures above 100 mm.

### Products Condensable in Liquid Nitrogen

In contrast to the behavior of the other cycloparaffins, a liquid was not observed to condense on the incident window of the reaction cell during irradiation. However, examination of the mass spectra of the condensables, obtained on a Consolidated mass spectrometer, Model 21-103, showed the presence of two $C_8$ compounds with molecular weights of 110 and 112. By comparison with the mass pattern of the *n*-butylcyclobutane, synthesized for this investigation, it was shown that the heavier $C_8$ product was identical with the synthetic compound. For reasons to be adduced later, the lighter $C_8$ product was assumed to be cyclobutylcyclobutane. No other condensable products were detected for runs less than one hour in duration. However, it should be noted that 2- to 4-hour runs produced a saturated $C_{12}H_{22}$ product which is assumed to arise from secondary reactions.

TABLE III. Runs with added hydrogen at a cyclobutane pressure of 52.5 mm.

| Mole fraction of hydrogen | Rate of pressure decrease moles/min $\times 10^6$ | $\phi P$ |
|---|---|---|
| 0.0 | 0.945 | $0.16_2$ |
| 0.06 | 0.666 | $0.11_4$ |
| 0.20 | 0.738 | $0.12_6$ |
| 0.44 | 0.705 | $0.12_1$ |
| 0.59 | 0.743 | $0.12_7$ |
| 0.82 | $0.62_8$ | $0.10_7$ |

A number of $C_8H_{14}$ isomers were eliminated as products by showing that the condensables contained no detectable unsaturation in titration with bromine in glacial acetic acid.[6]

## Runs with Added Hydrogen

Since it was suspected that H atoms were reacting hydrogenatively either with the substrate or with the cyclobutylcyclobutane, a series of runs was carried out in which the partial pressure of cyclobutane was kept constant while the mole fraction of added hydrogen was varied. The results are shown in Table III.

It can be seen from Table III that the quantum yield of pressure decrease remains substantially unchanged with mole fractions of added hydrogen greater than 0.06.

## The Mass Spectra of the Condensable Products

A careful study of the mass spectra of the condensable products showed, as previously noted, that *n*-butylcyclobutane was present together with a $C_8H_{14}$ compound. Collation of the mass spectra of other known cyclobutyl hydrocarbons, coupled with the fact that no unsaturation appeared to be present, led to the conclusion that the $C_8H_{14}$ product was cyclobutylcyclobutane. Since this product has not yet been synthesized, it was only possible to draw semiquantitative information from the mass spectra. It was concluded that the concentration ratio of *n*-butylcyclobutane to cyclobutylcyclobutane, designated as $BC/C_2$, was proportional to the ratio of the intensity of mass 69 to 88 percent of the intensity of mass 67. The data for runs with pure cyclobutane and for cyclobutane-hydrogen mixtures are shown in Table IV.

TABLE IV. Mass spectral data on the ratio of $C_8H_{16}$ to $C_8H_{14}$ in the products.

| Total pressure mm | Mole fraction of hydrogen | Duration of run min | Mass 69/0.88 Mass 67 |
|---|---|---|---|
| 2.5 | 0 | 60 | 1.44 |
| 51.0 | 0 | 60 | 0.50 |
| 70.0 | 0 | 10 | 0.31 |
| 70.0 | 0 | 60 | 0.54 |
| 123.0 | 0 | 60 | 0.35 |
| 160.4 | 0 | 60 | 0.41 |
| 245.6 | 0 | 60 | 0.30 |
| 52.0 | 0.0 | 60 | 1.1 |
| 65.9 | 0.20 | 60 | 1.9 |
| 92.4 | 0.44 | 60 | 2.3 |
| 126.0 | 0.59 | 60 | 2.7 |

From Table IV it is apparent that the ratio $(C_8H_{16})/(C_8H_{14})$, in the runs with pure substrate, decreases rapidly with increasing pressure, reaching a fairly constant value above approximately 120 mm. The two runs done at 70 mm indicate in addition that the ratio increases with duration of exposure.

The data on the cyclobutane-hydrogen mixtures in Table IV show that the ratio definitely increases with increasing quenching of the Hg $6(^3P_1)$ atoms by hydrogen.

## The Stoichiometry of the Reaction

In the mercury $6(^3P_1)$ photosensitized decomposition of cyclobutane (C), the only primary products would appear to be hydrogen, cyclobutylcyclobutane ($C_2$) and *n*-butylcyclobutane (BC). We may therefore represent the stoichiometry of the decomposition by the equations

$$2C \rightarrow BC, \tag{1}$$

$$2C \rightarrow C_2 + H_2. \tag{2}$$

TABLE V. Quantum yield data.

| Cyclobutane pressure mm | Pressure decrease ($\phi P$) | Hydrogen formation ($\phi_{H_2}$) | Cyclobutane consumption ($\phi C$) | $C_8H_{16}$ formation ($\phi_{BC}$) | $C_8H_{14}$ formation ($\phi_{C_2}$) |
|---|---|---|---|---|---|
| 41 | 0.16 | $0.06_5$ | 0.45 | 0.16 | 0.07 |
| 98 | 0.16 | $0.08_5$ | 0.49 | 0.16 | 0.09 |
| 145 | 0.16 | $0.10_3$ | 0.53 | 0.16 | 0.10 |
| 164 | 0.16 | $0.09_8$ | 0.52 | 0.16 | 0.10 |
| 215 | 0.16 | $0.10_6$ | 0.53 | 0.16 | 0.11 |

Hence the following relations must apply:

$$\phi_C = 2\phi_P + 2\phi_{H_2},$$

$$\phi_{C_2} = \phi_{H_2},$$

$$\phi_{BC} = \phi_P. \tag{3}$$

The calculated quantum yield data at selected pressures are presented in Table V.

## DISCUSSION

In order to facilitate discussion of the stoichiometry and mechanism of the reaction, the salient features of our findings are summarized below:

(a) The reaction is pressure decreasing. The quantum yield of pressure decrease attains a constant value of 0.16 at pressures greater than 35 mm.

(b) The quantum yield is independent of the light intensity.

(c) The primary products of the reaction are hydrogen, *n*-butylcyclobutane, and a $C_8H_{14}$ compound. Extensive decomposition produced in addition a saturated $C_{12}H_{22}$ product.

(d) From the absence of unsaturation in the condensable products, coupled with mass spectral evidence, it is concluded that the $C_8H_{14}$ compound must be the hitherto unsynthesized cyclobutylcyclobutane.

(e) The rate of formation of hydrogen, at constant substrate pressure, is independent of time, for at least the first half-hour of exposure.

(f) The quantum yield of hydrogen formation reaches a maximum value of 0.10 at substrate pressures greater than 120 mm.

(g) At a constant partial pressure of cyclobutane, added hydrogen reduces the quantum yield of pressure decrease to a new constant value of 0.12.

(h) A study of the mass patterns of the $C_8$ products indicates that the ratio $(C_8H_{16})/(C_8H_{14})$ (1) decreases rapidly with increasing cyclobutane pressure, reaching a constant value at approximately 120 mm, (2) increases with increasing duration of exposure, (3) increases with the mole fraction of added hydrogen at a constant partial pressure of cyclobutane.

(i) From the simple stoichiometry of the reaction, the quantum yields for substrate disappearance and product formation can be calculated. All these quantities achieve constant maximum values at cyclobutane pressures greater than approximately 120 mm. The values are $\phi_C=0.53$, $\phi_{H_2}=0.10$, $\phi_{BC}=0.16$, and $\phi_{C_2}=0.10$.

In the light of the foregoing facts, and by analogy with the reactions of the other cycloparaffins with Hg 6($^3P_1$) atoms, the cyclobutane decomposition will be discussed in terms of the following mechanism:

$$\text{cyclo } C_4H_8+\text{Hg } 6(^3P_1)\rightarrow\text{cyclo } C_4H_7+H+\text{Hg } 6(^1S_0), \quad (4)$$

$$H+\text{cyclo } C_4H_8\rightarrow\text{cyclo } C_4H_7+H_2, \quad (5)$$

$$2\text{ cyclo } C_4H_7\rightarrow\text{dicyclo } C_8H_{14}, \quad (6)$$

$$2\text{ cyclo } C_4H_7\rightarrow\text{cyclo } C_8H_{14}, \quad (7)$$

$$H+\text{cyclo } C_8H_{14}\rightarrow\text{cyclo } C_8H_{15}, \quad (8)$$

$$\text{cyclo } C_8H_{15}+\text{cyclo } C_4H_8\rightarrow\text{cyclo } C_4H_7+\text{cyclo } C_8H_{16}, \quad (9)$$

where dicyclo $C_8H_{14}$ represents cyclobutylcyclobutane; cyclo $C_8H_{14}$, cyclobutylbutene; cyclo $C_8H_{15}$, cyclobutylbutyl radicals; and cyclo $C_8H_{16}$, *n*-butylcyclobutane.

Equations (4), (5), and (6) account for two of the major products, hydrogen and cyclobutylcyclobutane. In this part of the mechanism, cyclobutane resembles the higher cycloparaffins. As an additional product of radical recombination, the reactive intermediate, cyclobutylbutene, is postulated in Eq. (7). It is assumed that the concentration of this olefinic product is negligibly small, owing to Eqs. (8) and (9). The observed product, *n*-butylcyclobutane therefore arises as a product of hydrogenation of the olefinic intermediate. Such a postulate is in consonance with the fact that cycloalkyl radicals show increasing tendency to isomerize with decreasnig ring size. Thus cyclopropyl radicals would appear to isomerize readily to allyl radicals,[3-5] whereas cyclopentyl radicals are fairly stable under similar conditions. Cyclobutyl radicals should be intermediate in stability between these two. That no direct isomerization of cyclobutyl to butenyl occurs is evident by the absence of butane or octanes in the products, expected products of the reactions of butenyl radicals, in the presence of H atoms and the substrate.

Steady-state calculations for the complete quenching region on the above mechanism yield $\phi_C=2K$, $\phi_{H_2}=K[k_4/k_3+k_4]$, where $K$ represents an inefficiency factor in the primary reaction between Hg 6($^3P_1$) and cyclobutane. Whence from Table V, $K=0.25$ and $k_3+k_4/k_3=\phi_C/2\phi_{H_2}=2.5$. Therefore $k_4/k_3=1.5$. The ratio (cyclo $C_8H_{16}$)/(dicyclo $C_8H_{14}$) is also equal to $k_4/k_3$, independent of pressure, in agreement with our findings. The increase in the ratio with increasing mole fraction of added hydrogen (Table IV) may be evidence for the reaction

$$H+\text{dicyclo } C_8H_{14}\rightarrow\text{cyclo } C_8H_{15} \quad (7)$$

under such high H-atom concentrations. It is pertinent to note here that H atoms react rapidly with dicyclopropyl in the mercury photosensitization of hydrogen-dicyclopropyl mixtures.[3]

The saturated $C_{12}H_{22}$ product, which appeared under prolonged exposure, could be explained by the addition of cyclobutyl radicals to the olefin formed in step (4), followed by stabilization of the radical by abstraction of an H atom from the substrate. The resulting $C_{12}H_{22}$ product would therefore be either 1,3-dicyclobutylbutane or 1,4-dicyclobutylbutane.

The disproportionation of cycloalkyl radicals, so important for cyclopentyl and cyclohexyl radicals, may well be of importance in the cyclobutane reaction. However, since the expected disproportionation product, cyclobutene, was not detected among the products, we may conclude either that disproportionation is unimportant in cyclobutyl radical reactions or that cyclobutene reacts so rapidly with H atoms that the stationary-state concentration is negligibly low under the conditions of our experiments.

## CONCLUSIONS

The data obtained in this first investigation of the reaction of cyclobutane with Hg 6($^3P_1$) atoms seem to be consistent with the assumption that the cycloparaffins differ one from another in degree not kind. Thus all the cycloalkanes appear to undergo C—H bond rupture in the primary process. With decreasing ring size, two factors become important. These are the increasing C—H bond strength of the cycloparaffin and the decreasing stability of the cycloalkyl radical.

## ACKNOWLEDGMENTS

The authors would like to thank Mr. D. V. Kniebes of the Institute of Gas Technology for assistance in the interpretation of the mass spectral patterns, Dr. R. B. Bernstein of this department for assistance in the analytical work and for many valuable discussions, and Mr. Hadley W. Ford of our laboratory for very helpful advice.

# A New Determination of the Half-Life of $Am^{242m}$; the Problem of Counting Short-Lived Activities*†

THOMAS K. KEENAN, ROBERT A. PENNEMAN, AND B. B. MCINTEER
*Los Alamos Scientific Laboratory, University of California, Los Alamos, New Mexico*

The half-life of $Am^{242m}$ has been redetermined to yield a value of $16.01\pm0.02$ hours (99 percent confidence level). A simple relationship is developed between experimentally measured average counts/minute and true $dN/dt$; a convenient rule of thumb states that there is <0.1 percent error between average disintegration rate (finite counting interval) and $dN/dt$ (at the mid-point of the counting interval) when the counting interval does not exceed 20 percent of the half-life.

THE americium isotope of mass 241 undergoes neutron capture to form $Am^{242m}$, which decays ~64 percent[1] by negative beta-particle emission to $Cm^{242}$. The half-life of $Am^{242m}$ has been previously measured as $16\pm3$ hr[2] and $15.75\pm0.25$ hr.[3]

An accurate value was necessary for the study of the exchange rate of Am(III)−Am(V) ions in solution using $Am^{242m}$ as tracer. Nitric acid solutions containing 1–2μg of pure $Am^{241}$ (>99 percent purity) were irradiated at a flux of $\sim5\times10^{11}$ n/cm²/sec in the homogeneous reactor[4] at Los Alamos. Aliquots were pipetted onto tantalum disks, ignited to a dull red heat, and counted. Duplicate counting results were observed whether the active samples were mounted on tantalum or platinum.

The beta particles were collected in a methane-flow external chamber which was fitted with a 7.8 mg/cm² aluminum window to block out the 5.48-Mev and 6.08-Mev alpha particles resulting from unconverted $Am^{241}$ and from $Cm^{242}$ daughter. The pulses were fed into a PA-2[5] pulse amplifier and recorded on an SC-3[6] binary scaler which had a factor of 1024. Careful experiments on coincidence loss in this counter resulted in an equation which was used to correct all counts exceeding 54 000 c/m. During each counting period, time was determined to the nearest second by standardizing a clock with WWV.

The decay of the ten samples was followed over a total time of $7\frac{1}{2}$ to 8 half-lives (>100 hours). A constant background is present because of the gammas from unconverted $Am^{241}$.[7] The samples were allowed to decay until this gamma background gave agreement within 0.1 percent in two counts taken 24 hours apart. This background was then subtracted from all previous counts, the resulting data then yielding a straight line when activity was plotted against time on semilog paper (see Fig. 1).

The best slope for this straight line was determined by the method of least squares and the half-life evaluated from the relationship,

$$t_{\frac{1}{2}}=-\frac{\ln 2}{(\text{slope})(2.303)}$$

The mean value of ten samples, which varied from 15.97 hr to 16.04 hr, yielded a half-life of $16.01\pm0.02$ hr (standard deviation). Using the "range" method[8] of determining reliability, the standard deviation is also 0.02 hr.

Some question arose as to the reliability of the lower counting-rate portion of the curve in Fig. 1. It was necessary to know whether $\Delta N/\Delta t$ was an accurate measure of $dN/dt$ at mean time $(\Delta t/2)$ when counting periods of 20 minutes were needed to collect 100 000 total counts. The following treatment was derived to clarify this situation.

I

From radioactive decay laws, $dN/dt=-\lambda N$.

$$\text{Average counts/min}=kN_0\frac{(1-e^{-\lambda\Delta t})}{\Delta t}, \quad (1)$$

$$\text{Actual counts/min at } \Delta t/2=k\lambda N_0 e^{-\lambda\Delta t/2}, \quad (2)$$

where $N_0$ = atoms initially present and $k$ = instrument constant, including geometry. Thus,

$$\frac{\text{average c/m}}{\text{actual c/m (at } \Delta t/2)}=\frac{1}{\lambda\Delta t}(e^{\lambda\Delta t/2}-e^{-\lambda\Delta t/2})=\frac{2}{\lambda\Delta t}\sinh(\lambda\Delta t/2). \quad (3)$$

The series expansion of Eq. (3),

$$1+\frac{(\lambda\Delta t)^2}{24}+\frac{(\lambda\Delta t)^4}{1920}+\cdots,$$

is identical with that obtained by Schuler.[9]

* Presented in part at the 313th meeting of the American Physical Society, Washington, D. C., May 1–3, 1952.
† This work was sponsored by the U. S. Atomic Energy Commission.

[1] Hanna, Harvey, and Moss, Phys. Rev. **81**, 486 (1951).
[2] W. M. Manning and L. B. Asprey, *The Transuranium Elements: Research Papers* (McGraw-Hill Book Company, Inc., New York, 1949), Paper No. 22.7. National Nuclear Energy Series, Plutonium Project Record, Vol. 14B, Div. IV.
[3] B. G. Harvey, Chalk River (private communication).
[4] L. D. P. King, AECD-3287.
[5] W. G. Rexroth, LA-1239. This and following reference are obtainable from Ref. Services Branch, Technical Information Service, USAEC, P. O. Box 62, Oak Ridge, Tennessee.
[6] E. L. Kemp, LA-1207.
[7] Asaro, Reynolds, and Perlman, UCRL-1681, Feb. 16, 1952; Beling, Newbon, and Rose, Phys. Rev. **86**, 797 (1952); **87**, 670 (1952).
[8] R. B. Dean and W. J. Nixon, Anal. Chem. **23**(4), 636 (1951).
[9] R. H. Schuler, Nucleonics **10**, 96 (1952).

II

The problem may be approached by considering that there is some fraction $\phi$ of the counting time ($\Delta t$) at which the actual c/m is equal to the observed average c/m. Equating these two quantities, then,

$$(kN_0)[(1-e^{-\lambda\Delta t})/(\Delta t)]=\lambda kN_0 e^{-\lambda\phi\Delta t}. \quad (4)$$

Thus,

$$\phi=\frac{1}{\lambda\Delta t}\ln\left[\frac{\lambda\Delta t}{1-e^{-\lambda\Delta t}}\right]=\frac{1}{2}-\frac{1}{\lambda\Delta t}\ln\left[\frac{2}{\lambda\Delta t}\sinh\lambda\Delta t/2\right]$$

$$=\frac{1}{2}-\frac{\lambda\Delta t}{24}+\frac{(\lambda\Delta t)^3}{2880}+\cdots. \quad (5)$$

Equation (5) obviously approaches $\frac{1}{2}$ as the limit as $\Delta t$ approaches zero. Since the major experimental error is associated with the determination of the average c/m rather than with time, it is convenient to apply Eq. (3) rather than Eq. (5). Indeed, the experimental data do not generally warrant application of the correction terms of Eq. (3) when $\lambda\Delta t$ is $\leqslant 0.1549$ ($\Delta t=22.35$ percent of $t_{\frac{1}{2}}$).

III

The half-life problem may be formulated as follows for two counting periods.

Let $\delta N_1$ be the number of atoms decaying during $0\leqslant t\leqslant t_1$; $\delta N_2$ those during $t_2\leqslant t\leqslant t_3$. Then

$$(\delta N_1)/(\delta N_2)=(1-e^{-\lambda t_1})/(e^{-\lambda t_2}-e^{-\lambda t_3}). \quad (6)$$

This expression represents an exact solution of the problem. If time intervals are chosen so that $t_3-t_2=t_1$ then Eq. (6) becomes simplified to the form

$$\frac{\delta N_1}{\delta N_2}=\frac{1}{e^{-\lambda t_2}},$$

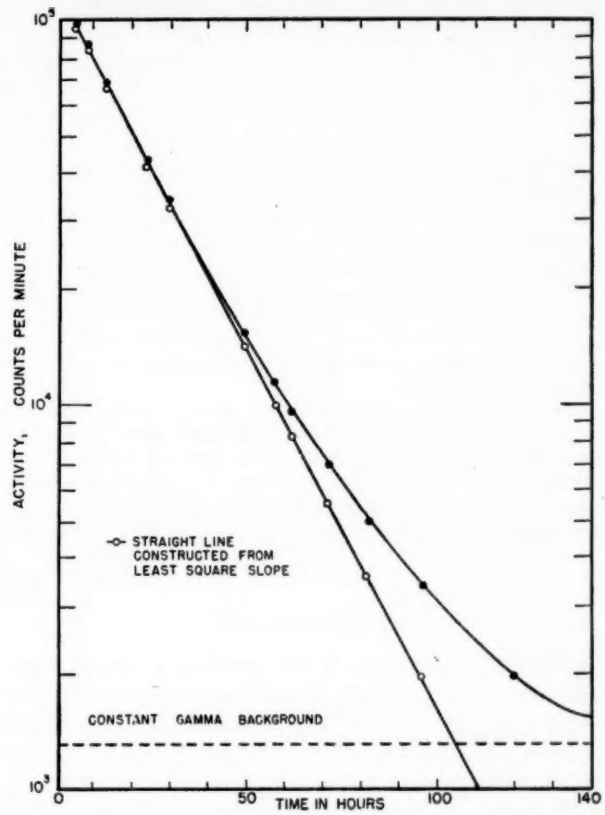


FIG. 1. Typical decay curve of $Am^{242m}$ activity. Solid circles are experimental points, open circles are points corrected for gamma background.

so

$$\lambda=\frac{\ln[(\delta N_1)/(\delta N_2)]}{t_2},$$

where $t_2$ is the time elapsed between time zero and the beginning of the second interval.

# The Methyl Alcohol Molecule and Its Microwave Spectrum

EUGENE V. IVASH* AND DAVID M. DENNISON
*Harrison M. Randall Laboratory of Physics, University of Michigan*

(Received March 27, 1953)

The theory of hindered rotation in methyl alcohol developed by Burkhard and Dennison has been extended to include the second-order Stark effect as well as a detailed discussion of $K$-type doubling. It has been applied to an interpretation of the microwave spectrum of normal methanol and of two isotopic molecules, $C^{13}H_3O^{16}H$ and $C^{12}H_3O^{18}H_3$ recently measured by Hughes, Good, and Coles. A very convincing fit between the predicted and observed lines is obtained which serves to determine many of the molecular constants, as well as providing a substantial number of self-consistency checks.

The height of the potential barrier (on the assumption of a sinusoidal potential) is found to be 374.8 $cm^{-1}$. The CH distance in the methyl group cannot be obtained with any accuracy from the present data but is consistent with the CH distance in methane, namely, 1.093A, and has been taken to have this value. The remaining dimensions are, however, well determined and are: OH distance = 0.937A, CO distance = 1.434A, COH angle = 105°56′, HCH angle = 109°30′. The symmetry axis of the methyl group passes between the H and O of the hydroxyl group and lies at a distance of 0.079A from the oxygen. The above values for the barrier height and molecular dimensions do not differ much from those found by Burkhard and Dennison but are believed to be considerably more accurate.

Using the molecular constants, the positions of all the observed microwave lines which can be identified have been calculated. In every case the agreement is good. Those discrepancies which do exist are of an order of magnitude which can be ascribed to higher-order effects not included in the present theory.

The Stark effect, both first and second order, has been computed for all identified lines. In all but one or two cases the agreement with experiment is found to be very satisfactory.

## INTRODUCTION

THE present paper is the third in a series[1,2] from this laboratory dealing with the theory of hindered rotation in the methyl alcohol molecule $CH_3OH$ and with the interpretation of its spectrum. A model of the molecule has been assumed which consists of a rigid methyl and a rigid hydroxyl group undergoing mutual rotation about the symmetry axis of the methyl group, subject to a hindering potential of the form $V=H/2(1-\cos 3x)$, where $H$ is the so-called height of the potential barrier, and $x$ is the angle measuring the relative rotation of one group with respect to the other. The advantages and limitations of this model have been discussed in the earlier papers.

The theory as developed by Koehler and Dennison,[1] in the first paper of the series further assumed the hydroxyl group to be a symmetric rotator, thus greatly simplifying the Hamiltonian of the system and making possible exact solutions for the wave functions and the energy levels. No appreciable progress could be made towards determining the molecular constants, however, since at the time it appeared impractical to interpret the portions of the infrared spectrum then known.

The microwave spectrum of methyl alcohol as measured by Hershberger and Turkevich,[3] by Dailey,[4] and by Coles[5] furnished new information which was utilized by Burkhard and Dennison,[2] who further extended the theory by considering the hydroxyl group not as a symmetric rotator but as an asymmetric rotator, corresponding to the actual situation. They were able to evaluate a number of the molecular constants but had few, if any, cross checks on the validity of their results.

A recent paper by Hughes, Coles, and Good[6] on the microwave spectrum of methanol has provided many further experimental data which may now be used to make a much more precise determination of the molecular constants, as well as providing a considerable number of cross checks. In general, the agreement between the present results and those of Burkhard and Dennison is good, although there are some minor changes, and there has been a substantial improvement in accuracy. The theory of hindered rotation has also been extended to take account of certain features of the microwave spectrum not originally considered.

## THEORY

### 1. Structure of the Energy Levels

The methods to be employed are essentially those used by Burkhard and Dennison and contain the following steps. The simplified model of reference 1, can be solved exactly and yields energy levels and wave functions described by the quantum numbers $J$, $M$, $K$, $\tau$, and $n$. The total angular momentum of the molecule (in units of $\hbar$) is given by $J$, while $K$ and $M$ represent the components of $J$ along the symmetry axis of the molecule and along some space fixed axis, respectively. $n$ is a quantum number describing the torsional oscillation. In the limit of very large values of $H$, that is, for high potential barriers, the energy becomes $(n+\frac{1}{2})h\nu_t$, where $\nu_t$ is the torsional frequency. The quantum number $\tau$ relates to the tunneling of the hydrogen of the hydroxyl group from one minimum to another and

* Present address: Department of Physics, University of Texas, Austin, Texas.

[1] J. S. Koehler and D. M. Dennison, Phys. Rev. **57**, 1006 (1940).
[2] D. G. Burkhard and D. M. Dennison, Phys. Rev. **84**, 408 (1951).
[3] W. D. Hershberger and J. Turkevich, Phys. Rev. **71**, 554 (1947).
[4] B. P. Dailey, Phys. Rev. **72**, 84 (1947).
[5] D. K. Coles, Phys. Rev. **74**, 1194 (1948).
[6] Hughes, Good, and Coles, Phys. Rev. **84**, 418 (1951).

may take on the values 1, 2, or 3. The magnitude of the threefold splitting of the levels, correlated with the three values of $\tau$, goes rapidly to zero for a very high potential barrier $H$.

The wave equation for the model in which the methyl group is represented by a symmetric rotator, but the hydroxyl group by an asymmetric rotator, is very complicated, but the matrix elements of its Hamiltonian may be evaluated using as a basis the wave functions of the symmetric model. Diagonalizing the Hamiltonian yields the energy levels and the wave functions describing the asymmetric model. Since the Hamiltonian now contains off-diagonal elements corresponding to changes in $K$, $\tau$, and $n$, these are no longer good quantum numbers. However, in the application of the theory to methyl alcohol, the asymmetry and consequently the off-diagonal elements are small, and therefore it is proper to retain these numbers as convenient labels for the levels.

If the second-order Stark effect is to be considered—as it will be in the present paper—the following elements should be added to those listed in reference 2:

$$H_{JK\tau n}{}^{J-1\,K\tau n}=\mu_{11}\mathcal{E}[(J^2-K^2)(J^2-M^2)]^{\frac{1}{2}}/J(4J^2-1)^{\frac{1}{2}}$$

$$H_{JK\tau n}{}^{J-1\,K\pm1\,\tau' n'}=\pm\mu_{\perp}\mathcal{E}[(J\mp K)(J\mp K-1)(J^2-M^2)]^{\frac{1}{2}}\int_0^{2\pi}P_{K\tau n}{}^{*}\exp(\mp ix)P_{K\pm1\,\tau' n'}dx/2J(4J^2-1)^{\frac{1}{2}}.$$

$\mu_{11}$ and $\mu_{\perp}$ are the components of the permanent electric moment parallel and perpendicular, respectively, to the symmetry axis of the methyl group, and $\mathcal{E}$ is the Stark electric field strength. $P_{K\tau n}$ is a periodic function of $x$ defined in reference 2. (The notation and definitions to be used here are similar to those appearing in reference 2.)

The energy levels may be found by solving the energy determinant (diagonalizing the Hamiltonian), and while their actual evaluation involves a considerable amount of calculation, the resulting structure of the energy levels may be described rather simply. In Fig. 1 the levels for which $J=3$ and $n=0$ are shown schematically for the following systems: (a) a symmetric rigid rotator, (b) a symmetric hindered rotator, (c) an asymmetric rigid rotator, and (d) an asymmetric hindered rotator.

Proceeding from left to right in the diagram, it is seen that the introduction of a hindering potential splits the levels of the rigid symmetrical rotator. If the potential has a periodicity of three, as it does in methyl alcohol, each level is split in three with the exception of the ones for which $K=0$, which split into only two levels. The magnitude of the splitting is a measure of the penetration of the potential barrier and hence is a very sensitive function of its height. $K$ is a good quantum number for both (a) and (b), but for the latter case one must add a new quantum number $\tau$, which determines the kind or type of level, and may assume the values 1, 2, or 3. The introduction of an asymmetry, in addition to the hindered rotation, results in a splitting of the type 3 level for $K=1$, type 2 for $K=2$, type 1 for $K=3$, etc. If the barrier height is now raised indefinitely without disturbing the asymmetry, one goes from (d) to (c). Finally, if the asymmetry of the rigid rotator is removed, the levels degenerate into those of the rigid symmetrical rotator. The splitting of the levels of the rigid rotator caused by the asymmetry is often called $K$-type doubling and was first discussed by Wang.[7] When the splitting is small, it is approximately given by the formula

$$\Delta E_K=4h^2c(b/8)^K(J+K)\,!/(J-K)\,!(K-1)\,!^2,$$

where

$$c=1/C-1/2A-1/2B,$$

$$2bc=1/B-1/A,$$

and $A$, $B$, $C$ are the principal moments of inertia of a nearly symmetric rigid top with $B\cong A$, and $C<B<A$.

It is evident from Fig. 1 that the levels of an asymmetric rotator subject to a threefold hindering potential exhibit both the features of the splitting which are due to the tunnel effect and also that which is due to the asymmetry. The latter effect, which by analogy with the rigid case will also be called $K$-type doubling, does not affect all levels but only one out of every three.

## 2. Theory of the $K$-Type Doubling

The problem of $K$-type doubling for the hindered asymmetric rotator is similar to that for the rigid

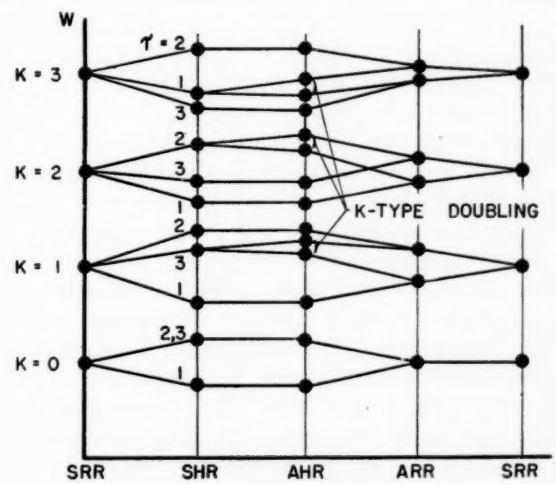


FIG. 1. Correlation of the rotational energy levels corresponding to various limiting cases for a molecule of the methyl alcohol type. $J=3$, $n=0$ for the above levels. SRR—symmetric rigid rotator, SHR—symmetric hindered rotator, AHR—asymmetric hindered rotator, ARR—asymmetric rigid rotator.

[7] S. C. Wang, Phys. Rev. 34, 243 (1929).

asymmetric rotator, though it differs from it in two respects. The dissimilarities are occasioned by the existence of the hindering potential, and by the presence of the cross product of inertia $D$. When proper account is taken of these two factors, it can be verified that the formulas developed for the hindered asymmetric rotator go over into those for the rigid asymmetric rotator as the potential barrier $H$ becomes indefinitely high.

As shown in reference 2 the energy determinant factors into three subdeterminants which are designated by the numbers 1, 2, and 3. The roots of subdeterminants 1 and 2 are identical, and the levels in question belong to the degenerate symmetry class $E$. Subdeterminant 3, however, yields pairs of roots whose separation constitutes the $K$-type doubling which we seek to calculate. It will prove convenient to include the Stark effect terms in the following discussion which for simplicity has been limited to the levels for which $n=0$. Evaluating the roots of subdeterminant 3 by standard perturbation methods, it can be shown that the structure of the levels is represented by the expression,

$$E_{JKM}=\bar{E}_{JK}+a_{JKM}\mathcal{E}^2 \pm\tfrac{1}{2}[b_{JKM}{}^2\mathcal{E}^2+(\Delta_{JK}+c_{JKM}\mathcal{E}^2)^2]^{\frac{1}{2}},$$

where $\mathcal{E}$ is the electric field strength, $a_{JKM}$ and $c_{JKM}$ involve the off-diagonal elements $J\rightarrow J\pm1$, $K\rightarrow K\pm1$ of the Hamiltonian, and $b_{JKM}=\mu_{11}KM/(J^2+J)$. $\bar{E}_{JK}$ is, of course, the center of gravity of the doublet levels in the absence of an electric field, and $\Delta_{JK}$ is the corresponding doublet separation.

From the foregoing formula it is clear that for low field strengths, where $\mathcal{E}(b_{JKM}{}^2+2\Delta_{JK}c_{JKM})^{\frac{1}{2}}\ll\Delta_{JK}$, the Stark effect will be of second order but that it will become of first order for such large values of $\mathcal{E}$ that $\mathcal{E}(b_{JKM}{}^2+2\Delta_{JK}c_{JKM})^{\frac{1}{2}}\gg\Delta_{JK}$.

Just as the symmetric rigid rotator possesses a linear Stark effect resulting from the degeneracy of its energy levels, while a quadratic Stark effect exists for the asymmetric rotator because the degeneracy has been removed, so also for the asymmetric hindered rotator, the removal of the degeneracy by the off-diagonal matrix elements produces a quadratic Stark effect. As the field strength $\mathcal{E}$ is increased, the quadratic approximation begins to lose its validity, breaking down completely when the Stark splitting is of the same order of magnitude as the $K$ type of splitting. For field strengths still higher, the Stark effect becomes linear. The latter situation is very likely to be the case for levels with high $K$, for which the $K$-type splitting is usually very small. Experimental examples of precisely this behavior will be encountered.

The $K$-type doubling in the absence of an electric field is of particular interest. It may be approximated through the off-diagonal elements of the Hamiltonian in the same manner as is done for the rigid asymmetrical rotator. In the following expressions the quantum number $\tau$ will be suppressed, since its values are uniquely determined by the values of $K$.

$$\Delta_{J0}=0 \quad \Delta_{J1}=2H_{J-1}{}^{J1}$$
$$\Delta_{J2}=2[H_{J0}{}^{J2}]^2/(E_{J2}{}^0-E_{J0}{}^0)$$
$$\Delta_{J3}=2[H_{J-1}{}^{J1}][H_{J1}{}^{J3}]^2/(E_{J3}{}^0-E_{J1}{}^0)^2$$
$$\Delta_{J4}=2[H_{J2}{}^{J4}]^2[H_{J0}{}^{J2}]^2/(E_{J4}{}^0-E_{J2}{}^0)^2(E_{J4}{}^0-E_{J0}{}^0),$$

where

$$E_{JK}{}^0=H_{JK}{}^{JK}.$$

The matrix elements as well as the energies $E_{JK}{}^0$ depend upon the molecular constants. A substitution of the methyl alcohol constants as determined in a later section gives rise to the following values expressed in mc/sec:

$$\Delta_{J1}=400(J^2+J),$$
$$\Delta_{J2}=0.086(J-1)(J)(J+1)(J+2),$$
$$\Delta_{J3}=2.12\times10^{-5}(J-2)(J-1)(J)(J+1)(J+2)(J+3),$$
$$\Delta_{J4}=1.91\times10^{-9}(J-3)(J-2)\cdots(J+4).$$

### 3. Selection Rules for the Asymmetric Hindered Rotator

The permanent electric moment of the molecule may be resolved into two components, $\mu_{11}$ lying along the symmetry axis of the methyl group, and $\mu_\perp$ normal to the symmetry axis and in the COH plane. The case for which there is no external field $\mathcal{E}$ will be first considered.

The wave function $\psi$ for the asymmetric hindered rotator can be expanded linearly in terms of the symmetric hindered rotator wave functions $u_{JK\tau nM}$. As a consequence of the threefold factoring of the secular determinant already discussed, however, there are three different possible classes of $\psi$, each class containing only those symmetric wave functions which are associated with a given subdeterminant. Thus, the $\psi$'s corresponding to an energy eigenvalue of subdeterminants 1, 2, and 3 will have the respective forms,

$$\psi_1=\cdots a_{-22}u_{-22}+a_{-11}u_{-11}+a_{03}u_{03}+a_{12}u_{12}+a_{21}u_{21}+\cdots$$
$$\psi_2=\cdots b_{-21}u_{-21}+b_{-13}u_{-13}+b_{02}u_{02}+b_{11}u_{11}+b_{23}u_{23}+\cdots$$
$$\psi_3=\cdots c_{-23}u_{-23}+c_{-12}u_{-12}+c_{01}u_{01}+c_{13}u_{13}+c_{22}u_{22}+\cdots.$$

The quantum numbers which are particularly pertinent to the present expansion are $K$ and $\tau$, and for this reason $u_{JK\tau nM}$ has been contracted to $u_{K\tau}$. It is to be noted that these expansions contain the wave functions $u_{K\tau}$ corresponding to all $K$ such that $|K|\leqslant J$, and that for every $K$ there is only one particular $\tau$.

To determine the selection rules one must calculate the matrix elements of the dipole moment along the space-fixed axes $X$, $Y$, and $Z$ between two states $a$ and $b$. These will have the usual form

$$(u_F)_{ab}=\int\psi_a{}^*\mu_F\psi_b dV,$$

where $F$ is either $X$, $Y$, or $Z$, and $\mu_F$ is the quantum-mechanical operator corresponding to the dipole moment along $F$. By using the above-mentioned expansions of $\psi$, one can reduce this integral to a sum of integrals over the symmetric wave functions, and hence, from a knowledge of the selection rules for the symmetric rotator, one may deduce those for the asymmetric hindered rotator.

It will be recalled[1] that, for the symmetric rotator, the only permitted transitions are those for which (a) $\Delta K=0$, $\Delta\tau=0$, corresponding to the component of the electric moment along the symmetry axis, or (b) $K\rightarrow K-1$, $\tau=1\rightarrow 2$, $2\rightarrow 3$, or $3\rightarrow 1$ and $K\rightarrow K+1$, $\tau=2\rightarrow 1$, $3\rightarrow 2$, or $1\rightarrow 3$ corresponding to the perpendicular component. For both (a) and (b) $\Delta J=\pm 1$, 0, and $\Delta n$ may have any value.

The first result of this calculation is that no transitions are possible between energy levels belonging to different subdeterminants. Moreover, since the matrix elements of the Hamiltonian are diagonal in $J$ and $M$, (i.e., $J$ and $M$ are good quantum numbers), the selection rules for $J$ and $M$ will be the same as those of the symmetric hindered rotator, namely, $\Delta J=0$, $\pm 1$, and $\Delta M=0$, $\pm 1$. As before, $\Delta n$ can be anything.

Transitions between all levels of subdeterminant 1 are, in general, possible, consistent, of course, with the requirement that $|K|\leqslant J$, while the same holds for levels of subdeterminant 2. It should, however, be remembered that the two determinants are degenerate with respect to each other, and that the energy levels of the two are identical although labeled differently. Thus, the transition $(K=1,\ \tau=1)\rightarrow(K=-1,\ \tau=3)$, for example, is effectively also a transition to the state $(K=1,\ \tau=2)$, since the $K=-1$, $\tau=3$ and the $K=1$, $\tau=2$ levels coincide. Since the methyl alcohol molecule is only slightly asymmetric, it may be expected that transitions that violate the selection rules for the symmetric rotator, though possible, will, in general, be weak.

The selection rules for transitions between energy states corresponding to subdeterminant 3, because of the degeneracy existing between diagonal elements of this determinant, must be considered separately from those for subdeterminants 1 and 2. It will be recalled that for subdeterminant 3, because of the off-diagonal elements, a $K$-type doubling or splitting of the energy levels occurs, thereby removing the degeneracy which exists for the symmetric hindered rotator.

An examination of determinant 3 shows that the wave function for a $K$-doublet level has one of the two following forms:

$$\psi_+=a_0u_0+a_1(u_{-1}-u_1)+a_2(u_{-2}+u_2)+a_3(u_{-3}-u_3)\cdots$$

and

$$\psi_-=b_1(u_{-1}+u_1)+b_2(u_{-2}-u_2)+b_3(u_{-3}+u_3)\cdots,$$

where the $u_K$ are the symmetric hindered rotator wave functions corresponding to the quantum number $K$, and the $a_K$ and the $b_K$ are development coefficients which depend on the molecular constants. The other quantum numbers $J$, $M$, $\tau$, and $n$ have been omitted for simplicity. The two members of a $K$-type doublet possess different forms of the wave function and the states belong to different symmetry classes. The two forms of wave functions will be designated as the $+$ and $-$ types, corresponding to the first and second equations, respectively.

Substituting these expressions for $\psi$ into the equation for $(\mu_F)_{ab}$, and making use of the symmetry properties of $u_K$, one obtains the following results for the energy levels of determinant 3:

Only $+\rightarrow+$ or $-\rightarrow-$ transitions are allowed for $\Delta n=$ even, $\Delta J=\pm 1$, or for $\Delta n=$ odd, $\Delta J=0$.

Only $+\rightarrow-$ or $-\rightarrow+$ transitions are allowed for $\Delta n=$ even, $\Delta J=0$, or for $\Delta n=$ odd, $\Delta J=\pm 1$.

Whether a given level is $+$ or $-$ can be determined, in general, only by an inspection of the secular determinant, since the ordering of the levels may change as the molecular parameters are varied. However, in the case of methyl alcohol for $n=0$ and for values of the molecular constants near those to be presented later, the result is quite simple. For a given value of $J$ the two lowest levels are $+$, the next two higher ones are $-$, the next two higher ones are $+$, etc. It may be noted that for the levels arising from subdeterminant 3, the selection rules for $\Delta n=$ even become formally the same as those for the case of the rigid asymmetric rotor with components of the permanent electric moment along the principal axes of the least and middle moments of inertia. For $\Delta n=$ odd the situation is analogous to that of the rigid rotator with the moment along the greatest moment of inertia axis.

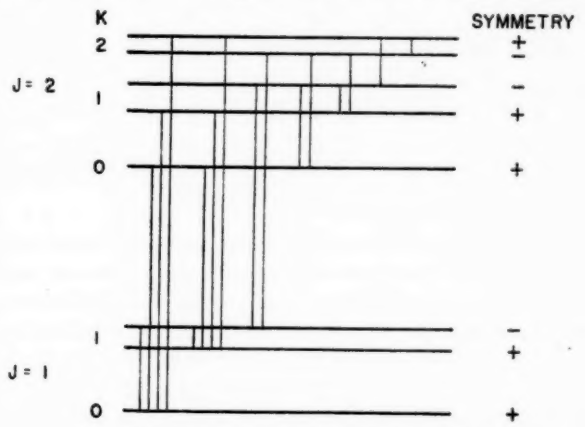


FIG. 2. Allowed transitions between levels with $J=2$, $n=0$ and $J=1$, $n=0$ for methyl alcohol.

The selection rules for the $n=0$ levels of methyl alcohol are illustrated in Fig. 2.

If, in addition to the moments along the $y$ and $z$ axes, a moment along the $x$ axis should also exist, the selection rules given above for levels of determinant 3 would break down and all transitions, in general, would

be possible between these levels. The rule relating to noncombination between the levels of different subdeterminants would still hold, however.

Until now it has been assumed that no external electric field $\mathcal{E}$ is present. If $\mathcal{E}$ is not zero, then the matrix elements of the Hamiltonian have $J\rightarrow J\pm1$ connections, and this results in the possibility of transitions with $\Delta J=\pm2$. The rule $\Delta M=0, \pm1$ is still valid, however, and intercombinations between levels of the different subdeterminants are forbidden as before. Since, however, the presence of the Stark energy matrix elements disturbs the symmetry of the secular determinant, the wave function for levels with $K$-type doubling is now no longer either a pure $+$ or $-$ type but is instead a mixture of the two. Consequently, all transitions between these levels are then permitted, so that previously forbidden lines become allowed, their intensities increasing with $\mathcal{E}$. Such lines have actually been observed, and will later be discussed in detail in connection with the so-called "mirror" lines.

### 4. Classification of Lines

As in the infrared spectrum, the principal classes of transitions in the microwave region are those for which (1) $\Delta J=\pm1$, $\Delta K=0$, (2) $\Delta J=0$, $\Delta K=\pm1$, and (3) $\Delta J=\pm1$, $\Delta K=\pm1$. These three different cases all occur in the observed microwave spectrum of methanol and have the following characteristics.

(1) In the first class only transitions for which $\tau\rightarrow\tau$ are allowed by the selection rules and, furthermore, only those lines for which $n\rightarrow n$ fall within the microwave region. Since $\Delta K=0$ and $\Delta\tau=0$ the internal energy terms largely drop out of the frequency expression, which is then dependent, at least in the first order, only on $J$. In the higher orders, however, a splitting occurs, a group of lines being formed for each value of $|K|$ less than or equal to the smaller $J$ involved in the transition, and for each value of $n$. Because of the different possible values of $\tau$ together with the phenomenon of $K$-type doubling, each such group with a given $n$ value will consist of two lines for $K=0$ and of four lines for $K\neq0$. For methyl alcohol, only the frequencies corresponding to the transitions $J=0\rightarrow1$, $K=0\rightarrow0$, $n\rightarrow n$, $\tau\rightarrow\tau$ fall within the present microwave region. For this case two lines may be expected for $n=0\rightarrow0$, two lines for $n=1\rightarrow1$, etc. The separation between the components of each of these doublets was estimated by Burkhard and Dennison and found to be small, of the order of a fraction of a mc/sec. The calculation, however, was somewhat sensitive to the order of the approximation and it is quite possible that these splittings may actually be as large as a few mc/sec. The separation between the lines corresponding to $n=0$, 1, 2, etc. depends upon a type of vibration-rotation interaction not described by the simple model in which the methyl and hydroxyl group are assumed to be rigid, and may be expected to be much larger. This effect has been observed in the microwave spectrum of methyl silane[8] where the $n=1\rightarrow1$ lines are displaced towards lower frequencies from the $n=0\rightarrow0$ lines by about 50 mc/sec.

(2) In the second class, that for which $\Delta J=0$, $\Delta K=\pm1$, the frequency is in first order independent of the value of $J$. The higher-order terms arising from the off-diagonal elements of the Hamiltonian, however, result in a small $J$ dependence. Thus for a transition with given values of $K$, $n$, and $\tau$, an entire series of lines exists corresponding to the values of $J$ equal to or greater than the largest $|K|$ involved. If the levels in question are those associated with the subdeterminant 3, there will exist, in addition, a $K$-type doubling of the lines. For methyl alcohol the only series thus far observed is that corresponding to the transitions $J\rightarrow J$, $K=1\rightarrow2$, $n=0\rightarrow0$, $\tau=2\rightarrow1$.

(3) Finally, there is the class for which $\Delta J=\pm1$, $\Delta K=\pm1$. A large number of lines of this type have been observed in the microwave spectrum of methanol. Most of them are due to transitions in which $J$ and $K$ change in opposite directions, though there are instances where the change is in the same direction. In general, the lines of this third class are irregularly spaced throughout the spectrum. The lines arising from the energy levels of subdeterminants 1 and 2 are single while those from subdeterminant 3 exhibit $K$-type doubling. There exists a type of combination relation which, while only approximate, may be of value in identifying the lines. Consider the two transitions $J\rightarrow J-1$, $K\rightarrow K-1$, $\tau\rightarrow\tau'$, and $J'-1\rightarrow J'$, $K-1\rightarrow K$, $\tau'\rightarrow\tau$. If these two frequencies are added, the internal energy terms cancel and the result in the first order will be $(J'-J)$ times the frequency of the line $J=0\rightarrow1$, $K=0\rightarrow0$, $\tau\rightarrow\tau$, $n\rightarrow n$. The deviation from this combination relation turns out to be of the order of a hundred mc/sec in methanol for $J=3$, $J'=4$ but may be expected to be greater for larger values of $J$ and $J'$.

It will be shown that the Stark effect of all lines for which $\Delta K=\pm1$ is of the first order when the levels are those associated with subdeterminants 1 and 2. The lines belonging to subdeterminant 3, however, all have a second-order Stark effect up to the point where the Stark splitting becomes of the same magnitude as the $K$-type doubling, in which case a first-order Stark effect appears.

It might also be pointed out that the selection rules for an asymmetric hindered rotator permit transitions in which $K$ changes by more than one unit. Such lines, however, will be relatively weak for molecules of the methyl alcohol type where the asymmetry is small.

## THE EXPERIMENTAL DATA

The line data which will be used in determining the molecular constants of methanol and in demonstrating the consistency of the solution so obtained may be divided into the three classifications just described.

[8] D. R. Lide and D. K. Coles, Phys. Rev. **80**, 911 (1950).

(1) The lines corresponding to the transitions $J=0\rightarrow1$, $K=0\rightarrow0$, $\tau\rightarrow\tau$, $n\rightarrow n$ may be expected to fall between 48 000 and 50 000 mc/sec. This region of the microwave spectrum has been investigated by Edwards, Gilliam, and Gordy[9] for both normal methanol and for the isotopic molecules $C^{13}H_3OH$, $C^{12}H_3OD$, and $C^{12}D_3OD$. The spectrum of normal methanol showed a considerable number of irregularly spaced lines of which two, a single line at 49 867 and a close doublet centered at 48 374 (doublet separation 4 mc/sec) were the strongest. Burkhard and Dennison picked the single line as the one to be identified with the $n=0\rightarrow0$ transition on the basis that with this choice lines could be found in the spectra of the isotopic molecules which were consistent with the dimensions of the molecule. If this choice were correct, the doublet at 48 374 might then be associated with the same $J$ and $K$ transition but with $n=1\rightarrow1$, although its separation from the $n=0\rightarrow0$ line would seem to be abnormally large.

Several recent pieces of experimental data are now available, however, which appear to show that Burkhard and Dennison made the incorrect identification and that the frequency corresponding to $J=0\rightarrow1$, $K=0\rightarrow0$, $\tau\rightarrow\tau$, $n=0\rightarrow0$ lies at 48 374 mc/sec. The frequency of this particular transition will be designated as $\nu_1$. The evidence is the following.

(a) Hughes, Good, and Coles[6] found a line at 28 316 mc/sec which, from its observed Stark pattern, can be assigned to $J=3\rightarrow4$, $K=1\rightarrow0$, $\tau=2\rightarrow3$, $n=0\rightarrow0$. Subsequent to the publication Hughes (private communication) has measured a line at 19 967 mc/sec which can be identified as one for which $J=3\rightarrow2$, $K=0\rightarrow1$, $\tau=3\rightarrow2$, $n=0\rightarrow0$. According to the approximate combination rule, the sum of these two frequencies, namely, 48 283 mc/sec, should be nearly equal to $\nu_1$. The observed deviation, 91 mc/sec, is of the right order of magnitude, and a calculation, based upon the molecular constants to be presented later, leads to a predicted deviation of 104 mc/sec.

(b) Dr. C. W. Peters at the University of Michigan has re-examined the fine structure of the parallel vibration-rotation band at 1034 $cm^{-1}$ of methyl alcohol. Although the individual lines were found to be split into a number of components, the positions of their centers agreed very accurately with the results obtained by Borden and Barker[10] using lower resolution, namely,

$$\nu=1034.18+1.5975J-0.0088J^2.$$

This formula leads to a prediction that the microwave line $\nu_1$ should fall at 48 160 mc/sec which is in reasonable agreement with the line at 48 374 but inconsistent with the line at 49 867.

[9] Edwards, Gilliam, and Gordy (to be published). We are very much indebted to Professor Gordy for sending us a preliminary account of their work.

[10] A. Borden and E. F. Barker, J. Chem. Phys. **6**, 553 (1938).

TABLE I.

| | $C^{13}H_3O^{16}H$ | $C^{12}H_3O^{16}H$ | $C^{12}H_3O^{18}H$ |
|---|---|---|---|
| $\nu_2$ | 24 948.04 | 27 065.58 | 33 918.57 |
| $a$ | −2.942 | −2.654 | −0.445 |
| $b$ | 0.1111 | 0.0901 | 0.0855 |
| $c$ | $-1.06\times10^{-5}$ | $3.36\times10^{-4}$ | $-2.97\times10^{-5}$ |
| $d$ | $-4.9\times10^{-7}$ | $-4.9\times10^{-6}$ | $-3.0\times10^{-8}$ |
| $A$ | 131.1 | 131.3 | 131.0 |
| $B$ | 1.710 | 1.751 | 2.646 |

(c) A recent announcement by Swan[11] states that the line at 49 867 shows a first-order Stark effect, whereas the line $\nu_1$ can only have a second-order Stark effect.

(2) The only lines of the second class so far observed in the microwave spectrum of methanol are those for which $J\rightarrow J$, $K=1\rightarrow2$, $\tau=2\rightarrow1$, and $n=0\rightarrow0$. These form a series corresponding to the values of $J\geqslant2$ and have been measured[6] for $C^{12}H_3O^{16}H$, $C^{13}H_3O^{16}H$, and $C^{12}H_3O^{18}H$ through $J=30$, 31, and 26, respectively. The positions of the individual lines of the series may be expressed as a power series expansion in $J^2+J$ as follows:

$$\nu=\nu_2+a(J^2+J)+b(J^2+J)^2+c(J^2+J)^3+d(J^2+J)^4+\cdots.$$

The values of these coefficients as determined from the first five members of each series are given in Table I in mc/sec. (The values for normal methanol presented here differ slightly from those given by Burkhard and Dennison since they used alternate rather than adjacent lines in their calculation. This difference illustrates the difficulty of obtaining accurate coefficients in a series expansion, and indicates that while $\nu_2$ is very reliably determined, the value of $b$, for example, may be in error by as much as 1 percent. While no explicit use is made of the constants $c$ and $d$, they have been included to show that they are small and that they contribute very little to the positions of the lines with low $J$ values. If this were not the case, the method employed for finding $a$ and $b$ would yield very inaccurate values.)

Hughes, Good, and Coles[6] have measured the Stark effect of these lines and found it to be predominantly of the first order, with the splitting given by the expression $M\mathcal{E}[A/(J^2+J)+B]$, where $M$ is the magnetic quantum number and $\mathcal{E}$ the electric field in esu. The experimental values of $A$ and $B$ in mc/sec–esu are listed in Table I.

(3) In addition to the series lines just discussed, Hughes, Good, and Coles observed a considerable number of lines irregularly spaced throughout the microwave region. These are to be ascribed to the third class of transitions in which both $J$ and $K$ change. From the Stark patterns it was possible in a number of cases to determine the values of $J$. This information, together with estimates for the internal energy levels,

[11] P. R. Swan, Jr., Mass. Inst. Technol. Quart. Progr. Rept., p. 30, April 15, 1952.

TABLE II.

| Designation | Frequency | Transition $J$ | $K$ | $\tau$ |
|---|---|---|---|---|
| $\nu_a$ | 19 967 | 3→2 | 0→1 | 3→2 |
| $\nu_b$ | 28 316 | 3→4 | 1→0 | 2→3 |
| $\nu_c$ | 36 169 | 3→4 | 0→1 | 2→1 |
| $\nu_d$ | 37 704 | 8→7 | 1→2 | 1→3 |
| $\nu_e'$ | 38 294 | 5→6 | 3→2 | 1→2 |
| $\nu_e''$ | 38 453 | 5→6 | 3→2 | 1→2 |

served to fix the transition in question. The lines which could be identified uniquely are listed in Table II in mc/sec. In all cases $n=0\rightarrow 0$. The lines $\nu_e'$ and $\nu_e''$ are the two components of a $K$-type doublet.

## CALCULATION OF THE MOLECULAR CONSTANTS OF $C^{12}H_3O^{16}H$

Seven molecular parameters appear in the matrix elements of the Hamiltonian. These are the four moments and products of inertia $A$, $C_1$, $C_2$, and $D$, the barrier height $H$ and the components of the permanent electric moment, namely, $\mu_{\|}$ and $\mu_{\perp}$. [$C_2$ is the moment of inertia of the rigid methyl group with respect to the symmetry axis of that group. The remaining quantities are defined as follows (see also reference 2): Consider a Cartesian coordinate system $\xi, \eta, \zeta$, whose origin lies at the center of gravity of the entire molecule. The $\zeta$ axis is parallel to the symmetry axis of the methyl group, and the $\eta$ axis lies in the plane defined by the $\zeta$ axis and the hydroxyl group. If the mass of any atom of the molecule be $\mu_i$ and its coordinates $\xi_i\eta_i\zeta_i$, then $A=\sum_i\mu_i(\eta_i^2+\zeta_i^2)$, $C=\sum_i\mu_i(\xi_i^2+\eta_i^2)$, and $D=\sum_i\mu_i\eta_i\zeta_i$. Further $C_1=C-C_2=A-B$.] Although in principle all seven parameters are determined by the spectrum, in practice neither $D$ nor $\mu_{\perp}$ can be obtained separately with any great accuracy but only their product $D\mu_{\perp}$. On the other hand, $\mu_{\|}$ is readily obtained, and hence, $\mu_{\perp}$ can be calculated using the experimental value for the total permanent dipole moment $\mu=[\mu_{\|}^2+\mu_{\perp}^2]^{\frac{1}{2}}=1.69\times10^{-18}$ esu found by Kubo.[12]

An examination of the energy expressions shows that the Stark energy of the series of lines belonging to transitions $J\rightarrow J$, $K=1\rightarrow 2$, $\tau=2\rightarrow 1$, $n=0\rightarrow 0$ depends linearly upon $\mu_{\|}$ and $D\mu_{\perp}$ but is relatively insensitive to the remaining parameters. The positions of the lines $\nu_1$, $\nu_2$, $\nu_b$, and $\nu_c$ on the other hand are sensitive functions of $A$, $C_1$, $C_2$, and $H$ and depend to only a small extent upon $D$. This suggests the employment of a cycle of calculations starting from the molecular parameters found by Burkhard and Dennison. The cycle is repeated until a set of parameters is found which correctly reproduces the observational data. The actual computations are quite lengthy since they involve the evaluation of the energy determinant by successive approximations, as well as the calculation of a number of matrix elements. The general procedure and the results may be readily summarized, however.

### 1. Evaluation of $D$, $\mu_{\|}$, and $\mu_{\perp}$

The Stark energy for the series lines of class two is predicted from the secular energy determinant to be mainly of first order but containing also a small admixture of second order which will be discussed later. The first-order expression for the splitting has the form $M\mathcal{E}[A/(J^2+J)+B]$ where $A$ and $B$ are linear functions of $\mu_{\|}$ and $D\mu_{\perp}$, respectively, but depend upon the remaining parameters in a complicated fashion. As has been seen, the experimental results are in the same form, and the values of $A$ and $B$ have been given in Table I. Identifying coefficients and making use of Kubo's value for the total permanent dipole moment,[12] one obtains

$$D=-0.107\times10^{-40}\ \text{g cm}^2,$$
$$\mu_{\|}=-0.885\times10^{-18}\ \text{esu},$$
$$\mu_{\perp}=1.44\times10^{-18}\ \text{esu}.$$

$\mu_{\|}$ is chosen to be negative in conformity with the requirement of atomic electronegativity which demands that the parallel component of the moment be directed along the symmetry axis in the direction from the O to the C atom. Similarly, $\mu_{\perp}$ must be directed from the O to the H atom and is therefore positive. Consequently the sign of $D$ must be negative. This conclusion, as will be seen later, is supported by the Stark data for the various isotopic molecules.

### 2. Calculation of $A$, $C_1$, $C_2$, and $H$

It proves convenient to express the four frequencies $\nu_1$, $\nu_2$, $\nu_b$, and $\nu_c$ as the sum of two sets of terms, (1) the large terms arising from the principal diagonal elements of the Hamiltonian, and (2) the small terms which have been grouped under the designation $\epsilon$. The

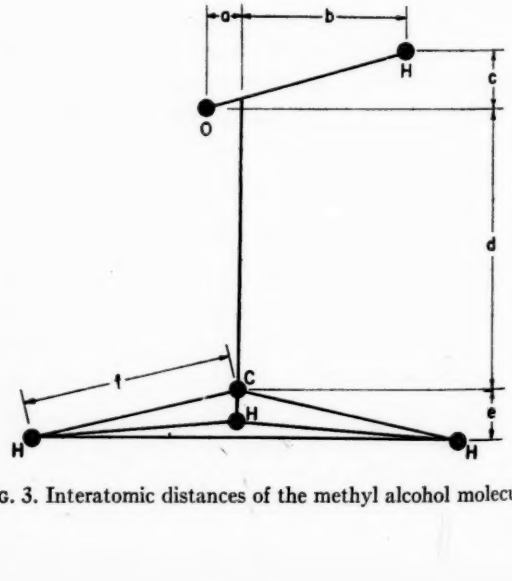


FIG. 3. Interatomic distances of the methyl alcohol molecule.

[12] M. Kubo, Sci. Papers Inst. Phys. Chem. Research Tokyo **26**, 242 (1935).

quantity $\epsilon$ contains the contributions from the off-diagonal elements of the Hamiltonian as well as the diagonal element

$$-[\hbar^2 D^2/2C_1(BC_1-D^2)]\int_0^{2\pi} P_{K\tau n}^* \frac{d^2}{dx^2} P_{K\tau n} dx.$$

$\nu_1 = 48\,374$ mc/sec
$$= (h/8\pi^2)[1/A + C_1/(BC_1-D^2)] + \epsilon_1,$$

$\nu_2 = 24\,948$ mc/sec
$$= -\tfrac{3}{2}\nu_1 + 3h/8\pi^2 C + (E_{210}-E_{120})/h + \epsilon_2,$$

$\nu_b = 28\,316$ mc/sec
$$= (9/2)\nu_1 - h/8\pi^2 C + (E_{030}-E_{120})/h + \epsilon_b,$$

$\nu_c = 36\,169$ mc/sec
$$= (7/2)\nu_1 + h/8\pi^2 C + (E_{110}-E_{020})/h + \epsilon_c.$$

The quantities $E_{K\tau n}$ are the hindered rotation energies defined in reference 2, p. 412 expressed in $cm^{-1}$. The small terms $\epsilon_1$, $\epsilon_2$, $\epsilon_b$, and $\epsilon_c$ have been calculated and are of the order of 100 mc/sec.

The foregoing expressions for the four frequencies are essentially functions only of the parameters $A$, $C_1$, $C_2$, and $H$. An examination of the equations shows that there exists a unique solution which may be obtained by successive approximations. The result is

$A = 35.341\times10^{-40}$ g cm$^2$ $\quad C_2 = 5.333\times10^{-40}$ g cm$^2$
$C_1 = 1.245$ g cm$^2$ $\quad H = 374.82$ cm$^{-1}$.

It is interesting to note that the value of $5.333\times10^{-40}$ g cm$^2$ for the moment of inertia of the methyl group in methyl alcohol is quite close to the corresponding moment of inertia of the methyl group in methane, namely, $5.330\times10^{-40}$ g cm$^2$.[13] This near equality of the two moments of inertia makes it plausible, though not certain, that the CH distance and the HCH angle of methyl alcohol do not differ much from those of methane.

It is impossible in the case of any molecule as complex as methanol to obtain a rigorously exact solution for the energy levels. In order to progress at all it is necessary to consider a simplified model which neglects certain of the higher-order effects. Among the effects neglected in the present paper, there is the centrifugal stretching of the molecule and also the interaction between the rotational energy and the normal vibrations. Estimates indicate that this influence will be relatively small on the low-lying levels under consideration. Some idea of the sensitivity of the equations may be gained by successively varying the frequencies of $\nu_1$, $\nu_2$, $\nu_b$, and $\nu_c$ by 100 mc/sec and solving for the new molecular parameters. The maximum changes in the constants were found to be $\Delta A = 0.07\times10^{-40}$ g cm$^2$, $\Delta C_1 = 0.003\times10^{-40}$ g cm$^2$, $\Delta C_2 = 0.02\times10^{-40}$ g cm$^2$, and $\Delta H = 0.3$ cm$^{-1}$.

[13] G. Herzberg, *Infrared and Raman Spectra of Polyatomic Spectra* (D. Van Nostrand Company, Inc., New York, 1945), p. 456.

TABLE III.

| $C^{12}H_3O^{16}H$ | $C^{13}H_3O^{16}H$ | $C^{12}H_3O^{18}H$ |
|---|---|---|
| $D=-0.107\times10^{-40}$ | $-0.126\times10^{-40}$ | $-0.250\times10^{-40}$ |
| $\mu_{\parallel}=-0.885\times10^{-18}$ | $-0.886\times10^{-18}$ | $-0.890\times10^{-18}$ |
| $\mu_{\perp}=1.44\times10^{-18}$ | $1.44\times10^{-18}$ | $1.44\times10^{-18}$ |

### 3. Interatomic Distances

The four inertial constants $A$, $C_1$, $C_2$, and $D$ of the normal molecule are insufficient to determine the six interatomic distances of the molecules which are shown in Fig. 3.

The additional data which would fix the values of the six distances could, of course, come from the spectra of isotopic molecules. At the present time the only lines which have been measured experimentally, and which are suitable because they involve only low $J$ values, are the class two series lines of the isotopic molecules, for which values of $\nu_2$ have been listed in Table I. The most convenient point of attack was found to be the utilization of the products of inertia $D$ and the components of the electric moment as determined by the Stark coefficient $A$ and $B$. The reason for this is that these coefficients depend insensitively upon small changes in the remaining moments of inertia, and, in any case, these small changes can be estimated quite reliably. The results of the analysis are shown in Table III where the figures obtained previously for normal methanol have been included. $D$ is in g cm$^2$, and the electric moments are in esu.

It is very satisfactory to find that the components of the electric moment for the three isotopic molecules agree within the limits of experimental error. In principle the two additional values of $D$ in conjunction with the $A$, $C_1$, $C_2$, and $D$ of the normal molecule should be sufficient to evaluate the six structural parameters. In fact, however, the constant $f$ cannot be determined with any accuracy but only its component perpendicular to the symmetry axis. For this reason it has seemed advisable to assume that $f$ has the same value that it has in methane, namely, 1.093A. Since the moment of inertia of methane is almost precisely equal to $C_2$, one could make the equivalent assumption that the HCH angle is equal to the methane angle of 109°28′. By using the $D$ of $C^{12}H_3O^{18}H$ together with the moments and products of inertia of normal methanol, the molecular dimensions may be calculated. These are listed in Table IV.

The product of inertia $D$ for the molecule $C^{13}H_3O^{16}H$ may now be calculated and is found to have the value $-0.124\times10^{-40}$ g cm$^2$, which should be compared with the observed figure of $-0.126\times10^{-40}$ g cm$^2$.

The following points in connection with the molecular dimensions should be noted: (1) The O atom is located 0.079A away from the symmetry axis on the opposite side from that of the H atom, which in turn is 0.807A from the symmetry axis. The center of gravity of the

TABLE IV.

| | |
|---|---|
| $a=0.079$A | $\overline{OH}=0.937$A |
| $b=0.807$A | $\overline{CO}=1.434$A |
| $c=0.306$A | $\sphericalangle HCH=109°30'$ |
| $d=1.432$A | $\sphericalangle COH=105°56'$ |
| $e=0.364$A | |
| $f=1.093$A (assumed) | |

OH group for the normal molecule lies between the O atom and the symmetry axis at a distance of 0.027A from the latter. Thus, neither the O atom nor the center of gravity of the OH group is situated precisely along the axis of symmetry, in agreement with the earlier results of Burkhard and Dennison. (2) Because of the general similarity between the COH portion of the $CH_3OH$ molecule and the $H_2O$ molecule, the OH distance and the COH angle of the former can be expected to be fairly close to the OH distance and the HOH angle of the latter, namely, 0.958A and 104°31′ respectively.[14] It is gratifying to find that this expectation is reasonably well fulfilled. (3) The CO distance as determined here is 1.434A, which is very close to the figure 1.44A found by electron diffraction methods. The actual value obtained, however, depends upon the dimensions assumed for the CH distance. In particular, a change of 0.01A from the adopted value of 1.093A for the CH distance will cause a change in the CO dimension of 0.008A. (4) The calculated value of 109°30′ for the HCH angle is very close to the figure of 109°28′ for the corresponding angle in methane. This agreement is, however, also dependent upon the exact value assumed for the CH distance.

The molecular dimensions which have been given are probably not accurate to the number of places listed, but rather represent a set which is consistent with the experimental data employed. The errors involved in the figures may arise from a number of causes such as: (a) experimental errors, which in many, but not all, instances are small because of the accuracy of the microwave measurements, and (b) the limitations of the present model in which, for example, the molecule is taken to be rigid, and a simple sinusoidal dependence is assumed for the hindering potential. The higher-order corrections introduced by these and other causes may influence some of the results, according to past experience, by one or two percent. An example of such effects is the discrepancy between the value of $-0.124\times10^{-40}$ g cm$^2$ for the $D$ of the $C^{13}H_3O^{16}H$ molecule based upon the calculated interatomic distances, and that of $-0.126\times10^{-40}$ g cm$^2$ obtained from the Stark data for this molecule. The difference of $0.002\times10^{-40}$ g cm$^2$ between the two figures is within the expected deviation.

An examination of the procedure used in determining the interatomic distances shows that most of the errors in the calculated values for the dimensions arise from the uncertainties in $D$ and in the assumed CH distance. If the possible variation in $D$ is taken to be $0.002\times10^{-40}$ g cm$^2$—a not unreasonable value as seen above—then the following changes result in the molecular dimensions:

$\Delta a=0.003$A, $\Delta b=0.003$A, $\Delta c=0.03$A, $\Delta d=0.002$A.

Likewise if the CH distance is altered by 0.01A from the assumed value of 1.093A, the changes are

$\Delta a=0.001$A, $\Delta b=0.001$A, $\Delta c=0.015$A, $\Delta d=0.008$A.

## CALCULATION OF ADDITIONAL LINES OF THE MICROWAVE SPECTRUM

The molecular constants of methanol which have been given make it possible to calculate the energy levels of the molecule and hence to determine the predicted spectrum, which may then be compared with the observed spectrum. Deviations between the predicted and observed lines are to be expected, and originate from (1) experimental errors, (2) inaccuracies in the molecular constants, and (3) to a great extent from the simplified model employed to represent the methyl alcohol molecule.

TABLE V.

| Molecule | $\nu_2$ (calc) | $\nu_2$ (obs) | $(\nu_2-\nu_2(N))$ calc | $(\nu_2-\nu_2(N))$ obs |
|---|---|---|---|---|
| $C^{13}H_3O^{16}H$ | 26 940 | 27 066 | 1992 | 2118 |
| $C^{12}H_3O^{18}H$ | 34 492 | 33 919 | 9544 | 8971 |

The hindered rotation energy levels $E_{K\tau n}$ as well as the Fourier coefficients used in the expansion of the wave functions are given in the Appendices for those states which occurred most frequently in the calculations. Additional levels and coefficients may, of course, be obtained through the use of the continued fractions described in reference 1. The process of diagonalizing the Hamiltonian was accomplished by the usual perturbation methods, which are here especially applicable since the off-diagonal elements are generally much smaller than the difference in the corresponding diagonal elements. These calculations are all straightforward but often very lengthy, and for that reason computations have been made only for those spectral lines which have been identified in the microwave spectrum. It will prove convenient to use the three classifications of lines already employed in discussing the experimental spectrum. Since, however, only one line of class 1 ($J\rightarrow J+1$, $K\rightarrow K$, $\tau\rightarrow\tau$, $n\rightarrow n$) has been observed, and this has been used earlier in determining the molecular constants, the first lines to be considered will be the series lines of class 2 ($J\rightarrow J$, $K=1\rightarrow2$, $\tau=2\rightarrow1$, $n=0\rightarrow0$).

### 1. The Class 2 Lines

The experimental data regarding these lines have been listed in Table I. Until now the only figures from

[14] B. T. Darling and D. M. Dennison, Phys. Rev. 57, 128 (1940).

this class that have been used in the calculations have been those for the origin of the series $\nu_2$ for normal methanol, and the Stark coefficients $A$ and $B$ for all three isotopic molecules. With the aid of the interatomic distances the moments and products of inertia of the isotopic molecules can be obtained, and these, together with the barrier height, which is independent of the isotopic masses, serve to fix the energy levels associated with the transition. In Table V the calculated and observed values of $\nu_2$ are listed as well as the shift in $\nu_2$ in going from the normal to the isotopic molecule. All frequencies are in mc/sec.

The agreement is quite satisfactory especially when one recalls that these frequencies are the result of the difference of two frequencies, one because of the normal rotation and the other because of the hindered rotation, each of which is approximately ten times larger than their difference. It was found that no reasonable change in the molecular dimensions would improve the agreement, and it was concluded that the discrepancies must arise from an oversimplification of the model, such as, for example, the assumption that the methyl and hydroxyl groups are rigid.

TABLE VI.

| Molecule | $b$ calc | $b$ obs |
|---|---|---|
| $C^{12}H_3O^{16}H$ | 0.1025 | 0.1111 |
| $C^{13}H_3O^{16}H$ | 0.0913 | 0.0901 |
| $C^{12}H_3O^{18}H$ | 0.0842 | 0.0855 |

The quantities $a$ and $b$ appearing in Table I describe the positions of the lines in the series and are the coefficients of the $J^2+J$ and $(J^2+J)^2$ terms, respectively. Each of these can be calculated since they are due principally to the off-diagonal elements $K\rightarrow K\pm1$ and $K\rightarrow K\pm2$ of the Hamiltonian. As explained by Burkhard and Dennison, the coefficient $a$, however, is not suitable as a check, since it is contaminated by terms arising from the centrifugal stretching, an effect not taken into account in the simple model. The results of comparing the calculated and observed values of $b$ are shown in Table VI and are given in mc/sec.

The agreement is moderately satisfactory since it is expected that higher-order effects could give contributions amounting to several percent. It is, however, somewhat puzzling that the discrepancy should be the largest for normal methanol.

### 2. The Class 3 Lines

The third classification of lines are those due to simultaneous changes in $J$ and $K$, and the only examples positively identified in the microwave spectrum of normal methyl alcohol are listed in Table II. Of the six frequencies appearing in the table, two, $\nu_b$ and $\nu_c$, have already been used to determine the molecular constants. The values of the remaining frequencies may be calculated and appear in Table VII in mc/sec.

TABLE VII.

| Designation | $\nu$ calc | $\nu$ obs | $B$ calc | $B$ obs |
|---|---|---|---|---|
| $\nu_a$ | 19 978 | 19 967 | 22 | — |
| $\nu_b$ | 28 316 | 28 316 | 11.7 | 11 |
| $\nu_c$ | 36 196 | 36 169 | 6.6 | 6.52 |
| $\nu_d$ | 37 799 | 37 704 | 2.9 | 3.09 |
| $\nu_e'$ | 38 605 | 38 294 | 13.4 | 13.0 |
| $\nu_e''$ | 38 749 | 38 453 | 13.4 | 13.0 |

The discrepancies between the observed and calculated frequencies are of the same order of magnitude as those appearing previously and are no doubt the result of the same type of higher-order effects. It is very satisfactory to find that the calculated difference between $\nu_e'$ and $\nu_e''$, namely, 144 mc/sec, is so close to the observed difference of 159 mc/sec, since this doublet is an example of $K$-type splitting, and to the first order should be independent of the higher-order terms.

All six lines should show a Stark dependence which is predominantly linear and of the form $\Delta\nu=BM\mathcal{E}$, where $M$ is the magnetic quantum number and $\mathcal{E}$ the field strength. Experimentally† the lines do show the predicted dependence, and the calculated and observed constants $B$ in mc/sec-esu are given in the last two columns of the table. It should be remarked that $\nu_e'$ and $\nu_e''$, being members of a $K$-type doublet, possess a quadratic Stark effect for sufficiently low fields which, however, becomes linear when $\alpha=KM\mathcal{E}\mu_{II}/(J^2+J)$ becomes larger than the $K$-type splitting $\Delta_{JK}$. For the upper level involved in the transition, $J=6$, $K=2$, calculations show that $\Delta_{JK}/h=144$ mc/sec, whereas $\alpha/h=6.4\,M\mathcal{E}$ mc/sec, and the Stark effect will therefore be quadratic for reasonable values of the field strength. For the lower level, on the other hand, for which $J=5$ and $K=3$, one obtains $\Delta_{JK}/h=0.43$ and $\alpha/h=13.4\,M\mathcal{E}$ and, consequently, here the Stark effect will be linear and will dominate the smaller quadratic effects.

### 3. The Second-Order Stark Effect

The second-order or quadratic Stark effect has been measured by Hughes, Good, and Coles for a number of lines in the microwave spectrum of methyl alcohol. These lines may be grouped into two classes: those for which the Stark effect is predominantly linear with a relatively slight quadratic admixture and those for which the effect is purely quadratic. An example of the former category is given by members of the $\nu_2$ series, and, indeed, by any first-order lines, while the latter is represented by lines of the $\nu_1$ type as well as by a number of other lines found in the microwave spectrum by Hughes, Good, and Coles. We shall consider each category separately.

† Hughes, Good, and Coles originally gave 3.4 mc/sec-esu as the value of $B$ for the line $\nu_b$. This figure has been subsequently redetermined by them (private communication) and found to be 11 mc/sec-esu.

TABLE VIII.

| $J$ | $M$ | $C$ calc | $C$ obs | $J$ | $D$ calc | $D$ obs |
|---|---|---|---|---|---|---|
| 2 | 2 | 0.31 | 0.37 | 7 | 0.024 | 0.024 |
| 2 | −2 | | | | | |
| 3 | −3 | 0.52 | 0.38 | 9 | 0.0155 | 0.0165 |

Besides possessing a linear Stark effect, the members of the $\nu_2$ series have also a quadratic dependence which may be represented by the equation

$$\Delta\nu=(C+DM^2)\mathcal{E}^2.$$

The coefficient of $\mathcal{E}^2$ for some of the components of lines of the normal molecule has been determined by Hughes, Good, and Coles, and the $M^2$ dependence for a fixed voltage has been also studied for the $J=7$ and $J=9$ lines. The values for the coefficient of $\mathcal{E}^2$ and for the coefficients of $M^2$ are believed to be accurate to within 15 percent and 10 percent, respectively, and are given in Table VIII together with the calculated values in units of mc/sec-esu$^2$. The latter have been obtained using expressions determined by the usual methods of perturbation theory. The agreement, except for the $J=3$, $M=-3$ line, is within experimental error and is quite gratifying, since the second-order effect is superimposed on a strong first-order effect.

The Stark effect of $\nu_1$, corresponding to $J=0\rightarrow1$, $K=0\rightarrow0$, $\tau=1\rightarrow1$, $2\rightarrow2$ or $3\rightarrow3$, and $n=0\rightarrow0$, has not as yet been measured experimentally, but is theoretically predicted to be pure second order, the line being shifted in position, but not split. As described earlier, $\nu_1$ should actually be a close doublet consisting of the $\tau=1$ line, and to the coincident lines $\tau=2$ and 3. The magnitude of the doublet separation is in some doubt; the provisional work of Edwards, Gilliam, and Gordy[9] showed a doublet separation of about 4 mc/sec, whereas the estimate by Burkhard and Dennison, based upon their theory, indicated a separation of only a fraction of a megacycle per second. In the following calculation, it will be assumed that the doublet separation is larger than the Stark energy. If this is not the case, a mixing of the levels would occur, complicating the equations.

The Stark energy $\Delta E_{JK\tau n}$ arises from the off-diagonal elements of the Hamiltonian $H_{J-1\,K\tau n}{}^{JK\tau n}$ and $H_{J-1\,K\pm1\,\tau'n'}{}^{JK\tau n}$, straightforward methods yielding the results

$$\Delta E_{00\tau n}=\mu_{11}{}^2\mathcal{E}^2/3(H_{00\tau n}{}^{00\tau n}-H_{10\tau n}{}^{10\tau n})+(\mu_\perp{}^2\mathcal{E}^2/6)\sum_{\tau'n'}[(-M_{0\tau n}{}^{1\tau'n'})^2/(H_{00\tau n}{}^{00\tau n}-H_{11\tau'n'}{}^{11\tau'n'})$$
$$+(+M_{0\tau n}{}^{-1\tau'n'})^2/(H_{00\tau n}{}^{00\tau n}-H_{1-1\,\tau'n'}{}^{1-1\,\tau'n'})],$$

$$\Delta E_{10\tau n}=\mu_{11}{}^2\mathcal{E}^2/3(H_{10\tau n}{}^{10\tau n}-H_{00\tau n}{}^{00\tau n})+4\mu_{11}{}^2\mathcal{E}^2/15(H_{10\tau n}{}^{10\tau n}-H_{20\tau n}{}^{20\tau n})$$
$$+(\mu_\perp{}^2\mathcal{E}^2/10)\sum_{\tau'n'}[(-M_{0\tau n}{}^{1\tau'n'})^2/(H_{10\tau n}{}^{10\tau n}-H_{21\tau'n'}{}^{21\tau'n'})+(+M_{0\tau n}{}^{-1\tau'n'})^2/(H_{10\tau n}{}^{10\tau n}-H_{2-1\,\tau'n'}{}^{2-1\,\tau'n'})],$$

where

$$\pm M_{K\tau n}{}^{K\mp1\,\tau'n'}=\int_0^{2\pi}P_{K\tau n}{}^*\exp(\pm ix)P_{K\pm1\,\tau'n'}dx.$$

The Stark change in the frequency is then given by

$$h\Delta\nu=\Delta E_{10\tau n}-\Delta E_{00\tau n}.$$

Substituting in the above formula and evaluating the matrix $\pm M$, the following expressions are obtained for the frequency shifts of the lines corresponding to $J=0\rightarrow1$, $K=0\rightarrow0$, $n=0\rightarrow0$, and $\tau=1\rightarrow1$, and $\tau=2\rightarrow2$ or $3\rightarrow3$, respectively:

$$\Delta\nu=0.22\,\mathcal{E}^2\text{ mc/sec}$$
$$\Delta\nu=0.20\,\mathcal{E}^2\text{ mc/sec}.$$

Among the many irregular spaced lines of methanol found by Hughes, Good, and Coles, there are a number which show a pure second-order Stark effect. These must be members of a $K$-type doublet for which the $K$-type splitting in both the initial and final states is large compared with the Stark energy. Most of the observed lines correspond to such high $J$ and $K$ values that the large size of the higher-order terms makes a unique identification impossible at present. An exception appears to be the line at 28 970 mc/sec which fits well with the identification $J=9\rightarrow8$, $K=1\rightarrow2$, $\tau=3\rightarrow2$, $n=0\rightarrow0$. The calculated position of this line is at 29 030 mc/sec. The Stark effect should be of second order, and a somewhat lengthy calculation gives

$$\Delta\nu=(-0.033M^2+0.09)\,\mathcal{E}^2\text{ mc/sec},$$

while the experimental result is

$$\Delta\nu=(-0.034M^2+0.16)\,\mathcal{E}^2\text{ mc/sec}.$$

Evidently the agreement is excellent for the coefficient of $M^2\mathcal{E}^2$, but less good for the $\mathcal{E}^2$ coefficient. It is possible that other effects may be contributing to the quadratic Stark effect. For example, the polarization

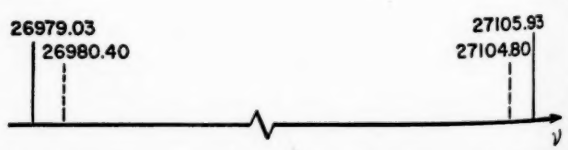


FIG. 4. Observed "mirror image pattern" of $C^{12}H_3O^{16}H$. The solid and dotted lines represent allowed and forbidden transitions, respectively.

of the molecule does produce a second-order effect, but its value for the case of the water molecule has been estimated[15] and found to be very small, of the order of $\Delta\nu = 10^{-4}\mathcal{E}^2$ mc/sec, and there seems to be no reason to believe that it would be essentially larger in methanol.

### 4. The "Mirror" Lines

Hughes, Good, and Coles have measured a set of four lines in the $C^{12}H_3O^{16}H$ microwave spectrum which they term a "mirror image pattern" because two of the lines bear a mirror-like resemblance to the other two. The observed pattern is illustrated in Fig. 4, where the observed frequencies are given in mc/sec.

The lines at 26 980.40 mc/sec and 27 104.80 mc/sec are forbidden in the absence of a field, that is, they appear only when a Stark voltage is applied, and become stronger as the voltage is increased. The allowed lines at 26 979.03 mc/sec and 27 105.93 mc/sec, which exhibit a second-order Stark effect at low field strengths, merge with the forbidden lines at a field of several volts/cm, the mixture yielding a first-order Stark effect at slightly higher voltages corresponding to a value of about 3.5 mc/sec-esu for the coefficient of $M\mathcal{E}$. The linear Stark patterns are slightly asymmetrical with frequency displacements on the low-frequency side being ten percent greater than those on the high-frequency side. From the Stark patterns it may be concluded that $\Delta J = \pm 1$ and that the $J$ of the lowest state is at least 12.

As Hughes, Good, and Coles point out, such a "mirror image" set of lines may be interpreted as being due to a transition between two $K$-type doublets. The transition in question appears to be one in which $J = 13 \rightarrow 12$, $K = 3 \rightarrow 4$, $\tau = 1 \rightarrow 3$, $n = 0 \rightarrow 0$. From the moments of inertia for the $C^{13}H_3O^{16}H$ molecule as obtained from the interatomic distances, the zeroth-order frequency due to the diagonal elements of the Hamiltonian may be calculated, and is found to be 27 300 mc/sec, in good agreement with the observed value of 27 140 mc/sec for the center of the pattern. Using the formulas developed for the $K$-type splitting, one obtains

$$\Delta_{13,3} = 122 \text{ mc/sec} \quad \Delta_{12,4} = 1.0 \text{ mc/sec}.$$

The energy-level diagram for the transitions involved is shown in Fig. 5, where the above calculated values are also indicated.

The + and − signs refer to the symmetry types of the levels. In the absence of a field only $+ \rightarrow +$, $- \rightarrow -$ transitions are allowed. When a field is applied, however, the other transitions $+ \rightarrow -$, $- \rightarrow +$ become possible, the probability increasing with the strength of the field. On the basis of this scheme, a separation between the allowed lines of 123 mc/sec and a forbidden-allowed splitting of 1.0 mc/sec are predicted. These values may be compared with the observed ones of 127 mc/sec and about 1.2 mc/sec, respectively.

[15] S. Golden and E. B. Wilson, Jr., J. Chem. Phys. **16**, 669 (1948).

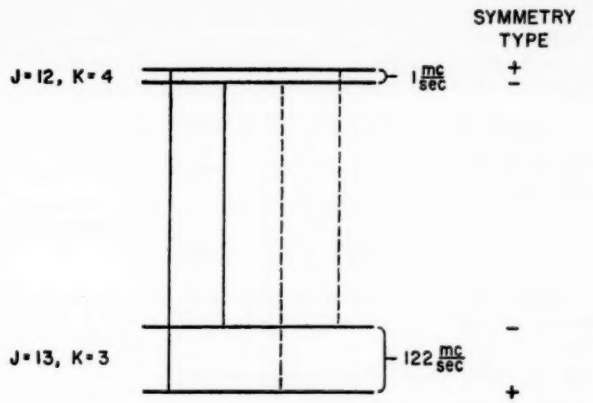


FIG. 5. Energy-level diagram for the "mirror image pattern" of Fig. 4. The allowed and forbidden transitions are indicated by solid and dotted lines, respectively.

According to previous results, a quadratic Stark effect for $K$-type doublets should be observed for sufficiently weak electric fields. As the field strength is increased to the point where the Stark splitting is larger than the $K$-type splitting, the Stark effect becomes predominantly linear. For the above particular case of "mirror" lines it is clear that the linear Stark effect will occur first for the $K = 4$ levels, since their splitting is very much less than that of the $K = 3$ levels. The linear Stark coefficient for the $K = 4$ state may be shown from the previous results to be $4\mu_{II}/(J^2+J)$, from which expression a calculated value of 3.4 mc/sec-esu for the coefficient is obtained, which may be compared with the observed value of 3.5 mc/sec-esu. The fact that the Stark pattern is slightly asymmetrical can be ascribed to the presence of energy terms in the $K$-type doubling expressions other than those linear in $\mathcal{E}$.

## APPENDIX

### 1. Energy Levels

As discussed in reference 2, the diagonal elements of the Hamiltonian in the absence of an external field consist of the sum of three terms. One of these is proportional to $D^2$ and for methanol is very small, in many calculations being negligible. Of the other terms, one represents the rotational energy of a symmetrical rotator and for methanol may be expressed in wave numbers by the formula

$$0.8066(J^2+J-K^2)+4.2544K^2.$$

The remaining term is the internal rotation energy $E_{K\tau n}$. The figures in Tables IX–XII were utilized in the present paper, and are based on the constants, $C_1/C = 0.189275$, $C_2 = 5.33265 \times 10^{-40}$ g cm$^2$, and $H = 374.821$ cm$^{-1}$. The energies are given for $n = 0$ and are expressed in wave numbers.

TABLE IX. $E_{K\tau 0}$.

| $K$ | $\tau=1$ | $\tau=2$ | $\tau=3$ |
|---|---|---|---|
| 0 | 128.8254 | 137.9489 | 137.9489 |
| 1 | 129.2529 | 140.0068 | 135.4901 |
| 2 | 130.4922 | 141.2561 | 133.0484 |
| 3 | 132.4105 | 141.4193 | 130.9748 |
| 4 | 134.7797 | 140.4585 | 129.5256 |

The internal rotational energy is a periodic function of $\gamma=2\pi C_1K/3C$ and hence, may be expanded as a Fourier series in $\gamma$. For the above molecular constants, $\gamma$ has the value of 22.71,30°K. The levels for $\tau=1$ and $n=0$ are well represented (in $cm^{-1}$) by

$$E_{K10}=134.922-6.320\cos\gamma+0.239\cos2\gamma-0.014\cos3\gamma.$$

The levels for $\tau=2$ and $\tau=3$ may be found by increasing $\gamma$ by 120° and 240°, respectively.

## 2. Wave Functions

The internal rotation wave functions of the symmetrical rotator are denoted by

$$P_{K\tau n}{}^{(x)}=2\pi^{-\frac{1}{2}}\sum_{m=-\infty}^{\infty}a_m\exp(imx),$$

where the normalization factor $2\pi^{-\frac{1}{2}}$ has been included so that

$$\int_0^{2\pi}P_{K\tau n}{}^{*(x)}P_{K\tau n}{}^{(x)}dx=\sum_{m=-\infty}^{\infty}a_m{}^2=1.$$

TABLE X. ($\tau=1$).

| | $K=0$ | 1 | 2 | 3 |
|---|---|---|---|---|
| $a_{-12}$ | 0.000024 | 0.000019 | 0.000015 | 0.000012 |
| $a_{-9}$ | 0.001035 | 0.000843 | 0.000690 | 0.000566 |
| $a_{-6}$ | 0.025430 | 0.021577 | 0.018369 | 0.015651 |
| $a_{-3}$ | 0.285724 | 0.257096 | 0.231585 | 0.208369 |
| $a_0$ | 0.914017 | 0.911676 | 0.904393 | 0.891392 |
| $a_3$ | 0.285724 | 0.318393 | 0.356104 | 0.399863 |
| $a_6$ | 0.025430 | 0.030129 | 0.035925 | 0.043130 |
| $a_9$ | 0.001035 | 0.001278 | 0.001591 | 0.001997 |
| $a_{12}$ | 0.000024 | 0.000030 | 0.000039 | 0.000051 |

TABLE XI. ($\tau=2$).

| | $K=0$ | 1 | 2 | 4 |
|---|---|---|---|---|
| $a_{-13}$ | 0.000007 | 0.000006 | 0.000005 | 0.000003 |
| $a_{-10}$ | 0.000356 | 0.000285 | 0.000225 | 0.000134 |
| $a_{-7}$ | 0.010692 | 0.008899 | 0.007292 | 0.004669 |
| $a_{-4}$ | 0.160297 | 0.140304 | 0.120826 | 0.085326 |
| $a_{-1}$ | 0.832730 | 0.790585 | 0.737563 | 0.609367 |
| $a_2$ | 0.525624 | 0.590463 | 0.657155 | 0.776626 |
| $a_5$ | 0.066764 | 0.080896 | 0.097287 | 0.134722 |
| $a_8$ | 0.003435 | 0.004366 | 0.005512 | 0.008426 |
| $a_{11}$ | 0.000095 | 0.000124 | 0.000163 | 0.000267 |

TABLE XII. ($\tau=3$).

| | $K=0$ | 1 | 3 |
|---|---|---|---|
| $a_{-11}$ | 0.000095 | 0.000072 | 0.000042 |
| $a_{-8}$ | 0.003435 | 0.002701 | 0.001696 |
| $a_{-5}$ | 0.066764 | 0.055017 | 0.037808 |
| $a_{-2}$ | 0.525624 | 0.466110 | 0.367846 |
| $a_1$ | 0.832730 | 0.864211 | 0.901337 |
| $a_4$ | 0.160297 | 0.180788 | 0.224808 |
| $a_7$ | 0.010692 | 0.012693 | 0.017555 |
| $a_{10}$ | 0.000356 | 0.000438 | 0.000652 |
| $a_{13}$ | 0.000007 | 0.000009 | 0.000014 |

The Fourier coefficients $a_m$ have been calculated for those $n=0$ levels which are of principal importance in the present paper, and appear in Tables X, XI, and XII for $\tau=1$, 2 and 3, respectively. From a knowledge of the structure of the wave functions (see reference 1), it is then possible through interpolation methods to obtain the coefficients for any $K$ or $\tau$ to a fair order of accuracy.

# Note on Some Regularities of the Absorption Band Maxima of Colored Alkali Metal Halides

A. GLASNER* AND F. C. TOMPKINS
*Department of Inorganic and Physical Chemistry, Imperial College of Science and Technology, London, S.W. 7, England*
(Received April 1, 1953)

The various relationships which exist between the absorption band maxima of colored alkali metal halides have been noted, and some simple empirical rules have been proposed for calculating certain crystal parameters from the position of these maxima.

ATTENTION is directed to some regularities of the absorption band maxima† of colored alkali metal halides and the relationships which exist between these and certain parameters of the crystal. These considerations have lead us to propose some simple rules for calculating certain of these parameters, although we have found no satisfying theoretical justification of the equations proposed.

*1. The first fundamental band $f_1$ [1,2] of the lattice and the F [3,4] band.* Table I gives the band maxima of these two bands and the difference, designated $f_1-F$, in electron volts. The latter, except for NaCl and NaBr, is constant for a series of halide ions and independent of the alkali metal. For theoretical considerations, data at as near 0°K as possible would be more valuable, but those given in Table I refer to room temperature at which a greater range of data are available. The shift in band maxima between −253°C and 20°C, where measured, is *ca* 0.1 ev, for the $F$ band[3] and 0.25 ev for the $f_1$ band[5] and is about the same for different salts—the agreement of different investigators for the same salt at the same temperature is also *ca* 0.1 v. The constant difference $(f_1-F)$ suggests that the electron transitions from the full band and from the $F$ center are to the same higher energy level and that the energy of transition is independent of the nature of the monovalent cation.

*2. The α and β bands.* The few data available are due to Pringsheim *et al.*,[6] who first recorded them in the long-wave tail of the first fundamental band, and to Martienssen[7] (see Table I). Now anion and cation vacancies are most probably present predominantly as pairs,[8] and in $F$-center production, by irradiation or additive coloration, the pairs dissociate giving isolated cation vacancies and $F$ centers. Similarly, during bleaching of $F$ centers anion vacancies are produced, and these are expected to associate with cation vacancies. The simultaneous production of the $\beta$ and $F$ band found experimentally and the fact that $f_1-\beta$ is roughly constant suggest therefore, that the $\beta$ band has its origin in the presence of isolated cation vacancies which cause a shift in the fundamental band maximum. On the other hand, the $\alpha$ band, which at low temperatures precedes the appearance of the $\beta$ band and is formed from it during bleaching, is evidently due to the presence of an intermediate complex formed under conditions where the mobility of the cation vacancy is restricted and where, therefore, the separation of the vacancy pair is incomplete.

*3. V centers* [9–12] ($V_1$, $V_2$, $V_3$). Table II shows that the difference $(V_3-V_1)$ is constant, independent of the cation and anion, but that $V_3-V_2$ varies with the anion. The regularities are consistent with the view that $V_1$ centers (stable only at low temperatures) arise from isolated positive holes; $V_3$ centers, from positive holes trapped at a cation vacancy; and $V_2$, as a pair of positive holes associated with a cation vacancy.[13,14] In the latter case, we note that "resonance" between the neighboring

TABLE I. Relationship between the first fundamental ($f_1$) and the $F$-band maxima, in electron volts.[a]

| Alkali metal halide | $f_1$ | $F$ | $f_1-F$ | $\beta$ | $\alpha$ | $f_1-\beta$ |
|---|---|---|---|---|---|---|
| NaF | 10.55 | 3.63 | 6.92 | | | |
| KF | 9.80 | 2.73 | 7.07 | | | |
| LiCl | 8.63 | 3.20 | 5.43 | | | |
| NaCl | 7.81 | 2.64 | 5.17 | | | |
| KCl | 7.62 | 2.19 | 5.43 | | | |
| RbCl | 7.43 | 2.00 | 5.43 | | | |
| CsCl | 7.62 | 2.03 | 5.59 | | | |
| NaBr | 6.56 | 2.29 | 4.27 | | | |
| KBr | 6.60 | 1.98 | 4.62 | 6.42 | 6.14 | 0.18 |
| RbBr | 6.46 | 1.85 | 4.61 | 6.27 | | 0.19 |
| KI | 5.63 | 1.80 | 3.83 | 5.46 | 5.18 | 0.17 |
| RbI | 5.55 | 1.60 | 3.95 | 5.33 | ··· | 0.22 |

[a] $f_1$—band maxima at room temperature; $\alpha$ and $\beta$ bands measured at liquid air temperature, since $\alpha$ bands are unstable at room temperatures.

*On leave from The Hebrew University, Jerusalem, Israel.

[1] R. Hilsch and R. W. Pohl, Z. Physik **57**, 145 (1929); **59**, 812 (1930).
[2] E. E. Schneider and H. M. O'Bryan, Phys. Rev. **51**, 293 (1937).
[3] Erich Mollwo, Z. Physik **85**, 56 (1933).
[4] R. W. Pohl, Proc. Phys. Soc. (London) **49**, 3 (1937).
[5] H. Fesefeldt, Z. Physik **64**, 623 (1930).
[6] Delberg, Pringsheim, and Yuster, J. Chem. Phys. **19**, 574 (1951); **20**, 746 (1952).
[7] W. Martienssen, Z. Physik **131**, 488 (1952).
[8] F. Seitz, Revs. Modern Phys. **18**, 396 (1946).
[9] E. Mollwo, Ann. Physik [5], **29**, 394 (1937).
[10] Casler, Pringsheim, and Yuster, J. Chem. Phys. **18**, 1564 (1950).
[11] H. Dorendorf, Z. Physik **129**, 317 (1951).
[12] W. H. Duerig and J. J. Markham, Phys. Rev. **88**, 1043 (1952).
[13] J. Alexander and E. E. Schneider, Nature **164**, 653 (1949).
[14] F. Seitz, Phys. Rev. **79**, 529 (1950).

TABLE II. Relationships between the various $V$ bands.[a]

| Alkali metal halide | $V_3$ | $V_2$ | $V_1$ | $V_3-V_1$ | $V_3-V_2$ |
|---|---|---|---|---|---|
| NaCl | 5.88 | 5.54 | 3.58 | 2.30 | 0.34 |
| KCl | 5.73 | 5.32 | 3.43 | 2.30 | 0.41 |
| KBr | 5.32 | 4.66 | 3.01 | 2.31 | 0.66 |
| KI | 4.41 | 3.53 | ··· | ··· | 0.88 |

[a] Values for the $V$-band maxima were taken from references 9 and 10, those for $V_1$ centers were obtained at liquid nitrogen temperature since these latter are unstable. $V_2$ and $V_3$ were measured at room temperatures.

positive holes will depend in magnitude on the nature of the positive holes (i.e., of the anions) and that this suggested "structure" is consistent with the experimental fact that the concentration of $V_2$ centers, mainly formed by additive coloration with the halogen gas, is proportional to the gas pressure.[9]

*4. Work of removal of anion to infinity, $W^-$.*[15,16] $W^-$ may be calculated empirically from

$$W^-=F+E-\tfrac{1}{2}H, \tag{1}$$

where $F$ = the energy corresponding to the absorption maxima of the $F$ band; $E$ and $H$ refer to the electron affinity of the halogen atom and the bond dissociation energy of the halogen molecule, respectively. Table III gives our calculated values compared with those obtained by Mott and Littleton by a rigorous calculation. The agreement is good.

*5. Work of removal of cation to infinity, $W^+$.* $W^+$ may be calculated from the equation

$$W^+=(U-F)+\tfrac{1}{2}W_0, \tag{2}$$

where $U$ is the energy maximum of the $U$ band,[7] and $\frac{1}{2}W_0$ is the (average) energy necessary to create a vacant lattice site. This latter has been calculated by Mott and Littleton[15] for three halides from

$$\tfrac{1}{2}W_0=W^-+W^+-U_0, \tag{3}$$

where $U_0$ is the lattice energy.

The values of $W^-$ calculated by Mott and Gurney[17] are NaCl, 0.95; KCl, 0.95; and KBr, 0.94 ev. We have found, however, that $W^-$ is approximated very closely by $E_v$, the energy of combination of a pair of vacances in uni-univalent salts having ions of roughly the same size. Using Seitz's formula

$$E_v=e^2/\mu r, \tag{4}$$

where $e$ is the electronic charge, $\mu$ is the static dielectric constant, and $r$ is the shortest distance between two ions of opposite charge in the lattice, we obtain the following values: NaCl, 0.92; KCl, 0.97; and KBr, 0.91, in good agreements with their $W^-$ values. Table III gives values of $W^+$ calculated from our formula

$$W^+=(U-F)+e^2/\mu r \tag{5}$$

and the only three values calculated by Mott and Littleton.

TABLE III. $W^+$ calculated by three different methods and $W^-$ calculated by two different methods.

| Alkali metal halide | $U-F+e^2/\mu r$ | $f_1-y$ | $W^-=F+E-\frac{1}{2}H$[a] |
|---|---|---|---|
| LiCl | ··· | 5.46 | 5.73 |
| NaCl | 4.65 | 4.64 (4.62)[b] | 5.17 (5.18)[b] |
| KCl | 4.52 | 4.45 (4.47) | 4.72 (4.79) |
| RbCl | 4.27 | 4.26 | 4.53 |
| CsCl | ··· | 4.45 | 4.56 |
| NaBr | 4.36 | 4.29 | 4.81 |
| KBr | 4.34 | 4.33 (4.23) | 4.50 (4.60) |
| RbBr | 4.19 | 4.19 | 4.37 |
| KI | 4.12 | [4.12] | 4.19 |
| RbI | ··· | 4.04 | 3.99 |

[a] $E$ (Cl, Br, I) = 3.78, 3.52, 3.17; $\frac{1}{2}H$ (Cl, Br, I) = 1.25, 1.00, 0.78 ev.
[b] Figures in parentheses indicate Mott and Littleton's values.

The third column gives $W^+$ calculated from $f_1-y$, where $f_1$ refers to the energy of the absorption maximum of the first fundamental band, and $y$ is an empirical constant independent of the cation but dependent on the nature of the anion; the values in ev used for $y$ to give the best agreement for the series of salts with the same anion were $Cl^-$ (3.17), $Br^-$ (2.27), and $I^-$ (1.51).

We believe that theoretical considerations of the nature of the processes accompanying light absorption by colored crystals and of the "structure" of the various centers must be consistent with the regularities noted above.

[15] N. F. Mott and M. J. Littleton, Trans. Faraday Soc. **34**, 485 (1938).
[16] N. F. Mott and R. W. Gurney, *Electronic Processes in Ionic Crystals* (Clarendon Press, Oxford, 1948), second edition.
[17] R. W. Gurney and N. F. Mott, Trans. Faraday Soc. **34**, 506 (1938).

# Investigations on Silver Sulfide

CARL WAGNER
*Department of Metallurgy, Massachusetts Institute of Technology, Cambridge, Massachusetts*
(Received March 31, 1953)

The variability of the Ag/S ratio in silver sulfide has been studied with the help of electrochemical measurements. Silver sulfide coexisting with metallic silver at 200°C contains a silver excess of $2.0\times10^{-3}$ *g*-atom Ag/mole $Ag_2S$, whereas silver sulfide coexisting with liquid sulfur has very nearly ideal stoichiometric composition. The variability of the Ag/S ratio in $\beta$ $Ag_2S$ at 160°C is of the order of $3\times10^{-5}$ *g*-atom Ag/mole $Ag_2S$.

The interdiffusion coefficient of silver in $Ag_2S$ at 220°C is about $3\times10^3$ times greater than the self-diffusion coefficient of silver in $Ag_2S$.

A thermodynamic calculation gives the result that the transformation temperature of $Ag_2S$ coexisting with metallic silver is about 1.7°C lower than the transformation temperature of $Ag_2S$ coexisting with liquid sulfur in accordance with observations made by Kracek.

## INTRODUCTION

A VARIABILITY of the Ag/S ratio in silver sulfide was first indicated by the dependence of the electrical conductivity on the sulfur partial pressure of the ambient gas found by Tubandt and Reinhold.[1] At 200°C the electrical conductivity of $Ag_2S$ decreases from about 900 to 45 $ohm^{-1}$ $cm^{-1}$ on increasing the sulfur partial pressure up to saturation. Further measurements have been made by Reinhold and Möhring[2] and Reinhold and Schmitt.[3] More recently, Hebb[4] deduced the electronic component of the conductivity of $\beta$ $Ag_2S$ at 27°C as a function of the chemical potential of silver from measurements on polarized samples.

The change in the Ag/S ratio in $Ag_2S$ has been determined by Reinhold and Schmitt[2] at sulfur partial pressures above 0.1 mm Hg. Since these measurements cover only a small range of the sulfur partial pressure, further experiments have been made in order to determine the variation of the Ag/S ratio as a function of the chemical potential of silver with the aid of an electrochemical method described below. The temperature range from 160 to 300°C was chosen in order to obtain results for both $\alpha$ $Ag_2S$ (stable above 178°C) and $\beta$ $Ag_2S$ (stable below 176°C).

## EXPERIMENTAL

### General Principles

In the galvanic cell

$$\mathrm{Ag}\,|\,\mathrm{AgI}\,|\,\mathrm{Ag_2S}\,|\,\mathrm{Pt},$$

silver iodide is essentially an ionic conductor.[5] The chemical potential of silver in the $Ag_2S$ phase, $\mu_{Ag}$, is therefore related to the electromotive force $E$ of the cell by[6]

$$\mu_{Ag}-\mu_{Ag}{}^0=-E\mathfrak{F}, \tag{1}$$

where $\mu_{Ag}{}^0$ is the chemical potential of silver in its pure state and $\mathfrak{F}$ is the Faraday constant.

From the equation

$$2\mathrm{Ag}+\mathrm{S}=\mathrm{Ag_2S}, \tag{2}$$

it follows that

$$2\mu_{Ag}+\mu_S=\mu_{Ag_2S}. \tag{3}$$

Since the variation of the Ag/S ratio is very small, the chemical potential of silver sulfide, $\mu_{Ag_2S}$, is practically constant and equal to the value $\mu_{Ag_2S}{}^0$ for the standard state. The value of $\mu_{Ag_2S}{}^0$ is determined by the chemical potentials of the pure components and the standard free energy of formation of $Ag_2S$, $\Delta F^0(2\mathrm{Ag}+\mathrm{S}=\mathrm{Ag_2S})$, which according to Reinhold[7] may be obtained from the electromotive force $E^0$ of the cell $\mathrm{Ag}\,|\,\mathrm{AgI}\,|\,\mathrm{Ag_2S}\,|\,\mathrm{Pt}+\mathrm{S(l)}$. Thus

$$\Delta F^0(2\mathrm{Ag}+\mathrm{S}=\mathrm{Ag_2S})=\mu_{Ag_2S}{}^0-2\mu_{Ag}{}^0-\mu_S{}^0=-2E^0\mathfrak{F}. \tag{4}$$

Upon combining Eqs. (1), (3), and (4), it follows that

$$\mu_S-\mu_S{}^0=-2(E^0-E)\mathfrak{F}. \tag{5}$$

Thus the electromotive force $E$ of the cell

$$\mathrm{Ag}\,|\,\mathrm{AgI}\,|\,\mathrm{Ag_2S}\,|\,\mathrm{Pt}$$

gives the chemical potentials of both components in $Ag_2S$.

To define the initial stage of the $Ag_2S$ sample, an initial potential of 0.05 volt may be forced on the foregoing cell.

A well-defined amount of silver may be added to, or removed from, the $Ag_2S$ sample by sending a current $i$ during time $t$ across the cell. If a positive current flows in the cell from the left to the right, $Ag^+$ ions enter the $Ag_2S$ pellet via the AgI pellet and electrons are furnished from the platinum electrode. In silver sulfide both $Ag^+$

[1] C. Tubandt and H. Reinhold, Z. Elektrochem. **37**, 589 (1931).
[2] H. Reinhold and H. Möhring, Z. physik. Chem. B **28**, 178 (1935).
[3] H. Reinhold and K. Schmitt, Z. physik. Chem. B **44**, 75 (1939).
[4] M. H. Hebb, J. Chem. Phys. **20**, 185 (1952).
[5] C. Tubandt, Z. anorg. u. allgem. Chem **115**, 105 (1921).
[6] C. Wagner, Z. Elektrochem. **40**, 364 (1934).
[7] H. Reinhold, Z. Elektrochem. **40**, 361 (1934).

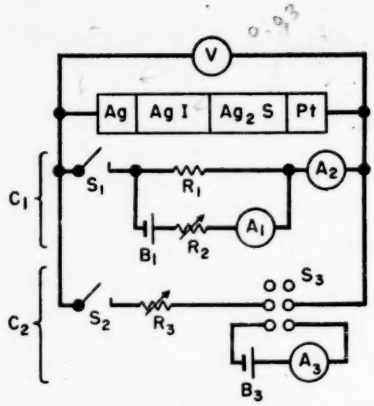


FIG. 1. Measuring circuit for the cell Ag|AgI|$Ag_2S$|Pt. $V$ tube voltmeter. $C_1$ circuit for applying a definite potential to cell, $S_1$ switch; $R_1$ resistor (1 ohm); $R_2$ variable resistor (30 ohms); $B_1$ battery (1.5 volt); $A_1$, $A_2$ milliammeters. $C_2$ circuit for passing current through cell; $S_2$ switch; $S_3$ reversing switch; $A_3$ multirange milliammeter; $R_3$ variable resistor ($10^6$ ohms); $B_3$ battery (30 volt).

ions and electrons are mobile,[8–10,2] and thus a uniform Ag/S ratio $r$ throughout the $Ag_2S$ sample is obtained. If the current is reversed, $Ag^+$ ions and electrons are removed.

The change in the Ag/S ratio $r$ in $Ag_2S$ with respect to the state of $Ag_2S$ in a cell involving $E=0.05$ volt is

$$|\Delta r| = q/n_S\mathfrak{F} = it/n_S\mathfrak{F}, \qquad (6)$$

where $q$ is the number of coulombs passed across the cell and $n_S$ is the number of $g$-atoms of sulfur in the $Ag_2S$ sample.

The method used in this investigation may be called a solid-state coulometric titration.

If the Ag/S ratio is increased so far that the potential of the cell becomes zero, an additional amount of charge passing through the cell leads to deposition of silver in $Ag_2S$.

On the other hand, if the Ag/S ratio is decreased by a certain critical amount, liquid sulfur will be formed as a new phase. Then the potential of the cell reaches the limiting value $E^0$. According to Reinhold,[7] $E^0$ equals 0.230 v at 200°C.

## Preparation of Samples

Silver sulfide was prepared by synthesis from the elements. The first batch of $Ag_2S$ was obtained by heating silver pellets and excess sulfur together in a boat in an atmosphere of purified argon at 220°C. Excess sulfur was removed by subsequent heating to 400°C. A second batch of $Ag_2S$ was prepared according to the procedure used by Hönigschmid and Sachtleben.[11] Sulfur was precipitated from a solution of sodium thiosulfate by adding sulfuric acid and was purified by vacuum distillation. To prepare silver sulfide, a boat containing purified sulfur was placed in a furnace together with a boat containing silver pellets, and a stream of argon was passed over the two boats.

Pellets of $Ag_2S$ with a diameter of 0.635 cm and a thickness of 0.1 to 0.4 cm were pressed in a die.

## Electrical Circuit

A cell consisting of a AgI and a $Ag_2S$ pellet between a silver and a platinum foil was assembled in a glass tube. Sufficient electrical contact was secured by applying a slight pressure with the aid of steel springs. All experiments were made in an atmosphere of purified argon.

The electrical circuit is shown in Fig. 1. To define the initial state, a potential of 0.05 volt was applied to the cell by passing a current of 0.05 amp through resistor $R_1$ (=1 ohm) and closing switch $S_1$.

To obtain $E-q$ curves, a current of appropriate intensity was sent through the cell by closing switch $S_2$ in Fig. 1. After each 5 seconds, switch $S_2$ was opened and the resulting potential was read. The intensity of the current was chosen so that the total time for increasing the potential from 0.01 to 0.20 volt was between 30 and 120 seconds. Thus currents of 0.002 to 0.010 amp for $\alpha$ $Ag_2S$ and of $3\times10^{-5}$ to $1\times10^{-4}$ amp for $\beta$ $Ag_2S$ were used.

## Experimental Results

### 1. *Results for* $\alpha$ $Ag_2S$

At 200 to 300°C steady potentials were obtained within a couple of seconds. This indicates that a virtually uniform Ag/S ratio presupposed in the derivation of Eq. (1) is reached within a very short time, as is expected in view of the high value of the interdiffusion coefficient of silver in $Ag_2S$ calculated below.

Up to a potential $E=0.2$ volt, the same potential $E$ is obtained by passing a given charge with different current intensities. Measurements with a graphite electrode instead of a platinum electrode gave essentially the same results.

Values of $q$ for a given change in the potential $E$ have been found to be proportional to the mass of the sample. Different batches of $Ag_2S$ gave practically equal results. Thus the potential $E$ is a single-valued function of the value $\Delta r$ calculated from Eq. (6). Results are shown in Figs. 2 and 3.

The potential changes are reversed when equivalent amounts of electrical charge are passed in the opposite direction. After completion of a cycle the initial potential of 0.05 volt was obtained provided that the potential did not exceed 0.20 volt, since sulfur vaporizes at higher potentials.

If the potential of the cell exceeded 0.2 volt, the potential dropped slowly after switch $S_2$ in Fig. 1 had been opened. Under these conditions the sulfur partial pressure is appreciable, and thus sulfur is lost by

[8] C. Tubandt and H. Reinhold, Z. anorg. u. allgem. Chem. **160**, 222 (1927).
[9] C. Wagner, Z. physik. Chem. B **21**, 42 (1933); **23**, 469 (1934).
[10] C. Tubandt and H. Reinhold, Z. physik. Chem. B **24**, 22 (1934).
[11] O. Hönigschmid and R. Sachtleben, Z. anorg. u. allgem. Chem. **195**, 207 (1931).

vaporization. Preuner and Schupp,[12] Braune, Peter, and Nevelling,[13] and Braune and Steinbacher[14] have shown that sulfur vapor contains various types of molecules, *viz.*, $S_2$, $S_4$, $S_6$, and $S_8$. The partial pressure $ps_\nu$ of molecules $S_\nu$ involving $\nu$ atoms of sulfur is related to the chemical potential by the general formula

$$ps_\nu/ps_\nu^0=\exp[\nu(\mu_S-\mu_S^0)/(RT)], \qquad (7)$$

where $ps_\nu^0$ is the partial pressure of molecules $S_\nu$ over liquid sulfur, which has been calculated by Braune, Peter, and Nevelling.[13] From Eqs. (5) and (7) and values of $E^0$ reported by Reinhold,[7] the partial pressure of each type of molecule as a function of the potential $E$ of the cell is obtained as

$$ps_\nu/ps_\nu^0=\exp[-2\nu(E^0-E)\mathfrak{F}/RT]. \qquad (8)$$

Numerical values are indicated on the right-hand side of Figs. 2 and 3. At 200°C the partial pressures of all types of sulfur molecules are lower than $10^{-6}$ atmos, and thus volatilization of sulfur is negligible. At potentials

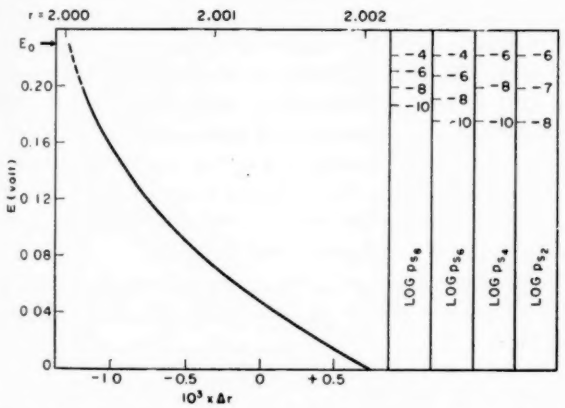


FIG. 2. Potential of cell Ag|AgI|$Ag_2S$|Pt *vs* Ag/S ratio $r$ at 200°C.

exceeding 0.2 volt, however, the volatility of sulfur increases rapidly.

Incidentally, the observation of steady potentials below $E=0.20$ volt seems to be in conflict with the results of conductivity measurements of previous authors. Tubandt and Reinhold[1] found that the electrical conductivity of $Ag_2S$ wires changed rapidly when a current of nitrogen loaded with sulfur was replaced by a current of pure nitrogen, or conversely. The electrical conductivity in nitrogen was essentially the same as the limiting value observed by Reinhold and Schmitt[3] without the presence of a carrier gas when the sulfur was frozen out below −80°C. If the sulfur partial pressure is lower than about $10^{-6}$ atmos or $E<0.2$ volt, vaporization of sulfur in a gentle stream of nitrogen is almost negligible as has been pointed out above. It is therefore probable that in the experiments of Tubandt and Reinhold[1] sulfur was not vaporized but removed by

[12] G. Preuner and W. Schupp, Z. physik. Chem. **68**, 129 (1909).
[13] Braune, Peter, and Nevelling, Z. Naturforsch. **6a**, 32 (1951).
[14] H. Braune and E. Steinbacher, Z. Naturforsch. **7a**, 486 (1952).

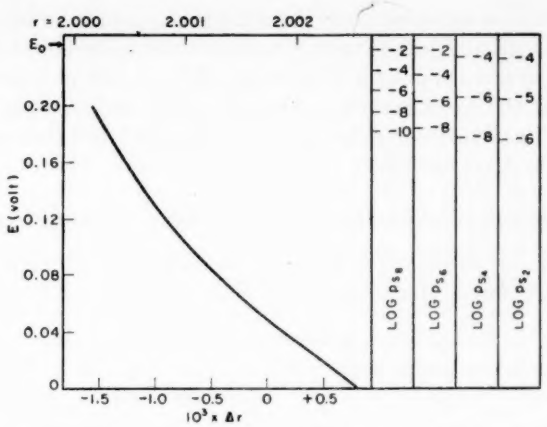


FIG. 3. Potential of cell Ag|AgI|$Ag_2S$|Pt *vs* Ag/S ratio $r$ at 300°C.

reaction with the nickel wires used as leads. If no sulfur in the gas phase is present, nickel may react with $Ag_2S$ and yield nickel sulfide and excess silver dissolved in $Ag_2S$ and finally metallic silver. This interpretation reconciles seemingly conflicting observations.

### 2. *Results for* β $Ag_2S$

At 160°C, considerable drifts of the potential were observed after a current had been passed through the cell. For samples about 0.1 cm thick, a nearly steady potential was obtained after 30 seconds. In spite of this relatively long waiting period, there were considerable hysteresis effects, i.e., the $E-q$ curves for removal and addition of silver did not coincide. Measurements with a graphite electrode instead of a platinum electrode showed hysteresis to about the same extent. It is therefore unlikely that hysteresis effects are caused by electrode reactions. In view of uncertainties due to hysteresis, only the order of magnitude of the variability of the Ag/S ratio can be reported. At 160°C, the change in the Ag/S ratio was found to be $3(\pm1)\times10^{-5}$ *g*-atom Ag/mole $Ag_2S$ for a change in the potential $E$ from 0.18 to 0.0 volt.

$E-q$ curves for β $Ag_2S$ show a maximum of the slope between $E=0.12$ and 0.15 volt. Wagner and Schottky[15] have pointed out that in disordered crystals a maximum of the slope of chemical potential *vs* composition curves occurs at the ideal stoichiometric composition if nonthermodynamic lattice imperfections can be disregarded, and the concentrations of "disorder centers" such as interstitial ions, ion vacancies, excess electrons, and electron holes are sufficiently small so that their interaction is negligible and classical statistics represents an adequate approximation. Although nonthermodynamic lattice imperfections in β $Ag_2S$ may play some part, the conclusion is drawn that the ideal stoichiometric Ag/S ratio in β $Ag_2S$ is reached between $E=0.12$ and 0.15 volt where the slope of the $E-q$ curves has a maximum value. For the following evalua-

[15] C. Wagner and W. Schottky, Z. physik. Chem. B **11**, 163 (1931).

tion it is assumed that the ideal stoichiometric ratio is reached at $E=0.15$ volt. Since the total variation of the Ag/S ratio in $\beta$ $Ag_2S$ is as low as $3\times10^{-5}$, it is estimated that the Ag/S ratio in $\beta$ $Ag_2S$ at 160°C and a potential $E=0.15$ volt differs by not more than $1\times10^{-5}$ from the ideal ratio $r_0=2.000$.

### 3. *Investigations on the $\beta-\alpha$ Phase Transformation of* $Ag_2S$

To determine the absolute value of the Ag/S ratio in $Ag_2S$ for a given potential $E$, the transformation of $\beta$ $Ag_2S$ to $\alpha$ $Ag_2S$ was studied in a furnace of low heat capacity whose temperature could be raised from 160 to 200 or 300°C in a couple of minutes.

TABLE I. Ag/S ratio $r$ in $\alpha$ $Ag_2S$ at $E=0.20$ volt.

| Temp. (°C) | Ag/S ratio $r$ from $\beta-\alpha$ transf. | Ag/S ratio $r$ from $\alpha-\beta$ transf. |
|---|---|---|
| 200 | 2.00010 | 2.00012 |
| 300 | 2.00016 | ... |

When a cell having an initial potential of 0.15 volt at 160°C was heated above the transformation temperature without passing a current, i.e., at constant composition of the sample, the potential rose to about 0.22 volt and then slowly drifted to lower values. This is characteristic of a cell with $Ag_2S$ from which sulfur vaporizes.

Sulfur losses may be prevented by adding silver to the sample during the transformation. To this end, switch $S_1$ of the circuit $C_1$ in Fig. 1 was closed and a potential of 0.15 volt was maintained across resistor $R_1$. The current passing through the cell was measured by a milliammeter $A_2$ having an internal resistance of 36 ohms. After two minutes the current had dropped to a relatively low value. Then switch $S_1$ was opened and the potential $E'$ (0.16 to 0.18 volt) was read after the final temperature had been reached. The change in the Ag/S ratio of the sample due to the flow of a current during the transformation was calculated from the current-time integral and the number $n_S$ of moles of $Ag_2S$ as

$$\delta=\left(\int idt\right)\Big/\mathfrak{F}n_S. \tag{9}$$

If it is assumed that the sample initially had ideal stoichiometric composition, i.e., $r=2$, the Ag/S ratio of the sample corresponding to a potential $E'$ after the transformation equals $r(E')=2+\delta$. Then the ratio $r(E)$ at any potential $E$ is obtained as

$$r(E)=2+\delta+[\Delta r(E)-\Delta r(E')], \tag{10}$$

where the values of $\Delta r(E)$ and $\Delta r(E')$ are to be taken from Figs. 2 and 3. Numerical values of $r$ for 200 and 300°C and $E=0.2$ volt are presented in Table I.

TABLE II. Ag/S ratio in $\alpha$ $Ag_2S$ coexisting with metallic silver.

| Temp. (°C) | $r$ |
|---|---|
| 200 | 2.0020 |
| 300 | 2.0025 |

### 4. *Investigations on the $\alpha-\beta$ Phase Transformation of* $Ag_2S$

When a cell having an initial potential between 0.0 and 0.2 volt is cooled from 200 to 160°C, the potential drops to zero. This indicates that $\alpha$ $Ag_2S$ decomposes to $\beta$ $Ag_2S$ and metallic silver if the initial potential is lower than 0.2 volt. To determine the Ag/S ratio in $\alpha$ $Ag_2S$ in a cell having an initial potential of $E=0.2$ volt at 200°C, the potentiometer of the circuit $C_1$ in Fig. 1 was set to 0.15 volt and switch $S_1$ was closed as soon as the transformation had started and the potential of the cell had dropped below 0.15 volt. Thus $\beta$ $Ag_2S$ with a virtually ideal Ag/S ratio $r=2$ was obtained. The amount of silver removed during the transformation was calculated from the current-time integral by recording the potential drop across a 2-ohm resistor in circuit $C_1$ (not shown in Fig. 1) by means of a Leeds and Northrup Speedomax recorder. The current was limited by a resistor of 100 ohms in series. As is shown in Table I, the value of $r(E=0.2$ v) obtained with this method agrees satisfactorily with that of the first method based on the $\beta-\alpha$ transformation.

Upon adding the difference in the Ag/S ratio between 0.20 and 0.0 volt to the value of $r$ at $E=0.20$ volt, the Ag/S ratio $r$ at $E=0.0$ volt, i.e., for $Ag_2S$ coexisting with metallic silver is obtained (see Table II).

Likewise, values of $r$ for other values of $E$ are obtained and are shown on the upper abscissa of Figs. 2 and 3.

## DISCUSSION

In view of the volatility of sulfur, the electrochemical method does not give results for $Ag_2S$ when nearly saturated with sulfur. By means of a gravimetric method, Reinhold and Schmitt[3] have determined the sulfur excess with respect to the composition of a sample coexisting with metallic silver. Sulfur partial pressures between 0.1 mm Hg and the saturation pressure of sulfur were used. Values for $Ag_2S$ wires were found to be higher than values for compressed $Ag_2S$ pellets. According to Reinhold and Schmitt,[3] this divergence suggests adsorption rather than a bulk phase equilibrium. This conclusion is supported by the peculiar dependence of the sulfur excess on the sulfur partial pressure. In the following discussion the behavior of silver sulfide at sulfur partial pressures exceeding 0.1 mm Hg is therefore disregarded.

Silver sulfide may be considered as an ionic compound. Disorder in the sublattice of sulfur ions seems negligible in view of the large size of sulfur ions and their extremely low diffusivity.[16–18]

[16] H. Braune and O. Kahn, Z. Elektrochem. **31**, 576 (1925).
[17] M. Haissinsky and D. Peschanski, J. chim. phys. **47**, 191 (1950).
[18] D. Peschanski, J. chim. phys. **47**, 933 (1950).

In $\alpha$ $Ag_2S$, silver ions are distributed virtually at random among a large number of nearly equivalent lattice sites as has been deduced from x-ray investigations by Rahlfs.[19] Accordingly, the chemical potential of $Ag^+$ ions, $\mu_{Ag^+}$, is essentially independent of deviations from the ideal stoichiometric ratio. Thus it follows from the general relation $\mu_{Ag^+}+\mu_e=\mu_{Ag}$ that the change in the chemical potential of the electrons, $\mu_e$, is essentially equal to the change in $\mu_{Ag}$, i.e., in view of Eq. (1),

$$d\mu_e \cong d\mu_{Ag} = -d(E\mathfrak{F}). \tag{11}$$

An excess of silver in $\alpha$ $Ag_2S$ corresponds to prevalence of excess electrons, i.e., $n$-type conduction. This is in accordance with the negative sign of the Hall effect found by Klaiber[20] and the fact that the electrical conductivity of $\alpha$ $Ag_2S$ increases with decreasing sulfur partial pressure.[1,3,21]

If the presence of electron holes and electrically neutral silver atoms is disregarded, the excess of silver, $(r-2)$ mole Ag/mole $Ag_2S$, is equivalent to the number of excess electrons per unit volume, $(N/V)$, i.e.,

$$[(r-2)/V_m]N_0=(N/V), \tag{12}$$

where $N_0$ is Avogadro's number and $V_m=35$ cm$^3$ is the molar volume of $Ag_2S$.

For a free-electron gas, Sommerfeld[22] has derived the formula

$$\left(\frac{N}{V}\right)\frac{2h^3}{\pi(8mkT)^{\frac{3}{2}}}=F(\mu_e/RT), \tag{13}$$

where $m$ is the electronic mass, $k$ is the Boltzmann constant, $h$ is Planck's constant, and the Fermi-Dirac function $F$ is defined by

$$F(\mu_e/RT)=\int_0^\infty \frac{u^{\frac{1}{2}}du}{\exp(u-\mu_e/RT)+1}. \tag{14}$$

Since according to Eqs. (12) and (13) $F$ is proportional to $(r-2)$ and therefore $d\ln F/d\ln(r-2)=1$, it follows that

$$\frac{d(\mu_e/RT)}{d\ln(r-2)}=\frac{d(\mu_e/RT)}{d\ln F}\,\frac{d\ln F}{d\ln(r-2)}=\frac{d(\mu_e/RT)}{d\ln F}. \tag{15}$$

Substitution of Eq. (11) in Eq. (15) yields

$$-\frac{d(E\mathfrak{F}/RT)}{d\ln(r-2)}=\left[\frac{d\ln F}{d(\mu_e/RT)}\right]^{-1}. \tag{16}$$

For $Ag_2S$ coexisting with metallic silver at 200°C, the left-hand member of Eq. (13) is found to be 0.61. According to tables of the Fermi-Dirac function computed by McDougall and Stoner,[23] a value of $F(\mu_e/RT)=0.61$ corresponds to $\mu_e/RT=-0.13$ and $[d\ln F/d(\mu_e/RT)]^{-1}=1.23$, slightly greater than the limiting value of 1.00 according to classical statistics, whereas a $(E\mathfrak{F}/RT)$ *vs* $\ln(r-2)$ plot gives a slope of $-3.0$ at $E=0$. Thus, the equality postulated in Eq. (16) is not confirmed.

Actually there is no free-electron gas in $Ag_2S$ in view of a nonuniform electrostatic potential. Also under these conditions, the number of states for electrons at the bottom of the conduction band is proportional to the square root of the energy $\epsilon$, but the proportionality factor differs from that for a free-electron gas. This divergence may be accounted for by introducing an effective electronic mass $m^*$ defined by the relation $d^2\epsilon/dk^2=h^2/4\pi^2m^*$ where $k$ is the wave number.[24] From the experimental results of the present investigation, the effective mass may be calculated in the following way. In view of Eq. (16) the negative slope of the $(E\mathfrak{F}/RT)$ *vs* $\ln(r-2)$ plot for $E=0$ is equal to $[d\ln F/d(\mu_e/RT)]^{-1}$ i.e., equal to 3.0, which corresponds to a value of $F(\mu_e/RT)=5.77$ according to tables computed by McDougall and Stoner.[23] Substituting this value in Eq. (13) with $m^*$ instead of $m$ and using Eq. (12), one may calculate $m^*$ and thus obtains the ratio of the effective mass to the electronic mass, $m^*/m=0.22$.

In $\beta$ $Ag_2S$ most $Ag^+$ ions occupy well-defined lattice sites as is indicated by the magnitude of the self-diffusion coefficient of $Ag^+$ ions, which is obtained as $7\times10^{-8}$ cm$^2$/sec from the transference number of cations and the electrical conductivity of $\beta$ $Ag_2S$ at 160°C[2]. The order of magnitude of the degree of disorder, i.e., the fraction of interstitial cations or cation vacancies may roughly be calculated as the ratio of the self-diffusion coefficient of silver in $\beta$ $Ag_2S$ to the self-diffusion coefficient in $\alpha$ $Ag_2S$ ($\sim1\times10^{-5}$ cm$^2$/sec).[25,26] This gives a degree of disorder of about $10^{-2}$, which is much greater than the variability of the Ag/S ratio. Consequently, the concentrations of interstitial cations and cation vacancies in $\beta$ $Ag_2S$ at 160°C are practically independent of variations of the Ag/S ratio. The same is true for the chemical potential of silver ions. Thus Eq. (11) also holds for $\beta$ $Ag_2S$. Since the electron concentration is very low, formulas derived from classical statistics apply. Consequently, the concentration $(N/V)$ of excess electrons in $\beta$ $Ag_2S$ is related to the chemical potential of silver by

$$(N/V)=\text{constant}\times\exp(\mu_{Ag}/RT).$$

The same dependence is obtained for the electronic conductivity if a contribution of the electron holes is disregarded and a constant mean free path is assumed. This is in accordance with considerations of Hebb[4] and his evaluation of experimental data for $\beta$ $Ag_2S$.

[19] P. Rahlfs, Z. physik. Chem. B **31**, 157 (1935).
[20] F. Klaiber, Ann. Physik (5) **3**, 229 (1929).
[21] C. Wagner, Z. physik. Chem. B **22**, 181 (1933).
[22] A. Sommerfeld, Z. Physik **47**, 1 (1928).
[23] J. McDougall and E. C. Stoner, Trans. Roy. Soc. (London) A **237**, 67 (1938).
[24] N. F. Mott and H. Jones, *Properties of Metals and Alloys* (Clarendon Press, Oxford, 1936), p. 95.
[25] Tubandt, Reinhold, and Jost, Z. anorg. u. allgem. Chem. **177**, 253 (1929).
[26] W. Jost and H. Rüter, Z. physik. Chem. B **21**, 48 (1933).

## THE USE OF SILVER SULFIDE FOR THE DETERMINATION OF THE ATOMIC WEIGHT OF SULFUR

The foregoing results are of special importance in conjunction with the use of silver sulfide by Hönigschmid and Sachtleben[11] for the determination of the atomic weight of sulfur. These authors synthesized $Ag_2S$ with a slight excess of sulfur, and then heated samples in a gentle stream of nitrogen at 300°C until no further weight change was observed during several hours. Assuming ideal stoichiometric composition of their samples, Hönigschmid and Sachtleben deduced an atomic weight of sulfur equal to 32.066, which has been confirmed by subsequent work by Hönigschmid.[27] This value is also in close agreement with the value of 32.063 derived from the density of gaseous $SO_2$ and $H_2S$ by Moles, Toral, and Escribano[28] and the value of 32.064 obtained from mass-spectroscopical investigations by Nier.[29]

From the data presented in Table II it follows that at 300°C silver sulfide may accomodate a silver excess as high as 0.12 percent. If, however, a sample containing excess sulfur is heated at 300°C, sulfur vaporizes with a noticeable rate only until a potential $E=0.20$ volt has been reached. At $E=0.20$ volt, the Ag/S ratio is 2.00016. This value would cause an error of $-0.002$ unit in the atomic weight of sulfur. The present investigation shows that the error in the atomic weight of sulfur due to deviations from the ideal stoichiometric ratio of $Ag_2S$ samples weighed by Hönigschmid and Sachtleben is relatively small, but a more definite conclusion cannot be drawn since volatilization of sulfur from $Ag_2S$ depends on too many unknown factors.

The results of the present investigation provide the possibility to prepare $Ag_2S$ with a known Ag/S ratio by using a controlled atmosphere, or a temperature below 178°C, since deviations from the ideal ratio in $\beta$ $Ag_2S$ are relatively small. Thus, in future work, one may either take into account or minimize deviations from the ideal Ag/S ratio.

## INTERDIFFUSION OF SILVER IN SILVER SULFIDE

The rate of the reaction $2Ag(s)+S(l)=Ag_2S(s)$ has been found to be inversely proportional to the instantaneous thickness $\Delta\xi$ of the reaction product, $Ag_2S$. Thus diffusion of one of the reactants determines the rate. According to Wagner,[30] silver ions and electrons are the migrating constituents. The rate, i.e., the number of equivalents of $Ag_2S$ formed per unit area per unit time, $\dot{n}/A$, equal to the number of moles Ag diffusing per unit area per unit times, is

$$\dot{n}/A=k_r/\Delta\xi, \tag{17}$$

where $k_r$ is the rational rate constant.

On the other hand, Fick's first law gives the relation

$$\dot{n}/A=-D(dc/d\xi), \tag{18}$$

where $c$ is the local concentration of silver in $Ag_2S$ in $g$-atom per unit volume, $\xi$ is the distance from the $Ag-Ag_2S$ interface, and $D$ is the interdiffusion coefficient of silver between $Ag_2S$ samples involving different Ag/S ratios. The value of $D$ depends on concentration $c$. Introducing an effective average interdiffusion coefficient $D_{\text{eff}}$, we may rewrite Eq. (18) as

$$\dot{n}/A=D_{\text{eff}}[c(Ag_2S+Ag)-c(Ag_2S+S)]/\Delta\xi, \tag{19}$$

where $c(Ag_2S+Ag)$ and $c(Ag_2S+S)$ are the silver concentrations in $Ag_2S$ coexisting with metallic silver and liquid sulfur, respectively. If the change in the lattice parameter with the Ag/S ratio is disregarded, we have

$$c(Ag_2S+Ag)-c(Ag_2S+S)=[r(Ag_2S+Ag)-r(Ag_2S+S)]/V_m, \tag{20}$$

where $V_m=35$ cm$^3$ is the molar volume of $Ag_2S$ and $r(Ag_2S+Ag)$ and $r(Ag_2S+S)$ are the Ag/S ratios for silver sulfide coexisting with metallic silver and liquid sulfur, respectively.

If we substitute Eq. (20) in Eq. (19) and compare Eqs. (17) and (19), we obtain

$$D_{\text{eff}}=k_rV_m/[r(Ag_2S+Ag)-r(Ag_2S+S)]. \tag{21}$$

The rate constant $k_r$ at 220°C equals about $1.6\times10^{-6}$ equivalent cm$^{-1}$ sec$^{-1}$ according to Wagner,[30] Reinhold and Seidel,[31] and Croatto.[32] Thus it follows from Eq. (21) that

$$D_{\text{eff}}\cong2.8\times10^{-2}\text{ cm}^2/\text{sec at }220°\text{C}. \tag{22}$$

This value is about three orders of magnitude greater than diffusion coefficients in liquid systems. It is also about $2.8\times10^3$ times greater than the self-diffusion coefficient $D^*$ of silver in $Ag_2S$, which is estimated to be of the order $1\times10^{-5}$ cm$^2$/sec according to diffusion measurements on the system $Ag_2S-Cu_2S$.[25,26]

The divergence between the interdiffusion and the self-diffusion coefficient is due to the fact that the mobility of electrons is much greater than the mobility of silver ions. When there is a gradient of the metal/nonmetal ratio, metal ions and electrons migrate in the same direction, electrons having the tendency to move faster than silver ions. Thus there results an electrical potential gradient[30] which decelerates electrons and accelerates silver ions so that the actual migration rates are equal, and each volume element remains essentially electrically neutral. In most cases the interdiffusion coefficient is only two or three times greater than the self-diffusion coefficient of an ion.[33,34] Exceptional conditions, however, are found in silver sulfide in which the concentration of excess electrons is substantially lower than the concentration of disordered ions but conduc-

[27] O. Hönigschmid, Ber. Deutsch. Chem. Gesellsch. **75**, 1814 (1942).
[28] Moles, Toral, and Escribano, Trans. Faraday Soc. **35**, 1439 (1939).
[29] A. O. Nier, Phys. Rev. (2) **53**, 282 (1938).
[30] C. Wagner, Z. physik. Chem. B **21**, 25 (1933).
[31] H. Reinhold and H. Seidel, Z. Elektrochem. **41**, 499 (1935).
[32] U. Croatto, Gazz. Chim. Ital. **79**, 458 (1949).

tion is preponderately electronic because the mobility of an excess electron is much greater than the mobility of an interstitial ion or an ion vacancy. This situation is encountered not only in $Ag_2S$ but also in $Cu_2S$,[33–35] $Cu_2Se$,[33–35] $Cu_2Te$,[36] and in KCl[33,37] having a potassium excess.

Since conduction in $\alpha$ $Ag_2S$ is mainly electronic, the diffusion rate of silver ions per unit area per unit time is obtained as[38]

$$\dot{n}/A = -D^*c(d\ \ln a_{Ag}/d\xi), \tag{23}$$

where $a_{Ag}$ is the activity of silver.

Upon comparing Eqs. (18) and (23), it follows that

$$D/D^* = d\ \ln a_{Ag}/d\ \ln c. \tag{24}$$

Upon introducing the average diffusion coefficient $D_{eff}$ and the Ag/S ratio $r$, Eq. (24) becomes

$$D_{eff}/D^* = \frac{r_0|\ln a_{Ag}(Ag_2S+S)|}{r(Ag_2S+Ag)-r(Ag_2S+S)}, \tag{25}$$

where $r_0=2$ is the ideal Ag/S ratio and $a_{Ag}(Ag_2S+S)$ is the activity of silver in $Ag_2S$ coexisting with liquid sulfur, the activity of pure silver being taken as unity. Numerical evaluation of Eq. (25) gives $D_{eff}/D^*=5\times10^3$.

Equation (25) may also be obtained from Darken's[39] theory of diffusion in metallic systems.[34] The extreme situation found in $Ag_2S$ strongly supports Darken's equation interrelating interdiffusion coefficient, self-diffusion coefficients, and activity coefficients in alloys.

## MEASUREMENT OF THE DIFFUSION POTENTIAL IN SILVER SULFIDE

The diffusion potential across a $Ag_2S$ pellet in contact with silver on one side and with liquid sulfur on the other side has been determined by measuring the potential difference between two silver wires coated with AgCl (see Fig. 4). Since AgCl is an ionic conductor having a definite chemical potential of silver ions and the chemical potential of silver ions in $\alpha$ $Ag_2S$ is virtually independent of the Ag/S ratio, the potential difference across the phase boundary AgCl/$Ag_2S$ is essentially the same for the two probes. Thus the potential difference between the two probes gives directly the potential difference between points adjacent to the probes 1 and 2 within the $Ag_2S$ pellet. At 200°C, a potential difference of 0.21 volt was observed. Probe 2 adjacent to liquid sulfur was found to be negative with respect to probe 1 corresponding to the negative space charge caused by electrons moving ahead toward the $Ag_2S$/S interface. Theoretically, a diffusion potential close to $E_0=0.23$ volt is expected,[30,33] if the probes are located exactly at the $Ag_2S$–Ag and the $Ag_2S$–S interface. In view of the finite size of the probes, the actual potential difference is somewhat lower.

## THERMODYNAMICS OF THE PHASE TRANSFORMATION OF SILVER SULFIDE BETWEEN 176 AND 178°C

Kracek[40] has found that the temperature for equilibrium between $\alpha$ and $\beta$ $Ag_2S$ in the presence of metallic silver is $1.6\pm1.1$°C lower than in the presence of liquid sulfur. This temperature difference may be calculated from available thermodynamic data by a method similar to that used by Hauffe and Wagner[41] for the discussion of the liquidus of intermetallic compounds.

In the following calculations, sulfur and silver are denoted as components 1 and 2 and their mole fractions as $x_1$ and $x_2$, respectively. Since $x_1=1-x_2$, the mole fraction $x_2$, temperature $T$, and pressure $P$ will be used as independent variables. The two phases, $\alpha$ and $\beta$, coexist if the chemical potentials of each component are equal, i.e.,

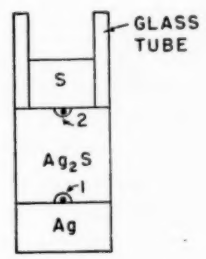


FIG. 4. Setup for the measurement of the diffusion potential across a $Ag_2S$ pellet in contact with silver on one side and with liquid sulfur on the other side. 1 and 2: Ag wires coated with AgCl. Diameter of the silver wires: 0.025 cm; height of the $Ag_2S$ pellet: 0.4 cm.

$$\mu_1'(x_2', T)-\mu_1''(x_2'', T)=0, \tag{26}$$

$$\mu_2'(x_2', T)-\mu_2''(x_2'', T)=0, \tag{27}$$

where quantities referring to $\alpha$ and $\beta$ $Ag_2S$ are marked by a prime and a double prime superscript, respectively.

The molar free energy of either phase, $F_m'$ and $F_m''$, respectively, may be expressed as the sum of the products of mole fractions and chemical potentials,

$$F_m'(x_2', T)=(1-x_2')\mu_1'(x_2', T)+x_2'\mu_2'(x_2', T), \tag{28}$$

$$F_m''(x_2'', T)=(1-x_2'')\mu_1''(x_2'', T)+x_2''\mu_2''(x_2'', T). \tag{29}$$

If instability with regard to the formation of liquid sulfur as another phase is disregarded, there is a temperature $T^*$ at which the compositions of the coexisting phases are equal to each other. For this particular mole fraction $x_2^*$ and temperature $T^*$ it

[33] C. Wagner, Z. physik. Chem. B **32**, 447 (1936).
[34] H. Reinhold and H. Möhring, Z. physik. Chem. B **38**, 221 (1937).
[35] H. Reinhold and H. Seidel, Z. physik. Chem. B **38**, 245 (1937).
[36] H. Reinhold and H. Bräuninger, Z. physik. Chem. B **41**, 397 (1939).
[37] O. Stasiw, Nachrichten Gesellsch. Wissenschaften Göttingen (N.F.) **1**, 147 (1935).
[38] C. Wagner, "Diffusion and High Temperature Oxidation of Metals" in: *Atom Movements* (American Society for Metals, Cleveland, Ohio, 1951), p. 153.
[39] L. S. Darken, Trans. Am. Inst. Met. Mining Eng. **178**, 184 (1948).
[40] F. C. Kracek, Trans. Am. Geophys. Union **27**, 364 (1946).
[41] K. Hauffe and C. Wagner, Z. Elektrochem. **46**, 160 (1940).

follows from Eqs. (26) to (29) that

$$F_m'(x_2^*, T^*)-F_m''(x_2^*, T^*)=0. \quad (30)$$

For the temperature dependence of the difference $F_m'(x_2^*, T)-F_m''(x_2^*, T)$ we have according to the Gibbs-Helmholtz equation

$$\frac{\partial}{\partial T}\frac{F_m'(x_2^*, T)-F_m''(x_2^*, T)}{T} = -\frac{H_m'(x_2^*, T)-H_m''(x_2^*, T)}{T^2}, \quad (31)$$

where $H_m'(x_2^*, T)-H_m''(x_2^*, T)$ is the increase in enthalpy for the transformation of $\beta$ phase containing $(1-x_2^*)\cong\frac{1}{3}$ g-atom sulfur and $x_2^*\cong\frac{2}{3}$ g-atom silver to $\alpha$ phase. Denoting the heat of transformation of one mole of $Ag_2S$ by $\Delta H_{tr}$ and neglecting the effect of deviations from the ideal stoichiometric composition and dependence on temperature, we have

$$H_m'(x_2^*, T)-H_m''(x_2^*, T)=\tfrac{1}{3}\Delta H_{tr}. \quad (32)$$

Integration of Eq. (31) with respect to $T$ yields in view of Eqs. (30) and (32)

$$F_m'(x_2^*, T)-F_m''(x_2^*, T)=\tfrac{1}{3}(T^*-T)\Delta H_{tr}/T^*. \quad (33)$$

From the Gibbs-Duhem equation

$$(1-x_2)(\partial\mu_1/\partial x_2)+x_2(\partial\mu_2/\partial x_2)=0, \quad (34)$$

it follows by integration between mole fractions $x_2^*$ and $x_2$ that

$$\mu_1(x_2, T)=\mu_1(x_2^*, T)-\int_{x_2^*}^{x_2}\frac{x_2}{1-x_2}\frac{\partial\mu_2}{\partial x_2}dx_2, \quad (35)$$

which applies to either phase.

If we multiply Eqs. (26) and (27) through by $(1-x_2^*)$ and $x_2^*$, respectively, add corresponding sides, substitute Eq. (35) for either phase, and rearrange terms, we have

$$\begin{aligned}&[(1-x_2^*)\mu_1'(x_2^*, T)+x_2^*\mu_2'(x_2^*, T)]\\ &\quad-[(1-x_2^*)\mu_1''(x_2^*, T)+x_2^*\mu_2''(x_2'', T)]\\ &\quad+\left\{x_2^*[\mu_2'(x_2', T)-\mu_2'(x_2^*, T)]\right.\\ &\quad\left.-(1-x_2^*)\int_{x_2^*}^{x_2}\frac{x_2'}{1-x_2'}\frac{\partial\mu_2'}{\partial x_2'}dx_2'\right\}\\ &\quad-\left\{x_2^*[\mu_2''(x_2'', T)-\mu_2''(x_2^*, T)]\right.\\ &\quad\left.-(1-x_2^*)\int_{x_2^*}^{x_2''}\frac{x_2''}{1-x_2''}\frac{\partial\mu_2''}{\partial x_2''}dx_2''\right\}=0. \quad (36)\end{aligned}$$

Equation (36) may be simplified by the following mathematical transformation

$$\begin{aligned}&x_2^*[\mu_2(x_2, T)-\mu_2(x_2^*, T)]-(1-x_2^*)\int_{x_2^*}^{x_2}\frac{x_2}{1-x_2}\frac{\partial\mu_2}{\partial x_2}dx_2\\ &\quad=-\int_{\mu_2(x_2^*, T)}^{\mu_2(x_2, T)}\frac{x_2-x_2^*}{1-x_2}d\mu_2\\ &\quad\cong-\frac{1}{1-x_2^*}\int_{\mu_2(x_2^*, T)}^{\mu_2(x_2, T)}(x_2-x_2^*)d\mu_2, \quad (37)\end{aligned}$$

which applies to either phase if $x_2\cong x_2^*$.

If we use Eqs. (28) for $x_2'=x_2^*$ and (29) for $x_2''=x_2^*$ in Eq. (36), substitute Eqs. (33) and (37) in Eq. (36), and solve for $T^*-T$, we obtain

$$\begin{aligned}T^*-T=\frac{T^*}{\tfrac{1}{3}(1-x_2^*)\Delta H_{tr}}&\left[\int_{\mu_2'(x_2^*, T)}^{\mu_2'(x_2', T)}(x_2'-x_2^*)d\mu_2'\right.\\ &\left.-\int_{\mu_2''(x_2^*, T)}^{\mu_2''(x_2'', T)}(x_2''-x_2^*)d\mu_2''\right]. \quad (38)\end{aligned}$$

The difference $x_2-x_2^*$ in either phase may be expressed in terms of $r$,

$$\begin{aligned}x_2-x_2^*&=r/(1+r)-r^*/(1+r^*)\\ &=(r-r^*)/[(1+r)(1+r^*)]\cong\frac{1}{9}(r-r^*) \quad (39)\end{aligned}$$

where $r^*$ is the Ag/S ratio corresponding to the mole fraction $x_2^*$ at which the compositions of coexisting $\alpha$ $Ag_2S$ and $\beta$ $Ag_2S$ are equal, i.e., at which transformation from $\beta$ $Ag_2S$ to $\alpha$ $Ag_2S$ takes place without change in $\mu_{Ag}-\mu_{Ag}^0$ or $E$. In view of the small variability of $r$ for the $\beta$ phase, $r^*$ may be assumed to be equal to the ideal value $r_0=2.000$.

If we denote the limiting values of $\mu_{Ag}$ in $\alpha$ and $\beta$ $Ag_2S$ coexisting with metallic silver and elemental sulfur by $\mu_{Ag}(\alpha+Ag)$, $\mu_{Ag}(\beta+Ag)$, $\mu_{Ag}(\alpha+S)$, and $\mu_{Ag}(\beta+S)$, respectively, substitute Eqs. (39) in Eq. (38) applied (1) to the three-phase equilibrium $\alpha$ $Ag_2S+\beta$ $Ag_2S+Ag$ and (2) to the three-phase equilibrium $\alpha$ $Ag_2S+\beta$ $Ag_2S+S$, and subtract corresponding sides, we obtain the difference of the two three-phase equilibrium temperatures as

$$\begin{aligned}&T(\alpha+\beta+S)-T(\alpha+\beta+\mathrm{Ag})\\ &\quad=\frac{1}{3}\frac{T^*}{(1-x_2^*)\Delta H_{tr}}\left[\int_{\mu_2'(\alpha+S)}^{\mu_2'(\alpha+\mathrm{Ag})}(r'-r^*)d\mu_2'\right.\\ &\quad\left.-\int_{\mu_2''(\beta+S)}^{\mu_2''(\beta+\mathrm{Ag})}(r''-r^*)d\mu_2''\right]. \quad (40)\end{aligned}$$

Since the temperature dependence of the $E$ *vs* $r$ curves for $\alpha$ $Ag_2S$ is relatively small, the value of the first integral may be obtained from Eq. (1) and Fig. 2. The value of the second integral is negligible since the maximum value of $r''-r^*$ for $\beta$ $Ag_2S$ is much less than the corresponding difference for $\alpha$ $Ag_2S$. The heat of transformation equals $\Delta H_{tr}=1050$ cal/mole $Ag_2S$ according to Kapustinskiĭ and Vesoloviskiĭ.[42] Hence it follows from Eq. (40) that

$$T(\alpha+\beta+S)-T(\alpha+\beta+\mathrm{Ag})=1.7°, \qquad (41)$$

in accordance with the value of $1.6\pm1.1°$ observed by Kracek.[40]

[42] A. F. Kapustinskii and B. K. Vesolovskii, J. Phys. Chem. U. S. S. R. **11**, 68 (1938); Chem. Abstracts **32**, 8251 (1938).


### ACKNOWLEDGMENT

This work was done as a part of an investigation sponsored by the U. S. Atomic Energy Commission under Contract No. AT-30-Gen-1002.


THE JOURNAL OF CHEMICAL PHYSICS VOLUME 21, NUMBER 10 OCTOBER, 1953

# The Correct Application of the Gibbs-Helmholtz Equation to Reversible Galvanic Cells in Which the Compositions of Some of the Phases Vary with Temperature

R. E. Barieau
*California Research Corporation, Richmond, California*
(Received March 16, 1953)

The detailed proof is given that the Gibbs-Helmholtz equation $d\Delta F_{\text{cell}}/dT=-\Delta S_{\text{cell}}$ is directly applicable to any reversible galvanic cell, regardless of how the compositions of any phases present may vary with the temperature.

IN 1950 the present writer[1] published a paper dealing with the general application of the Gibbs-Helmholtz equation to reversible galvanic cells. In this paper it was stated, "The Gibbs-Helmholtz equation is derivable from very general principles, since it involves the relationship of the temperature coefficient of reversible work and the corresponding isothermal entropy change. For this reason, it may be stated with confidence that the Gibbs-Helmholtz equation is directly applicable to any reversible galvanic cell." It was thought at the time that the quoted paragraph would be a sufficient statement of the validity of the Gibbs-Helmholtz equation and that it would not be necessary to give the proof in detail. However, it has recently been pointed out to the writer that Li[2] has objected to the statement quoted. In fact, Li says, "Since Eq. (1) $[d\Delta F/dT=-\Delta S]$ has originated from the fundamental form $dF/dT=-S$, which is derived for systems with temperature as the only independent variable, it is obvious that Eq. (1) is not applicable to any reversible galvanic cell operated at variable concentration, as pointed out by Brickwedde and Brickwedde."[3]

Although it is true that the Gibbs-Helmholtz equation is usually derived in the manner indicated by Li, it is more general than this particular derivation indicates. The general derivation was first given by Helmholtz[4] in the form $(\partial\mathcal{E}/\partial T)_Q=1/T(\partial q/\partial Q)_T$, where $(\partial\mathcal{E}/\partial T)_Q$ is the temperature coefficient of emf when no charge is allowed to flow and $(\partial q/\partial Q)_T$ is the isothermal absorption of heat by the cell from the surroundings per unit of charge flow. Helmholtz's equation as derived is strictly accurate, only if the volume of the cell is kept constant during the isothermal change and also during the temperature change. Gibbs[5] was the first to derive the equation strictly applicable to reversible galvanic cells in which the pressure is maintained constant—thus the name, the Gibbs-Helmholtz equation. The general proof is as follows.

We take as our system the entire galvanic cell, which is in contact with a thermostat at temperature $T$. From the First Law of Thermodynamics, we may write for any change of the cell $\Delta E=q-w$ where $\Delta E$ is the change in internal energy of the galvanic cell, $q$ is the heat absorbed by the cell during the change, and $w$ is the total work done by the cell, which includes work done against the atmosphere and also the electrical work. Now let us allow an infinitesimal change to take place reversibly. Then by the Second Law of Thermodynamics, $q=TdS$ and we have $dE=TdS-PdV-\mathcal{E}dQ$ where $\mathcal{E}$ is the emf of the cell and $dQ$ is the infinitesimal amount of charge transferred during the infinitesimal change. $dQ=\mathfrak{F}dN$ where $\mathfrak{F}$ is the faraday and $dN$ is the infinitesimal number of equivalents of electricity transferred. Thus $dE=TdS-PdV-\mathcal{E}\mathfrak{F}dN$. Except for a change in symbolism and for a term involving gravitational forces this last equation has been given by Gibbs.[6]

[1] R. E. Barieau, J. Am. Chem. Soc. **72**, 4023 (1950).
[2] J. C. M. Li, J. Chem. Phys. **19**, 1059 (1951).
[3] F. G. Brickwedde and L. H. Brickwedde, Phys. Rev. (II) **60**, 172 (1941).
[4] H. Helmholtz, Sitzber. Akad. Wiss. Berlin **1**, 22 (1882).
[5] *The Scientific Papers of J. Willard Gibbs* (Longmans, Green and Company, New York, New York, 1906), Vol. I, p. 411.
[6] Reference 5, p. 338.

We define $F=E+PV-TS$

$$dF=dE+PdV+VdP-TdS-SdT,$$

or on substituting for $dE$, $dF=-SdT+VdP-\mathcal{E}\mathfrak{F}dN$. Then for a reversible process at constant $T$ and $P$, we have $dF=-\mathcal{E}\mathfrak{F}dN$. Since $F$ for a reversible galvanic cell is a function of three variables, it follows from the elementary laws of partial differentiation:

$$(\partial F/\partial T)_{P,N}=-S,$$
$$(\partial F/\partial N)_{T,P}=-\mathcal{E}\mathfrak{F}.$$

Differentiating the first of these with regard to $N$ and the second with regard to $T$, it follows:

$$(\partial^2 F/\partial T\partial N)_P=-(\partial S/\partial N)_{T,P}=-\mathfrak{F}(\partial\mathcal{E}/\partial T)_{N,P}.$$

The last equation means that the change in emf of a reversible galvanic cell with change in temperature, keeping pressure constant and allowing no charge to flow, is proportional to the entropy change of the cell as we allow current to flow in a reversible manner at constant pressure and temperature. During this derivation we have said nothing about the phases present nor their composition nor how they change with temperature. The last equation is therefore applicable to any reversible galvanic cell.

The chemist, by convention, has taken to expressing

$$\left(\frac{\partial S}{\partial N}\right)_{P,T}=\left(\frac{\Delta S}{N}\right)_{P,T} \quad \text{and} \quad \left(\frac{\partial F}{\partial N}\right)_{P,T}=\left(\frac{\Delta F}{N}\right)_{P,T}.$$

Thus, the more familiar forms follow:

$$\Delta F_{\text{cell}}=-N\mathcal{E}\mathfrak{F}$$

$$N\mathfrak{F}\left(\frac{d\mathcal{E}}{dT}\right)_{P,N}=\Delta S_{\text{cell}} \quad \text{and} \quad \left(\frac{d\Delta F_{\text{cell}}}{dT}\right)_{P,N}=-\Delta S_{\text{cell}}.$$

Thus we see that the Gibbs-Helmholtz equation is applicable to any reversible galvanic cell.

If we allow the cell to discharge reversibly and isothermally, the cell undergoes an entropy change which can be calculated from the heat absorbed by the cell from the surroundings. Now there is some process taking place within the cell which when expressed as a chemical equation will have an entropy change equal to the entropy change of the cell. This is the correct cell reaction, and it is the only correct cell reaction because it is the only equation which actually expresses what is taking place within the cell when it discharges reversibly and isothermally.

Li[2] also says, "As an example, for cells of the following type:

$$H_2(g)\,|\,H_2SO_4(m) \text{ saturated with } CuSO_4\cdot 5H_2O(s)\,|\,Cu(s),$$

where m is the molality of $H_2SO_4$ which is independent of temperature, the "correct" reaction is found to be:

$$H_2(g)+\frac{x+5y}{1+5y}CuSO_4 \text{ (in solution)}$$
$$+\frac{1-x}{1+5y}CuSO_4\cdot 5H_2O(s)=H_2SO_4 \text{ (in solution)}$$
$$+\frac{5-5x}{1+5y}H_2O \text{ (in solution)}+Cu(s),$$

where

$$x=\left(\frac{\partial\bar{F}_{H_2SO_4}}{\partial\bar{F}_{CuSO_4}}\right)_T \quad \text{and} \quad y=\left(\frac{\partial\bar{F}_{H_2O}}{\partial\bar{F}_{CuSO_4}}\right)_T.$$

This reaction can no longer be written from Barieau's principle···."

The answer to this criticism is that the system as postulated as being set up by Li would not be a reversible cell. $CuSO_4$ is supposed to react with $H_2$, but since these are in contact at the anode, they would react irreversibly at the electrode. The Gibbs-Helmholtz equation cannot, of course, be applied to such a system.

# The Thermodynamics of Reversible Galvanic Cells in Which the Compositions of Some of the Phases Vary with Temperature

J. W. Stout
*Institute for the Study of Metals, The University of Chicago, Chicago, Illinois*
(Received July 1, 1953)

The entropy change calculated from the temperature coefficient of electromotive force of a reversible galvanic cell, in which the compositions of some of the phases vary with temperature, corresponds to a unique correct chemical reaction. The equivalence of methods suggested by Barieau and by Li for determining this correct reaction is shown. The method of Barieau is simpler and more direct and presents the results in a more convenient form.

In many galvanic cells two or more phases are in equilibrium and consequently, at constant temperature, there is more than one possible chemical reaction whose free energy change may be identified with the reversible electromotive force of the cell. If the temperature is varied, however, the compositions of the phases in general will change, and since the partial molal entropy of a component of the cell will be different in different phases, there is only one correct chemical reaction whose entropy change corresponds to the temperature coefficient of reversible electromotive force of the cell. The choice of this correct reaction has been treated by Barieau[1] who stated the following principle: "The processes that will take place between the phases in equilibrium are those that will maintain the phases in equilibrium." From this point of view, which is certainly correct, the entropy change occurring in the complete cell is calculated from the Gibbs-Helmholtz equation and then Barieau's principle is used to determine the correct cell reaction.

An alternative point of view has been taken by Brickwedde and Brickwedde[2] and more recently by Li.[3] These authors prefer to speak of the free energy changes accompanying the separate reactions, each involving one of the phases that are in equilibrium. These $\Delta F$'s are functions of composition as well as temperature and consequently in their temperature derivatives a term involving the change of $\Delta F$ with composition appears. As has been pointed out by Barieau,[4] Li's contention that the Gibbs-Helmholtz equation cannot be applied to a reversible cell whose composition varies with temperature is not correct. Li further incorrectly stated that it was not possible to apply Barieau's principle to a cell in which there was more than one concentration variable. It is, however, possible to determine the correct cell reaction with Li's approach and the purpose of this note is to show the equivalence of the two methods.

For simplicity we consider a cell in which the equilibrium between only two phases need be considered, a pure solid phase $R_0$, and a liquid phase which contains $m+1$ components, $R_0$, $R_1$, . . . $R_m$. As the cell discharges, the chemical reaction that occurs may be written

$$qR_0(\text{soln})+(\nu_0-q)R_0(\text{solid})+\sum_{j=1}^{m}\nu_jR_j=0. \quad (1)$$

$R_j$ is the formula of the $j$-th chemical species and $\nu_j$ is its coefficient in the chemical reaction, negative for reactants, positive for products, and zero for chemical species which are unchanged. As the reaction proceeds by an amount $d\epsilon$ then, in the solution, the change in the number of moles of component $R_0$ is $dn_0=qd\epsilon$ and that of any other component $R_j$ is $dn_j=\nu_jd\epsilon$. In order to write expressions in terms of intensive properties of the solution, it is desirable to introduce concentration variables. A convenient choice is $c_i=n_i/n_1$. Then

$$dc_0=(1/n_1)(q-c_0\nu_1)d\epsilon, \quad (2)$$

$$dc_j=(1/n_1)(\nu_j-c_j\nu_1)d\epsilon. \quad (3)$$

The principle stated by Barieau[1] that the phases remain in equilibrium requires in this case the constancy of $\mu_0$, the partial molal free energy of the species $R_0$. At constant pressure and temperature

$$d\mu_0=(\partial\mu_0/\partial c_0)dc_0+\sum_{j=2}^{m}(\partial\mu_0/\partial c_j)_T dc_j=0. \quad (4)$$

In the partial derivatives, pressure and all concentration variables except those occurring explicitly as differentials, as well as the quantities indicated explicitly as subscripts outside the parentheses, are to be held constant.

Substituting (2) and (3) in (4) one obtains

$$q=c_0\nu_1+\sum_{j=2}^{m}(\partial c_0/\partial c_j)_{T,\mu_0}(\nu_j-c_j\nu_1). \quad (5)$$

In the alternative method the free energy change of the reaction is written

$$\Delta F=\sum_{j=1}^{m}\nu_j\mu_j+q\mu_0(\text{soln})+(\nu_0-q)\mu_0(\text{solid}). \quad (6)$$

One considers $\Delta F$ a function of concentration variables as well as pressure and temperature. However, as the

[1] R. E. Barieau, J. Am. Chem. Soc. **72**, 4023 (1950).
[2] F. G. Brickwedde and L. H. Brickwedde, Phys. Rev. **60**, 172 (1941).
[3] J. C. M. Li, J. Chem. Phys. **19**, 1059 (1951).
[4] R. E. Barieau, J. Chem. Phys. **21**, 1827 (1953).

temperature changes, the only concentration variables which may be permitted to change are those arising from redistribution of material among the different phases. In this case, therefore, all concentration variables except $c_0$ are independent of temperature. One then writes

$$d\Delta F/dT=(\partial\Delta F/\partial T)+(\partial\Delta F/\partial c_0)_T(dc_0/dT)$$
$$=-\Delta S+(\partial\Delta F/\partial c_0)_T(dc_0/dT) \quad (7)$$

($d\Delta F/dq=0$ since $\mu_0$ is equal in the two phases).

In order that the entropy change of the reaction be given by the temperature coefficient of electromotive force of the cell, it is necessary that the second term be zero. If there is zero temperature coefficient of the solubility of the solid phase then $d\Delta F/dT$ gives the correct $\Delta S$ regardless of the value of $q$, and one would have to ask about the higher derivatives such as $\Delta C_p$ to determine the correct value of $q$. In general, however, $dc_0/dT$ is not zero and the equation determining $q$ is therefore $(\partial\Delta F/\partial c_0)_T=0$, or

$$\sum_{j=1}^{m}\nu_j(\partial\mu_j/\partial c_0)_T+q(\partial\mu_0/\partial c_0)_T=0, \quad (8)$$

or

$$q=-\sum_{j=1}^{m}\nu_j(\partial\mu_j/\partial\mu_0)_T. \quad (9)$$

This corresponds to the result obtained by Li.[3] It should be emphasized that in the partial derivative $(\partial\mu_j/\partial\mu_0)_T$ all concentration variables except $c_0$ are held constant. The equivalence of (9) and (5) is readily shown. One may write the Gibbs-Duhem equation

$$c_0+(\partial\mu_1/\partial\mu_0)+\sum_{j=2}^{m}c_j(\partial\mu_j/\partial\mu_0)_T=0. \quad (10)$$

Substituting (10) in (9) one obtains

$$q=c_0\nu_1-\sum_{j=2}^{m}(\nu_j-c_j\nu_1)(\partial\mu_j/\partial\mu_0)_T. \quad (11)$$

From the definition of partial molal quantities

$$(\partial\mu_j/\partial c_0)_T=(\partial\mu_0/\partial c_j)_T.$$

Therefore

$$(\partial\mu_j/\partial\mu_0)_T=(\partial\mu_0/\partial c_j)_T/(\partial\mu_0/\partial c_0)_T$$
$$=-(\partial c_0/\partial c_j)_{T,\,\mu_0}. \quad (12)$$

Substituting (12) in (11) one obtains (5).

The cell treated by Li[3] has been criticized by Barieau[4] because in it there would be an irreversible reaction of hydrogen gas and copper sulfate. As an example we shall choose a cell* which does not suffer from this defect, but has the characteristic present in Li's cell that there is more than one concentration variable in the aqueous phase. Consider the cell $H_2(g)\,|\,HCl(c_2)$, NaCl (sat)$\,|\,$NaCl, AgCl, Ag. The reaction may be written

$$H_2(g)+2AgCl(s)-qNaCl(c_0)+qNaCl(s)$$
$$=2HCl(c_2)+2Ag(s)$$

where $c_0$ and $c_2$ are concentrations (moles per mole water) in the aqueous phase of NaCl and HCl, respectively. The other component (water) is designated by the subscript 1. Then $\nu_0=0$, $\nu_1=0$, $\nu_2=2$, and from Eq. (5)

$$q=2(\partial c_0/\partial c_2)_{T,\mu_0}. \quad (13)$$

The equivalent expression from (9) is

$$q=-2(\partial\mu_2/\partial\mu_0)_{T,c_2}. \quad (14)$$

In contrast to Eq. (14), Eq. (13) is in a form convenient for the introduction of experimental data since by using it $q$ may be calculated from measurements of the solubility of NaCl in solutions of varying HCl concentration.

The extension of the above treatment to cells where additional pure solid phases are present is not difficult. When a solid phase of variable composition is present, as is the case with two-phase amalgam electrodes, the method suggested by Li becomes more complicated since the variations of composition variables in the two phases are not independent. In all cases the method of Barieau is simpler and more direct and the results appear in a convenient form.

Barieau[1] noted that in the cases considered by him the correct reaction involved total phase so that the change in thermodynamic properties could be written as differences between total quantities for the various phases rather than involving partial molal quantities. This is because in his examples the number of phases in equilibrium is equal to the number of components and so at constant pressure and temperature the composition of the phases must remain constant if they are to remain in equilibrium as the cell discharges. Therefore total quantities of the equilibrium phase concentrations must be used up or produced. In fact the correct equation in all the cases treated by Barieau may be immediately written down by requiring that total quantities are involved and that the reaction be balanced. When, however, the number of components exceeds the number of phases, as in the example treated in this paper, then the composition of the phases may change as the cell discharges and partial molal quantities are involved in the change of thermodynamic quantities.

* I am indebted to Dr. R. E. Barieau for suggesting this cell.

# Surface Migration of Water Molecules in Ice

E. J. MURPHY
*Bell Telephone Laboratories, Inc., Murray Hill, New Jersey*
(Received March 16, 1953)

This paper continues the discussion of data given in a previous paper on the second term in the "local conductivity" of ice. It is inferred that the $H_2O$ molecules in internal surfaces are engaged in a special kind of random walk, in which the molecule is always attached to the surface by one chemical bond. This is described as bipedal random walk. It occurs with an activation energy of 5.2 kcal/mole (0.23-electron volt per molecule). On the other hand, molecules which jump up into field-free space and return to the surface have to acquire an energy of 11.5 kcal/mole (0.5 ev/molecule). The ratio of the corresponding Boltzmann factors is about $10^{-5}$ at 0°C and about $10^{-8}$ at −100°C; this implies that the dominant mode of diffusion in internal surfaces in ice is bipedal random walk.

The migration of a water molecule on an ice surface is a special type of diffusion process. The general formulas of the theory of stochastic processes and diffusion become available for the description of the diffusion of water molecules in a surface if the appropriate expression for the diffusion constant $D$ is substituted in the formulas. A new procedure is used to calculate $D$ from the Einstein relation. Instead of using the direct-current conductivity, the second term of the local conductivity is used. The expression for the diffusion constant derived from the model for local conductivity is $D_L=3.5\times10^{-4}\exp(-5.2\times10^3/RT)$ cm²/sec, where the activation energy $5.2\times10^3$ cal/mole, is derived from the second term in the local conductivity of ice. This leads to a rather explicit model of the diffusion process: it may be described as bipedal random walk of the water molecule by the breaking of one bond at a time with an activation energy of 0.23-electron volt associated with each step.

It is pointed out also that the water molecule on an internal surface has a polarizability characteristic of the surface structure.

## INTRODUCTION

IN a preceding paper a method of determining the concentration of molecules on internal surfaces in ice was described and illustrated.[1] The experimental relations described there will be used here to derive further information regarding the conditions prevailing in surfaces, internal or external.

A part of the significance of the present discussion lies in showing that while a surface has a crystalline structure, its molecules are in a state of rather active continual migration—an internal surface can be pictured as having a great deal more migrational activity than the homogeneous parts of the crystal. The quantitative basis for this is derived from measurements of the activation energy for the *local conductivity* of ice.

Moreover, while it is evident that in general the molecules of a surface migrate about in some kind of diffusional motion (random flight), we attempt here to show that there is sufficient evidence in available experimental relations to reduce this general motion to a more regular motion which we describe as *bipedal random walk*.

## MODEL OF SURFACE POLARIZATION AND MIGRATION

### A. The Water Molecule on an Ice Surface

When we picture how a water molecule is attached to an internal surface in ice, some interesting things appear. The water molecule is a tetrahedral structure with an oxygen atom at the center, a proton at each of two vertices, and centers of negative charge at the other two vertices.[2] (This structure is derived mainly from infrared spectra and from the electric moment of the $H_2O$ molecule.) Each proton can then form a hydrogen bond to a complementary point or spot on an adjacent molecule. For the present purpose no features of the structure of the water molecule are needed other than that it is attached to the "surface" of the ice by *two* geometrically distinct chemical bonds and that it has an electric moment different from zero.

### B. A Characteristic Surface Polarization

Such a molecule can pivot on the one bond while the other bond dances back and forth between two attracting points on the surface at each of which it forms momentarily a hydrogen bond. During this oscillation the molecule is contributing to the second term of the local conductivity. The activation energy for this process is 5.2 kcal/mole, or 0.23 ev per molecule. The distance moved by the proton in the oscillatory motion may be assumed to be about 0.78A, that is, about the same distance as in the interior of the crystal. Therefore, the conduction formula used in a preceding paper[3] should also apply to the local conductivity contributed by this type of motion, but the concentration factor ($n$) will, of course, be much smaller than the total number of hydrogen bonds per cc.

### C. Comparison with Orientational Polarization and Interfacial Polarization

The polarization process described above may also be put in terms of the effect of the applied field upon the distribution of the orientations of the electric moment vectors of the surface molecules as they step from one point of attachment to the surface to the next. Since the internal surfaces are oriented at random with respect to the direction of the applied field, the distribution of the orientations of the molecules can be influenced by it in much the same way as in the Debye theory for the

[1] E. J. Murphy, J. Chem. Phys. **19**, 1516 (1951).
[2] See Bernal and Fowler, J. Chem. Phys. **1**, 515 (1933).
[3] E. J. Murphy, Phys. Rev. **79**, 396 (1950).

polarization due to free polar molecules. In fact, this polarization is a special type of *orientational polarization.*

The *internal surface polarization* which we have been discussing is, however, quite different from *interfacial polarization* or *Maxwell-Wagner polarization* (with which it might be confused). The latter is not a molecular polarization: it has its origin in the existence of differences between the conductivities or dielectric constants (or both) of different parts of the dielectric; thus its properties are determined by the properties of the different homogeneous parts of a heterogeneous system. The internal surface polarization, on the other hand, is a molecular polarization; it derives its properties from the characteristics of the structure of the internal surface itself. Its properties refer both to the static or average aspects of structure and to the lability or local mobility of the surface structure.

### D. Migration by Bipedal Random Walk

The two hydrogen bonds of the $H_2O$ molecules are completely equivalent. Therefore, after the molecule has

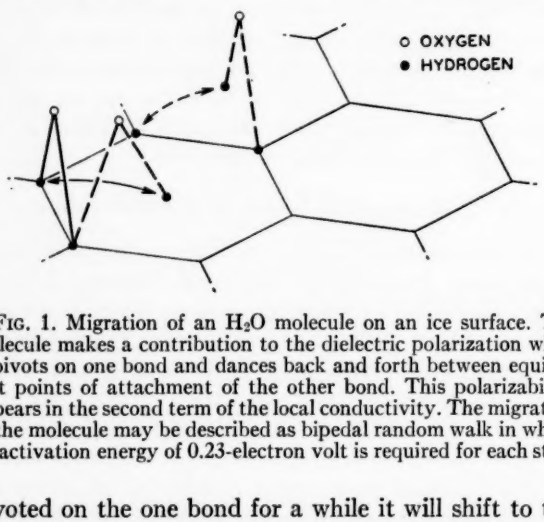


FIG. 1. Migration of an $H_2O$ molecule on an ice surface. The molecule makes a contribution to the dielectric polarization while it pivots on one bond and dances back and forth between equivalent points of attachment of the other bond. This polarizability appears in the second term of the local conductivity. The migration of the molecule may be described as bipedal random walk in which an activation energy of 0.23-electron volt is required for each step.

pivoted on the one bond for a while it will shift to the other. Though the molecule is a tetrahedral structure, it will be convenient for our present purpose to confine attention to two of the vertices and picture it as a triangular molecule. (This is simply to avoid unnecessary complication.) Then the motion of the triangular molecule on the surface is similar, for example, to the motion of a draughtsman's dividers on a sheet of paper when it is pivoted first on one leg (bond) and caused to oscillate between two fixed points with the other. If the dividers are placed at the points of intersection of a triangular net or two-dimensional lattice as in Fig. 1 and the dividers span the distance between adjacent lattice points, all lattice positions are accessible to the dividers (molecule) without change of its radius (angular distance between bonds). Similarly, the $H_2O$ molecule can move about on an ice surface by pivoting alternately on the one bond and then on the other, and all parts of the surface are accessible to the molecule by this type of motion.

This is, in fact, essentially the motion of a biped in walking. This comes about because a biped has certain rigidities of structure which admit only certain motions. The motion of the biped, the motion of the dividers, and the motion of the molecule on a surface are all abstractly equivalent; they are realizations of a general type of motion which we may describe as *bipedal random walk.*

The triangular or bipedal molecule is engaged in a random walk motion in two senses: first, the motion is actually abstractly equivalent, as has just been said, to a general bipedal walking motion; and second, it is random walk in the sense of the theory of stochastic processes.[4] It is a special kind of random walk of the surface molecule which specifies in some detail one of the ways by which diffusion takes place in this type of surface structure. *In this type of random walk each step requires a definite activation energy. In the present case the value of the activation energy is known (0.23 ev per molecule), and the physical process with which it is associated has been demonstrated to correspond to the breaking of one hydrogen bond.* Later on we shall discuss briefly the relation of bipedal random walk to other diffusion processes.

### E. Structure of the Surface

The bonding points or spots on the internal surface are arranged in a way corresponding to the symmetries of the internal structure of the crystal. But the arrangement in the surface is actually not the intersection of the internal structure with some plane "surface" to which the molecules are attached—for no plane surface is involved, nor any other continuous surface for that matter, but merely a set of discrete points or spots on the water molecules in the crystal. With this picture in mind, we see that the motion of the molecule in an actual physical "surface" (as distinguished from a continuous geometric surface) is equivalent to that of a biped walking on stepping stones arranged in a three-dimensional space in which there is no gravitational field. These "stones" are arranged tetrahedrally in the space, and we can imagine the biped (molecule) as proceeding in a gingerly way by moving one leg back and forth several times between adjacent stones before changing to the new "stone" (bonding point) and the other "leg" (bond). During a similar motion on the part of the molecule, it is contributing to the second term in the local conductivity. *The polarization associated with this term in the local conductivity is characteristic of the molecular structure of the surface;* we may call it the *internal surface polarization.*

## THE DOMINANT TYPE OF SURFACE MIGRATION OR DIFFUSION

An important aspect of bipedal random walk is the fact that the molecule can "step" or rotate from one lattice point to the next neighboring one, proceeding in this way all over the internal surface (or for that matter

[4] S. Chandrasakar, Revs. Modern Phys. **15**, 1 (1943).

over an external surface), without ever breaking two bonds simultaneously, because the two bonds of the molecule span exactly the space between corresponding points in the lattice (see Fig. 1). As the probability of two independent events is the product of their individual probabilities, and the probability of the breaking of a hydrogen bond is given by a Boltzmann factor, the activation energy for the simultaneous breaking of two hydrogen bonds is twice that for the breaking of one bond. Consequently, the kind of diffusional motion which should predominate in an internal surface is bipedal random walk.

The basis for this in quantitative terms is as follows: When two bonds of a surface molecule break simultaneously, the molecule has acquired the heat of sublimation and is in the vapor state. But the relative frequency of this occurrence ($p_{vap}/p_{bip}$) in the case of ice is given approximately by the ratio of the Boltzmann factors for the two states, namely,

$$p_{vap}/p_{bip}=C[\exp(-11.5\times10^3/RT)]/[\exp(-5.2\times10^3/RT)]. \quad (1)$$

$C$ is a constant which will be discussed later on. At 0°C this fraction has approximately the value $10^{-5}$ and at −100°C about $10^{-8}$. The fraction $p_{vap}/p_{bip}$ represents the ratio of the number of surface molecules in the *vapor state* to the number of surface molecules in the *state of bipedal random walk*. This calculation shows that the dominant mode of migration in the surface is random walk by molecules attached by one bond to the surface (bipedal random walk), rather than by the random flight of molecules going into the vapor state and later recombining with the surface.

There is another mode of migration which should be discussed in this connection; it may be described, to be consistent in terminology, as unipedal migration. This is just hopping from one point of attachment to the lattice to an adjacent one. By definition it involves the breaking of all bonds to the surface simultaneously. It is similar to vaporization followed by recondensation on the surface, except that the point of reattachment in the latter case may be remote from the initial point of attachment. The ratio $p_{uni}/p_{bip}$ of the number of molecules in the state of unipedal migration to those in the state of bipedal migration is

$$p_{uni}/p_{bip}=[(\exp(-11.5\times10^3/RT)]/[\exp(-5.2\times10^3/RT)]. \quad (2)$$

This gives essentially the same ratios as Eq. (1).

There is an approximation in the two calculations made in Eqs. (1) and (2). The population of molecules in the vapor state depends not only upon the energy difference between the two states but on the volume available to the molecule in the vapor state. This factor was represented in Eq. (1) by the constant $C$. In small internal surfaces the volume available to molecules which have evaporated into the comparatively field-free space associated with the surface would only be larger by a small factor than the volume available to the molecule while it is in the surface. Therefore, it was simply assumed that $C$ is small as compared with the exponential factors in Eq. (1). This introduces no essential error since we are at present only concerned to show which mode of migration is the dominant one, rather than to obtain the exact ratios of their contributions. In Eq. (2) the volume factors for unipedal and bipedal migration may be considered to be essentially equal; therefore we let $C=1$.

The conclusion from the above discussion is that random walk with one bond attached to the surface (bipedal random walk) is the dominant mode of migration in internal surfaces in ice. It dominates over both hopping by the breaking of two bonds and evaporation and recondensation as a mode of transport. This should also apply to external surfaces if surface diffusion is suitably restricted by definition.

### Activity in Internal Surfaces

On account of the comparatively high lability and diffusional mobility in internal surfaces, we may picture them as places in the crystal where there is a considerable amount of translational motion going on continually; they are, in a sense, especially busy places. Conditions in internal surfaces may be described as being halfway between the liquid state and the crystalline state, because the molecules are attached to the surface by only one chemical bond, for ice the energy of liquefaction (solid to surface liquid) is about 5.2 kcal/mole. The molecules on internal surfaces in freshly formed ice are therefore engaged in an annealing process in which the form of the internal surface is changing toward the form corresponding to thermodynamical equilibrium in the crystal structure of ice. If the internal surface is small, it should also migrate in the crystal with a Brownian motion of significant magnitude, for when a molecule moves from one end of the surface to another, the volume enclosed by the surface moves in the opposite direction in the crystal. The activation energy for the mobility of these small surfaces in their Brownian motion is equal to the activation energy derived from the second term in the local conductivity. It is due to the breaking of one hydrogen bond and has the value 0.23-electron volt per molecule.

## RELATION TO DIFFUSION IN GENERAL

### A. A Sequence of Increasing Specialization of the Model

The model we have described here may be regarded for heuristic convenience as a result of a sequence of steps, each increasing the specialization of the model of the process of diffusion. The motions involved in the formation of the orientational polarization of a free molecule (the Debye theory) involve essentially random flight. The molecule experiences random flight in the coordinates of its center of gravity and also in three

angles, that is, the uncorrelated increments in the three Euler angles. When the molecule becomes attached to a surface lattice, random flight is reduced to random walk; the steps are now of equal length, determined by the binding points in a regular lattice. This is the first step in the specialization of the diffusion process.

The second step is to associate an activation energy with the diffusion process. In general, the solutions of the diffusion equation and of related equations, contain the diffusion constant $D$. Theories involving the diffusion process often extend, for example, only to expressing $D$ as a function of the macroscopic viscosity and the radius of the particle, using Stokes' law. However, the data for the second term in the local conductivity of ice enable us to associate an activation energy with surface diffusion, namely, 0.23-electron volt per $H_2O$ molecule. It is an advance in the analysis of a process when we can substitute an activation energy for a viscosity; but so long as the activation energy is itself an empirical constant, it is not a large advance.

The third step is the identification of the source of the empirical activation energy with a definite physical process, the breaking of a chemical bond. The experimental relation which enables us to do this is the numerical coincidence between the activation energy for local conductivity and the heat of sublimation of ice.[5] This also employs the fact that the heat of sublimation of ice has been shown to be largely accounted for by the breaking of hydrogen bonds. Moreover, the model[1,3] used in the interpretation of the local conductivity also enters in an essential way into the identification which makes it possible to say that the diffusion process in a surface of ice depends upon the breaking of one hydrogen bond.

The fourth step is the one taken here, namely, making use of the tetrahedral structure of the water molecule to show that there are two geometrically distinct bonds to the surface—rather than a single bond of twice the strength. This has led to the conclusion that surface migration is predominantly bipedal random walk, rather than a hopping motion or a general vaporization-recondensation process. The surface molecules migrate by stepping to the *nearest* lattice point; this gives the migration about as much regularity as it can have and still be random walk. (The regularity of surface diffusion is of interest, for example, in connection with crystal growth.) There is a fifth step in this sequence, but it will be necessary to discuss the relation of mobility to diffusion in more detail before stating it.

### B. The Einstein Relation Applied to Local Mobility

The mobility $\mu$ is derived ordinarily from the direct-current conductivity. The diffusion constant $D$ can then be calculated by means of the Einstein relation

$$D=kT\mu/e. \tag{3}$$

This relation is so general that it imposes only weak restrictions on the model; it can be applied to diffusion of many kinds.

Let us now apply the Einstein relation to the local mobility $\mu_L$ derived from the local conductivity $\sigma_p$ by the relation

$$\mu_L=9\times10^{11}\sigma_p/ne. \tag{4}$$

In this expression, $n$ is the concentration of surface molecules and $e$ the elementary charge. The constant $9\times10^{11}$ converts $\sigma_p$ from (ohm cm)$^{-1}$ to esu. (The elementary charge $e$ appears in this expression, though the molecule is neutral, because of the nature of the model for the local conductivity.) We now have

$$D_L=kT\mu_L/e \tag{5}$$

for the diffusion constant as calculated from the local conductivity.

The expression for the local conductivity is

$$\sigma_p=[ne^2d^2\exp(-W/kT)][9\times10^{11}h]^{-1} \tag{6}$$

on the basis of the model which we have used in the study of ice.[1] Substituting this expression in Eq. (4), we have

$$\mu_L=h^{-1}ed^2\exp(-W/kT), \tag{7}$$

and for $D_L$ we have

$$D_L=h^{-1}kTd^2\exp(-W/kT)$$
$$=2.12\times10^{10}Td^2\exp(-W/kT). \tag{8}$$

We may substitute into this expression the following numerical values appropriate to ice: $T=273°C$, $d=0.78\times10^{-8}$ cm, and the ratio $W/kT=5.2\times10^3/RT$. This gives

$$D_L=3.5\times10^{-4}\exp(-5.2\times10^3/RT)\ \text{cm}^2/\text{sec} \tag{9}$$

for the local diffusion constant of ice in internal surfaces (and in external surfaces under suitable restrictions). This can be written in the form $D_L=D_0\exp(-W/kT)$. $D_0$ then has the value $3.5\times10^{-4}$ cm$^2$/sec. This "constant" varies with $T$, but in the range of temperatures with which we are usually concerned this variation is small as compared with the variation in $D_L$ due to the exponential factor. The value of $D_0$ is sensitive to variations in $d$ the length of the unit step. It is interesting that $D_L$ depends mainly on the activation energy and $d$.

The calculation of a diffusion constant by putting the *local* conductivity rather than the ordinary direct-current conductivity (the migrational conductivity) into the Einstein relation, is a new procedure, and it will be desirable to discuss its meaning. The physical significance of local conductivity has been discussed at considerable length in a preceding paper[6] where it was called the "polarization conductivity." The local conductivity measures the local mobility involved in the formation of a dielectric polarization. In the model which we have used to explain the data for the local

[5] E. J. Murphy, Phys. Rev. **79**, 203 (1950).

[6] E. J. Murphy and S. O. Morgan, Bell System Tech. J. **38**, 502 (1939).

conductivity of ice, it depends upon the local translational motion of a proton between two sites $0.78\times10^{-8}$ cm apart. This activation energy for local mobility is a quantity which can be associated with *each step* in the random walk process. The diffusion constant $D$ calculated from direct-current conductivity measurements can only be associated with each step by assuming that the steps are alike or by ascribing to each the average value. The two procedures should in many cases reach the same result. The local conductivity method gives a sharper picture of the diffusion process; or at least reaches it more directly.

### C. Random Walk with an Activation Energy for Each Step

In order to make this statement more definite, let us picture random walk more explicitly. Consider the integers to be arranged on a line with equal spacing ($d$) between them, and let a particle be associated with one of them, say $i_0$. Let this particle be able to jump forward or backward by one integer at a time. Let the probability of jumping forward be some definite number $p$; that of jumping backward is then $1-p$. There is then a definite probability that the particle starting from an initial position $i_0$ will be found after a specified time $t$ to be associated with another selected integer $i_n$. This is a discrete random walk process. In the case described above the discrete steps are on a line, but there is no change in principle if the steps occur between points arranged in a lattice of two or more dimensions. Thus the bipedal migration of a water molecule on a surface of lattice points is a discrete random walk process to which the general theory of stochastic processes applies.

It has been shown in the theory of stochastic processes that discrete random walk leads in the limit of arbitrarily large number of steps to the same expressions as are obtained from the solution of the diffusion equation.[7,8] Moreover, it has been shown that the difference equation which expresses discrete random walk becomes, in the limit of continuous variables, the differential equation for diffusion. In consequence of this, it is only necessary for us to substitute the expression for $D_L$ given in Eq. (9) for $D$ wherever it appears in the solutions of the diffusion equation for given boundary conditions, in order to have available expressions for diffusion in ice surfaces, based upon the underlying general theory of diffusion together with the special model which has been described here. For example, in the transport of water molecules by diffusion in a concentration gradient, we have

$$\frac{\partial P}{\partial t}=D\left(\frac{\partial^2 P}{\partial x^2}+\frac{\partial^2 P}{\partial y^2}+\frac{\partial^2 P}{\partial z^2}\right), \tag{10}$$

where $P$ is a probability function, or alternatively a concentration function, and we substitute the expression given for $D_L$ in Eq. (9) for $D$ in the solutions of Eq. (10).[4]

[7] See reference 4, p. 5.
[8] See M. Kac, Am. Math. Soc. Monthly **54**, 369 (1947).

Similarly, for diffusion in a constant field or in an harmonically varying field, we can substitute the expression for $D_L$ given in Eq. (9) for $D$ in the solutions of the appropriate differential equations.

The fifth step in specializing the picture of the diffusion process in ice surfaces is now evident. Since $D_L$ is calculated from the *local* conductivity, we can associate with *each step* in the diffusion process an activation energy of 0.23-electron volt.[9] We may picture this activation energy as determining the time that the molecule is in a state of "indecision" as to when and in which direction to take the next step. In this we assume that the time of indecision is long as compared with the time of action. The time of indecision represents the time of waiting for a fluctuation which breaks a hydrogen bond.

## CONCLUDING DISCUSSION

The theory of surface migration of water molecules which has been developed here is based upon the study of the local conductivity (or polarization conductivity) of ice. It depends primarily on the fact that the local conductivity of ice exhibits two terms, and that the activation energy for the second term is about one half of that for the first term. (This is interpreted by considering that the $H_2O$ molecule in the interior is held in place by four hydrogen bonds while the $H_2O$ molecule in the surface is held in position by only two bonds.) Three other experimental relations are used in developing the model. One of them is the fact that the activation energy for the main term in the local conductivity of ice is about equal to the heat of sublimation of ice, and that this in turn is the energy for the breaking of two hydrogen bonds per molecule (or four bonds between the molecule and its environment). A second consideration refers to the nature of local conductivity as contrasted with the direct-current conductivity: the activation energy for local conductivity is the activation energy for mobility. (This will be discussed further in another place.) The fourth experimental relation used in the model is the evidence (from x-ray diffraction, infrared absorption, and chemical properties) that the bonds between molecules have tetrahedral symmetry, so that a walking type of motion is available to the molecule by the alternate breaking of two distinct bonds.

These considerations have lead to a rather sharply defined model for the diffusion of water molecules in surfaces. Each step in the increasing specialization of the model represents an independent experimental relation. The several aspects of the model should therefore have recognizable consequences when the present theory of surface migration of water molecules is applied to various physical processes. The theory derived for ice should apply in principle, and perhaps even reasonably quantitatively, to the diffusion of water in any surface to which the water molecules are attached by hydrogen bonds.

[9] See reference 1 (footnote §) with regard to the accuracy of the value 0.23 ev.

# The Fundamental Absorption Bands in the Infrared Spectrum of Phosphine*

V. M. McConaghie and H. H. Nielsen
*Department of Physics and Astronomy, The Ohio State University, Columbus, Ohio*

(Received January 12, 1953)

The four fundamental bands in the infrared spectrum of $PH_3$ have been analyzed. The bands $\nu_1$ and $\nu_3$ yield values of $B^{(xz)}$ and $[(1-\zeta_2^{(z)})B^{(xz)}-B^{(xz)}]$ as well as values for the centers of the bands. The method of Nielsen for arriving at explicit expressions for the rotation term values of $\nu_2$ and $\nu_4$ has permitted the evaluation also of the quantity $(1-\zeta_4^{(z)})B^{(xz)}$ and to infer the centers of these bands. The structure of the molecule has been derived from this information and the zeta sums. The PH distance $r_0$ obtained is equal to 1.42A, and the H−P−H angle is equal to 93° 50′.

## I. INTRODUCTION

THE fundamental bands in the infrared spectrum of phosphine, two of which lie near 4.2$\mu$ and two of which lie near 10$\mu$, were studied first by Robertson and Fox[1] using a prism spectrometer. Subsequently the spectrum was remeasured by Fung and Barker[2] who used a prism-grating spectrometer. More recently these bands have been studied in this laboratory with still higher resolving power, using a vacuum grating instrument.[3] We shall here report more fully on this work and evaluate certain of the constants of the molecule from the data obtained.

## II. EXPERIMENTAL DETAILS

The phosphine used in this experiment was generated in an atmosphere of nitrogen by dropping water slowly on to calcium phosphide contained in a 300-cc round-bottom flask. The phosphine generated was passed through successive tubes containing calcium chloride and phosphorous pentoxide and finally into a condenser immersed in liquid air. A calcium chloride drying tube and a gas bubbler containing copper sulfate solution was connected to the exit of this trap. The phosphine was purified by fractional distillation using a method described by Durrant, Pearson, and Robinson,[4] the distillation, in this instance, taking place with the condenser immersed in a dry-ice bath.

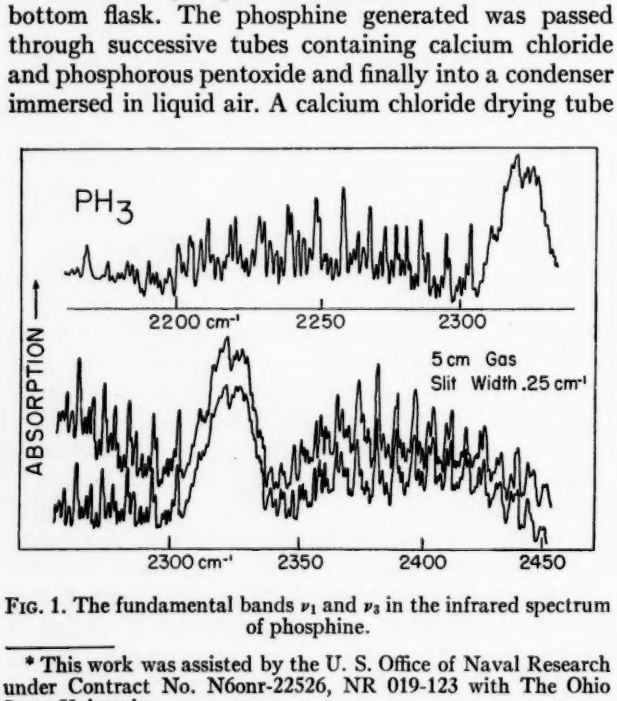


FIG. 1. The fundamental bands $\nu_1$ and $\nu_3$ in the infrared spectrum of phosphine.

The spectrograph used was the vacuum grating instrument described by Bell, Noble, and Nielsen.[5] A vacuum spectrograph was most advantageous in examining the 4.2$\mu$ region which overlaps badly with the atmospheric $CO_2$ fundamental band $\nu_3$. Two replica echellette gratings made by Wood were used to measure the bands reported here. The one, used to study the 4.2$\mu$ region, had 7500 lines per inch; the other, used to examine the 10$\mu$ region, had 3600 lines per inch. Throughout slit widths were maintained which subtended a frequency interval of about 0.3 cm$^{-1}$.

## III. DISCUSSION OF THE DATA

### The 4.2$\mu$ Region

Figure 1 shows the region near 4.2$\mu$ which has been redrawn from the original records. Two separate recordings over a portion of this region are shown to illustrate the extent to which the data were reproducible. This region is interpreted to be due to the two fundamental bands $\nu_1$ and $\nu_3$, the first of which is a parallel band and the second of which is a perpendicular band. The frequencies $\nu_1$ and $\nu_3$, while coupled through a Coriolis interaction, perturb each other only very slightly.[6] One may, therefore, proceed to analyze them by standard methods. The frequency positions of the more important lines in this region, reduced to vacuum, are given in Table I, in particular those which were used to obtain the molecular constants. The identifications given to the lines are set down in the first, third, and fifth columns in Table I.

Many of the lines in the $P$ and $R$ branches of $\nu_1$ overlap with lines belonging to the band $\nu_3$, and the positions of these cannot, therefore, be determined with high accuracy. This is particularly true in the instances of $P(12)$, $P(11)$, and $R(2)$ which have been indicated in the table with asterisks. The values of $B^{(xz)''}$ and $B^{(xz)'}$ are

* This work was assisted by the U. S. Office of Naval Research under Contract No. N6onr-22526, NR 019-123 with The Ohio State University.

[1] R. Robertson and J. J. Fox, Proc. Roy. Soc. (London) **A120**, 128 (1928).

[2] L. W. Fung and E. F. Barker, Phys. Rev. **45**, 238 (1934).

[3] V. M. McConaghie and H. H. Nielsen, Proc. Natl. Acad. Sci. U. S. **34**, 455 (1948).

[4] Durrant, Pearson, and Robinson, J. Chem. Soc. **28**, 730 (1934).

[5] Bell, Noble, and Nielsen, Rev. Sci. Instr. **18**, 48 (1947).

[6] H. H. Nielsen, J. Chem. Phys. **21**, 142 (1953).

obtained by application of the usual combination relations; the differences having been corrected for centrifugal distortion. The centrifugal distortion constant $D_J$ which has been used in this correction is the one obtained by Wright and Randall[7] from their measurements on the rotation spectrum. The values obtained for $B^{(xz)''}$ and $B^{(xz)'}$ are the following: $B^{(xz)''}=4.45$ cm$^{-1}$ and $B^{(xz)'}=4.39$ cm$^{-1}$. The value obtained for $B^{(xz)''}$ here we shall regard as in satisfactory agreement with the value 4.446 cm$^{-1}$ given by Wright and Randall. The latter value, which is undoubtedly more accurate than the one given by us, will be used hereafter in our calculations. The following value for the band center, $\nu_1=2322.9$ cm$^{-1}$, is obtained from the combination relations.

The lines comprising the $^PP$ and $^RR$ branches of the perpendicular band $\nu_3$ are difficult to identify because they overlap the $P$ and $R$ lines of $\nu_1$ badly in many cases. An attempt has, nevertheless, been made to make such an assignment, but the positions of the lines can in many instances not be established with great precision.

TABLE I. Frequency positions and identifications of lines in the bands $\nu_1$ and $\nu_3$.

| | | | | | |
|---|---|---|---|---|---|
| $P(12)$* | 2209.7 | $^PP(5,1)$ | 2284.5 | $^RR(5,4)$ | 2376.3 |
| $P(11)$* | 2219.6 | $^PP(5,2)$ | 2286.1 | $^RR(5,3)$ | 2377.3 |
| $P(10)$ | 2229.0 | $^PP(5,3)$, $P(4)$ | 2287.0 | $^RR(5,2)$ | 2378.3 |
| $P(9)$ | 2238.9 | $^PP(5,4)$ | 2288.5 | $^RR(5,1)$ | 2379.1 |
| $P(8)$ | 2248.8 | $^PP(4,1)$ | 2292.5 | $^RR(5,0)$ | 2380.7 |
| $^PP(8,2)$ | 2255.5 | $^PP(4,2)$ | 2294.0 | $^RR(6,6)$, $R(6)$ | 2382.3 |
| $P(7)$ | 2258.2 | $^PP(4,3)$ | 2295.2 | $^RR(6,5)$ | 2383.0 |
| $^PP(8,3)$ | 2258.9 | $P(3)$ | 2295.6 | $^RR(6,4)$ | 2384.7 |
| $^PP(8,4)$ | 2260.7 | $P(2)$ | 2304.0 | $^RR(6,3)$ | 2385.0 |
| $^PP(8,5)$ | 2261.7 | $P(1)$ | 2314.0 | $^RR(6,2)$ | 2386.6 |
| $^PP(8,6)$ | 2263.3 | $R(2)$* | 2349.0 | $^RR(6,1)$ | 2387.6 |
| $^PP(8,7)$ | 2265.0 | $R(3)$ | 2357.1 | $^RR(7,7)$, $^RR(6,0)$ | 2389.1 |
| $^PP(7,1)$ | 2265.5 | $^RR(3,3)$ | 2359.2 | $^RR(7,6)$, $R(7)$ | 2390.2 |
| $^PP(7,2)$, $P(6)$ | 2267.6 | $^RR(3,2)$ | 2360.4 | $^RR(7,5)$ | 2391.4 |
| $^PP(7,3)$ | 2268.4 | $^RR(3,1)$ | 2361.4 | $^RR(7,4)$ | 2392.9 |
| $^PP(7,4)$ | 2270.5 | $^RR(3,0)$ | 2362.8 | $^RR(7,3)$ | 2394.8 |
| $^PP(7,5)$ | 2271.5 | $R(4)$ | 2365.5 | $^RR(7,2)$ | 2395.8 |
| $^PP(7,6)$ | 2272.8 | $^RR(4,4)$ | 2366.5 | $^RR(7,1)$ | 2397.1 |
| $^PP(6,1)$ | 2275.5 | $^RR(4,3)$ | 2367.8 | $R(8)$ | 2397.9 |
| $^PP(6,2)$, $P(5)$ | 2277.0 | $^RR(4,2)$ | 2369.5 | $R(9)$ | 2405.5 |
| $^PP(6,3)$ | 2278.0 | $^RR(4,1)$ | 2370.8 | $R(10)$ | 2413.2 |
| $^PP(6,4)$ | 2279.4 | $^RR(4,0)$ | 2371.9 | $R(11)$ | 2419.0 |
| $^PP(6,5)$ | 2280.9 | $R(5)$ | 2373.8 | $R(12)$ | 2426.8 |
| | | $^RR(5,5)$ | 2374.8 | | |

No attempt to identify the $^PR$ and $^RP$ lines has been made since, in general, these may be expected to be weak. The $^RR$ and $^PP$ lines occur here, more or less, in groups. Each group has a common $J$ value and consists of $J+1$ components. The frequency of a line within a group in the $^RR$ branch will be designated as $^RR(J-1,K)$, and the frequency of a line within the $^PP$ branch will be designated by $^PP(J,K)$. Their frequencies will be approximately

$$^RR(J-1,K)=\nu_0-[B^{(zz)}-B^{(xz)}]+2JB^{(xz)}+2(K+1)[(1-\zeta_3^{(z)})B^{(zz)}-B^{(xz)}] \quad (1)$$

and

$$^PP(J,K)=\nu_0-[B^{(zz)}-B^{(xz)}]-2JB^{(xz)}-2(K-1)[(1-\zeta_3^{(z)})B^{(zz)}-B^{(xz)}]. \quad (2)$$

Taking the difference $^RR(J-1,K)-^PP(J,K)$, one obtains

$$^RR(J-1,K)-^PP(J,K)=4JB^{(xz)}+4K[(1-\zeta_3^{(z)})B^{(zz)}-B^{(xz)}]. \quad (3)$$

If the differences (3) are divided by $4J$ and then plotted against $(K/J)$, a straight line will result of which $[(1-\zeta_3^{(z)})B^{(zz)}-B^{(xz)}]$ will be the slope and of which $B^{(xz)}$ will be the intercept. Such a graph has been prepared using the values of $J=4$, 5, 6, 7, and 8. This is shown in Fig. 2 and from this the values $[(1-\zeta_3^{(z)})B^{(zz)}-B^{(xz)}]=-0.6$ and $B^{(xz)}=4.445$ cm$^{-1}$ are obtained. The value of $B^{(xz)}$ obtained here must be regarded as in satisfactory agreement with those obtained earlier, when one considers that again here the accuracy of the frequency positions of the $^RR$ and $^PP$ lines is reduced by the overlapping of the bands $\nu_1$ and $\nu_3$. The sum of (1) and (2) will be seen to be equal to

$$\tfrac{1}{2}[^RR(J-1,K)+^PP(J,K)]=[\nu_3-\zeta_3^{(z)}B^{(zz)}]+[(1-\zeta_3^{(z)})B^{(zz)}-B^{(xz)}]. \quad (4)$$

Using the value $-0.6$ for $[(1-\zeta_3^{(z)})B^{(zz)}-B^{(xz)}]$, one obtains the value $[\nu_3-\zeta_3^{(z)}B^{(zz)}]=2327.7$ cm$^{-1}$.

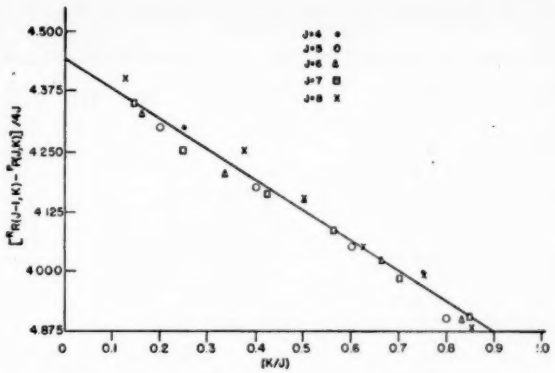


FIG. 2. The differences $^RR(J-1,K)-^PP(J,K)$ divided by $4J$ for the lines in the fundamental band $\nu_3$ in the spectrum of phosphine plotted against $(K/J)$.

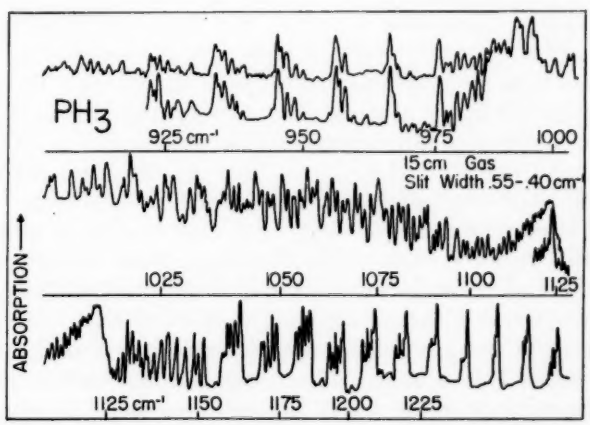


FIG. 3. The fundamental bands $\nu_2$ and $\nu_3$ in the infrared spectrum of phosphine.

[7] N. Wright and H. M. Randall, Phys. Rev. 44, 391 (1933).

TABLE II. Frequency positions and identifications of lines in the bands $\nu_2$ and $\nu_4$.

| | | | |
|---|---|---|---|
| $P(8,0)$ | 912.3 | ${}^RR(5,5)$ | 1187.4 |
| $P(7,0)$ | 923.3 | ${}^RR(6,5)$ | 1198.0 |
| $P(6,0)$ | 934.0 | ${}^RR(6,6)$ | 1198.7 |
| $P(5,0)$ | 944.4 | ${}^RR(7,6)$ | 1209.4 |
| $P(4,0)$ | 954.7 | ${}^RR(7,7)$ | 1209.7 |
| $P(3,0)$ | 964.6 | ${}^RR(8,7)$ | 1220.4 |
| $P(2,0)$ | 974.3 | ${}^RR(8,8)$ | 1220.7 |
| ${}^RR(3,2)$ | 1163.6 | ${}^RR(9,8)$, ${}^RR(9,9)$ | 1231.4 |
| ${}^RR(3,3)$ | 1164.4 | ${}^RR(10,9)$, ${}^RR(10,10)$ | 1242.7 |
| ${}^RR(4,3)$ | 1174.9 | ${}^RR(11,10)$, ${}^RR(11,11)$ | 1254.2 |
| ${}^RR(4,4)$ | 1176.3 | ${}^RR(12)$ | 1265.7 |
| ${}^RR(5,4)$ | 1186.3 | ${}^RR(13)$ | 1277.5 |

### The 8μ to 11μ Region

The two bands which comprise the region $8\mu$ to $11\mu$ in the spectrum of $PH_3$ are shown in Fig. 3. The lower-frequency band is identified as $\nu_2$ and the higher-frequency band as $\nu_4$. Two separate recordings are shown over the $P$ branch of the band $\nu_2$ with different amounts of gas. They serve to show the fidelity of the data.

The bands $\nu_2$ and $\nu_4$ are coupled by strong Coriolis interaction. The effect of this has been discussed in reference 6 and may be summarized by saying that the perturbation manifests itself in the respect that the sub-bands which make up $\nu_2$ become resolvable and that the degenerate Coriolis coupling factor, $\zeta_4^{(z)}$, must be replaced by an effective Coriolis coupling factor $(\zeta_4^{(z)})_e$ which depends upon the value of $K$. It is shown in reference 6 that the lines in $\nu_4$ which it is convenient to use to determine the quantity $(1-\zeta_4^{(z)})B^{(zz)}$ are the ${}^RR(J,J)$ and the ${}^RR(J,J-1)$ lines and that the lines $P(J,K=0)$ in the band $\nu_2$ are the ones which may conveniently be used to verify the magnitude of the Coriolis resonance interaction between $\nu_2$ and $\nu_4$. These lines in the two bands have been identified, and their frequency positions, reduced to vacuum, are given in Table II.

Straight lines will result if the frequencies of the ${}^RR(J,J)$ and the ${}^RR(J,J-1)$ lines given in Table II are plotted, respectively, against $2J$ and $2(J-1)$, the slopes of which will be $\{(1-\zeta_4^{(z)})B^{(zz)}+2(\zeta_{2,4}{}^{(x)}B^{(xx)})^2/\delta\}$ and $\{(1-\zeta_4^{(z)})B^{(zz)}+4(\zeta_{2,4}{}^{(x)}B^{(xx)})^2/\delta\}$. These slopes are read from the graphs to be 5.64 $cm^{-1}$ and 5.72 $cm^{-1}$, their difference being equal to $2(\zeta_{2,4}{}^{(x)})^2/\delta=0.09$ $cm^{-1}$. The intercepts of the above straight lines will, respectively, be $\nu_4$ and $\nu_4+2B^{(xx)}[1+2(\zeta_{2,4}{}^{(x)})^2B^{(xx)}/\delta]$. We infer from the intercepts that $\nu_4$ may be set equal to 1122.4 $cm^{-1}$.

It may be seen from Fig. 3 that the band $\nu_2$ is split into its $J+1$ component sub-bands. This frequency might, moreover, be expected to show inversion doubling, in which case these close-lying component lines would occur in two groups, a group with each inversion component. This is quite evidently not the case, and as in the instance of the arsine molecule[8] one is led to conclude that only in vibration levels of vibration quantum numbers greater than one does inversion doubling become large enough to make itself evident experimentally. It is safe, therefore, to use Eq. (7), reference 6, to calculate the term values for the state $\nu_2$ in $PH_3$. One obtains $\nu_2$ if the lines identified with the frequencies given by Eq. (8), reference 6, are plotted against $J$ and the curve is extrapolated to $J=0$. The value appears to be $\nu_2=992$ $cm^{-1}$. Using the frequency positions of the lines $P(J,K=0)$ given in Table II and Eq. (8), reference 6, replacing $\omega_2$ and $\omega_4$ in it by the band centers $\nu_2$ and $\nu_4$, we may proceed independently to evaluate the quantity $2(\zeta_{2,4}{}^{(x)}B^{(xx)})^2/\delta$, setting $\delta\cong 130$ $cm^{-1}$. The value obtained for this constant calculated from $\nu_2$ is $2(\zeta_{2,4}{}^{(x)}B^{(xx)})^2/\delta=0.09$ $cm^{-1}$ which is in good agreement with the value determined from $\nu_4$. We can therefore evaluate also the quantity $(1-\zeta_4^{(z)})B^{(zz)}$ and for it we have 5.54 $cm^{-1}$.

### IV. EVALUATION OF THE MOLECULAR CONSTANTS

The information gathered in the preceding section permits the evaluation of $B^{(zz)}$ when account is taken of the fact that $\zeta_3^{(z)}+\zeta_4^{(z)}=-1+(B^{(xx)}/2B^{(zz)})$. The value 3.87 $cm^{-1}$ is determined for $B^{(zz)}$. The values of $B^{(xx)}$ and $B^{(zz)}$ yield these values for the two principal moments of inertia, $I_{xx}=6.29\times10^{-40}$ g-cm² and $I_{zz}=7.23\times10^{-40}$ gm-cm². These latter are related to the altitude $h$ of the pyramid and the angle $\beta$, between the altitude and a PH distance, in the following manner; $I_{xx}=\frac{1}{2}I_{zz}+[3mM/(3m+M)]h^2$ and $I_{zz}=3mh^2\tan^2\beta$, where $m$ and $M$ are the masses of the hydrogen and the phosphorous atoms. A little arithmetic yields $h=0.764\times10^{-8}$A and $\beta=57°\,30'$. In terms of the PH distances and the H−P−H angle, we have $r_0=1.42$A and $\alpha=93°\,50'$. These values we regard to be in substantial agreement with the values $r_0=1.419$A and $\alpha=93°\,30'$ obtained by Loomis and Strandberg[9] for $PH_3$ from a study of the microwave spectra of the hybrid phosphine molecules.

TABLE III. Constants of the $PH_3$ molecule derived from the infrared spectrum.

| | | | |
|---|---|---|---|
| $B^{(xx)''}$ | 4.45 $cm^{-1}$ | $I^{(xx)}$ | $6.29\times10^{-40}$ gm-cm² |
| $B^{(xx)'}$ | 4.39 $cm^{-1}$ | $I^{(zz)}$ | $7.24\times10^{-40}$ gm-cm² |
| $[(1-\zeta_3^{(z)})B^{(zz)}-B^{(xx)}]$ | −0.06 | $\nu_1$ | 2322.9 $cm^{-1}$ |
| $(1-\zeta_4^{(z)})B^{(zz)}$ | 5.54 $cm^{-1}$ | $\nu_2$ | 992.0 $cm^{-1}$ |
| $\zeta_3^{(z)}$ | 0.01 | $\nu_3$ | 2327.7 $cm^{-1}$ |
| $\zeta_4^{(z)}$ | −0.43 | $\nu_4$ | 1122.4 $cm^{-1}$ |
| $B^{(zz)}$ | 3.87 $cm^{-1}$ | $r_0$ | 1.42A |
| | | $\alpha$ | 93° 50′ |

The constants derived from the spectrum of $PH_3$ in the infrared are summarized for convenience in Table III.

[8] H. H. Nielsen, Disc. Faraday Soc. **9**, 85 (1950).

[9] C. C. Loomis and M. W. P. Strandberg, Phys. Rev. **81**, 798 (1951).

# The Fundamental Absorption Bands in the Infrared Spectrum of Stibine and Deuterated Stibine*

W. H. HAYNIE† AND H. H. NIELSEN
*Department of Physics and Astronomy, The Ohio State University, Columbus, Ohio*

(Received March 6, 1953)

The four fundamental bands in the infrared spectrum of stibine and the two high-frequency bands in deutero-stibine have been measured. These bands have been sufficiently well analyzed to permit the determination of the size and the shape of the molecule. It has been possible, moreover, to correct the band centers for anharmonicity so as to estimate with considerable accuracy the values of the normal frequencies. The constants arrived at for the molecule are as follows: the SbH distance $r_0=1.71$A, the H−Sb−H angle $\alpha=91°\,30'$, the normal frequencies for stibine $\omega_1=1988.9$, $\omega_2=795.9$, $\omega_3=1974.5$, $\omega_4=844.7$, and for deutero-stibine the values $\omega_1^*=1409.4$, $\omega_2^*=568.5$, $\omega_3^*=1403.5$, and $\omega_4^*=599.5$ cm$^{-1}$ are obtained.

## I. INTRODUCTION

A CONSIDERABLE amount of work has been reported recently concerning the infrared spectra and the molecular structure of molecules belonging to the pyramidal $XH_3$ variety.[1–7] The last molecule in this series which is stable chemically is the stibine molecule, $SbH_3$. A preliminary investigation of this spectrum has been reported by Smith,[8] and we shall here report on high-dispersion measurements on the four fundamental bands of stibine and on the two high-frequency fundamental bands in deuterated stibine. The two low-frequency fundamental bands in deuterated stibine have been located, but not resolved into rotational structure.

## II. EXPERIMENTAL DETAILS

The stibine gas was prepared by dropping sulphuric acid of 0.2$N$ concentration on to lathe turnings of an alloy composed of 80 percent zinc and 20 percent antimony. This reaction yielded a 3 percent concentration of stibine gas in hydrogen. Attempts to separate the stibine from the hydrogen failed in all cases, probably due to the decomposition of the stibine. The deuterium compound was produced in the same manner, using deuterated sulphuric acid diluted with heavy water. As nearly as could be determined the percentage yield of $SbD_3$ in $D_2$ was the same as the $SbH_3$ in $H_2$.

While the stibine gas is, indeed, unstable it was found that at room temperatures the gas could be used in an absorption cell, made of clean Pyrex glass, fitted with windows of polished sodium chloride or potassium bromide, for two or three days before the absorption by the gas became too weak for measurements to be practicable. Three absorption cells were used, one of length 5 cm for use at relatively low dispersion and two of lengths 15 cm and 25 cm for measurements at high dispersion. The low-dispersion spectra were obtained with a Beckmann IR-3 spectrophotometer and covered the entire region from 2$\mu$ to 15$\mu$. They showed only the four fundamental bands and indicated clearly that the long-wavelength bands at 12$\mu$–13$\mu$ are relatively much weaker than the short-wavelength bands near 5.3$\mu$. No prism spectra were recorded of $SbD_3$ in an attempt to conserve $SbD_3$ gas.

The high-dispersion spectra were recorded with a vacuum grating spectrometer described elsewhere.[9] The instrument was, in this instance, used with a Golay pneumatic detector and associated amplifier which fed into a Speedomax strip chart recorder. Two gratings were used in this work; one was a replica echellette grating made by Wood with 3600 lines per inch and the other was a replica echellette made by Wood with 1800 lines per inch. The former was used to measure the bands in $SbH_3$ at 5.3$\mu$, the bands in $SbD_3$ at 7.5$\mu$, and the short-wavelength half of the bands at 12$\mu$. The long-wavelength half of the 12$\mu$ region was measured using the grating with 1800 lines per inch. Near 5.3$\mu$ and 7.5$\mu$ slits were used subtending a frequency interval of about 0.4 cm$^{-1}$ and at 12$\mu$–14$\mu$ the slits subtended frequency intervals from 0.3 cm$^{-1}$ to 0.5 cm$^{-1}$.

## III. DISCUSSION OF THE DATA

### The 5.3μ Region in the Spectrum of $SbH_3$ and the 7.5μ Region in $SbD_3$

The 5.3$\mu$ region in the spectrum of $SbH_3$ is interpreted to consist of two fundamental bands $\nu_1$ and $\nu_3$. The first of these is a parallel band and the second is a perpendicular band. The data, redrawn from the original records are shown in Fig. 1, and the frequency positions of the lines in the two bands, reduced to vacuum, are given in Table I. As in other molecules in this series[1,10] $\nu_1$

* This work was assisted by the U. S. Office of Naval Research under Contract No. N6 onr-22526, NR 019-123 with The Ohio State University.

† Now at Eastman Kodak Company, Rochester, New York.

[1] V. M. McConaghie and H. H. Nielsen, Proc. Nat. Acad. Sci. 34, 455 (1948).
[2] V. M. McConaghie and H. H. Nielsen, Phys. Rev. **75**, 633 (1949).
[3] H. H. Nielsen, Disc. Faraday Soc. **9**, 85 (1950).
[4] H. H. Nielsen, J. Chem. Phys. **20**, 759 (1952).
[5] H. H. Nielsen, Bull. Am. Phys. Soc. **27**, 685 (T2) (1952).
[6] H. H. Nielsen, J. Chem. Phys. **20**, 1955 (1952).
[7] H. H. Nielsen, J. Chem. Phys. **21**, 142 (1952).
[8] D. C. Smith, J. Chem. Phys. **19**, 384 (1951).
[9] Bell, Noble, and Nielsen, Rev. Sci. Instr. **18**, 48 (1948).
[10] V. M. McConaghie and H. H. Nielsen, J. Chem. Phys. **21**, 1836 (1953).

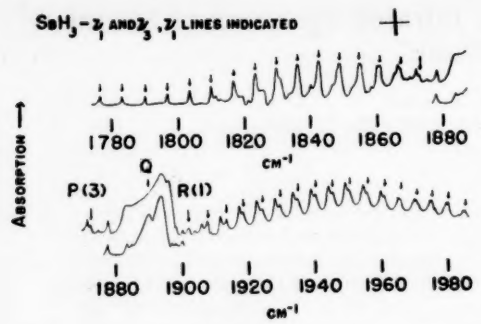


FIG. 1. Absorption pattern of the fundamental bands 2 and $2_3$ in the infrared spectrum of $SbH_3$.

and $\nu_3$ are very loosely coupled through Coriolis interactions and the perturbation is only slight. One may, therefore, analyze $\nu_1$ by the standard methods where use is made of the combination relations. These lead to the following values for $B^{(xx)''}$, $B^{(xx)'}$, and $\nu_1$: $B^{(xx)''}=2.94$ cm$^{-1}$, $B^{(xx)'}=2.90$ cm$^{-1}$, and $\nu_1=1890.9$ cm$^{-1}$.

TABLE I. Frequency positions of lines in the bands[a] $\nu_1$ and $\nu_3$ in the infrared spectrum of $SbH_3$.

| | | | |
|---|---|---|---|
| $R(1)$ | 1902.4<br>1906.4 | $P(2)$ | 1877.7 |
| $R(2)$ | 1908.2<br>1912.0 | $P(3)$ | 1873.4 |
| $R(3)$ | 1913.4<br>1917.5 | $P(4)$ | 1867.0<br>1866.2 |
| $R(4)$ | 1919.0<br>1923.2 | $P(5)$ | 1860.9<br>1859.6 |
| $R(5)$ | 1924.9<br>1928.8 | $P(6)$ | 1854.6<br>1853.0 |
| $R(6)$ | 1930.2<br>1934.2 | $P(7)$ | 1848.5 |
| $R(7)$ | 1935.7<br>1939.4 | $P(8)$ | 1842.3 |
| $R(8)$ | 1941.0<br>1945.2 | $P(9)$ | 1836.0 |
| $R(9)$ | 1946.2<br>1950.2 | $P(10)$ | 1829.6 |
| $R(10)$ | 1951.2<br>1955.4 | $P(11)$ | 1823.1 |
| $R(11)$ | 1956.6<br>1960.7 | $P(12)$ | 1816.6 |
| $R(12)$ | 1961.9<br>1965.5 | $P(13)$ | 1809.9 |
| $R(13)$ | 1966.7<br>1970.7 | $P(14)$ | 1803.3 |
| $R(14)$ | 1971.5<br>1975.8 | $P(15)$ | 1796.6 |
| $R(15)$ | 1976.8 | $P(16)$ | 1789.8 |
| $R(16)$ | 1981.2 | $P(17)$ | 1782.8 |
| $R(17)$ | 1986.2 | $P(18)$ | 1776.2 |

[a] The lines to which an assignment is made are attributed to $\nu_1$.

The corresponding region of absorption for $SbD_3$ lies near 7.5$\mu$. The data is shown redrawn from the original recordings in Fig. 2, and the frequency positions of the lines reduced to vacuum are given in Table II. As in the instance of $SbH_3$ the standard methods of analysis may be used. They lead in the case of $SbD_3$ to these values $B^{*(xx)''}=1.49$ cm$^{-1}$, $B^{*(xx)'}=1.48$ cm$^{-1}$, and $\nu_1{}^*=1358.8$ cm$^{-1}$, the asterisk being used to indicate that these constants relate to the isotopic molecule.

The method by which we have dealt with the frequency $\nu_3$ in the spectra of $SbH_3$ and $SbD_3$ is entirely similar to that by which $\nu_3$ was treated in the case of the spectrum of $AsH_3$ and $AsD_3$.[1] The band resembles a parallel band in the spectrum of both $SbH_3$ and $SbD_3$ indicating that the quantity $[(1-\zeta_3{}^{(z)})B^{(zz)}-B^{(xx)}]$ is nearly zero. In both spectra, the lines of $\nu_3$ overlap the lines of $\nu_1$ in such a manner that they are difficult to distinguish, especially in the $P$ branches. While no apparent $K$ splitting occurs in either band it may be seen, particularly in the band $\nu_1$ due to $SbH_3$, that the unresolved line groups are sharper on the high-frequency side and more diffuse on the low-frequency side. This indicates, as is the case in the spectra of $AsH_3$ and

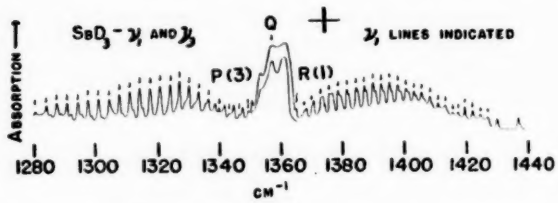


FIG. 2. Absorption pattern of the fundamental bands 2 and $2_3$ in the infrared spectrum of $SbD_3$.

$AsD_3$, that the coefficients of $K$ and $K^2$ in the expression for the frequencies of the lines must nearly cancel on the one side (in this case the high-frequency side) and add up on the low-frequency side. It is difficult to fix exactly for what value of $K$ these two quantities are the same, but we estimate it to be close to $K=10$. From the width of the unresolved line groups on the low-frequency side we have estimated the quantity $[(1-\zeta_3{}^{(z)})B^{(zz)}-B^{(xx)}]$ to be about 0.04 cm$^{-1}$. The algebraic sign to be attached to $[(1-\zeta_3{}^{(z)})B^{(zz)}-B^{(xx)}]$ can be fixed only from the manner in which the $Q$ branches converge. It appears, from Fig. 1, that the $Q$ branches of $\nu_3$ must converge on the high-frequency side. This would indicate that the term $[(1-\zeta_3{}^{(z)})B^{(zz)}-B^{(xx)}]$ is positive and that the coefficient of $K^2$ in the relation for the frequencies is negative.

In the band $\nu_3$ in the spectrum of $SbD_3$ the lines remain rather sharp on both sides of the band center, as nearly as one can tell. This indicates that the coefficients of $K$ and $K^2$ are both very nearly equal to zero. The band centers $\nu_3$ and $\nu_3{}^*$ for the molecules $SbH_3$ and $SbD_3$ are estimated to be, respectively, at 1894.2 cm$^{-1}$ and 1362.0 cm$^{-1}$.

### The 12μ–13μ Region in the Spectrum of $SbH_3$

This region consists also of two overlapping bands. The low-frequency one of these is the parallel band $\nu_2$ and the other is the perpendicular band $\nu_4$. The more significant lines in these two bands are given in Table III together with their frequency positions reduced to vacuum. Figure 3 shows a reproduction of the data of this region redrawn to a frequency scale.

The value of $(1-\zeta_4^{(z)})B^{(zz)}$ for $SbH_3$ is derived in the same manner as this quantity was obtained for $PH_3$ and $AsH_3$ from the analysis of those spectra and as outlined in reference 4. The ${}^RR(J, K)$ lines in the band $\nu_4$ are here not well resolved from the ${}^RR(J, K-1)$ lines, as is the case in the spectra of $PH_3$ and $AsH_3$;[5,6] in fact all the ${}^RR(J, K)$ lines occur as a single line beyond the ${}^RR(9, K)$ line. At values of $J$ less than 9 some degree of resolution has been achieved. Taking, however, $R(14,14)$ and ${}^RR(14,13)$ to have the same frequencies, i.e., 949.8 $cm^{-1}$ and ${}^RR(6,6)$ and ${}^RR(6,5)$ to be 885.8 $cm^{-1}$ and 884.9 $cm^{-1}$, respectively, we estimate the quantities $[(1-\zeta_4^{(z)})B^{(zz)}+2(\zeta_{2,4}{}^{(x)}B^{(xx)})^2/\delta]$ and $[(1-\zeta_4^{(z)})B^{(zz)}+4(\zeta_{2,4}{}^{(x)}B^{(xx)})^2/\delta]$ to be 4.05 $cm^{-1}$ and 4.15 $cm^{-1}$, respectively. This gives the values $(1-\zeta_4^{(z)})B^{(zz)}=3.95$ $cm^{-1}$ and $2(\zeta_{2,4}{}^{(x)}B^{(xx)})^2/\delta=0.1$ $cm^{-1}$. Moreover, if we take the frequency values of the lines $P(1)$ and $P(6)$ given in Table III and verify independently from the band $\nu_2$ what the value $2(\zeta_{2,4}{}^{(x)}B^{(xx)})^2/\delta$ may be expected to be (see reference 4) we obtain $2(\zeta_{2,4}{}^{(x)}B^{(xx)})^2/\delta=0.1$ which we regard as being in satisfactory agreement with the value obtained from $\nu_4$. It is not practicable to determine the band centers $\nu_2$ and $\nu_4$ with great precision. They are estimated, however, to have the values $\nu_2=781.5$ $cm^{-1}$ and $\nu_4=830.9$ $cm^{-1}$.

TABLE II. Frequency positions of lines in the band $\nu_1$ in the infrared spectrum of $SbD_3$.

| | | | | | |
|---|---|---|---|---|---|
| $R(1)$ | 1365.3 | $R(14)$ | 1400.9 | $P(8)$ | 1334.3 |
| $R(2)$ | 1368.0 | $R(15)$ | 1403.5 | $P(9)$ | 1331.1 |
| $R(3)$ | 1370.5 | $R(16)$ | 1405.9 | $P(10)$ | 1328.0 |
| $R(4)$ | 1373.4 | $R(17)$ | 1408.6 | $P(11)$ | 1324.9 |
| $R(5)$ | 1376.2 | $R(18)$ | 1411.2 | $P(12)$ | 1321.7 |
| $R(6)$ | 1379.0 | $R(19)$ | 1413.5 | $P(13)$ | 1318.4 |
| $R(7)$ | 1381.8 | $R(20)$ | 1415.8 | $P(14)$ | 1315.5 |
| $R(8)$ | 1384.7 | | | $P(15)$ | 1312.0 |
| $R(9)$ | 1387.5 | $P(3)$ | 1349.9 | $P(16)$ | 1308.7 |
| $R(10)$ | 1390.2 | $P(4)$ | 1347.0 | $P(17)$ | 1305.3 |
| $R(11)$ | 1392.9 | $P(5)$ | 1343.7 | $P(18)$ | 1302.0 |
| $R(12)$ | 1395.6 | $P(6)$ | 1340.6 | $P(19)$ | 1298.6 |
| $R(13)$ | 1398.2 | $P(7)$ | 1337.3 | $P(20)$ | 1295.3 |

Insufficient $SbD_3$ gas was available to measure these bands in the spectrum of that molecule. The $Q$ branch of the band $\nu_2$ was located, however, as was the composite $Q$ branches of the band $\nu_4$. These are $\nu_2{}^*=561.1$ $cm^{-1}$ and $\nu_4{}^*=592.5$ $cm^{-1}$.

## IV. EVALUATION OF THE MOLECULAR CONSTANTS

The rotational constants $B^{(xx)\prime\prime}$ and $B^{(xx)\prime}$ have been given in Sec. III. One may now proceed to evaluate also the rotational constant $B^{(zz)}$ with the information obtained in earlier sections remembering, of course, that $\zeta_3^{(z)}+\zeta_4^{(z)}=1-B^{(xx)}/2B^{(zz)}$. We obtain the value 2.80 $cm^{-1}$ for $B^{(zz)}$. These values of $B^{(xx)}$ and $B^{(zz)}$ yield for the principal moments of inertia $I^{(xx)}=9.53\times10^{-40}$ g $cm^2$ and $I^{(zz)}=10.00\times10^{-40}$ g $cm^2$. These are, in terms of the molecular dimensions and atomic masses $I^{(xx)}=\frac{1}{2}I^{(zz)}+(3mM/3m+M)h^2$ and $I^{(zz)}=3mh^2\tan^2\beta$, where $m$ and $M$ are the masses of the hydrogen atoms and the antimony atoms and $\beta$ is the angle between the altitude of the pyramid and the Sb–H distance. One quickly arrives at the values $h=0.96$A and $\beta=55°\,46'$. For the Sb–H distance and for the H–Sb–H angle, we obtain these values $r_0=1.71$A and $\alpha=91°\,30'$. These values agree very satisfactorily with those arrived at by Loomis and Strandberg[11] from the data taken on the microwave spectra of the hybrid molecules of stibine. Their values for $r_0$ and $\alpha$ are, respectively, 1.712A and 91.5°. It is of interest to compare the values of $r_0$ and $\alpha$ obtained in this manner with those obtained from the ratio of $I^{(xx)}$ and $I^{(xx)*}$. By this method the value we obtain is $r_0=1.69$A and $\alpha=89°\,40'$. The quantities $\zeta_3^{(z)}$ and $\zeta_4^{(z)}$ may also be evaluated. For these we obtain $\zeta_3^{(z)}=0.01$ and $\zeta_4^{(z)}=-0.43$. Shaffer[12] has shown, more-

TABLE III. Frequency positions of lines in the bands $\nu_2$ and $\nu_4$ in the infrared spectrum of $SbH_3$.

| | | | |
|---|---|---|---|
| $P(5,0)$ | 734.2 | ${}^RR(7,6)$ | 892.2 |
| | | ${}^RR(7,7)$ | 893.9 |
| $P(4,0)$ | 742.2 | | |
| | | ${}^RR(8,7)$ | 900.8 |
| $P(3,0)$ | 749.5 | ${}^RR(8,8)$ | 901.9 |
| $P(2,0)$ | 756.6 | ${}^RR(9,8)$ | 908.8 |
| | | ${}^RR(9,9)$ | 909.9 |
| $P(1,0)$ | 763.6 | | |
| | | ${}^RR(10,10)$ | 917.8 |
| $P(0,0)$ | 770.2 | | |
| | | ${}^RR(11,11)$ | 925.7 |
| ${}^RR(4,4)$ | 869.7 | | |
| | | ${}^RR(12,12)$ | 933.6 |
| ${}^RR(5,5)$ | 877.7 | | |
| | | ${}^RR(13,13)$ | 941.6 |
| ${}^RR(6,5)$ | 884.9 | | |
| | | ${}^RR(14,14)$ | 949.8 |
| ${}^RR(6,6)$ | 885.8 | | |

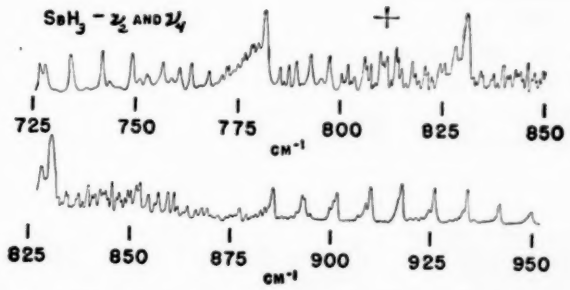


FIG. 3. Absorption pattern of the fundamental bands $2_2$ and $2_4$ in the infrared spectrum of $SbH_3$.

[11] C. C. Loomis and M. W. P. Strandberg, Phys. Rev. **81**, 798 (1951).
[12] W. H. Shaffer, J. Chem. Phys. **9**, 607 (1941).

TABLE IV. Vibrational frequencies and potential energy constants for the $SbH_3$ and $SbD_3$ molecules.

| | $SbH_3$ | $SbD_3$ |
|---|---|---|
| $\nu_1$ ($cm^{-1}$) | 1890.9 | 1358.8 |
| $\nu_2$ | 781.5 | 561.1 |
| $\nu_3$ | 1894.2 | 1362.0 |
| $\nu_4$ | 830.9 | 592.5 |
| $\omega_1$ | 1988.9 | 1409.4 |
| $\omega_2$ | 795.9 | 568.5 |
| $\omega_3$ | 1974.5 | 1403.5 |
| $\omega_4$ | 844.5 | 599.5 |
| $\alpha$ ($10^5$ dynes/cm) | 2.256 | 2.256 |
| $\beta$ | 1.269 | 1.269 |
| $\nu$ | 1.026 | 1.026 |
| $k_1$ | 1.900 | 1.900 |
| $k_2$ | 1.599 | 1.599 |
| $k_3$ | 2.075 | 2.075 |

over, that $(\zeta_3^{(z)})^2+(\zeta_4^{(z)})^2+2(\zeta_{3,4}^{(z)})^2$ †$=1+(Izz/2Ixx)^2$, where $(\zeta_{3,4}^{(z)})$ is the Coriolis coupling constant between the two perpendicular frequencies $\omega_3$ and $\omega_4$. While this constant plays no significant role here we have, nevertheless, evaluated it and find it to be $|\zeta_{3,4}^{(z)}|=0.73$.

It is, in addition, possible now to correct the frequencies for anharmonicity and to make rather accurate estimates of the values of the harmonic frequencies themselves. We shall here follow the method for computing the perpendicular frequencies $\omega_3$ and $\omega_4$ developed by Dennison[13] for pyramidal $XY_3$ molecules. The method may be expected to be valid so long as the frequencies in the isotopic molecules $XH_3$ and $XD_3$ all transform by about the same factor. The method will not be reviewed here except to point out that it depends upon the Teller-Redlich product rule $(4I_{xx}\mu^*/I_{xx}^*\mu)=(\omega_3\omega_4)^2/(\omega_3^*\omega_4^*)^2$, and a second relation which is derived from a knowledge of how $\zeta_3^{(z)}$ (or $\zeta_4^{(z)}$) depends upon the potential energy constants $\alpha$, $\beta$, and $\gamma$[14] in Dennison's notation. The starred quantities refer to the deuterated molecule and $\mu=3mM/(3m+M)$. The method leads to these values for $\omega_3$ and $\omega_4$, $\omega_3=1974.5$ $cm^{-1}$, $\omega_4=844.7$ $cm^{-1}$, $\omega_3^*=1430.5$ $cm^{-1}$, and $\omega_4^*=599.5$ $cm^{-1}$.

To correct the parallel frequencies for anharmonicity and make a reliable estimate of the values of the harmonic frequencies $\omega_1$ and $\omega_2$, we follow the method of McConaghie and Nielsen[1] which we shall not repeat here except to say that it depends also upon a product rule $(\omega_1\omega_2/\omega_1^*\omega_2^*)^2=(m^*\mu^*/m\mu)$ and a relation

$$\mu(\omega_1^2+\omega_2^2)-\mu^*(\omega_1^{*2}+\omega_2^{*2})=\{[(C-1)/2C]\omega_1^2+[(C+1)/2C]\omega_3^2\}(\mu-\mu^*/2),$$

where‡

$$C=\{[4k_2^2/\mu m+(k_1/\mu-k_3/m)^2]^{\frac{1}{2}}/[(k_1/\mu)-(k_3/m)]\}$$

and the $k_i$ are in Shaffer's notation. Once $\omega_3$ and $\omega_4$ are known and the quantity $\zeta_{3,4}^{(z)}$ has been determined from experiment, it is possible to evaluate $C$. We obtain,

TABLE V. Rotational constants and dimensions of the $SbH_3$ and $SbD_3$ molecules.

| | $SbH_3$ | $SbD_3$ |
|---|---|---|
| $B^{(xz)''}$ | 2.94 $cm^{-1}$ | 1.49 $cm^{-1}$ |
| $B^{(xz)'}(\nu_1)$ | 2.96 $cm^{-1}$ | 1.48 $cm^{-1}$ |
| $B^{(zz)}$ | 2.80 $cm^{-1}$ | |
| $I_{xx}$ | $9.53\times10^{-40}$ g $cm^2$ | |
| $I_{zz}$ | $10.00\times10^{-40}$ g $cm^2$ | |
| $r_0$(A) | 1.71 | 1.71 |
| $h_0$(A) | 0.96 | 0.96 |
| $\angle\beta$ | 55° 46′ | 55° 46′ |
| $\angle\alpha$ | 91° 30′ | 91° 30′ |

for $C$, the value $C=-1.1447$. The values we arrive at for $\omega_1$, $\omega_2$, $\omega_1^*$, $\omega_2^*$ are $\omega_1=1988.9$ $cm^{-1}$, $\omega_2=795.9$ $cm^{-1}$, $\omega_1^*=1409.4$ $cm^{-1}$, and $\omega_2^*=568.5$.

It is possible from these corrected frequencies to compute force constants of the molecule. We obtain for these $\alpha=2.256\times10^5$ dynes/cm, $\beta=1.269\times10^5$ dynes/cm, $\gamma=1.026\times10^5$ dynes/cm and§ $k_1=1.900\times10^5$ dynes/cm, $k_2=1.599\times10^5$ dynes/cm, $k_3=2.075\times10^5$ dynes/cm.

The information obtained from this investigation is summarized in Tables IV and V.

† The two before the quantity $(\zeta_{3,4}^{(z)})^2$ has been omitted in Shaffer's paper through a typographical error.

[13] D. M. Dennison, Revs. Modern Phys. **12**, 175 (1940).

[14] The constants $\alpha$, $\beta$ and $\gamma$ are, respectively, equal to the constants $(I^{(e)}{}_{zz}/2I^{(e)}{}_{xx})^2n_1$, $(I^{(e)}{}_{zz}/2I^{(e)}{}_{xx})n_2$, and $n_3$ in Shaffer's notation.

‡ Reference 1 defines $C=[(k_1/\mu)-(k_3/m)]$. This is a typographical error.

§ The $k_1$, $k_2$, and $k_3$ are Shaffer's notation.

# Comparative Retentions of the Nuclear Isomers of $Br^{80}$ in the Propyl Bromides

P. C. CAPRON AND E. CRÈVECOEUR
*Institut Interuniversitaire des Sciences Nucléaires, University of Louvain, Louvain, Belgium*
(Received March 11, 1953)

By experiments on retention, which is defined as the fraction of the radioactivity resisting aqueous extraction, we find, for propyl bromides irradiated in paraffin at a distance of two centimeters from the source with unfiltered neutrons:

| | $R_{(Br^{80}(18\ min))}$ | $R_{(Br^{80}(4.4\ hr))}$ |
|---|---|---|
| Normal propyl bromide | $0.72\pm0.05$ | $0.85\pm0.05$ |
| Isopropyl bromide | $0.37\pm0.02$ | $0.58\pm0.03$ |

The different sources of error are examined and eliminated.

The addition of free bromine, with the purpose of blocking the impurities, left a difference in the retention of the two isomers.

An interpretation is suggested.

The percentage of Br(18 min) of isomeric transition in the free state proceeding from Br(4.4 hr) in the bound state, is found to be 16 percent for the normal propyl bromide and 40 percent for the isopropyl bromide.

## I. INTRODUCTION

IT has been shown before that the nuclear isomers of bromine-80 are produced in different capture levels[1,2] and that there is a difference in the behavior of these isomers following the emission of capture gamma rays.[3]

The energy of the gamma rays, accompanying the isomeric transition has been studied thoroughly, since this radiation undergoes a violent conversion. However, the energy of the capture gamma rays, i.e., which effects the transition from the excited state of the complex nucleus to the two isomeric states, has not been exactly determined up to now.

Given the difficulty of determining rigorously the energy of the capture gamma rays, one can see that the study of this energy by comparison will be of more interest. This is the case in the formation of isomeric pairs.

Before, it had been hoped that it would be possible to do this by an indirect method: the retention in liquids[4,5] following the theoretical works of W. F. Libby;[6] and Miller, Gryder, and Dodson.[7]

According to these theoretical views, one could expect it to be possible to determine these recoil energies from the retentions. Going back to the theoretical views and considering only the "billiard ball" type collisions,[8] the total retention is obtained as the sum of the partial retentions for an infinite number of collisions. Calculations have shown that it is impossible to determine the initial recoil energy by retention and that one cannot discuss the result without taking into account important secondary effects.[9]

In a preceding work[5] it has been shown by multiplying the number of experiments that the retentions of both isomers are different. With slow neutrons (not filtered with Cd) for monobromobenzene, one obtains

$$R_{(Br^{80}(18\ min))}=0.50\pm0.06,$$
$$R_{(Br^{80}(4.4\ hr))}=0.65\pm0.03.$$

In the same work, it has been shown that the retention varied with the energy of the incident neutrons.

For bromoform[8] in the same conditions, one obtains

$$R_{(Br^{80}(18\ min))}=0.53\pm0.02,$$
$$R_{(Br^{80}(4.4\ hr))}=0.69\pm0.04.$$

On the other hand, Friedman and Libby,[10] and Fox and Libby,[11] studying the retention on normal and isopropyl bromide in the liquid and the solid state do not find any difference between the retentions of the isomers and conclude that they have the same mean recoil energy. These authors give the results reproduced in Table I.

Since the results which we obtained with $C_6H_5Br$ and $CHBr_3$ were different from those that Fox and Libby obtained with the isopropyl bromide, we also tried these products and as in the case of $C_6H_5Br$ and

TABLE I. Retention of radiobromine isotopes in isopropyl bromide, produced by $(n,\gamma)$ reaction.

| | 25°C | −196°C |
|---|---|---|
| $Br^{80}$(18 min) | $33.7\pm2.0\%$ | $81.6\pm2.0\%$ |
| $Br^{80}$(4.4 hr) | $33.9\pm2.0\%$ | $79.9\pm1.0\%$ |

[1] P. Capron and A. Verhoeve-Stokkink, Phys. Rev. **81**, 336 (1951).
[2] P. Capron, Bull. acad. roy. Belg. **27**, 524 (1941).
[3] Capron, Crèvecoeur, and Faes, J. Chem. Phys. **17**, 349 (1949).
[4] P. Capron and E. Crèvecoeur, Bull. Cong. Nat. Sci. Bruxelles (1950).
[5] P. Capron and E. Crèvecoeur, J. chim. phys. **49**, 29 (1952).
[6] W. F. Libby, J. Am. Chem. Soc. **69**, 2523 (1947).
[7] Miller, Gryder, and Dodson, J. Chem. Phys. **18**, 579 (1950).
[8] P. Capron and Y. Oshima, J. Chem. Phys. **20**, 1403 (1952).
[9] E. Broda, *Advances in Radiochemistry* (Cambridge University Press, Cambridge, 1950).
[10] L. Friedman and W. F. Libby, J. Chem. Phys. **17**, 647 (1949).
[11] M. S. Fox and W. F. Libby, J. Chem. Phys. **20**, 487 (1952).

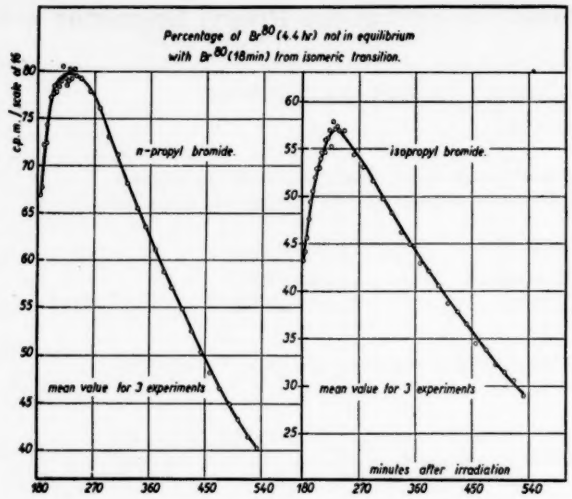
Percentage of Br80(4.4 hr) not in equilibrium with Br80(18min) from isomeric transition.
c.p.m. / scale of 10
n-propyl bromide.
isopropyl bromide.
mean value for 3 experiments
mean value for 3 experiments
minutes after irradiation

FIG. 1. FIG. 2.

$CHBr_3$ we find a difference in the retention of the two isomers.

Three important objections can be found to the interpretation of our experiments.

### 1. Possible Error from the Concentration of $Br^{80}$ (18 min) on the Walls of the Counter

There is a possibility, in fact, the washed liquid, being not perfectly dry, that the water remaining in it would form a thin film on the glass walls of the Geiger counter. As a result, this water would concentrate the $Br^{80}$(18 min) of isomeric transition (I. T.) on the walls of the counter. Thus the electrons of disintegration would have an efficiency greater than if the radioactive bromine was uniformly distributed in the liquid; so, the $Br^{80}$(4.4 hr) would appear more active and would show a too great retention.

We have theoretically and experimentally answered to this objection. The fact that we find no difference between the ratios of the activities in experiments made with liquid counters of different volumes, shows that this effect is negligible.

### 2. Possible Error Due To the Concentration of One Isomer on the Walls of the Vessel During the Irradiation

If one isomer is more adsorbed to the walls of the vessel than the other, the observed activities in the irradiated liquid are not the true ones and must be corrected.[12,13]

The experiments show that the verified difference of retention for the two isomers cannot be attributed to this effect.

[12] Goldhaber, Chiang, and Willard, J. Am. Chem. Soc. **73**, 2271 (1951).

[13] S. Goldhaber and J. Willard, J. Am. Chem. Soc. **74**, 318 (1952).

### 3. Possible Error from the Isomeric Transition

It is possible that in the washed liquid the quantity of bounded $Br^{80}$(4.4 hr) was not in equilibrium with its $Br^{80}$(18 min) of I.T. If this one is in a free state it is carried off by the water in washing.

The experiments show that the quantity of $Br^{80}$(4.4 hr) not in equilibrium with its $Br^{80}$(18 min) of I.T. is 40 percent. One can account for this percentage in the calculations of the original activities, or wait until the 75th minute. At this moment the equilibrium between the $Br^{80}$(4.4 hr) and its $Br^{80}$(18 min) of I.T. is realized.

## II. EXPERIMENTS

### A. Product

The normal and isopropyl bromide come from Light and Company. The small amount of impurities which they may contain are due to the alcohol. The purification did not seem necessary for the following reasons.

1. Since we are looking for the retentions of the isomers, any impurity would influence each isomer in the same way.

TABLE II.

| Normal propyl bromide | Isopropyl bromide |
|---|---|
| $N_2=5716$<br>$N_1=6665$<br>$p_{172}=156.9$<br>$N_1-N_2=949$<br>$y=54.5$<br>The percentage of $Br^{80}$(4.4 hr) not in equilibrium with its $Br^{80}$(18 min) of I.T. is 54.5/156.9=34.7%. | $N_2=3945$<br>$N_1=4702$<br>$p_{172}=110.7$<br>$N_1-N_2=757$<br>$y=43.5$<br>The percentage of $Br^{80}$(4.4 hr) not in equilibrium with its $Br^{80}$(18 min) of I.T. is 43.5/110.7=39.3%. |

2. Instead of eliminating the impurities (olefines) we have fixed them in a few experiments by adding free bromine.

### B. Extraction

We prefer the washing with water to the washing with bisulfite or sodium bromide, even if this does give a poorer reproducibility of the results.[14] Indeed we feared that the addition of sodium bisulfite or bromide would influence the secondary reactions. Trials have shown that after three minutes heavy mechanical washing of the irradiated liquid with distilled water in equal quantities, a second washing was unnecessary.

### C. Irradiation

The irradiation was carried out in a cylinder of paraffin; of height 45 cm and diameter 40 cm. A Ra–Be source of 1400 mC was slid to the center of the cylinder through an opening situated at 20 cm from the base. Above the source a cylindrical opening of 10 cm diameter was used to introduce the vessel containing the

[14] P. F. Shaw and C. H. Collie, J. Chem. Soc. **17**, 1217 (1949).

liquid. This opening was closed with a paraffin bloc. Between source and vessel there were 2 cm of paraffin. The results were not corrected for the accuracy of the source.

### D. Radioactivity

The activities were measured with liquid counters type M6, from Twentieth Century Ltd. A scale of 64 was followed by a mechanical register L.K.B. The resolving time of the whole system is of $3\times10^{-4}$ minute.

Preliminary experiments have shown that $Br^{82}$(34 hr) should not be taken into account, due to the very weak activity of that isotope after a short time of irradiation.

### E. Experiments

*1. Determination of the percentage of $Br^{80}$(4.4 hr) which is not in equilibrium with $Br^{80}$(18 min) of I.T., by washing*

(*a*) *Procedure.*—After 180 minutes irradiation, the liquid is left to stand for 172 minutes to eliminate the $Br^{80}$(18 min) directly formed. By washing, the $Br^{80}$(4.4 hr) and the $Br^{80}$(18 min) of I.T. in the free state are extracted. Since the latter can come from $Br^{80}$(4.4 hr) in free or bounded state, it is possible that in the washed liquid the $Br^{80}$(4.4 hr) will not have been in equilibrium with its $Br^{80}$(18 min) of I.T. It is necessary to know the percentage of $Br^{80}$(4.4 hr) which is not in equilibrium with its $Br^{80}$(18 min) of I.T. to effect the necessary corrections.

(*b*) *Calculations.*—If one carries out a washing and measures the washed liquid at the 172nd minute, after an irradiation of 180 minutes, the decrease of the activity is not found to be exponential, but passes through a maximum value as shown on Figs. 1 and 2. This is due to the fact that a part of the $Br^{80}$(4.4 hr) is not in equilibrium with its $Br^{80}$(18 min) of I.T., eliminated by washing. By the extrapolation of the measured activities between 255th and 540th minutes, when the whole system is in equilibrium, one can calculate the number of disintegrations $N_1$ which would have been produced if the system had been in equilibrium since the beginning:

$$N_1=(x+y)\int_{t_1=180}^{t_2=255} e^{-\lambda_1\cdot t}dt.$$

Experimentally we found the number of disintegrations to be smaller than $N_1$. This value $N_2$ is given by the formula,

$$N_2=x\int_{t_1=180}^{t_2=255} e^{-\lambda_1\cdot t}dt+y\int_{t_1=180}^{t_2=255}(e^{-\lambda_1 t}-e^{-\lambda_2 t})dt,$$

where $x$ is the quantity of $Br^{80}$(4.4 hr) in the bound state and in equilibrium with its $Br^{80}$(18 min) of I.T., and $y$ is the quantity of $Br^{80}$(4.4 hr) in the bound state which is not in equilibrium with its $Br^{80}$(18 min) of I.T. by

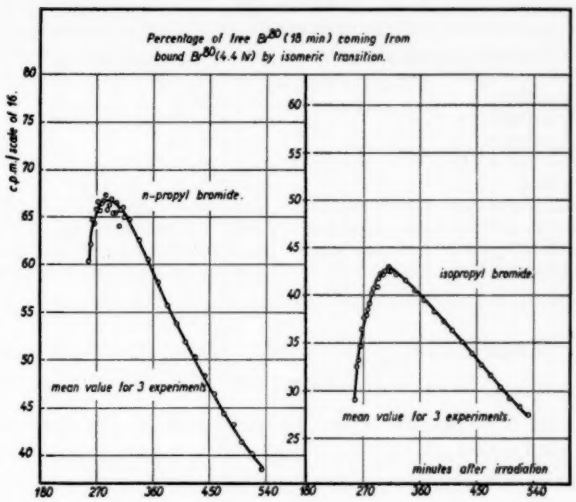


FIG. 3. FIG. 4.

washing. The difference between $N_1$ and $N_2$ allows us to determine the percentage of $Br^{80}$(4.4 hr) which by washing is not in equilibrium with its $Br^{80}$(18 min) of I.T.,

$$N_1-N_2=y\int_{t_1=180}^{t_2=255} e^{-\lambda_2\cdot t}dt.$$

Evaluating $y$,

$$y=\frac{-\lambda_2(N_1-N_2)}{e^{-\lambda_2 t_2}-e^{-\lambda_2 t_1}}.$$

The value of $y$ divided by the activity of $Br^{80}$(4.4 hr) which is supposed to be in equilibrium with its $Br^{80}$(18 min) of I.T. after 172 minutes, gives the percentage of $Br^{80}$(4.4 hr) in the bound state which is not in equilibrium with its $Br^{80}$(18 min) of I.T. in the washed liquid.

(*c*) *Experimental results.*—The application of these formulas to the results of the experiments gave the results shown in Table II for the mean value of three experiments.

*2. Determination of the percentage of $Br^{80}$(18 min) of isomeric transition in a free state, proceeding from $Br^{80}$(4.4 hr) in bound state*

(*a*) *Procedure.*—The $Br^{80}$(4.4 hr) and $Br^{80}$(18 min) were taken off in the free state by a first washing done at the 172nd minute. A second washing done at the 246th minute removed the $Br^{80}$(18 min) of I.T. in the free state and coming from the $Br^{80}$(4.4 hr) in a bounded state.

(*b*) *Calculations.*—See 1. (*b*)

(*c*) *Experimental results* (*Figs. 3 and 4*).—Results of Table III are the mean value of three experiments. The experimental results show a difference for normal and isopropyl bromide.

TABLE III.

| Normal propyl bromide | Isopropyl bromide |
|---|---|
| $N_2'=4821$<br>$N_1'=5249$<br>$p_{246}=150.6$<br>$N_1'-N_2'=428$<br>$y=24.6$<br>The percentage of $Br^{80}$(18 min) of I.T. in free state proceeding from $Br^{80}$(4.4 hr) in bound state is given by 24.6/150.6=16.3%. | $N_2'=2890$<br>$N_1'=3595$<br>$p_{246}=103.1$<br>$N_1'-N_2'=705$<br>$y=40.5$<br>The percentage of $Br^{80}$(18 min) of I.T. in free state proceeding from $Br^{80}$(4.4 hr) in bound state is given by 40.5/103.1=39.3%. |

### 3. *Determination of the activity picked up by the walls of the vessel*

(*a*) *Procedure.*—After 180 minutes irradiation, the vessel was washed thoroughly with a liquid of which the activity was afterwards measured.

(*b*) *Experimental results.*—The quantities of $Br^{80}$(18 min) and $Br^{80}$(4.4 hr) which are picked up by the walls of the vessel during irradiation are determined by a washing of the vessel by: (1) distilled water, (2) concentrated NaOH (10 *N*).

Table IV gives the quantities of isomers picked up by the walls of the vessel, and by comparison with the total activities given in Table V, we have the percentage of the activity of the deposit on the walls of the vessel and the activity of the normal liquid.

The activity of washed liquid cannot be influenced by the activity picked up by the walls of the vessel, since it is taken off by a water washing. Only the unwashed liquid can be influenced, but we can neglect them because: (1) the percentage is weak; (2) the two isomers are influenced in the same proportion.

### 4. *Determination of the ratios of activity and the retentions of the two isomers*

(*a*) *Procedure.*—After an irradiation of 180 minutes and a washing, we measured the activities of the unwashed and the washed liquid. Readings were made every three minutes from the 12th minute to the 60th minute and every 15 minutes until the 390th minute.

(*b*) *Calculations.*—The activities at the time $t=0$ after the irradiation are calculated by the integral method.

Calculation of $C_{2.0}$: Activity originating in $Br^{80}$(4.4 hr) extrapolated at $t=0$ after the irradiation. If $n_0$ is the number of Br(4.4 hr) which are formed per unit time, $T$ the time of irradiation, $t$ the time after the irradiation, $\lambda_1$ the disintegration constant of the $Br^{80}$(4.4 hr), and $b=(1-e^{-\lambda_1 t})/\lambda_1$, then the quantity of $Br^{80}$(4.4 hr) disintegrating is given by,

$$P\cdot\lambda_1=n_0\cdot b\cdot\lambda_1\cdot e^{-\lambda_1 t}. \qquad (1)$$

The $Br^{80}$(4.4 hr) is not directly registered by the counter. It is measured by $Br^{80}$(18 min) of I.T. of which the quantity disintegrating per unit time is given by,

$$Q\cdot\lambda_2=n_0\cdot\frac{\lambda_1\cdot\lambda_2}{\lambda_2-\lambda_1}(b\cdot e^{-\lambda_1 t}-a\cdot e^{-\lambda_2 t}), \qquad (2)$$

where $\lambda_2$ is the disintegration constant of $Br^{80}$(18 min) and $a=1-e^{-\lambda_2 t}/\lambda_2$. The quantity $C_{2.0}$ assignable to $Br^{80}$(4.4 hr) is obtained by applying the formula,

$$C_{2.0}=\frac{Pt_1-Pt_2}{e^{-\lambda_1 t_2}-e^{-\lambda_1 t_1}}\lambda_1, \qquad (3)$$

which is obtained by integrating formula (2) where the expression $e^{-\lambda_2 t}$ is considered as being 0 between $t_1=390$ minutes and $t_2=180$ minutes, and where the activity $C_{2.0}$ is $\lambda_2/(\lambda_2-\lambda_1)=1.073$ times greater than the actual quantity of $Br^{80}$(4.4 hr).

Calculation of $C_{1.0}$.—Activity of $Br^{80}$(18 min) directly formed at $t=0$ after irradiation. Both isomers being present between the 15th and 150th minutes, one must subtract from the total activity the activity of $Br^{80}$(4.4 hr) which has disintegrated in the mean time.

For the first readings, the expression $e^{-\lambda_2 t}$ of formula (2) is not to be neglected. It gives the activity due to $Br^{80}$(4.4 hr). Calculations and experiments show that the two expressions $b\cdot e^{-\lambda_1 t}$ and $a\cdot e^{-\lambda_2 t}$ may vary in importance: (1) before washing it depends only on the irradiation time; (2) after washing it depends on the irradiation time and on the percentage of $Br^{80}$(4.4 hr) not in equilibrium with its $Br^{80}$(18 min) of I.T.

*Unwashed liquid.*—If equilibrium between $Br^{80}$(4.4 hr) and its $Br^{80}$(18 min) of I.T. is established at 100 percent, the activity measured between the 15th and 150th minutes will be proportional to

$$\int_{15}^{150} e^{-\lambda_1 t}dt=109.3.$$

If the equilibrium between $Br^{80}$(4.4 hr) and its $Br^{80}$(18 min) of I.T. is zero percent at $t=0$, the activity measured between the 15th and 150th minutes will be proportional to

$$\int_{15}^{150}(e^{-\lambda_1 t}-e^{-\lambda_2 t})dt=94.8.$$

Let 1.0 be the measured activity of $Br^{80}$(4.4 hr) 100 percent in equilibrium between the 15th and 150th minutes, then the activity of $Br^{80}$(4.4 hr) which is not in equilibrium, is given by

$$94.8/109.3=0.867.$$

As in the unwashed liquid, after three hours irradiation the quantity of $Br^{80}$(4.4 hr) which is not in equi-

TABLE IV.

| Washing | Activities Br(18 min) | Activities Br(4.4 hr) | Ratios | % deposit on the walls of the vessel Br(18 min) | % deposit on the walls of the vessel Br(4.4 hr) |
|---|---|---|---|---|---|
| Distilled $H_2O$ | 25.7 | 4.2 | 6.06 | 7.5 | 9.0 |
| NaOH (10 N) | 35.8 | 5.3 | 6.70 | 10.4 | 11.4 |

librium is equal to

$$a/b = 25/143 = 0.18,$$

the activity of $Br^{80}$(4.4 hr) is corrected by the coefficient,

$$0.82 \times 1.0 + 0.18 \times 0.867 = 0.976.$$

From the total activity, measured between the 15th and 150th minutes assignable to both isomers, the quantity of Br (4.4 hr) to subtract is

$$0.976 \times C_{2.0} \int_{15}^{150} e^{-\lambda_1 t} dt.$$

The remainder $Q_{t_3} - Q_{t_4}$ gives the initial activity of $Br^{80}$(18 min) directly formed by the formula,

$$C_{1.0} = \lambda_2 \frac{Q_{t_3} - Q_{t_4}}{e^{-\lambda_2 t_4} - e^{-\lambda_2 t_3}}.$$

Washed liquid.—In the washed liquid we have: (1) 18 percent $Br^{80}$(4.4 hr) which is not in equilibrium because of irradiation and which is measured by the counter only after washing; (2) in the remaining 82 percent, experiments described under 1, determined that there was 40 percent not in equilibrium. We have thus $0.18 + 0.82 \times 0.40 = 0.508$ not in equilibrium, and 0.492 in equilibrium.

Since we have 0.508 of $Br^{80}$(4.4 hr) not in equilibrium the activity is to be corrected by:

$$0.492 \times 1.0 + 0.508 \times 0.867 = 0.933.$$

From the total activity measured between the 15th and the 150th minutes assignable to both isomers, the quantity of $Br^{80}$(4.4 hr) to subtract is equal to:

$$0.933 \times C_{2.0} \int_{15}^{150} e^{-\lambda_1 t} dt.$$

The calculation of initial activity of directly formed $Br^{80}$(18 min) is made in the same way as for unwashed liquid.

(c) *Experimental results.*—

Three hours of irradiation.—Mean average life is given by the formula,

$$\bar{\theta} = \frac{1 - e^{-\lambda T}(\lambda T + 1)}{\lambda(1 - e^{-\lambda T})},$$

where $T$ is the time of irradiation. We find for $Br^{80}$(18 min): 25.8 min and for $Br^{80}$(4.4 hr): 81.3 min.

The measurements of ratios of activities and retentions in normal and isopropyl bromide have been made in three conditions: (1) Without adding free bromine: Table V. (2) With addition of $10^{-4}$ mole of bromine: Table VI. (3) With addition of $10^{-2}$ mole of bromine: Table VII.

In the tables the symbols employed are:

TABLE V.

Without addition of free bromine

Normal propyl bromide

| Unwashed liquid $C_{1.0}$ | Unwashed liquid $C_{2.0}$ | Unwashed liquid Ratios | Washed liquid $C_{1.0}$ | Washed liquid $C_{2.0}$ | Washed liquid Ratios |
|---|---|---|---|---|---|
| 247.1 | 31.1 | 7.94 | 145.0 | 25.4 | 5.70 |
| 248.6 | 32.9 | 7.55 | 186.6 | 28.9 | 6.45 |
| 225.3 | 30.0 | 7.51 | 172.3 | 25.9 | 6.65 |
| 304.9 | 40.7 | 7.49 | 192.5 | 30.5 | 6.31 |
| 267.5 | 36.7 | 7.28 | 231.4 | 35.2 | 6.57 |
| 411.0 | 44.4 | 9.25 | 203.4 | 33.0 | 6.16 |
| 274.9 | 40.0 | 6.87 | 278.1 | 39.6 | 7.02 |
| 310.5 | 39.8 | 7.80 | 227.9 | 37.1 | 6.14 |
| 288.6 | 39.8 | 7.25 | 233.6 | 36.6 | 6.38 |
| 342.1 | 40.8 | 8.38 | 236.5 | 36.9 | 6.40 |
| 284.6 | 39.0 | 7.29 | | | |
| 298.4 | 39.0 | 7.65 | | | |
| 287.6 | 41.4 | 6.94 | | | |
| 304.3 | 40.0 | 7.60 | | | |
| 280.0 | 41.2 | 6.79 | | | |
| 327.3 | 39.5 | 8.28 | | | |
| 277.9 | 41.2 | 6.74 | | | |
| 290.9 | 38.3 | 7.59 | | | |
| $(C_{1.0})_{Av} = 292.8 \pm 9.4$ | | | $(C_{1.0})_{Av} = 210.7 \pm 11.5$ | | |
| $(C_{2.0})_{Av} = 38.6 \pm 0.9$ | | | $(C_{2.0})_{Av} = 32.9 \pm 1.5$ | | |
| $R_M = 7.58 \pm 0.20$ | | | $R_M = 6.40 \pm 0.10$ | | |
| $R_{Av} = 7.58 \pm 0.29$ | | | $R_{Av} = 6.40 \pm 0.45$ | | |
| Ret. Br(18 min) $= 0.72 \pm 0.05$ | | | Ret. Br(4.4 hr) $= 0.85 \pm 0.05$ | | |

Isopropyl bromide

| Unwashed liquid $C_{1.0}$ | Unwashed liquid $C_{2.0}$ | Unwashed liquid Ratios | Washed liquid $C_{1.0}$ | Washed liquid $C_{2.0}$ | Washed liquid Ratios |
|---|---|---|---|---|---|
| 364.1 | 54.5 | 6.68 | 102.1 | 19.4 | 5.26 |
| 305.6 | 43.5 | 7.02 | 112.3 | 23.7 | 4.73 |
| 334.1 | 47.5 | 7.03 | 122.3 | 23.1 | 5.29 |
| 434.0 | 55.7 | 7.79 | 106.1 | 22.7 | 4.67 |
| 345.5 | 49.2 | 7.02 | 166.2 | 29.9 | 5.55 |
| 346.2 | 44.7 | 7.74 | 113.3 | 21.9 | 5.17 |
| 295.2 | 41.4 | 7.13 | 117.8 | 24.8 | 4.75 |
| 452.9 | 49.4 | 9.16 | 94.4 | 25.3 | 3.73 |
| 285.7 | 40.9 | 6.98 | 146.9 | 28.7 | 5.11 |
| 344.5 | 41.0 | 8.40 | 100.6 | 19.5 | 5.13 |
| 253.4 | 34.0 | 7.45 | | | |
| 262.3 | 33.4 | 7.85 | | | |
| 267.1 | 37.4 | 7.14 | | | |
| 323.1 | 37.7 | 8.57 | | | |
| 266.3 | 35.4 | 7.52 | | | |
| 294.8 | 35.3 | 8.35 | | | |
| 267.2 | 34.4 | 7.76 | | | |
| 275.2 | 32.9 | 8.36 | | | |
| $(C_{1.0})_{Av} = 317.6 \pm 13.7$ | | | $(C_{1.0})_{Av} = 118.2 \pm 6.7$ | | |
| $(C_{2.0})_{Av} = 41.5 \pm 1.7$ | | | $(C_{2.0})_{Av} = 23.9 \pm 1.0$ | | |
| $R_M = 7.65 \pm 0.23$ | | | $R_M = 4.94 \pm 0.15$ | | |
| $R_{Av} = 7.65 \pm 0.45$ | | | $R_{Av} = 4.94 \pm 0.35$ | | |
| Ret. Br(18 min): $0.37 \pm 0.02$ | | | Ret. Br(4.4 hr): $0.58 \pm 0.03$ | | |

$(C_{1.0})_{Av}$ = average activity of $Br^{80}$(18 min), $(C_{2.0})_{Av}$ = average activity of $Br^{80}$(4.4 hr), $R_M$ = mean of the ratios of the activities: $Br^{80}$(18 min)/$Br^{80}$(4.4 hr), $R_{Av}$ = ratio of the average activities: $(C_{1.0})_{Av}/(C_{2.0})_{Av}$, $\mathfrak{R}_M = R_M$ washed liquid/$R_M$ unwashed liquid. $\mathfrak{R}_{Av} = R_{Av}$ washed liquid/$R_{Av}$ unwashed liquid. Ret = retention.

One hour of irradiation.—Only with isopropyl bromide + $10^{-4}$ mole of bromine. Mean average life is found to be 19.3 min for $Br^{80}$(18 min), and 29.2 min for $Br^{80}$(4.4 hr)* (Tables VIII and IX).

* These experiments of one-hour irradiation were suggested by Professor W. F. Libby who kindly read our manuscript. We thank him very much.

TABLE VI.

With addition of $10^{-4}$ mole of bromine

Normal propyl bromide

| Unwashed liquid | | | Washed liquid | | |
|---|---|---|---|---|---|
| $C_{1.0}$ | $C_{2.0}$ | Ratios | $C_{1.0}$ | $C_{2.0}$ | Ratios |
| 204.8 | 27.4 | 7.47 | 170.9 | 23.9 | 7.15 |
| 266.0 | 33.9 | 7.84 | 128.3 | 21.1 | 6.08 |
| 225.4 | 30.4 | 7.41 | 169.9 | 25.3 | 6.71 |
| 319.4 | 35.4 | 9.02 | 140.9 | 24.1 | 5.84 |
| $(C_{1.0})_{Av}=253.9\pm21.9$ | | | $(C_{1.0})_{Av}=152.5\pm9.2$ | | |
| $(C_{2.0})_{Av}=31.8\pm1.5$ | | | $(C_{2.0})_{Av}=23.6\pm0.8$ | | |
| $R_M=7.98\pm0.32$ | | | $R_M=6.46\pm0.26$ | | |
| $R_{Av}=7.98\pm0.79$ | | | $R_{Av}=6.46\pm0.44$ | | |
| Ret. Br(18 min) : $0.60\pm0.06$ | | | Ret. Br(4.4 hr) : $0.74\pm0.04$ | | |

Isopropyl bromide

| Unwashed liquid | | | Washed liquid | | |
|---|---|---|---|---|---|
| $C_{1.0}$ | $C_{2.0}$ | Ratios | $C_{1.0}$ | $C_{2.0}$ | Ratios |
| 261.4 | 40.0 | 6.53 | 90.9 | 14.4 | 6.31 |
| 301.4 | 38.1 | 7.91 | 70.7 | 13.1 | 5.40 |
| 219.4 | 28.7 | 7.64 | 93.7 | 15.3 | 6.12 |
| 336.2 | 42.3 | 7.94 | 76.1 | 15.9 | 4.78 |
| $(C_{1.0})_{Av}=279.6\pm21.8$ | | | $(C_{1.0})_{Av}=82.8\pm4.8$ | | |
| $(C_{2.0})_{Av}=37.3\pm2.6$ | | | $(C_{2.0})_{Av}=14.7\pm0.5$ | | |
| $R_M=7.49\pm0.28$ | | | $R_M=5.63\pm0.30$ | | |
| $R_{Av}=7.49\pm0.78$ | | | $R_{Av}=5.63\pm0.38$ | | |
| Ret. Br(18 min) : $0.30\pm0.03$ | | | Ret. Br(4.4 hr) : $0.39\pm0.03$ | | |

## CONCLUSIONS

### 1. The Existence of a Difference in the Retentions of the Two Isomers of Bromine in the Liquid Phase

As we have previously pointed out, in considering the ratios of activities Br(18 min)/Br(4.4 hr), distinction must be made between $R_M$: the mean of the ratios of the activities and $R_{Av}$ the ratio of the average activity. $R_M$ yields a more accurate result than $R_{Av}$ because $R_M$ does not include the experimental errors of the activities, which vary from one experiment to another. Our argument is that a difference between the $R_M$ of the washed liquid and the $R_M$ of the unwashed liquid proves undoubtedly a difference in the retentions whatever the true retention may be. A great number of experiments will reduce the experimental error on $R_{Av}$ as we have already shown for $C_6H_5Br$ and for normal and isopropyl bromide without bromine. The results compiled in Table IX show that in every case "$R_M$ washed" is different from "$R_M$ unwashed." The same is also found for the ratio $\Re_M=R_M$ washed/$R_M$ unwashed. The results obtained by using $\Re_{Av}=R_{Av}$ washed/$R_{Av}$ unwashed are not so conclusive and this is due only to the fact that $R_{Av}$ includes the experimental errors on the absolute activities. Our object is not to obtain the real value of the retention, but only to show there exists a difference in the retentions of the isomers.

The impurities do not have to be taken into account in the determination differences, by the fact that the value of $R_M$ is different for the washed and unwashed liquid: (a) with or without added bromine; (b) with different average life—one hour and three hours of irradiation; (c) with the neutron energy (4). The impurities should play a role in the measurement of the true retention.

TABLE VII.

With addition of $10^{-2}$ mole of bromine

Normal propyl bromide

| Unwashed liquid | | | Washed liquid | | |
|---|---|---|---|---|---|
| $C_{1.0}$ | $C_{2.0}$ | Ratios | $C_{1.0}$ | $C_{2.0}$ | Ratios |
| 181.1 | 23.9 | 7.57 | 131.8 | 17.1 | 7.70 |
| 324.7 | 34.8 | 9.33 | 138.5 | 20.3 | 6.82 |
| 234.6 | 28.1 | 8.34 | 173.9 | 25.1 | 6.92 |
| 337.5 | 34.9 | 9.67 | 137.3 | 19.1 | 7.18 |
| $(C_{1.0})_{Av}=269.5\pm32.3$ | | | $(C_{1.0})_{Av}=145.4\pm8.3$ | | |
| $(C_{2.0})_{Av}=30.4\pm2.3$ | | | $(C_{2.0})_{Av}=20.4\pm1.5$ | | |
| $R_M=8.86\pm0.40$ | | | $R_M=7.12\pm0.18$ | | |
| $R_{Av}=8.86\pm1.26$ | | | $R_{Av}=7.12\pm0.66$ | | |
| Ret. Br(18 min) $=0.54\pm0.07$ | | | Ret. Br(4.4 hr) $=0.67\pm0.07$ | | |

Isopropyl bromide

| Unwashed liquid | | | Washed liquid | | |
|---|---|---|---|---|---|
| $C_{1.0}$ | $C_{2.0}$ | Ratios | $C_{1.0}$ | $C_{2.0}$ | Ratios |
| 211.2 | 28.6 | 7.38 | 78.1 | 11.4 | 6.85 |
| 131.0 | 17.9 | 7.31 | 57.6 | 9.3 | 6.19 |
| 119.9 | 17.4 | 6.89 | 71.0 | 10.1 | 7.03 |
| 148.7 | 16.5 | 9.01 | 60.4 | 10.7 | 5.64 |
| $(C_{1.0})_{Av}=152.7\pm17.6$ | | | $(C_{1.0})_{Av}=66.8\pm4.1$ | | |
| $(C_{2.0})_{Av}=20.1\pm2.5$ | | | $(C_{2.0})_{Av}=10.4\pm0.4$ | | |
| $R_M=7.59\pm0.30$ | | | $R_M=6.42\pm0.34$ | | |
| $R_{Av}=7.59\pm1.28$ | | | $R_{Av}=6.42\pm0.46$ | | |
| Ret. Br(18 min) : $0.44\pm0.05$ | | | Ret. Br(4.4 hr) : $0.52\pm0.08$ | | |

TABLE VIII.

Isopropyl bromide $+10^{-4}$ mole of bromine

| Unwashed liquid | | | Washed liquid | | |
|---|---|---|---|---|---|
| $C_{1.0}$ | $C_{2.0}$ | Ratios | $C_{1.0}$ | $C_{2.0}$ | Ratios |
| 254.0 | 14.9 | 17.0 | 105.6 | 7.4 | 14.3 |
| 213.1 | 12.7 | 16.8 | 129.6 | 8.4 | 15.4 |
| 200.9 | 12.1 | 16.6 | 113.6 | 7.2 | 14.7 |
| 254.2 | 14.3 | 17.8 | 102.3 | 7.6 | 13.5 |
| $(C_{1.0})_{Av}=230.5\pm12.0$ | | | $(C_{1.0})_{Av}=112.8\pm5.3$ | | |
| $(C_{2.0})_{Av}=13.5\pm0.6$ | | | $(C_{2.0})_{Av}=7.6\pm0.25$ | | |
| $R_{Av}=17.1\pm1.16$ | | | $R_{Av}=14.8\pm0.84$ | | |
| $R_M=17.1\pm0.23$ | | | $R_M=14.8\pm0.34$ | | |
| Ret. Br(18 min) : $0.49\pm0.03$ | | | Ret. Br(4.4 hr) : $0.56\pm0.03$ | | |

### 2. Interpretation

1. The fact of finding different retentions for the isomers of bromine with the propyl bromide only goes to confirm that which had been obtained by the authors with monobromobenzene[5] and bromoform[8] and by other authors under different conditions.[15]

It corroborates that which we know about the capture levels of bromine[1] and the differences in the formation of the two isomers as a function of the energy of the neutrons.[16] On the other hand, these experiments

[15] A. Maddock and J. Green, J. chim. phys. **48**, 207 (1951).
[16] Katz, Pease, and Moody, Can. J. Phys. **30**, 476 (1952).

TABLE IX.

| | Without bromine | | Three hours of irradiation $+10^{-4}$ mole of $Br_2$ | | $+10^{-2}$ mole of $Br_2$ | | One hour $+10^{-4}$ mole of $Br_2$ |
|---|---|---|---|---|---|---|---|
| | n. Prop. Brom. | Isopr. Brom. | n. Prop. Brom. | Isopr. Brom. | n. Prop. Brom. | Isopr. Brom. | Isoprop. Br. |
| $R_M$ washed liquid | 6.40±0.10 | 4.94±0.15 | 6.46±0.26 | 5.63±0.30 | 7.12±0.18 | 6.42±0.34 | 14.5 ±0.34 |
| $R_M$ unwashed liquid | 7.58±0.20 | 7.65±0.23 | 7.98±0.32 | 7.49±0.28 | 8.86±0.40 | 7.59±0.30 | 17.1 ±0.23 |
| $\mathcal{R}_M$ | 0.84±0.04 | 0.65±0.07 | 0.81±0.07 | 0.75±0.09 | 0.80±0.06 | 0.85±0.08 | 0.85±0.03 |
| $R_W$ washed liquid | 6.40±0.45 | 4.94±0.35 | 6.46±0.44 | 5.63±0.38 | 7.12±0.66 | 6.42±0.46 | 14.5 ±0.84 |
| $R_W$ unwashed liquid | 7.58±0.29 | 7.65±0.45 | 7.98±0.80 | 7.49±0.78 | 8.86±1.26 | 7.59±1.28 | 17.1 ±1.16 |
| $\mathcal{R}_W$ | 0.84±0.09 | 0.65±0.14 | 0.81±0.12 | 0.75±0.16 | 0.80±0.21 | 0.85±0.21 | 0.85±0.09 |
| Ret. Br(18 min) | 0.72±0.05 | 0.37±0.02 | 0.60±0.06 | 0.30±0.03 | 0.54±0.07 | 0.44±0.05 | 0.49±0.03 |
| Ret. Br(4.4 hr) | 0.85±0.05 | 0.58±0.03 | 0.74±0.04 | 0.39±0.03 | 0.67±0.07 | 0.52±0.07 | 0.56±0.03 |

lead to a conclusion different from that of Fox and Libby[11] who do not find any difference between the retentions of isomers for the propyl bromides. It is difficult to see how to explain this disagreement between Fox and Libby and the authors. The greatest differences seem to lie in the intensity of irradiation which is $5\times10^4$ neutrons/sec/cm$^2$ for us and $10^7$ for Fox and Libby. One might well wonder whether the great density of the neutrons could have a positive action in the secondary effects.

2. The differences between the retentions must come, finally, from a difference at the moment of the complex dissociation.

Among numerous hypotheses which can be put forward let us retain only the following:

(a) If the first gamma of the cascade is powerful enough and is not subject to internal conversion, one can speak of the dissociation of the molecule by recoil. It will result in the possibility of a "hot atom reaction" and also in all the effects discussed by Goldhaber and Willard.[13]

(b) If the first gamma of the cascade is not very powerful and is subject to internal conversion, one will see the bromine ionize many times by the Auger effect, the molecule break up by repulsion, and one will not be able to speak of the recoil effect as such. It is this which goes on in the I.T.

It does not seem that the first hypothesis in itself can explain the differences obtained between the retentions of the two isomers.

On one hand, in order for this hypothesis to be correct, it would be necessary for the first capture gamma to be very powerful and therefore come from the levels of a very short average life. It follows, consequently, a great possibility in order that the second capture gamma, also very powerful, might be emitted rapidly and annul the effect of the first,[17] "the cancellation of $\gamma$ recoil momenta is extensive."

On the other hand, it has shown theoretically that the difference between the retentions could not be explained exclusively by the "billiard ball process" as it is only eventually for recoil energies of a few volts.[8]

[17] Cleary, Hamill, and Williams, J. Am. Chem. Soc. **74**, 4675 (1952).

Several experimenters[6,12,13,17–19] have foreseen all the consecutive effects both primary and secondary, on the recoil of bromine.

The second hypothesis, on the contrary, seems to have certain advantages.[20–27] For an atom already heavy, as bromine, the complex capture levels are close. It is therefore probable that the first gamma might not be very powerful, falling into a level of relatively long average life, so that the second gamma does not annul the effect of the first. This would be in agreement with the experiments of Wexler and Davies[26] who show the existence of not very powerful capture gammas, strongly converted. The phenomena of retention of $Br^{80}$(4.4 hr) and $Br^{80}$(18 min) formed in the capture would be of a similar mechanism to that which occurs for $Br^{80}$(18 min) in the I.T. One would be tempted to conclude like Hornig, Levey, and Willard[19] as we have already said that "it appears likely that reaction results directly or indirectly from the charge."

"The value of +10 for the charge of the fragments from I.T." obtained by Wexler and Davies[26] must lead to the existence of an ion of which it would be interesting to know the life, and which should be put in relation to the long life of $Br^{80}$(4.4 hr) encountered experimentally.[3]

The mechanisms of charge and discharge would be clearly different for the two isomers and would be able to explain the difference found in the retentions.[28,29]

3. We do not know whether the difference found between there tentions for the normal propyl bromide and isopropyl bromide should be attributed to the chemical nature of the molecules or to the impurities. The fact of seeing the same variation in the presence of bromine, that is to say in the blocking up of the impurities seems to give strength to the first hypothesis. This seems also

[18] Hamill, Williams, Schwarz, and Voiland, U. S. Atomic Energy Commission (U.) Report March 1, 1951.
[19] Hornig, Levey, and Willard, J. Chem. Phys. **20**, 1556 (1952).
[20] S. Wexler and T. Davies, J. Chem. Phys. **20**, 1688 (1952).
[21] B. Hamermesh and V. Hummel, Phys. Rev. **83**, 663 (1951).
[22] M. Goldhaber and A. Sunyar, Phys. Rev. **83**, 906 (1951).
[23] E. Amaldi and F. Rasetti, Ricerca Sci. **10**, 115 (1939).
[24] S. Yosim and T. Davies, J. Phys. Chem. **56**, 599 (1952).
[25] E. Jacobi, Helv. Chem. Acta **35**, 1480 (1952).
[26] S. Wexler and T. Davies, Phys. Rev. **88**, 203 (1952).
[27] S. Wexler and T. Davies, J. Chem. Phys. **18**, 376 (1950).
[28] W. H. Hamill and J. Young, J. Chem. Phys. **20**, 888 (1952).
[29] J. Magee and E. Gurnee, J. Chem. Phys. **20**, 894 (1952).

to be confirmed by the fact that at the time of the I.T. starting from $Br^{80}$(4.4 hr) bounded, the isopropyl bromide gives 40 percent of $Br^{80}$(18 min) free, whereas the normal propyl bromide gives only 16 percent.

We want to express our sincere thanks to the Union Minière du Haut Katanga, who has most generously lent us the radium-beryllium sources used in these experiments.

THE JOURNAL OF CHEMICAL PHYSICS VOLUME 21, NUMBER 10 OCTOBER, 1953

# Segmental Mobility of Polymers Near Their Glass Temperature

F. BUECHE*
*Department of Physics, University of Wyoming, Laramie, Wyoming*
(Received March 19, 1953)

Glass forming polymers exhibit a rapid rise of activation energy for molecular motion as $T$ is lowered through the glass temperature. This phenomena is explained here in two different but largely equivalent ways. The first method assumes that in order for a polymer segment to move (i.e., rotate or jump) an energy greater than a critical energy $E$ must be localized on it and its neighbors. The second approach stipulates that a segment may not move unless more than a certain critical amount of free volume is associated with it and its neighbors. Both approaches lead to good agreement with experimental data available for polystyrene and polyisobutylene. The critical values of $E$ and the free volume for these polymers are found and shown to be reasonable. Conclusions are drawn concerning factors influencing the glass temperature.

## INTRODUCTION

IT has been known for some time that many liquids which do not crystallize upon cooling undergo a transformation in many of their properties at a so-called glass temperature.[1] Above this temperature these substances behave much like normal liquids and below they appear to be typical noncrystalline solids. In the neighborhood of the glass temperature $T_g$ peculiar effects are observed.

Even though the glass temperature is now generally recognized to be the temperature at which the period of molecular motion approaches the time scale of experiments, some of the accompanying phenomena are still only vaguely understood. Of these, one of the most puzzling is the fact that the activation energy for molecular motion increases many-fold as $T_g$ is approached from above. In this paper we shall offer a simple theory for this effect. The theory will be outlined in two different ways, the first based upon the concept of activation energy and the second based upon the concept of free volume. Although the end results appear to be largely equivalent, each formalism has features which make it more easily applied to certain problems than the other. The treatment will be limited to the case of glass forming polymers, but its wider application should be obvious.

Striking evidence of the changing activation energy for molecular motion is shown by various data taken on bulk polymers near their glass temperature (sometimes called the "apparent second-order transition temperature"). For example, Fox and Flory have carried out extensive viscosity measurements on the two polymers, polystyrene[2] and polyisobutylene.[3] They find that the activation energy for viscous flow is far from constant for these materials, being both a function of temperature and molecular weight. A study of the system polystyrene —diethyl benzene shows that the activation energy is highly dependent upon diluent concentration as well.[4]

Recently some progress has been made towards interpreting bulk viscosity data on high polymers.[5] It has been shown both experimentally and theoretically that the activation energy for viscous flow is identical to that for diffusion and for dipole rotation when the dipole is attached directly to the chain. In fact a relation was derived which states that the bulk viscosity of a polymer is given by

$$\eta=\frac{R^2}{M}\frac{\rho A}{16}\frac{kT}{a^2P}N^*, \tag{1}$$

where $R$ is the mean square end-to-end chain length for a molecular weight $M$, $\rho$ is the density of polymer in the mixture, $A$ is Avogadro's number, $k$ is Boltzman's constant, $T$ is the absolute temperature, $a$ is the segmental jump distance, and $N^*$ is an effective molecular weight. $P$ is the jump frequency for the segments of the polymer. Since $P$ is by far the most temperature sensitive quantity in the above expression, a calculation of the activation energy for viscous flow reduces essentially to a calculation of the jump frequency of the

* Present address: Rohm and Haas Research Laboratories, 5000 Richmond Street, Philadelphia, Pennsylvania.

[1] R. Boyer and R. Spencer, *Advances in Colloid Science* (Interscience Publishing Company, New York, 1946), Vol. 2.

[2] T. G. Fox and P. J. Flory, J. Appl. Phys. **21**, 581 (1950).

[3] T. G. Fox and P. J. Flory, J. Phys. and Colloid Chem. **55**, 221 (1951).

[4] F. Bueche, J. Appl. Phys. **24**, 423 (1953).

[5] F. Bueche, J. Chem. Phys. **20**, 1959 (1952).

polymer segments. This is also the important temperature sensitive factor for dielectric phenomena and for diffusion. It is this quantity we propose to calculate.

Our method of calculation is actually a modification of one first presented by Eyring.[6] His method was originally proposed for small molecules, but it has been used in a much more general field. Essentially he postulated that two things are necessary for molecular motion: (1) an energy $\epsilon_1$ must be available to provide a hole into which the molecule can move, and (2) an energy $\epsilon_2$ must be furnished to the molecule in order for it to break free from its neighbors and pass into the hole. It was then found that the jumping frequency was given by

$$P_E = A \exp[-(\epsilon_1+\epsilon_2)/RT], \tag{2}$$

where $A$ is a frequency factor which Eyring was able to express in terms of known physical constants and the entropy of activation. Since the entropy of activation is not easily calculated without recourse to experiment, we shall not attempt its calculation here. We shall assume it to be negligibly temperature-dependent in comparison to the energy factor.

Eyring's model has been shown to be somewhat incorrect for diffusion in even fairly simple crystalline substances.[7] A more realistic model (particularly for nonsymmetric molecules) is one which allows a cooperative movement of molecules or polymer segments. In such a model, the movement of a single segment is accompanied by a compensating movement of several other segments. A hole the size of the moving segment is not necessary. It is this picture which we wish to put on a quantitative basis. In the next section we treat the problem from an energy viewpoint, and, in the section following that, we attack the problem from the standpoint of free volume.

## ENERGY CONSIDERATIONS

We shall assume that for one segment to move or rotate, an energy $E$ must be localized on it and its neighbors. The exact number of participating segments will not be needed but for convenience we shall say that $q$ segments are involved. Our problem of calculating the segmental jumping frequency therefore reduces to the problem of calculating the probability that thermal energy fluctuations will lead to an energy of $E$ or more localized on $q$ segments. This is a simple calculation in fluctuation theory and it is carried out below.

It is known that the distribution function for fluctuations of a variable such as the energy $\epsilon$ is given by

$$f(\epsilon) = C \exp\{-[U(\epsilon)-TS(\epsilon)]/RT\}, \tag{3}$$

where $C$ is a normalization constant.[8] $U(\epsilon)$ is the energy associated with a system in a state $\epsilon$ (in our case $U(\epsilon)=\epsilon$), and $S(\epsilon)$ is the entropy associated with a system in a state $\epsilon$. $T$ is the absolute temperature, and $R$ is the gas constant. The main assumption made in the derivation of this relation is that $f(\epsilon)$ have a rather sharp peak. This condition will be satisfied unless $T$ becomes very large compared to the glass temperature and so it may be used as a good approximation for our present purposes.

The usual procedure is to expand the exponent in a Taylor series about the maximum of the function and drop higher terms. We cannot do that here, since our main interest will be in the region of the tail of the distribution. However, we can go ahead and carry out the expansion making use of the facts that $\partial\epsilon/\partial\epsilon=1$, $\partial^2\epsilon/\partial\epsilon^2=0$, and $\partial S/\partial\epsilon=1/T$, $\partial^2 S/\partial\epsilon^2=-C/T^2$, etc., where $C$ is the specific heat of the $q$ segments under consideration. Actually some uncertainty exists as to whether one should use $C_p$ or $C_v$ under these conditions. This is of minor consequence, however, since it may be shown that they differ by only a few percent in the case of polymers. After carrying out the expansion one finds that the series can be summed so as to give

$$\epsilon - TS = \epsilon_0 - TS_0 + C[\ln(1+\beta)-\beta],$$

where $\beta=(\epsilon-\epsilon_0)/CT$ and the subscript zero indicates values at the maximum of $f(\epsilon)$. Substitution back into the expression for $f(\epsilon)$ leads to

$$f(\epsilon) = K \exp\{(C/R)[\ln(1+\beta)-\beta]\}, \tag{4}$$

where $K$ is the normalization constant and is essentially given by

$$K = (\pi RCT^2)^{-\frac{1}{2}}.$$

If we multiply $f(\epsilon)$ by a frequency factor $B$ analogous to but not equal to the factor $A$ used above, we can obtain the segmental jumping frequency by integrating over all values of $\epsilon > E$. Doing this we obtain for the jumping frequency $P$,

$$P = P_0\{\exp(-E/Rt)\}\sum_0^{\alpha}(E/RT)^n/n!$$

or (5)

$$P = P_0\{1-[\exp(-E/RT)]\sum_{\alpha+1}^{\infty}(E/RT)^n/n!\},$$

where

$$P_0 = B(C/\pi R)^{\frac{1}{2}}(\alpha!/\alpha^{\alpha+1})\exp(-\alpha)$$

and

$$\alpha = C/R.$$

In deriving these relations we have made the substitution that $\epsilon_0=CT$. This is not precisely correct since it assumes $C$ to be constant for all temperatures. However, the above relations still hold provided we redefine $E$ as being the former $E$ plus the error in the above relation. That is, if $\epsilon_0=CT-\delta$, then $E$ should really be our original value plus $\delta$. Within the range of experiments

[6] H. Eyring, J. Chem. Phys. 4, 283 (1936).

[7] See, for example, the chapter by C. Zener in *Imperfections in Nearly Perfect Crystals* (John Wiley and Sons, Inc., New York, 1952).

[8] See, for example, J. C. Slater, *Introduction to Chemical Physics* (McGraw-Hill Book Company, Inc., New York, 1939).

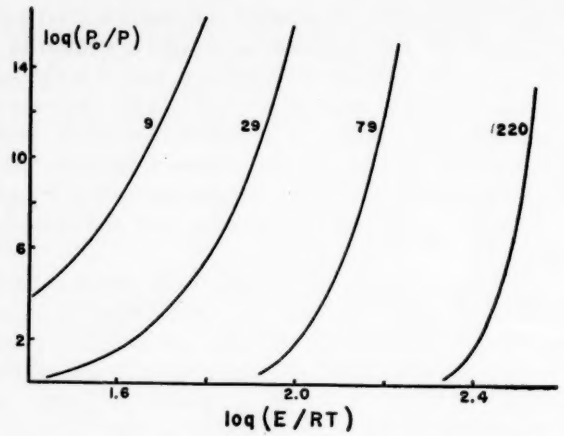


FIG. 1. Theoretical curves showing the variation of jump frequency with temperature as found from energy considerations. The $\alpha$-values are indicated on the curves.

we will be considering (i.e., from $T_g$ to about $T_g+150$) the quantity $\delta$ will not vary appreciably and so $E$ will still be essentially constant with temperature.

It is clear that the above expressions involve only two parameters other than the proportionality constant $P_0$. They are $E$ and $C$. To best illustrate our result we have plotted a family of curves in Fig. 1 relating $\log(P_0/P)$ and $\log(E/RT)$ for different $\alpha=C/R$ values.

But from Eq. (1) we have

$$\log\eta=\log(1/P)+\log[(R^2\rho AkTN^*)/(16Ma^2)]. \quad (6)$$

Since the factor in square brackets is only slowly varying in comparison to $P$, we see that a plot of any experimental viscosity data in the form of $\log\eta$ *vs* $\log(1/T)$ should be able to be fitted to one of the theoretical curves by a simple shifting of axes. Of course the axes must be kept parallel. After a fit has been obtained, the vertical line $\log(1/T)=0$ of the experimental curve will coincide with the vertical line $\log(E/R)$ of the theoretical curve and so $E$ is determined. The value of $C$ is characteristic of the curve which provides a fit and so it too is determined.

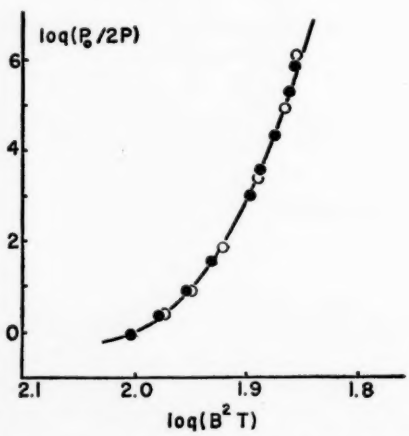


FIG. 2. Comparison between experiment and theory for polystyrene. The experimental points are from the data of Fox and Flory. $\alpha$ was taken equal to 220.

To test the theory we have made use of the extensive data of Fox and Flory[2,3] on the temperature and molecular weight dependence of the viscosity of polystyrene and polyisobutylene. Their data have been treated as outlined above and have been found to fit the theory quite accurately. This is shown in Figs. 2 and 3. In each case the line was calculated from theory. The experimental points were fitted as outlined above. Not all the data on either polystyrene or polyisobutylene were used for these figures, but it all fits equally well. The data shown are in each case for two of the most extensively measured fractions.

Figure 2 shows the polystyrene data using Fox and Flory's fractions *C*8 ($M=3000$) and *B*6 ($M=5600$). From these data we conclude that $C/R=220$. The error in $C$ is of the order of 8 percent due to uncertainty in which curve fits most accurately. Using the fact that $C_p$

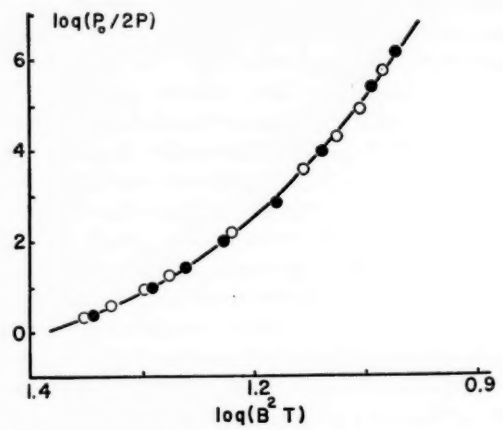


FIG. 3. Comparison between experiment and theory for polyisobutylene. The experimental points are from the data of Fox and Flory. $\alpha$ was taken equal to 29.

above the transition temperature for polystyrene is about 48 cal/mole styrene unit,[9] we see that $q$, the number of participating segments, must be about 9. This is certainly in a reasonable range.

Figure 3 shows the data on polyisobutylene obtained by Fox and Flory. The fractions used were *PR7F3* ($M=5400$) and *PB4F1* ($M=80\,000$). Again the data fit the theoretical curve within the experimental accuracy. In this case $C/R=29$ with an uncertainty of about $\pm5$ percent. It is seen that the number of cooperating segments for this polymer is much smaller than for polystyrene. Probably the number is only 3 or 4. This is not unexpected since polyisobutylene has a much less bulky structure than polystyrene.

In all of the above discussion we have tacitly assumed that variation of molecular weight (i.e., addition of chain ends) does not alter the number of cooperating segments (i.e., $C$) but only influences $E$. This cannot be

[9] R. Buchdahl and L. E. Nielsen, J. Appl. Phys. **21**, 482 (1950).

expected to be true for an indefinite lowering of $M$, but it appears to be satisfactory within the ranges studied. However, we can now show how $E$ varies with $M$ since $E$ also is obtained from our curve fitting. We would expect $E$ to decrease linearly with the number of chain ends or as $M^{-1}$. The values of $E$ are plotted against $M^{-1}$ in Figs. 4 and 5.

The data on polystyrene shown in Fig. 4 definitely bear out this assumption. Unfortunately, the polyisobutylene data in Fig. 5 are not sufficiently accurate to allow us to draw any conclusion in that case. It is seen that the limiting $E$ for high molecular weight is 240 kcal/mole and 35 kcal/mole for polystyrene and polyisobutylene, respectively.

Although the above treatment is seen to lead to reasonable results, it has the disadvantage that its results are expressed in terms of energy. Such a result is not easily applied to data dealing with the effects of diluents since, even at moderate diluent concentrations,

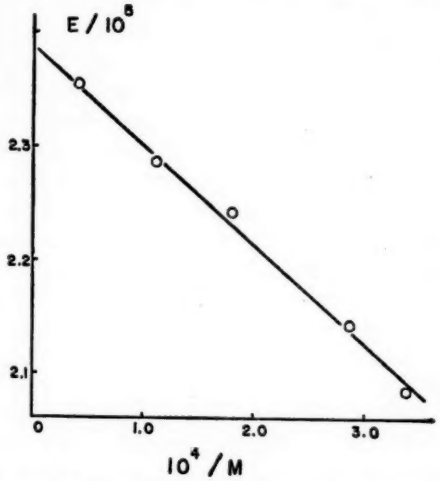


FIG. 4. Variation of the critical energy with molecular weight for polystyrene. $E$ is in cal/mole.

both $C$ and $E$ will vary. Also, the above treatment will not be easy to apply at the transition temperature itself since $C$ varies rather rapidly within a few degrees of $T_g$. For these reasons it was felt that a similar treatment based upon a free volume viewpoint might be of considerable value. This has been carried out, and the results are summarized in the following paragraphs.

## VOLUME CONSIDERATIONS

In this section we shall assume that a polymer segment will be able to jump or rotate whenever the density of segments around that segment becomes smaller than a certain critical value. Stated mathematically, we shall stipulate that it is possible for a segment to move whenever a certain number of segments normally occupying a volume $V_0$ has its volume enlarged to $Q$ or greater due to thermal density fluctuations.

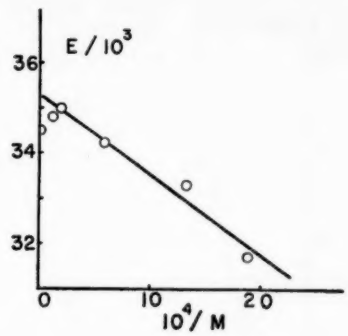


FIG. 5. Variation of the critical energy with molecular weight for polyisobutylene. $E$ is in cal/mole.

This again is a problem in fluctuation theory and we must find the distribution function for density fluctuations. From Eq. (3) we have that the probability that a group of segments which on the average occupy a volume equal to $V_0$ finds itself in a volume $V$ is given by

$$f(V)\sim\exp\{-[U(V)-TS(V)]/RT\}.$$

Expanding about the most probable volume ($V_0$) gives

$$U-TS=U_0-TS_0+(V-V_0)^2/(2\beta V_0),$$

where $\beta$ is the isothermal compressibility. This then gives

$$f(V)=(2\pi\beta V_0RT)^{-\frac{1}{2}}\exp\{-(V-V_0)^2/(2\beta V_0RT)\}.$$

The number of segments able to move is proportional to the number having a volume greater than $Q$. Therefore it is given by

$$\int_Q^\infty f(V)dV,$$

which is equal to

$$\tfrac{1}{2}\{1-\mathcal{E}_2[(Q-V_0)/(2\beta V_0RT)^{\frac{1}{2}}]\},$$

where

$$\mathcal{E}_2(x)=(4/\pi)^{\frac{1}{2}}\int_0^x\exp(-y^2)dy.$$

This is a well-known tabulated function.

Or, for the frequency of rotation we have

$$P=\tfrac{1}{2}P_0\{1-\mathcal{E}_2[(Q-V_0)/(2\beta V_0RT)^{\frac{1}{2}}]\}. \qquad (7)$$

The proportionality constant $P_0$ used here is not equal to the similar quantity used in the first part of this paper. However, its significance is essentially the same.

Here, as was done with the previous result, we can compare experiment and theory by plotting $\log(P_0/P)$ against some variable and comparing it with an experimental plot of $\log\eta$ against the same variable provided we ignore slowly varying factors. Again, aside from the proportionality constant $P_0$, we have two parameters, in this case $V_0$ and $Q$. The parameter $V_0$ will be proportional to the specific volume of the polymer and so can be written as

$$V_0=V_{00}[1+(\alpha_1+\alpha_2)T] \quad \text{for} \quad T>T_g. \qquad (8)$$

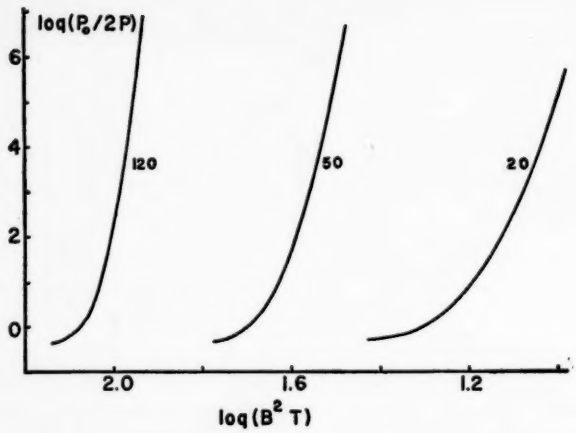


FIG. 6. Theoretical curves showing the variation of jump frequency with temperature as found from free volume considerations. The numbers on the curves indicate the value used for $A$.

In this expression $\alpha_1$ is the volume thermal expansion coefficient characteristic of the solid-like expansion of the polymer and $\alpha_1+\alpha_2$ is the total expansion coefficient in the liquid like region, i.e., $T>T_g$.

The quantity $Q$ is not so well known. It is, of course, the critical volume necessary for rotation. Although no proof has been presented for the assertion, many authors assume that free volume (volume effective in allowing rotations) is the volume in excess of that which the substance occupies due to actual solid-like expansion. The argument often used to justify this assumption is that thermal vibrations actually account for the solid-like expansion and this volume is not available for rotation purposes. The validity of this assumption is supported by comparing our above result with experiment.

If we accept that $T_g$ actually represents the temperature at which $P$ takes on a certain critical value (shown to be about 0.1 in reference 5 and fairly well confirmed by the work of Baker *et al.*[10]), we see that from Eq. (7) this must represent a condition where

$$(Q-V_0)/(V_0T)^{\frac{1}{2}}=\text{constant}. \tag{9}$$

But Fox and Flory[2] have shown that $T_g$ actually occurs at a fixed free volume defined in the sense indicated above as closely as their experiments can tell. Since this was true even though $T_g$ was varied through a range of about 50 degrees, it is clear that $Q$ cannot be independent of temperature. In fact it is required that $Q=(Q_{00}+\alpha_1V_{00}T)$ in order for the above experiments to be satisfied. This in effect shows that the solid-like expansion of the polymer does not yield appreciable volume which is effective in aiding segmental movements.

Taking this form for $Q$ and using the value of $V_0$ from Eq. (8) we find that for the region $T>T_g$

$$P=\tfrac{1}{2}P_0\{1-\mathcal{E}_2[A/(BT^{\frac{1}{2}})-BT^{\frac{1}{2}}]\}, \tag{10}$$

where

$$B=\alpha_2(V_{00}/2\beta R)^{\frac{1}{2}} \quad \text{and} \quad A=\alpha_2(Q_{00}-V_{00})/2\beta R.$$

In arriving at this result we have neglected small terms in $\alpha^2$. The error introduced by this may be shown to be negligible for our purposes.

From the form of the above relation it seems that the best comparison between experiment and theory may be obtained by comparing plots of $\log(P_0/2P)$ *vs* $\log(B^2T)$ and $\log\eta$ *vs* $\log(T)$ using $A$ as a parameter. A family of curves showing $\log(P_0/2P)$ *vs* $\log(B^2T)$ for different values of $A$ is plotted in Fig. 6. As in the previous section we have fitted Fox and Flory's data on polystyrene and polyisobutylene with our theoretical formula. The results are shown in Figs. 7 and 8. It is clear that the theory is capable of fitting the experimental data.

The values obtained from the curve fitting are that $A=100\pm10$ and $B=0.45$ for polystyrene ($M=3000$). For polyisobutylene we have $A=20\pm3$ and $B=0.19$ for $M=5400$. From these values we can compute $Q_{00}$ and $V_{00}$ provided the compressibility $\beta$ and the expansion factor $\alpha_2$ are known. Fortunately, neither one of these quantities is very critical for this computation.

Using $\beta=0.7\times10^{-10}$ dyne$^{-1}$ and $\alpha_2=4\times10^{-4}$ degree$^{-1}$ as the constants for both polymers (which seem to be about an average of the literature data), one finds that $V_{00}=4300$ cubic angstroms for polyisobutylene and 24 000 for polystyrene. The ratio $Q_{00}/V_{00}$ is 1.22 for polyisobutylene and 1.20 for polystyrene. These latter two values are amazingly close together and indicate that about the same percentage of free volume is needed for rotation in both polymers.

The values for $V_{00}$ might at first sight seem too large to be reasonable, representing cubes of sides 16 and 28 angstroms. Certainly the number of segments in such volumes are much larger than the number of cooperating segments found by our first method of calculation. However, a simple approximate calculation shows that the energy found by method one is about that which

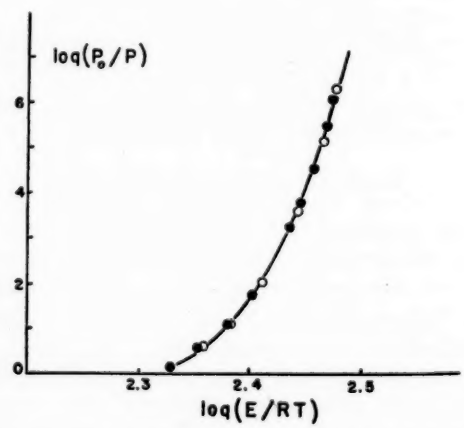


FIG. 7. Comparison between experiment and theory for polystyrene. $A$ was taken to be 100.

[10] Baker, Auty, and Ritenour, J. Chem. Phys. **21**, 159 (1953).

would be needed to expand a volume $V_0$ to the critical size found by method two. From this one is led to the following interrelation between the results of the two methods. In order for a segment to rotate, a certain energy $E$ must be localized on it and its neighboring segments as found by method one. This energy is then at least partly dissipated in doing work against the surroundings so as to expand the volume available to these and the neighbor segments. If the energy was $E$ or larger, the free volume thus provided will be large enough so that rotation can take place.

## CONCLUSION

It appears that each of the two methods outlined here can adequately describe the mobility of polymer segments near $T_g$. The first method, utilizing energy concepts, is most valuable in describing phenomena which can be related directly to the energy needed for segmental movement. On the other hand, it is difficult to apply that result to problems where free volume is the more easily evaluated quantity. For such problems the result of method two should prove useful. In particular, Eq. (9) can serve as a powerful tool in predicting transition temperatures as a function of any quantity which affects the specific volume in a known fashion. However, method two also has limitations. For example, strictly speaking it is not correct to represent the data for two molecular weights using the same value of $A$, since $A$ probably varies somewhat with molecular weight. We therefore see that each formalism has its own particular advantages, and even though they are largely equivalent, one may be more easily applied to a particular problem than the other.

It should also be pointed out that these calculations provide considerable insight into the factors affecting the value of $T_g$. As a general rule it would appear that any factor which increases the volume disturbed by a rotating segment or which increases the density of the solid will in turn cause $T_g$ to become higher. Increasing chain stiffness and addition of bulky, but stiff, chain side groups will increase $T_g$. The affect of polar groups, although admittedly being very important in regard to crystallization phenomena, will apparently affect $T_g$ only in as much as they increase the density of the polymer or contribute to adhesion of one group to another. It is significant to note that although the transition temperatures of polystyrene and polyisobutylene are far different, the ratio $V_{00}/E$ is about the same for the two polymers. It would therefore seem that the big difference in transition temperature between the two is nearly all the result of the increased bulk of the styrene unit.

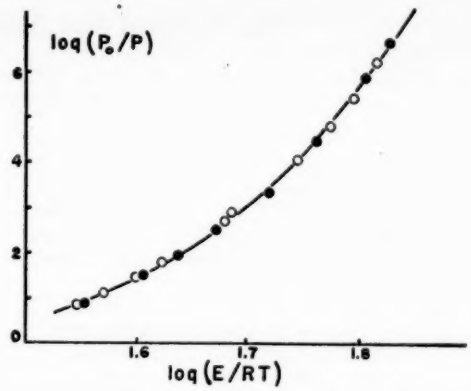


FIG. 8. Comparison between experiment and theory for polyisobutylene. $A$ was taken to be 20.

# The Crystal and Molecular Structure of Tetraborane

CHRISTER E. NORDMAN* AND WILLIAM N. LIPSCOMB
*School of Chemistry, University of Minnesota, Minneapolis 14, Minnesota*

(Received July 11, 1953)

The molecular structure of tetraborane $B_4H_{10}$ has been determined from 616 observed reflections from single crystals. The ordered phase is monoclinic $P2_1/n$, with four molecules in a unit cell with parameters, $a=8.68$, $b=10.14$, $c=5.78$A, and $\beta=105.9°$. Complete three-dimensional Fourier syntheses, including one from which the boron atoms had been subtracted, were employed to locate unambiguously the positions of all atoms.

Molecular dimensions indicate that the isolated molecule has symmetry $C_{2v}$. The boron atoms form two triangles $B_IB_IB_{II}$ with a common edge $B_I-B_I$ the angle between the planes of the triangles being 118.1°. Each of the two $B_I$ borons has one attached hydrogen atom, and each $B_{II}$ has two attached hydrogen atoms. The remaining four hydrogen atoms form bridges between the four $B_I-B_{II}$ pairs. Molecular parameters are four $B_I-B_{II}=1.845\pm0.002$A, $B_I-B_I=1.750$A, $B_{II}-B_{II}=2.786$A, six $B-H=1.11\pm0.04$A, four $B_I-H$ (bridge) $=1.21\pm0.03$A, and four $B_{II}-H$ (bridge) $=1.37\pm0.10$A. Mean values and their average deviations have been given on the assumptions that the molecular symmetry is $C_{2v}$ and that the six $B-H$ distances are equal.

There is an interesting false, incorrect structure which almost satisfies the x-ray diffraction data.

A metastable modification, obtained by sudden freezing of the super-cooled liquid, has spherically disordered molecules in hexagonal close packing. There are two molecules in a unit cell of dimensions, $a=5.79$ and $c=9.36$A.

## INTRODUCTION

THE structures of the numerous hydrides of boron have long been the subject of considerable interest because of their electron deficiency and their seemingly peculiar valence relationships. This interest, however, has largely been of a speculative nature, with only meager experimental support. Because of preparative difficulties, the chemical instability and the low melting points of most of the boron hydrides, experimental work is difficult. Early results obtained by electron diffraction studies in the gas phase were of limited reliability, particularly in the case of the higher hydrides, giving only vague indications of possible boron arrangements. As a result, the early literature contains many incorrect conclusions regarding the structures of the boron hydrides.

In recent years, however, single crystal x-ray diffraction studies have shed new light on the problems in this field. Improved electron diffraction methods have added to the progress, and produced substantial support of the results obtained. The structures of decaborane ($B_{10}H_{14}$)[1] and stable pentaborane[2,3] ($B_5H_9$) have recently been established and are quite different from those originally suggested. It was therefore considered highly desirable to carry out additional x-ray diffraction studies in the field of the higher boron hydrides. For this reason the present investigation of the structure of tetraborane $B_4H_{10}$ was undertaken.

## EXPERIMENTAL

Since the melting point of tetraborane is $-120$°C, a previously described low-temperature technique was used in taking the x-ray photographs.[4] The substance was vacuum-distilled into the tips of thin-walled Pyrex capillaries, about 1 mm in diameter, which were subsequently sealed off. To reduce the risk of explosion or decomposition through contact with air, the vacuum line was previously rinsed out with dry nitrogen, carefully evacuated, and the $B_4H_{10}$ permitted to enter from a Breakoffsky which was broken by means of a glass covered, magnetically controlled iron breaker. As the thermal decomposition of tetraborane is quite rapid at room temperature, the distillation was performed at a low pressure, maintaining the Breakoffsky as well as the receiving capillary immersed in a cooling bath. For the same reason all samples and capillaries were stored under dry ice at all times.

The Buerger precession camera was used throughout the work, and the photographs were taken with the sample at about $-150$°C. A capillary was mounted on the goniometer head and a crystal grown in a stream of cold nitrogen gas. In this manner, monoclinic single crystals of tetraborane were readily obtained. Zero-level photographs were taken using $M_0K\alpha$ radiation and a precession angle of $\mu=30°$. With the reciprocal $c$ axis parallel to the spindle axis, complete sets of nets were photographed giving a total of 616 observed $hkl$ reflections. For correlation purposes, 5 more nets, not containing $OOl$, were photographed after reorienting the crystal. All but the weakest nets were photographed from 2 to 5 times with varying exposures in order to facilitate the estimation of intensities. A standard intensity scale containing varying exposures of two neighboring reflections from a $B_4H_{10}$ crystal was used

* Present address: Institute for Cancer Research and the Lankenau Hospital Research Institute, 7701 Burholme Avenue, Philadelphia 11, Pennsylvania.

[1] Kasper, Lucht, and Harker, Acta Cryst. **3**, 436 (1950).

[2] W. J. Dulmage and W. N. Lipscomb, Acta Cryst. **5**, 260 (1952).

[3] Hedberg, Jones, and Schomaker, Proc. Nat. Acad. Sci. U. S. **38**, 679 (1952).

[4] T. B. Reed and W. N. Lipscomb, Acta Cryst. **6**, 45 (1953).

for visual estimation of the observed intensities. By means of the cross nets, the entire set of photographs was standardized to a common scale. Lorentz and polarization corrections were conveniently applied with the use of a transparent template made by reproducing a published graph.[5]

The liquid $B_4H_{10}$ showed a considerable tendency to supercool. However, when supercooling was carried far enough, instantaneous freezing took place giving a strongly disordered, hexagonal modification. It was possible to obtain single crystals of this phase and to observe seven different reflections. In addition, an incomplete set of photographs was obtained for a third modification, seemingly also hexagonal.

No phase transitions were observed when the monoclinic phase was cooled to −175°C.

## UNIT CELL AND SPACE GROUP

The symmetry of the reciprocal lattice is $C_{2h}$. The dimensions of the monoclinic unit cell are $a=8.68\pm0.02$A, $b=10.14\pm0.03$A, $c=5.78\pm0.02$A, and $\beta=105.9°\pm0.3°$. With this choice of axes, the extinctions of *hOl* when $h+l$ is odd and of *OkO* when $k$ is odd were observed. These extinctions indicate the presence of an $n$ glide plane and a twofold screw axis. Thus, the space group is $C_{2h}{}^5-P2_1/n$. The unit cell volume is 489A$^3$. The density of $B_4H_{10}$ can be expected to have a value slightly lower than that of 0.761 g cm$^{-3}$ reported[2] for $B_5H_9$. It follows that the unit cell contains four molecules, giving a calculated density of 0.725 g cm$^{-3}$. Since the multiplicity of the general position of the space group is also four, no molecular symmetry is demanded.

## DETERMINATION OF THE STRUCTURE

As a first step toward finding a trial structure, sharpened Patterson projections were made of the three principal zones. The *hkO* and *hOl* projections showed a considerable concentration of peaks at or near $x=0$ and $x=\frac{1}{2}$, indicating a layer-like arrangement of scattering matter parallel to the *bc* plane. A conclusion drawn from this was that the boron skeleton of the molecule could not extend more than about 1.4A in the $x$ direction. The extension of the molecule in other directions was brought out by an unsharpened *Okl* Patterson section at $x=0$ and by a half-cell Patterson projection (Fig. 1) along $a$ from $x=-\frac{1}{4}$ to $x=\frac{1}{4}$. Both of these showed short intramolecular vectors clearly separated from the far-out intermolecular peaks. Thus it became clear at this stage that the boron arrangement in the tetraborane molecule is a fairly compact one, extending no more than about one B−B bond length in the direction of any one of the axes.

Another noteworthy feature present in the Patterson function was a strong tendency toward undemanded symmetry observed in the *Okl* projection as well as in the $x=0$ section and the half-cell projection (Fig. 1). All of these contained what resembled a center of symmetry at $y=\frac{1}{4}$, $z=\frac{1}{4}$, and, corresponding to the origin peak, a very high maximum at $y=\frac{1}{2}$, $z=\frac{1}{2}$. It was therefore concluded that the above-mentioned layers are "almost centered" with respect to the *bc* face. In order to satisfy this requirement, it is necessary for the layers to lie at the same $x$ values as the twofold screw axes and for the individual molecules to be so located that the operation of the screw axis produces a "centering" effect, resembling a translation of $\frac{1}{2}(b+c)$. If a center of symmetry is chosen as the origin, the screw axes are at $x=\pm\frac{1}{4}$, $z=\pm\frac{1}{4}$. Thus, the boron layers were found to lie approximately at $x=\frac{1}{4}$ and $\frac{3}{4}$ with molecules in the neighborhood of $x=0$ and $\frac{1}{2}$. Similarly, from the appropriate Patterson projections as well as the $P(\frac{1}{2}, y, \frac{1}{2})$ Patterson-Harker section approximate $y$ coordinates were obtained.

In the foregoing, the reasoning has been outlined which led to the assignment of approximate molecular

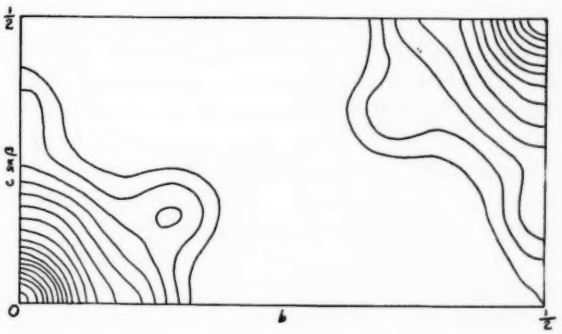


FIG. 1. Unsharpened Patterson half-cell projection along $a$ from $x=-\frac{1}{4}$ to $+\frac{1}{4}$.

positions. Although these were subsequently found to be correct, some difficulty was experienced in finding the true molecular structure. This difficulty arose from the existence of a "false solution," i.e., a model giving reasonably good agreement with the experimental evidence while actually being significantly different from the true solution.

With regard to the molecular structure, the "false symmetry" in the *Okl* Patterson functions demands that the projection of the molecule has $C_i$ symmetry about the $b$ axis. Obviously this is an idealization, in so far as the corresponding Patterson symmetry is not actually present, though nearly so. It was felt, however, that this hypothesis presented a workable first approximation, and that the manner in which the symmetry was violated would become evident during the Fourier refinement process.

The first trial model consisted of a distorted boron tetrahedron, with one bond slightly shorter than the others. This model gave good agreement with the Patterson function. An *hOl* Fourier projection was made, which after a slight refinement gave the result

[5] J. Waser, Rev. Sci. Instr. 22, 567 (1951).

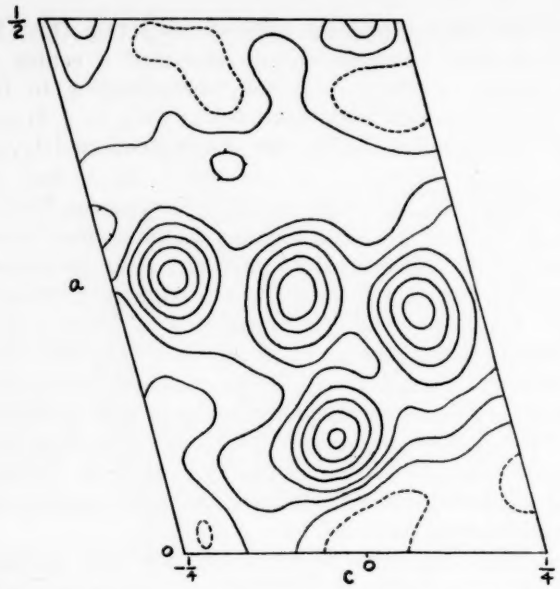


FIG. 2. *hOl* Fourier projection of the original (false) model.

shown in Fig. 2. A comparison of observed and calculated *hOl* structure factors was subsequently made. Aside from moderate discrepancies for small-angle reflections, to be expected from the omission of the hydrogen atoms, the structure factor agreement was remarkably good. Similarly, the *hkO* Fourier projection presented a seemingly unambiguous support of the assumed model. As the next step a three-dimensional Fourier synthesis was carried out. Although one of the four boron peaks was somewhat lower than the others, there were no significant subsidiary maxima or other

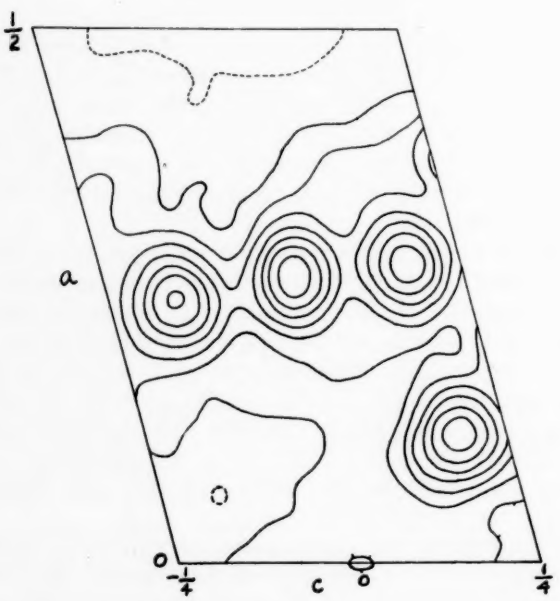


FIG. 3. *hOl* Fourier projection of the revised (true) model. The electron density scale is the same as that in Fig. 2.

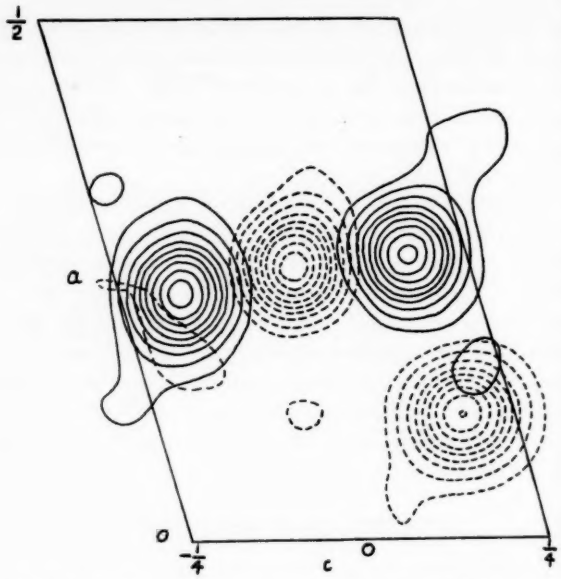


FIG. 4. Superposition of two sections of the final Fourier synthesis showing the boron positions. The sections are perpendicular to the *b* axis, at $y=26/60$ (solid contours) and $y=17/60$ (broken contours), respectively.

indications of the false character of the model. Although the peak shifts were slight, a series of refinements were carried out in the hope of locating the hydrogen atoms. In its final form the three-dimensional Fourier synthesis

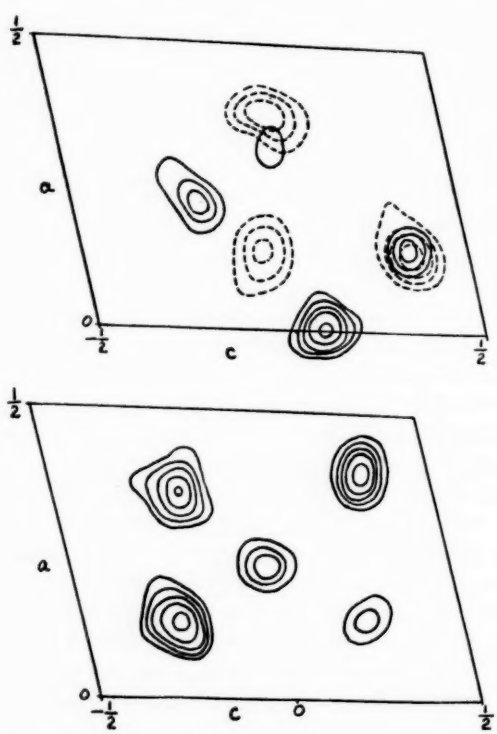


FIG. 5. Three sections of the Fourier difference synthesis showing the hydrogen positions. The sections are perpendicular to the *b* axis at $y=13/60$ (top, broken contours), $y=17/60$ (top, solid contours) and $y=28/60$ (bottom picture). Overlaps in the top picture do not indicate different hydrogen atoms.

TABLE I. Atomic coordinates.

| Atom | Type | $x$ | $y$ | $z$ |
|---|---|---|---|---|
| $B_1$ | $B_I$ | 0.277 | 0.415 | 0.172 |
| $B_2$ | $B_{II}$ | 0.117 | 0.296 | 0.179 |
| $B_3$ | $B_I$ | 0.267 | 0.268 | 0.010 |
| $B_4$ | $B_{II}$ | 0.243 | 0.425 | 0.844 |
| $H_1$ | $H_I$ | 0.396 | 0.444 | 0.307 |
| $H_2$ | $H_{IV}$ | 0.160 | 0.431 | 0.246 |
| $H_3$ | $H_{II}$ | 0.141 | 0.239 | 0.350 |
| $H_4$ | $H_{III}$ | 0.000 | 0.311 | 0.066 |
| $H_5$ | $H_{IV}$ | 0.144 | 0.200 | 0.998 |
| $H_6$ | $H_I$ | 0.367 | 0.198 | 0.080 |
| $H_7$ | $H_{IV}$ | 0.232 | 0.299 | 0.805 |
| $H_8$ | $H_{II}$ | 0.366 | 0.456 | 0.815 |
| $H_9$ | $H_{III}$ | 0.131 | 0.452 | 0.744 |
| $H_{10}$ | $H_{IV}$ | 0.240 | 0.494 | 0.022 |

showed boron maxima[6] whose heights were, on a relative scale, 9, 9, 9, and 7.5, respectively. All other maxima were less than 2. The hydrogen atoms could not be located with any certainty. In spite of the evidence supporting the correctness of the boron positions, the result appeared doubtful because one of the B–B bond lengths was found to be about 1.35A, considerably shorter then expected.

The problem was now re-examined in the light of the sharpened Patterson-Harker section, $P(x, \frac{1}{2}, z)$. Although this section was essentially consistent with the *h*0*l* Patterson projection, a significant peak was discovered which, although present, was hardly noticeable in the projection. This peak called for a considerable shift in the position of one of the boron atoms and, consequently, a reassignment of a number of vectors shown in the Patterson function. Although the new boron position violated the almost-present false *Okl* symmetry, it was found possible to account satisfactorily for all vectors in terms of the *Okl* Patterson projection as well as the other principal Patterson projections. However, an unexplained inconsistency remained in the *Okl*

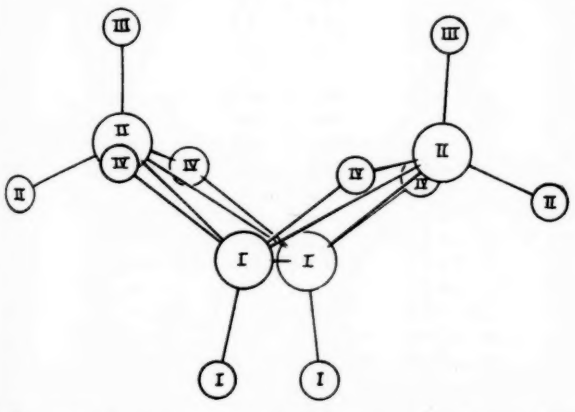


FIG. 6. The molecule of tetraborane. The boron (large circles) and hydrogen (small circles) atoms are numbered according to Table I.

[6] The $x$, $y$, $z$ coordinates of the four boron atoms in the false model are 0.235, 0.420, 0.160; 0.120, 0.398, 0.010; 0.260, 0.280, 0.025; and 0.260, 0.425, 0.835.

TABLE II. Interatomic distances[a] and bond angles.

(a) B–B bonds

$B_1-B_2=1.848$A
$B_2-B_3=1.847$A
$B_3-B_4=1.842$A
$B_4-B_1=1.844$A
Average $B_I-B_{II}$ $=1.845\pm0.002$A
$B_I-B_I=1.750$A
$B_{II}-B_{II}=2.786$A

(b) Regular B–H bonds

$B_1-H_1=1.16$A
$B_3-H_6=1.11$A
$B_2-H_3=1.12$A
$B_4-H_8=1.17$A
$B_2-H_4=1.07$A
$B_4-H_9=1.03$A
Average B–H (regular) $=1.11\pm0.04$A

(c) Bridge B–H bonds

$B_1-H_2=1.21$A
$B_1-H_{10}=1.16$A
$B_3-H_5=1.26$A
$B_3-H_7=1.19$A
Average $B_I-H_{IV}$ $=1.21\pm0.03$A

$B_2-H_5=1.44$A
$B_4-H_{10}=1.25$A
$B_2-H_5=1.49$A
$B_4-H_7=1.30$A
Average $B_{II}-H_{IV}$ $=1.37\pm0.10$A

(d) H–H distances

$H_I-H_I=2.80$A
$H_{II}-H_{II}=4.62$A
$H_{III}-H_{III}=2.81$A
$H_{II}-H_{III}=1.95\pm0.03$A
$H_I-H_{IV}=1.94\pm0.05$A
$H_{II}-H_{IV}=1.99\pm0.08$A
$H_{III}-H_{IV}=1.80\pm0.07$A
$H_{IV}-H_{IV}$ (parallel to $B_{II}-B_{II}$) $=1.78\pm0.04$A
$H_{IV}-H_{IV}$ (parallel to $B_I-B_I$) $=2.54\pm0.19$A

(e) Molecular angles

$\angle B_I-B_{II}-B_I=56.6°$
$\angle B_I-B_I-B_{II}=61.7°$
$\angle B_{II}-B_I-B_{II}=98.0°$
$\angle B_I-B_I-H_I=118°$
$\angle$ Between Planes of $B_IB_IB_{II}=118.1°$
$\angle$ Plane of $B_IB_IB_{II}$ to $B_{II}-H_{II}=112°$
$\angle$ Plane of $B_IB_IB_{II}$ to $B_{II}-H_{III}=122°$
$\angle$ Plane of $B_IB_IB_{II}$ to plane of $B_IB_{II}H_{IV}=170°$

(f) Close intermolecular distances

| Symmetry operation relating neighboring molecules | |
|---|---|
| $2_1$ | $H_3-H_{10}=2.72$A |
| $2_1-c$ | $H_6-H_9=3.12$A |
| $n$ | $H_4-H_6=2.75$A |
| $n-c$ | $H_2-H_6=3.08$A |
| $c$ | $H_3-H_7=2.61$A |
| $2_1-n$ | $H_9-H_2=2.80$A |
| $2_1+n-c$ | $H_8-H_1=2.56$A |

[a] Unfortunately, we have not corrected for series termination, which may be responsible for our small B–H distances and therefore for the small boron radius. However, we feel that this contribution to the B–B distances is very small and that there is no doubt about the molecular geometry.

TABLE III. Calculated bond orders in $B_4H_{10}$.

| Bond | $n$ | Number of equivalent bonds |
|---|---|---|
| $B_I-B_I$ | 0.38 | 1 |
| $B_I-B_{II}$ | 0.27 | 4 |
| $B_{II}-B_{II}$ | 0.01 | 1 |
| B–H (regular) | 0.96 | 6 |
| $B_I-H_{IV}$ (bridge) | 0.65 | 4 |
| $B_{II}-H_{IV}$ (bridge) | 0.35 | 4 |

TABLE IV. The atomic scattering factor for boron.

| $\sin\theta/\lambda$A$^{-1}$ | Int. Tabellen | This paper |
|---|---|---|
| 0.0 | 5.0 | 5.0 |
| 0.1 | 3.5 | 3.5 |
| 0.2 | 2.4 | 2.3 |
| 0.3 | 1.9 | 1.7 |
| 0.4 | 1.7 | 1.48 |
| 0.5 | 1.5 | 1.42 |
| 0.6 | 1.4 | 1.40 |
| 0.7 | 1.2 | 1.34 |

TABLE V. Observed and calculated structure factors.[a]

| *hkl* | $F_{calc}$ | $F_{obs}$ | *hkl* | $F_{calc}$ | $F_{obs}$ | *hkl* | $F_{calc}$ | $F_{obs}$ | *hkl* | $F_{calc}$ | $F_{obs}$ |
|---|---|---|---|---|---|---|---|---|---|---|---|
| 000 | +120.0 | ... | 103 | −2.4 | 3.2 | 193 | −6.6 | 6.2 | 261 | +3.5 | 3.9 |
| 002 | −7.6 | 7.0 | 107 | −2.3 | 2.5 | 1,10,$\bar{4}$ | +3.7 | 4.0 | 262 | −2.5 | 3.0 |
| 006 | +7.8 | 7.7 | 11$\bar{5}$ | −6.6 | 6.9 | 1,10,$\bar{3}$ | −1.6 | 1.9 | 263 | −3.7 | 3.7 |
| 011 | −17.5 | 16.2 | 11$\bar{3}$ | +2.2 | 2.2 | 1,10,$\bar{2}$ | +3.1 | 3.1 | 266 | +3.3 | 3.1 |
| 012 | −6.5 | 6.9 | 11$\bar{1}$ | −18.0 | 16.5 | 1,10,$\bar{1}$ | +3.2 | 3.7 | 27$\bar{5}$ | −3.1 | 3.6 |
| 013 | +10.1 | 9.6 | 111 | −30.0 | 26.8 | 1,10,0 | −1.8 | 1.4 | 27$\bar{3}$ | +2.8 | 2.1 |
| 015 | −3.2 | 3.2 | 113 | +2.9 | 2.3 | 1,10,1 | −1.6 | 2.4 | 27$\bar{2}$ | +2.2 | 3.0 |
| 016 | −2.2 | 2.4 | 115 | −3.8 | 3.6 | 1,10,2 | +4.0 | 4.0 | 271 | −3.6 | 3.7 |
| 017 | −1.7 | 2.1 | 117 | −2.7 | 2.5 | 1,10,4 | +2.4 | 2.8 | 270 | −2.2 | 2.3 |
| 020 | −10.1 | 9.3 | 12$\bar{6}$ | +4.0 | 4.6 | 1,10,5 | +1.8 | 2.9 | 271 | −6.6 | 6.9 |
| 021 | +5.8 | 6.3 | 12$\bar{2}$ | −14.5 | 13.4 | 1,12,0 | −2.1 | 1.9 | 273 | +3.2 | 3.4 |
| 022 | −11.1 | 10.7 | 12$\bar{1}$ | −10.3 | 10.1 | 20$\bar{6}$ | −5.1 | 5.8 | 275 | −1.6 | 2.3 |
| 023 | −1.7 | 1.5 | 120 | +31.6 | 28.4 | 20$\bar{4}$ | −4.1 | 4.1 | 276 | −1.3 | 2.3 |
| 024 | −3.9 | 3.7 | 121 | +4.1 | 4.9 | 20$\bar{2}$ | +2.6 | 2.9 | 28$\bar{4}$ | −1.6 | 1.9 |
| 026 | −1.3 | 1.5 | 122 | −6.0 | 4.8 | 200 | −38.4 | 33.0 | 28$\bar{3}$ | +2.0 | 1.9 |
| 027 | +1.6 | 1.7 | 123 | +4.3 | 4.2 | 202 | −2.1 | 1.8 | 28$\bar{2}$ | −4.8 | 5.2 |
| 031 | +2.5 | 3.9 | 124 | −3.0 | 2.4 | 204 | +2.6 | 2.5 | 280 | +1.5 | 1.7 |
| 032 | +5.3 | 4.7 | 126 | +4.4 | 3.9 | 206 | −5.5 | 5.1 | 283 | +1.5 | 2.0 |
| 033 | −2.9 | 2.7 | 13$\bar{5}$ | +2.6 | 2.3 | 21$\bar{7}$ | +1.8 | 2.1 | 284 | −3.4 | 3.2 |
| 035 | +2.2 | 2.4 | 13$\bar{4}$ | −3.3 | 3.6 | 21$\bar{6}$ | −2.5 | 3.1 | 29$\bar{5}$ | +1.8 | 2.4 |
| 040 | +9.9 | 9.1 | 13$\bar{3}$ | +13.1 | 13.5 | 21$\bar{5}$ | +2.2 | 2.6 | 29$\bar{3}$ | +3.2 | 3.6 |
| 041 | −4.6 | 4.5 | 13$\bar{2}$ | +1.1 | 1.6 | 21$\bar{3}$ | −8.9 | 8.4 | 290 | +1.9 | 1.4 |
| 042 | +6.2 | 6.2 | 13$\bar{1}$ | −4.6 | 3.7 | 21$\bar{2}$ | +8.5 | 8.1 | 291 | +2.8 | 3.5 |
| 043 | −0.9 | 1.5 | 130 | +7.6 | 7.4 | 21$\bar{1}$ | +13.3 | 13.3 | 293 | +2.3 | 2.8 |
| 044 | +3.9 | 3.9 | 131 | +7.8 | 8.7 | 210 | −10.2 | 8.4 | 2,10,$\bar{2}$ | +2.5 | 2.7 |
| 045 | +1.7 | 1.9 | 132 | −5.0 | 4.8 | 211 | +9.6 | 8.2 | 2,10,3 | −2.1 | 2.2 |
| 051 | −1.5 | 2.1 | 133 | +10.3 | 10.4 | 212 | +3.5 | 3.7 | 2,11,$\bar{3}$ | −3.9 | 4.4 |
| 052 | +2.1 | 2.3 | 14$\bar{4}$ | −5.6 | 5.6 | 213 | −6.5 | 6.6 | 2,11,0 | −2.1 | 1.7 |
| 053 | −3.7 | 3.5 | 14$\bar{2}$ | −1.3 | 2.3 | 214 | +1.5 | 2.1 | 2,11,2 | +1.7 | 1.9 |
| 054 | −0.9 | 1.5 | 14$\bar{1}$ | +0.6 | 1.6 | 215 | +2.2 | 2.2 | 2,11,3 | −3.4 | 3.3 |
| 055 | −1.5 | 1.7 | 140 | +11.4 | 9.9 | 217 | +1.3 | 1.4 | 2,12,$\bar{4}$ | +2.5 | 2.2 |
| 056 | −1.3 | 1.9 | 142 | −8.9 | 9.4 | 22$\bar{4}$ | +8.4 | 8.7 | 2,12,0 | −3.5 | 2.7 |
| 060 | −12.8 | 12.7 | 143 | −2.8 | 3.2 | 22$\bar{3}$ | −3.5 | 4.2 | 2,12,2 | +2.6 | 2.7 |
| 062 | +1.9 | 2.1 | 144 | −1.6 | 2.1 | 22$\bar{2}$ | +6.9 | 7.3 | 2,13,0 | +1.4 | 1.4 |
| 064 | +0.8 | 1.5 | 15$\bar{7}$ | −2.1 | 1.9 | 220 | −1.6 | 3.3 | 30$\bar{5}$ | −3.5 | 4.1 |
| 066 | −4.0 | 3.9 | 15$\bar{5}$ | −3.0 | 2.8 | 222 | +9.2 | 8.4 | 30$\bar{1}$ | +12.9 | 12.8 |
| 067 | +1.2 | 1.2 | 15$\bar{1}$ | −8.4 | 8.2 | 224 | +1.8 | 1.8 | 301 | −3.8 | 2.2 |
| 071 | +7.1 | 6.9 | 150 | −5.6 | 5.6 | 23$\bar{5}$ | −1.8 | 2.5 | 303 | +1.5 | 1.5 |
| 073 | −6.1 | 5.9 | 151 | −7.8 | 7.3 | 23$\bar{3}$ | −1.8 | 1.9 | 305 | +2.5 | 2.9 |
| 075 | +3.9 | 4.0 | 152 | +4.0 | 4.1 | 23$\bar{2}$ | −4.6 | 3.7 | 307 | +0.2 | 0.9 |
| 080 | −5.9 | 5.7 | 155 | −2.5 | 2.4 | 23$\bar{1}$ | +7.2 | 6.0 | 31$\bar{7}$ | +2.1 | 2.0 |
| 081 | −3.4 | 3.9 | 157 | −1.6 | 1.3 | 230 | +6.5 | 7.5 | 31$\bar{5}$ | +3.1 | 3.6 |
| 082 | +5.0 | 4.9 | 16$\bar{6}$ | +1.8 | 2.2 | 231 | −4.1 | 3.5 | 31$\bar{3}$ | +4.8 | 4.5 |
| 084 | +3.0 | 3.6 | 16$\bar{4}$ | +2.9 | 2.5 | 232 | −3.8 | 3.9 | 31$\bar{1}$ | +6.9 | 6.5 |
| 086 | −1.6 | 1.7 | 16$\bar{2}$ | −4.8 | 4.1 | 234 | −2.9 | 3.5 | 310 | −0.8 | 1.6 |
| 091 | −2.5 | 2.4 | 160 | +8.7 | 9.0 | 24$\bar{4}$ | −6.5 | 5.9 | 311 | +8.6 | 7.9 |
| 092 | +1.8 | 2.1 | 161 | +2.3 | 2.7 | 24$\bar{3}$ | +4.5 | 4.2 | 317 | +1.6 | 1.0 |
| 093 | −1.5 | 2.1 | 162 | +2.0 | 2.0 | 24$\bar{2}$ | −6.0 | 6.3 | 32$\bar{6}$ | −2.6 | 3.2 |
| 094 | −2.2 | 2.6 | 163 | −1.2 | 1.7 | 240 | −2.2 | 2.4 | 32$\bar{5}$ | +2.2 | 2.6 |
| 095 | −1.9 | 2.4 | 166 | +2.6 | 2.2 | 241 | −3.7 | 3.1 | 32$\bar{4}$ | +2.3 | 1.9 |
| 0,10,0 | +2.7 | 3.2 | 17$\bar{6}$ | +2.4 | 2.2 | 242 | −8.1 | 7.3 | 32$\bar{3}$ | −2.1 | 1.9 |
| 0,10,2 | −2.5 | 2.4 | 17$\bar{4}$ | −1.5 | 2.1 | 243 | +5.7 | 5.2 | 32$\bar{1}$ | −7.8 | 7.5 |
| 0,10,3 | +0.7 | 1.5 | 17$\bar{1}$ | +3.8 | 3.9 | 25$\bar{5}$ | +1.8 | 2.1 | 320 | −10.2 | 9.2 |
| 0,11,2 | −2.4 | 2.3 | 170 | +2.1 | 1.6 | 25$\bar{3}$ | +8.2 | 8.4 | 321 | +4.6 | 3.6 |
| 0,11,3 | +3.9 | 4.0 | 172 | −2.1 | 2.0 | 25$\bar{2}$ | +2.1 | 2.2 | 323 | −4.8 | 4.5 |
| 0,11,4 | +2.0 | 1.7 | 175 | +1.8 | 2.4 | 25$\bar{1}$ | −7.8 | 6.9 | 326 | −2.2 | 2.2 |
| 0,12,0 | +1.7 | 1.7 | 18$\bar{6}$ | −3.4 | 3.3 | 251 | +4.4 | 5.1 | 33$\bar{3}$ | −14.9 | 14.8 |
| 0,12,1 | +1.4 | 1.5 | 18$\bar{3}$ | +2.0 | 2.1 | 253 | +6.3 | 6.6 | 33$\bar{2}$ | +5.8 | 5.8 |
| 0,13,1 | −2.4 | 2.4 | 180 | −8.5 | 8.6 | 25$\bar{5}$ | −2.2 | 2.2 | 33$\bar{1}$ | +7.6 | 7.5 |
| 0,14,0 | +2.3 | 2.4 | 186 | −3.4 | 3.2 | 26$\bar{6}$ | +4.6 | 4.5 | 331 | −2.4 | 1.7 |
| 10$\bar{7}$ | +2.3 | 2.6 | 19$\bar{5}$ | +1.5 | 2.0 | 26$\bar{5}$ | +2.5 | 3.0 | 333 | −10.1 | 9.6 |
| 10$\bar{5}$ | +1.8 | 2.0 | 19$\bar{3}$ | −6.4 | 6.2 | 26$\bar{4}$ | −2.3 | 2.3 | 334 | +2.3 | 2.4 |
| 10$\bar{3}$ | −2.5 | 1.3 | 19$\bar{2}$ | −1.5 | 1.8 | 26$\bar{3}$ | −3.9 | 4.3 | 335 | +2.4 | 2.6 |
| 10$\bar{1}$ | +14.6 | 15.2 | 191 | +3.0 | 3.2 | 26$\bar{1}$ | −1.0 | 1.5 | 34$\bar{6}$ | −3.9 | 3.7 |
| 101 | −5.0 | 4.2 | 192 | +3.0 | 3.2 | 260 | +11.7 | 11.3 | 34$\bar{5}$ | −1.6 | 1.9 |

TABLE V.—*Continued.*

| *hkl* | $F_{calc}$ | $F_{obs}$ | *hkl* | $F_{calc}$ | $F_{obs}$ | *hkl* | $F_{calc}$ | $F_{obs}$ | *hkl* | $F_{calc}$ | $F_{obs}$ |
|---|---|---|---|---|---|---|---|---|---|---|---|
| 34$\bar{4}$ | +8.0 | 9.1 | 416 | −1.3 | 1.5 | 52$\bar{4}$ | −6.0 | 5.6 | 62$\bar{6}$ | +1.4 | 1.7 |
| 34$\bar{2}$ | +3.2 | 4.1 | 42$\bar{8}$ | −1.8 | 1.1 | 52$\bar{2}$ | +5.3 | 5.6 | 62$\bar{5}$ | −1.4 | 1.7 |
| 34$\bar{1}$ | +3.3 | 3.2 | 42$\bar{4}$ | −6.6 | 6.9 | 52$\bar{1}$ | +5.2 | 4.8 | 62$\bar{4}$ | +3.2 | 3.3 |
| 340 | −7.5 | 6.9 | 42$\bar{3}$ | −2.4 | 2.3 | 520 | +5.9 | 5.5 | 62$\bar{3}$ | +2.4 | 2.5 |
| 341 | −1.5 | 2.7 | 42$\bar{2}$ | −5.9 | 6.0 | 522 | −4.0 | 3.7 | 62$\bar{2}$ | +2.3 | 2.4 |
| 342 | +8.5 | 8.5 | 42$\bar{1}$ | +5.1 | 5.1 | 523 | +1.2 | 1.9 | 62$\bar{1}$ | −2.8 | 2.9 |
| 343 | +2.9 | 2.9 | 420 | +4.4 | 4.2 | 524 | +1.3 | 1.8 | 621 | −1.4 | 2.3 |
| 344 | +1.4 | 1.8 | 422 | −5.4 | 4.9 | 525 | +1.7 | 1.8 | 622 | +1.9 | 1.6 |
| 346 | −2.5 | 1.9 | 424 | −3.2 | 3.4 | 53$\bar{6}$ | −1.8 | 2.4 | 623 | +2.0 | 2.3 |
| 35$\bar{7}$ | +2.5 | 2.2 | 425 | +2.2 | 2.3 | 53$\bar{3}$ | +8.1 | 7.7 | 624 | +2.4 | 2.0 |
| 35$\bar{5}$ | +2.3 | 2.3 | 426 | +1.4 | 1.3 | 530 | −3.5 | 3.2 | 63$\bar{7}$ | −1.3 | 1.3 |
| 35$\bar{4}$ | +2.4 | 2.7 | 43$\bar{3}$ | +4.1 | 4.8 | 533 | +6.5 | 6.6 | 63$\bar{6}$ | −1.2 | 1.6 |
| 35$\bar{2}$ | −5.9 | 6.2 | 43$\bar{2}$ | +3.3 | 3.5 | 54$\bar{6}$ | +2.1 | 2.2 | 63$\bar{4}$ | −1.9 | 1.6 |
| 35$\bar{1}$ | +6.9 | 6.3 | 43$\bar{1}$ | +2.4 | 2.5 | 54$\bar{4}$ | −4.2 | 4.2 | 63$\bar{1}$ | −3.5 | 3.7 |
| 350 | +2.6 | 2.5 | 430 | +0.6 | 1.2 | 54$\bar{2}$ | −3.5 | 4.1 | 630 | −2.2 | 1.9 |
| 351 | +5.7 | 5.7 | 433 | +3.3 | 3.1 | 54$\bar{1}$ | −2.4 | 2.2 | 631 | +1.5 | 1.5 |
| 354 | −3.9 | 3.9 | 434 | +3.3 | 3.5 | 540 | +3.7 | 3.1 | 632 | −3.2 | 2.8 |
| 355 | +2.9 | 1.8 | 44$\bar{4}$ | +5.0 | 4.6 | 542 | −3.8 | 3.6 | 64$\bar{5}$ | +2.3 | 2.7 |
| 36$\bar{4}$ | −3.2 | 3.9 | 44$\bar{2}$ | +6.2 | 5.1 | 543 | −1.7 | 2.2 | 64$\bar{4}$ | −3.2 | 3.2 |
| 36$\bar{2}$ | −2.5 | 2.6 | 44$\bar{1}$ | −3.2 | 3.6 | 544 | −2.6 | 2.6 | 64$\bar{2}$ | −2.6 | 2.7 |
| 361 | −2.0 | 2.3 | 440 | −2.0 | 2.0 | 55$\bar{7}$ | −2.6 | 2.8 | 640 | −0.9 | 1.2 |
| 362 | −5.3 | 5.3 | 441 | +2.1 | 1.7 | 55$\bar{1}$ | −6.0 | 5.5 | 641 | +2.8 | 3.3 |
| 37$\bar{5}$ | −1.7 | 1.9 | 442 | +5.8 | 5.7 | 550 | +1.6 | 2.0 | 642 | −2.5 | 3.0 |
| 37$\bar{2}$ | +4.2 | 4.2 | 443 | −3.1 | 3.6 | 551 | −2.4 | 2.2 | 65$\bar{3}$ | +3.2 | 3.3 |
| 37$\bar{1}$ | −5.2 | 5.0 | 444 | +2.2 | 2.3 | 56$\bar{2}$ | +5.4 | 6.0 | 650 | +2.4 | 2.1 |
| 371 | −2.5 | 1.7 | 45$\bar{3}$ | −9.8 | 8.7 | 560 | +1.1 | 1.4 | 653 | +2.7 | 2.2 |
| 374 | +2.2 | 1.9 | 45$\bar{2}$ | −1.8 | 1.6 | 57$\bar{5}$ | +1.9 | 2.2 | 66$\bar{6}$ | +3.2 | 3.1 |
| 375 | −2.5 | 2.4 | 45$\bar{1}$ | +2.0 | 1.6 | 57$\bar{1}$ | +3.4 | 2.9 | 66$\bar{2}$ | +2.4 | 2.0 |
| 38$\bar{6}$ | +2.0 | 2.2 | 450 | −1.4 | 1.4 | 570 | −3.8 | 4.4 | 66$\bar{1}$ | −1.8 | 2.0 |
| 38$\bar{5}$ | +1.9 | 1.8 | 453 | −7.3 | 6.2 | 571 | +2.2 | 1.8 | 660 | +5.0 | 4.9 |
| 38$\bar{2}$ | +1.3 | 1.7 | 46$\bar{6}$ | −4.3 | 4.2 | 58$\bar{6}$ | −2.7 | 3.7 | 661 | −1.7 | 2.0 |
| 38$\bar{1}$ | −1.9 | 2.2 | 46$\bar{4}$ | +2.4 | 2.9 | 58$\bar{4}$ | +2.2 | 1.9 | 68$\bar{5}$ | +2.0 | 2.0 |
| 380 | +4.9 | 4.9 | 46$\bar{2}$ | −2.1 | 1.6 | 58$\bar{3}$ | −1.7 | 1.9 | 68$\bar{4}$ | −4.5 | 4.5 |
| 381 | +3.3 | 3.2 | 46$\bar{1}$ | +4.8 | 5.3 | 58$\bar{2}$ | −3.6 | 4.5 | 68$\bar{1}$ | +2.0 | 2.0 |
| 39$\bar{3}$ | +3.0 | 3.0 | 460 | −7.9 | 6.8 | 58$\bar{1}$ | +1.7 | 2.1 | 680 | +1.3 | 1.2 |
| 392 | −1.2 | 2.1 | 461 | −2.3 | 1.9 | 580 | −3.8 | 3.6 | 681 | +2.4 | 2.5 |
| 393 | +3.2 | 2.6 | 462 | +2.3 | 2.3 | 582 | +1.8 | 1.9 | 682 | −3.4 | 2.5 |
| 3,10,$\bar{4}$ | −4.3 | 4.9 | 465 | +2.3 | 2.2 | 583 | −2.1 | 1.9 | 69$\bar{5}$ | +0.9 | 1.6 |
| 3,10,$\bar{2}$ | −2.5 | 2.8 | 466 | −2.0 | 1.1 | 584 | −2.0 | 2.1 | 69$\bar{3}$ | +1.5 | 1.9 |
| 3,10,0 | +2.2 | 1.6 | 47$\bar{7}$ | +2.6 | 1.9 | 59$\bar{5}$ | −2.2 | 1.9 | 69$\bar{2}$ | +1.7 | 1.9 |
| 3,10,2 | −4.4 | 4.7 | 47$\bar{2}$ | −1.4 | 2.2 | 59$\bar{3}$ | −3.7 | 2.6 | 69$\bar{1}$ | +1.9 | 2.2 |
| 3,10,4 | −1.7 | 2.4 | 47$\bar{1}$ | +5.9 | 6.2 | 59$\bar{1}$ | +3.3 | 2.5 | 690 | −2.1 | 2.4 |
| 3,11,$\bar{3}$ | +3.0 | 3.5 | 470 | +1.7 | 1.3 | 590 | +2.2 | 2.3 | 6,10,$\bar{4}$ | +2.7 | 1.5 |
| 3,11,$\bar{1}$ | −4.0 | 3.5 | 472 | +1.9 | 2.3 | 591 | −2.6 | 2.3 | 6,10,2 | +2.5 | 1.9 |
| 3,11,3 | +2.2 | 2.3 | 475 | +1.5 | 1.9 | 593 | −2.0 | 1.5 | 6,10,3 | −1.1 | 1.5 |
| 3,12,0 | +2.8 | 2.8 | 48$\bar{4}$ | +3.6 | 3.3 | 5,10,$\bar{5}$ | −1.0 | 2.0 | 6,11,0 | +1.0 | 1.4 |
| 3,12,1 | +2.0 | 2.0 | 48$\bar{1}$ | −3.0 | 3.1 | 5,10,$\bar{4}$ | +3.6 | 3.3 | 70$\bar{5}$ | +2.5 | 2.8 |
| 3,12,3 | −1.4 | 1.6 | 482 | +2.3 | 2.4 | 5,10,$\bar{3}$ | +2.5 | 2.4 | 70$\bar{1}$ | +2.5 | 2.0 |
| 40$\bar{8}$ | +2.3 | 2.2 | 485 | −1.7 | 1.8 | 5,10,$\bar{2}$ | +1.9 | 2.1 | 701 | +3.9 | 4.2 |
| 40$\bar{6}$ | +4.2 | 4.6 | 490 | +0.9 | 1.4 | 5,10,2 | +3.2 | 2.6 | 703 | −1.0 | 1.5 |
| 40$\bar{4}$ | −3.0 | 2.8 | 4,12,$\bar{4}$ | −1.4 | 1.9 | 5,12,0 | −2.1 | 2.0 | 705 | +2.0 | 2.2 |
| 40$\bar{2}$ | +13.4 | 13.7 | 4,12,0 | +4.1 | 3.1 | 60$\bar{8}$ | −1.6 | 1.3 | 71$\bar{7}$ | +3.2 | 2.9 |
| 400 | +6.8 | 6.7 | 4,12,2 | −2.0 | 2.1 | 60$\bar{6}$ | −6.3 | 6.2 | 71$\bar{5}$ | +2.2 | 2.1 |
| 404 | +2.2 | 2.2 | 50$\bar{5}$ | −1.5 | 1.5 | 60$\bar{4}$ | +6.3 | 6.0 | 71$\bar{3}$ | −2.2 | 1.7 |
| 406 | +2.0 | 2.2 | 50$\bar{3}$ | +3.4 | 3.3 | 60$\bar{2}$ | −6.6 | 6.5 | 71$\bar{1}$ | +8.2 | 7.6 |
| 41$\bar{7}$ | −2.8 | 3.0 | 50$\bar{1}$ | −8.6 | 7.5 | 600 | −9.1 | 8.5 | 710 | −2.3 | 2.3 |
| 41$\bar{4}$ | +3.1 | 3.5 | 503 | +2.4 | 2.8 | 602 | +5.0 | 4.7 | 715 | +2.3 | 1.3 |
| 41$\bar{3}$ | +4.2 | 3.7 | 505 | −4.4 | 4.0 | 604 | −3.1 | 2.3 | 72$\bar{6}$ | −3.2 | 3.6 |
| 41$\bar{2}$ | −4.9 | 4.2 | 51$\bar{7}$ | −4.4 | 4.2 | 61$\bar{7}$ | +3.2 | 2.9 | 72$\bar{5}$ | −2.9 | 3.2 |
| 41$\bar{1}$ | −10.4 | 9.8 | 51$\bar{1}$ | −10.3 | 9.4 | 61$\bar{6}$ | +2.2 | 2.4 | 72$\bar{4}$ | +4.2 | 4.4 |
| 410 | −3.6 | 3.3 | 510 | +2.2 | 2.8 | 61$\bar{3}$ | −3.8 | 3.7 | 72$\bar{3}$ | −1.9 | 1.7 |
| 411 | −3.2 | 3.5 | 512 | −2.4 | 1.7 | 61$\bar{1}$ | +7.6 | 6.9 | 72$\bar{2}$ | −1.7 | 2.1 |
| 413 | +3.4 | 3.7 | 515 | −2.4 | 2.4 | 610 | +6.8 | 6.7 | 720 | −5.2 | 5.2 |
| 414 | −3.2 | 3.0 | 516 | +1.3 | 1.6 | 613 | −2.6 | 2.4 | 721 | −4.6 | 4.1 |
| 415 | −2.1 | 2.3 | 52$\bar{6}$ | +3.2 | 3.2 | 615 | +2.2 | 2.1 | 722 | +3.8 | 4.0 |

TABLE V.—*Continued.*

| *hkl* | $F_{calc}$ | $F_{obs}$ | *hkl* | $F_{calc}$ | $F_{obs}$ | *hkl* | $F_{calc}$ | $F_{obs}$ | *hkl* | $F_{calc}$ | $F_{obs}$ |
|---|---|---|---|---|---|---|---|---|---|---|---|
| $73\bar{5}$ | −3.6 | 3.6 | $81\bar{4}$ | −2.5 | 2.6 | $86\bar{4}$ | +2.1 | 1.9 | 960 | +1.5 | 1.4 |
| $73\bar{4}$ | +1.9 | 2.2 | $81\bar{3}$ | +3.0 | 2.5 | $86\bar{3}$ | +2.3 | 2.7 | $97\bar{2}$ | −2.2 | 1.9 |
| $73\bar{3}$ | −3.9 | 3.6 | $81\bar{1}$ | −4.7 | 4.1 | $86\bar{2}$ | −2.7 | 2.7 | $97\bar{1}$ | +2.2 | 2.2 |
| $73\bar{2}$ | −1.7 | <1.8 | 810 | −1.8 | 1.9 | 860 | −2.7 | 2.4 | 980 | −1.6 | 1.2 |
| $73\bar{1}$ | +1.4 | 1.8 | 812 | −2.5 | 2.1 | 870 | +2.2 | 1.9 | $99\bar{3}$ | −1.6 | 1.6 |
| 730 | +1.8 | 2.1 | $82\bar{4}$ | −4.0 | 4.5 | $88\bar{4}$ | +2.2 | 2.0 | $10,0,\bar{2}$ | −2.2 | 1.8 |
| 731 | −2.5 | 2.8 | 820 | −1.9 | 1.9 | 880 | −1.7 | 1.4 | 10,1,0 | +0.6 | 1.2 |
| 732 | +1.6 | 1.9 | 822 | −2.3 | 1.8 | 882 | +1.7 | 2.0 | $10,2,\bar{4}$ | +4.0 | 3.7 |
| 733 | −2.3 | 1.9 | $83\bar{5}$ | +1.9 | 2.3 | $90\bar{3}$ | −2.6 | 2.9 | $10,2,\bar{1}$ | −2.0 | 1.9 |
| $74\bar{4}$ | +3.7 | 3.1 | $83\bar{4}$ | +3.6 | 3.4 | $90\bar{1}$ | −2.3 | 2.0 | 10,2,2 | +2.5 | 2.0 |
| 742 | +1.7 | 1.9 | $83\bar{3}$ | −0.6 | 1.8 | $92\bar{3}$ | +3.6 | 3.7 | 10,4,2 | −1.4 | 1.1 |
| $75\bar{4}$ | −2.8 | 3.3 | 832 | +4.7 | 4.6 | 920 | +2.2 | 1.7 | $10,5,\bar{5}$ | +1.6 | 1.8 |
| $75\bar{1}$ | +4.5 | 5.1 | $84\bar{6}$ | +0.9 | 1.4 | 921 | +2.1 | 1.8 | $10,5,\bar{3}$ | +2.4 | 2.2 |
| 752 | −3.1 | 3.6 | $84\bar{5}$ | −1.3 | 1.6 | 923 | +2.6 | 3.0 | $10,5,\bar{2}$ | +2.0 | 1.6 |
| $76\bar{6}$ | −2.5 | 2.6 | $84\bar{4}$ | +3.3 | 3.3 | $93\bar{5}$ | +3.7 | 3.7 | $10,5,\bar{1}$ | −3.2 | 3.0 |
| 760 | −3.8 | 3.7 | $84\bar{3}$ | −2.4 | 3.2 | $93\bar{4}$ | −1.3 | 1.8 | 10,5,0 | +1.2 | 1.4 |
| $77\bar{3}$ | −1.2 | 2.1 | $84\bar{1}$ | +3.3 | 2.8 | $93\bar{3}$ | +3.3 | 2.8 | 10,5,1 | +1.9 | 1.6 |
| 770 | +2.8 | 3.0 | 840 | +1.5 | 1.6 | $93\bar{1}$ | −3.4 | 3.2 | 10,6,$\bar{3}$ | −2.0 | 1.9 |
| 780 | +3.8 | 3.2 | 841 | −2.8 | 2.0 | 931 | +3.3 | 2.9 | 10,6,0 | +1.6 | 1.6 |
| 790 | −1.6 | 1.6 | 842 | +2.0 | 1.8 | $94\bar{4}$ | −4.9 | 4.1 | 10,7,0 | −1.6 | 1.4 |
| $80\bar{6}$ | +4.4 | 4.4 | 843 | −1.8 | 1.8 | $94\bar{2}$ | +2.5 | 2.6 | $11,0,\bar{1}$ | +4.3 | 3.6 |
| $80\bar{4}$ | −1.9 | 1.8 | $85\bar{5}$ | −3.4 | 3.2 | 942 | −3.1 | 2.5 | 11,4,0 | −1.5 | 1.1 |
| 800 | +7.8 | 7.1 | 850 | −1.8 | 1.7 | 950 | −2.0 | 1.7 | $12,0,\bar{2}$ | +2.7 | 2.2 |
| 802 | −2.5 | 2.3 | 851 | −3.1 | 2.9 | $96\bar{4}$ | +1.6 | 1.9 | | | |
| $81\bar{7}$ | −2.1 | 2.4 | $86\bar{6}$ | −2.1 | 2.0 | $96\bar{1}$ | +2.9 | 2.2 | | | |

[a] A total of 429 reflections (not listed) which could have occurred on our films were below the limits of observations. For only 13 of these reflections was $F_{calc}$ greater than its observational limit, and no reflection was greater than 1.5 times its corresponding limit.

half-cell Patterson projection (Fig. 1). Its failure to reveal the peak violating the false symmetry may possibly be due to lack of resolution in this unsharpened map. The final *hOl* Fourier projection of the correct model is shown in Fig. 3.

A three-dimensional Fourier synthesis was then carried out with the revised model, from which accurate boron positions were obtained. All hydrogen atoms could be located in this synthesis, but in order to achieve a higher reliability a three-dimensional difference Fourier was made. The coefficients of the latter were obtained by subtracting the calculated boron contributions from the observed structure factors, and assigning to the unobserved $F$'s a hydrogen contribution equal and opposite to the calculated boron contribution. Figure 4 shows a superposition of two sections of the three-dimensional Fourier synthesis, giving the boron positions. Selected sections of the difference synthesis are shown in Fig. 5.

## FINAL MODEL AND DISCUSSION OF RESULTS

The final atomic coordinates as obtained from the three-dimensional Fourier syntheses are listed in Table I.

A drawing of the molecule is shown in Fig. 6. While no molecular symmetry is demanded by the space group, the results strongly indicate that the molecule possesses $C_{2v}$ symmetry. Thus, the notation in the second column of Table I identifies symmetrically equivalent atoms. The coordinates were used to calculate interatomic distances and bond angles. The results are given in Table II with the average deviations from the mean, in cases where several equivalent distances occur. The probable errors in the boron-boron bond lengths are estimated at about 0.02A for $B_I-B_I$ and $B_{II}-B_{II}$, and about 0.01A for $B_I-B_{II}$. For the B−H and H−H distances the mean deviations may be considered about equal to the probable error.

Referring to Fig. 6, it should be pointed out that the bridge hydrogens do not lie in the plane of $B_IB_IB_{II}$, but are displaced by about 0.16A toward the concave side of the molecule, giving a basket-like structure.

As the Pauling theory of partial single bonds has shown considerable success in explaining the bond distances in other electron deficient compounds,[7-9] it is interesting to examine the $B_4H_{10}$ molecule from this point of view. Assigning a bond order $n=1$ to a full 2-electron bond, the Pauling relation between bond distance $D$ and bond order $n$ is

$$D(1)-D(n)=0.6\log n.$$

Assuming the covalent radii of boron and hydrogen equal to 0.75 and 0.36A, respectively, the single bond distances are 1.50A for B−B and 1.10 for B−H. The

[7] L. Pauling, J. Am. Chem. Soc. **69**, 542 (1947).
[8] W. J. Dulmage and W. N. Lipscomb, J. Am. Chem. Soc. **73**, 3539 (1951).
[9] K. Hedberg, J. Am. Chem. Soc. **74**, 3486 (1952).

latter value includes an electronegativity correction of −0.01A. The calculated bond orders are given in Table III. The total bond order is 11.23 in satisfactory agreement with the value 11 expected on the grounds that the molecule contains 22 valence electrons. The calculated valence of boron is 3.17 to 3.18 and that of hydrogen is 0.96 to 1.00.

It is of interest that the $B_{II}-B_I-B_{II}$ bond angle is 98°, about midway between the corresponding angle of 90° in the octahedron and 108° in the icosahedron. Thus, the boron arrangement may be regarded as a fragment from either the octahedron or the icosahedron. The relatively open structure of this, the first member of the $B_NH_{N+6}$ series compared with the relatively compact higher $B_NH_{N+4}$ structures, probably is a factor relating to the comparatively greater reactivity.

The observed and calculated structure factors were adjusted to a common scale by plotting $\log F_0/F_c$ *vs* $(\sin\theta/\lambda)^2$ and finding the scale and temperature factor constants from the expression

$$\log F_0/F_c=\log A-(B/2.303)(\sin\theta/\lambda)^2.$$

However, when atomic scattering factors given in *Internationale Tabellen* (vol. 2, p. 571, 1935) were used, a straight line was not obtained. The deviations, though not large, were consistent in so far as they occurred independently in all three principal zones and in the plot of general *hkl* structure factors. It was therefore felt that the disagreement could not be accounted for in terms of a failure of the assumption of spherical atoms. A revised $f$ curve for boron as given in Table IV was therefore used in calculating the final $F_c$'s. With this assumption the value found for B was 3.4A². The observed and calculated structure factors are listed in Table V. The index of reliability $R=\Sigma||F_0|-|F_c||/\Sigma|F_0|$ for the 616 observed reflections is 10.7 percent. Including the 430 unobserved reflections and assuming their $F_0$ values to be equal to one-half the estimated maximum values, the index of reliability is 14.6 percent. The agreement can be considered very good.†

## DISORDERED PHASES

As mentioned earlier, a hexagonal modification was almost consistently obtained by crystallizing from a supercooled liquid. The axial lengths of this phase were found to be $a=5.79\pm0.03$A and $c=9.36\pm0.05$A, giving a cell volume of 272A³. Assuming 2 molecules per unit cell, the molecular volume is 136A³, or somewhat larger than the value of about 122A³ found for the monoclinic phase. Strong disorder was indicated by a very rapid, isotropic decrease of reflected intensities with increasing angle of reflection. The latter circumstance prevented the observation of more than 7 different reflections, which however, are consistent with the space group $D_{6h}^4-C6_3/mmc$. These facts as well as the axial ratio $c/a=1.62$ offer strong support of the view that the structure consists of a hexagonally close-packed arrangement of molecules randomly oriented in three dimensions. This hypothesis was tested by direct comparison of observed and calculated intensities.

The center of rotation of the molecule was assumed to lie on the twofold axis present in the molecule. Its exact location was arrived at by a trial and error method. Thus, it was found that the best agreement with the observed values was obtained when the center of rotation was chosen at a point 0.80A from the midpoint of the line joining the $B_I$ atoms, on the side of the $B_{II}$ atoms. This point is very close to the center of the smallest possible sphere circumscribed about the molecule.

A molecular form factor was calculated in the customary manner, using the assumed center of rotation. Within the unit cell the centers were located at

$$x=\tfrac{1}{3},\tfrac{2}{3};\quad y=\tfrac{2}{3},\tfrac{1}{2};\quad z=\tfrac{1}{4},\tfrac{3}{4},$$

as demanded in a close-packed arrangement.

TABLE VI. Observed and calculated structure factors for the disordered phase.

| *hkl* | $F_{calc}$ | $F_{obs}$ |
|---|---|---|
| 00.0 | +108.5 | ... |
| 00.2 | −29.4 | 30.0 |
| 00.4 | −2.1 | 1.7 |
| 10.0 | −18.1 | 16.1 |
| 10.1 | −21.9 | 22.1 |
| 10.2 | +4.4 | 5.3 |
| 10.3 | −0.3 | <1.3 |
| 11.0 | +1.9 | 1.9 |
| 20.0 | +0.7 | <1.3 |
| 20.1 | −2.0 | 2.1 |

Table VI shows the agreement between observed and calculated structure factors. The 7 observed reflections give $R=5.3$ percent. Thus, the good agreement strongly supports our assumption of randomly oriented, close-packed molecules.

What seemed like a second disordered modification of $B_4H_{10}$ was observed once, and an incomplete set of pictures was obtained. According to these pictures, the cell was hexagonal with $a=11.6$A, $c=16.7$A, suggesting $Z=16$ and a molecular volume almost exactly equal to that in the monoclinic phase. The unexpected value of $Z$ as well as the peculiar fact that $F_{00l}$ was observed for $l=4n$ only led us to doubt the reality of this phase. It was indeed found possible to account for all observations in terms of the monoclinic modification. The *hOl* reciprocal lattice net of this pseudohexagonal phase was

† *Note added in proof:*—If contributions of only boron atoms are employed, values of $R$ are 38 percent for *hOl* and 33 percent for *hkO* reflections for the false model, and 20 percent for either *hOl* or *hkO* reflections for the correct model. Thus the detailed agreement is really significantly worse for the false model. In the early stages of this study we could not estimate the effect of the hydrogen atoms on $R$, which their contribution eventually reduced as described above.

actually a superposition with equal weight of the nets $hkO$, $hkk$, and $h\bar{k}\bar{k}$ belonging to the monoclinic phase. The fact that this type of "triple twinning" is possible without producing diffraction effects typical of a badly split crystal seems to be a consequence of some peculiar geometrical relationships. In order for, say, $h20$ and $h11$ to fall on the same row line it is required that $b=c\sqrt{3}$ in the monoclinic phase, a condition which is indeed very closely fulfilled. Similarly, it must be considered a coincidence that, for example, the reciprocal lattice point 111 falls almost halfway between 020 and 120 so as to produce an apparent doubling of the pseudohexagonal $c$ axis.

The packing of molecules in the monoclinic phase suggests simple mechanisms for the formation of the disordered as well as the pseudohexagonal phases. The monoclinic form can be approximately described as having molecules stacked in layers parallel to the $bc$ plane, at $x=\frac{1}{4}$ and $\frac{3}{4}$. Within each such layer the packing of the molecular centers is approximately hexagonal, which is reflected in the axial ratio $b/c=\sqrt{3}$. The location of neighboring layers with respect to each other closely resembles a hexagonal close packing, except for a monoclinic translation of $\frac{1}{2}$ a $\cos\beta$ in the $c$ direction. Thus, the "formation" of the close packed disordered phase must be understood as a slight translation of adjacent layers producing a change in $\beta$ from 105.7° to 90°, accompanied by "free rotation" of the molecules.

This relationship between the monoclinic and the disordered, hexagonal phase explains the "triple twinning" responsible for the pseudohexagonal modification. In going from the disordered to the ordered form, there are evidently three different directions, 120 degrees apart, in which the monoclinic tilt can occur. Since the ordering process does not appreciably affect the location of individual molecules within the layers, or the lattice in the layer directions, one may assume that the tilt can occur randomly in the three directions. This would produce a hexagonal modification of the kind observed.

It is a pleasure to make the following acknowledgments. Financial support of this research was granted by the Office of Naval Research, Contract N8-onr-66203. Dr. L. V. McCarty of the General Electric Company, Schenectady, New York, very kindly supplied us with a pure sample of tetraborane. Mr. L. R. Lavine and Mr. M. Atoji assisted in the experimental work. Finally, it is a pleasure to acknowledge the cooperation of Professor R. Pepinsky, through whose courtesy the three-dimensional syntheses were carried out on the X−RAC.

THE JOURNAL OF CHEMICAL PHYSICS VOLUME 21, NUMBER 10 OCTOBER, 1953

# Electronic States of Diatomic Molecules: The Oxygen Molecule*

FAUSTO G. FUMI† AND ROBERT G. PARR
*Department of Chemistry, Carnegie Institute of Technology, Pittsburgh, Pennsylvania*

(Received March 6, 1953)

A scheme is proposed for the computation of electronic energy levels of diatomic molecules with fair accuracy and minimum labor. The theoretical LCAO MO method including configuration interaction is employed. However, the number of configurations considered is kept small; the energies of the asymptotic dissociation products for the various states are taken from atomic data in the manner of Pariser; the calculation of the interaction energies is simplified by the neglect of overlap in all terms and by the neglect of differential overlap in the electronic repulsion terms; and certain core parameters are fitted empirically. The first application is made to the oxygen molecule, using one empirical parameter. The vertical excitation energies from the ground state to the $^1\Delta_g$, $^1\Sigma_g^+$, $^3\Sigma_u^+$, and $^3\Sigma_u^-$ states are computed as functions of distance between 1.16A and 1.63A, and they agree with the observed values within 0.2 ev; excitation energies to the unobserved $^1\Sigma_u^-$, $^3\Delta_u$, $^1\Delta_u$, and $^1\Sigma_u^+$ states are also computed. The results are in substantial accord with a previous more involved calculation by Moffitt. A justification of the proposed scheme is presented which makes use of the orthonormalized atomic orbitals of Löwdin.

## 1.

THE availability of a large amount of accurate experimental data on the electronic levels of diatomic molecules provides an ideal background for theoretical work, and yet few quantitative calculations have been made on diatomic molecules other than hydrogen since the early applications of perturbational and variational techniques. The present work is not of comparable rigor but rather involves the development and application of a scheme to compute with minimum labor and fair accuracy electronic excitation energies in diatomic molecules involving several valence electrons, without necessarily obtaining a good approximation to the ground state.

The scheme is essentially the one proposed by Pariser and Parr[1] for the computation of the energy levels of complex unsaturated molecules. It falls within the

* This paper was presented by F. G. F. at the St. Louis Meeting of the American Physical Society, November 28–29, 1952. The work was supported in part by the U. S. Office of Naval Research, through Contract Nonr-493(00) with Carnegie Institute of Technology, in part by a grant from Research Corporation.

† Research Corporation Postdoctoral Fellow. Permanent address: Department of Physics, University of Milan, Milan, Italy.

[1] R. Pariser and R. G. Parr, J. Chem. Phys. **21**, 466, 767 (1953).

TABLE I. Wave functions for some electronic states of $O_2$.

| Configuration | States | Wave functions[a] |
|---|---|---|
| $A$ and $C$ | $^3\Sigma_g^-$ | $(u^+\bar{u}^+u^-\bar{u}^-g^+g^-)$ and $(g^+\mathbf{g}^+g^-\mathbf{g}^-u^+u^-)$ |
| | $^1\Sigma_g^+$ | $2^{-\frac{1}{2}}[(u^+\bar{u}^+u^-\bar{u}^-g^+\mathbf{g}^-)-(u^+\bar{u}^+u^-\bar{u}^-\mathbf{g}^+g^-)]$ and $2^{-\frac{1}{2}}[(g^+\mathbf{g}^+g^-\mathbf{g}^-u^+\bar{u}^-)-(g^+\mathbf{g}^+g^-\mathbf{g}^-\bar{u}^+u^-)]$ |
| | $^1\Delta_g$ | $(u^+\bar{u}^+u^-\bar{u}^-g^+\mathbf{g}^+)$ and $(g^+\mathbf{g}^+g^-\mathbf{g}^-u^+\bar{u}^+)$ |
| $B$ | $^3\Sigma_u^+$ | $2^{-\frac{1}{2}}[(u^+\bar{u}^+g^-\mathbf{g}^-u^-g^+)+(u^-\bar{u}^-g^+\mathbf{g}^+u^+g^-)]$ |
| | $^3\Sigma_u^-$ | $2^{-\frac{1}{2}}[(u^+\bar{u}^+g^-\mathbf{g}^-u^-g^+)-(u^-\bar{u}^-g^+\mathbf{g}^+u^+g^-)]$ |
| | $^3\Delta_u$ | $(u^+\bar{u}^+g^+\mathbf{g}^+u^-g^-)$ |
| | $^1\Sigma_u^+$ | $2^{-1}[(u^+\bar{u}^+g^-\mathbf{g}^-\bar{u}^-g^+)+(u^-\bar{u}^-g^+\mathbf{g}^+\bar{u}^+g^-)-(u^+\bar{u}^+g^-\mathbf{g}^-u^-\mathbf{g}^+)-(u^-\bar{u}^-g^+\mathbf{g}^+u^+\mathbf{g}^-)]$ |
| | $^1\Sigma_u^-$ | $2^{-1}[(u^+\bar{u}^+g^-\mathbf{g}^-\bar{u}^-g^+)-(u^-\bar{u}^-g^+\mathbf{g}^+\bar{u}^+g^-)-(u^+\bar{u}^+g^-\mathbf{g}^-u^-\mathbf{g}^+)+(u^-\bar{u}^-g^+\mathbf{g}^+u^+\mathbf{g}^-)]$ |
| | $^1\Delta_u$ | $2^{-\frac{1}{2}}[(u^+\bar{u}^+g^+\mathbf{g}^+\bar{u}^-g^-)-(u^+\bar{u}^+g^+\mathbf{g}^+u^-\mathbf{g}^-)]$ |

[a] Here $(u^+\bar{u}^+u^-\bar{u}^-g^+g^-)$, for example, represents the normalized Slater determinant, a typical term in the expansion of which is $(6!)^{-\frac{1}{2}}[(\pi_u^+\alpha)^1(\pi_u^+\beta)^2\cdot(\pi_u^-\alpha)^3(\pi_u^-\beta)^4(\pi_g^+\alpha)^5(\pi_g^-\alpha)^6]$, where $\alpha$ and $\beta$ are one-electron spin functions and superscripts denote electrons.

framework of one-electron theories and uses the formalism of molecular orbital theory in the approximation in which molecular orbitals (MO) are expressed as linear combinations of atomic orbitals (LCAO). However, we consider the possibility that molecular states might not be properly described in simple configurational language, where a configuration is defined by assigning electrons to MO's; we allow for configuration interaction. The choice of molecular orbital language is suggested by the availability of much outstanding qualitative work by Mulliken and others on the interpretation of the electronic spectra of diatomic molecules in terms of MO configurations.

The important features of the scheme[1] are the obtainment of the energies of the asymptotic dissociation products of molecular states from atomic data;[2,3] a considerable simplification of molecular algebra[4] effected by the neglect of overlap in the core terms and by the neglect of differential overlap in the electronic repulsion terms, and the treatment of certain molecular core parameters as empirical quantities.[1,5]

For a first application of the scheme we have chosen the oxygen molecule. Here the quantitative treatment is simplified by the possibility of accounting qualitatively for the low excited states on the $\pi$-electron approximation. Moffitt[5] and Meckler[6] have also recently treated $O_2$. Meckler was interested in the magnetic properties of the ground state of the molecule over a wide range of distance and used Gaussian atomic functions; consequently he had to include a large amount of configuration interaction. Moffitt set out to test conventional LCAO MO theory with configuration interaction, and he arrived at a preliminary formulation and made a first application of his important "atoms in molecules" idea. In his formulation one constructs molecular wave functions of proper behaviour at infinite distance; this is not required in the present formulation.

TABLE II. Energy formulas in terms of integrals over molecular orbitals.[a,b]

| | $I(\pi_u)$ | $I(\pi_g)$ | $J(\pi_u^+,\pi_u^+)$ | $J(\pi_g^+,\pi_g^+)$ | $J(\pi_u^+,\pi_g^+)$ | $K(\pi_u^+,\pi_u^-)$ | $K(\pi_g^+,\pi_g^-)$ | $K(\pi_u^+,\pi_g^-)$ | $K(\pi_u^+,\pi_g^+)$ | $(\pi_u^+\pi_u^+\|\pi_g^-\pi_g^-)$ |
|---|---|---|---|---|---|---|---|---|---|---|
| $^3\Sigma_g^-(A)$ | 4 | 2 | 6 | 1 | 8 | −2 | −1 | −2 | −2 | 0 |
| $^3\Sigma_g^-(C)$ | 2 | 4 | 1 | 6 | 8 | −1 | −2 | −2 | −2 | 0 |
| $H_{AC}$ | | | | | | | | −1 | 1 | |
| $^1\Sigma_g^+(A)$ | 4 | 2 | 6 | 1 | 8 | −2 | 1 | −2 | −2 | 0 |
| $^1\Sigma_g^+(C)$ | 2 | 4 | 1 | 6 | 8 | 1 | −2 | −2 | −2 | 0 |
| $H_{AC}$ | | | | | | | | 1 | 1 | |
| $^1\Delta_g(A)$ | 4 | 2 | 6 | 1 | 8 | −2 | 0 | −2 | −2 | 0 |
| $^1\Delta_g(C)$ | 2 | 4 | 1 | 6 | 8 | 0 | −2 | −2 | −2 | 0 |
| $H_{AC}$ | | | | | | | | 0 | 1 | |
| $^3\Sigma_u^+(B)$ | 3 | 3 | 3 | 3 | 9 | −1 | −1 | −3 | −3 | 1 |
| $^3\Sigma_u^-(B)$ | 3 | 3 | 3 | 3 | 9 | −1 | −1 | −3 | −1 | −1 |
| $^3\Delta_u(B)$ | 3 | 3 | 3 | 3 | 9 | −1 | −1 | −2 | −3 | 0 |
| $^1\Sigma_u^+(B)$ | 3 | 3 | 3 | 3 | 9 | −1 | −1 | −1 | −1 | 1 |
| $^1\Sigma_u^-(B)$ | 3 | 3 | 3 | 3 | 9 | −1 | −1 | −1 | −3 | −1 |
| $^1\Delta_u(B)$ | 3 | 3 | 3 | 3 | 9 | −1 | −1 | −2 | −1 | 0 |

[a] Except for the $H_{AC}$, the formulas given are for the energies of states of the indicated symmetries for the indicated configurations. The $H_{AC}$ are interaction elements between the $(A)$ and $(C)$ configurations.

[b] Definitions of integrals are $I(\phi)=\int\phi^*H_{\text{core}}\phi d\tau$, $J(\phi_i,\phi_j)=\int\phi_i^*(1)\phi_j^*(2)\,(e^2/r_{12})\phi_i(1)\phi_j(2)d\tau$, $K(\phi_i,\phi_j)=\int\phi_i^*(1)\phi_j^*(2)\,(e^2/r_{12})\phi_j(1)\phi_i(2)d\tau$, and $(\phi_i\phi_i|\phi_j\phi_j)=\int\phi_i(1)\phi_j(2)\,(e^2/r_{12})\phi_i(1)\phi_j(2)d\tau$.

[2] W. Moffitt, Proc. Roy. Soc. (London) **A210**, 246 (1951).
[3] R. Pariser, J. Chem. Phys. **21**, 568 (1953).
[4] R. G. Parr, J. Chem. Phys. **20**, 1499 (1952).
[5] W. Moffitt, Proc. Roy. Soc. (London) **A210**, 224 (1951).
[6] A. Meckler, Quarterly Progress Reports, Solid State and Molecular Theory Group, M.I.T., July 15 and October 15, 1952.

TABLE III. Energy formulas in terms of integrals over atomic orbitals—($A$) and ($C$) configurations.[a,b]

| | $\frac{1}{4}(aa\|aa)$ | $\frac{1}{4}(aa\|a_sa_s)$ | $\frac{1}{4}(aa\|bb)$ | $\frac{1}{4}(aa\|b_sb_s)$ | Core contribution |
|---|---|---|---|---|---|
| $^3\Sigma_g^-(A)$ | 3 | 23 | 15 | 19 | $6\alpha+2\beta$ |
| $^3\Sigma_g^-(C)$ | 3 | 23 | 15 | 19 | $6\alpha-2\beta$ |
| $H_{AC}$ | −1 | 3 | 1 | −3 | 0 |
| $^1\Sigma_g^+(A)$ | 7 | 19 | 19 | 15 | $6\alpha+2\beta$ |
| $^1\Sigma_g^+(C)$ | 7 | 19 | 19 | 15 | $6\alpha-2\beta$ |
| $H_{AC}$ | 3 | −1 | −3 | 1 | 0 |
| $^1\Delta_g(A)$ | 5 | 21 | 17 | 17 | $6\alpha+2\beta$ |
| $^1\Delta_g(C)$ | 5 | 21 | 17 | 17 | $6\alpha-2\beta$ |
| $H_{AC}$ | 1 | 1 | −1 | −1 | 0 |

[a] See Table II, footnote a.
[b] Definitions of integrals are $(pq|rs)=\int\chi_p(1)\chi_q(1)(e^2/r_{12})\chi_r(2)\chi_s(2)dv$, $\alpha=\int\chi_aH_{core}\chi_adv$, and $\beta=\int\chi_bH_{core}\chi_adv$, where $\chi_p$, $\chi_q$, $\chi_r$, and $\chi_s$ are Slater AO's from the set, $a$, $a_s$, $b$, $b_s$.

TABLE IV. Energy formulas in terms of integrals over atomic orbitals—($B$) configuration.[a,b]

| | $\frac{1}{4}(aa\|aa)$ | $\frac{1}{4}(aa\|a_sa_s)$ | $\frac{1}{4}(aa\|bb)$ | $\frac{1}{4}(aa\|b_sb_s)$ | Core contribution |
|---|---|---|---|---|---|
| $^3\Sigma_u^+$ | 2 | 10 | 11 | 7 | $6\alpha$ |
| $^3\Sigma_u^-$ | 1 | 13 | 8 | 8 | $6\alpha$ |
| $^3\Delta_u$ | 2 | 10 | 9 | 9 | $6\alpha$ |
| $^1\Sigma_u^+$ | 5 | 9 | 8 | 8 | $6\alpha$ |
| $^1\Sigma_u^-$ | 2 | 10 | 7 | 11 | $6\alpha$ |
| $^1\Delta_u$ | 3 | 11 | 8 | 8 | $6\alpha$ |

[a] See Table II, footnote a.
[b] See Table III, footnote b.

## 2.

The qualitative interpretation of the low excited states of $O_2$ involves only two configurations:[7,5]

$$[(KK)(\sigma_g2s)^2(\sigma_u2s)^2(\sigma_g2p)^2](\pi_u2p)^4(\pi_g2p)^2, \quad (A)$$

$$[(KK)(\sigma_g2s)^2(\sigma_u2s)^2(\sigma_g2p)^2](\pi_u2p)^3(\pi_g2p)^3. \quad (B)$$

Indeed one can show by using the vector model and Pauli principle that the (A) configuration gives the states $^3\Sigma_g^-$, $^1\Sigma_g^+$, and $^1\Delta_g$, while the (B) configuration gives the states $^3\Sigma_u^+$, $^3\Sigma_u^-$, $^3\Delta_u$, $^1\Sigma_u^+$, $^1\Sigma_u^-$, and $^1\Delta_u$. These include the observed low excited states of $O_2$.

It seems reasonable to try and develop a quantitative treatment of these states on the $\pi$-electron approximation.[5] There is then only one configuration to consider besides (A) and (B):

$$[(KK)(\sigma_g2s)^2(\sigma_u2s)^2(\sigma_g2p)^2](\pi_u2p)^2(\pi_g2p)^4. \quad (C)$$

TABLE V. Values of integrals (ev).[a]

| | Internuclear distance (A) 0 | 1.163 | 1.279 | 1.396 | 1.512 | 1.628 |
|---|---|---|---|---|---|---|
| $(aa\|bb)$ | 14.52 | 11.213 | 10.350 | 9.601 | 8.947 | 8.372 |
| $(aa\|b_sb_s)$ | 12.62 | 11.019 | 10.216 | 9.507 | 8.880 | 8.324 |
| $-\beta$ | | 5.381 | 3.283 | 2.390 | 1.956 | 1.689 |

[a] See Table III, footnote b, for definitions of integrals.

[7] G. Herzberg, *Spectra of Diatomic Molecules* (D. Van Nostrand Company, Inc., New York, 1950), pp. 345–346, 559–560.

This gives rise to states of the same type as does configuration (A), so that for the states $^3\Sigma_g^-$, $^1\Sigma_g^+$, and $^1\Delta_g$ there will be configuration interaction.

To construct the wave functions for these states we have to resolve the degeneracy of the Slater determinants going with each configuration by using the operators which commute with the Hamiltonian, the angular momentum around the molecular axis, and the total spin. $\Sigma$ states must also be eigenstates of the reflections in planes through the molecular axis. The resolution of the degeneracy is facilitated by the use of $\pi$-electron MO's having a definite value of the angular momentum about the molecular axis; we call them $\pi^+$, $\pi^-$ depending on whether this value is $\hbar$, $-\hbar$. The results are given in Table I; only the simplest multiplet component is given for each state, since we neglect spin-orbit coupling.

TABLE VI. Valence states of O, $O^+$ and $O^-$.

| State[a] | Schematic representation[b] $\pi^+$ $\pi^-$ | Energy formula[c] |
|---|---|---|
| $O^-$, $V_1$ | O O O O | $6J_{\pi\pi}-2K_{\pi\pi}+4\alpha(O^-)$ |
| O, $V_2$ | {O O / O} {O / O O} | $3J_{\pi\pi}-K_{\pi\pi}+3\alpha(O)$ |
| $O^+$, $V_1$ | {O O / O O} | $J_{\pi\pi}+2\alpha(O^+)$ |
| $O^+$, $^3V_1$ | {O / O} {O / O} | $J_{\pi\pi}-K_{\pi\pi}+2\alpha(O^+)$ |
| $O^+$, $^1V_1$ | (O / O O / O) | $J_{\pi\pi}+K_{\pi\pi}+2\alpha(O^+)$ |

[a] The notation for the valence states is that of Moffitt, reference 5.
[b] A $o$ in the $\left\{\begin{matrix}\text{first}\\\text{second}\end{matrix}\right\}$ column under $\left\{\begin{matrix}\pi^+\\\pi^-\end{matrix}\right\}$ indicates occupancy of $\left\{\begin{matrix}\pi^+\\\pi^-\end{matrix}\right\}$ by an electron of spin $\left\{\begin{matrix}\alpha\\\beta\end{matrix}\right\}$. Brackets denote alternative, parentheses coupled situations.
[c] $\alpha(O^-)$, $\alpha(O)$ and $\alpha(O^+)$ denote the core energies of a $2p\pi$ electron in $O^-$, O and $O^+$, respectively. $J_{\pi\pi}$ is the Coulomb integral, $K_{\pi\pi}$ the exchange integral between two $2p\pi$ electrons.

## 3.

The energy formulas for the states of the (A), (C), and (B) configurations in terms of integrals over MO's are given in Table II.

Energy formulas in terms of integrals over AO's are given in Tables III and IV. To obtain these formulas, one uses the LCAO approximation, the assumption of zero overlap, and the assumption of zero differential overlap. That is, one writes

$$\begin{aligned}\pi_u^{\pm}&=\tfrac{1}{2}[(a+b)\pm i(a_s+b_s)],\\ \pi_g^{\pm}&=\tfrac{1}{2}[(a-b)\pm i(a_s-b_s)],\end{aligned} \quad (1)$$

where $a$, $a_s$ and $b$, $b_s$ are atomic $2p\pi_x$, $2p\pi_y$ Slater orbitals on the two atoms; one assumes in computing all terms in the energy formulas that

$$S=\int abdv=\int a_sb_sdv=0; \quad (2)$$

and one assumes in computing electronic repulsion terms that

$$abdv \equiv ab_sdv \equiv a_sbdv \equiv a_sb_sdv \equiv 0 \quad \text{(zero differential overlap)}. \quad (3)$$

The relevant consequence of Eq. (2) is that the MO's as given in Eq. (1) are normalized. The relevant consequence of Eq. (3) is that in the electronic repulsion parts of the final energy formulas only atomic Coulomb repulsion integrals appear. Thus, for example, one writes for the molecular Coulomb integral $J(\pi_u^+, \pi_u^+)$ the formula (see Tables II and IV for definitions and notations for integrals)

$$4J(\pi_u^+, \pi_u^+) = (aa|aa)+(aa|a_sa_s) + (aa|bb)+(aa|b_sb_s) \quad (4)$$

instead of the more complex formula

$$4J(\pi_u^+, \pi_u^+) = [1/(1+S)^2][(aa|aa)+(aa|a_sa_s) + (aa|bb)+(aa|b_sb_s)+4(aa|ab)+4(aa|a_sb_s) + 2(ab|ab)+2(ab|a_sb_s)]. \quad (5)$$

TABLE VII. Energies of spectroscopic and valence states of O, $O^+$, and $O^-$ (ev).

| State | Energy | Details of energy calculation[a,b] |
|---|---|---|
| $0^+, {}^1V_1 \equiv O^+, {}^2P$ | 18.6 | $18.6 = 13.6 + 5.0$, 5.0 from spectral data for $O^+$ |
| $0^+, V_1 \equiv O^+, {}^2D$ | 16.9 | $16.9 = 13.6 + 3.3$, 3.3 from spectral data for $O^+$ |
| $O^+, {}^3V_1$ | 14.7 | $14.7 = 13.6 + 1.1$, $1.1 = -\frac{1}{2}\left[\frac{{}^2P - {}^4S}{5} + \frac{{}^2D - {}^4S}{3}\right]$, using spectral data for $O^+$ |
| $O^+, {}^4S$ | 13.6 | ionization potential of O |
| O, $V_2$ | 0.5 | $0.5 = -\frac{1}{4}\left[\frac{{}^1D - {}^3P}{2} + \frac{{}^1S - {}^3P}{5}\right]$, using spectral data for O |
| O, $^3P$ | 0.0 | arbitrary energy zero |
| $0^-, V_1 \equiv O^-, {}^2P$ | −2.2 | negative electron affinity of O |

[a] Spectral data for O and for $O^+$ and the ionization potential and electron affinity for O are taken from Landolt-Bornstein Tables, Vol. I, 1950.
[b] In the two cases in which averages of spectroscopic states are taken, alternative averaging processes are possible which give slightly different results.

Mulliken[8] has shown that what is involved in passing from Eq. (5) to (Eq. (4) is a cancellation of the effect of certain terms in the numerator of (5) by the effect of $S$ in the denominator, so that our replacing formulas like (5) by formulas like (4) is not as unreasonable as may first appear. Indeed, a rather complete justification of this procedure is given in the Appendix below, where the neglect of overlap in the treatment of the core is also rationalized.

## 4.

Table V gives the values used for the integrals over atomic orbitals which appear in Tables III and IV.

The choice of values for the one-center integrals $(aa|aa)$ and $(aa|a_sa_s)$ is a crucial point in the scheme. Moffitt[2] and Pariser[3] have independently pointed out that a major source of error in LCAO MO calculations of excitation energies using Slater AO's is the inaccuracy of the energies of dissociation products, and they have given ways of eliminating this error which involve taking data from atomic spectroscopy and using atomic wave functions only to compute the properly molecular part of the energy. We take this attitude and extend the method of Pariser,[3,1] determining the values of $(aa|aa)$ and $(aa|a_sa_s)$ from an analysis of the valence states of O, $O^+$, and $O^-$ which are relevant to the molecular states being considered. The identification of these valence states is schematically described in Table VI; Table VII gives their location in energy as derived from a Mulliken-type treatment.[9] Values of $(aa|aa)$ and $(aa|a_sa_s)$ are obtained by a least-squares method from the following equations relating theoretical and experimental energy changes for dissociation processes:[3,1]

$$2O(V_2) \rightarrow O^+({}^1V_1)+O^-(V_1), \quad \Delta E = (aa|aa)+(aa_s|aa_s) = 15.4 \text{ ev},$$
$$2O(V_2) \rightarrow O^+(V_1)+O^-(V_1), \quad \Delta E = (aa|aa)-(aa_s|aa_s) = 13.7 \text{ ev}, \quad (6)$$
$$2O(V_2) \rightarrow O^+({}^3V_1)+O^-(V_1), \quad \Delta E = (aa|aa)-3(aa_s|aa_s) = 11.6 \text{ ev}.$$

For the two-center integrals $(aa|bb)$ and $(aa|b_sb_s)$ we take the values given by Kopineck[10] for Slater $2p\pi$ AO's of effective charge 4.55. "Ball" values for these integrals[4] were discarded because they do not satisfy the integral trigonometric identity,

$$(aa|bb)-(aa|b_sb_s) \equiv 2(aa_s|bb_s), \quad (7)$$

which relates integrals over Slater orbitals, and this identity is used in obtaining the one-center integrals from valence-state data. We have also found that lowering the values of $(aa|bb)$ and $(aa|b_sb_s)$ as suggested by Pariser and Parr[1] lessens the agreement with experiment of the final excitation energies.

TABLE VIII. Electronic excitation energies in $O_2$ (ev).[a]

| | | Internuclear distance (A)[b] 1.163 | 1.279 | 1.396 | 1.512 | 1.628 |
|---|---|---|---|---|---|---|
| $^1\Delta_g$ | calculated | 0.98 | 0.86 | 0.72 | 0.59 | 0.48 |
| | observed | 1.01 | 0.94 | 0.84 | 0.73 | 0.62 |
| $^1\Sigma_g^+$ | calculated | 1.90 | 1.61 | 1.30 | 1.04 | 0.83 |
| | observed | 1.70 | 1.55 | 1.37 | 1.17 | 0.97 |
| $^1\Sigma_u^-$ | calculated | 10.39 | 5.85 | 3.80 | 2.75 | 2.09 |
| | observed | — | — | — | — | — |
| $^3\Delta_u$ | calculated | 10.59 | 5.98 | 3.90 | 2.81 | 2.14 |
| | observed | — | — | — | — | — |
| $^3\Sigma_u^+$ | calculated | 10.78 | 6.12 | 3.99 | 2.88 | 2.18 |
| | observed | 10.78 | 6.12 | 3.99 | 2.88 | 2.18 |
| $^3\Sigma_u^-$ | calculated | 11.14 | 7.37 | 6.01 | 5.57 | 5.46 |
| | observed | 11.26 | 7.94 | 5.91 | 4.65 | 3.83 |
| $^1\Delta_u$ | calculated | 13.16 | 9.84 | 7.81 | 6.55 | 5.73 |
| | observed | — | — | — | — | — |
| $^1\Sigma_u^+$ | calculated | 15.06 | 11.74 | 9.71 | 8.45 | 7.63 |
| | observed | — | — | — | — | — |

[a] Excitation energies are relative to the $^3\Sigma_g^-$ ground state.
[b] The equilibrium internuclear distance for the ground state is 1.208A.

[8] R. S. Mulliken, J. Chim. Phys. 46, 497 (1949).

[9] R. S. Mulliken, J. Chem. Phys. 2, 782 (1934).
[10] H. J. Kopineck, Z. Naturforsch. 5a, 420 (1950).

The value of the core parameter $\alpha$ is not needed for the calculation of the excitation energies. We choose to consider $\beta$ an empirical quantity, fitting it to the observed excitation energy ${}^3\Sigma_g^- \rightarrow {}^3\Sigma_u^+$ obtained from Morse curves for these two states. (Moffitt[5] in effect did this also.) The resulting values of $\beta$ are included in Table V.

## 5.

Table VIII gives the electronic excitation energies from the ${}^3\Sigma_g^-$ ground state to the low excited states of $O_2$ calculated using the energy formulas of Tables III and IV and the values for the integrals given in Table V. The experimental values for the excitation energies quoted in Table VIII are obtained by computing Morse curves for the ground state and for each of the excited states using the experimental values for the equilibrium distance $r_e$, the dissociation energy $D_e$ and the harmonic vibration frequency $\omega_e$.[7,11] For the states ${}^1\Sigma_g^+$ and ${}^1\Delta_g$ the resulting experimental excitation energies are reliable to a few thousandths of an ev, but for the states ${}^3\Sigma_u^+$ and ${}^3\Sigma_u^-$ the precision drops to a few hundredths and a few tenths of an ev, respectively.

Our theoretical results agree with the experimental values within 0.2 ev. For the state ${}^3\Sigma_u^-$, however, the agreement is somewhat uncertain since the experimental values are not known accurately; anyhow, it is clear that for this state the $\pi$-electron approximation breaks down at the larger distances considered, as Moffitt[5] has also noted.

A comparison of our calculated values with those of Moffitt[5] reveals very good general agreement. The approximation of zero differential overlap may be said to be thus vindicated.

The predicted excitation energies to the non-observed states ${}^1\Sigma_u^-$, ${}^3\Delta_u$, ${}^1\Delta_u$ and ${}^1\Sigma_u^+$ should be somewhat qualified. We regard with some confidence the predictions for the states ${}^1\Sigma_u^-$ and ${}^3\Delta_u$, which should be stable and have a value for $D_e$ of the order of 1 ev. The predictions for the more excited states ${}^1\Delta_u$ and ${}^1\Sigma_u^+$, on the other hand, probably have only a qualitative value, giving the general location and the order in energy of these two states; whether they should be stable remains open to question.

## APPENDIX. A JUSTIFICATION OF THE SCHEME

The features of the scheme that need to be justified are the neglect of overlap in all energy terms and the neglect of differential overlap in the electronic repulsion terms, together with the use of Slater AO's to compute the integrals which are not assumed equal to zero.

Löwdin[12] has proved elegantly that his orthonormalized atomic orbitals ("Löwdin orbitals"),[13] which are defined to satisfy exactly the condition of zero overlap, satisfy approximately the condition of zero differential overlap. Here we shall consider in detail the case of diatomic molecules, deriving the relations between integrals over Löwdin orbitals and integrals over Slater orbitals. We shall see that the corrections are important only for the core integrals while for the electronic repulsion integrals the corrections may ordinarily be neglected.

Consider first a homonuclear diatomic molecule with equivalent Slater AO's $\chi_a$ and $\chi_b$ on the two atoms. Denoting by $\lambda_a$ and $\lambda_b$ the corresponding Löwdin orbitals, we have

$$\begin{aligned}\lambda_a &= A\chi_a + B\chi_b,\\ \lambda_b &= B\chi_a + A\chi_b,\end{aligned} \tag{8}$$

where

$$\begin{aligned}2A &= (1+S)^{-\frac{1}{2}} + (1-S)^{-\frac{1}{2}} = 2 + \tfrac{3}{4}S^2 + \cdots,\\ 2B &= (1+S)^{-\frac{1}{2}} - (1-S)^{-\frac{1}{2}} = -S + \cdots,\end{aligned}$$

in which $S = \int \chi_a \chi_b dv$. Then, denoting integrals over Löwdin orbitals by superscripts $\lambda$,

$$S^\lambda = 0, \tag{9}$$

$$\alpha^\lambda = (\alpha - S\beta)/(1-S^2) \simeq \alpha - \beta S, \tag{10}$$

$$\beta^\lambda = (\beta - S\alpha)/(1-S^2) \simeq \beta - S\alpha, \tag{11}$$

where $\alpha = \int \chi_a H_{\text{core}} \chi_a dv$ and $\beta = \int \chi_b H_{\text{core}} \chi_a dv$ are the Coulomb and resonance core integrals. The formula for $\beta^\lambda$ is indeed the one that Pariser and Parr[1] propose to apply in computing the core resonance integral to be used in the energy formulas whenever one does not want to consider this integral an empirical quantity. If we use the Mulliken[8] approximate formulas for the hybrid Coulomb-exchange and the exchange integral between $\chi_a$ and $\chi_b$ (tantamount to considering the first term in a certain infinite series expansion[14]),

$$\begin{aligned}(aa|ab) &= \tfrac{1}{2}S[(aa|aa) + (aa|bb)];\\ (ab|ab) &= S(aa|ab);\end{aligned} \tag{12}$$

we obtain also

$$\begin{aligned}(aa|aa)^\lambda &= (aa|aa) + [S^2/(2-2S^2)]\\ &\quad \times [(aa|aa) - (aa|bb)] \simeq (aa|aa);\\ (aa|bb)^\lambda &= (aa|bb) - [S^2/(2-2S^2)]\\ &\quad \times [(aa|aa) - (aa|bb)] \simeq (aa|bb);\\ (aa|ab)^\lambda &= (ab|ab)^\lambda = 0.\end{aligned} \tag{13}$$

Suppression of the Mulliken approximation would cause terms in $S^3$ to appear in these last formulas.

If each atom of the diatomic molecule carries two orthogonal Slater AO's, say $\chi_a$ and $\chi_{a_s}$ on the first atom, and $\chi_b$ and $\chi_{b_s}$ on the second, as in $O_2$, the argument can be generalized without difficulty. In particular, one finds that the integrals over Löwdin orbitals satisfy the identity, Eq. (7), which relates integrals over Slater orbitals.

[11] G. Herzberg, Can. J. Phys. **30**, 185 (1952).
[12] P. O. Löwdin (private communication).
[13] P. O. Löwdin, J. Chem. Phys. **18**, 365 (1950).
[14] K. Ruedenberg, J. Chem. Phys. **19**, 1433 (1951).

# Work Function in Field Emission. Chemisorption*

ROBERT GOMER
*Institute for the Study of Metals, The University of Chicago, Chicago, Illinois*
(Received April 27, 1953)

Analogs to the contact potential are calculated for the work function increase in field emission caused by polar chemisorbates. It is found that the discreteness of the dipoles constituting the layer leads to a work function increment smaller than the corresponding contact potential. The discrepancy becomes more marked at low coverages and high fields. A simple Fermi-Thomas calculation for estimating the depolarization of the electron cloud at a metal surface is given. It is probable that observed depolarizations of oxygen and nitrogen on tungsten can be explained in terms of this factor. The effect of the high fields used in cold emission on the work function is estimated and found to be of the order of 0.1 volt. Arguments are presented to show that a recent explanation of the fall in heats of chemisorption with coverage may need revision.

IT has been known for many years that adsorbates generally cause a change in the work function of the substrate. The work of de Boer,[1] Rideal,[2] Bosworth,[3] Mignolet,[4] and others has utilized this phenomenon to obtain information on the absorption of various substances on metal substrates. The chemisorption of oxygen, nitrogen, and hydrogen seems to increase the work function of metals, so that a negative contact potential results between a clean surface and one contaminated with one of these gases. It further appears that the contact potential varies almost linearly with the degree of coverage of the surface.[1,3] These facts are most simply and reasonably explained by assuming that the individual adsorption complexes (ad-atom-substrate or ad-molecule-substrate) have dipole moments and are but weakly polarizable. The contact potential is then given by $V_\infty = 2\pi M$, where $M$ is the dipole moment per unit area, so that $V_\infty$ is a linear function of the coverage $\theta$, if the dipole moment per adatom is constant.

The origin of the dipole moments of individual adatom complexes is not well understood. It is probably more or less correct that adsorbate atoms can be considered to have a slight excess charge, which, with its image in the metal, gives rise to a dipole of moment $M = 2dq$, $d$ being the distance of the center of the adatom to the surface and $q$ its effective charge. For simplicity, the latter is considered spherically symmetric, so that higher moments are ignored. It must be pointed out that this model is somewhat idealized, since it is doubtful whether surfaces can be considered smooth on the atomic scale, or rather whether the image plane can thus be described. Boudart[5] has pointed out that ad-atoms of slight positive charge can give rise to negative contact potentials if the adatom fits into holes actually below the surface, so that the positive end of the dipole points inward. It is doubtful whether this situation exists with adsorbates other than hydrogen. Even in the latter instance it may be that the effect exists only on certain loosely packed planes. The device described below will be able to answer this question.

The method of following chemisorption by contact potential measurements is relatively simple and fairly clearcut. It suffers from the fundamental disadvantage that the adsorption area must be macroscopic. This means in practice that wires or evaporated films are used, so that polycrystalline surfaces of unknown structure are involved.

The advent of Müller's field emission microscope[6] has supplied a tool singularly suited for the study of individual crystal surfaces under absolutely determinable conditions. It seems close at hand to apply this device to a study of chemisorption. Very interesting patterns have been noted by Müller,[6] Becker,[7] the author,[8a] and others. If a means can be found of determining the contact potentials of individual crystal faces of the single crystal emitter under various conditions of chemisorption, much valuable information can be obtained. Drechsler and Müller have already determined the work function of two crystallographic directions in clean tungsten by field emission.[9] Their method consisted of cutting a small hole in a metal plate, coated with fluorescent material, on which the field emission pattern was allowed to impinge. The portion of the beam penetrating through the hole was then measured separately and represented the current from a small region of the emitting crystal. By opening the tube and rotating the tip, emission from various directions could thus be measured and compared with the total emission. A very similar device has recently been built in this laboratory, consisting of a field

* This work was supported in part by Contract AF 33(038)-6534 with the United States Air Force.

[1] J. H. De Boer, *Electron Emission and Adsorption Phenomena*, (Cambridge University Press, Cambridge, 1935).

[2] R. C. L. Bosworth and E. K. Rideal, Physica **4**, 925 (1937).

[3] (a) Reference 2, this paper; (b) R. C. L. Bosworth, Proc. Cambridge Phil. Soc. **33**, 394 (1937); (c) R. C. L. Bosworth, Trans. Roy. Soc. N.S.W. **79**, 53 and 166 (1946).

[4] J. C. P. Mignolet, *Discussions on Heterogeneous Catalysis* (Faraday Society, 1950), p. 105.

[5] M. Boudart, J. Am. Chem. Soc. **74**, 3556 (1952).

[6] E. W. Müller, Z. Physik **131**, 136 (and previous papers).

[7] J. A. Becker, Bell System Tech. J. **30**, 907 (1951) and unpublished work.

[8] (a) R. Gomer, J. Chem. Phys. **21**, 293 (1953); (b) J. Chem. Phys. **20**, 1772.

[9] M. Drechsler and E. W. Müller, Z. Physik **134**, 208 (1953).

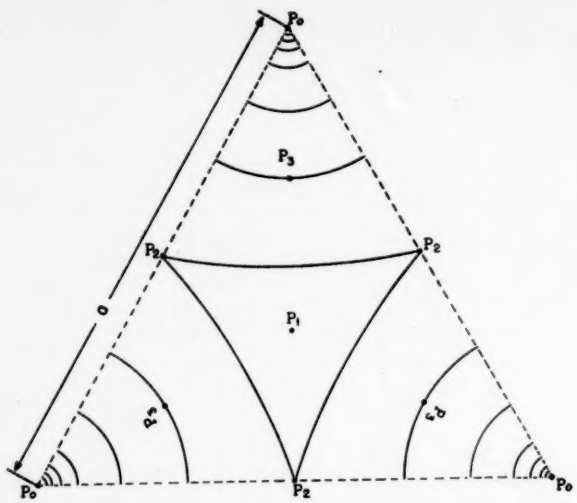


FIG. 1. Unit cell of triangular dipole array. Dipole-dipole distance is $a$ [dotted line connecting dipole sites ($P_0$)]. Equipotentials represented by solid lines. Points $P_1$, $P_2$, $P_3$ represent points for which potentials have been calculated.

emission tube with a hole in the spherical envelope leading to a suitably constructed Faraday cage. In our arrangement the emitter is mounted in a way permitting its rotation (by means of magnetically operated levers and bearings) about 2 azimuths, so that any part of the field emission pattern may be brought to bear on the analyzer cage.

It is apparent that this device enables one to measure the effective work function of individual crystallographic directions by use of the Fowler-Nordheim equation,[10] which relates field current to applied field in terms of a work function. Unfortunately, the evaluation of the results is not as direct as in the case of contact potential measurements. In the latter case one measures the maximum potential barrier that electrons must go over, whether this maximum occurs at the site of the double layer (which would be the case for a completely smeared-out dipole sheet, i.e., a condenser) or whether it is found at a much larger distance from the emitting surface. In our case the details of the structure of the potential in the vicinity of the surface are important, since field emission depends on a tunnel phenomenon taking place within 10–15A from the surface. Thus one must consider that the potential will vary with position between individual dipoles, and that it will only build up to the final value of the contact potential in a distance much larger than the dipole half-length $d$.

The chief object of this paper is, therefore, the determination of the potential curves for the emission of electrons from surfaces containing layers of dipoles. The determination of these curves is carried out by summation of individual dipole potentials. The calculations are thus analogous to those of patch theory in thermionic emission.[11] From these potential curves a graphical determination of the effective potential barriers in field emission will then be carried out for various fields, so that the effective work function can be found. Similar graphical determinations have been used by Drechsler and Müller[9] to obtain effective work functions for clean tungsten, taking into account surface roughness and local field enhancement. It will be obvious that the effective increment in work function in field emission will always be less than the corresponding contact potential, since the latter builds up to its full value at distances which increase with decreasing coverage. The effect of the high fields used in cold emission on the work function of the clean and gas-covered surface will be estimated in connection with polarization effects. Finally, some interesting conclusions regarding chemisorption can be drawn from the results on the structure of the electric potential within the ad-layer.

[10] R. H. Fowler and L. W. Nordheim, Proc. Roy. Soc. (London) A111, 173 (1928).
[11] J. A. Becker, Revs. Modern Phys. 7, 95 (1935).

## ELECTRIC POTENTIALS DUE TO DISCRETE DIPOLE LAYERS

For the purposes of this paper, individual dipoles will be considered as already described. The potential $P$

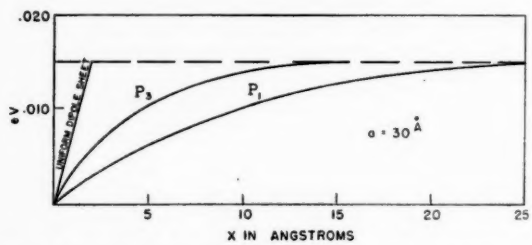


FIG. 2. Representative potential curves for nitrogen on tungsten, as functions of the distance $x$ from the surface.

due to a single dipole of this kind is then

$$P=14.4\alpha(1/[y^2+(x-d)^2]^{\frac{1}{2}}-1/[y^2+(x+d)^2]^{\frac{1}{2}}) \text{ ev}, \quad (1)$$

where $\alpha$ is the charge on the adatom in electron charges $d$ the dipole half-length, $x$ the Cartesian coordinate parallel to the dipole axis, and $y$ the coordinate perpendicular to it. The origin is taken at the center of the dipole. $P$ is given in electron volts if all distances are expressed in angstroms. $P$ given by Eq. (1) approaches the value for the potential due to a point dipole at large $x$ and $y$.

Our task is now the summation of the contributions of individual dipoles to the total potential at a given point. We shall consider only regular arrays of dipoles. This assumption is probably a good one for mobile chemisorbed layers, where dipole repulsion will tend to maintain the layer with maximum dipole-dipole distances. It may be possible to extend the present calculations to layers of other types; however, the present paper shows fundamental properties quite clearly and is an obvious starting point. Calculations were carried out for regular square and triangular

(hexagonal) arrays. The results proved to be almost identical when translated into terms of coverage $\theta$. Hence only triangular arrays will be discussed. Three points within the triangular "unit cell" containing half a dipole were considered, as indicated in Fig. 1. Summations, using the potential of Eq. (1) were then carried out for several values of the closest dipole-dipole distance $a$, extending to distances of $4a$. At distances greater than $4a$, direct summation was replaced by integration, using the potential due to a point dipole,

$$P_{4a-\infty}=\frac{4\pi d\alpha\cdot x\cdot 14.4}{.865a^2}\int_{4a}^{\infty}\frac{ydy}{(x^2+y^2)^{\frac{3}{2}}}$$
$$=209d\alpha x/a^2(x^2+16a^2)^{\frac{1}{2}}\text{ ev.} \quad (2)$$

The total potential at a given point and a given distance from the surface $x$ is then the sum of the corresponding summation and integration. Typical curves for $P_1$ and $P_3$ with $a=30$A are shown in Fig. 2. $\alpha$ is of the order of

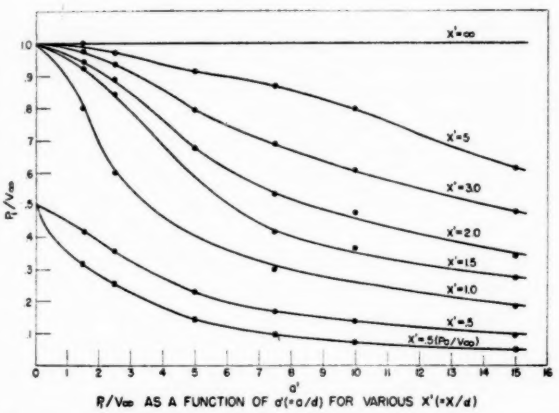


FIG. 3. Nondimensional plot of $P_1$ in terms of contact potential $V_\infty$, as a function of distance from the surface, $x$, and dipole-dipole distance $a$. $x$ and $a$ are expressed in terms of the dipole half-length $d$. A curve for $P_0$ at $x'=0.5$ is shown for comparison.

1/30 electron charges.[3] It is seen that the potential does not rise as steeply as it would in the case of a uniform dipole sheet, but builds up gradually, reaching the value of the contact potential $2\pi M$ at large distances. It is interesting to note that

$$\lim_{x\to\infty} P_{4a-\infty}=2\pi M. \quad (3)$$

Perhaps it should be stated explicitly that these results are strictly true only for infinite plane surfaces, corresponding to an upper limit of infinity in the integral of Eq. (2) or to a solid angle $2\pi$ in the formula $2\pi M$. For finite surfaces the upper limit of integration (or the corresponding solid angle at large $x$) would be less, bringing the potential back to zero at $x=\infty$. This is why finite crystals may have different work functions on various faces (caused by effective dipole layers), but the same inner chemical potential; calculations for infinite crystals lead to different inner potentials,

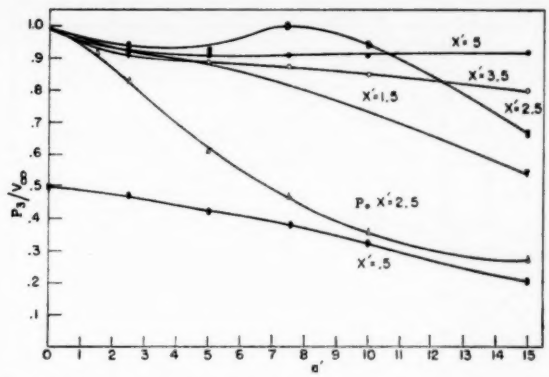


FIG. 4. Nondimensional plot of $P_3$ in terms of contact potential and dipole-dipole spacing as function of $x$. Symbols as in Fig. 3. A curve for $P_0$ at $x'=2.5$ is included for comparison. Note that the crossing over of curves implies that $P_3$ may have slight maxima before leveling off to the value of $V_\infty$ at $x=\infty$.

depending on the face by which the crystal is entered. The reason for this is obvious from the above. While it is true that the contact potential for finite crystals will fall off eventually, the region of interest in field emission is so close to the surface that this effect can be ignored.

The curves shown in Fig. 2 are based on a dipole half-length $d=2$A. All subsequent calculations will employ this value as most reasonable for actual cases. It is possible, however, to express the potentials nondimensionally as fractions of the contact potential $V_\infty$ and to express $a$ and $x$ in terms of $d$. The results for $P_1/V_\infty$ are summarized in this way in Fig. 3.

Calculations for $P_2$ and $P_3$ were not extended as far as those for $P_1$. Since the values of $P_2$ lie between the corresponding ones for $P_1$ and $P_3$, they are omitted. In general the values for $P_3$ are fairly close to those for $P_1$. Thus the region enclosed by equipotentials up to and including the points $P_3$ can be approximated as having a potential somewhere between $P_1$ and $P_3$; roughly 80 percent of the surface is thus accounted for. For $x'=0.5$ and 2.5 calculations were also made for $P_0$, representing the potential at an unfilled lattice site. Data for $P_0$ and $P_3$ are shown in Fig. 4. It is seen that $P_0$ is appreciably lower than the other potentials considered.

## EFFECTIVE WORK FUNCTION INCREMENTS RESULTING FROM DIPOLE LAYERS

The results of the previous section will now be applied to field emission. Before doing so, it may be useful to give a very simple rationale for the Fowler-Nordheim equation. Figure 5a shows a one-dimensional potential energy diagram for electrons in a metal and surrounding space, in the presence and absence of an applied external field. The penetration coefficient of the barrier in the presence of a field is given by

$$D=\text{const}\exp[-(m^{\frac{1}{2}}/\hbar)\int_0^l\sqrt{(V-E)}dx]. \quad (4)$$

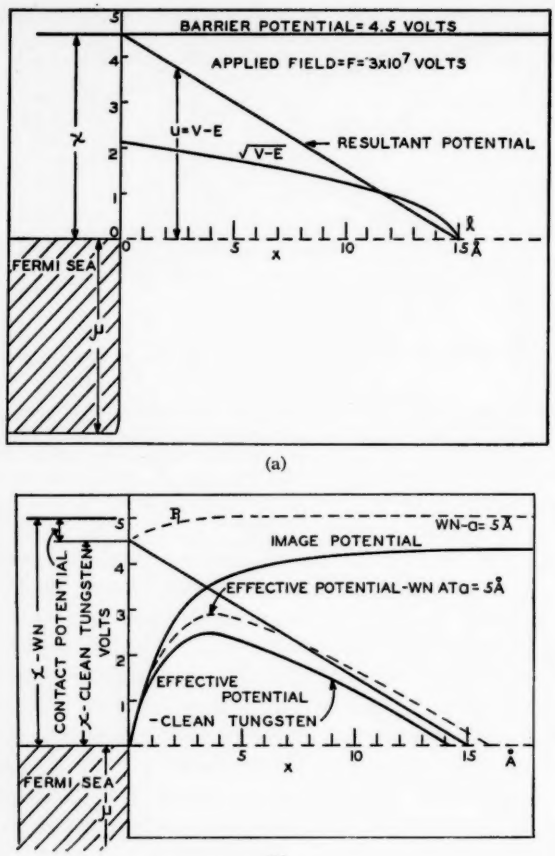


FIG. 5. Schematic potential diagrams for metal surfaces with applied external potentials. (a) Clean metal, no image potential assumed. $\chi$ represents work function, $\mu$ the depth of the Fermi sea. (b) Same as (a) but based on image potential. Barriers are shown for clean metal and metal with a dipole layer of nitrogen. The upper dotted curve represents $P_1$ alone and is drawn from an origin at 4.5 volts on the diagram.

The exponent is thus proportional to the area under the curve traced by the square root of the ordinate $u=V-E$ in Fig. 5a, since (to a good approximation[8b]) only electrons very near the top of the Fermi sea contribute to emission. The area $A$ is nearly triangular and hence given by

$$\tfrac{2}{3}\chi^{\frac{1}{2}}\cdot l=\tfrac{2}{3}\chi^{\frac{3}{2}}/F, \tag{5}$$

where $F$ is the applied field. Thus the dependence on work function and field of the Fowler-Nordheim exponent seems reasonable. In this simple picture image potential was neglected. It can readily be seen that its effect would be to decrease the effective barrier, which amounts to increasing the effective field. This is the nature of the image correction later introduced by Nordheim.[12]

In order to determine the effective increase in work function caused by a dipole layer, we proceed as follows. For a given field a plot of the potential barrier and its square root is constructed for the clean metal. The contribution of the dipole layer potential to the barrier is then added, using the $P_1$ values corresponding to the coverage (or dipole-dipole distance) under consideration. The square root areas for the clean and contaminated cases are then determined by cutting out and weighing. It is now assumed that the pre-exponential parts of the penetration coefficients and of the Fowler-Nordheim equation change negligibly compared to the exponential parts, so that

$$\chi+\Delta\chi=\chi\cdot\left(\frac{A+\Delta A}{A}\right)^{\frac{3}{2}}, \tag{5}$$

where $\chi$ represents the work function of the clean metal, $\Delta\chi$ the increment due to the double layer, $A$ the area of the square root barrier for the clean metal, and $A+\Delta A$ the area of the square root barrier for the metal in the presence of the layer. Figure 5b shows the barriers for a representative case. The classical image potential has been used and is blended smoothly into the Fermi level. It is clearly not correct to relate the simple Fowler-Nordheim equation to a potential barrier based on image potential. The following correction is therefore made: A third barrier is plotted, consisting of the clean metal barrier plus a uniform linear additional potential of known value (approximately equal to the mean value of the actual layer potential under consideration). The procedure outlined above is then used to determine the apparent $\chi+\Delta\chi$ for this case. A correction factor given by $(\chi+\Delta\chi)$ apparent/$(\chi+\Delta\chi)$ can thus be found and applied to the effective work function for the actual barrier. The effective $\Delta\chi$ for the layer can then be compared with the corresponding contact potential. These results are plotted for a range of fields and $\theta$ values in Fig. 6.

These data are based on values of $P_1$. A more correct procedure would require similar calculations for $P_2$, $P_3$, and so on. The resultant values of the work function would then have to be weighted by the corresponding emitting areas to determine the emission current at a given voltage. In practice, the error introduced by using $P_1$ is small, since $P_3$ is quite close to $P_1$ at all except very low coverages (large $a$). The effect of neglecting areas of higher work function than $P_1$ is to give slightly low values for the effective work functions at low coverage.

A previous investigation of the velocity distribution of electrons in field emission[8b] has shown that emerging electrons may be expected to have energies of the order of 0.1 ev transverse to the direction of emission. This energy is sufficient to prevent focussing effects by the lateral potential gradients existing in the region of the potential barrier. It can readily be shown that potential differences between $P_1$ and points as close as 1A to a dipole site do not exceed 0.1 ev.

A clean metal work function of $\chi=4.5$ ev was used. Effective dipole moments per ad-atom were those of nitrogen on tungsten, based on Bosworth's[3] value of

[12] L. W. Nordheim, Proc. Roy. Soc. (London) A121, 628 (1928).

the contact potential. In order to convert from values of $a$ to the equivalent values of $\theta$, a mean number of sites/cm$^2$ equal to $1.2\times10^{15}$ was assumed. $\theta$ is then given by

$$\theta=(3.1/a)^2, \tag{6}$$

i.e., the nearest neighbor distance at $\theta=1$ is taken as 3.1A. The contact potentials for oxygen and hydrogen on tungsten are so close to that for nitrogen that it is probably safe to use the percentage values given in Fig. 6 when dealing with these gases.

Two facts emerge from Fig. 6. There is a marked decrease in effective contact potential with increase in field. Comparison of Figs. 3 and 6 shows that the effective contribution to the work function can be expressed empirically by the potential due to the layer existing at a distance from the surface $x=5$A at $F=3\times10^7$ v/cm, and 2A at $F=6\times10^7$ v/cm. Over this range the relation is more or less linear. Second, the decrease in effective potential becomes less important at higher coverage, since a uniform dipole sheet is more closely approximated.

The curves of Fig. 6 indicate that one should not expect strictly linear Fowler-Nordheim plots in the case of contaminated surfaces, since the effective work function changes with field. While this is true, it is possible to work at fields of the order of $3-4\times10^7$ volts/cm and to stick to a very small range, so that the variation of work function over the working range is small.

## DEPOLARIZATION EFFECTS

The calculations to this point have been expressed in terms of the contact potentials existing at a given coverage $\theta$; these are average values based on measurements made on polycrystalline samples.

It is interesting to ask what causes the slight depolarizations observed by Bosworth.[3c] Two factors must be considered. The first is the depolarization of the adsorbate complex itself under the influence of neighboring dipoles. The existence of very strong potential gradients in dipole arrays was recognized many years ago by Langmuir.[13] A second factor which seems to have been overlooked is the following: Common sense shows that the electron cloud in a metal does not terminate sharply at the surface, since this would lead to infinite gradients of the wave function and hence infinite kinetic energies. The calculations of Bardeen[14] show that a spilling over of the electrons takes place and gives rise to a double layer with the negative end directed outward. The contribution to the work function by this layer is of the order of 1 ev. Smoluchowski's[14,15] refined considerations show that the details of

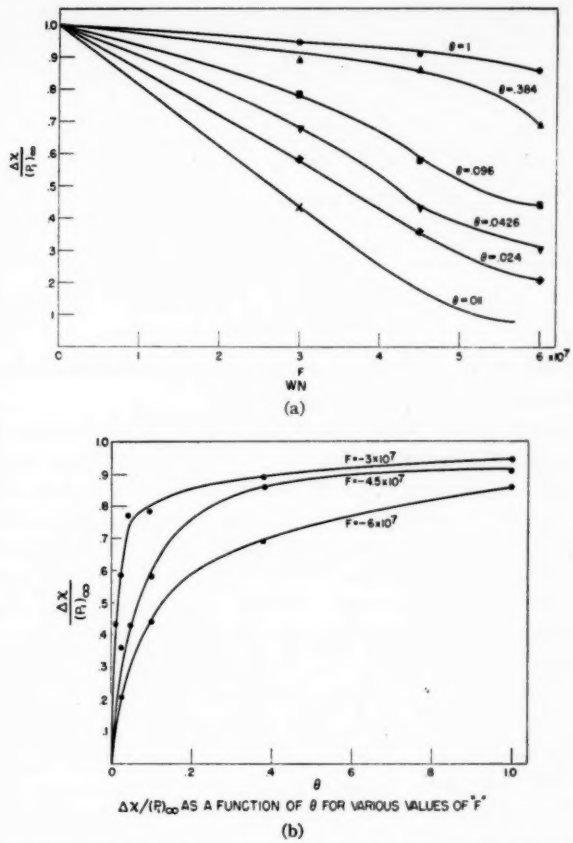


FIG. 6. (a) Work function increment $\Delta\chi$ in field emission in terms of the corresponding contact potentials $P_{1\infty}$ as functions of the applied field for various coverages $\theta$. (b) $\Delta\chi/P_{1\infty}$ as functions of $\theta$ for various applied fields $F$.

the surface, i.e., the exact boundaries of the "$S$ polyhedra" are subject to similar considerations, so that electron spillover is possible from the hills to the troughs of a surface; this produces a double layer of opposite sign to that previously mentioned. These facts are responsible for the differences in work function of various faces of clean metal crystals.

It is apparent that external fields will polarize the electron cloud at the metal surface. It will now be shown that the observed self-depolarizations of chemisorbed electronegative layers can be rather well explained by assuming that the effect is almost wholly due to a depolarization of this electron cloud by the dipoles constituting the layer. In order to calculate the effect, we resort essentially to the Fermi-Thomas method. We assume that the chemical potential ($\mu$) of electrons in the interior of the metal is equal to that of electrons in the external cloud. If the latter is subjected to an external potential not experienced by electrons in the interior, e.g., that due to an applied field or that resulting from a chemisorbed polar layer, a reduction in electron density $\rho$ will occur in the external cloud. If Fermi statistics are applicable, we can write

$$\rho_P/\rho=(1-P/\mu)^{\frac{1}{2}} \tag{7}$$

[13] I. Langmuir, J. Am. Chem. Soc. **54**, 2798 (1932).

[14] Excellent summaries, with references, are given in C. Herring and M. H. Nichols, Revs. Modern Phys. **21**, 185–270 (1949) and in the chapter by C. Herring in *Metal Interfaces* (American Society for Metals, Cleveland, 1950).

[15] R. Smoluchowski, Phys. Rev. **60**, 661 (1941).

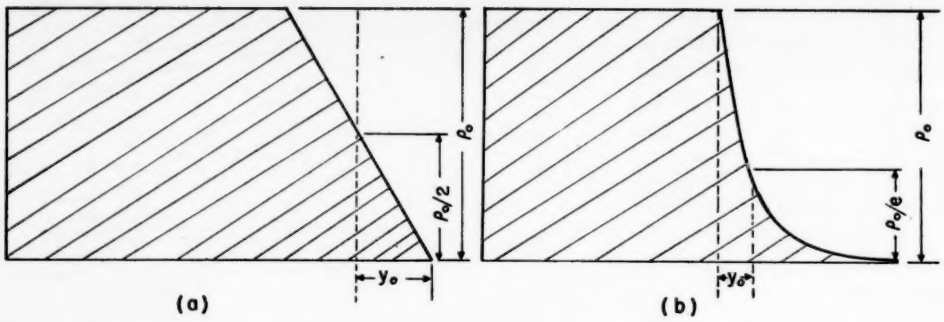


FIG. 7. Schematic diagram for the electron density $\rho$ at a metal surface. $\rho_0$ density in the interior. (a) linear decrease; (b) exponential decrease.

for the ratio of densities in the cloud in the absence and presence of an external potential $P$.

There is very good reason to believe that the electron cloud at the metal surface is sufficiently dense to obey Fermi statistics. Thus field emission experiments on tantalum carried out between room temperature and 2°K showed no appreciable change in the work functions or their relative values.[16] Experiments by Dyke[17] and his associates not only confirm the validity of the exponential part of the Fowler-Nordheim equation, but show that it is valid at very high fields; also, his patterns for tungsten look exactly like those obtained by other workers at lower fields. This indicates that the effect of fields on the work function is small. All these facts can be true only for virtual fermions.

The Thomas-Fermi method is strictly applicable only to systems in which the density gradient of fermions varies slowly, compared to their de Broglie wavelength. In connection with nuclear statistics, von Weizsäcker[18] has developed a correction to the Fermi energy, which depends on this density gradient. Figure 7 shows two models of the electron cloud at the surface. A linear decrease of density is assumed in Fig. 7a and an exponential one in Fig. 7b. In terms of the chemical potential the Weizsäcker correction $\mu_w$ turns out to be

$$\mu_w=\frac{d}{d\rho}\left[\frac{\hbar^2}{8m}\frac{[\text{grad}\rho]^2}{\rho}\right]=(1/\rho^2)\left[2\rho\frac{d^2\rho}{dx^2}-\left(\frac{d\rho}{dx}\right)^2\right]\frac{\hbar^2}{8m}. \quad (8)$$

Application to the two cases shows that a term

$$\mu_w=-\hbar^2/2my_0^2 \text{ at } \rho=\rho_0/4 \quad (9a)$$

results for the linear decrease and a similar one but of opposite sign

$$\mu_w=\hbar^2/8my_0^2 \text{ at } \rho<\rho_0 \quad (9b)$$

for the exponential decay. $y_0$ represents the distance in which the charge density drops from $\frac{1}{2}\rho_0$ to zero in the linear case and the distance in which it drops from $\rho_0$ to $\rho_0/e$ in the exponential one. It is seen that the Weizsäcker energies for these cases are almost identical but of opposite sign. If $y_0$ is expressed in angstroms, the corrections to the energy in ev amount to roughly $1/y_0^2$. Since $y_0$ is of the order of 1A, no serious error results from neglecting the Weizsäcker term.

Strictly speaking, Eq. (7) should be applied at each point of the cloud and the resultant densities used for the determination of the new electron layer potential. For simplicity, however, it is assumed that the mean density in the cloud outside the metal can be taken as $\frac{1}{4}\rho_0$, and that the effect of external potentials consists merely in a reduction of this value, leaving the effective dipole distance unchanged. Then the ratio $\rho_P/\rho$ represents the fractional decrease in the electron layer contribution to the work function. $\mu$ in Eq. (7) must therefore be divided by $4^{\frac{1}{3}}$. A value of $\mu_0=6$ ev was used for the normal chemical potential. It is further necessary to carry out the solution self-consistently, that is, to consider the repolarization of the electron layer by the decrease in its self-potential. This is done by using Eq. (7) to calculate a first value of the new electron layer potential, subtracting this from the original value, and using this difference as the first repolarization potential. This is subtracted from the original external potential to obtain a new effective external potential for use in Eq. (7). Iteration is continued until a consistent value is reached. Calculations were carried out for assumed initial double-layer potentials of 0.5 and 1 ev. The results are shown in Fig. 8.

It is possible to apply these results to Bosworth's[3b,c] values of the contact potential for oxygen, nitrogen, and

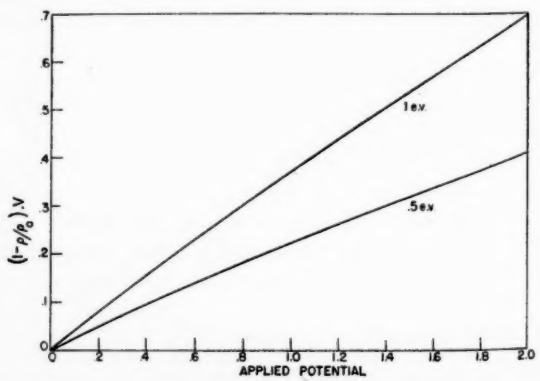


FIG. 8. Decrease in potential $V$ due to electron layer at a metal surface with applied depolarizing potential for two initial potentials of the layer.

[16] R. Gomer and J. K. Hulm, J. Chem. Phys. **20**, 1500 (1952).
[17] W. P. Dyke and J. K. Trolan, Phys. Rev. **89**, 799 (1953).
[18] C. F. v. Weizsäcker, Z. Physik **96**, 436 (1935).

hydrogen on tungsten. For this purpose $P_1$ at $x=1$A is used as the depolarizing potential. Strictly, this $P_1$ (at a given $\theta$) must be based on the dipole moment per complex at zero coverage, i.e., on the initial slope of the $V_\infty$ *vs* $\theta$ plot. The results for nitrogen and oxygen are shown in Figs. 9 and 10. The points represent sums of the depolarization and the actual contact potentials. The straight lines represent the initial slopes of the $V_\infty$ *vs* $\theta$ plots, i.e., the contact potentials that would result if there were no depolarization. It will be seen that both oxygen and nitrogen can be fitted very well. To obtain this fit, the electron cloud was assigned an initial potential of 0.5 volt in both cases. For hydrogen the $V_\infty$ *vs* $\theta$ plot shows almost no deviation from linearity up to the highest values of $\theta$ reached by Bosworth.[3b] There is some question whether this value is 1, as believed by Bosworth,[3b] or 0.7.[19] In any case, there should be very little depolarization below a contact potential of 1 volt on the basis of the present calculations.

It should be emphasized that we do not attempt to calculate the electron layer potential a *priori*; the latter is taken empirically to give the best fit with experiment. We crudely estimate the perturbation of this potential by external fields. It should also be pointed out that the $V_\infty$ *vs* $\theta$ curves taken from Bosworth[3] are not directly determined and thus subject to quite some uncertainty. On the whole, however, it seems reasonable to explain the observed depolarizations of slightly polarizable electronegative layers on the basis of electron layer depolarization. This result will certainly not be valid for electropositive adsorbates like cesium or barium on tungsten.

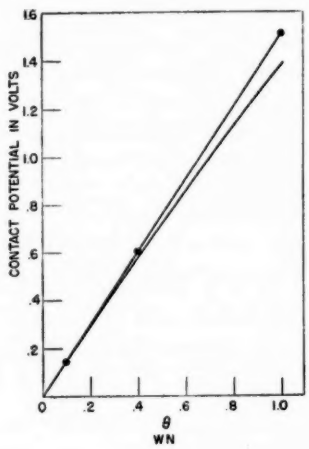


FIG. 9. Contact potential *vs* coverage $\theta$ for nitrogen on tungsten after Bosworth, reference 3, (curved line). Straight line represents initial slope, solid points the sum of the contact potential and the calculated depolarization.

The conclusion just reached enables one to estimate the effect on the work function of the fields necessary for cold emission. If the reasoning of this section is correct, ad-atom-surface complexes like *N–W* are very poorly polarizable so that experimentally produced fields would be quite insufficient to cause polarization, the more so as these fields ($3-5\times10^7$ v/cm) are smaller than the inherent fields existing in the dipole layer. Thus for both clean and contaminated surfaces the effect on the electron cloud only need be considered. It turns out from Fig. 8 that at fields of $3\times10^7$ v/cm a polarization of 0.07 volt should take place, thus increasing the work function by that amount over the weak field work function.

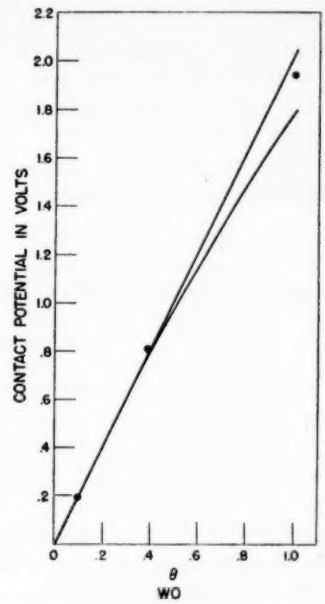


FIG. 10. Oxygen on tungsten. Same as Fig. 9.

## ELECTROSTATIC EFFECTS ON HEATS OF CHEMISORPTION

Experimental measurements of heats of chemisorption show that initially very high differential heats drop remarkably with increasing coverage. It has been realized for some time that Coulomb repulsion of the dipoles, depolarization effects, and so on are quite insufficient to explain more than a small fraction of this drop.[5] The latter may amount in the case of oxygen on tungsten to 60 kcal at $\theta=.5$. Boudart[5] has recently made the following very interesting suggestion: it is assumed that a small integral number of electrons is involved per ad-atom-substrate bond, and is thus localized in a region between the adatom and the surface; on the average these electrons will find themselves more or less halfway between atom and surface, i.e., at $\frac{1}{2}d$. If a given heat of formation $H_0$ corresponds to each bond of this kind, the observed heat of formation $H$ will be smaller than $H_0$ by the electrostatic energy of the bonding electrons in the potential of the layer at $\frac{1}{2}d$. Boudart now assumes that the potential at this point can be taken as half the contact potential $V_\infty$ at a given coverage; since $V_\infty$ varies linearly with $\theta$, linear decreases in $H$ and their order of magnitude would thus be explained.

If the model of the chemisorbed layer used by us is

[19] E. K. Rideal and B. M. W. Trapnell, J. chim. phys. **47**, 126 (1950).

correct, Boudart's argument unfortunately no longer gives correct magnitudes and should not lead to linear changes in $H$. It turns out that $P_0$ at $x'=0.5$ is very much smaller than $V_\infty/2$ (see lowest curve in Fig. 3) for all conceivable values of $a'$. Furthermore, it is possible to express $P_0$ at $x=1$A for $d=2$A (the most reasonable actual assignment) by

$$P_0=18.1Ma^{-2.85}\text{ ev} \quad (M \text{ in Debye}) \tag{10}$$

from which it follows that the dependence on $\theta$ is

$$P_0=.724M\theta^{1.43}\text{ ev}. \tag{11}$$

If depolarization is taken into account, the result of Eq. (11) must be multiplied by the factor $(1-0.064\theta^{.43})$. This does not change the result significantly. Thus at $\theta=0.5$, Boudart's effect can account for only about 8 kcal in the case of oxygen, assuming two electrons per bond. It follows that Boudart's effect can account for the observed changes in $H$ only if individual adatom-surface complexes are far from being the simple dipoles by which we have represented them and have a charge distribution which leads to effectively continuous dipole sheets even at low coverages. It seems likely that there is considerable deviation from spherical charge distribution in the direction normal to the surface. This deviation should not affect our arguments too much. A spreading of the charge parallel to the surface would be needed to effect quasicontinuity of the dipole sheet. This does not seem probable for electronegative adsorbates.

Calculations similar to those of the first section of this paper show that dipole repulsion energies $E_p$ for a triangular lattice can be expressed by

$$E_p=.076M^2\theta^{1.39}\text{ ev} \quad (M \text{ in Debye}). \tag{12}$$

Equation (12) leads to effects of the same order of magnitude as that of Topping,[19] but is based on a dipole model with $d=2$A rather than on point dipoles. As Rideal and Trapnell[20] point out, and as is apparent from Eq. (12), this energy amounts to at most 2 kcal.

Electrostatic interactions of the dipoles with the electron cloud at the surface may also be considered. A little thought will show that this effect, while small, must lead to an increase in $H$, since the only nonlinear part can arise from the cumulative effect of the dipole layer potential on the cloud. This effect, as we have seen, is to drive the cloud back into the metal, hence reducing the net electrostatic interaction of the dipoles with the electron cloud.

If these arguments are correct, it would appear that ordinary electrostatic effects are insufficient to explain observed decreases in $H$. Two possibilities remain. The first is connected with the fact that wires and films used in heat experiments are polycrystalline and thus may be sufficiently heterogeneous from the heat point of view. The second possibility is that the effect exists even on uniform surfaces and is caused by an increase in the kinetic energy of the electron cloud, resulting from the change in the gradient of the wave function when the cloud is partially driven back into the metal by the dipole layer potential. However, this effect cannot exceed the original Coulomb interaction, unless other quantum mechanical, essentially tunnel, effects set in.

## ACKNOWLEDGMENT

It is a pleasure to acknowledge many stimulating discussions with Dr. Morrell H. Cohen of this Institute. I also wish to thank Mr. Matthew Prastein for performing many of the numerical computations.

# Vibration Spectrum of a Simple Cubic Lattice*†

GORDON F. NEWELL‡
*Institute for Fluid Dynamics and Applied Mathematics, University of Maryland, College Park, Maryland*
(Received March 27, 1953)

Analytic expressions are derived for the frequency distribution function $g(f)$ of a simple cubic monoatomic lattice. Only nearest and next-nearest neighbor interactions are considered, and the latter are assumed to be weak compared with the former. The procedure is based upon considering the next-nearest neighbor interactions as a perturbation, and the results are correct to the first power of a parameter $\tau$ which is essentially a measure of strength of the next-nearest neighbor forces as compared with the nearest neighbor forces.

It has been known for some time that a simple cubic lattice with only nearest neighbor interactions degenerates into the equivalent of three independent one-dimensional lattices giving a nonzero $g(f)$ for $f=0$ and an infinite value at the maximum frequency. If, however, one includes even a small interaction between next-nearest neighbors, the behavior of $g(f)$ near both ends of the spectrum changes considerably; in fact it vanishes at both ends. For intermediate frequencies, $g(f)$ is continuous but has four analytic singularities with vertical tangents of the type predicted by van Hove for a quite general type of crystal. Although the calculated $g(f)$ is exact only in the limit $\tau\to 0$, it does properly describe the exact location and type of singularities for $0\leq\tau\leq 1/10$.

## I. INTRODUCTION

A NEW wave of interest in the vibration spectra of crystals has developed in recent years. Although new applications, particularly in the theory of superconductors, have given this subject new importance, renewed popularity has also centered around recent developments in the determination of the analytic form for the frequency distribution of the lattice vibrations. Interest in the latter was instigated some years ago by an exact evaluation of the frequency distribution for a two-dimensional square lattice with vibration couplings between nearest and next-nearest neighbors only in a monoatomic lattice.[1] Montroll found that the frequency distribution function $g(f)$ contained two logarithmic singularities.

More recently, Smollett[2] showed that logarithmic singularities also appear in the frequency distribution function for a two-dimensional crystal with long-range Coulomb forces. He also noted that these singularities were caused by saddle points in the surface which expresses the frequency of vibration as a function of the propagation vector.

The most recent contribution to this subject was an analysis by Van Hove[3] of the types of singularities to be expected in the frequency distribution $g(f)$ for a quite general type of crystal lattice with harmonic forces. Van Hove showed that, assuming a periodic structure in the lattice, the frequency distribution of a crystal must contain a certain minimum number of analytic singularities and that, except under very special conditions, the nature of these singularities depends only upon the dimensionality of the crystal. For any two-dimensional crystal, one should expect to find at least one finite discontinuity and at least one logarithmic singularity in $g(f)$ whereas for any three-dimensional crystal, one should find that $dg/df$ has at least two infinite discontinuities and is also negatively infinite at the maximum frequency.

The calculations by Montroll and Smollett clearly illustrate these theorems of van Hove as applied to a two-dimensional system. The following gives an illustration of how these theorems apply in a three-dimensional system.

The system to be considered here is one that has been studied many times before by various approximations.[4] The lattice is simple cubic and monoatomic. The forces are harmonic and act between nearest and next-nearest neighbors only along the line joining the particles. None of the previous investigations of this problem showed the detailed analytic character of the frequency distribution, because the approximations were not of such a type as to give exact details with a finite amount of labor. Although the following is also an approximate procedure, it does give exactly the location and the type of singularities in addition to giving an accurate evaluation of $g(f)$ under well-defined conditions.

The following notation, much of which is in common use, will be used to describe the problem:

$\alpha$ = force constant for nearest neighbors
$2\gamma$ = force constant for next-nearest neighbors
$\tau = 2\gamma/(\alpha+4\gamma)$
$\nu$ = fundamental frequency of some normal mode
$\nu_L$ = the largest value of $\nu$
$f=\nu/\nu_L$ = dimensionless unit of frequency, $0\leq f\leq 1$
$(\phi_1, \phi_2, \phi_3)$ = coordinates in the reciprocal space, $-\pi\leq\phi_j\leq\pi$.

* Partially supported by U. S. Office of Naval Research.
† A preliminary report of this paper was given at the American Physical Society meeting at North Carolina, March, 1953.
‡ Present address: Graduate Division of Applied Mathematics, Brown University, Providence, Rhode Island.
[1] E. Montroll, J. Chem. Phys. **15**, 575 (1947).
[2] M. Smollett, Proc. Phys. Soc. (London) **A65**, 109 (1952).
[3] L. Van Hove, Phys. Rev. **89**, 1189 (1953).
[4] M. Blackman, Repts. Progr. in Phys. **8**, 11 (1941). E. Montroll, J. Chem. Phys. **10**, 219 (1942).

The frequency of the normal modes for any finite lattice are found by solving for $f$ the secular equation[4]

$$\begin{vmatrix} a_{11}-2f^2 & a_{12} & a_{13} \\ a_{12} & a_{22}-2f^2 & a_{23} \\ a_{13} & a_{23} & a_{33}-2f^2 \end{vmatrix}=0 \qquad (1)$$

in which

$$a_{ii}=1-\cos\phi_i(1-2\tau+\tau\cos\phi_j+\tau\cos\phi_k)$$
$$a_{jk}=\tau\sin\phi_j\sin\phi_k, \quad j\neq k.$$

$i$, $j$, $k$ is any permutation of 1, 2, 3, and the points $(\phi_1, \phi_2, \phi_3)$ are given discreet values on a fine mesh square lattice in the reciprocal space. As the system becomes arbitrarily large, the points in the reciprocal lattice become uniformly dense, and the frequency spectrum becomes continuous. It is then meaningful to seek a density distribution of the frequencies of the normal modes.

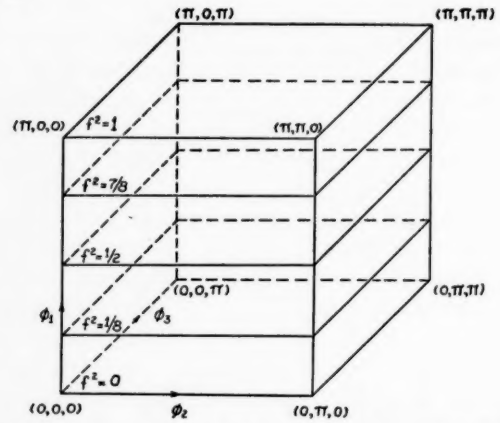


FIG. 1. Surfaces of constant $f$ for several values of $f$ and $\tau=0$ are represented by planes parallel to the coordinate planes. One branch is shown above. The other two branches are identical except for a permutation of the axes.

The manner by which one should calculate this frequency distribution is quite straightforward. The chief barrier to a complete solution of this problem is purely algebraic. By solving (1) for $f$ as a function of $(\phi_1, \phi_2, \phi_3)$, one can construct in the space $(\phi_1, \phi_2, \phi_3)$ surfaces of constant $f$. Since (1) is a cubic equation, there will be 3 values of $f$ for each $(\phi_1, \phi_2, \phi_3)$. It is usually convenient to separate these three solutions in some systematic way so as to establish a one-to-one correspondence between values of $f$ and values of $(\phi_1, \phi_2, \phi_3)$ on three separate spaces or branches. The frequency distribution function $g(f)$ is then defined such that $g(f)\,df$ is that fraction of the total volume in the three branches for which $f(\phi_1, \phi_2, \phi_3)$ lies between $f$ and $f+df$. If we let $f_i(\phi_1, \phi_2, \phi_3)$ be the frequencies at points of the $i$th branch, then

$$g(f)=\frac{1}{3(2\pi)^3}\frac{d}{df}\sum_{i=1}^{3}\int\int\int d\phi_1 d\phi_2 d\phi_3$$
$$f_i(\phi_1, \phi_2, \phi_3)\leq f, \quad -\pi\leq\phi_i\leq\pi. \qquad (2)$$

$g(f)$ has been so defined that $\int_0^1 g(f)df=1$.

The roots of (1) are invariant to changing $\phi_i$ to $-\phi_i$. In the following we shall therefore consider only the cube $0\leq\phi_i\leq\pi$ in which case (2) takes the form

$$g(f)=\frac{1}{3\pi^3}\frac{d}{df}\sum_{i=1}^{3}\int\int\int d\phi_1 d\phi_2 d\phi_3$$
$$f_i(\phi_1, \phi_2, \phi_3)\leq f, \quad 0\leq\phi_i\leq\pi. \qquad (2a)$$

## II. ANALYSIS FOR $\tau=0$

In the crystal model we are considering, only those interactions between nearest and next-nearest neighbors have been considered. It is intended to represent a crystal with only short-range forces. In keeping with this, it is also proper to assume that $\tau$ is small.

By setting $\tau=0$, however, one obtains a frequency distribution which does not give a proper behavior at either low or high frequencies. In order to understand the effects of a small next-nearest neighbor interaction, we shall begin the investigation with a review of the case $\tau=0$ for, despite its failures, it will serve as a guide to the later developments.

If we set $\tau=0$ in Eq. (1), the secular equation separates trivially to give three roots

$$2f_i^2=1-\cos\phi_i=2\sin^2(\phi_i/2). \qquad (3)$$

The reason for this simple decomposition is that the vibrations along the three crystal axis are not coupled with each other. The vertical vibrations of one particle are coupled only with the vertical vibrations of its nearest neighbors in the vertical direction. They are not affected by the vibrations of its neighbors along the other crystal axes. Thus the system behaves as three independent one-dimensional systems.

For the purpose of constructing surfaces of constant frequency, there are two convenient ways of separating the three solutions of (3) into three separate branches. One way is to use the separation implied by (3), i.e., to choose the first branch to have surfaces of constant $f$ which are planes of constant $\phi_1$. This scheme is illustrated in Fig. 1. The other two branches are identical except that the planes are perpendicular to the $\phi_2$ and $\phi_3$ axes in the other two branches.

One is not, however, compelled to separate the solutions in this manner. Wherever a degeneracy occurs, i.e., wherever the surfaces for the same value of $f$ from two different branches would cross if placed in the same space, we have a choice of reconnecting the branches in a different manner without destroying the continuity of the surfaces. Of course, any scheme other than the one above would have surfaces with right angle turns.

A second convenient choice of separation is to make each branch symmetric in $\phi_1$, $\phi_2$, and $\phi_3$. This scheme is illustrated in Fig. 2. Note that if one superimposes the three branches on the same space, the surfaces of constant $f$ form three intersecting planes parallel to the

three coordinate planes. Although we shall use simple modifications of the first scheme in most of the later discussions, the latter scheme is important because for $\tau \neq 0$, the off-diagonal elements of Eq. (1) cause discontinuities to appear in the surfaces approximated by Fig. 1, whereas they merely round the sharp corners of Fig. 2 to make a smooth surface.

The calculation of $g(f)$ for $\tau=0$ is quite trivial. If we use the scheme illustrated by Fig. 1, the contributions to $g(f)$ are the same from the three branches; thus

$$\begin{aligned} g(f) &= \pi^{-3} \frac{d}{df} \int_{f_1(\phi_1,\phi_2,\phi_3)\leq f} d\phi_1 d\phi_2 d\phi_3 \\ &= \pi^{-1} \frac{d}{df} \int_{\sin(\phi_1/2)\leq f} d\phi_1 \\ &= 2\pi^{-1}(1-f^2)^{-\frac{1}{2}}. \end{aligned} \tag{4}$$

One notices that $g(f)$ has a singularity at $f=1$ and approaches the limit $2/\pi$ for $f=0$. (The latter feature means that this distribution will not give the familiar Debye $T^3$ law for the specific heat.) In later discussions, we will also find it convenient to observe the shape of the distribution of $f^2$ values. If we let $G(f^2)$ be the normalized distribution of the values of $f^2$, $\int_0^1 G(f^2)df^2 = 1$, then

$$G(f^2) = g(f)/2f = \pi^{-1}[f^2(1-f^2)]^{-\frac{1}{2}}.$$

$G(f^2)$ has singularities at both $f^2=0$, and $f^2=1$ and is also symmetric about $f^2=\frac{1}{2}$.

Before proceeding with the analysis for $0<\tau\ll 1$, it is interesting to consider quite generally the conditions under which an approximate expression for $f_i(\phi_1, \phi_2, \phi_3)$ can lead to large deviations in the curve for $g(f)$. Suppose $f_i^0(\phi_1, \phi_2, \phi_3)$ is some approximation for the frequency of the $i$th branch and $\Delta_i(\phi_1, \phi_2, \phi_3)$ the error, $f_i(\phi_1, \phi_2, \phi_3) = f_i^0(\phi_1, \phi_2, \phi_3) + \Delta_i(\phi_1, \phi_2, \phi_3)$. Then

$$\begin{aligned} g(f) &= \frac{1}{3\pi^3} \frac{d}{df} \sum_{i=1}^{3} \int\int\int_{0\leq f_i^0+\Delta_i\leq f} d\phi_1 d\phi_2 d\phi_3 \\ &\sim \frac{1}{3\pi^3} \frac{d}{df} \sum_{i=1}^{3} \left\{ \int\int\int_{0\leq f_i^0\leq f} d\phi_1 d\phi_2 d\phi_3 \right. \\ &\qquad \left. - \int\int_{S(f)} \frac{\Delta_i(\phi_1,\phi_2,\phi_3)\,dS}{|\operatorname{grad} f_i^0(\phi_1,\phi_2,\phi_3)|} \right\}. \end{aligned} \tag{5}$$

$\Delta_i$ is assumed to be small in the approximation above, and the second integral is a surface integral over the surface $f_i^0(\phi_1, \phi_2, \phi_3) = f$.

We might expect unusual things to happen if any of the following should take place.

(a) $\Delta_i$ is large
(b) $\operatorname{grad}\Delta_i$ is large
(c) $\operatorname{grad} f^0$ vanishes
(d) derivatives of $\operatorname{grad} f^0$ diverge
(e) the boundary of $S$ varies rapidly with $f$.

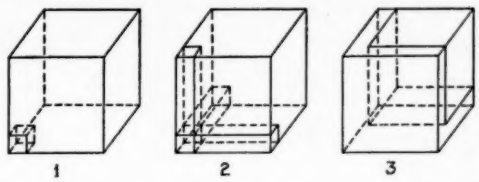


FIG. 2. A surface $f$=constant has three branches. In Fig. 1 they are represented by planes parallel to the coordinate planes. It is also possible to separate the three roots of the secular equation into three branches in such a way that in each branch, $f$ is symmetric in $\phi_1$, $\phi_2$, and $\phi_3$. This scheme is illustrated above. A superposition of these three branches gives again the three branches of which one would appear as in Fig. 1.

We shall presently see how some of these cause gross distortion of the frequency distribution despite the fact that $\Delta$ is small over most of the space. The vanishing of $\operatorname{grad} f^0$ is also the cause of singularities in the approximate $G(f^2)$. Thus we anticipate unusually large errors in $G(f^2)$ in the vicinity of singularities of the approximate $G(f^2)$. In particular, we shall see that even a small $\tau$ greatly distorts the $G(f^2)$ for $\tau=0$ in the neighborhood of $f^2=0$ or 1.

### III. SURFACES OF CONSTANT $f$, $0<\tau\ll 1$

To solve (1) for small $\tau$, we propose to use the conventional first-order perturbation theory. This will suffice to determine $f$ to order $\tau$ except at such $\phi_i$ for which two or more of the $f_i$ are nearly degenerate. As the next approximation, therefore, we consider

$$2f_i^2 = 1 - \cos\phi_i(1 - 2\tau + \tau\cos\phi_j + \tau\cos\phi_k), \tag{6}$$

where $i$, $j$, and $k$ are some cyclic permutation of 1, 2, and 3. This approximation (as well as the higher perturbation approximations) breaks down when two of the diagonal elements of (1) are nearly equal, thus when

$$\begin{aligned} &\cos\phi_i(1-2\tau+\tau\cos\phi_j+\tau\cos\phi_k) \\ &\qquad \sim \cos\phi_j(1-2\tau+\tau\cos\phi_i+\tau\cos\phi_k) \\ &(\cos\phi_i-\cos\phi_j)(1-2\tau+\tau\cos\phi_k)\sim 0. \end{aligned}$$

The second factor cannot vanish unless $\tau \geq \frac{1}{3}$. For $\tau<\frac{1}{3}$, the degeneracies occur only along the diagonal planes of the cube,

$$\phi_1=\phi_2, \quad \phi_2=\phi_3, \quad \text{and} \quad \phi_1=\phi_3. \tag{7}$$

For now, we shall disregard the effect of these degeneracies on the values of $f_i$ and assume that (6) is approximately correct everywhere. The error in $g(f)$ due to this assumption will be considered in Sec. 5 along with other errors.

The separation of the three roots of (6) into three branches can still be accomplished in many ways. In this respect the situation here is no different than in the previous section. Whenever a surface of constant $f$ crosses a degeneracy surface, one has a certain degree of liberty in the manner of connecting the surfaces. These degeneracy surfaces as given by (7) are indeed the same as for $\tau=0$. If we use the separation implied

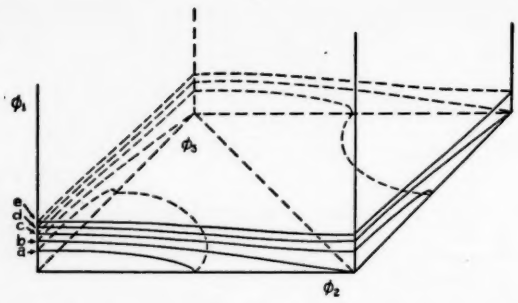


FIG. 3. The shape of the surfaces of constant $f$ for $0<\tau\ll 1$ is illustrated above in which only a section of the cube for $\phi_1$ small appears. The surfaces shown correspond to the following values of $f$: a) $f^2=\frac{1}{2}\tau$, b) $f^2=\tau$, c) $f^2=3\tau/2$, d) $f^2=2\tau$ and e) $f^2=5\tau/2$. The surfaces assimilate the planes of Fig. 1 except that for $\tau>0$, the surfaces bend downward into the $\phi_2-\phi_3$ plane for $f^2<2\tau$. The other two branches are obtained by permuting the axes.

by (6), the three branches are identical except for a permutation of the axis. The surfaces approach those of Fig. 1 as $\tau\to 0$. A scheme corresponding to that of Fig. 2 can also be used and would indeed be the appropriate one to use in considering higher approximations that cause a splitting of the degeneracies.

For the present, we shall continue to use the former scheme because the surfaces are somewhat easier to visualize, and we need consider only one branch. Whereas the surfaces of constant $f$ for $\tau=0$ were planes parallel to the coordinate planes, the corresponding surfaces for $\tau\neq 0$ are

$$\cos\phi_1=(1-2f^2)[1-\tau(2-\cos\phi_3-\cos\phi_2)]^{-1}. \quad (8)$$

($i$ has been chosen as 1 in Eq. (6).)

We first observe that for $0<\tau<\frac{1}{4}$, the second factor in (8) is always positive. Thus $\cos\phi_1$ is positive or negative accordingly as $f^2$ is less than or greater than $\frac{1}{2}$. Furthermore, if we replace $f^2$ by $1-f^2$ and $\phi_1$ by $\pi-\phi_1$, (8) remains invariant. This means that the surface $1-f^2=$constant is obtained from the surface $f^2=$constant by reflecting across the plane $\phi_1=\pi/2$. The symmetry, of course, also holds for $\tau=0$ and causes $G(f^2)$ to be symmetric about $f^2=\frac{1}{2}$. (This symmetry will be destroyed, however, by higher approximations.)

For purposes of analyzing the shape of the constant frequency surfaces, it is sufficient to consider only the surfaces $f^2\leq\frac{1}{2}$ which lie in the half cube $\phi_1\leq\pi/2$. The distinguishing features of these surfaces are illustrated in Fig. 3. The value of $\phi_1$ at $\phi_2=\phi_3=0$ is independent of $\tau$ but for $\tau>0$, $\phi_1$ is a monotone decreasing function of $\phi_2$ and $\phi_3$. If $f^2<2\tau$, the surfaces of constant $f$ will not extend over all values of $\phi_2$ and $\phi_3$ because of the necessary restriction $|\cos\phi_1|\leq 1$. $\phi_1$ vanishes when

$$\begin{aligned} 2f^2&=\tau(2-\cos\phi_3-\cos\phi_2)\\ f^2&=\tau[\sin^2(\phi_3/2)+\sin^2(\phi_2/2)]. \end{aligned} \quad (9)$$

Since (8) is an equation involving only the cosines of the angles and since $d\cos\phi/d\phi=0$ at $\phi=0$ or $\pi$, the surfaces of constant $f$ will, with but a few exceptions, intersect faces of the cube at right angles. The exceptions to this are quite obvious from either analytic or geometrical reasoning. A surface that intersects a corner of the tube cannot be perpendicular to all three faces. The surfaces $f^2=\tau$ which intersects the corners $(0,\pi,0)$ and $(0,0,\pi)$ is shown in Fig. 3 as well as the surface $f^2=2\tau$ which intersects the corner $(0,\pi,\pi)$. The surface $f^2=0$ contains only the single point $(0,0,0)$. In each case the surfaces in the neighborhood of the corners are quadratic functions of the displacements from the corners.

As anticipated in the previous section, we see that drastic changes are taking place in the surfaces of constant $f$ as $\tau$ becomes greater than zero. These changes will be particularly pronounced for $f^2$ of order $\tau$ or less and by symmetry also for $1-f^2$ of order $\tau$ or less. Whereas for $\tau=0$, $G(f^2)$ diverges as $f^2\to 0$; for $\tau\neq 0$, $G(0)=0$. As a consequence of the "saddle points" at the corners of the cube, we expect, in accordance with Van Hove's analysis, that $g(f)$ and $G(f^2)$ will have vertical tangents at $f^2=\tau$ and $f^2=2\tau$, also at $1-f^2=\tau$ and $1-f^2=2\tau$.

To rigorously prove that the above conclusions are not invalidated by better approximations than Eq. (6) requires a somewhat more detailed analysis (see Sec. 5). One may well question these conclusions on the grounds that the eigenvalues are degenerate at all corners of the cube and grad$f$ vanishes at all corners.

## IV. EVALUATION OF $G(f^2)$

The actual calculation of $G(f^2)$ is not difficult even though the integrals can apparently not be evaluated in closed form. It is, however, possible to express $G(f^2)$ in terms of integrals that depend only upon one parameter instead of two ($f^2$ and $\tau$).

The function we seek to determine is

$$G(f^2)=\pi^{-3}\frac{d}{df^2}\int\int\int d\phi_1 d\phi_2 d\phi_3$$

integrated over the region

$$0\leq\phi_i\leq\pi$$

and

$$2f^2\geq 1-\cos\phi_1(1-2\tau+\tau\cos\phi_2+\tau\cos\phi_3)$$

or for $f^2\leq\frac{1}{2}$,

$$G(f^2)=\pi^{-3}\frac{d}{df^2}\int\int d\phi_2 d\phi_3 \times\cos^{-1}\{(1-2f^2)[1-\tau(2-\cos\phi_2-\cos\phi_c)]^{-1}\}$$

integrated over the region

$$0\leq\phi_2,\phi_3\leq\pi \quad\text{and}\quad 2f^2\geq\tau(2-\cos\phi_2-\cos\phi_3) \quad (11)$$

Since the integrand vanishes at that boundary which is a function of $f^2$, the differentiation of the integral pro-

duces no surface terms and thus gives

$$G(f^2)=2\pi^{-3}\int\int d\phi_2 d\phi_3$$

$$\times\{[1-\tau(2-\cos\phi_2-\cos\phi_3)]^2-(1-2f^2)^2\}^{-\frac{1}{2}} \quad (12)$$

integrated still over the region (11).

It is convenient to factor the integrand of (12) into

$$[2f^2-\tau(2-\cos\phi_3-\cos\phi_2)]^{-\frac{1}{2}}$$
$$\times[2(1-f^2)-\tau(2-\cos\phi_3-\cos\phi_2)]^{-\frac{1}{2}}$$
$$=\tfrac{1}{2}\{f^2-\tau[\sin^2(\phi_3/2)+\sin^2(\phi_2/2)]\}^{-\frac{1}{2}}$$
$$\times\{1-f^2-\tau[\sin^2(\phi_3/2)+\sin^2(\phi_2/2)]\}^{-\frac{1}{2}}. \quad (13)$$

Inasmuch as we neglected the off-diagonal terms in (1), it is consistent for us to make any desirable expansions based upon the assumption $\tau\ll 1$ and keep only linear terms in $\tau$. We shall not attempt to expand the first factor when $f^2<\frac{1}{2}$ because this will not be justified

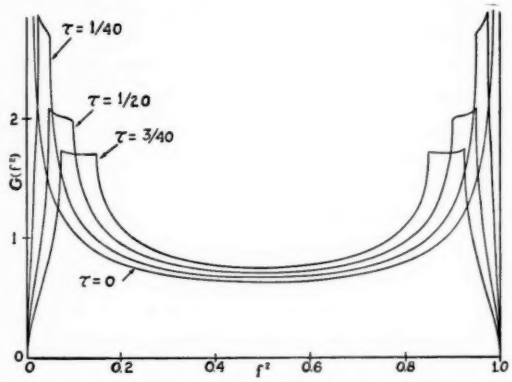


FIG. 4. The density of values of $f^2$, $G(f^2)$, is plotted *vs* $f^2$ for several values of $\tau$, $0\leq\tau<1/10$. The curves have vertical tangents at $f^2=0$, $\tau$, $2\tau$, $1-2\tau$, $1-\tau$, and 1.

for arbitrarily small $f^2$. However, we are justified in expanding the second factor in powers of $\tau$ on the basis that $\tau\ll\frac{1}{2}\leq 1-f^2$. We write the result of this expansion of (13) in the form

$$\tfrac{1}{2}\tau^{-\frac{1}{2}}(1-f^2)^{-\frac{1}{2}}\{(1-f^2/2)[\kappa-\sin^2(\phi_3/2)-\sin^2(\phi_2/2)]^{-\frac{1}{2}}$$
$$-\tfrac{1}{2}\tau[\kappa-\sin^2(\phi_3/2)-\sin^2(\phi_2/2)]^{\frac{1}{2}}\}$$

in which

$$\kappa=f^2/\tau. \quad (14)$$

We insert this into (12) and rewrite (12) in the form

$$G(f^2)=4\pi^{-3}\tau^{-\frac{1}{2}}(1-f^2)^{-\frac{1}{2}}\{(1-f^2/2)I(\kappa)-\tfrac{1}{2}\tau J(\kappa)\} \quad (15)$$

$$I(\kappa)=\tfrac{1}{4}\int\int d\phi_2 d\phi_3[\kappa-\sin^2(\phi_3/2)-\sin^2(\phi_2/2)]^{-\frac{1}{2}} \quad (16)$$

$$J(\kappa)=\tfrac{1}{4}\int\int d\phi_2 d\phi_3[\kappa-\sin^2(\phi_3/2)-\sin^2(\phi_2/2)]^{\frac{1}{2}}. \quad (17)$$

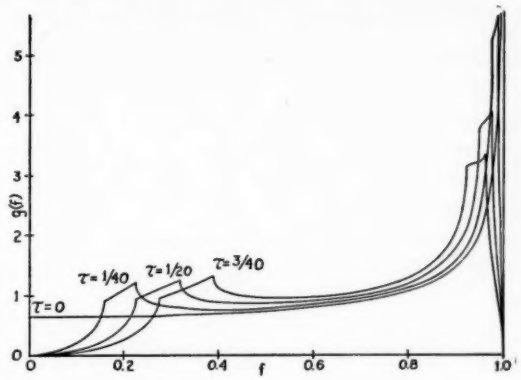


FIG. 5. The density of values of $f$, $g(f)$, is plotted against $f$ for several values of $\tau$, $0\leq\tau<1/10$. These curves have vertical tangents at $f^2=\tau$, $2\tau$, $1-2\tau$, $1-\tau$, and 1.

The limits of integration in (16) and (17) correspond to those in (11) which we rewrite as

$$0\leq\phi_2,\phi_3\leq\pi, \quad \kappa\geq\sin^2(\phi_3/2)+\sin^2(\phi_2/2). \quad (18)$$

The calculation of $G(f^2)$ is thus essentially reduced to the evaluation of two integrals $I(\kappa)$ and $J(\kappa)$. Actually one need labor over only one of them since they are related by

$$J(\kappa)=\tfrac{1}{2}\int_0^\kappa I(\kappa)d\kappa. \quad (19)$$

Two analytic singularities in $I(\kappa)$ are caused primarily by a change in the shape of the boundary (18) at $\kappa=1$ and $\kappa=2$. This region of integration is the projection of the surfaces of Fig. 3 onto the $\phi_2-\phi_3$ plane which for $\kappa\leq 2$ is defined by the intersection of the surface with the $\phi_2-\phi_3$ plane. For $\kappa\geq 2$, the second condition in (18) is satisfied everywhere in the square $0\leq\phi_2,\phi_3\leq\pi$.

Although it seems that there should be an elegant way of treating this integral for arbitrary $\kappa$, no such method was found. $I(\kappa)$ and $J(\kappa)$ were actually evaluated by some combinations of analytic and numerical procedures that are hardly worth detailed description here.

The interesting regions are for $\kappa$ near 0, 1, and 2. For $\kappa\ll 1$, $I(\kappa)\sim\frac{1}{2}\pi\kappa^{\frac{1}{2}}$ plus terms of order $\kappa^{\frac{1}{2}}$. Near $\kappa=1$, $I(1)-I(\kappa)$ is proportional to $(1-\kappa)^{\frac{1}{2}}$ for $\kappa\leq 1$ and $dI(\kappa)/d\kappa$ has an infinite discontinuity at $\kappa=1$. Near $\kappa=2$, $I(2)-I(\kappa)$ is proportional to $(\kappa-2)^{\frac{1}{2}}$ for $\kappa\geq 2$ and $dI(\kappa)/d\kappa$ has another infinite discontinuity at $\kappa=2$.

From graphs of $I(\kappa)$ and $J(\kappa)$, one can construct a family of curves for $G(f^2)$ for various small values of $\tau$. Several such curves are shown in Fig. 4. It is interesting to notice how for small $\tau$, these curves approach the curve $\tau=0$. The corresponding curves for $g(f)$ are shown in Fig. 5. They show discontinuities in slope at $f=\tau^{\frac{1}{2}}$, $(2\tau)^{\frac{1}{2}}$, $(1-\tau)^{\frac{1}{2}}$, and $(1-2\tau)^{\frac{1}{2}}$.

Except for these singularities, the curves have very much the same general shape as previous approximate curves.[4]

## V. ACCURACY OF RESULTS

The discussions in the previous sections were based upon the assumption that for sufficiently small $\tau$, one could neglect the off-diagonal terms of (1). We shall now give a more rigorous justification for this assumption and determine the limits of its validity. We are not particularly interested in evaluating explictly the errors of order $\tau^2$ that are to be normally expected in such an approximation, but rather we wish to investigate if any of the possible sources of exceptionally large errors listed at the end of Sec. 2 can cause a serious distortion of the curves given in the last section. Except near degeneracies, the error in the evaluation of $f$ itself is of order $\tau^2$. If none of these listed anomalies takes place on or near a surface of constant $f$, the calculated value of $G(f^2)$ or $g(f)$ will be correct at that value of $f$ to order $\tau$ with the error of order $\tau^2$.

We first consider the possibility of large errors in $f$, which could, of course, arise only near the planes of degeneracy. Even near these planes, however, the error in $f$ can at most be of order $\tau$. Unless the curves of constant $f$ run tangent to the planes of degeneracy at some point, the error due to this alone will, however, not cause a serious distortion of distribution curve because the error in $f$ will be of order $\tau$ only on a small fraction (generally of order $\tau$) of the total area of the surface over which one must integrate to find $G(f^2)$. We still expect $G(f^2)$ to be correct at most values of $f$ to order $\tau$, but since any curve $f^2=$ constant will generally intersect one or more of these degeneracy planes, the error in $G(f^2)$ could be of order $\tau^2 \log\tau$. [We would expect this to cause errors of order $\tau^2 \log\tau$ in the contribution to $G(f^2)$ from any given branch, but the errors due to different branches usually have a tendency to nearly cancel.]

The possibility of degeneracy planes running nearly tangent to the surfaces of constant $f$ can be ruled out, in general, on the grounds that the degeneracy planes are the diagonal planes of the cube, whereas, the constant frequency surfaces are nearly parallel to the coordinate planes. The only possible exceptions to this are near the corners of the cube where the corrected curves of constant $f$ are appreciably distorted from planes. The corners of the cube are also vulnerable positions for other errors and must be given special consideration. We notice, for example, that grad$f$ vanishes at the corners.

Since all off-diagonal elements in (1) vanish at the corners, the frequency at the corner is given exactly by (6). The off diagonal terms vanish as the square of the distance from the corner (in addition to being of order $\tau$). Wherever grad$f$ vanishes so also does the error and the gradient of the error. It turns out that this is just sufficient to prevent the off-diagonal terms from causing any error of order $\tau$ (even percentagewise) in the $g(f)$ curve. Near the origin for example, we can expand the sines and cosines to give

$$\begin{vmatrix} \frac{1}{2}\phi_1^2+\frac{1}{2}\tau(\phi_2^2+\phi_3^2)-2f^2 & \tau\phi_1\phi_2 & \tau\phi_1\phi_3 \\ \tau\phi_1\phi_2 & \frac{1}{2}\phi_2^2+\frac{1}{2}\tau(\phi_1^2+\phi_3^2)-2f^2 & \tau\phi_2\phi_3 \\ \tau\phi_1\phi_3 & \tau\phi_2\phi_3 & \frac{1}{2}\phi_3^2+\frac{1}{2}\tau(\phi_1^2+\phi_2^2)-2f^2 \end{vmatrix}=0. \tag{20}$$

The off-diagonal terms are still smaller by a factor of $\tau$ than the diagonal terms. The same arguments used previously to show that $g(f)$ was correct to order $\tau$ at points other than the corners can be used again to show that $g(f)$ is percentagewise correct to order $\tau$ for small $f$ near the origin of the cube. An inspection of the situation at the other corners will convince the reader that the curve derived for $g(f)$ is also correct to order $\tau$ for those values of $f$ at points near the other corners of the cube.

The most critical point of the cube is the corner $(\pi, \pi, \pi)$. The curves of constant frequency must "turn the corner" where a threefold degeneracy exists. Although the above conclusions regarding the accuracy are still valid here, it is at this corner that the approximation first breaks down if $\tau$ is chosen too large.

To see what sort of things could cause a break down in the above method, it is helpful to consider the exact analysis of the corresponding two-dimensional problem given by Montroll.[1] The present method can, of course, also be applied to the two-dimensional problem, in fact the frequencies of two branches along the three faces $\phi_1=0$, $\phi_2=0$, and $\phi_3=0$ are exactly those frequencies for the two branches of the two-dimensional problem. We expect that any anomaly of the two-dimensional problem will appear in some form or other also in the three-dimensional case.

In two dimensions, one observes from Montroll's analysis that for $\tau<\frac{1}{5}$, there is a saddle point at the corner $(\pi, \pi)$ of one of the branches if frequency is plotted against $\phi_1$ and $\phi_2$. As $\tau$ increases past $\frac{1}{5}$, this saddle point changes into a local minimum and a new saddle point develops and starts to move down the main diagonal from this corner. One can locate this new saddle by observing that $f$ has a maximum along this diagonal of the square.

The approximation scheme described here does not properly describe this phenomena. It takes place when the curves of constant frequency try to approach the corner nearly tangent to the diagonal line of degeneracy. Actually the off-diagonal terms cause the curves of constant $f$ to come into the corner even closer to the diagonal than the approximation predicts (at least on the one branch of interest here).

This breakdown of the approximation in two dimensions means also a breakdown of the approximation in

three dimensions at $\tau=\frac{1}{5}$ in the vicinity of the points $(0, \pi, \pi)$, $(\pi, 0, \pi)$, and $(\pi, \pi, 0)$ or at the frequency $f^2=2\tau$. Although the breakdown at these points is not the first one that takes place as $\tau$ increases, a study of it at least gives some indication of what sort of behavior to look for at the point $(\pi, \pi, \pi)$.

In three dimensions near the point $(\pi, \pi, \pi)$, one can detect unusual developments by observing the frequencies along the main diagonal from (0, 0, 0) to $(\pi, \pi, \pi)$. One expects, just as in two dimensions, that the distortion will be greatest along this line of maximum degeneracy. Because of the symmetry of the matrix (1) when $\phi_1=\phi_2=\phi_3$, the three roots $f_1$, $f_2$, and $f_3$ of (1) are easily found to be

$$\begin{aligned} 2f_1^2&=(1+2\tau)-(1-2\tau)\cos\phi-4\tau\cos^2\phi \\ 2f_2^2&=2f_3^2=(1-\tau)-(1-2\tau)\cos\phi-\tau\cos^2\phi \end{aligned} \tag{21}$$

with $\phi=\phi_1=\phi_2=\phi_3$. It is the first of these that is of particular interest. In addition to $f_1^2$ having the expected stationary values at $\phi=0$ and $\phi=\pi$, it also has a maximum at $\cos\phi=-(1-2\tau)/8\tau$. This maximum will be meaningful only if $-1\leq\cos\phi$ or if

$$\tau\geq\tfrac{1}{10}.$$

When $\tau$ reaches $\frac{1}{10}$, we know that the shape of the surfaces near $(\pi, \pi, \pi)$ undergoes some change that the approximate procedure does not predict. Apparently, as in the two-dimensional problem, a new saddle point is developing at $\tau=\frac{1}{10}$ which for $\tau>\frac{1}{10}$ moves down the main diagonal leaving a local minimum at the point $(\pi, \pi, \pi)$. We expect that this breakdown will take place quite suddenly as $\tau$ approaches $\frac{1}{10}$ and for $\tau$ near $\frac{1}{10}$ will be localized near $f^2=1-2\tau$. Since there is no apparent source of difficulties for $\tau<\frac{1}{10}$, the curves of the last section appear to be accurate to within a few percent up to $\tau$ almost $\frac{1}{10}$.

No serious attempt has been made to analyze in detail what happens for $\tau\geq\frac{1}{10}$. The problem becomes quite tedious, and one is discouraged by the expectation that the approximations will break down again at other points when $\tau=\frac{1}{5}$ and will go completely wild at $\tau=\frac{1}{3}$ when a new set of degeneracy planes appears. $\tau=\frac{1}{4}$ will also be a critical value and possibly also $\tau=1/7$.

Some three-dimensional wave surfaces for $\tau=\frac{1}{3}$ have been plotted numerically to investigate qualitatively what to expect. For $\tau=\frac{1}{3}$, it is possible to obtain expansions for $g(f)$ at small $f$ and for $f$ near 1. It is also possible to detect and analyze a logarithmic singularity in $g(f)$, a feature one does not expect except for certain critical values of $\tau$. Aside from this, the only significant conclusion to be drawn from this study of $\tau=\frac{1}{3}$ is that one can generally expect the surfaces of constant $f$ to be far more complex than most people have anticipated.

In conclusion, it should be noted that although the method employed here can be applied to a few other problems, it certainly cannot be classified as a procedure for handling general vibration problems. The success of the procedure in this case rests upon knowing a rather simple solution of the problem for $\tau=0$.

**ACKNOWLEDGMENT**

The author is indebted to Drs. Elliott Montroll and Richard Wallis for many helpful discussions and for checking the manuscript.

# The Heat Capacity of Thorium Dioxide from 10 to 305°K. The Heat Capacity Anomalies in Uranium Dioxide and Neptunium Dioxide

DARREL W. OSBORNE AND EDGAR F. WESTRUM, JR.*
*Argonne National Laboratory, Lemont, Illinois*

(Received July 8, 1953)

The heat capacity of thorium dioxide was determined from 10 to 305°K in an adiabatic calorimeter. As expected, no anomaly was observed in the heat capacity. The enthalpy, entropy, and free energy were calculated from the heat-capacity data and are tabulated for several temperatures. At 298.16°K the entropy and the enthalpy are, respectively, $15.593 \pm 0.02$ cal deg$^{-1}$ mole$^{-1}$ and $2524.4 \pm 3$ cal mole$^{-1}$. By assuming the lattice entropy of uranium dioxide and of neptunium dioxide to be equal to the entropy of thorium dioxide, the magnetic entropy contributions at 298.16°K were evaluated as 3.0 cal deg$^{-1}$ mole$^{-1}$ for uranium dioxide and 3.6 cal deg$^{-1}$ mole$^{-1}$ for neptunium dioxide. These values are somewhat greater than the spin-only values ($R \ln 3 = 2.18$ cal deg$^{-1}$ mole$^{-1}$ for uranium dioxide and $R \ln 4 = 2.75$ cal deg$^{-1}$ mole$^{-1}$ for neptunium dioxide). The entropies of the other isomorphous actinide dioxides at 298.16°K are estimated to be (in cal deg$^{-1}$ mole$^{-1}$) 17.8 for $PaO_2$, 19.7 for $PuO_2$, 20.0 for $AmO_2$, 20.3 for $CmO_2$, 20.6 for $BkO_2$, and 20.3 for $CfO_2$.

ANOMALIES have been observed in the heat capacity of uranium dioxide at 28.7°K[1] and of neptunium dioxide at 25.3°K[2] that are presumably related to the magnetic behavior of these substances. In order to obtain an estimate of the contribution of the lattice vibrations to the heat capacities of uranium dioxide and of neptunium dioxide, so that the magnetic contributions can be resolved, measurements have been made of the heat capacity of thorium dioxide.

Inasmuch as the electronic structure of the $Th^{+4}$ ion is of the rare gas type, with a $^1S_0$ ground state, and thorium dioxide is diamagnetic,[3] the heat capacity of thorium dioxide arises entirely from the lattice vibrations and should not show an anomaly. Further, the dioxides of thorium, uranium, and neptunium, as well as those of protactinium, plutonium, and americium, all have the fluorite structure. The lattice parameter[4] is 5.597A for thorium dioxide, 5.468A for uranium dioxide, and 5.436A for neptunium dioxide, and the masses of the isotopes of the cations employed are 232, 238, and 237, respectively. Because of the similar structure and the small percentage differences between the lattice dimensions and between the atomic masses, it seems reasonable to assume that the heat capacity of thorium dioxide is a good approximation for the lattice contribution to the heat capacities of uranium dioxide, neptunium dioxide, and the other actinide dioxides.

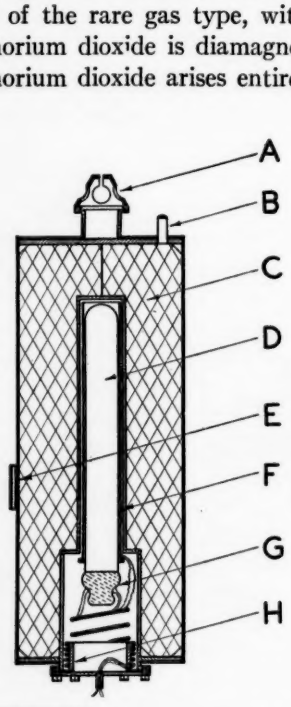


FIG. 1. The calorimeter: *A*, cone for cooling; *B*, monel tube; *C*, copper vanes; *D* and *G* platinum resistance thermometer; *E*, thermocouple well; *F*, constantan heater; *H*, spool for leads.

## THORIUM DIOXIDE SAMPLE

A very pure sample of electrically fused thorium dioxide that had been ground and sieved to 200 mesh was ignited to constant weight at 800°C in a platinum dish and then weighted directly into the calorimeter. Gravimetric analyses on the thorium dioxide (before ignition) by A. R. Mendenhall, Jr., indicated 750 ppm of water and 40 ppm of carbon. It is believed that the traces of water and carbon were removed by ignition. Thorium determinations by K. J. Jensen using gravimetric oxalate precipitation were 87.93, 87.54, and 87.88 percent thorium (theoretical, 87.88 percent). Spectrochemical analyses by J. P. Faris and J. A. Goleb revealed the following impurities in ppm: 50 of Al, 10 of Fe, 50 of Si, less than 5 of B, Be, Bi, Co, Cr, Cu, K, Li, Mg, Mn, Na, Ni, Pb, Sb, and Sn.

Analyses for the rare earth elements were performed by K. J. Jensen and J. P. Faris by a procedure involving extraction of the thorium into thenoyltrifluoro-acetone and spectroscopic examination of the raffinate for the rare earths. Checks were made to determine the validity and sensitivity of the method. The only rare earth element detected was lanthanum (40 ppm). The upper

* Chemistry Department, University of Michigan, Ann Arbor Michigan.

[1] Jones, Gordon, and Long, J. Chem. Phys. **20**, 695 (1952).
[2] Westrum, Hatcher, and Osborne, J. Chem. Phys. **21**, 419 (1953).
[3] W. Trzebiatowski and P. W. Selwood, J. Am. Chem. Soc. **72**, 4504 (1950).
[4] W. H. Zachariasen, Acta Cryst. **2**, 388 (1949).

limit of the sum of all the other rare earth elements was 150 ppm.

The mass of the sample used in the calorimeter was 185.504 g.

## CRYOSTAT AND CALORIMETER

The cryostat used in these measurements has been previously described[2] and was modified only by substitution of a copper "floating" ring[5] for the outer adiabatic shield and by increasing the dimensions of the remaining adiabatic shield to inside diameter 4.8 cm, length 12 cm, and thickness 0.75 mm, in order to accommodate a larger calorimeter.

The gold-plated copper calorimeter, 2.8 cm in diameter and 6.4 cm long, is shown in schematic section in Fig. 1. The thickness of the shell is 0.25 mm. A carefully machined copper cone (*A*) at the top provides thermal contact with the adiabatic shield when it is desired to cool the calorimeter. The lid of the calorimeter is soft-soldered in place after filling. Six vanes (*C*) of 0.1 mm copper foil, soft-soldered to the re-entrant well, aid in establishing temperature equilibrium. Pure helium gas, at a pressure of one atmosphere at 25°C, is used to provide thermal conductivity between the sample and the calorimeter. A small hole drilled in the end of a thin-walled Monel tube (*B*) serves for evacuation and filling with helium. The amount of solder used for soldering the lid and closing the hole in the tube (*B*) is determined by reweighing the closed calorimeter.

The re-entrant well contains a 25-ohm capsule type platinum resistance thermometer[6] (*D*) (Laboratory designation A-1) within a cylindrical copper heater tube (*F*). The heater tube is wound bifilarly with 160 ohms of B and S No. 40 double glass insulated constantan wire, which is cemented in place with baked Formvar. The glass head (*G*) through which the thermometer leads are sealed is entirely within the enlarged portion of the well, and the lead wires to both the thermometer and the heater are brought to temperature equilibrium with the outside of the calorimeter by means of a small copper spool (*H*) around which the leads are wound and cemented with baked Formvar. The spool is bolted in place with 00–90 brass cap screws. A copper-constantan differential thermocouple junction coated with baked Formvar makes a snug fit in a small tube (*E*) soldered to the calorimeter. A weighed amount of Lubriseal stopcock grease is used to establish thermal contact between the calorimeter, thermometer, heater, thermocouple, and spool. The amount of stopcock grease is carefully maintained constant to a few tenths of a mg in the heat-capacity measurements on the empty and on the full calorimeter. The mass of the empty calorimeter including thermometer, heater, spool, and grease is 45.7 g.

[5] Yost, Garner, Osborne, Rubin, and Russell, J. Am. Chem. Soc. **63**, 3488 (1941).

[6] H. J. Hoge and F. G. Brickwedde, J. Research Natl. Bur. Standards **22**, 351 (1939).

TABLE I. Heat capacity of $ThO_2$. Molecular Weight = 264.12; 0°C = 273.16°K

| $\bar{T}$ (°K) | $C_p$ (cal deg$^{-1}$ mole$^{-1}$) | $\bar{T}$ (°K) | $C_p$ (cal deg$^{-1}$ mole$^{-1}$) | $\bar{T}$ (°K) | $C_p$ (cal deg$^{-1}$ mole$^{-1}$) |
|---|---|---|---|---|---|
| 10.19 | 0.034 | 61.43 | 3.340 | 166.27 | 10.43 |
| 11.85 | 0.048 | 67.15 | 3.786 | 175.73 | 10.90 |
| 13.44 | 0.070 | 72.93 | 4.230 | 185.75 | 11.36 |
| 15.15 | 0.099 | 79.41 | 4.722 | 195.89 | 11.80 |
| 17.09 | 0.142 | 86.35 | 5.257 | 185.66 | 11.35 |
| 19.14 | 0.207 | 61.39 | 3.337 | 195.64 | 11.78 |
| 21.18 | 0.290 | 67.11 | 3.784 | 205.69 | 12.19 |
| 23.27 | 0.394 | 74.95 | 4.380 | 215.83 | 12.56 |
| 25.46 | 0.521 | 84.37 | 5.103 | 226.06 | 12.91 |
| 27.83 | 0.674 | 92.34 | 5.697 | 236.26 | 13.24 |
| 30.52 | 0.865 | 99.61 | 6.219 | 246.35 | 13.54 |
| 33.59 | 1.100 | 106.97 | 6.745 | 256.45 | 13.81 |
| 37.00 | 1.369 | 114.43 | 7.269 | 266.58 | 14.07 |
| 40.93 | 1.693 | 122.30 | 7.804 | 276.62 | 14.31 |
| 45.48 | 2.061 | 130.77 | 8.359 | 286.58 | 14.53 |
| 50.49 | 2.470 | 139.55 | 8.924 | 296.52 | 14.73 |
| 55.86 | 2.898 | 148.37 | 9.450 | 305.40 | 14.91 |
| 61.63 | 3.356 | 157.30 | 9.956 | | |

The calibration of thermometer A-1 and the method of making the heat capacity measurements have been described previously.[2]

## EXPERIMENTAL RESULTS

The molal heat capacities are listed in Table I in chronological sequence. The temperature intervals can usually be estimated from the difference between the average temperatures for successive runs. A correction for curvature, amounting at most to 0.001 cal deg$^{-1}$ mole$^{-1}$, has been made. Also, small corrections were made for the difference in the amount of helium and of solder in the measurements on the empty and on the full calorimeter. The results are expressed in terms of the defined thermochemical calorie equal to 4.1840 absolute joules. The molecular weight of thorium dioxide was taken to be 264.12, and the ice point was taken to be 273.16°K.

The rate of heating was 1 deg/min or less, except in a few duplicate runs where it was varied intentionally. For example, the runs at mean temperatures of 61.63 and 61.39°K had a temperature rise of 5.9° and a rate of 1.2 deg/min; the run at 61.43°K had the same temperature rise but half the rate. The run at 74.95°K had an abnormally high rate (2.1 deg/min) and a large temperature rise (10.1°). The duplicate runs of varying heating rate agree within 0.1 percent and indicate that the shield control was satisfactory.

Values of the molal heat capacity at selected temperatures, read from a smooth curve through the experimental points, are presented in Table II. These values are considered to have a probable error of 0.1 percent above 25°K; at 14°K the probable error may be 1 percent, and at 10°K it may be 3 percent as a consequence of the decreased sensitivity of the resistance thermometer and the provisional nature of the temperature scale below 14°K.

TABLE II. Thermodynamic properties of $ThO_2$.

| $T$ (°K) | $C_p$ (cal deg$^{-1}$ mole$^{-1}$) | $H°-H_0°$ (cal mole$^{-1}$) | $S°$ (cal deg$^{-1}$ mole$^{-1}$) | $-\frac{F°-H_0°}{T}$ (cal deg$^{-1}$ mole$^{-1}$) |
|---|---|---|---|---|
| 10 | 0.032 | 0.08 | 0.011 | 0.003 |
| 15 | 0.096 | | | |
| 20 | 0.240 | | | |
| 25 | 0.492 | | | |
| 30 | 0.827 | | | |
| 40 | 1.614 | | | |
| 50 | 2.430 | 38.60 | 1.068 | 0.296 |
| 60 | 3.226 | | | |
| 70 | 4.006 | | | |
| 80 | 4.767 | | | |
| 90 | 5.525 | | | |
| 100 | 6.246 | 257.3 | 3.948 | 1.375 |
| 110 | 6.960 | | | |
| 120 | 7.649 | | | |
| 130 | 8.315 | | | |
| 140 | 8.951 | | | |
| 150 | 9.546 | 655.1 | 7.129 | 2.762 |
| 160 | 10.10 | | | |
| 170 | 10.62 | | | |
| 180 | 11.10 | | | |
| 190 | 11.55 | | | |
| 200 | 11.97 | 1196.5 | 10.227 | 4.244 |
| 210 | 12.35 | | | |
| 220 | 12.71 | | | |
| 230 | 13.04 | | | |
| 240 | 13.35 | | | |
| 250 | 13.64 | 1839.1 | 13.088 | 5.732 |
| 260 | 13.90 | | | |
| 270 | 14.15 | | | |
| 280 | 14.38 | | | |
| 290 | 14.60 | | | |
| 300 | 14.80 | 2551.6 | 15.683 | 7.159 |
| 298.16 | 14.76 ±0.015 | 2524.4 ±3 | 15.593 ±0.02 | 7.126 ±0.01 |

The heat content or enthalpy was calculated by numerical quadrature of the heat capacity *versus* the temperature, the entropy by numerical quadrature of the heat capacity *versus* the logarithm of the temperature, and the free energy from the relation $F=H-TS$. The extrapolation below 10°K was made with a Debye function. The values of these thermodynamic functions at 50° intervals are given in Table II. The estimated probable error in each function is 0.2 percent at 50°K and 0.1 percent at temperatures above 50°K, but in order to make the table internally consistent, one more figure is given for some of the values than is justified by the experimental accuracy.

## DISCUSSION

The heat capacities of thorium dioxide, uranium dioxide,[1] and neptunium dioxide[2] are presented graphically in Fig. 2. As anticipated, thorium dioxide, unlike the other two dioxides, does not have an anomaly in its heat capacity.

On the assumption that the lattice heat capacity of the actinide dioxides is equal to the heat capacity of thorium dioxide, the magnetic contributions to the heat capacities of uranium dioxide and of neptunium dioxide can be obtained by taking the difference between the thorium dioxide curve and the other curves in Fig. 2. The magnetic heat-capacity curves resemble those calculated for a cooperative transition from an ordered antiferromagnetic state at low temperatures to a disordered state at temperatures above the anomaly,[7] except that they are appreciably different from zero at temperatures far above the anomaly.

Similarly, the magnetic contributions to the entropies can be obtained by subtracting the entropy of thorium dioxide from the entropies of uranium dioxide[1] and of neptunium dioxide.[2] The results are shown in Fig. 3.

It is of interest to compare these results with the magnetic entropies calculated on the basis of the spin-only and the free ion approximations and also to compare them with the magnetic susceptibility data. In uranium dioxide, with two unpaired electrons, the magnetic entropy at high temperatures is $R \ln (2S+1) = R \ln 3 = 2.18$ cal deg$^{-1}$ mole$^{-1}$ if the orbital contribution to the magnetic moment is completely quenched. On the other hand, the magnetic entropy of free $U^{+4}$ ions at high temperatures is $R \ln (2J+1) = R \ln 5 = 3.20$ cal deg$^{-1}$ mole$^{-1}$ if the ground state is $6d^2\ {}^3F_2$, or $R \ln 9 = 4.37$ cal deg$^{-1}$ mole$^{-1}$ if the ground state is $5f^1 6d^1\ {}^3H^4$ or $5f^2\ {}^3H_4$. (Hund's rules are assumed. The term symbols are given for $LS$ coupling, but $J$ in the ground state will be the same for $jj$ coupling as for $LS$ coupling.) It can be seen from Fig. 3 that the magnetic entropy of uranium dioxide attains the spin-only value of $R \ln 3$ at about 73°K and increases steadily with temperature. At 298.16°K it is 3.04 cal deg$^{-1}$ mole$^{-1}$, corresponding to partial but not complete quenching of the orbital angular momentum. Extrapolation indicates that the magnetic entropy exceeds $R \ln 5$ above 370°K, and this may be an argument against the $6d^2$ electronic configuration for the ground state.

The effective magnetic moment of uranium dioxide derived from susceptibility measurements extending down to 80°K is 3.20 Bohr magnetons.[3,8] This magnetic moment is intermediate between the spin-only value (2.83 Bohr magnetons) and that for the free ions with

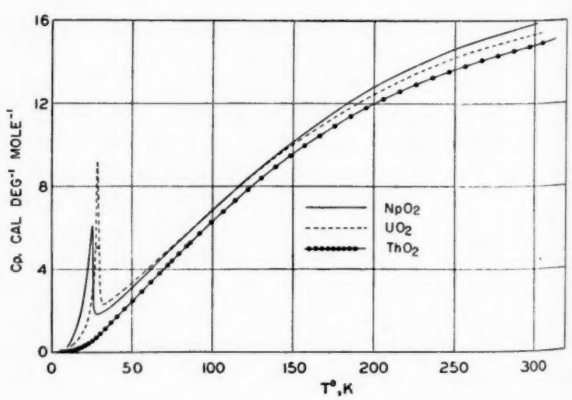


FIG. 2. Heat capacities of $ThO_2$, $UO_2$, and $NpO_2$.

[7] R. Kikuchi, Phys. Rev. **81**, 988 (1951).
[8] J. K. Dawson and M. W. Lister, J. Chem. Soc. **1950**, 2181.

a $5f^2\ ^3H_4$ or $5f^16d^1\ ^3H_4$ ground state (3.58 Bohr magnetons), and it is much larger than the magnetic moment for the free ions with a $6d^2\ ^3F_2$ ground state (1.63 Bohr magnetons). Hence, the magnetic moment of uranium dioxide corresponds to a $5f^2$ or $5f^16d^1$ configuration and partial quenching of the orbital angular momentum. However, Trzebiatowski and Selwood[3] and Dawson[9] have found that in $UO_2$-$ThO_2$ solid solutions the magnetic moment of $U^{+4}$ approaches the spin-only value at infinite dilution. On the assumption that quenching would occur for $6d$ but not for $5f$ electrons, they concluded that the configuration in the ground state is $6d^2$. The magnetic entropy curve, on the other hand, seems to indicate that the configuration is $5f^16d^1$ or $5f^2$ rather than $6d^2$.

The only measurement of the magnetic susceptibility of uranium dioxide below 80°K is a single determination by Trapnell and Selwood[10] at 20°K. It would be desirable to have further measurements to give the shape of the magnetic susceptibility curve in the region of the heat capacity anomaly (29°K), in order to determine whether uranium dioxide is antiferromagnetic below 29°K, as suggested by Jones, Gordon, and Long.[1]

In neptunium dioxide, with three unpaired electrons, the spin-only value for the magnetic entropy at high temperatures is $R$ ln 4=2.75 cal deg$^{-1}$ mole$^{-1}$, whereas the magnetic entropy of free $Np^{+4}$ ions at high temperatures is $R$ ln 10=4.58 cal deg$^{-1}$ mole$^{-1}$ if the ground state is $5f^3\ ^4I_{9/2}$, and $R$ ln 4=2.75 cal deg$^{-1}$ mole$^{-1}$ if it is $6d^3\ ^4F_{3/2}$. Other possible ground states for free $Np^{+4}$ ions and the corresponding magnetic entropies at high temperatures are $R$ ln 12=4.94 cal deg$^{-1}$ mole$^{-1}$ for $5f^26d^1\ ^4K_{11/2}$ and $R$ ln 8=4.13 cal deg$^{-1}$mole$^{-1}$ for $5f6d^2\ ^4H_{7/2}$. As shown in Fig. 3, the spin-only value of $R$ ln 4 is attained at 95°K, and at 298.16°K the magnetic entropy of neptunium dioxide is 3.60 cal deg$^{-1}$ mole$^{-1}$. These results seem to indicate that there is partial quenching of the orbital angular momentum and that the configuration in the ground state is not $6d^2$.

Susceptibility measurements have not been made on neptunium dioxide, but data on another quadrivalent neptunium compound, $KNpF_5$, indicate partial quenching of the orbital angular momentum.[11]

It would be difficult to measure the low-temperature heat capacities and thus obtain the entropies of the other actinide dioxides, because the half-lives of the available isotopes are too short. The rate of energy liberation by radioactive decay is so large that it would be difficult to achieve thermal equilibrium between the sample, calorimeter, and thermometer. For example, if the heat capacity of $Pu^{239}O_2$ is approximately the same as that of $NpO_2$, the radioactive decay would cause the temperature to rise more than 3 deg/min at 30°K. Therefore, it is desirable to attempt to estimate the entropies of the other actinide dioxides.

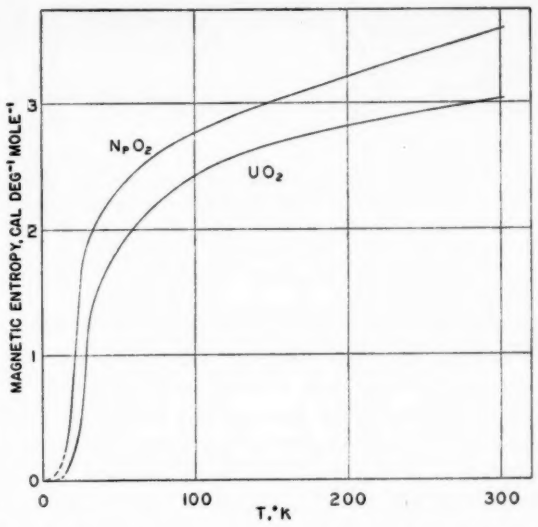


FIG. 3. Magnetic entropies of $UO_2$ and of $NpO_2$, obtained by subtracting the entropy of $ThO_2$ from the entropies of $UO_2$ and of $NpO_2$.

It will be noted that at 298.16°K the magnetic entropy of uranium dioxide exceeds the spin-only value for two unpaired electrons by 0.86 cal deg$^{-1}$ mole$^{-1}$, and the magnetic entropy of neptunium dioxide exceeds the spin-only value for three unpaired electrons by 0.85 cal deg$^{-1}$ mole$^{-1}$. We assume that the difference between the magnetic entropy and the spin-only value is roughly constant for the isomorphous actinide dioxides, and accordingly estimate that the entropy of each actinide dioxide at 298.16°K is given approximately by the entropy of thorium dioxide at this temperature (i.e., the lattice contribution) plus $R$ ln $(2S+1)$ plus 0.86 cal deg$^{-1}$ mole$^{-1}$. In this manner the following estimates were obtained for the entropies at 298.16°K, in cal deg$^{-1}$ mole$^{-1}$: $PaO_2$, 17.8; $PuO_2$, 19.7; $AmO_2$, 20.0; $CmO_2$, 20.3; $BkO_2$, 20.6; and $CfO_2$, 20.3. For completeness, the experimental entropies of $ThO_2$, $UO_2$[1], and $NpO_2$[2] at 298.16°K are listed here also, in cal deg$^{-1}$ mole$^{-1}$: $ThO_2$, 15.59±0.02; $UO_2$, 18.63±0.1; and $NpO_2$, 19.19±0.1.

[9] J. K. Dawson, J. Chem. Soc. **1951**, 2889.
[10] B. M. W. Trapnell and P. W. Selwood, Nature **169**, 840 (1952).
[11] D. M. Gruen, dissertation, University of Chicago, 1951.

# On Rates of Approach to Equilibrium

S. H. BAUER
*Department of Chemistry, Cornell University, Ithaca, New York*
(Received March 31, 1953)

The limiting conditions on the applicability of an exponential decay law for the rate of approach to equilibrium of a system which is near but not at equilibrium are discussed. Attention is called to a solution which is more general; it consists of a superposition of exponentials, with a spectrum of relaxation times.

A NUMBER of interesting discussions have appeared in the literature[1,2] regarding the rate of approach to equilibrium of a chemical reaction which is near but not at that state. Using essentially a Taylor's expansion for the free energy function in terms of the variables which characterize the system and neglecting all terms involving increments raised to a power higher than unity, one can show that the rate of return to equilibrium is directly proportional to the magnitude of the instantaneous free energy displacement from equilibrium: $\partial\Delta F/\partial t \doteq -k\Delta F$, and is independent of the detailed mechanism for the reaction. To my knowledge, the criterion for proximity and proof that mere proximity is a sufficient as well as necessary condition for this rate law to be valid for cases where the displacement from equilibrium is finite though small, have not been discussed. The question whether different types of perturbations with equal $\Delta F$'s (or of other gauges for departure from equilibrium) are equivalent, merits careful discussion: for example, can one treat displacements from equilibrium due to a sudden injection of enthalpy in the same way as perturbations induced by sudden concentration changes?

Manes *et al.*[2] have indicated that the exponential law for approach to equilibrium is limited to reactions which can be represented by a single over-all equation. In this note I shall first point to the severity of this restriction; I shall then briefly discuss a case wherein the perturbation is induced by an injection of enthalpy, to demonstrate that the above law is not always valid, even when the displacement from equilibrium is as small as one chooses; and then I shall discuss some sufficiency conditions.

(1) Consider the double equilibrium,

$$A \underset{k_1}{\overset{k_1'}{\rightleftharpoons}} B \underset{k_2}{\overset{k_2'}{\rightleftharpoons}} C, \text{ with } (k_1, k_1') > (k_2, k_2').$$

If a displacement from equilibrium is induced by a sudden injection of $A$, *no matter how small in amount*, it is obvious that the concentration of $B$ will first rise and then fall to its final value. Further, the concentration of $A$ will first decline rapidly to one level, and then more slowly to its final level. Similarly, the approach to equilibrium will not follow a simple exponential decline if the system were ever so slightly perturbed by the injection of $B$. Only the sudden injection of a small amount of $C$ will produce a displacement for which the free energy increment will follow a first-order decline. Hence the restricting condition[2] for the applicability of the simple rate law implies not only that the over-all (thermodynamic) reaction could be written as one equation, but also (kinetically), that either

(a) the concentrations of all the metastable intermediates remain less than the sensitivity of the analytical procedures available for their detection, and that the precision of the analytical methods for the stable reactants and products is so low that the maximum accumulation of intermediates is not detectable as a net deficiency, or (b) that the mean lifetime of the intermediates is shorter than the effective time constant of the analytical devices used. The criterion is operational, but of temporal duration, depending as it does on developments in the art of analysis. One may safely predict that numerous systems which may be treated at present as "single over-all reactions" will have to be reconsidered in the future utilizing descriptions which involve more than one reaction.

Since the rate of change of the free energy during approach to equilibrium is in general some function of the magnitude of the free energy departure from equilibrium, the principle of continuity of enthalpy and entropy assures us that this function is analytic. The formal reason for the failure of the exponential law lies, then, in neglecting all but the first term in the Taylor's expansion. In principle, one could allow for multivalued variations with time (for instance, the concentration of $B$ above) if the higher terms were included. This would necessitate that the rate be measured sufficiently precisely at and immediately adjacent the equilibrium point to permit evaluation of the higher derivatives.

(2) Suppose the system

$$A_2 \rightleftharpoons 2A, \quad \text{with} \quad (\Delta H^0/RT) \geqslant 40$$

in equilibrium, is suddenly perturbed by an instantaneous compression. A sudden pressure rise will be noted due both to the decrease in volume and the simultaneous rise in translational temperature, since work was injected adiabatically into the system. A rapid distribution of energy between translational and vibra-

[1] Gilkerson, Jones, and Gallup, J. Chem. Phys. **20**, 1182 (1952).
[2] Manes, Hoffer, and Weller, J. Chem. Phys. **18**, 1355 (1950). Refer to these papers [1 and 2] for extensive references to previous publications.

tional modes will take place and a corresponding fall in total pressure will be observed. Final equilibrium will be reached relatively slowly, corresponding to the slower redistribution of energy among the chemical as well as thermal degrees of freedom. Hence a further slow fall in pressure will be noted. I wish to emphasize that the above pattern will be followed regardless of the magnitude of the initial perturbation.

The departure from equilibrium is more serious in such instances. Indeed, only when equilibrium within groups of degrees of freedom is maintained, but disequilibrium exists between these groups (translational-vibrational-chemical) can one introduce local values for thermodynamic variables for the purpose of treating their equalization between the groups.

Examination of the above two cases shows the trap into which the unwary may fall. Except for reactions which proceed "practically" according to a one-step mechanism, it is not only the *magnitude of the perturbation* but also the *age of the system* which control its behavior with time. We have thus deduced a sufficiency condition. If one does not wish to consider the manner of displacement from equilibrium, he may apply the first-order rate law to old systems only, those in which the kinetics are controlled by the longest time constant; i.e., after the perturbation he must wait for a time $t \simeq \tau_{\max}$. On the other hand, if he can brook no delay, he must restrict displacements from equilibrium to be induced by selected perturbations; i.e., those which are associated with the step in the mechanism which has the longest time constant.

To arrive at a quantitative formulation of the above, consider a system near equilibrium, represented by the following sequence of steps which show its ultimate mechanism:

$$[X_1] \underset{k_1}{\overset{k_1'}{\rightleftharpoons}} [X_2] \rightleftharpoons \cdots \underset{k_{n-1}}{\overset{k'_{n-1}}{\rightleftharpoons}} [X_n],$$

where each bracket symbolically stands for the participating reactants, which need not all be isolatable.[3] Also, let the instantaneous departure of each unit from its equilibrium concentration (or temperature, or both) be designated by the collective symbol $x_1, x_2 \cdots x_n$. Then

$x_i = (X_i) - (X_2)_{eq}$

$x_i(0) = x_i^0$, is the given initial perturbation

$x_i \to 0$ at $t \to \infty$.

Since no metastable intermediates exist between adjacent pairs, the previous arguments[1,2] are valid, and the *rates of the individual transformations* may be approximated by first-order equations, when the departure from *local equilibrium* is not too great. To make the treatment sufficiently simple, we must assume that the driving force for reaction is proportional to the displacement from ultimate equilibrium. Then we get $n$ simultaneous rate equations

$$\begin{aligned} (p+k_1)x_1 - k_1'x_2 &= 0 \\ -k_1x_1 + (p+k_1'+k_2)x_2 - k_2'x_3 &= 0 \\ -k_{n-1}x_{n-1} + (p+k'_{n-1})_n &= 0, \end{aligned} \quad (1)$$

where $p \equiv d/dt$.

The solutions[4] $x_i(t)$ are sums of exponentials,

$$x_i(t) = \sum_{j=1}^{n} A_{ij} e^{-p_j t}; \quad i = 1, 2, \cdots n$$

$A_{ij}$ may be either $>$ or $<0$.[5] (2)

From inspection of this equation it is clear that in general $x_i(t)$ will reduce to a single exponential only when $(p_{\min} t) > 1$; i.e. $t > \tau_{\max}$; further, that the relaxation times are related to the unimolecular rate constants but not in a simple manner, being the reciprocal of the roots of the determinantal equation.

Two additional points of interest should be mentioned. In closed systems one may select appropriate definitions for measurement of the $x_i$'s, such that the conservation laws may be simply expressed as $\sum_{i=1}^{n} x_i(t) = 0$. This additional restraint adds little to the above arguments, except for the case $i=2$. Then the two roots must be equal. Further, for systems which are not closed, and in which perturbations are introduced continuously, rather than merely initially, the solution of the problem may be obtained by "folding" the exponential solution (2) into the rate of injection of the perturbation, *provided* the effects are linear.

[3] The argument may be readily generalized to include the possibility of mutual interconversion of all pairs of brackets. The solution for the sequential case used as an example requires obtaining the roots of a determinant with only two nonvanishing diagonal rows on each side of the main diagonal, whereas the general case leads to a determinant with no vanishing terms.

[4] The indicated procedure for treating chemical lag by means of a spectrum in a relaxation times has been used by J. G. Kirkwood and Bryce Crawford, Jr. [J. Phys. Chem. **56**, 1048 1952] in their formulation of the macroscopic equations of transport.

[5] The significance of the coefficients may be determined as follows: Let

$$a_{ii} \equiv k_{i-1}' + k_i; \; a_{i,i-1} \equiv -k_{i-1}'; \; a_{i,i+1} \equiv -k_i'.$$

In this case, $k_n = 0$, and all other $a_{ij} = 0$. After substitution of the trial solution (2) into the linear equations, the set may be written in the form

$$\sum_{l=1}^{n} \sum_{j=1}^{n} (A_{lj} a_{il} - A_{ij} p_j) e^{-p_j t} = 0, \quad \text{for all } i. \quad (a)$$

But this must be valid for any value of $t$, and hence independent of the index $j$; i.e.,

$$\sum_{l=1}^{n} (A_{lj} a_{il}) - A_{ij} p_j = 0, \quad \text{for all } i \text{ and } j. \quad (b)$$

The determinantal condition for the existence of a nontrivial solution is

$$|a_{il} - \delta_{il} p_j| = 0, \quad (c)$$

the solution of which gives $n$ roots, $p_1 \cdots p_j \cdots p_n$. These are the coefficients of the time variable in (2) and have the dimensions of a reciprocal time. Now, for each root there are $n$ unknown $A_{lj}$'s, but there are also $n$ equations, since (b) is valid for each $i$ from 1 to $n$.

$$\sum_{l=1}^{n} A_{lj} (a_{il} - \delta_{il} p_j) = 0 \quad \text{for any selected } j' \quad (d)$$

$$\text{for } i = 1, 2, 3 \cdots n.$$

Solution of the $n$ sets of $n$ simultaneous linear equations will give the coefficients $A_{lj}$ to within $n$ constant factors. The latter are determined by the boundary conditions

$$x_i(0) = \sum_{j=1}^{n} A_{ij} = x_i^0. \quad (e)$$

Again, since $x_i^0(0)$ may be either positive or negative, so may the $A_{ij}$'s.

# Letters to the Editor

*THIS section will accept reports of new work, provided these are terse and contain few figures, and especially few half-tone cuts. The Editorial Board will not hold itself responsible for opinions expressed by the correspondents. Contributions to this section should not exceed 600 words in length and must reach the office of the Editor not later than the 15th of the second month preceding that of the issue in which the Letter is to appear. No proof will be sent to the authors. A publication charge of $15.00 per Letter is made which, when honored, will entitle the Institution to 100 free reprints.*

## Correlation between Photoconductance and Ultraviolet Spectrum of Anthracene Crystals

D. J. CARSWELL
*Physical Chemistry Department, University of Sydney, Sydney, Australia*
(Received August 10, 1953)

BAYLISS[1] has discussed the known[2] photoconductance effect of anthracene. A correlation between the threshold of the photoconductance, the optical absorption, and thermal excitation energy has been shown[3] to hold for violanthrone, isoviolanthrone, and pyranthrone.

We now report that for single anthracene crystals the plot of the photocurrent against the frequency of incident light reproduces closely the optical spectrum[4] of the crystal, as can be seen from Fig. 1. No extinction coefficients are reported for the second

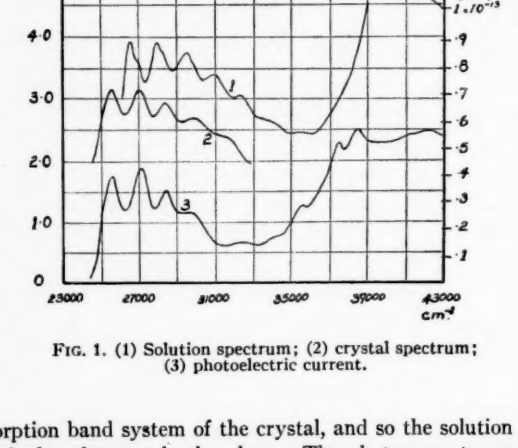


FIG. 1. (1) Solution spectrum; (2) crystal spectrum; (3) photoelectric current.

absorption band system of the crystal, and so the solution spectrum[5] of anthracene is also shown. The photocurrents were observed with very nearly monochromatic light and varied with the angle between its vibration direction and the crystal axes. The characteristic[2] buildup and decay of the photocurrent with time was observed, the current-potential relation was found to be ohmic up to a limiting potential, and the current was proportional to the light intensity. Experimental detail and theoretical discussion will be published shortly. I am indebted to the Vacuum Oil Company for a scholarship and wish to thank Dr. T. Iredale and Dr. L. E. Lyons for their interest in the work.

[1] N. S. Bayliss, Rev. Pure Appl. Chem. 1, 64 (1951).
[2] A. T. Vartanyan, Doklady Akad. Nauk. S.S.S.R. 71, 631 (1950).
[3] H. Akamatu and H. Inokuchi, J. Chem. Phys. 20, 1481 (1952).
[4] G. Kortum and B. Finckh, Z. physik. Chem. B52, 263 (1942).
[5] "Catalog of Ultraviolet Spectrograms," A.P.I. Project, 44 National Bureau of Standards, No. 170.

## Mass Spectrum of Gallium Vapor

STEPHEN ANTKIW AND VERNON H. DIBELER
*National Bureau of Standards, Washington 25, D. C.*
(Received August 10, 1953)

MASS spectrometric studies of the vapors of carbon[1,2] and other Group IV elements[3] have revealed relatively high concentrations of polyatomic molecules in addition to the monatomic species. Thus previous calculations of vapor pressure and heats of vaporization based on the assumption of monatomic vapors must be corrected for some of these elements.

Computations of the vapor pressure of gallium, made by assuming a monatomic vapor,[4,5] prompted us to investigate the mass spectrum of this element. The experiment was also considered particularly suitable for testing a recently developed high-temperature furnace for a mass spectrometer ion source.

Mass spectra were obtained with a Consolidated 21–102 mass spectrometer. The ion-source furnace, developed for the thermal decomposition of organic and semiorganic molecules introduced in the vapor phase, consisted of a quartz tube with an inside diameter of 1 mm wound with a bifilar tungsten heater. A nichrome radiation shield enclosing the tube and heater had the same dimensions as the original ion-repeller assembly of the ion source, which it was designed to replace. Thus vapors entered the ionization chamber from the end of the furnace at a point approximately one millimeter above the electron beam. A platinum, platinum-rhodium thermocouple was used to obtain a curve of temperature *versus* heater current to a maximum temperature of 1025°C. In order to prevent possible reaction of the gallium with platinum, the thermocouple was removed before introducing the sample.

Gallium metal, obtained from the Eagle-Picher Company through Mr. B. F. Scribner, was of high purity, containing less than 25 ppm total impurities. These were principally lead, copper, manganese, and aluminum. The sample was melted by holding the container in the hands, and about 10 mg was drawn into a previously flamed quartz capillary tube. This tube was placed inside the furnace and the mass spectrometer was assembled and evacuated. Raising the temperature of the furnace to about 750°C permitted satisfactory outgasing of the furnace assemply and ion source without evaporating detectable amounts of gallium. The sample was further heated several hours at 1000°C before the results reported here were obtained.

Mass spectra and isotope ratios were obtained by using conventional procedures at a number of equilibrium temperatures in the range 865 to 1025°C. Ion currents of about $3\times10^{-12}$ amp were obtained for the $Ga^+$ ion at the highest temperature. The very simple spectra showed only the ions $Ga^+$, $Ga_2O^+$, and $Ga_2^+$ with relative total isotopic abundances of 100:10:1, respectively, varying only slightly with temperature. The $Ga_2O^+/Ga_2^+$ ratio was essentially constant giving some evidence that the diatomic ions might be fragment ions of the oxide rather than molecule ions. However, by assuming comparable ionization cross sections, upper limits of one percent for the diatomic molecule and 0.1 percent for triatomic and higher species are estimated for the composition of the vapor. It seems certain therefore that the previous assumption of monatomic gallium vapor is entirely justified.

The observation of $Ga_2O^+$ ions is of particular interest. Although Speiser and Johnston reported no evidence of reaction between gallium and quartz, visual examination of the sample remaining in the capillary at the end of our experiments showed appreciable areas of the metal-quartz interface apparently separated by an oxide film. As the existence of univalent gallium seems doubtful,[6] the presence of $Ga_2O^+$ suggests an ion fragment of the sesqui oxide, $Ga_2O_3$. However, there is no other evidence of this molecule although the mass spectrum is unknown and the molecule ion may be unstable. These points deserve further investigation.

A series of isotopic measurements was also made of the $Ga^+$ ion at three temperatures; *viz.*, 865, 935, and 1025°C. The $Ga^{69}/Ga^{71}$ ratios were 1.51, 1.53, and 1.53, respectively, with approximately

one percent deviation from the mean of at least nine determinations at each temperature. The ratio 1.53 corresponds to the isotopic abundances of $Ga^{69}=60.5$ and $Ga^{71}=39.5$. These are considered in good agreement with the values reported by Inghram[7] from measurements made on thermionic $Ga^+$ ions from the oxide.

We wish to acknowledge our indebtedness to Mr. William B. Haliday for construction of the furnace and to Dr. Fred L. Mohler for many helpful discussions.

[1] W. A. Chupka and M. G. Inghram, J. Chem. Phys. **21**, 371 (1953).
[2] R. E. Honig, Bull. Am. Phys. Soc. **28**, No. 3, 41 (1953).
[3] R. E. Honig, J. Chem. Phys. **21**, 573 (1953).
[4] P. Harteck, Z. Physik. Chem. **134**, 1 (1928).
[5] R. Speiser and H. L. Johnston, J. Am. Chem. Soc. **75**, 1469 (1953).
[6] N. V. Sidgwick, *The Chemical Elements and Their Compounds* (Clarendon Press, Oxford, 1950), Vol. I, p. 480.
[7] Inghram, Hess, Brown, and Goldberg, Phys. Rev. **74**, 343 (1948).

## Hindered Molecular Rotation in Liquid Crystals*

R. D. SPENCE, *Michigan State College, East Lansing, Michigan*
AND
H. S. GUTOWSKY AND C. H. HOLM, *Noyes Chemical Laboratory, Urbana, Illinois*
(Received July 24, 1953)

THE proton magnetic resonance absorption in the liquid crystal phase of para-azoxyanisole was reported earlier.[1] At 7300 gauss the resonance had three components with intensities of 2:3:2, and the outer peaks were separated by 3.3 gauss. We have since plotted[2] the line shapes at 6365 and 4175 gauss. The results at the three fields agree within an experimental error of ±2 percent, so the line structure cannot arise from a field dependent interaction. We propose that the line structure is produced by the net nuclear magnetic dipolar fields associated with restriction of the molecules in the liquid crystal phase to rotation about their long axis.

A scale drawing of para-azoxyanisole is shown in Fig. 1. The molecule is long and thin; on steric grounds the benzene groups can reorient about the C−N bonds (rotate about $\alpha$) much more easily than the molecule can turn about any other axis. In addition, the $CH_3$ groups are certainly in motion about the C−O bonds[3] (rotating about $\beta$). The liquid crystal phase is anisotropic, presumably with ordered micro = regions where the long molecules are stacked up side by side. The observed line should be a composite of the absorption from protons in the $CH_3$ groups and protons attached to the benzene rings, with the absorption of each set determined by its structure and motions.

There are three protons in $CH_3$ groups to four on the benzene, with relative absorptions of 3/7 and 4/7. In a crystal powder the second moment, $\Delta H_2^2$, for a rigid methyl group is 21.7 gauss[2]; rotation about $\beta$ reduces this by a factor of 1/4 and rotation about $\alpha$ by 1/10 giving 0.5 gauss[2] for the composite motions.[4] Rotation about $\alpha$ reduces only[3] the intermolecular broadening of the protons on the benzene; these protons occur in pairs separated by 2.45A and their second moment is 1.65 gauss[2]. The net second moment predicted for the sample is

$$\Delta H_2^2=(3/7(0.5)+(4/7)(1.65)=1.16 \text{ gauss}^2.$$

The value observed at 132°C is 1.07 gauss[2].

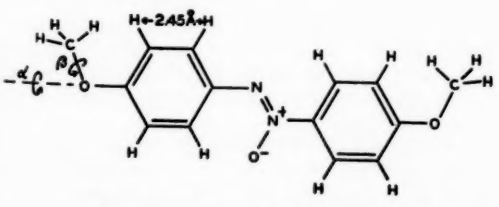


FIG. 1. Scale model for para-azoxyanisole.

The proton pairs on the benzene ring should give a doublet line[3] with a separation of $3\mu r^{-3}$, i.e., 2.9 gauss, where $\mu$ is the proton magnetic moment and $r$ is the proton-proton distance, 2.45A. The small value of $\Delta H_2^2$ calculated for the $CH_3$ group protons indicates a single line less than a gauss wide. Combining these, a triplet line is predicted, with relative intensities of 2:3:2, and a separation between outer peaks of 2.9 gauss. The observed separation ranges from 3.9 gauss at 117°C, the transition point, to 2.25 gauss at 135°C, the clear point.

The agreement between theory and experiment is well within the uncertainties introduced by intermolecular line broadening and low-frequency thermal motions other than the main ones postulated. A further complication arises from the diamagnetic anisotropy of the molecule which tends to align the long axis parallel to an external magnetic field. The analysis given above assumes a random crystal powder. For oriented molecules, the doublet line separation would be 2.9 $(3\cos^2\theta-1)$ gauss. Partially effective orientation, decreasing with increasing temperature, would help account for the wide range of line separation observed in the liquid crystal phase.

The derivative of the absorption in the solid at room temperature is a broad line with a width, $\delta H$, of 6.3 gauss, and a narrow central spike. The second moment is 5.3 gauss[2] which agrees fairly well with the 3.3 gauss[2] predicted for a rigid molecule with rotating $CH_3$ groups, allowing for increased intermolecular broadening in the solid phase. The narrow spike is probably the central component of the triplet line from the rotating $CH_3$ groups with the other structure washed out by intermolecular broadening and superposition of the different line shapes.

It appears that analyses similar to the above will explain the more complex experimental findings in liquid crystals of other materials.[5]

We wish to thank Dr. L. H. Meyer for several interesting discussions of this research and for his assistance with the measurements at 6365 gauss.

* Supported in part by the U. S. Office of Naval Research.
[1] Spence, Moses, and Jain, J. Chem. Phys. **21**, 380 (1953).
[2] Gutowsky, Meyer, and McClure, Rev. Sci. Instr. **24**, 1953 (to be published).
[3] H. S. Gutowsky and G. E. Pake, J. Chem. Phys. **18**, 162 (1950); line width changes associated with rotation of $CH_3$ groups are ordinarily observed at temperatures below −150°C.
[4] J. G. Powles and H. S. Gutowsky, J. Chem. Phys. **21** (to be published, 1953).
[5] Jain, Moses, Lee, and Spence, Bull. Am. Phys. Soc. **28**, No. 4, 8 (1953).

## Polarized Infrared Spectrum of $KAu(CN)_2$*

LLEWELLYN H. JONES
*Los Alamos Scientific Laboratory, Univeristy of California, Los Alamos, New Mexico*
(Received July 1, 1953)

A STRUCTURAL examination of inorganic complex cyanides, using polarized infrared spectra, is in progress. The monovalent gold-potassium-cyanide system is the simplest, as only one complex is formed. The purpose of this letter is to present some results on the structure of potassium gold dicyanide.

A crystallographic[1] and an x-ray[2] examination of $KAu(CN)_2$ shows that it crystallizes in the rhombohedral system and suggests an arrangement of linear groups parallel to the C-axis.

A single crystal of $KAu(CN)_2$ was mounted at the focus of a reflecting microscope consisting of two American Optical Company reflecting objectives. The crystal was about 300 microns long (along the C-axis), 150 microns wide, and 50 microns thick.

The incident light was polarized by a standard Perkin-Elmer polarizer consisting of 6 thin silver chloride plates inclined at the polarizing angle. The plane of polarization was changed by rotating the polarizer while the sample remained fixed.

The results are illustrated in Fig. 1. In the region 400 $cm^{-1}$ to 4000 $cm^{-1}$, there are two strong infrared absorption bands, at 427 $cm^{-1}$ and 2140 $cm^{-1}$, both polarized along the C-axis. The

band at 2140 $cm^{-1}$ undoubtedly arises from the asymmetric carbon-nitrogen stretching vibration, $\nu_3$.

This shows that the linear N−C−Au−C−N groups do indeed lie along the C-axis. The results also show that the band at 427 $cm^{-1}$ arises from the other asymmetric stretching vibration, $\nu_4$, which is polarized in the same direction as $\nu_3$, while the bending vibrations are polarized perpendicular to the linear group. $\nu_4$ is essentially an asymmetric vibration of the gold atom against the two cyanide groups.

The small absorption peak at 2100 $cm^{-1}$ arises from $NC^{13}AuC^{12}N$, as determined by the spectrum of $KAu(CN)_2$ enriched in $C^{13}$. A valence force calculation yields 2091 $cm^{-1}$ as $\nu_3$ for the $C^{12}-C^{13}$ isotopic species, based on 2140 $cm^{-1}$ for the $C^{12}-C^{12}$ species. Similarly, the weak peak at about 2117 $cm^{-1}$ probably arises from $N^{15}CAuCN^{14}$ (a simple valence force calculation yields about 2112 $cm^{-1}$). The intensities cannot be compared, as the sample was of varying thickness and was not perfectly masked.

From the frequencies of $\nu_3$ and $\nu_4$, a simple valence force treatment yields force constants of $2.30\times10^5$ dynes/cm for the Au−C bond and $16.78\times10^5$ dynes/cm for the C−N bond. However, these values cannot be considered as reliable, as the interaction constants may be considerable. More reliable values will be obtained from a complete analysis of the combination bands of $KAu(CN)_2$ and the $C^{12}-C^{13}$ and $C^{13}-C^{13}$ species.

* This work was sponsored by the U. S. Atomic Energy Commission.
[1] Unpublished work by E. Staritzky of this Laboratory.
[2] Unpublished work by F. H. Ellinger of this Laboratory.

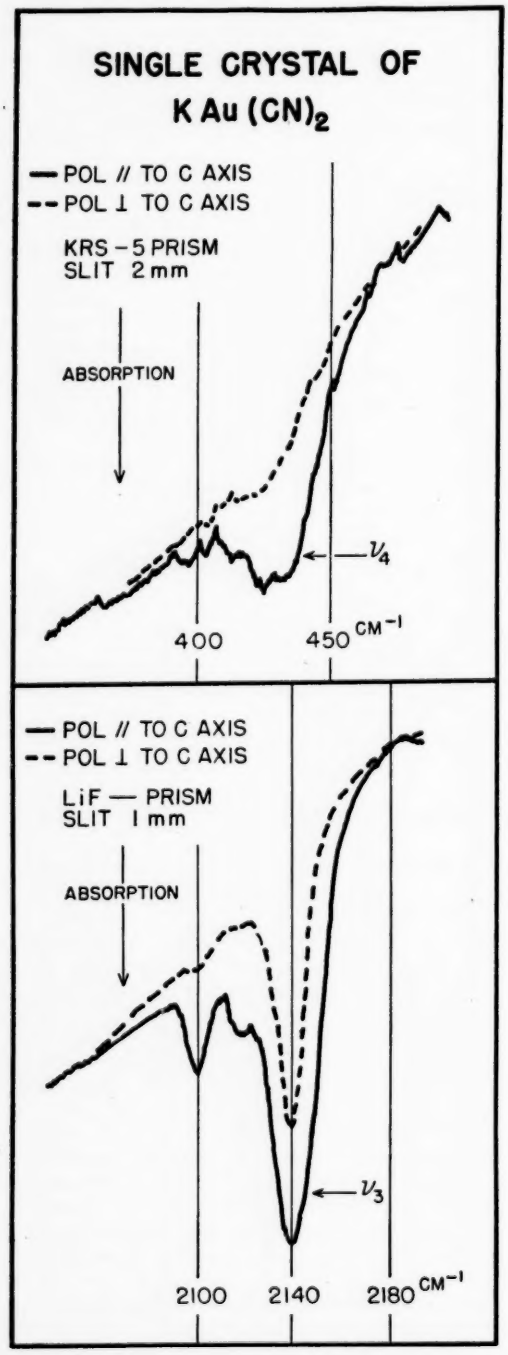


FIG. 1. Polarized infrared spectrum of a single crystal of $KAu(CN)_2$.

## The Refractive Index Correction in Light-Scattering Measurements

D. J. MEIER
*Shell Development Company, Emeryville, California*
(Received August 3, 1953)

VARIOUS correction factors have been described in the literature to account for the refractive effects produced by liquids of different refractive indices in light-scattering measurements. Most of the formulas have been derived by assuming the scattering volume to be a point source, which leads to correction factors proportional to $n^2$ for rectangular cells, to $n$ for cylindrical cells and unity for spherical cells.[1] Hermans and Levinson,[2] by considering the finite extension of the scattering volume, have derived equations which show the correction factor to be proportional to $n^2$, irrespective of the shape of the cell, provided that the photometer does not see past the edges of the beam. However, the experimental evidence presented by the authors only demonstrates the geometrical variables in their equation relating to slit widths and spacing to be correct. It is important to know the correction factor exactly for the various cell shapes, since it may readily amount to a 30 percent correction in the measurement of absolute turbidities or in comparing solvents, as for example, when a liquid of known scattering power is used to calibrate a light-scattering instrument for use with other solvents. Consequently, we believe that it will be of interest to present our results, which determine experimentally the correction factor.

Relative scattering in rectangular and conical cells was determined for several liquids having widely different refractive indices. Considering the geometry of our light-scattering instrument, every formula for the correction factor for rectangular cells agrees that it is proportional to $n^2$ (the "volume correction" discussed by Carr and Zimm[1] was negligible in these experiments). Thus, after multiplying the observed intensities of the scattered light by $n^2$, a figure is obtained which is proportional to the absolute scattering power of the liquid. By suitably normalizing these figures and comparing them with the normalized results obtained with conical cells after applying correction factors of unity, $n$ and $n^2$, it should be possible to make an unequivocal choice of the refractive index correction for conical cells and thence to determine the correction for cylindrical and spherical cells.

The following data were obtained in a light-scattering instrument similar to that described by Zimm.[3] The rectangular cells were 25×25×30 mm, with optically-polished faces. The conical cells were hand-blown in the shape of an ellipsoid of revolution with a volume of approximately 6 ml. Measurements with the conical cells were conducted with the cells immersed in an outer bath of hexadecane.

The various liquids were purified by distillation, followed by filtration through Seitz filter pads which had been impregnated with an EPON resin and baked. It was found that better results were obtained with water if the EPON-impregnated filter pad

TABLE I. Relative scattering of liquids. $T=25°C$. Unpolarized incident light, $\lambda=5780A$.

| Liquid | $n$ | Rectangular cell $i_{90}\times n^2$ | Conical cell $i_{90}$ | Conical cell $i_{90}\times n$ | Conical cell $i_{90}\times n^2$ |
|---|---|---|---|---|---|
| Benzene | 1.501 | 1.00 | 1.00 | 1.00 | 1.00 |
| 1-Methylnaphthalene | 1.613 | 4.39 | 3.79 | 4.08 | 4.39 |
| Carbon tetrachloride | 1.460 | 0.350 | 0.371 | 0.361 | 0.351 |
| Hexadecane | 1.434 | 0.390 | 0.418 | 0.401 | 0.383 |
| Methyl isobutyl ketone | 1.396 | 0.282 | 0.331 | 0.308 | 0.287 |
| Water | 1.333 | 0.089 | 0.117 | 0.104 | 0.0925 |
| Methyl alcohol | 1.330 | 0.170 | 0.219 | 0.194 | 0.172 |

was also made hydrophobic by application of a silicone resin.[4] That the samples were free of dust was shown by the absence of dissymmetry with the conical cells and by visual inspection at low scattering angles with the rectangular cells.

Table I presents the experimental results for the rectangular and conical cells, in each case normalized to those of benzene. By comparing the data given in Table I for the rectangular cells with those for the conical cells and assuming corrections of unity, $n$ and $n^2$, it is seen that the $n^2$ correction is correct for the conical cells. The average deviation between the results with the rectangular cells and the conical cells with the $n^2$ correction is slightly over 1 percent while the average deviation with the $n$ correction is over 8 percent, and correspondingly greater for the unity correction. The conclusions of Hermans and Levinson are thus quite satisfactorily verified.

Values for the relative scattering of carbon tetrachloride and benzene agree very well with those obtained by Carr and Zimm.[1] For 30°C and 5461A light, they found the ratio of scattering to be 0.348, as compared to our value of 0.350 at 25° and 5780A light.

[1] C. I. Carr, Jr., and B. H. Zimm, J. Chem. Phys. **18**, 1616 (1950).
[2] J. J. Hermans and S. Levinson, J. Opt. Soc. Am. **41**, 460 (1951).
[3] B. H. Zimm, J. Chem. Phys. **16**, 1099 (1948).
[4] General Electric Silicone Resin SR-53.

## Does Carbon Utilize 3*d* Orbitals in Bonding?

H. H. JAFFÉ
*Venereal Disease Experimental Laboratory, U. S. Public Health Service School of Public Health, University of North Carolina, Chapel Hill, North Carolina*
(Received May 25, 1953)

GILLESPIE has recently proposed that carbon (and nitrogen) may use 3*d* orbitals for bonding in several types of combinations: in the transition states of Walden inversion-type reactions, in electron deficient compounds, and in the transition states in carbonium-ion rearrangements.[1] He has attempted to estimate the promotion energy required to reach these orbitals, and by comparison with sulfur and phosphorus concluded that the energy is not prohibitive. However, the comparison does not appear valid. In the compounds of phosphorus and sulfur considered, one and two of the 3*sp* electrons, respectively, are completely transferred to atoms bonded to the central atom, leaving this atom with substantial affinity for 3*d* electrons. This affinity is further enhanced by the electronegativity of the elements bonded to the central atom.[2] In the carbon compounds considered by Gillespie no transfer of entire electrons occurs; they are further, in general, bonded only to one or two strongly electronegative groups; finally these bonds are either very weak bonds or half-bonds. Hence the central carbon atoms can hardly have a large amount of electron affinity. Accordingly Gillespie's arguments concerning the promotion energy are not convincing.

After discussing the promotion energy, Gillespie has constructed various *spd* hybrid orbitals, and concluded that they overlap very efficiently with the orbitals of the atoms bonded to the carbon atom.[1] This conclusion is based on a consideration of the angular dependence of the *spd* hybrid orbitals. Unfortunately, however, no overlap integrals were available to evaluate the extent of this overlap quantitatively. The relevant overlap integrals have recently been evaluated in this laboratory.[3] If Slater's formula[4] for the effective nuclear charges ($Z_{eff}$) is accepted, the overlap integrals of the 3*d* orbitals of the neutral carbon atom with any other orbital vanish, since $Z_{eff}$ is 0, and $\tau=1$. Although Slater's formula probably underestimates the penetration of *d* orbitals, no reasonable values for the effective nuclear charges would lead to appreciable overlap integrals.[5] Therefore, the promotion energy cannot be balanced by binding energy, and it must be concluded that the 3*d* orbitals cannot be of importance in bonding by carbon (and nitrogen). An alternative interpretation of the transition state of the Walden inversion-type reactions and of bonding in electron deficient compounds and the carbonium ion rearrangement transition states will be proposed in later papers.

[1] R. J. Gillespie, J. Chem. Soc. **1952**, 1002.
[2] Moffitt's evaluation of the promotion energy for sulfur shows the importance of the electron affinity. See Moffitt, Proc. Roy. Soc. (London) **A200**, 409 (1950).
[3] H. H. Jaffé and G. O. Doak, J. Chem. Phys. **21**, 196 (1953).
[4] J. C. Slater, Phys. Rev. **36**, 57 (1930).
[5] In a reply to this note, Gillespie [J. Chem. Phys. **21**, 1893 (1953)] states that the extremely small overlap integrals can probably be traced to inaccuracies in Slater's formula. Although this formula undoubtedly is a crude approximation, it is doubtful that overlap integrals calculated from better orbitals would be much larger. Gillespie quotes unpublished work by Craig, Maccoll, Nyholm, Orgel, and Sutton on $PCl_5$ as evidence that difficulties with Slater's rules are encountered in the presumably similar situation, which also involves an expansion of the valence shell. Although the present author has not seen the work of these authors, he has experienced no difficulties with Slater's rules in compounds of phosphorus, provided corrections were made for the ionic character of the bonds. (Jaffé, unpublished results). For the *d* orbital in Gillespie's hybrid orbital, $\psi_4''$, $Z_{eff}=\frac{1}{3}$, $\mu=0.167$; for the carbonium ion transition state $\tau\sim0.821$, $\rho\sim2.7$, $S\sim-0.04$.

## The Use of 3*d* Orbitals in Bonding by Carbon

R. J. GILLESPIE
*William Ramsay and Ralph Forster Laboratories, University College, London, W. C. 1., England*
(Received June 15, 1953)

GILLESPIE showed recently[1] by comparison with the cases of phosphorus and sulfur that the promotion energy involved in the use of 3*d* orbitals by the carbon atom was not prohibitively large. Jaffé[2] has objected that this comparison is not valid since expansion of the valence shell only occurs in phosphorus and sulfur in compounds with strongly electronegative elements.[3] This was in fact pointed out by Gillespie,[1] who suggested that carbon may be expected to utilize its 3*d* orbital only under similar circumstances. Thus in the transition state of a bimolecular substitution reaction the bonds in which a *d* orbital was supposed to be involved were those to the entering and leaving groups, both of which are in general electronegative groups such as OH, Cl, or F. In the carbonium ion rearrangements that were also considered the migrating methyl group is bound to two carbon atoms, each of which carries a formal $+\frac{1}{2}$ charge and which may therefore be regarded as strongly electronegative and capable of stabilizing a 3*d* orbital on the carbon atom of the migrating methyl group.

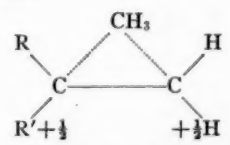


A similar situation occurs in the electron deficient compounds such as $Al_2(CH_3)_6$ in which it was pointed out[1] that the aluminium atoms may be regarded as being strongly electronegative in the direction of their unfilled $sp^4$ orbitals.

Jaffé has also stated[2] that for the 3*d* orbitals of carbon, Slater's rules[4] give the effective nuclear charge as zero and therefore all

overlap integrals involving the carbon $3d$ orbitals must vanish. The Slater effective nuclear charge is, however, only zero for the negative carbon atom $C^-$ appropriate to the bimolecular substitution transition state. In the carbonium-ion rearrangement transition state and metal alkyl compounds the carbon atom that is being considered is neutral, and for this case Slater's rules give $Z_{eff}=1$. In any case it must be emphasized that Slater's rules are only approximate. It has been shown recently[5] that they may be particularly inaccurate in rather similar cases to those under consideration, such as, for example, the $3d$ orbitals of the phosphorus atom in $PCl_5$, for which it appears that the value of $Z_{eff}$ given by Slater's rules is appreciably too small. The estimation of a reasonable value for the effective nuclear charge in the type of compound we are considering is a matter of some difficulty (this will be further discussed in a later paper) but there seems to be little justification at present for concluding that overlap integrals involving carbon $3d$ orbitals are necessarily inappreciable, and that therefore the carbon atom cannot utilize $3d$ orbitals for bond formation.

[1] R. J. Gillespie, J. Chem. Soc. **1952**, 1002.
[2] H. H. Jaffé, J. Chem. Phys. **21**, 1893 (1953).
[3] Jaffé's further objection that in the compounds of phosphorus and sulfur so far considered there is a complete transfer of one or two electrons from the phosphorus or sulfur atom to the attached atoms, whereas this does not occur in carbon compounds, is not sound. It may be *assumed* that a transfer of one or two electrons occurs in these compounds of phosphorus and sulfur, and their structures may then be described in terms of *sp*-hybrid orbitals and ionic-covalent resonance without involving the use of $3d$ orbitals at all. If, however, *spd* hybrid orbitals are used in the description of these structures than all the valency electrons of phosphorus and sulfur must be regarded as being involved in covalent bonding and none of them can be considered to have been completely transferred to the attached atoms.
[4] J. C. Slater, Phys. Rev. **36**, 57 (1930).
[5] Craig, Maccoll, Nyholm, Orgel, and Sutton, J. Chem. Soc. (to be published).

## Moderation of Hot Methyl Radicals in Photolysis of Methyl Iodide*

FRANK P. HUDSON, RUSSELL R. WILLIAMS, JR., AND WILLIAM H. HAMILL
*Department of Chemistry, University of Notre Dame, Notre Dame, Indiana*
(Received August 13, 1953)

THE study of the photolysis of methyl iodide vapor by Schultz and Taylor[1] was interpreted to show that methane production is by a hot radical mechanism. Since the energy of a light quantum of 2537A is approximately 50–60 kcal greater than the C—I bond strength in methyl iodide and the masses of the radical and atom are so different, the methyl radical produced in the primary process must have most of this excess energy, largely as kinetic energy. Production of methane in this system is proposed to occur mainly in early, hot collisions of the energetic methyl radicals with methyl iodide. Two important consequences of this mechanism are a temperature-independent rate of methane production, found by Schultz and Taylor and moderation of the rate of methane production by inert gases added, shown qualitatively for carbon dioxide by Schultz and Taylor. However, it is possible that this substance might exert a specific chemical effect other than moderation. We have shown[2] that an analogous mechanism may be applied to the photolysis of hydrogen iodide and have also investigated methyl-iodide photolysis to test further and to develop the hot radical hypothesis. We have photolyzed methyl iodide with light from a Hanovia SC2537 lamp, filtered through Corning 7910 glass. Noncondensable products have been analyzed with a Consolidated 21-103A mass spectrometer. At constant light absorption, we find the rate of methane production to be experimentally independent of temperature over the range 25–100°C in pure methyl iodide and in methyl iodide plus neon at a pressure six times that of the methyl iodide.

We have examined the effect of moderating gases on the rate of methane production in methyl iodide at constant partial pressure of 100 mm Hg, as shown in Fig. 1. Here we find a regular decrease in the rate of product formation with decreasing ratio of methyl iodide to moderator. In all cases, it appears that the rate approaches zero at infinite dilution by moderator. We also note that, if fused silica is used instead of Corning 7910 glass (which cuts off at approximately 2200A), carbon dioxide is not as effective as a moderator. This may be because of formation of still more energetic radicals by absorption of the 1849A mercury line of the resonance lamp.

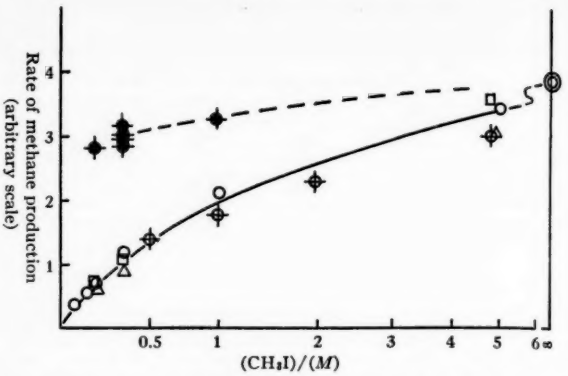


FIG. 1. Rate of methane production in the presence of added inert gases ($M$). Legend: open circle, neon; triangle, argon; square, helium; crossed open circle, carbon dioxide (all in 7910 glass); crossed closed circle, carbon dioxide in quartz.

We believe that the comparable effects of the various moderators rules out the possibility of a specific chemical effect and strengthens the hot radical hypothesis. Analysis of other products of this reaction and of reaction of hot methyl radicals with various substrates will be reported later.

* Taken from the Ph.D thesis of Frank P. Hudson. Work supported in part by U. S. Atomic Energy Commission under contract At (11-1)-38.
[1] R. D. Schultz and H. A. Taylor, J. Chem. Phys. **18**, 194 (1950).
[2] Schwarz, Williams, and Hamill, J. Am. Chem. Soc. **74**, 6007 (1952).

## Crystal Structure of Silanols and their Infrared Spectra

MASAO KAKUDO, P. NOBUTAMI KASAI, AND TAKEO WATASE
*Department of Applied Chemistry, Faculty of Engineering, Osaka University, Osaka, Japan*
(Received July 22, 1953)

CRYSTAL structures of diethylsilanediol[1] and diphenylsilanediol[2] have been previously reported. We have now added diallylsilanediol $(C_3H_5)_2Si(OH)_2$,[3] bis-(dimethylhydroxysilyl) methane $OH(CH_3)_2SiCH_2Si(CH_3)_2OH$,[4] and tetramethyldisiloxanediol-1,3 $OH(CH_3)_2SiOSi(CH_3)_2OH$ in our study on crystal analysis. Their crystallographic data are given in Table I. The molecular arrangement of diallylsilanediol is similar to diethylsilanediol, while the diols having OH groups at both ends of their molecules such as $OH(CH_3)SiCH_2Si(CH_3)_2OH$ form a chain

TABLE I.

| | $(C_3H_7)_2Si(OH)_2$ | $(OH(CH_3)_2Si)_2O$ | $(OH(CH_3)_2Si)_2CH_2$ |
|---|---|---|---|
| Density | 1.105(10°C) | 1.118(16°C) | 1.078(20°C) |
| System | Monoclinic Flat prismatic | Monoclinic Needle | Orthorhombic Needle |
| Unit cell | $a=14.59$ kX.<br>$b=4.94$<br>$c=13.37$<br>$\beta=114°30'$ | $a=21.28$ kX.<br>$b=5.86$<br>$c=8.46$<br>$\beta=111°00'$ | $a=14.50$ kX.<br>$b=11.31$<br>$c=6.14$ |
| Space group | $C_{2h}^5-P2_1/a$ | $C_{2h}^5-P2_1/a$ | $D_2^4-P2_12_12_1$ |
| Moles in a unit cell | 4 | 4 | 4 |

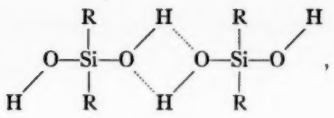

Type 1

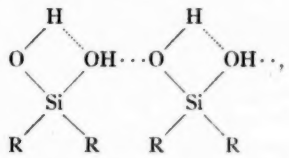

Type 2

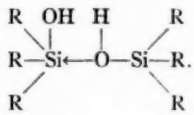

Type 3

structure against the layer structure in the case of alkylsilanediols. However, it may be said that all these silanols take a similar structure from the viewpoint that the molecular chains linearly joined by two OH groups of each molecule are gathered side by side and parallel to an axis according to their own lateral interactions. As regards these strong hydroxyl associations, the relation between the arrangement of OH groups and the infrared absorption spectra of diethylsilanediol has been examined.* The nearest OH···OH distances in diethylsilanediol are 2.56 and 2.64A, and the others are longer than 3.5A.

On the basis of these inter-hydroxyl distances, it is proposed that the formula for the hydrogen bondings is of types 1 or 2.[5] The infrared absorption spectra of the O−H bond were shown in Fig. 1. Curve 1 shows only a broad band with a maximum at 3.1$\mu$, while the absorption maximum expected from the relation between O−H O distances and shifts of O−H stretching frequency reported by Kuhn[6] and Lord,[7] must be at 4.1$\mu$ in the case of diethylsilanediol.

This indicated that the type 2, which has the same numbers intra- and inter-molecular hydrogen bond with different O−H stretching frequency, cannot exist in crystal. The O−H stretching vibration in Si−OH of afwillite, in which there are both a hydrogen bond and a nearly free O−H bond, was observed at 3.03, 2.95, and 3.3∼4.0$\mu$ by Megaw.[8]

From these facts, it is reasonable to suppose that the molecular chain in crystalline silanol is formed by hydroxyl association as shown by type 1, in which there is only a kind of O−H bond. In its dilute solution, the free O−H vibration at 2.72, and 2.77$\mu$ appears, and these figures are similar to those for the absorption of an orgainc alcohol solution. This shows that the molecules of silanol in solution are not associated with each other in the way of type 3 expressing the pentavalent coordination of the silicon atom, but are linked by a hydrogen bond of type 1 or 2, as predicted in the case of tri-ethylsilanol solution by Grubb and Osthoff.[9] It can be considered as a property of the hydroxyl group in silanols, which may throw light on the study of their physico-chemical behavior.

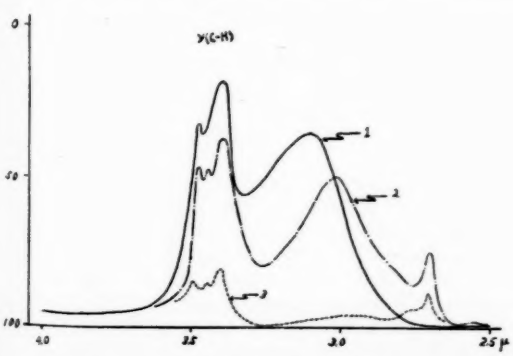

FIG. 1. Absorption spectra of $(C_2H_5)_2Si(OH)_2$: (1) crystal, in Nujol mull; (2) 0.01 $M/L$; in $CCl_4$; (3) 0.001 $M/L$, in $CCl_4$.

A more detailed study on the hydroxyl bond in various types of crystalline silanols such as tetramethyldisiloxanediol-1,3 etc. has now been progressing.

We wish to offer our sincere thanks to Dr. W. L. Roth and his co-workers who kindly sent us their recent papers about silanols, and encouraged us.

We are grateful for the kindness of Mr. T. Kanzawa and Mr. T. Ôkawa in the taking of the infrared absorption spectra.

[1] M. Kakudo and T. Watase, Technol. Repts. Osaka Univ. **2**, 50 (1952).
[2] Eatase, Kakudo, and Kasai, Ann. Repts. Textile Research Inst. Osaka Univ. **6**, 38 (1952).
[3] K. Hashitani and R. Ôkawara, Bull. Chem. Soc. Japan **26**, 279 (1953).
[4] M. Kakudo and T. Watase, Ann. Repts. Textile Research Inst. Osaka Univ. **7** (1953).
* The infrared spectra were taken by the Perkin-Elmer Recording Spectrometer at the Osaka City University and the Laboratory of the Takeda Pharmaceutical Industry Company & Ltd.
[5] M. Kakudo and T. Watase, J. Chem. Phys. **21**, 167 (1953).
[6] L. P. Kuhn, J. Am. Chem. Soc. **74**, 2492 (1952).
[7] R. C. Lord and R. E. Merrifield, J. Chem. Phys. **21**, 166 (1953).
[8] Megaw, Acta Cryst. **5**, 397 (1952).
[9] W. T. Grubb and R. C. Osthoff (private communication).

## Proton Magnetic Resonance Experiment on a Single Crystal of Oxalic Acid Dihydrate, $(COOH)_2 \cdot 2H_2O$

J. ITOH, R. KUSAKA, R. KIRIYAMA, AND S. YABUMOTO
*Department of Physics and Department of Chemistry, Osaka University, Osaka, Japan*
(Received July 20, 1953)

THE crystal structure of oxalic acid dihydrate has already been determined rather precisely by many investigators[1] (space group, $C_{2h}^5-P2_1/a$; $Z=2$). The atomic positions are shown in Fig. 1. No information about the positions of the hydrogen atoms, however, have been given by x-ray analyses.

Richards and Smith[2] made a proton magnetic resonance experiment on a polycrystal of this acid hydrate and proposed a proton configuration for the interpretation of the second moments of the absorption lines. But their suggestion involves, as they stated, ambiguities about the distance and the direction of the lines joining protons.

We have carried out a proton magnetic resonance experiment with a single crystal at a frequency of 6.1 Mc/sec. When the crystal was rotated about the $b$ axis, the line shape was observed at a particular angle, which was composed of seven components, not well resolved owing to the broadness of each component line. Since it is known that, in the case of $b$-axis rotation, proton magnetic resonance lines for each of four molecules in the unit cell coincide with each other, this appearance of seven lines suggests the existence of a three-proton system in the crystal. We made further measurements at various other orientations of the crystal. Although, in general, lines expected from the three-proton interaction are not resolved clearly, the most separated components were well resolved in some cases. Assuming suitable configurations of three protons, the resonance line positions and relative intensities are calculated for various orientations of the crystal, using the formula of Andrew and Bersohn.[3] Satisfactory agreement with the experimental results is obtained, when it is assumed that the triangle composed of three protons has the sides of 1.65, 1.92, and 2.30A, and the angles between the $a$ axis and the projections of the sides of 1.65 and 1.92A onto the $ac$ place are ∼51° and ∼28°, respectively. These two sides make angles of ∼57.5° and ∼90° with the $b$ axis.

Now the position of the three-proton triangle in the lattice will be considered. Firstly, the proton-proton distance between

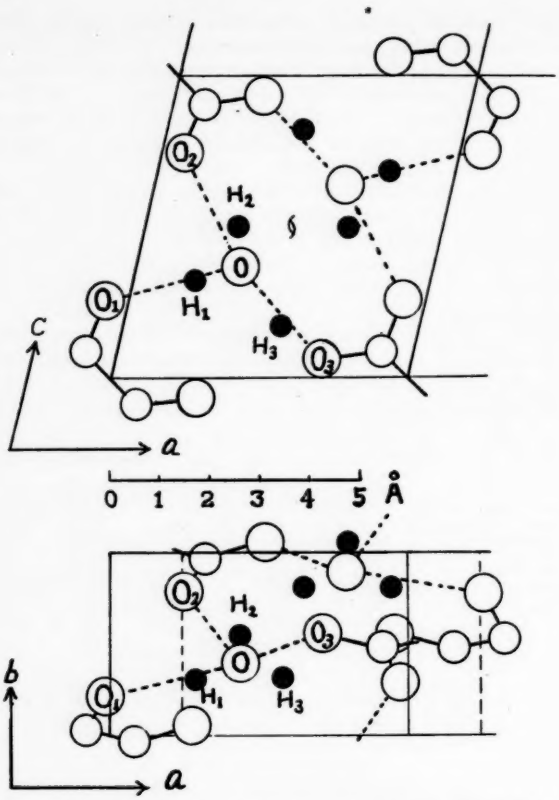


Fig. 1. Projections of one-half of the unit cell on the *ac* plane and also on the *ab* plane. Positions of C and O atoms are those determined by the x-ray analyses, while those of H atoms are determined by the present experiment. The cell dimension is $a=11.88$, $b=3.60$, $c=6.12$A, and $\beta=76.5°$. The distances between the water oxygen and the surrounding atoms are: $O-O_1=2.85$, $O-O_2=2.90$, $O-O_3=2.50$, $O-H_1=1.00$, $O-H_2=0.96$, and $O-H_3=1.43$. The distance between $O_3$ and $H_3$ is 1.41A. The sides of the proton triangle are: $H_1-H_2=1.65$, $H_1-H_3=1.92$, and $H_2-H_3=2.30$A.

the neighboring proton triangles, which are equivalent to each other, must not be less than 2.5A, as the width of each component line is less than about 4 gauss. Next, since one of the sides is 1.65A which is approximately equal to the proton-proton distance in a water molecule in some hydrated crystals,[4] this proton pair seems to correspond to two protons in the water molecule. Then the distances between these protons and the oxygen atom of the water molecule will be both equal to about 1A. In view of these considerations, the position of the proton triangle in the lattice is determined as in Fig. 1.

One of the two protons of the water molecule lies roughly on the line of a longer hydrogen bond predicted by x-ray analyses. But another proton and the third proton both deviate considerably from lines of the hydrogen bonds. It may be considered that the third proton, which belonged originally to the OH radical of oxalic acid, has been attracted to some extent towards the water molecule and influenced also by the surrounding oxygen atoms. From these considerations, it would hardly be said that this crystal consists of hydroxonium ions and oxalic ions. Our conclusion agrees fairly well with a recent x-ray result[5] which presumed the nonexistence of hydroxonium ions in accordance with the asymmetric C—O distances of carboxylic acid.

Full accounts of the experiment will be published shortly in *Journal of the Physical Society of Japan*.

[1] For instance, W. H. Zachariasen, Z. Krist. **89**, 442 (1934); Brill, Herman Peters, Ann. Physik **42**, 357 (1942); J. D. Dunitz and J. M. Robertson, J. Chem. Soc. **1947**, 142.
[2] R. E. Richards and J. A. S. Smith, Trans. Faraday Soc. **47**, 1261 (1951).
[3] E. R. Andrew and R. Bersohn, J. Chem. Phys. **18**, 159 (1950).
[4] G. E. Pake, J. Chem. Phys. **16**, 327 (1948). Itoh, Kiriyama, *et al.*, J. Phys. Soc. Japan **8**, 293 (1953).
[5] F. R. Ahmed and D. W. J. Cruickshank, Acta Cryst. **6**, 385 (1953).

## Assignment of the O—H Deformation Frequency

JAMES R. QUINAN AND STEPHEN E. WIBERLEY
*Rensselaer Polytechnic Institute, Troy, New York*
(Received August 3, 1953)

THE vibrational assignment of the O—H deformation frequency of alcohols in which the hydrogen atom moves perpendicular to the O—H bond and in the COH plane has not yet been definitely established. The disagreement in the literature has been pointed out by Sutherland,[1] who suggested that more experimental work should be carried out on the alcohols and their corresponding OD compounds.

The tabulated heavy alcohols have been prepared in this laboratory by the decomposition of the corresponding dry magnesium alkoxides with $D_2O$. The infrared spectra were obtained using a Perkin-Elmer Model 12B Recording Spectrometer with both sodium chloride and lithium fluoride prisms. Raman measurements were made with a medium spectrograph and a Raman source manufactured by Hilger.

All of the work reported to date has been carried out with methyl and ethyl alcohols and their corresponding deuterated compounds. It is generally agreed that the OD deformation band in $CH_3OD$ vapor lies at 863 $cm^{-1}$ [2,3] and is shifted to 940 $cm^{-1}$ [4,5] on association. The corresponding frequency in the undeuterated methyl alcohol vapor has not been found in the infrared, but Borden and Barker,[6] taking the value of 1110 $cm^{-1}$ assigned to the OH bending in Raman studies of Halford, Anderson, and Kissin,[5] calculate a value of about 1030 $cm^{-1}$ in the vapor. Davies[4] also assigned a value of 1110 $cm^{-1}$ to this mode in methanol. More recently Barrow[7] assigned a value of 803 $cm^{-1}$ to the $\delta$(OD) in $C_2H_5OD$ vapor. By the product rule he calculated a value of 1050 $cm^{-1}$ for the corresponding frequency of the undeuterated alcohol in the vapor state.

As a result of observations made with deuterated methanol vapor Noether[3] suggested 1340 $cm^{-1}$ as the $\delta$(OH) rather than the $\delta$(CO) as ascribed by Borden. Davies[4] after considering the spectra of the methyl halides reported that 1340 $cm^{-1}$ is probably a vibration between the methyl and hydroxyl groups. Herzberg[8] has stated that the OH deformation may be identified with either the polarized Raman line at 1056 $cm^{-1}$ in the liquid or the infrared band at 1340 $cm^{-1}$ in the vapor, which probably corresponds to the polarized 1370 $cm^{-1}$ Raman line in $CH_3OH$. While Herzberg favors a value of 1340 $cm^{-1}$, the work of Davies on the halides and the fact that the Raman line at 1370 $cm^{-1}$ is found in $CH_3OD$ as well as in $CH_3OH$, but not in $CH_2DOD$,[5] indicates that 1370 $cm^{-1}$ is probably a methyl deformation.

As indicated by Table I, our work agrees with the alternate

TABLE I. Hydroxyl deformation frequencies ($cm^{-1}$) for a series of alcohols.

| | OH | OD |
|---|---|---|
| Methanol | ··· | 940 |
| Ethanol | ··· | 940 |
| *n*-Propanol | ··· | ··· |
| *n*-Butanol | 1010 | 915 |
| *n*-Pentanol | ··· | 938 |
| *n*-Hexanol | 1021 | 949 |
| *n*-Octanol | 1020 | 944 |
| *n*-Decanol | 1035 | 944 |
| 2-Butanol | ··· | 947 |

suggestion of 1056 $cm^{-1}$ by Herzberg and the similar assignment by Barnes *et al.*,[9] Thompson,[10] and Hibben.[11] In this series of alcohols the infrared and Raman spectrum of each deuterated alcohol is similar to the regular alcohol through the range 1300–1450 $cm^{-1}$. Similarly, a band at 1100–1120 $cm^{-1}$ which disappears in the vapor state does not change in the liquid upon deuteration. The only significant difference is the disappearance of the band at about 1020 $cm^{-1}$ upon deuteration and the simultaneous appearance of a band at 940 $cm^{-1}$. This 1020 $cm^{-1}$ band cannot be found in methyl, ethyl, propyl, or amyl alcohols because of the

strong absorption in this region caused by the CO stretching frequency as well as by the aliphatic groups themselves. However, the corresponding $\delta$(OD) appears at 940 cm$^{-1}$ in each case except propanol, where it is again obscured by another band.

The OH deformation in the vapor has not been found, but the OD occurs at 860 cm$^{-1}$ in deuterated methanol and secondary butanol. The lower alcohols have absorption bands in the vapor which probably obscure the deformation bands. Butyl and amyl alcohols show a series of weak absorptions in this region which cannot be significantly evaluated even using a one-meter gas cell. Alcohols above amyl have such a low vapor pressure that adequate vapor spectra have not as yet been obtained.

[1] G. B. B. M. Sutherland, Disc. Faraday Soc. **9**, 274 (1950).
[2] E. F. Barker and G. Bosschieter, J. Chem. Phys. **6**, 563 (1938).
[3] H. E. Noether, J. Chem. Phys. **10**, 693 (1942).
[4] M. Davies, J. Chem. Phys. **16**, 267 (1948).
[5] Halford, Anderson, and Kissin, J. Chem. Phys. **5**, 927 (1937).
[6] A. Borden and E. F. Barker, J. Chem. Phys. **6**, 553 (1938).
[7] G. M. Barrow, J. Chem. Phys. **20**, 1739 (1952).
[8] G. Herzberg, *Infrared and Raman Spectra of Polyatomic Molecules* (D. Van Nostrand Company, Inc., New York, 1945), p. 334.
[9] Barnes, Gore, Stafford, and Williams, Anal. Chem. **20**, 402 (1948).
[10] H. W. Thompson, J. Chem. Soc. (London) **1948**, 328.
[11] J. H. Hibben, *The Raman Effect and its Chemical Application* (Reinhold Publishing Corporation, New York, 1939), p. 148.

## A New Structure Type for Metallic Oxides of Formula $A_6BO_8$*

JOHN S. KASPER, *Research Laboratory, General Electric Company, Schenectady, New York*
AND
C. L. CHRIST, *U. S. Geological Survey, Washington 25, D. C.*
(Received August 10, 1953)

WE wish to report a new and simple structure type which each of us has found independently for metallic oxides of composition $A_6BO_8$. The two examples are $Mg_6MnO_8$ (J.S.K.) and $Cu_6PbO_8$ (C.L.C.). The former was synthesized from MgO and $MnCO_3$, the latter occurs in nature as a mineral.

The structure can be described as follows: The cubic unit cell contains 32 oxygen ions in an essentially close-packed arrangement; there is, then, an ordered distribution of 4 tetravalent ions, 24 divalent ions, and 4 vacancies among the 32 octahedral interstices. This distribution is given below and is illustrated in Fig. 1 by means of sections perpendicular to the $z$ axis.

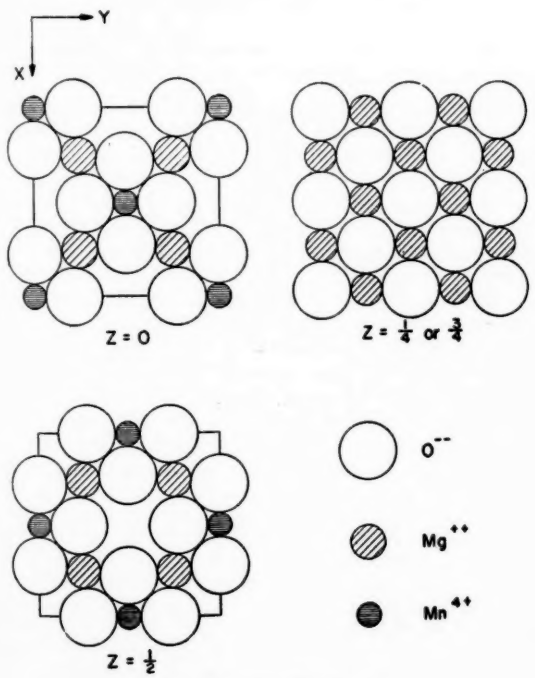


FIG. 1. Structure of $Mg_6MnO_8$.

4 $Mg_6MnO_8$ per unit cell; $a_0$=8.381A
Space group $Fm3M-O_h^5$
(000; 0 1/2 1/2; 1/2 0 1/2; 1/2 1/2 0)+
4 Mn at (a) 000
24 Mg at (d) 0 1/4 1/4; 1/4 0 1/4; 1/4 1/4 0;
0 1/4 3/4; 3/4 0 1/4; 1/4 3/4 0
8 $O_I$ at (c) 1/4 1/4 1/4; 3/4 3/4 3/4
24 $O_{II}$ at (e) XOO; OXO; OOX
$\overline{X}$OO; O$\overline{X}$O; OO$\overline{X}$
4 vacancies at (b) 1/2 1/2 1/2.

For $Mg_6MnO_8$, X has been determined as 0.230±0.003.

In the case of $Cu_6PbO_8$ for which $a_0$=9.210A, the intensity data at hand do not permit a decision as to whether there is a statistical distribution of the 24 Cu on the 28 sites (b) and (d), or whether X differs significantly from 1/4. From Bertaut's calculations[1] on the ordering of vacancies in ionic structures it would be expected that $Cu_6PbO_8$ has exactly the same structure as $Mg_6MnO_8$. This point is being further investigated.

The structure can be regarded as an "ordered NaCl type," and it would seem that more examples could be found, since the requirements for its formation appear to be simply:

(a) a ratio of 6 to 1 of a divalent ion and a tetravalent ion.
(b) a coordination number for oxygen of 6 for each ion.

It is planned to attempt the synthesis of other compounds for which these requirements are satisfied.

The detailed studies of the two compounds will be published separately.

* Publication authorized by the Director, U. S. Geological Survey.
[1] E. F. Bertaut, Acta Cryst. **6**, 557 (1953).

## Homogeneous Gas Processes and Time Dependent Perturbation Theory

HENRY AROESTE*
*Cornell University, Ithaca, New York*
(Received August 3, 1953)

THE time dependent perturbation theory of Dirac has been applied to both intramolecular[1] and intermolecular[2] gas processes. Since the same basic method is applied to both types of process one may then question to what extent a unified theory may result.

Let us first consider the differences in the processes as they are measured in the laboratory. The measurements for intramolecular processes are not very precise. For instance, in the racemization of pinene, the following statement is made, "The reaction in all cases was slow enough and the time of reaction long enough to make negligible the time of heating and cooling."[3] This heating and cooling, however, becomes more significant the less complex the molecule. Contrariwise, in an intermolecular process the reactants are heated in different vessels to a certain temperature, and the rate of reaction at that temperature is measured. We do not discuss how the molecules in the two vessels get to the temperature, but assume they are both equilibrated before we bring them together. This is not quite so reasonable in the intramolecular case as it is not easy to keep the reactant at a high temperature without its reacting.

The unity in the two theories lies only in that the same method is applied to two different dynamic problems. The intermolecular theory has more epistemic[4] or phenomenological value than the intramolecular case. To quote Born, contrary to classical theory, dynamical problems in quantum mechanics "cannot be defined without a subjective, more or less arbitrary decision about what you are interested in."[5] This arises from the fact that $H$, the

Hamiltonian of the total system may be taken to be $H=H_0+V$, where $V$ is the perturbation and $H_0$ the unperturbed Hamiltonian. The choice of $V$ and $H_0$ is more or less arbitrary. The most convenient natural choice of $V$ for the intermolecular problem is the interaction between the molecules, and this is the choice usually made. The choice of $V$ in the intramolecular problem is less easy to make, the parts of the molecule being much less well defined. The choice is therefore much more arbitrary, and further, as is admitted, the perturbation may well be too large for the validity of the Dirac theory.

Thus, the unperturbed wave functions which are used for molecules in the intermolecular case have been experimentally verified and may easily be considered as representing the molecules as existing alone, and a simple "rule of correspondence"[4] between the mathematics and an imagined experiment exists. No such rule is evident in the intramolecular case. Another statement of this is that though in the intermolecular case time $t=0$ may be approximated in the laboratory by bringing two or more vessels together, time $t=0$ in the intramolecular case is purely a mathematical artifice as the perturbation in reality has lasted for all time.

The author wishes to thank Dr. John K. Bragg of the General Electric Research Laboratory for helpful discussion.

* Present address: Guggenheim Jet Propulsion Center, California Institute of Technology, Pasadena, California.

[1] N. Rosen, J. Chem. Phys. 1, 319 (1933).
[2] C. Zener, Phys. Rev. 37, 556 (1931) and, more recently, S. Golden, J. Chem. Phys. 17, 620 (1949).
[3] D. Smith, J. Am. Chem. Soc. 49, 43 (1927).
[4] H. Margenau, *The Nature of Physical Reality* (McGraw-Hill Book Company, Inc., New York, 1950).
[5] M. Born, *Natural Philosophy of Cause and Chance* (Oxford University Press, London, 1949).

## The Geometry of Ketene*

WILLIAM F. ARENDALE AND WILLIAM H. FLETCHER
*Department of Chemistry, University of Tennessee, Knoxville, Tennessee*
(Received August 13, 1953)

THE geometry of ketene has been discussed several times within the last few years, but no one has given a definite set of values for all of the internuclear distances plus the H−C−H angle. Two investigations of the microwave spectrum of $CH_2CO$, CDHCO, and $CD_2CO$ have yielded accurate values for the large moments of inertia,[1,2] and a recent investigation by electron diffraction[3] produced results in reasonable agreement with the microwave data. We have been investigating the spectrum of $CH_2CO$ and $CD_2CO$ with a grating spectrometer[4] and have obtained $B_0$ values for both molecules which are in excellent agreement with those reported by Johnson and Strandberg,[2] but we disagree seriously with the value of $A_0$ obtained from their data. They give 0.9399A as the perpendicular distance from the hydrogen atoms to the figure axis, which corresponds to a value of $A_0$ just slightly less than 9.47 $cm^{-1}$ for the light molecule. From the analysis of some of the perpendicular bands we find $A_0=9.41$ $cm^{-1}$ and it seems very unlikely that this figure is low by any significant amount.

There are only three independent pieces of data available, one $A_0$ and two $B_0$'s while there are four internal parameters to be determined. Another independent moment of inertia could be obtained from a microwave or infrared investigation of ketene containing a heavier isotope of carbon or oxygen, but since this new datum is not likely to be forthcoming, we have examined the data at hand and conclude that it is possible to fix the C−C and C−O distances within ±0.015A at worst. This uncertainty has very little effect on the other parameters.

We have used $B_0$ values obtained from the microwave data and $A_0=9.41$ $cm^{-1}$ in the calculations.[5] One of the carbons is so close to the center of mass that its contribution to the moment of inertia is negligible, but its position can be fixed by using the condition

$$\Sigma m_i x_i = 0.$$

TABLE I. Geometrical parameters of ketene.

| $r_{CO}$ | $r_{CC}$ | $r_{CH}$ | $\gamma$ | $r_{CO}+r_{CC}$ |
|---|---|---|---|---|
| 1.135A | 1.345A | 1.069A | 123°50′ | 2.480A |
| 1.150 | 1.329 | 1.071 | 123°20′ | 2.479 |
| 1.165 | 1.313 | 1.073 | 122°50′ | 2.478 |

By combining the two equations for $I_B$ one gets an equation in terms of $r_{CO}$ and $r_{CC}$ which can be used to calculate a number of consistent sets of the internal parameters. Three sets which lie in a reasonable range are given in Table I.

The variation of $r_{CO}+r_{CC}$ is small enough that $r_{CH}$ and $\gamma$ are essentially independent of the larger uncertainty in $r_{CO}$ and $r_{CC}$. It is reasonable now to choose the most probable pair of values for these by considering carbon monoxide and carbon dioxide. The C−O distance in ketene would be expected to be longer than in carbon monoxide, but probably not longer than in carbon dioxide. These distances are 1.131A and 1.163A, respectively. The extreme values given above for $r_{CO}$ would then fix the range of reasonable values as accurately as possible without the help of additional data. No help is gained by considering the C−C distance in ethylene (1.353A), but it is interesting to note that in any case this distance is less in ketene than in ethylene.

The values for the structural parameters obtained from the moments of inertia may be summarized: $r_{CH}=1.071\pm0.003$A, $r_{CO}=1.150\pm0.015$A, $r_{CC}=1.329\pm0.015$A, and $\gamma=123.3°\pm1.5°$.

* This work was supported by a Frederick Gardner Cottrell grant from Research Corporation.
[1] Bak, Kundsen, Madsen, and Rastrup-Anderson, Phys. Rev. 79, 190 (1950).
[2] H. R. Johnson and M. W. P. Strandberg, J. Chem. Phys. 20, 687 (1952).
[3] T. Taylor Broun and R. L. Livingston, J. Am. Chem. Soc. 74, 6085 (1952).
[4] Loaned by the Department of Physics, University of Tennessee.
[5] The physical constants used were those given by J. W. M. DuMond and E. R. Cohen, Phys. Rev. 73, 51 (1948).

## Complex Dielectric Constants of Some Aliphatic Alcohols at 9733 mc/sec*

NAOKAZU KOIZUMI
*Institute for Chemical Research, Kyoto University, Takatsuki, Osaka-Fu, Japan*
(Received July 24, 1953)

THERE have been many reports on the dielectric properties of alcohols at ultra-high frequencies in connection with the problem of the dielectric dispersion and absorption.[1] However, the values of the complex dielectric constant for alcohols appearing in these papers are not always in good agreement. In performing some studies on dielectric properties of alcohols and glycols, it was necessary to obtain the dielectric constants at microwave frequencies.

For this reason the complex dielectric constants for nine aliphatic alcohols have been measured at a frequency of 9733 mc/sec over the range of temperature 5° to 50°C with the wave-guide apparatus similar to those reported by Surber,[2] Crouch,[3] and Lacquer and Smyth.[4] In this method, the wavelength of radiation in the dielectric-filled wave guide $\lambda_d$ and the dielectric attenuation per wavelength $\alpha_d\lambda_d$ are obtained from the variation of magnitude of reflection coefficient at the face of liquid with the length of the liquid column. Hence, the real and imaginary parts of the dielectric constant are calculated from the equations,

$$\epsilon' = (\lambda_0/\lambda_c)^2+(\lambda_0/\lambda_d)^2[1-(\alpha_d\lambda_d/2\pi)^2]$$

$$\epsilon'' = (1/\pi)(\lambda_0/\lambda_d)^2\alpha_d\lambda_d,$$

where $\lambda_0$ is the wavelength in free space of the excitation frequency and $\lambda_c$ the cut-off wavelength of the empty wave guide. The observed values of dielectric constants are given in Table I. The values for methanol were fairly consistent with Lane and

TABLE I. Complex dielectric constants $\epsilon^* = \epsilon' - j\epsilon''$ of some aliphatic alcohols at 9733 mc/sec.

| | Temperature°C 5 | | 20 | | 35 | | 50 | |
|---|---|---|---|---|---|---|---|---|
| | $\epsilon'$ | $\epsilon''$ | $\epsilon'$ | $\epsilon''$ | $\epsilon'$ | $\epsilon''$ | $\epsilon'$ | $\epsilon''$ |
| Methanol | 7.25 | 5.71 | 8.35 | 7.20 | 9.69 | 9.37 | 10.87 | 9.48 |
| Ethanol | 4.37 | 1.93 | 4.38 | 2.19 | 4.46 | 2.70 | 4.71 | 3.79 |
| n- Propanol | 3.42 | 1.06 | 3.45 | 1.30 | 3.50 | 1.72 | 3.61 | 2.26 |
| iso-Propanol | 3.20 | 0.74 | 3.25 | 1.00 | 3.32 | 1.53 | 3.58 | 2.07 |
| n- Butanol | 3.05 | 0.67 | 3.10 | 0.81 | 3.19 | 1.17 | 3.29 | 1.35 |
| iso-Butanol | 2.89 | 0.51 | 2.97 | 0.73 | 3.08 | 1.00 | 3.24 | 1.25 |
| tert-Butanol | ... | ...[a] | 2.87 | 0.70[b] | 3.00 | 0.86 | 3.24 | 1.24 |
| n- Pentanol | 2.75 | 0.49 | 2.83 | 0.64 | 2.94 | 0.91 | 3.05 | 1.13 |
| iso-Pentanol | 2.75 | 0.49 | 2.81 | 0.59 | 2.92 | 0.76 | 2.95 | 1.02 |

[a] Solid, not measured.
[b] Values at 26°.

Saxton's data[5] but larger than those obtained with the plane wave method in free space by Bäz[6] and Yasumi *et al.*[7]

It is well known that the critical frequency of the dielectric relaxation for lower carbon-membered alcohols appears in the decimeter- and meter-wave regions at or near room temperature, and the dispersion form at the low-frequency side is nearly consistent with that for a single relaxation system.[8] Hence, assuming that the dispersion curve corresponding to the single relaxation system holds for these aliphatic alcohols, the apparent high-frequency limits of dielectric constants $\epsilon_{h,\,App}$ were extrapolated from the values in Table I and the static dielectric constants.[9] The values of $\epsilon_{h,\,App}$ are plotted against temperature in Fig. 1.

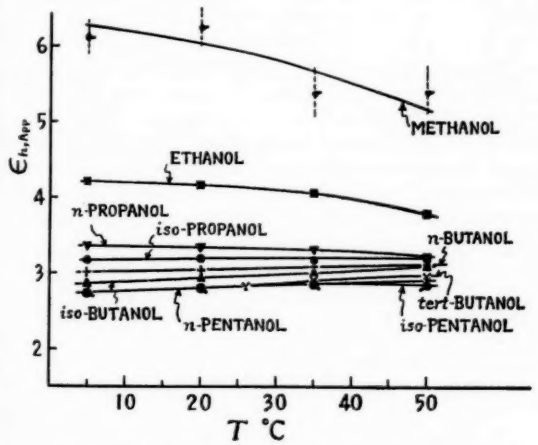


FIG. 1. Plot of the apparent high frequency $\epsilon_{h,\,App}$ of dielectric constant against temperature.

Girard and Abadie[10] have reported that there exist two distinct regions of dielectric dispersion for *n*-octanol. Recently, more detailed evidence for such dielectric dispersion has been presented by Cole and Davison[11] who pointed out that, in the supercooled liquid of *n*-propanol there exist two dispersion regions at the high-frequency side in addition to the first dispersion, and evaluated the critical frequency and the high-frequency limit for each dispersion region. Powles[12] has also discussed such distribution of relaxation time from the standpoint of the internal field in dielectric.

As shown in Fig. 1, it was found that the value of $\epsilon_{h,\,App}$ is much larger than the square of the optical refractive index $n^2$. This leads to the existence of other dispersion regions at higher frequencies. Although the values of $\epsilon_{h,\,App}$ in Fig. 1 may be somewhat different from the correct ones for the high-frequency limit of the first dispersion as was discussed by Cole and Davison, and Powles, the values of $\epsilon_{h,\,App}$ in the cases of methanol and ethanol may be nearly consistent with the high-frequency limit, because the present frequency is near the critical frequency of the first dispersion. As seen from Fig. 1, $\epsilon_{h,\,App}$ for these alcohols decreased with increasing temperature. From this temperature dependence of $\epsilon_{h,\,App}$, it may be deduced that most of the high-frequency dispersion is due to the dipole relaxation.

On the other hand, in the cases of butanols and pentanols, $\epsilon_{h,\,App}$ increased slightly with increasing temperature. This effect may be explained by the following speculation: The value of $\epsilon_{h,\,App}$ for these alcohols is smaller than the true high-frequency limit of the first dispersion, and the deviation of $\epsilon_{h,\,App}$ from the true value is more considerable with decreasing temperature, because the critical frequency of dielectric dispersion for these butanols and pentanols exists in the meter-wave region at ordinary temperature, so that the dielectric constants at the present frequency correspond to the values in an overlapping region of the first and the second dispersions, which shifts rapidly to lower frequencies with decreasing temperature, owing to the temperature dependent character of orientation polarization.

From the present results it was considered that there seems to be some evidence for the high-frequency dispersion due to dipole relaxation, though concerning the origin of the difference between $\epsilon_{h,\,App}$ and $n^2$, it may be necessary to take account of the partial contribution of the atomic polarization in the liquid state.[7]

The detailed description will appear elsewhere.

The author wishes to thank Professor R. Goto for his valuable advice in this work and also Mr. N. Hayama for his aid in purification of materials.

* Supported in part by the Scientific Research Encouragement Grant from the Ministry of Education.

[1] Cited in the following literatures, J. A. Saxton, Proc. Roy. Soc. (London) **A213**, 473 (1952); Dalbert, Magat, and Surdut, Bull. Soc. Chim. France **16**, D345 (1949).
[2] W. H. Surber, Jr., J. Appl. Phys. **19**, 514 (1948).
[3] G. E. Crouch, Jr., J. Chem. Phys. **16**, 364 (1948).
[4] H. L. Lacquer and C. P. Smyth, J. Am. Chem. Soc. **70**, 4097 (1948).
[5] J. A. Lane and J. A. Saxton, Proc. Roy. Soc. (London) **A213**, 400 (1952).
[6] G. Bäz, Physik. Z. **40**, 394 (1939).
[7] Yasumi, Shirai, and Mizushima, Bull. Chem. Soc. Japan **25**, 133 (1952).
[8] K. S. Cole and R. H. Cole, J. Chem. Phys. **9**, 341 (1941); D. W. Davison and R. H. Cole, J. Chem. Phys. **19**, 1484 (1951).
[9] N. Koizumi and T. Hanai (to be published). The values observed at audio-frequencies for the same specimens used in this work.
[10] P. Girard and P. Abadie, Trans. Faraday Soc. **42A**, 40 (1946).
[11] R. H. Cole and D. W. Davison, J. Chem. Phys. **20**, 1389 (1952).
[12] J. G. Powles, J. Chem. Phys. **21**, 633 (1953).

## Correlation of Proton Magnetic Resonance Chemical Shifts with Electronegativities of Substituents

JAMES N. SHOOLERY
*Varian Associates, Palo Alto, California*
(Received July 29, 1953)

A FINE structure in the nuclear induction signals from some alcohols was reported recently by Arnold, Dharmatti, and Packard.[1] Since then, a number of other organic liquids have been investigated with similar apparatus and with the results reported briefly here.

Fine structure in the proton magnetic resonance in organic liquids arises from the interaction of the molecular electrons with the applied magnetic field. Ramsey[2] has shown that when there is a near degeneracy of energy levels it is possible for both paramagnetic and diamagnetic terms to contribute to the shielding of a given nucleus. Differences in these terms at nonequivalent nuclei are proposed as an explanation for the observed chemical shift. One might reasonably expect that frequently the terms related to a simple diamagnetic circulation of electrons about the nuclei under observation predominate. For protons, these electrons are valence electrons, for which the ground-state wave functions are frequently regarded as linear combinations of atomic wave functions forming covalent bonding functions with admixtures of ionic states. Changing the type of atomic orbitals available, such as the introduction of a multiple bond nearby, might be expected to affect principally the covalent part of the wave func-

TABLE I. Chemical shifts in substituted ethanes.

| Compound | $\delta CH_3$ | $\delta CH_2$ | $\delta CH_2-\delta CH_3$ | $2.1+4.5(\delta CH_2-\delta CH_3)$ | Pauling electronegativity |
|---|---|---|---|---|---|
| $C_2H_6$ | 0.00 | 0.00 | 0.00 | 2.1 | 2.1 |
| $C_2H_5SH$ | 0.00 | 0.12 | 0.12 | 2.64 | 2.5 |
| $C_2H_5I$ | 0.05 | 0.18 | 0.13 | 2.68 | 2.5 |
| $C_2H_5Br$ | 0.05 | 0.21 | 0.16 | 2.82 | 2.8 |
| $C_2H_5NH_2$ | 0.00 | 0.17 | 0.17 | 2.86 | 3.0 |
| $C_2H_5Cl$ | 0.02 | 0.22 | 0.20 | 3.00 | 3.0 |
| $C_2H_5OH$ | 0.01 | 0.25 | 0.24 | 3.18 | 3.5 |
| $C_2H_5OCOCH_3$ | 0.01[a] | 0.31 | 0.30 | 3.45 | 3.5 |

[a] $CH_3$ in ethyl group.

tion, while introducing an electronegative element would affect the ionic part.

An interaction of the nuclear spins in molecules has been observed to lead to a further splitting of the chemically shifted signals. This interaction has the form $J(\boldsymbol{\mu}_1\cdot\boldsymbol{\mu}_2)$ and is usually of the order of a few cycles splitting. These effects have been studied and discussed in detail by other authors.[3,4] Figure 1 illustrates both the chemical shifts and spin-spin multiplets occurring in ethyl acetate under fractional milligauss resolution.

A number of saturated hydrocarbons, $C_nH_{2n+2}$, both normal and branched, have been investigated at 30 Mc in the vicinity of 7059 gauss. Terminal hydrogen nuclei appear to be better shielded by the bonding electrons than protons in $CH_2$ groups by about 2 milligauss. The chemical shifts $\delta$ reported here have been measured with respect to the terminal hydrogen in normal hexane. Following other workers,[5] we define $\delta$ by

$$\delta=10^5\times(Hr-Hc)/Hr,$$

where $Hr$ = resonance field for the reference compound and $Hc$ = resonance field for the comparison resonance. The $\delta$ for $CH_2$ groups in saturated hydrocarbons is approximately 0.03.

In order to determine whether changing just the ionic part of the wave function at the protons can be correlated with the chemical shift, a series of substituted ethanes were examined and the results are reported in Table I. Values of $\delta$ are given for the centers of the $CH_2$ and $CH_3$ spin-spin multiplets. From the table, the $\delta_{CH_3}$ values are much smaller than the $\delta_{CH_2}$, since electronegativity effects must be transmitted to the $CH_3$ protons through the $CH_2$ group. One would expect the largest $\delta_{CH_3}$ from the ethanes with the most electronegative substituents; however, ethyl bromide and iodide are exceptions to this trend, and, because of their large size, may be contributing some change in the covalent part of the CH bonds through distortion of the bond angles.

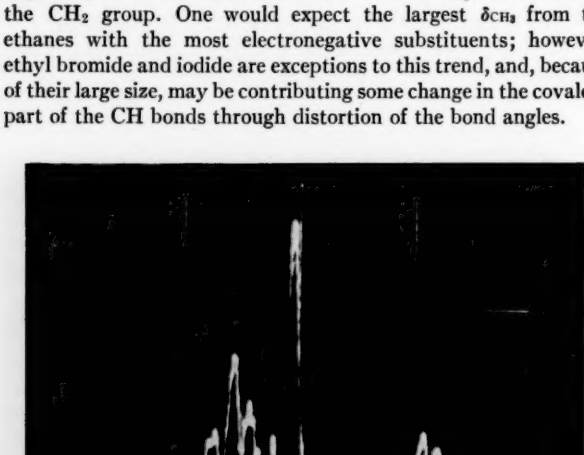

FIG. 1. Fine structure in ethyl acetate. The three signals on the left and the four on the right represent the $CH_3$ and $CH_2$ groups of the ethyl radical. The high, sharp peak in the center is the $CH_2$ group in the acetate radical. Total sweep width is 50 milligauss, the field decreasing from left to right.

It is possible to obtain a rough correlation between the difference in the $\delta$'s (splitting of the ethyl group) and the electronegativities, $E_s$, of the substituent elements responsible for the splitting through the empirical relation

$$E_s=2.1+4.5(\delta_{CH_2}-\delta_{CH_3}),$$

in which two parameters are adjusted to fit the data for ethane and ethyl chloride.

Substitution of various groups for hydrogen in benzene molecules results in electron transfer to or withdrawal from the ring, with consequent directive effects. As an example of the effect

TABLE II. Chemical shift of ring protons in benzene and its derivatives.

| Compound | $\delta C_6H_5$ | Electron density at ring protons |
|---|---|---|
| $C_6H_6$ | $0.62\pm0.015$ | ... |
| $C_6H_5NH_2$ | $0.56\pm0.015$ | increased |
| $C_6H_5CHO$ | $0.66\pm0.015$ | decreased |

of changes in the electron distribution from resonance of the ring with the substituent, chemical shifts for benzene and some of its derivatives are given in Table II. The increased electron density at the ring protons in aniline and the decrease in benzaldehyde are compatible with the inclusion of the following resonating structures

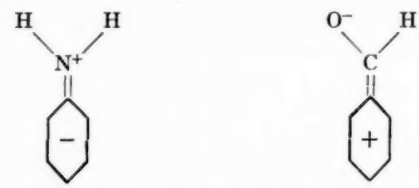

which are usually proposed for these molecules. The figures given represent the average shielding of the ring protons, but variations in shielding at the ortho-, meta-, and para-positions can be observed as partially resolved fine structure.

[1] Arnold, Dharmatti, and Packard, J. Chem. Phys. **19**, 507 (1951).
[2] N. F. Ramsey, Phys. Rev. **78**, 699 (1950).
[3] E. L. Hahn and D. E. Maxwell, Phys. Rev. **88**, 1070 (1952).
[4] Gutowsky, McCall, and Slichter, J. Chem. Phys. **21**, 279 (1953).
[5] Gutowsky, McCall, McGarvey, and Meyer, J. Chem. Phys. **19**, 1328 (1951).

## Thermodynamic Functions of FCN

N. W. LUFT
*Cheadle Hulme, Cheshire, England*
(Received July 27, 1953)

IN a recent edition of this Journal[1] Thomas calculated some molecular data for FCN, which he obtained by a semi-empirical correlation of corresponding data for the series of compounds XCN with X=H, Cl, Br, I. He proposed the following values for the CN distance and the two stretching frequencies:

$$r_{CN}=1.165\text{A};\ \omega_1=2294,\ \omega_2=1052\ \text{cm}^{-1}.$$

The other missing data may be estimated by a similar procedure. The doubly degenerate bending frequency $\omega_3$ is obtained by plotting

$$\mu_X=(r_{CN}/r_{CX})(1/m_X+1/m_C)+2/m_C+(r_{CX}/r_{CN})(1/m_C+1/m_N)$$

against the frequencies $\omega_3$ for the molecules XCN with X=D, Cl, Br, I. For a simple valence force field $\mu_X\omega_3^2$ is proportional to the bending force constant which seems to vary smoothly in this series of molecules. An assumed $r_{CF}=1.35\pm0.05$ gives

$$\mu_F=(2.791\pm0.013)\times10^{-23}\quad\text{and}\quad\omega_3=410\ \text{cm}^{-1}$$

for FCN. A more accurate value $r_{CF}=1.30\pm0.03$A was obtained

TABLE I. Estimated thermodynamic data of FCN.

| $T$°K | $-(F^0-H_0^0)/T$ | $S^0$ | $(H^0-H_0^0)/T$ | $C_p^0$ |
|---|---|---|---|---|
| 298.16 | 45.69 | 53.97 | 8.28 | 10.18 |
| 300 | 45.74 | 54.03 | 8.29 | 10.20 |
| 400 | 48.21 | 57.09 | 8.88 | 11.01 |
| 500 | 50.24 | 59.60 | 9.36 | 11.59 |
| 600 | 51.99 | 61.76 | 9.77 | 12.08 |
| 700 | 53.52 | 63.65 | 10.13 | 12.47 |
| 800 | 54.89 | 65.34 | 10.45 | 12.80 |
| 900 | 56.16 | 66.86 | 10.72 | 13.09 |
| 1000 | 57.68 | 68.65 | 10.97 | 13.32 |

by plotting the reduced masses $m_X m_{CN}/(m_X+m_{CN})$ against the difference between $r_{CX}$(XCN) and $r_{CX}$ (standard). Thus the principal moment of inertia is $I=81.06\times10^{-40}$ g cm².

These approximate molecular data may now be used for calculating the themodynamic functions of ideal FCN gas at a pressure of 1 atmos. These are given in Table I. Although the accuracy of these data is probably not quite as good as it is usually expected to be for tri-atomic molecules, they might prove useful in the future investigations and in experimental redetermination.

[1] W. J. O. Thomas, J. Chem. Phys. **20**, 920 (1952).

## The Temperature Dependence of the Thermal Diffusion Ratio

EUGENE M. HOLLERAN
*St. John's University, Brooklyn, New York*
(Received August 5, 1953)

THE thermal diffusion ratio of a binary gas mixture is measured by determining the composition change that occurs when the gas is confined in two connected vessels kept at two different temperatures. Since the thermal diffusion ratio $R_T$ varies with temperature, there arises the problem of assigning the correct average temperature to the measured value of $R_T$. According to the kinetic theory

$$R_T(\bar{T})=\left(\ln\frac{T_2}{T_1}\right)^{-1}\int_{T_1}^{T_2}R_T\,d\ln T, \tag{1}$$

from which the temperature $\bar{T}$ to be assigned to the measured value $R_T(\bar{T})$, determined between the experimental temperatures $T_1$ and $T_2$, can be found if the temperature dependence of $R_T$ is known. Brown has shown[1] that if $R_T$ is a linear function of $1/T$, the assigned temperature should be given by

$$\bar{T}=\frac{T_1T_2}{T_2-T_1}\ln\frac{T_2}{T_1}. \tag{2}$$

Using assigned temperatures found from Eq. (2), Stier[2] noted that his experimental $R_T$ values for argon and neon obeyed an empirical equation of the form

$$R_T=a\ln\frac{T}{b}, \tag{3}$$

where $a$ and $b$ are constants. Srivastava and Madan[3] have pointed out that Eq. (3) becomes inconsistent with the temperature dependence assumed in deriving Eq. (2). As these authors also note, an assumed temperature dependence for $R_T$ can be correct only if it fits the experimental measurements after these have been assigned the average temperatures determined by this temperature dependence through Eq. (1). Srivastava and Madan assume the temperature dependence for $R_T$ predicted by the Lennard-Jones 12, 6 intermolecular potential and calculate from this the temperatures to be assigned to the experimental $R_T$ values for the case of argon. (The experimental results for neon cannot be fitted by the 12, 6 model, which predicts a maximum $R_T$ smaller than several of the observed values.) They then find that the assumed temperature dependence fits the argon data well enough

TABLE I. Comparison of observed values of $R_T$ for argon and neon with those calculated from Eqs. (5) and (6).

| $T$ range °K | $(T_1T_2)^{\frac{1}{2}}$ | Argon $R_T$ (obs) | Argon $R_T$ Eq. (5) | Neon $R_T$ (obs) | Neon $R_T$ Eq. (6) |
|---|---|---|---|---|---|
| 90–195 | 132 | 0.067 | 0.095 | 0.382 | 0.387 |
| 90–296 | 163 | 0.151 | 0.150 | 0.441 | 0.441 |
| 195–296 | 240 | 0.248 | 0.249 | 0.550 | 0.542 |
| 195–490 | 309 | ··· | ··· | 0.599 | 0.607 |
| 195–495 | 311 | 0.312 | 0.315 | ··· | ··· |
| 273–623 | 412 | 0.389 | 0.387 | ··· | ··· |
| 302–645 | 441 | ··· | ··· | 0.713 | 0.699 |
| 460–638 | 542 | ··· | ··· | 0.750 | 0.753 |
| 455–685 | 558 | 0.466 | 0.465 | ··· | ··· |
| 621–819 | 713 | ··· | ··· | 0.817 | 0.824 |
| 638–833 | 729 | 0.534 | 0.534 | ··· | ··· |

to justify the assigned temperatures, but poorly enough to require certain modifications in the 12, 6 potential. The present point of interest is that they also find that Eq. (3) still fits the experimental data over a large part of the temperature range.

It therefore appears to be of interest to investigate directly the temperature dependence given by Eq. (3). Substitution of this into Eq. (1) yields the very simple expression for the assigned temperature:

$$\bar{T}=(T_1T_2)^{\frac{1}{2}}. \tag{4}$$

Plots of Stier's $R_T$ values for argon and neon against $\log T_1T_2$ show straight lines except for argon's lowest value, for which the large experimental error of ±10 percent is reported. Omitting this point, the values of the constants in Eq. (3) were found by the method of least squares. Table I shows that the resulting equations

$$R_T=0.2566\ln\frac{T}{91.01} \tag{5}$$

for argon, and

$$R_T=0.2591\ln\frac{T}{29.68} \tag{6}$$

for neon, fit the experimental data to within 2 percent over the entire temperature range for neon (132° to 713°K) and within 1 percent above about 150°K for argon. Since the reported probable experimental error is ±5 percent, the values of the constants in Eqs. (5) and (6) must be considered uncertain by several percent.

It has thus been confirmed in the most direct and self-consistent manner that $R_T$ is a linear function of $\ln T$ over a wide range of temperature for argon and neon, the two cases for which fairly extensive measurements have been made.

If the deviation for argon at the lowest temperature is real, the continued adherence of neon to Eq. (6) to lower temperatures would be consistent with the law of corresponding states and the lower value of $b$ for neon.

The author wishes to express his gratitude to St. John's University for the extension of a Summer Research Grant.

[1] H. Brown, Phys. Rev. **58**, 661 (1940).
[2] L. G. Stier, Phys. Rev. **62**, 548 (1942).
[3] B. N. Srivastava and M. P. Madan, J. Chem. Phys. **21**, 807 (1953).

## The $\nu_2$ Infrared Band in Gaseous Fluoroform*

WALTER F. EDGELL AND CHARLES MAY
*Department of Chemistry, Purdue University, Lafayette, Indiana*
(Received August 7, 1953)

A RECENT study[1] of the infrared bands of fluoroform calls attention to the fundamental difficulties in the spectra of this molecule. The Raman spectrum[2,3] of the liquid at −95°C shows a strong line at 1117 cm$^{-1}$ due to the symmetrical $CF_3$ stretching vibration ($\nu_2$) and a weak line at 1160 cm$^{-1}$ corresponding to the antisymmetrical stretching vibration ($\nu_5$). In this same region the infrared spectrum[1,4,5] of the gas consists of a very strong, single maximum band at 1152 cm$^{-1}$ and a moderately in-

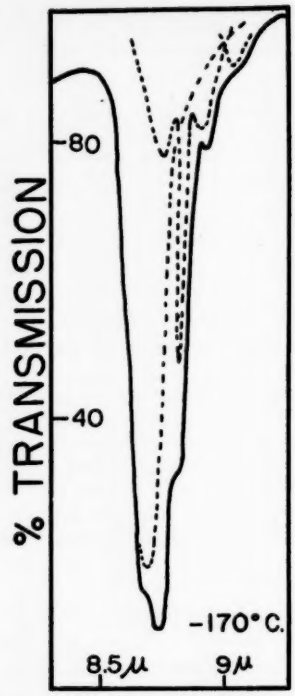


FIG. 1. The 8.7$\mu$ band of gaseous $CF_3H$ at low temperatures.

tense band at 1209 $cm^{-1}$ with $PQR$ branches and a $P-R$ separation of about 32 $cm^{-1}$. The band at 1152 $cm^{-1}$ has been assigned to $\nu_5$. Two interpretations have been advanced regarding $\nu_2$. Either it has been assigned to the 1209-$cm^{-1}$ band[1,4] or assumed to be too weak for observation or overlapped by $\nu_5$.[3,5]

It has occurred to us that lower temperatures might sharpen the 1152-$cm^{-1}$ band sufficiently to reveal any overlapping. A two-cm, low-temperature gas cell was filled to a pressure of 125-mm Hg at 30°C. As the temperature of the cell was lowered, the 1152-$cm^{-1}$ band became sharper and a shoulder at 1130 $cm^{-1}$ began to appear at −50°C. Finally at a cell temperature of −170°C,[6] the 1152-$cm^{-1}$ band was so narrow that well-defined shoulders were visible at 1116, 1130, 1140, and 1160 $cm^{-1}$ (see Fig. 1). At lower temperatures the gas completely condensed.

The only plausible explanation for the complexity of this band is the overlapping of $\nu_2$ and $\nu_5$. One interpretation,[7] illustrated in Fig. 1 places the $Q$ branch of $\nu_2$ at 1140 $cm^{-1}$ with its $P$ and $R$ branches at 1130 and 1152 $cm^{-1}$. The $\nu_5$ band (with one or possibly two peaks) centers at about 1157 $cm^{-1}$. The weak peak at 1116 $cm^{-1}$ is believed due to $\nu_2$ arising from a small amount of liquid on the windows. This is not unreasonable since most of the gas has condensed on the metal cell walls at this temperature.

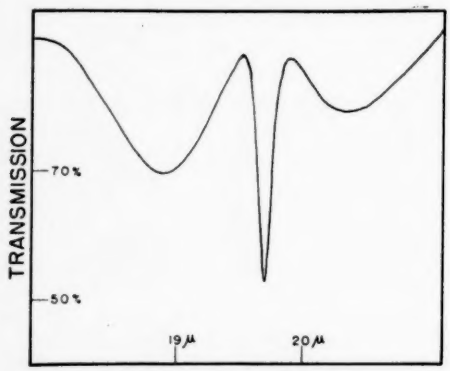


FIG. 2. The 19.7$\mu$ band of $CF_3H$.

There remains the matter of the 1209-$cm^{-1}$ band and its envelope. Recent work in this laboratory and at Harvard[8] has re-emphasized the important role of Coriolis coupling in influencing the shape of band envelopes arising from degenerative modes. In the absence of coupling or other complicating features, an $E$ band would consist of $PQR$ branches[9] with a $P-R$ separation of about 24 $cm^{-1}$. The 1209-$cm^{-1}$ band is assigned to the combination 508+699, an $E$ band with a modified envelope. This would be consistent with a similarly modified envelope for the 508-$cm^{-1}$ $E$ band. A question exists regarding the shape of this band.[1,5] Figure 2 shows it as obtained with a double-beam spectrometer using a KBr prism and a 10-$cm^{-1}$ cell with 70-mm pressure in agreement with the work of Plyler and Benedict.[5] The same envelope was also found at greater resolution with a CsBr prism in a double-pass spectrometer. The $P-R$ separation is 38 $cm^{-1}$ and corresponds to a value of roughly −0.8 for the Coriolis coupling constant $\zeta$.

This work, as well as the recent Raman data for the gas obtained by Claassen and Nielsen,[10] shows that the $\nu_2$ fundamental of gaseous $CF_3H$ lies near 1140 $cm^{-1}$ and removes the major difficulties relating to the fundamentals.

Support of this research by the U. S. Atomic Energy Commission is gratefully acknowledged.

* Based on the Ph.D. thesis of C. May; June, 1953.
[1] H. D. Rix, J. Chem. Phys. **21**, 1077 (1953).
[2] George Glockler and Walter F. Edgell, J. Chem. Phys. **9**, 224 (1941).
[3] Rank, Shull, and Pace, J. Chem. Phys. **18**, 855 (1950).
[4] W. C. Price as quoted by H. Bernstein and G. Herzberg, J. Chem. Phys. **16**, 30 (1948).
[5] E. K. Plyler and W. S. Benedict, J. Research Natl. Bur. Standards **47**, 202 (1951).
[6] The temperature of the gas was somewhat greater than that of the cell.
[7] An alternate solution places the $PQR$ branches at 1116, 1130, and 1140 $cm^{-1}$.
[8] S. Polo, private communication.
[9] S. L. Gerhardt and D. M. Dennison **43**, 197 (1933).
[10] H. Claassen and J. R. Nielsen, J. Opt. Soc. Am. **43**, 352 (1953).

## Intramolecular Isotope Effects* in the Reactions of Benzoic-α-$C^{14}$ Anhydride

VERNON F. RAAEN AND GUS A. ROPP
*Chemistry Division, Oak Ridge National Laboratory, Oak Ridge, Tennessee*
(Received July 20, 1953)

COMPARISONS of experimentally measured values of *intramolecular* carbon isotope effects with theoretically calculated values are of particular interest since the theory[1] appears to predict very definite and easily calculated ratios of rate constants. Out of the theory it developes also that the rate constant ratio for a given *intramolecular* isotope effect should have the same value at all temperatures in contrast to *intermolecular* isotope effects which vary decidedly with temperature.

The present *intramolecular* isotope effect study, which concerns the reactions of the symmetrical compound, benzoic-α-$C^{14}$ anhydride (I), is one of a series[2] of studies of various aspects of isotope effects. The reactions involved are

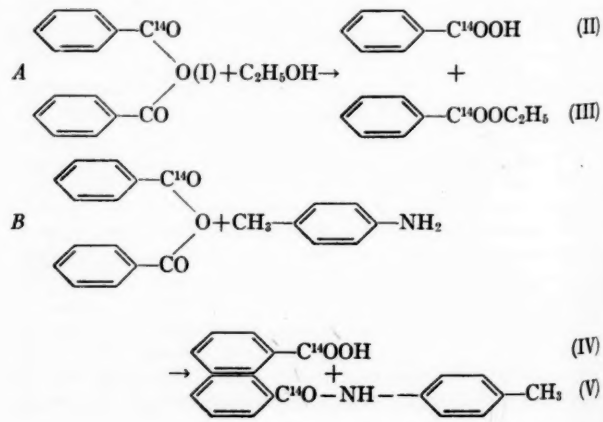

TABLE I.

| Reaction | Temperature 0°C | Specific activities μc/m mole | | $k_{12}/k_{14}$ | Theoretical value[a] |
|---|---|---|---|---|---|
| *A* | 30° | II = 3.99 | III = 3.54 | 1.127 | C—O bond making: 1.043 |
| | 78° | II = 4.03 | III = 3.57 | 1.129 | |
| *B* | 30° | IV = 3.92 | V = 3.65 | 1.073 | C—N bond making: 1.041 |
| | 138° | IV = 3.86 | V = 3.60 | 1.071 | |

[a] See reference 2.

The ethanolysis reaction, *A*, was carried out in ethanol solution at two temperatures and each isotope effect value was calculated as the ratio of specific activities of III and II. The specific activity of III was measured after the ester was isolated and completely hydrolyzed to benzoic-α-$C^{14}$ acid. The ethanolysis, *A*, was very slow, particularly at the lower temperature, 30°C, where thirty-three days was the time necessary to effect 93 percent reaction as measured by titration of the acid II. The reaction, *B*, was carried out in dry hydrocarbon solvents and went to completion rapidly. However, the *intramolecular* isotope effect ratios for *A* or *B* can be calculated at any stage during the reaction as the specific activity ratios II/III and IV/V.

It is believed that for reactions *A* and *B*, the symmetry-destroying steps (and hence the steps which decide the distribution of isotopes between the two products of each reaction) are, respectively, *A′* and *B′*, which involve attacks at the labeled carbon of the carbonyl group:

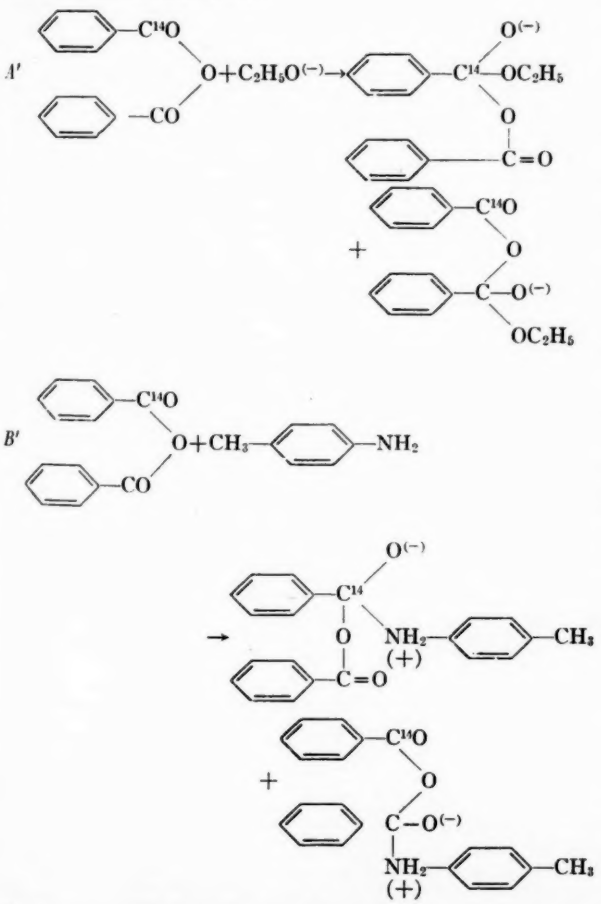

Results are presented in Table I. From Table I it appears that there is no appreciable variation of these isotope effect ratios with temperature in agreement with the theory. However, the lack of agreement between experimental and calculated isotope fractionation factors which is apparent in Table I has also been noted in other *intramolecular* isotope effect studies.[3] The presently described isotope fractionation studies are being extended, and when completed will be published with further discussion of the results. Studies now going on include the effect of nuclear substituents in the two rings of benzoic-α-$C^{14}$ anhydride on the *intramolecular* isotope effects in reactions such as *A* and *B*.

* This document is based upon work performed under Contract Number W-7405-eng. 26 for the U. S. Atomic Energy Commission at the Oak Ridge National Laboratory.

[1] J. Bigeleisen, J. Chem. Phys. **17**, 425 (1949); J. Bigeleisen, Brookhaven National Laboratory Report 1068 (1952). The latter is an unclassified report which can be obtained from the U. S. Atomic Energy Commission Technical Information Division.

[2] Ropp, Weinberger, and Neville, J. Am. Chem. Soc. **73**, 5573 (1951); G. A. Ropp and V. F. Raaen, J. Am. Chem. Soc. **74**, 4992 (1952); G. A. Ropp and V. F. Raaen, J. Chem. Phys. **20**, 1823 (1952).

[3] The extent of agreement between theory and experiment for carbon-14 *intramolecular* isotope effects has been tabulated by G. A. Ropp, Nucleonics **10**, 22-7 (1952).

## Substituted Methanes. XIX. $C^{13}$ Isotopic Shifts in the Vibrational Spectrum of Methanol

RICHARD B. BERNSTEIN,* *Department of Chemistry*
JAMES E. LAMPORT AND FORREST F. CLEVELAND, *Spectroscopy Laboratory,† Department of Physics, Illinois Institute of Technology, Chicago 16, Illinois*
(Received August 13, 1953)

USING a sample containing 9.3 atom percent $C^{13}$, it was possible to measure several isotopic frequency shifts in the Raman and infrared spectra of methanol. The material was prepared from $C^{13}$-enriched $BaCO_3$ (Eastman Kodak Company) by the lithium aluminum hydride reduction of enriched carbon dioxide.[1,2] The product was fractionated in a small packed column and was vacuum-distilled before use.

Raman spectrograms of the liquid were obtained with a 2-prism spectrograph[3] having a dispersion of 33A/mm at 4500A, using Hg 4358A and 4047A exciting lines with appropriate filters. Infrared spectra of the vapor were obtained with a Perkin-Elmer Model 12C spectrometer (NaCl optics), using a 10-cm cell. A confirmatory differential spectrum (enriched *vs* normal methanol) was obtained with a Baird Associates double-beam spectrophotometer. Comparison spectra of normal methanol were run under identical conditions in all cases.

From six Raman spectrograms of the $C^{13}$-enriched sample, obtained under various conditions, it was possible to identify and measure two lines resulting from $C^{13}H_3OH$. A third line of low intensity, attributed to $C^{13}H_3OH$, also was measured. From the infrared spectrograms only one band due to $C^{13}H_3OH$ could be observed with certainty; this was the *Q* branch of the band corresponding to the $C^{13}$-O stretching vibration, $\nu_4^{CO}(a')$, which was superimposed on the *P* branch of the corresponding band of $C^{12}H_3OH$. A second band lying between the two strong $C^{12}H_3OH$ bands near 2830 and 2970 $cm^{-1}$ was indicated, but it was not resolved. The data are summarized in Table I.

The $C^{13}$ shift observed for the C—O stretching frequency may be fairly well estimated by use of the simple pseudo-diatomic approximation. Assuming two pseudo-diatomic molecules,

TABLE I. Infrared and Raman spectral data for $C^{12}H_3OH$ and $C^{13}H_3OH$.

| Raman displacements ($cm^{-1}$) | | | Infrared wave numbers ($cm^{-1}$) | | | |
|---|---|---|---|---|---|---|
| | Liquid | | | Vapor | | |
| $C^{13}H_3OH$ | $C^{12}H_3OH$ | Shift | $C^{13}H_3OH$ | $C^{12}H_3OH$ | Shift | Assignment[a] |
| 1036 | 1021 | −15±1 | 1034 | 1018 | −16±1 | $\nu_4^{CO}(a')$ |
| 2835 | (2823)[b] | (−12±2)[b] | ··· | ··· | ··· | $\nu_2^{CH}(a')$ |
| 2943 | 2924 | −19±2 | ··· | ··· | ··· | $2\nu_6^{11}(A')$ |

[a] Designation from G. Herzberg, *Infrared and Raman Spectra of Polyatomic Molecules* (D. Van Nostrand Company, Inc., New York, 1945), first edition, Vol. 1, p. 335.
[b] Values somewhat uncertain.

$H_3C^{13}-OH$ and $H_3C^{12}-OH$, one may calculate the shift as $-17\ cm^{-1}$.

The authors appreciate the help of Miss E. L. Flaherty and Mr. P. C. Hutchinson of Baird Associates who obtained the confirmatory differential infrared spectrum. This research was aided by the U. S. Atomic Energy Commission; the Office of Ordnance Research, U. S. Army; and the Society of the Sigma Xi.

* Present address: Department of Chemistry, University of Michigan, Ann Arbor, Michigan.
† Publication No. 94.
[1] Nystrom, Yanko, and Brown, J. Am. Chem. Soc. **70**, 441 (1948).
[2] Cox, Turner, and Warne, J. Chem. Soc. **1950**, 3167.
[3] F. F. Cleveland, J. Chem. Phys. **11**, 1, 227 (1943).

## Kinetics of Fixation of Atmospheric Nitrogen at Elevated Temperatures*

HENRY WISE AND DWIGHT I. BAKER
*Jet Propulsion Laboratory, California Institute of Technology, Pasadena, California*
(Received August 10, 1953)

RECENT measurements of the kinetics of reaction of nitric oxide[1-3] permit a quantitative analysis of the problem of nitrogen fixation from air at elevated temperatures. Such calculations are of special practical value since experiments carried out by Daniels and co-workers[4,5] have indicated the feasibility of industrially producing nitric oxide from air in a furnace containing magnesia refractories. Such a procedure can supplement the production potential for the various oxides of nitrogen which at the present time is based to a large extent on the synthesis of nitric oxide by the oxidation of ammonia on a catalytic surface.

Kinetically the problem of nitrogen fixation requires an analysis of (1) the residence time required to form a given concentration of nitric oxide from air at a specified temperature and (2) the rate of cooling of the product gases required to "freeze" the composition of the gas mixture attained at the reactor temperature. From the rate expression for the net rate of formation of nitric oxide

$$+dp_{NO}/dt = k_{-1}(Kp_{N_2}p_{O_2} - p_{NO}^2), \tag{1}$$

where $k_{-1}$ refers to the specific reaction rate constant for the decomposition of NO (see reference 3) and $K$, the equilibrium constant for the system

$$N_2 + O_2 \underset{k_{-1}}{\overset{k_1}{\rightleftarrows}} 2NO,$$

the partial pressure of nitric oxide as a function of residence time and reactor temperature may be evaluated† (Table I).

In order to obtain a high yield of nitric oxide from the process of fixation of atmospheric nitrogen by suitable choice of gas-flow rate and reaction temperature, the rate of cooling of the product gases must also be adjusted in order to minimize any shift in composition from that attained in the reactor. For a system displaced from equilibrium the rate of formation of nitric oxide during the cooling process may be assumed to make a negligible contribution to the partial pressure of nitric oxide attained in the reactor. In the analysis which follows consideration is given only to the kinetics of decomposition of nitric oxide (excluding the reverse reaction). The results obtained refer to the maximum amount of product decomposed at a given cooling rate. Experimental measurements of the kinetics of thermal decomposition of nitric oxide have shown that the reaction is catalyzed by oxygen,[3] as given by the following rate expression:

$$-dp_{NO}/dt = k_{-1}p_{NO}^2 + k_2 p_{NO}\cdot p_{O_2}^{\frac{1}{2}}. \tag{2}$$

For large departures from chemical equilibrium, an approximate relation may be used in the evaluation of the cooling rate required to keep the decomposition of nitric oxide below a given value. Thus, the concentration of oxygen remains essentially constant, since the equilibrium partial pressure of nitric oxide (Table I) represents only a small fraction of the pressure of oxygen in the mixture, and since the rate of reformation of nitric oxide from the elements is considered to be negligibly small. On substitution of average values over a given temperature interval for the various quantities, one obtains from Eq. (2)

$$-\frac{dT}{dt} = [(\bar{k}_1\bar{p}_{NO} + \bar{k}_2 p_{O_2}^{\frac{1}{2}})\Delta T]/(\Delta p_{NO}/\bar{p}_{NO}). \tag{3}$$

It is apparent that the ratio $\Delta p_{NO}/\bar{p}_{NO}$ is equal to the fractional change in the number of moles of NO, a quantity that is independent of the equation of state of the gas and therefore a direct measure of the change produced by chemical reaction. The computations cover a temperature range from 2000°K to 3000°K (see Fig. 1). These results indicate that in the operating range of

TABLE I. Rate of attainment of equilibrium composition in air.[a] $p_T = 1$ atmos, $p_{NO}$ (atmos).

| $t$(sec) | 2000°K | 2400°K | 2800°K | 3000°K |
|---|---|---|---|---|
| 100 | $\sim 8.5\times10^{-3}$ | $\sim 2.1\times10^{-2}$ | $\sim 3.9\times10^{-2}$ | $\sim 5.2\times10^{-2}$ |
| 10 | $2.9\times10^{-3}$ | $\sim 2.1\times10^{-2}$ | $\sim 3.9\times10^{-2}$ | $\sim 5.2\times10^{-2}$ |
| 1 | $3.0\times10^{-4}$ | $2.0\times10^{-2}$ | $3.8\times10^{-2}$ | $\sim 5.2\times10^{-2}$ |
| $10^{-1}$ | $2.9\times10^{-5}$ | $3.9\times10^{-3}$ | $3.8\times10^{-2}$ | $\sim 5.2\times10^{-2}$ |
| $10^{-2}$ | $2.9\times10^{-6}$ | $3.9\times10^{-4}$ | $1.2\times10^{-2}$ | $3.9\times10^{-2}$ |
| $10^{-3}$ | $2.9\times10^{-7}$ | $3.9\times10^{-5}$ | $1.2\times10^{-3}$ | $5.0\times10^{-3}$ |
| $10^{-4}$ | $2.9\times10^{-8}$ | $3.9\times10^{-6}$ | $1.2\times10^{-4}$ | $5.0\times10^{-4}$ |
| $10^{-5}$ | $2.9\times10^{-9}$ | $3.9\times10^{-7}$ | $1.2\times10^{-5}$ | $5.0\times10^{-5}$ |
| $10^{-6}$ | $2.9\times10^{-10}$ | $3.9\times10^{-8}$ | $1.2\times10^{-6}$ | $5.0\times10^{-6}$ |
| [b]Equilibr. part. press. | $8.5\times10^{-3}$ | $2.1\times10^{-2}$ | $3.9\times10^{-2}$ | $5.2\times10^{-2}$ |

[a] Composition of air: 80 vol. percent $N_2$; 20 vol. percent $O_2$.
[b] National Bureau of Standards, *Selected Values of Chemical Thermodynamic Properties*, Series III, Vol. I.

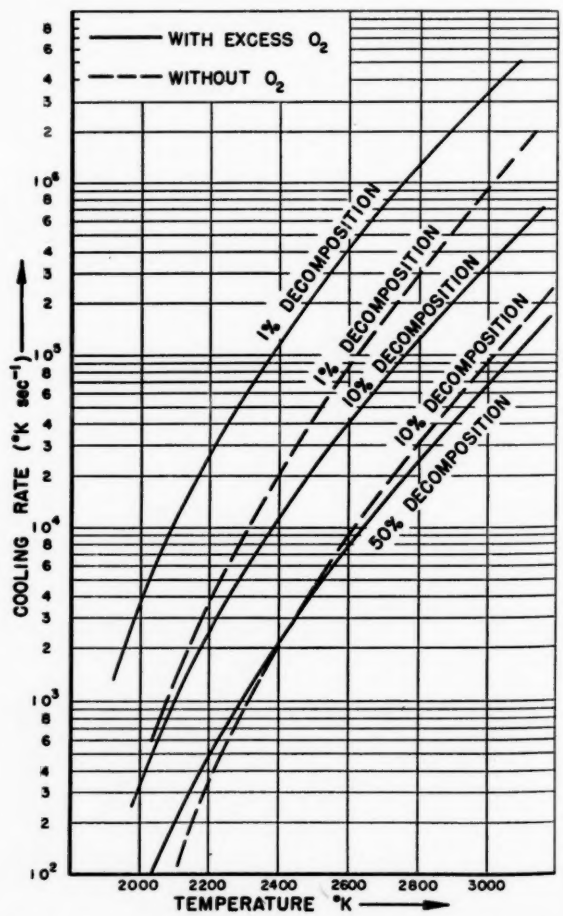


FIG. 1. Decomposition of nitric oxide as a function of cooling rate (excess $O_2$ represents 0.20 atmos).

2800°K the cooling rates required to freeze the composition of the gas mixture at 90 percent of the equilibrium value of NO are of the order of $10^5$ to $10^6$ °K per sec. It should be noted that the cooling requirements are increased by a factor of more than three in the presence of excess oxygen. It is evident, therefore, that an increase in the yield of NO necessitates high temperatures in the combustion zone and also high cooling rates. Thus, the equilibrium concentration of nitric oxide can be doubled by increasing the operating temperature from 2400 to 2800°K (Table I). However, it is important to note that little would be gained by this rise in reaction temperature unless it is accompanied by a corresponding increase in the cooling rate of the product gases. At low rates of cooling the final yield of NO becomes relatively independent of the composition of the gases attained in the reactor.

The method employing the passage of the gas mixture through a pebble-bed of magnesium oxide has shown some promise. Rates of heat exchange of the order of $10^4$ °K per second at a maximum gas temperature of 2400°K have been calculated for this type of heat exchanger.[4]

Application of the principle of adiabatic, isentropic expansion through a De Laval Nozzle offers another obviously interesting possibility. In such an expansion process a rate of temperature change of the order of $10^6$ °K per second has been calculated[6] in the temperature region of interest to the problem of atmospheric nitrogen fixation.

* This paper presents the results of one phase of research carried out at the Jet Propulsion Laboratory, California Institute of Technology, under Contract No. DA-04-495-ORD 18, sponsored by the Department of the U. S. Army Ordnance Corps.

[1] W. E. Koerner, thesis, University of Wisconsin, Madison, Wisconsin, 1949, (unpublished).

[2] H. Wise and M. Frech, J. Chem. Phys. **20**, 22 (1952).

[3] H. Wise and M. Frech, J. Chem. Phys. **20**, 1724 (1952).

[4] N. Gilbert and F. Daniels, Ind. Eng. Chem. **40**, 1719 (1948).

[5] W. G. Hendrickson, thesis, University of Wisconsin, Madison, Wisconsin, 1946 (unpublished).

† The influence of oxygen on the reaction kinetics (see reference 2) is neglected in these calculations for both the forward and reverse reactions. Also the approximation is made that the partial pressures of $N_2$ and $O_2$ do not change appreciably during the process of synthesis of nitric oxide from air. [K. J. Laidler, *Chemical Kinetics* (McGraw-Hill Book Company, Inc., New York, 1950), p. 51].

[6] D. Altman and S. S. Penner, J. Chem. Phys. **17**, 56 (1949).

## Paramagnetic Resonance Hyperfine Structure of the Free Radical $(SO_3)_2NO^-$

B. SMALLER AND E. L. YASAITIS
*Chemistry Division, Argonne National Laboratory, Lemont, Illinois*
(Received May 11, 1953)

THE paramagnetic properties of the free radical peroxylamine disulfonate have been discovered recently by Pake, Townsend, and Wiessman.[1] Their results both at 9000 Mc and 9.2 Mc were in agreement with the existence of a nuclear spin of one, attributed to the nitrogen nucleus, with an interaction energy of about 55 Mc causing a hyperfine splitting of the resonance. We considered it of interest to investigate more thoroughly this resonance in regard to signal shape and width and to determine the splitting constant more accurately.

TABLE I. Determination of $W_0$ (Mc/sec).

| Transition line designation | Zero field transitions | Weak field transitions | Strong field transitions |
|---|---|---|---|
| $\pi_1$ | | $55.2 \pm 0.3$ | $55.6 \pm 0.2$ |
| $\pi_2$ | | $54.8 \pm 0.3$ | $58.0 \pm 2.0$ |
| $\pi_3$ | | $55.0 \pm 1.0$ | $54.0 \pm 0.4$ |
| $\pi_4$ | | $55.5 \pm 0.5$ | |
| $\pi_5$ | | $56.5 \pm 1.0$ | |
| $\pi_6$ | | $55.0 \pm 0.5$ | |
| $\pi_1+\pi_2+\pi_6$ | $54.8 \pm 0.2$ | | |

The salt was prepared as potassium peroxylamine disulfonate with dilute NaOH used as solvent to inhibit polymerization. Tetraphenyl arsonium peroxylamine disulfonate, soluble in chloroform, was also prepared and found to have a similar paramagnetic behavior.

The detection system was a modification of the one used for nuclear resonance studies,[2] designed for a dual field modulation.[3] Signal detection was accomplished by a regenerative oscillator or amplifier.

The spectrum was first investigated in the strong field region. With excitation at 300 Mc the resonances occur because of the $\pi_1$, $\pi_2$, and $\pi_3$ transitions, the notations being those given by Nafe and Nelson.[4] A more accurate determination of the splitting constant, $W_0$, was achieved by investigation of the $\pi_1$, $\pi_2$, and $\pi_6$ transitions at very weak fields or zero field, for their resonant

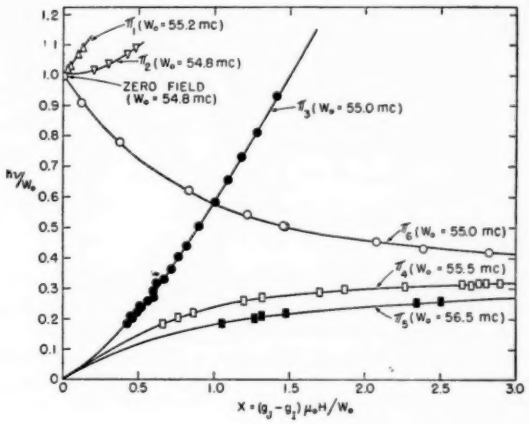


FIG. 1.

frequencies become equal to $W_0$ at zero field. The value of $W_0$ was thus determined by observing the coalescence of these resonances as the excitation frequency was varied through the $W_0$ point. Similarly the $\pi_4$, $\pi_5$, and $\pi_6$ transitions were studied especially near their asymptotic value of $W_0/3$ for strong fields where an accurate determination of $W_0$ can be made. The results for the various transitions are listed in Table I and, along with the best fitting theoretical curves, are plotted in Fig. 1. The mean value of $W_0 = 54.9 \pm 0.2$ Mc/sec is in agreement with that recently determined by Townsend *et al.*, in a re-investigation of this radical.[5]

The relationship between the line shape of a magnetic resonance signal and the distribution of the perturbing interactions has been considered by Pake and Purcell.[6] A useful criterion of the nature of the distribution is the shape of the dispersion-derivative signal as presented at the output of a phase sensitive lock-in detector, for the ratio of the field displacement between maximum negative signal response to that of the full width at half-maximum of the positive signal response is unique to the distribution. Thus, for a Gaussian distribution the ratio is 2.7 while for a Lorentzian, indicative of exchange narrowing,[7] the ratio is 3.5. A survey of the electronic transitions gave agreement with a Gaussian distribution with line width and shape independent of magnetic field.

The $\pi_4$, $\pi_5$, and $\pi_6$ resonances correspond, in strong fields, to nuclear spin transitions (i.e., $\Delta m_s = 0$, $\Delta m_I = \pm 1$) and thus should afford one an opportunity to measure a nuclear magnetic moment in a paramagnetic salt. In particular, the $\pi_4$ transition is of doublet structure with a separation proportional to the nuclear magnetic moment. For an isolated spin system the detection of this transition would be feasible despite its very weak intensity, yet because of the interactions present here one might expect that the relaxation time of the various spin states resulting from the electronic spin transitions would result in a pronounced broadening of the nuclear spin resonances. This effect is shown in Fig. 2 where the experimental line width is plotted as a function of resonance field strength for the $\pi_4$ transition. For comparison, the theoretical curve represents the variation in line width to be expected if the energy level broadening was contributed almost solely by the

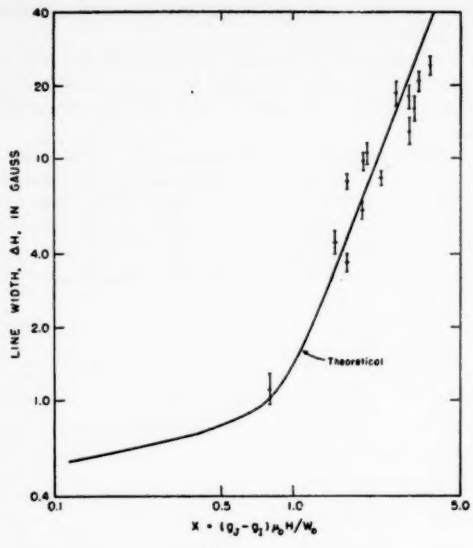


FIG. 2.

electronic spin transitions and was thus independent of field strength. With this prohibitively large line width, a direct measurement of the nuclear moment is obviously unfeasible.

We are indebted to M. Brachman for the theoretical intensity calculations and wish to express our appreciation to J. Katz and W. Sykes for the preparation of the potassium salt and tetraphenyl arsonium salt, respectively.

[1] Pake, Townsend, and Weissman, Phys. Rev. **85**, 682 (1952).
[2] G. Breit and I. I. Rabi, Phys. Rev. **38**, 2082 (1931).
[3] B. Smaller and E. Yasaitis, Rev. Sci. Instr. (to be published).
[4] J. E. Nafe and E. B. Nelson, Phys. Rev. **73**, 718 (1948).
[5] Townsend, Weissman, and Pake, Phys. Rev. **89**, 606 (1953). Apparently this recent work had been undertaken simultaneously with our own.
[6] G. E. Pake and E. M. Purcell, Phys. Rev. **74**, 1184 (1948).
[7] P. W. Anderson and P. R. Weiss, Revs. Modern Phys. **25**, 269 (1953).

## $n-\pi$ Emission Spectra*

C. REID†
*Laboratory of Molecular Structure and Spectra, Department of Physics, The University of Chicago, Chicago 37, Illinois*
(Received August 3, 1953)

MOLECULES containing a hetero-atom (O, N, S, etc.) with an "unshared pair" of electrons adjacent to a conjugated system usually show light absorption to longer wavelengths than do the corresponding conjugated molecules with no hetero-atom.

This absorption has been attributed to "$n-\pi$" transitions in which one of the unshared pair electrons is excited into the lowest unfilled level of the conjugated system.[1-3] Most such molecules also show phosphorescence, of lifetime ranging from *ca* $10^{-3}$ second for aromatic ketones to several seconds for pyridine. Phosphorescences of this kind have been attributed variously as due to singlet $n-\pi$ transitions, (formaldehyde[4]) triplet $n-\pi$ transitions, (formaldehyde,[5] pyridine,[2,3] etc.) and triplet $\pi-\pi$ transitions, (pyridine[6]). It is not always possible unambiguously to decide between these possibilities. The following argument clears up some of the difficulties.

Elementary MO considerations show that the singlet-triplet separation $=2\int\psi_n H\psi_\pi d\tau$, where $\psi_n$ and $\psi_\pi$ are the one-electron $n$ and $\pi$ orbital wave functions, respectively. We can expect this integral to be very small for two reasons. First, the amount of spatial overlap between these two orbitals is small, particularly if the conjugated system is an extended one. Second, symmetry considerations suggest that the integral should be zero, any positive part being balanced by an equal negative contribution.

Triplet transitions are often observed in emission only, the corresponding absorption being too weak to observe. This emission is thus well to the red of the longest wavelength (allowed) absorption. However, the above argument suggests that in the case of $n-\pi$ transitions, $T\rightarrow S$ emission should be much closer to the corresponding *singlet* absorption. Using as a guide an average $S-T$ separation for $\pi-\pi$ transitions of 6–7000 cm$^{-1}$, and assuming that the splitting will decrease in $n-\pi$ transitions in about the same ratio that the intensities of these transitions bear to those of $\pi-\pi$ transitions (about 0.02), we can expect that only a hundred cm$^{-1}$ or so will separate singlet absorption and triplet emission.

This allows us to say at once that the observed long-lived phosphorescence of pyridine at 27 000 cm$^{-1}$ (nearest appreciable absorption $\simeq$36 000 cm$^{-1}$) is not $n-\pi$ as has been suggested,[2,3] but $\pi-\pi$.

The correctness of this argument has been confirmed in this Laboratory by a comparison of the emission spectrum of pyridine in a rigid glass (EPA) with that of pyridine in concentrated sulfuric acid. For an $n-\pi$ transition the emission of pyridinium salts should be much weakened or absent, since the $n$ electrons are no longer excitable at such low energy. In fact, the emission is not only present but enhanced by a factor of about 10 in intensity. Accordingly it is certainly $\pi-\pi$, as was suggested tentatively by Sponer and Rush.[6]

Using the above picture, it is also possible to explain why the lifetimes of the emitting states of aldehydes and ketones are about 100–1000 times longer (*ca* $10^{-3}$ second) than is calculated from the extinction coefficient of what looks like the corresponding absorption band ($\epsilon\simeq$200). It is also possible to explain the conflicting results of the detailed analysis of the wave absorption and emission of formaldehyde.[4,5] The explanation suggests that the emission is not homogeneous, but comes partly from the $n-\pi$ singlet and partly from the triplet state. Experiments to confirm or disprove the correctness of this explanation are underway.

* This work was assisted by the Office of Ordnance Research under Project TB2-0001 (505) of Contract DA-11-022-ORD-1002 with The University of Chicago.
† On leave of absence from The University of British Columbia, Vancouver, British Columbia, Canada.
[1] H. L. McMurray and R. S. Mulliken, Proc. Nat. Acad. Sci. U. S. **26**, 312 (1940).
[2] M. Kasha, Disc. Faraday Soc. **9**, 14 (1950).
[3] C. Reid, J. Chem. Phys. **18**, 1673 (1950).
[4] P. J. Dyne, J. Chem. Phys. **20**, 811 (1952), and references contained therein.
[5] A. D. Walsh, J. Chem. Phys. **20**, 1502 (1952).
[6] J. H. Rush and H. Sponer, J. Chem. Phys. **20**, 1847 (1952).

## Specific Heat of Diamond at Low Temperatures

R. BERMAN AND J. POULTER
*Clarendon Laboratory, Oxford, England*
(Received July 20, 1953)

DESORBO has recently published measurements of the specific heat of diamond from room temperature down to liquid hydrogen temperatures.[1] The values are markedly lower than those found by Pitzer,[2] whose measurements extended down to 70°K, and the discrepancy is clearly shown by the comparison, given by DeSorbo, of the derived values of the Debye characteristic temperature $\theta$. DeSorbo points out that this may be due to differences in (1) impurity content; (2) imperfections in the lattice; or (3) the relative amounts of type I and type II diamonds in the samples.

We have constructed an apparatus in which we determine the difference in heat content of a specimen between two fixed temperatures and can measure the enthalpy difference between 4° and 90°K or 90°K and room temperature for diamond to an accuracy of 1 percent using 100–200 mg. With this apparatus we have made measurements on gem quality samples consisting entirely of type I and of type II stones (the classification being according to the ultraviolet transparency limit) and also on completely opaque "bortz" diamonds. Although the purity of these samples has not yet been ascertained, it is instructive to compare our results with those of Pitzer and of DeSorbo, as given in Table I.

TABLE I. Enthalpy differences—cal/g-atom.

| | 4.2°–90.1°K | 90.1°–291.2°K |
|---|---|---|
| Pitzer | (1.07) | 116.0 |
| DeSorbo | 0.81 (±0.04)[a] | 114.0 |
| This research: | | |
| Type I | 0.85$_8$±0.01 | 113.5±1.0 |
| Type II | 0.84$_8$±0.01 | 112.0±1.0 |
| Bortz | 1.08$_8$±0.01 | ··· |

[a] This probable error has been estimated using DeSorbo's assessment of the accuracy of his specific heat measurements at these temperatures.

The value we have ascribed to Pitzer for the 4° to 90°K interval was calculated on the assumption that the Debye $\theta$ remains at about 1930°K, which is the value he finds at 70° and is also calculated by Smith[3] as the value at 0°K. The enthalpy will not, in any case, be very sensitive to changes in the value of $\theta$ at temperatures below 70°K.

It will be seen that we have detected no difference greater than 1 percent between type I and type II diamonds, which rules this out as a source of difference between various sets of results. The marked discrepancy at low temperatures between our results on gem quality stones and Pitzer's on reasonably clear bortz led us to investigate stones of still poorer quality. As our values for bortz are very little greater than Pitzer's, it seems likely that his values of specific heat are genuinely too high in the lower temperature region.

Our results for gem stones agree (within the limits of experimental uncertainties) with those of DeSorbo, and this suggests that the imperfections which are present in his stones have little effect on the specific heat.

Details of our apparatus and of the experimental results will be published elsewhere.

[1] W. DeSorbo, J. Chem. Phys. **21**, 876 (1953).
[2] K. S. Pitzer, J. Chem. Phys. **6**, 68 (1938).
[3] H. M. J. Smith, Trans. Roy. Soc. (London) **241**, 105 (1948).

## Importance of $\nu_{11}e_{12}$ (849) Vibration of Benzene in Determining the Structure of Monosubstituted Benzenes

SATYA NARAIN GARG
*Department of Spectroscopy, Banaras Hindu University, Banaras, India*
(Received July 24, 1953)

EARLIER workers[1] have considered molecules like toluene, phenol, aniline, benzonitrile, benzotrifluoride, etc., as *approximately* belonging to $C_{2v}$ symmetry* group, and it has been unquestioningly believed that the monohalogen derivatives of benzene belong *rigorously* to $C_{2v}$ symmetry.* Perhaps the outstanding discrepancy between the observed and calculated $f$ values[2,3] and between the observed and calculated shifts[2] of origin (compared to benzene) of the first uv absorption band

TABLE I.

| Molecule | Frequency | I | $\rho\times100$ | Species from uv analysis |
|---|---|---|---|---|
| Toluene[a] | 842 | weak | Dep. | totally symmetric |
| Fluorobenzene[b] | 807 or 831 | strong | 12 | totally symmetric |
| Benzonitrile[a] | 842 | weak | | totally symmetric (totally symmetric) |
| Benzaldehyde[c] | 827 | medium | 7 | Analysis of absorption spectrum[d] independently shows a symmetry lower than $C_{2v}$ for this molecule. |

[a] Bass, J. Chem. Phys. **18**, 1403 (1950).
[b] Bass and Sponer, J. Opt. Soc. Am. **40**, 389 (1950).
[c] Bär, Z. Physik **79**, 455 (1932).
[d] Garg, J. Sci. Research, Banaras Hindu Univ. **II**, 153 (1951–52), Part I; **IV** (to be published), Parts II–IV.

system of fluorobenzene is due to this tacit belief. While toulene and benzotrifluoride *unquestionably* do not have $C_{2v}$ symmetry† (since the phenyl group has a $C_2$ axis while the attached part has a $C_3$ axis), the purpose of this note is to stress upon this fact further and to show that even fluorobenzene does not possess any symmetry.

Interest centers round vibration frequencies‡ of species $e_{1g}$ (Raman active) and $e_{2u}$ (inactive) of benzene whose values in $a_2$ part for a substituted benzene having $C_{2v}$ symmetry (even approximately) should remain unaltered.[4–6] A frequency of substituted benzenes in the neighborhood of 849, generally 800–849, has been assigned to $a_2$ part of $\nu_{11}e_{1g}$ (849) of benzene. This is correct in so far as the visualization of the mode of oscillation in this frequency of substituted benzenes is concerned.[6] But when ultimate question of the *rigorous* structure of the substituted benzene is taken up, the Raman depolarization factor and/or the symmetry species of this frequency as concluded from uv absorption or fluorescence spectrum, more often than not, go against the assumption of $C_{2v}$ symmetry. Reduction of the symmetry species to the corresponding ones of various lower symmetry groups is shown below.

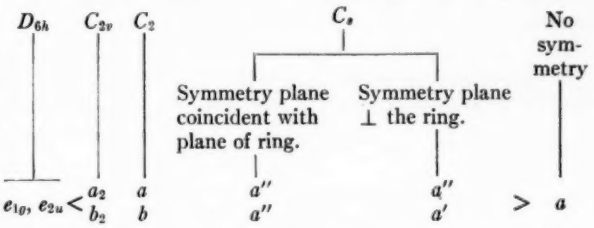


Thus, if the frequency 800–849 of a substituted benzene seems to belong to totally symmetric species on account of low Raman depolarization factor and/or the analysis of uv spectrum, the molecule should possess§ either $C_2$ symmetry or *no* symmetry. The former possibility $C_2$ can arise only for such substituted benzenes in which the phenyl group is attached to a part having a $C_2$ axis. In the case of the attached part having a $C_\infty$ axis (i.e., an atom or a linear part), the possibility of $C_2$ symmetry automatically means $C_{2v}$ symmetry, and therefore, is not be be considered. The observations on this frequency in a few compounds are given below.

Thus, it is interesting in its *implications* to see that *even* fluorobenzene does not have any symmetry, so that the F atom lies neither in the plane of the phenyl group nor in a plane perpendicular to it passing through the $C_2$ axis of the phenyl group.

The author wishes to thank Dr. R. K. Asundi for his keen interest in the problem and Dr. N. L. Singh for valuable discussions.

[1] See the extensive work of Sponer and collaborators.
* Most of the discrepancies in the analysis of the ultraviolet spectrum of these compounds seem to be due to this supposition.
[2] Sklar, Revs. Modern Phys. **14**, 232 (1942).
[3] Matsen, J. Am. Chem. Soc. **72**, 5243 (1950).
† Structurally, there are four possibilities for them: (1) First alternative (see text) in the $C_s$ group when one H (or F) atom of the $-CH_3$ (or $-CF_3$) part is in the plane of the ring and one above the plane and one correspondingly below it; (2) Second alternative (see text) in the $C_s$ group when two H (or F) atoms of the $-CH_3$ (or $-CF_3$) are above the plane of the ring and the third one is below the plane; (3) Completely unsymmetrical molecule so that neither the plane of the phenyl group nor the plane perpendicular to it passing through its $C_2$ axis has an H (or F) atom of the $-CH_3$ (or $-CF_3$) group; and (4) There is a pronounced internal rotation of $-CH_3$ (or $-CF_3$) against the phenyl group.
‡ Frequency numbering and other notations are those used by Herzberg, *Infrared and Raman Spectra of Polyatomic Molecules.*
[4] Pitzer and Scott, J. Am. Chem. Soc. **65**, 803 (1943).
[5] Ingold *et al.*, J. Chem. Soc. **1946**, 222–333; **1948**, 406–517.
[6] Garg, "Correlation of vibration frequencies of a molecule with those of its parts: calculation of some vibration frequencies of mono-substituted benzenes," J. Sci. Research, Banaras Hindu Univ. **IV** (to be published). See a short account of the same elsewhere.
§ The assignaments of not only those other frequencies of a mono-substituted benzene which have been correlated (reference 6) with the rest of the corresponding frequencies of benzene in regard to numerical relation and approximate mode of oscillation on the basis of approximate symmetry $C_{2v}$, but also of the remaining frequencies (due to the part attached to the phenyl group) can be shown to be satisfactory as regards species characteristics, *if* the symmetry group to which the mono-substituted benzene *really* belongs is settled with the help of observations on this frequency.

## Energetics of the Adsorption Process Responsible for the Joshi Effect

S. R. MOHANTY
*Chemical Laboratories, Banaras Hindu University, India*
(Received August 10, 1953)

THE Joshi effect,[1] *viz.*, an instantaneous and reversible photovariation (enhancement $+\Delta i$ and diminution $-\Delta i$) of the rms current $i$ under silent electric discharge, is negligibly small in a *freshly prepared* tube, and increases with the duration of exposure to discharge, at constant applied potential $V$ ($>V_m$ the minimum "threshold potential" for self-maintainance of the discharge), to a stationary maximum value after a certain "aging."[1,2] Joshi's theory[3-6] of the phenomenon contemplates: (1) Formation on the electrodes of an adsorption-like layer of electrons, ions, and excited gas particles derived from the discharge space; (2) emission from this layer of electrons by the external light; and (3) current decrease $-\Delta i$, as space charge effect, due to formation of (slow-moving) negative ions from electrons capture by the excited particles. Conditions disfavoring (3) give rise to the *positive effect* $+\Delta i$. Since stages (2) and (3) are instantaneous and fully reversible, the development with time $t$ of $\pm\Delta i$ is attributable to that of adsorption in (1) of Joshi's theory.

The author[2] has shown earlier that the $-\Delta i$-$t$ data are represented by the equation

$$(-\Delta i_{\max})-(-\Delta i_t)=[(-\Delta i_{\max})-(-\Delta i_0)]e^{-kt},$$

where $-\Delta i_0$ and $-\Delta i_t$ are the $-\Delta i$ values at the commencement of the discharge ($t=0$) and at time $t$, respectively, $-\Delta i_{\max}$ that of the final maximum, and $k$ a constant. The equation has a formal resemblance to that of the (chemical) reaction of the first order.

Other conditions remaining the same, $k$ increases with the temperature $T$. Thus, e.g., in a certain typical set of observations with all-glass Siemens' tubes ($p_{O_2}=52$ mm, $V=1.33$ kv rms, 50~), values for $k$ at 22.0 and 27.0°C are, respectively, 0.0229 and 0.0411 min$^{-1}$. The energy of activation, calculated from the Arrhenius equation, is 20.72 kcal/mole. The fact that this energy, while excluding that resulting from electrical activation, is still of the order of magnitude of activation energies in chemical reactions substantiates the observation[3] that the type of adsorption responsible for $\pm\Delta i$ is chemical in nature. Indeed, the energy of activation of physical adsorption is an order of magnitude smaller.[7,8]

The rate constant $k$ also increases with $V(>V_m)$. The thermal equivalent of the activation due to $V$ is being investigated.

[1] S. S. Joshi, Proc. Indian Sci. Congr., Presidential Address, Chemistry Section (1943).
[2] S. R. Mohanty, J. Indian Chem. Soc. **28**, 487 (1951).
[3] S. S. Joshi, Proc. Indian Sci. Congr., Part III, Physics Section, Abstract 26 (1946).
[4] S. S. Joshi, Proc. Indian Sci. Congr., Part III, Physics Section, Abstract 25 (1947).
[5] S. S. Joshi, Current Sci. (India) **15**, 281 (1946).
[6] S. S. Joshi, Current Sci. (India) **16**, 19 (1947).
[7] E. Berl and E. Weingaertner, Z. physik. Chem. **A173**, 35 (1935).
[8] S. Brunauer, *The Adsorption of Gases and Vapours* (Oxford University Press, London, 1942), Vol. I, "Physical Adsorption."

## The Thermodynamic Functions of Potassium Vapor*

MAURICE GRIFFEL
*Institute for Atomic Research, Iowa State College, Ames, Iowa*
(Received August 6, 1953)

THE thermodynamic functions of the monatomic and diatomic species of potassium vapor over the temperature interval 100 to 3000°K have been calculated from spectroscopic data. Ideality of the vapors was assumed. The physical constants used were those given by DuMond and Cohen,[1] and the spectroscopic data for the monatomic and diatomic species were taken from the compilations of Moore[2] and Herzberg.[3]

The methods for the rigid rotator-harmonic oscillator molecular model including high-temperature anharmonicity corrections were employed. In Table I are presented the results for the Gibbs function, $F_0-E_0^0/T$, the enthalpy function $H^0-E_0^0/T$, and the heat capacity. The entropy may be calculated from the first two. The dissociation equilibrium constant $K_p$, also given in Table I was calculated from the Gibbs function at each temperature. The dissociation energy $D_0^0\equiv\Delta E_0^0$ was taken to be 0.514 ev=11 854 cal/mole. In evaluating the vibrational contributions to the various functions, the tables of Johnston, Savedoff, and Belzer[4] were used.

* Contribution No. 244 from the Institute for Atomic Research and Department of Chemistry, Iowa State College, Ames, Iowa. Work was performed in the Ames Laboratory of the Atomic Energy Commission.
[1] J. W. M. DuMond and E. R. Cohen, Phys. Rev. **82**, 555 (1951).
[2] C. E. Moore, *Atomic Energy Levels*, Vol. **I**, Circular 467 (National Bureau of Standards, U. S. Department of Commerce, 1949).
[3] G. Herzberg, *Molecular Spectra and Molecular Structure* I. "Spectra of Diatomic Molecules" (D. Van Nostrand Company, Inc., New York, 1950).
[4] Johnston, Savedoff, and Belzer, *Contributions of the Thermodynamic Functions by a Planck-Einstein Oscillator in One Degree of Freedom* (U. S. Office of Naval Research, 1949).

TABLE I. Thermodynamic functions for monatomic and diatomic potassium vapor. Standard state is ideal gas at one atmosphere[a] cal/mole deg K.

| $T$°K | $-\left(\frac{F_0-E_0^0}{T}\right)_1$ | $-\left(\frac{F_0-E_0^0}{T}\right)_2$ | $K_p$ | $\left(\frac{H^0-E_0^0}{T}\right)_1$ | $\left(\frac{H^0-E_0^0}{T}\right)_2$ | $C_{p_1}^0$ | $C_{p_2}^0$ |
|---|---|---|---|---|---|---|---|
| 100 | 27.900 | 41.992 | $7.73\times10^{22}$ | 4.9680 | 7.9295 | 4.9680 | 8.7207 |
| 298.16 | 33.327 | 51.059 | $1.906\times10^{5}$ | 4.9680 | 8.6048 | 4.9680 | 9.0565 |
| 335.5 | 33.913 | 52.077 | $1.905\times10^{4}$ | 4.9680 | 8.6565 | 4.9680 | 9.0817 |
| 500 | 35.895 | 55.563 | 43.10 | 4.9680 | 8.8123 | 4.9680 | 9.1769 |
| 760 | 37.975 | 59.283 | 0.5831 | 4.9680 | 8.9604 | 4.9680 | 9.3117 |
| 1000 | 39.339 | 61.757 | 0.07809 | 4.9680 | 9.0592 | 4.9680 | 9.4320 |
| 1200 | 40.244 | 63.415 | 0.02676 | 4.9680 | 9.1296 | 4.9680 | 9.5314 |
| 1400 | 41.010 | 64.827 | 0.01239 | 4.9680 | 9.1942 | 4.9680 | 9.6305 |
| 1600 | 41.674 | 66.059 | 0.006931 | 4.9680 | 9.2548 | 4.9680 | 9.7294 |
| 1800 | 42.259 | 67.152 | 0.004406 | 4.9680 | 9.3131 | 4.9680 | 9.8282 |
| 2000 | 42.783 | 68.136 | 0.003062 | 4.9680 | 9.3695 | 4.9680 | 9.9268 |
| 2200 | 43.257 | 69.032 | 0.002275 | 4.9680 | 9.4247 | 4.9680 | 10.0255 |
| 2400 | 43.691 | 69.854 | 0.001773 | 4.9680 | 9.4788 | 4.9680 | 10.1241 |
| 2600 | 44.090 | 70.615 | 0.001437 | 4.9680 | 9.5323 | 4.9680 | 10.2227 |
| 2800 | 44.461 | 71.324 | 0.001201 | 4.9680 | 9.5851 | 4.9680 | 10.3213 |
| 3000 | 44.809 | 71.987 | 0.001024 | 4.9680 | 9.6375 | 4.9680 | 10.4020 |

[a] Subscript 1 refers to monatomic vapor; subscript 2 to diatomic vapor.